Doctoral theses at NTNU, 2012:49

Rune Schlanbusch

Control of rigid bodies

with applications to leader-follower spacecraft formations

ISBN 978-82-471-3365-1 (printed ver.)
ISBN 978-82-471-3366-8 (electronic ver.)
ISSN 1503-8181

Rune Schlanbusch
Doctoral Thesis

NTNU
Norwegian University of
Science and Technology

Thesis for the degree of
philosophiae doctor
Faculty of Information Technology, Mathematics, and
Electrical Engineering
Department of Engineering Cybernetics

NTNU
Norwegian University of
Science and Technology

Doctoral theses at NTNU, 2012:49

NTNU

NTNU
Norwegian University of
Science and Technology

Rune Schlanbusch

Control of rigid bodies

with applications to leader-follower spacecraft formations

Thesis for the degree of philosophiae doctor

Trondheim, March 2012

Norwegian University of
Science and Technology
Faculty of Information Technology, Mathematics, and Electrical Engineering
Department of Engineering Cybernetics

NTNU
Norwegian University of Science and Technology

Thesis for the degree of philosophiae doctor

Faculty of Information Technology, Mathematics, and Electrical Engineering
Department of Engineering Cybernetics

ISBN 978-82-471-3365-1 (printed ver.)
ISBN 978-82-471-3366-8 (electronic ver.)
ISSN 1503-8181

Doctoral Theses at NTNU, 2012:49

Printed by Fagtrykk, Trondheim

Summary

This thesis addresses the control problem of rigid bodies with applications to controlled synchronization of leader-follower spacecraft formations for both the rotational and translational cases. All control solutions throughout this thesis are based on the robotic controllers of Paden and Panja, and Slotine and Li necessarily adopted to fit the appropriate models and quaternion parametrization. After a short introduction including previous work, contributions and delimitations, the thesis is divided into three parts.

The first part is named "Modeling of leader-follower spacecraft formations" containing Chapter 2 which includes presentation of the classical equations of motion of ideal Keplerian orbits, attitude kinematics and dynamics, relative attitude and translational dynamics for leader-follower spacecraft formations; the latter parameterized using the different representations including true anomaly of the leader spacecraft and Euclidian parameters represented in either leader orbit frame or follower body frame. Furthermore, we present mathematical models of the most common orbital perturbing forces and torques and show through simulations how these forces affect the relative orbits.

The second part is named "Control of rigid bodies" and is divided into three chapters where we treat continuous and hybrid tracking control of rigid bodies, respectively in Chapter 3 and 4, while we discuss the choice of preferable equilibrium point for rotational maneuvers in Chapter 5. In the third chapter the attitude tracking control problem is considered where uniform exponential stability in the large of the equilibrium point is obtained for state feedback where disturbances are assumed to be known, while uniform practical exponential stability in the large of the equilibrium point is obtained for unknown but bounded disturbances; additional analysis also shows that the equilibrium point of the system in closed loop with the sliding surface-based control law can be proven uniformly asymptotically stable, almost in the large. Next, we introduce state dependent gains where the idea is to have large gains while working away from the equilibrium for fast trajectory convergence and small gains close to the equilibrium point to reduce sensitivity to measurement noise. We also treat the topic of "output" feedback (without velocity measurement) using similar non-linear gains proving uniform practical asymptotical stability of the equilibrium point. All results (except the result called "almost in the large") are based on the assumption that the attitude error never increases beyond 180 degrees relative to the chosen equilibrium point[1] and similar restrictions are

[1] By choosing between two equilibria we in some sense choose the rotational direction for a maneuver.

made for the estimated attitude error. In Chapter 4 we remove this assumption by introducing switching control laws with hysteresis, and similar stability results are obtained except that they are asymptotic instead of exponential for state feedback. We combine the two presented control laws through a hybrid supervisor, showing improved performance compared to using each one individually, and furthermore, revisit the output feedback controller applying switching for both the dynamics and observer, entirely removing the previous mentioned assumption on maximum allowed attitude error. In Chapter 5 we present two different schemes to choose the preferable equilibrium point based on either numerical analysis of simulation results or using an optimization technique on the linearized equations. Both methods include the initial rotational motion into the analysis where previous results usually choose equilibrium point based on the shortest rotation only.

The third part is named "Applications" where we consider the synchronization problem of leader-follower spacecraft formations in Chapter 6, autonomously generated references in Chapter 7 and collision avoidance in Chapter 8. In Chapter 6 we present two different control laws for attitude synchronization of rigid bodies where uniform asymptotic stability of the equilibrium point is obtained for known disturbances while practical results for unknown but bounded disturbances, where both analysis are based on cascaded theory; a similar result is also obtained for a leader-follower spacecraft formation based on the hybrid control solution; for relative translational control we show uniform global practical exponential stability of the equilibrium point. The latter result is extended in two different directions; first we assume that the total disturbance has a constant mean and by adding I^2 action we show that the residual can be reduced, and secondly by implementing exponential varying gain matrices where the gains are individually varying along each axis, we show that the performance for maneuvers can be increased from a fuel consumption point of view without increasing sensitivity to measurement noise compared to our previous results on state dependent gains. In Chapter 7 we present two different schemes for autonomously generated references based on leader and relative position coordinates for a leader-follower formation. In the first scheme considered the leader spacecraft is assumed to be nadir pointing while the reference for the follower spacecraft is generated to point at the leader nadir foot-print[2] at all time, even during formation reconfiguration while in the second scheme, references are generated for both the leader and follower to point their instruments at a common fixed or time varying target on the Earth surface specified by longitudinal and latitudinal coordinates. In Chapter 8 we treat the problem of collision avoidance during spacecraft reconfiguration utilizing what is called the null-space based (NSB) behavioral control concept where different tasks are merged together through use of a supervisor. We propose three different collision avoidance tasks where collision spheres[3] are either statically sized or dynamically sized along with a move to target-task which are combined with the control law through stability analysis to prove that collisions will not occur.

[2]By nadir foot-print we here mean the longitude and latitude obtained in the intersection between the Earth surface and a vector pointing from an orbiting spacecraft pointing towards the center of the Earth.

[3]When these spheres - which are located around each member - are entered, evasive maneuvers are performed.

Preface

This thesis is submitted in partial fulfillment of the requirements for Philosophiae Doctor Degree (PhD) at the Norwegian University of Science and Technology (NTNU), and presents the research results from my doctoral studies from October 2007 to March 2011 at the department of technology, Narvik University College (NUC). The research has been financially supported by the research council of Norway under project number 182731/V10 which is part of the activity "Strategic Projects - University Colleges".

First of all I want to thank my supervisor Professor Per Johan Nicklasson for introducing me to the world of spacecraft control and by giving me the possibility to spend more than three years of my life specializing in the enjoyable world of control theory and stability analysis. I also want to thank my co-supervisor Professor Jan Tommy Gravdahl at NTNU for his support and help throughout these years, both academic and administrative. I am indescribably grateful to Dr. Raymond Kristiansen whom has invested numerous hours of his time in my work through interesting academic discussions, calculations, simulations and the art of writing and at the same time developing a friendship which is much appreciated, in my heart you are my third supervisor. I would especially like to thank Dr. Antonio Loría and his wife Dr. Elena Panteley which I visited with my family for three months during the autumn of 2009 at Laboratoire des signaux et systèms, Supélec in Paris. Much of what I have learned these last years is through our joint work where all my elementary questions have been answered, which is a significant proof of their infinite patience.

During these last years I have also been fortunate to collaborate with my best friend and colleague Espen Oland which now has started on his own pursue for the doctoral degree and in some sense move the research baton further down the road here at NUC. I also want to thank my previous PhD colleague, now post doctor Esten Ingar Grøtli at NTNU for interesting discussions when we met in the Netherlands and for his contribution, comments and guidance during our joint work. Frode Einarsen and Bjarte Hoff, in addition to the rest of my colleagues here at NUC are people I also want to thank for the opportunity to befriend during the last years, especially during social hours. The administrative staff, especially Ellen Julin and Sidsel Kruuse-Meyer at the library also deserve attention for their work of providing me with all necessary material.

Although a lot of people have contributed in various ways there are none who have contributed more than my wife Siri and my son William. By them I have received all the patience and support I could dream of while at the same time

making every day joyous, constantly reminding me that life apart from research also is meaningful. For this I am forever indebted and I love you both. The contribution from the rest of my family has also been significant and I want to thank my mother, father and big brother Kristian for their support, inspiration and interest throughout these years. I would also like to thank my parents in law Terje and Gro-Heidi Korneliussen for the chance of getting to know you, your warm acceptance of me into your family and your pleasant company during these years in the cold, harsh north.

Contents

List of Figures

List of Tables

Chapter 1

Introduction

The work presented in this thesis are various results on control of rigid bodies with a special focus on leader-follower spacecraft formations. While working on this topic, new ideas were constantly appearing as the work proceeded and obstacles were encountered. The development has been as follows. In previous work typically only the relative motion between the leader and follower is analyzed while the leader is assumed to be perfectly controlled. This leads to results more similar to tracking control than synchronization, and thus we started investigating control of rigid bodies in general, extending the synchronization analysis through use of cascaded theory. Since fuel and energy consumption are very important aspects concerning orbiting spacecraft, we have focused on developing methods to reduce energy consumption without reducing overall performance. This has been done by introducing variable gains to reduce sensitivity to measurement noise and hybrid supervisory control. Furthermore, the problem of choosing preferable rotational direction during attitude stabilization has received some attention of ours, comparing both continuous and hybrid control and also through use of energy functions or optimization. The topic of output feedback has also been addressed because of the possibility to reduce spacecraft mass and volume and then cost by replacing physical equipment with observers. Since many of the planned missions contain up to 30 members, we have investigated the topic of autonomous obstacle and collision avoidance showing that by introducing a dynamical scheme, the allowed passing distance between members can be reduced leading to a possible reduction in energy consumption during formation maneuvers. Also, because of the large number of members, we have developed schemes for autonomous attitude reference generation where each follower points at the same location on the Earth surface as the leader to reduce the workload of ground station personnel.

As a lot of the presented results are in some sense reducing energy consumption or external workload we do not speak of optimality as in the sense of the word from an engineering point of view. We want our work to be autonomous without needing large amount of computation - since computational resources often are spares on board a spacecraft - which often is required for optimal control solutions. We want to keep the onboard computations and ground station workload at a minimum because in our vision, the members of a spacecraft formation should be small, light

and cheap to reduce cost, while on the other hand be able to perform accurate maneuvers to bring out the best from the concept of spacecraft formations.

1.1 Control of rigid bodies

Attitude control of rigid bodies is an interesting control problem which has a lot of applications including control of aircraft, unmanned aerial vehicles (UAV), helicopters, spacecraft and autonomous underwater vehicles (AUV) to name a few, and has also many similarities to robotic control. The dynamics of rigid bodies are described by the Euler equations, with the angular velocity vector and the tensor of inertia appearing as necessary components also referred to as Euler's moment equations or the Euler-Poisson equations (Euler, 1752). The integration problem of these equations has been widely studied by the most outstanding scientists throughout time similar to Fermat's Last Theorem (Wiles, 1995). See (Kovalev and Savchenko, 2001) and references therein for a selection of the most important results in rigid body dynamics obtained in 20th century as well as a statement of the problems representing the greatest interest and promoting to the completion of solution, and the work of Tsiotras and Longuski (1996) for an example of what kind of solutions which are already obtained.

A lot of results have been presented yielding different solutions to the problem of controlling the angular motion of rigid bodies using the Lyapunov method. Mortensen (1963) used the second Lyapunov method to construct the external control torques ensuring the asymptotic stabilization of the rotation of a rigid body. The result was later extended in Mortensen (1968) where a linear feedback law with constant coefficients for attitude control of an arbitrary rigid body was designed through use of Lyapunov techniques. In most cases these designs are based on sound physical insight, but they result in systems that are difficult to analyze, and the analysis is not carried out. It is, therefore, desirable to approach the design problem from a general point of view by taking advantage of the basic similarity of all attitude control systems; namely, that their primary control objective is to maintain the real attitude as close to the desired attitude as is necessary for successful operation, and their basic nonlinearity is that of three-dimensional rotations which were generalized by Meyer (1971). Smirnov (1974) studied the active control of the rotational motion of a rigid body using the Lyapunov function. In such study, a non-linear control law was derived with the help of the Lyapunov technique. The stability of uniform rotations of a rigid body with a fixed point about its first principal axis was studied by Kovalev and Savchenko (1975), while Belikov (1981) investigated the effect of gyroscopic forces on the stability of uniform rotation of a rigid body about its principal axis. In (Lebedev, 1981) triaxial orientation was investigated for a rigid body with an arbitrary mass geometry in the case when the constraints on the components of the controlling moment, which is a linear combination of independent vectors, are specified in implicit form, and control problems for both time-optimality and asymptotic stability were investigated. Brockett (1983) presented both necessary and sufficient conditions for existence of a smooth feedback which renders an equilibrium point of a nonlinear system locally asymptotically stable by means of two torques, each applied along a principal axis. It was later

Figure 1.1: Robots can do jobs faster and better than humans with precision, intelligence and endless energy levels making them an integral part of industry. Reproduced with courtesy to Asea Brown Boveri (ABB).

shown by Aeyels (1985) that the results also hold for one available torque along an appropriately chosen principal axis, while Crouch (1984) reported similar results for attitude control using geometric control. Furthermore, Aeyels and Szafranski (1988) showed that single control aligned with a principal axis cannot asymptotically stabilize the system. Sontag and Sussmann (1988) complimented this result by proving that the angular velocity equations can be smoothly stabilized with a single torque controller for bodies having an axis of symmetry. Byrnes and Isidori published a series of papers on global results for state feedback, but showed in (Byrnes and Isidori, 1989) (see references within) that a system which can be globally stabilized using state feedback, cannot be locally asymptotically stabilized by static output feedback. The problem was revisited by Outbib and Sallet (1992) using the Jurdjevic-Quinn techniques, leading to simpler feedback laws than previous results.

As most of the cited work above is concerned with control of the dynamic equations, results on attitude control have been developed in parallel. The rotation

Figure 1.2: A Remotely Operated Vehicle (ROV) in support of oil and gas drilling, construction, and production activities working in ocean depths inaccessible for most human activity. Reproduced with courtesy to Oceaneering.

between two frames is usually given by the *rotation matrix* also called the *direction cosine matrix* where many different parameterizations have been proposed over time. A widely used set of parameters for the rotation matrix is called the *Euler angles* where the rotation matrix is given as a composite rotation of selected combinations of rotations about the three principal axis often called *roll-pitch-yaw* (Egeland and Gravdahl, 2002). This representation has an inherent singularity at $\theta = 90^\circ$ which justifies use of other parameterizations such as the *angle-axis parametrization* which has four parameters; three parameters describing a rotation vector while one parameter describing the rotation angle about this vector; the parametrization is based on Euler's theorem stating that any rotation of a rigid body can be described by a single rotation about a fixed axis. *Euler parameters* and especially the *unit quaternion* (Hamilton, 1844) are both singularity free parameterizations based on the angle-axis parametrization, where the latter has been developed and utilized for representation of the rotational motion of rigid bodies as early as the 1950's; see (Shuster, 2008) for a historically retrospective, problems and formulations. Among other three parameter representations utilized we find the *Euler rotation vector*, the (modified) *Euler-Rodrigues parameters* and the $\boldsymbol{w}$ parameter (Tsiotras and Longuski, 1995) to name a few. See Tsiotras (1996) for a discussion on how different choices of parameters may suit different control problems and Shuster (1993) for a survey of representations.

Early results on attitude control were reported by the National Aeronautics and Space Administration (NASA) (Meyer, 1971) presenting quaternion-based control laws and the European Space Agency (ESA) (Crouch *et al.*, 1980) among others,

Figure 1.3: Unmanned Aerial Vehicles (UAV)s have become increasingly popular in military industry for reconnaissance as well as attack missions along with civil applications, such as firefighting or security work, such as surveillance of pipelines. Reproduced with courtesy to Andøya Rocket Range (ARR).

which in some sense serves as what can be called a base for later work. A linear decoupled model-independent control law based on quaternion feedback was presented by Wie and Barba (1985), control laws where the inertia matrix is represented along with constrained gain matrices based on unit-quaternion representation in (Wie *et al.*, 1989), while Koditschek (1988) reported adaptive results obtaining what was called "almost-global" asymptotically exact tracking. An important paper on the subject of attitude control was written by Wen and Kreutz-Delgado (1991) where a thorough review of previous work was given along with a general framework for the analysis of the attitude tracking control problem for rigid bodies. These results only hold for three independent actuators, and the case of feedback stabilization using only two independent controls was investigated in (Byrnes and Isidori, 1991), and furthermore, it was shown by Morin *et al.* (1995); Morin and Samson (1997) that asymptotic/exponential convergence can be obtained by letting the feedback be time-varying. Joshi *et al.* (1995) also studied the problem of global asymptotic stability of the attitude of a rigid spacecraft using model-independent quaternion feedback with gain matrices and simpler Lyapunov function and stability proof compared to what was reported in (Wen and Kreutz-Delgado, 1991). A different approach was proposed by Bullo and Murray (1999) where they use the Riemannian

structure of the configuration manifold of a fully actuated simple mechanical control system to derive a full state, coordinate-free feedback-plus-feedforward controller that locally exponentially tracks a general bounded reference trajectory.

As can be seen, the control solutions span in a lot of different directions, but naturally, attitude tracking control lies on a bulk of literature on tracking control of robot manipulators and, more generally Euler-Lagrange (EL) systems –*cf.* Ortega *et al.* (1998); see also Van der Schaft (1996) and references within for more on passivity and applications. The so-called *passivity-based approach* to robot control has gained much attention, which, contrary to computed torque control, handles the robot control problem by exploiting the robots' physical structure (Berghuis and Nijmeijer, 1993). A simple solution to the closed-loop passivity approach was proposed by Takegaki and Arimoto (1981) on the robot position control problem. The natural extension and a classic in robot control literature is the PD+ controller of Paden and Panja –*cf.* (Paden and Panja, 1988) which, together with the Slotine and Li controller –(Slotine and Li, 1987), were the first algorithms for which global asymptotic stability was demonstrated.

The passivity-based approach has successfully been applied to the rigid body control problem in numerous examples such as in (Slotine and Di Benedetto, 1990) where accurate attitude tracking control of rigid spacecraft handling large loads of unknown mass properties were investigated, Egeland and Godhavn (1994) presented an adaptive control scheme using a linear parametrization of the equation of motion, while Quottrup *et al.* (2001) obtained similar passive results for the Rømer satellite and global asymptotic stability for an input and output strictly passive system in feedback interconnection. In (Li *et al.*, 2006) the authors presented a passivity-based nonlinear attitude regulator for a rigid spacecraft subjected to control saturation, and in the recent paper by Casagrande *et al.* (2011) the authors proposed a controller that asymptotically stabilizes a passive system feeding back only the integral of the output based on the sampled integral stabilization technique.

Along with the passivity based approach, examples of other design methods that appeared in the eighties were called (integrator) backstepping and adaptive backstepping which yield the advantage of design flexibility compared to other design methods; see (Krstić *et al.*, 1995; Fossen, 2002) and references within for thorough presentations. The techniques have successfully been utilized on rigid bodies in many forms over the years –*cf.* *e.g.* (Wie *et al.*, 1989; Joshi *et al.*, 1995; Jensen and Wisniewski, 2001; Kristiansen *et al.*, 2009).

Output feedback control has received an increased amount of attention the last years, where for rigid bodies the technique is mostly used for angular velocity estimation by replacing measurement instruments such as gyroscopes, thus saving weight and money. Typically by output it is meant measurement of position or attitude but, although the phrase *output feedback* often is used, the correct term for rotational control would be *without velocity measurement* since the output from the sensors are measurement vectors of *e.g.* sun, stars, magnetic field and then the attitude is propagated through use of algorithms such geometric-based methods (TRIAD) (Wertz, 1978), QUEST (Shuster and Oh, 1981), Kalman filters (Lefferts *et al.*, 1982) etc. Such an angular velocity observer was presented by Salcudean (1991) using unit quaternions and a mechanical energy function approach which were proven globally convergent, while a passivity approach was considered by

Figure 1.4: The Hubble telescope is one of the largest and most versatile space telescopes, and is well-known as both a vital research tool and a public relations boon for astronomy. Reproduced with courtesy to NASA.

Lizarralde and Wen (1996) where the passivity properties were exploited in a non-linear controller to ensure asymptotic stability without need of a model-based observer for angular velocity reconstruction. Similar results were presented in (Ortega *et al.*, 1994) where a class of EL systems were determined, satisfying a dissipation propagation condition, while output feedback tracking control of a class of EL systems subjected to monotonic loads were investigated in (Aamo *et al.*, 2000). Tsiotras (1998) established passivity for the rigid body attitude equations where linear asymptotical stabilizing controllers and control laws followed naturally, while Astolfi (1999) revisited the problem of stabilizing the angular velocity of a rigid body where only two of the three states are measured and showed construction of a hybrid control law yielding exponential convergence. In (Caccavale and Villani, 1999) two different schemes were presented based on results for output control of robot manipulators –*cf.* (Berghuis and Nijmeijer, 1993); in the first scheme, a second-order model-based observer is adopted for estimation of the angular velocity, while the second scheme is based on a lead-filter for estimation of the angular velocity error. An alternative approach using Modified Rodrigues Parameters (MRP) was presented in (Akella, 2001) simplifying the structure of the control law. The topic of output feedback was further pursued for spacecraft control in (Costic *et al.*, 2000), where the inertia matrix was assumed unknown and the problem was solved using a quaternion-based adaptive approach while Wong *et al.* (2001*b*) reported similar results using the MRP kinematic representation. Maithripala *et al.* (2004) presented an intrinsic formulation of an observer for a class of simple mechanical systems on a Lie group, that is, no coordinates are needed to be introduced on the

Figure 1.5: The International Space Station (ISS) as seen from *Discovery*, serves as a research laboratory that has a microgravity environment in which crews conduct experiments in biology, human biology, physics, astronomy and meteorology, among other things. Reproduced with courtesy to NASA.

manifold which is a Lie group, hence a single formulation is valid for all coordinate patches, followed by an output feedback reference tracking controller based on the same principles converging from almost every initial condition (Maithripala *et al.*, 2006). Tayebi (2006) presented a scheme based on a unit quaternion observer and a linear feedback control law to prove asymptotic stability of the equilibrium point, thus avoiding the use of lead filter. The problem was further pursued in Astolfi and Lovera (2002); Tayebi (2008) where first-order dynamic output feedback controllers based on unit-quaternion representations were proposed obtaining global and almost global results, respectively, and almost global exponential stability for stabilization on SE(3) in (Cunha *et al.*, 2008). Bertrand *et al.* (2009) obtained results working directly on SO(3) where the gains in the control design can be tuned in advance to ensure that the torque inputs satisfy arbitrary saturation bounds.

The problem of global stability for manifolds in general and especially on $SO(3)$ has submerged as an interesting problem which has received some attention the last couple of years but surprisingly little in general. It is well known that representation on $SO(3)$ has four equilibria and that all three-parameter parameterizations such as Euler angles have singularities (Hughes, 1986). Euler parameters and unit quaternions are non-singular parameterizations of $SO(3)$ though the mapping from S^3 to $SO(3)$ is two-to-one on the manifold, that is, for each point $\mathbf{p} \in SO(3)$, there are exactly two unit quaternions, $\pm\mathbf{q}$. From an analytical view-point the two equilibria must be considered as different hence, one may not expect to achieve *global* stability properties in closed-loop using continuous feedback (Bhat and Bernstein, 2000). It was shown in (Mayhew *et al.*, 2009) that global stability properties of the

dual equilibrium points is achievable by lifting the trajectory in $SO(3)$ to a continuous path on S^3 through use of hybrid feedback, hence the global stabilization problem *on* $SO(3)$ is equivalent to stabilizing both quaternions corresponding to the same attitude, but, if one takes a look at the literature well known text books such as Hahn (1967) and Khalil (2002) clearly states that the term *global* refers to the whole state space $\mathbb{R}^n$ which is not the case for systems working on a manifold such as $SO(3)$, S^3 etc.; from this point of view, the term global has widely been misused in literature.

As previously mentioned, hybrid control is a suitable tool for solving the problem of the dual equilibrium points associated with quaternion feedback, among other things. Hybrid systems are dynamic systems that exhibits both continuous and discontinuous dynamic behavior that is, the system can both *flow* and *jump*. The field has gained a lot of attention the recent years; see *e.g.* (Van der Schaft and Schumacher, 2000; Goebel *et al.*, 2009) and references within for a thorough tutorial on modeling the dynamics of hybrid systems, on the elements of stability theory for hybrid systems, and on the basics of hybrid control; also see Liberzon (2003) for a thorough introduction on switching control. Discontinuous feedback has successfully been applied on rigid bodies such as in (Krishnan *et al.*, 1995) where the authors considered the case of two momentum wheel actuators using *pseudo-Euler's angles* where the spacecraft equations are not asymptotically stabilized to any equilibrium attitude using a time-invariant continuous feedback control law, but showed that it can be accomplished using discontinuous feedback control. A discontinuous control approach was also presented by Fragopoulos and Innocenti (2004), inspired by the work of Fjellstad and Fossen (1994*b*), where a signum function was utilized in the feedback controller, but, as pointed out by Mayhew *et al.* (2009), does not lead to a *robust* result because the rigid body may be stuck 180 degrees away from the equilibrium for infinite time when measurement noise is introduced. This particular problem was solved by including hysteresis to the switching (Mayhew *et al.*, 2009).

Numerous other techniques and applications for control of rigid bodies can be found such as time and fuel optimal control (Junkins and Turner, 1986; Spindler, 1996; Tsiotras *et al.*, 1996; Krstić and Tsiotras, 1997; Ioslovich, 2003; Lee *et al.*, 2008; El-Gohary and Tawfik, 2010); magnetic attitude control (Wiśniewski and Blanke, 1999; Lovera and Astolfi, 2004; Bhat, 2005); solar panel deployment (Kuang *et al.*, 2004); underactuated control (Tsiotras and Luo, 2000; Casagrande *et al.*, 2008); actuator failure (Tsiotras and Doumtchenko, 2000); flexible spacecraft (Bloch *et al.*, 1992; Song and Agrawal, 2001; Di Gennaro, 2003; Bang and Oh, 2004; Erdong and Zhaowei, 2010) and underwater vehicles (Fjellstad and Fossen, 1994*a*; Pettersen and Egeland, 1999; Astolfi *et al.*, 2002) to name a few. Target tracking for spacecraft is another application that has been addressed, such as in (Goerre and Shucker, 1999; Chen *et al.*, 2000; Tsiotras *et al.*, 2001; Steyn, 2006). To generate target tracking references usually a vector pointing from the spacecraft towards the desired point along with the first and second derivatives of the vector is calculated and then transformed into desired quaternions and angular velocities to ensure high accuracy tracking of the specified target point when fed as desired trajectories into the control law.

1.2 Synchronization

Synchronization in nature has puzzled and inspired scientists for centuries. The thought of termites and ants organizing and construct their mounds and anthills without any work leaders or architectures, based on very limited local information of the whole process (no global overview) spanning over several lifetimes of the participants, is fascinating. This kind of synchronization is rather ordinary in biological systems and are called *self-organization* or *self-synchronization*, defined as (Camazine *et al.*, 2003)

Self-organization is a process in which pattern at the global level of a system emerges solely from numerous interactions among the lower-level components of the system. Moreover, the rules specifying interactions among the systems' components are executed using only local information, without reference to the global pattern.

It should be noted that even as we often talk of biological systems such as fish schools, bird formations, flashing of fire flies *etc.* when synchronization is discussed, patterns of wind-blown ripples on the surface of a sand dune is also an example of self-synchronization. The group behavior is motivated by increased benefits for each member compared to living on its own. Typically this includes better protection against predators and increased probability to find food; also aero- and hydro-dynamical effects because of group behavior leads to *e.g.* increased range for geese flying in their characteristic V-formation. The control of self-organization is divided into two basic modes of interaction: positive and negative feedback. The first one enables phenomenons as flocking or schooling where birds nesting or fishes in schools attracts new members based on the total size of their formations, that is, the reason for a specific bird to nest at a specific mountain is not necessarily that it finds this particular place as the best but, because so many other birds are nesting there it has to assume that this is a good spot. Negative feedback is typically information which is gathered on small scale such as the distance towards the neighbors of each member thus, the size and shape of a formation can typically be described by the two previous mentioned mechanisms.

Although self-organization is particulary present in nature, alternatives are often observed, such as patterns formed by humans, since the pattern-formation processes with human groups are easily perceived, and are divided into four groups: leader, blueprint, recipe and template (Camazine *et al.*, 2003). The *leader* directs the building activity of the group and provide each group member with detailed instructions about what to do to contribute to building the overall pattern; the *blueprint* forms a compact representation of the spatial or temporal relationships of the parts of a pattern, the *recipe* which can be understood as sequential instructions that precisely specify the spatial and temporal actions of the individual's contribution to the whole pattern, and the *templates* can be understood as a full-size guide or mold that specifies the final pattern and strongly steers the pattern-formation process. Examples of the alternatives in order could be the rowing crew, where stroke synchronization and coordinated shifts in stroke frequency are largely responses to the coxswain's commands; a crew of construction workers receiving a detailed and virtually complete description through a blueprint; a cook

Figure 1.6: Ducks swimming in formation. The V-formation allows birds to communicate more easily and provides them with good visual contact of each other to keep the flock together. Reproduced with courtesy to the U. S. Fish and Wildlife Service Refuge Staff.

preparing food using a detailed recipe (without introducing feedback through tasting); and a die or mold used as template for *e.g.* producing tools or minting coins. This is according to Blekhman *et al.* (1997) called *controlled synchronization*, –see Blekhman *et al.* (1997) for a formalized mathematical definition. In addition to self-synchronization and controlled-synchronization Blekhman *et al.* (1997) also defines *natural-synchronization* as disconnected systems that present synchronous behavior, and refers to the example that *all precise clocks are synchronized in the sense of frequency*. Controlled-synchronization is divided by Nijmeijer and Rodriguez-Angeles (2003) into *internal (mutual) synchronization*, where all synchronized objects occur on equal terms in the unified-multi-composed system, and *external synchronization*, where it is supposed that one object in the multi-composed system is more powerful than the others and its motion can be considered as independent of the motion of the other objects. Kyrkjebø (2007) defined it as *degree of synchronization* where *cooperation* reflects internal synchronization while *coordination* reflects external synchronization.

Synchronization of dynamical systems was first studied by Christian Huygens in the XVIIth century where he studied two clocks operating simultaneously from the practical requirement of redundancy for maritime clocks (Huygens, 1669), whereas he later found that the pendulum clocks swung in exactly the same frequency and 180° out of phase (Huygens, 1673; Bennett *et al.*, 2002). Ultimately, the innovation of the pendulum clock did not solve the longitude problem, however, Huygens's synchronization observations have served to inspire study of sympathetic rhythms of interacting nonlinear oscillators in many areas of science. Another interesting observation was done by Cassini (1693) and formulated as

Cassini's first law: *the Moon has 1:1 spin-orbit resonance. This means that the rotation / orbit ratio of the Moon is such that the same face is always facing the Earth.*

Strutt (1896) also made an important discovery on self-synchronization for two tuning forks with electromagnetic excitation which were coupled either electrically, mechanically or by using a resonator box. The phenomenon of self-synchronization was in some sense "rediscovered" when a particular case of self-synchronizing mechanical vibro-exciters mounted on the same vibrating organ was discovered by chance in the U.S.S.R (Blekhman, 1988). Blekhman (1988) describes the synchronization phenomenon as

several man-made or natural objects performing in the absence of interaction oscillations or rotational motions with different frequencies (angular velocities); the start moving with the same multiple or commensurable frequencies (angular velocities) in the presence of even very weak interactions. In such cases, definite phase correlations between oscillations and rotations are being established.

In recent years, the problem has obtained increasing interest in various research areas due to its impact in technology development and challenges it imposes –see *e.g.* (Blekhman, 1988; Rodriguez-Angeles, 2002; Nijmeijer and Rodriguez-Angeles, 2003; Efimov, 2005; Kyrkjebø, 2007) and references within for more detailed and mathematical rigorous definitions and general results. In (Kyrkjebø, 2007) controlled synchronization is divided into three main approaches: *model-based*, *behavioral* and *virtual object*.

Model-based controlled synchronization consists in using the laws of physics and control theory in order to induce synchronization in dynamical systems. Successful instances include synchronization of robot manipulators (Rodriguez-Angeles and Nijmeijer, 2001; Bondhus *et al.*, 2004), leader-follower spacecraft formations (Lawton and Beard, 2000; Bondhus *et al.*, 2005; Kristiansen, 2008; Grøtli, 2010), ship replenishment operations (Fu *et al.*, 2004; Kyrkjebø *et al.*, 2006), rigid bodies (Bai *et al.*, 2008, 2009; Sarlette *et al.*, 2010) to name a few, and even synchronization schemes with multiple leaders have been considered as in (Meng *et al.*, 2010).

Behavioral based controlled synchronization is based on a group of systems which is controlled in a way such that each member collaborate in order to achieve a task as a team of agents. Examples may be found in the areas of autonomous vehicles (Lawton *et al.*, 2000; Ögren *et al.*, 2004; Antonelli and Chiaverini, 2006; Arrichiello, 2006), under-actuated marine vessels (Arrichiello *et al.*, 2006; Cui *et al.*, 2010) and rigid bodies (Nair and Leonard, 2007; Bai *et al.*, 2007, 2009; Sarlette *et al.*, 2009; Dimarogonas *et al.*, 2009). An instance of behavioral based control is *consensus*, in which a group of systems coordinate their motion without any subsystem having a higher hierarchy with respect to the others –see (Ren and Beard, 2008) and references within.

Virtual structure controlled synchronization was defined by Tan and Lewis (1996) as *a collection of elements,e.g. robots, which maintain a (semi) rigid geo-*

Figure 1.7: Navy and Japan Air Self-Defense Force aircraft fly in formation over U.S. Navy and Japan Maritime Self-Defense Force ships. In military activities traveling and maneuvering together in a disciplined, synchronized, predetermined manner, reduces losses and increases the chance of victory. Reproduced with courtesy to the United States Navy.

metric relationship to each other and to a frame of reference. The overall motion of this structure is then utilized to generate translational and rotational references for each individual member to track using individual tracking controllers, thus transforming the regulation problem into several local tracking-control problems and also removing the need of a leader. The approach has successfully been utilized in areas such as control of mobile robots/vehicles (Tan and Lewis, 1996; Young *et al.*, 2001; Egerstedt *et al.*, 2001; Lalish *et al.*, 2006) and marine crafts (Skjetne *et al.*, 2002), but can also be utilized in combination with model-based and behavioral approaches to achieve synchronization on different levels of abstraction as in (Beard *et al.*, 1998, 1999, 2001; Ren and Beard, 2004; Ögren *et al.*, 2004; Cong *et al.*, 2011) for control of spacecraft formations and mobile robot sensor networks, and consensus. The adjective *virtual* has also been used in other forms such as *virtual vehicle* (Crowley, 1989; Kyrkjebø *et al.*, 2006), *virtual leader* (Leonard and Fiorelli, 2001; Gu *et al.*, 2006) and *virtual center* (Tillerson *et al.*, 2003).

For large systems, *e.g.* complex dynamical systems such as spacecraft formations, the expression *divide and conquer* may seem appealing, and for good reasons; by dividing a system into smaller parts, the difficulties of stability analysis and control design can be greatly reduced. A particular case of such systems is the cascaded structure which consists of a *driving* system working as an input to the *driven* system through an *interconnection*, similar to leader-follower[1] based dynam-

[1]Note that leader-follower also in literature is referred to as master-slave, chief-deputy or

ical systems. Correspondingly, the synchronization controller inevitably couples the follower to the dynamics of the leader. However, the synchronization controller is demanded to achieve the task regardless of the leader dynamics as well as the reference that system intends to track. The ability to control two coupled systems separately, is called *separation principle* and is known *not* to hold in general for nonlinear systems –see (Mazenc *et al.*, 1994) for examples. This is where cascades theory enters in play –see (Loría and Panteley, 2005) and references therein and Appendix A.5 for more details on stability of cascaded systems.

A general result on autonomous cascaded system was presented by Seibert and Suarez (1990) where they proved that two interconnected systems with globally asymptotically stable (GAS) equilibria with bounded solutions (BS) resulted in GAS for the equilibrium point of the total system. Janković *et al.* (1996) studied the problem of global stabilizability of feed-forward systems by a systematic recursive design procedure for autonomous systems and linear growth restrictions of the interconnection term. Time-varying systems were considered in (Jiang and Mareels, 1997) for stabilization of robust control, while Panteley and Loría (1998) established sufficient conditions for uniform global asymptotical stability (UGAS) of cascaded nonlinear time-varying systems. The aspect of practical and semi-global asymptotic stability for nonlinear time-varying systems in cascade were pursued in (Chaillet, 2006; Chaillet and Loría, 2008) while exponential results were reported by Grøtli (2010). Cascaded systems have successfully been applied to a wide number of applications; in (Fossen and Fjellstad, 1993) a cascaded adaptive control scheme for marine vehicles including actuator dynamics was introduced, while Loría *et al.* (1998) solved the problem of synchronizing two pendula through use of cascades, and dynamic positioning of ships where discussed by (Loría *et al.*, 2000) applying output feedback control. Stability analysis of leader-follower spacecraft formations was presented in (Grøtli, 2010) where the controller-observer scheme is proven input-to-state-stable; in (Cui *et al.*, 2010) tracking errors of a leader-follower formation of n autonomous underwater vehicles (AUVs) was proven to be bounded and converging to a compact set through use of output feedback and backstepping design.

1.3 Spacecraft formations

In the last two decades formation flying has become an increasingly popular subject of study. This is a new method of performing space operations, by replacing large and complex spacecraft with an array of simpler micro-spacecraft bringing out new possibilities and opportunities of cost reduction, redundancy and improved resolution aspects of onboard payload. Formation flying is defined by Scharf *et al.* (2003) and Scharf *et al.* (2004) as *a set of more than one spacecraft whose dynamic states are coupled through a common control law. In particular, at least one member of the set must*

1. *track a desired state relative to another member, and*

target-chaser to name a few.

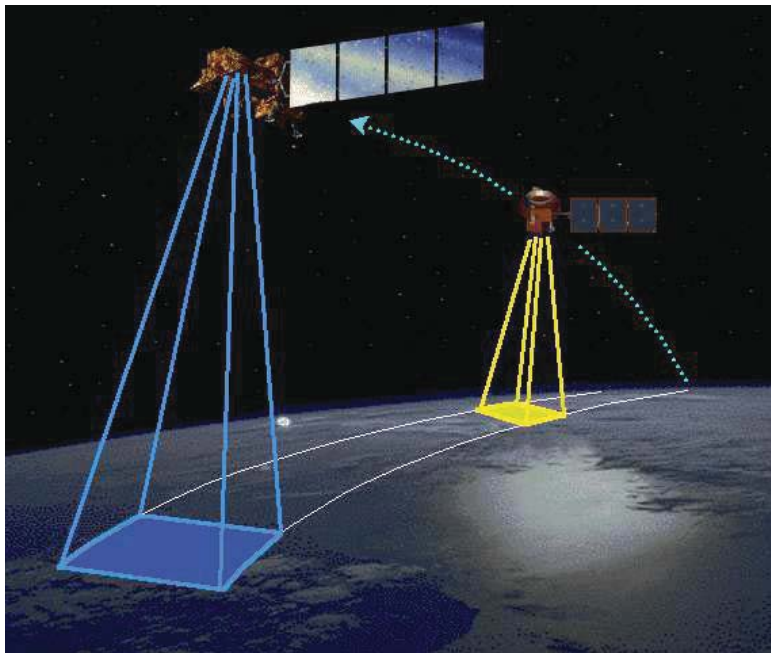

Figure 1.8: The Earth Observing-1 (EO-1) satellite in formation with Landsat 7 trailing by one minute, permitting scientists to obtain unique measurements by combining data from several satellites rather than by flying the full complement of instruments on one costly satellite. Reproduced with courtesy to NASA.

2. *the tracking control law must at the minimum depend upon the state of this other member.*

The key point is the word *relative* which marks the difference between formations and *constellations* such as the Global Positioning System (GPS) since each satellite only require an individual satellite's position and velocity for orbit corrections (Scharf *et al.*, 2003).

One of the main challenges is the requirement of synchronization between spacecraft; robust and reliable control of relative position and attitude are necessary to make the spacecraft cooperate to gain the possible advantages made feasible by spacecraft formations. For fully autonomous spacecraft formations both path- and attitude-planning must be performed on-line which introduces challenges like collision avoidance and restrictions on instrument pointing requirements, with the lowest possible fuel expenditure. For spacecraft formations one typically differs between *deep-space* missions where the relative spacecraft translational dynamics are approximated by a double integrator, and *planetary orbital environments* where spacecraft are subjected to significant orbital dynamics and environmental disturbances. The latter is furthermore divided into two categories: *active relative orbits* which are periodic relative spacecraft trajectories that require open loop control to maintain their periodicity, and *passive relative orbits* which are orbits that remain

constant in *e.g.* geometry or size throughout the orbit or at certain points on the orbit without active control, although many of these kind of orbits are ruined when disturbances are added to the analysis (Scharf *et al.*, 2003).

The system model is a key element to achieve an reliable and robust controller. Basically there are two different approaches for modeling spacecraft formations: *Cartesian coordinates* and *orbital elements* which both have their pros and cons. The orbital element method is often used to design formations concerning low fuel expenditure because of the relationship towards natural orbits, typically passive relative orbits, while Cartesian models often are used where orbits with fixed dimensions are studied, typically active relative orbits. Also for both modeling and control of spacecraft formation we divide into two areas: relative *translation* and *rotation* whereas some consider both with or without coupling.

The simplest model of relative translation between two spacecraft is linear and known as the Hill (Hill, 1878) or Clohessy-Wiltshire equations (Clohessy and Wiltshire, 1960). These linear models are based on assumptions of circular orbits, no orbital perturbations and small relative distance between spacecraft compared with the distance from the formation to the center of the Earth. Another model, known as the Lawden equations (Lawden, 1954), or Tschauner-Hempel equations (Tschauner, 1967), is an extension to the elliptical Keplerian orbits which neither considers orbital perturbations. Based on the Hill's equations Sabol *et al.* (2001) investigated four formation classes: *in-plane*, *in-track*, *circular* and *projected circular* designs and investigated the stability based on realistic perturbations through simulations, concluding that an active control action is needed to keep the satellites in any formation. As new mission applications appeared, the need of more detailed models arose, such as the problem of multiple-satellite rings (McInnes, 1995), nonlinear models for relative rotation and translation (Wang and Hadaegh, 1996), and later in (Yan *et al.*, 2000*b*; Schaub and Junkins, 2003; Ploen *et al.*, 2004*a*) and (Kristiansen, 2008) derived for arbitrary orbital eccentricity and with added terms for orbital perturbations; see (Alfriend *et al.*, 2010) and reference within for a thorough presentation. Although most previous work focus on relative translation, authors such as Wang and Hadaegh (1996); Pan and Kapila (2001); Ploen *et al.* (2004*b*); Kristiansen *et al.* (2007); Svendsen *et al.* (2007) presents coupled models of both relative translation and rotation.

Lawton (2000) defined three main formation flying control architectures, namely *leader-follower*, *behavior-based* and *virtual structure* strategies which are similar to the definitions for controlled synchronization in the previous section. Furthermore, Scharf *et al.* (2004) adds to the previous list *multiple-input, multiple-output* (MIMO) and *cyclic* architectures. In MIMO architecture a dynamical model for the total formation is used similar to a multivariable plant, thus all the tools available for this kind of system are applicable, at the cost of heavy communication requirements. Cyclic architecture on the other hand is more similar to leader-follower control where each member is connected to at least one other member, but not hierarchical, thus not too different from consensus algorithms.

A lot of work on relative control of spacecraft formations has been presented over the last two decades including numerous different techniques; see (Scharf *et al.*, 2004; Kristiansen and Nicklasson, 2009) for thorough reviews, and utilization of PD+, sliding surface, different techniques of backstepping and output feedback

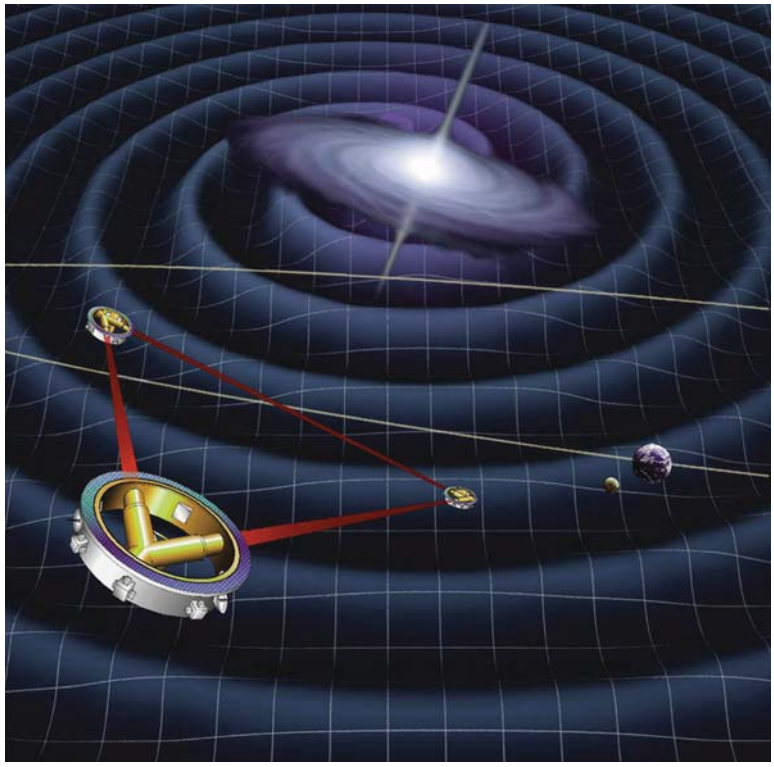

Figure 1.9: The Laser Interferometer Space Antenna (LISA) constellation is a joint NASA-ESA mission to detect and accurately measure gravitational waves from astronomical sources, possibly from sources of cosmological origin, such as the very early phase of the Big Bang, and test Einstein's theory of gravity. Reproduced with courtesy to Astrium.

in the latter reference. Notable results are (Wang and Hadaegh, 1996) where a thorough discussion on the formation control problem is presented including control laws for formation keeping and relative attitude alignment based on nearest neighbor-tracking, which later was extended in (Wang *et al.*, 1999) obtaining exponential stability of the equilibrium points. A different approach was presented by Yeh *et al.* (2000) based on Hill's equations using a sliding mode approach to minimize fuel required to maintain a rigid formation, while Lawton and Beard (2002) considered the problem of maintaining attitude alignment throughout a formation maneuver based on behavior approaches. Behavior-based control was also utilized by VanDyke and Hall (2006) for designing a class of decentralized attitude control laws.

By including adaptation laws Hadaegh *et al.* (1998) proved that the relative translational tracking error converges towards zero with time for constant disturbances, while de Queiroz *et al.* (2000) develops a globally adaptive feedback controller despite the presence of unknown, constant, or slow-varying spacecraft masses,

disturbance forces and gravity forces for a leader in circular orbit, later developed for elliptic orbits in (Yan *et al.*, 2000*b*). Similar results were also reported by Pan and Kapila (2001) proving global asymptotic convergence of the error states for both translational and rotational tracking control, while Wong *et al.* (2001*a*) reports similar results for translational tracking based on a learning controller which also accounts for periodic disturbances. The mass uncertainty problem is also considered by Lawton *et al.* (1999) where the derived control law under certain conditions ensures that the relative tracking error is kept within certain bounds during a formation rotational maneuver. The results of Wong *et al.* (2001*a*) were later extended by Pongvthithum *et al.* (2005) with a series of new features including independency for the control law of both satellites' parameters, leader position, orbit and control inputs, allowing unknown and time varying parameters, no requirement for periodic disturbances, although, it is assumed among other things, that the relative position is bounded. Another adaptive solution for relative attitude was presented in (Krogstad and Gravdahl, 2006*b*) where two control laws were presented; one for the leader and an adaptive synchronizing for the follower, though without considering disturbances. Consensus-based algorithm has also been presented as in *e.g.* Sarlette *et al.* (2007) driving the satellite swarm towards attitude synchronization from any initial configuration, without using any leader or external reference, and for various satellite interconnection topologies. Pan and Kapila (2001); Kristiansen *et al.* (2008); Krogstad and Gravdahl (2006*a*) also presented solutions to the 6DOF control problem where the first considered mutual synchronization of a fleet of followers and the second and third considered leader-follower formations, all obtaining asymptotic results although the latter utilized deep-space translational dynamics (double integrator). A different approach was proposed by Shan (2008) utilizing the concept of adaptive coupling control introduced by Sun (2003) although asymptotic properties were not proven, and Chang *et al.* (2010) presented a cooperative control law using adaptive time-varying Laplacian gains proving incremental input-to-state stability based on contraction analysis.

Output feedback control has also been utilized on spacecraft formations where the earliest result to the authors knowledge is the work of de Queiroz *et al.* (1999) using a model-independent velocity "observer" with a high-pass filter like structure yielding global uniform ultimate boundedness[2] of the relative position and velocity tracking errors; similar results also appeared in (Yan *et al.*, 2000*a*; Wang *et al.*, 2000). The results were later extended by Wong *et al.* (2002) assuming that the leader spacecraft in the formation follows a no-thrust, natural, elliptical orbit, while Pan *et al.* (2004); Wong *et al.* (2005) obtained similar results for the 6DOF case, also here through use of a high-pass filters.

Relative translational control was considered by Serrani (2003) where a robust decentralized controller using an internal model based approach was derived, handling parametric uncertainties, unknown disturbances and uncertainties on the reference trajectory. Kristiansen *et al.* (2006) obtained δ-weak uniform semi-global practical asymptotic stability[3] where adaptation of true anomaly rate and rate of change bounds for the leader spacecraft and spacecraft masses in the control

[2] See (Khalil, 2002) for definition of ultimate boundedness.
[3] See (Chaillet, 2006) for definition.

law were included. Grøtli and Gravdahl (2007) presented two different controller-observer schemes based on the sliding surface (Slotine and Li) and PD+ (Paden and Panja) control laws, obtaining exponential results for both controllers assuming known disturbances, and asymptotic results for unknown but bounded disturbances, which in (Grøtli *et al.*, 2008) was improved to exponential stability using presented definitions and theorems of sufficient conditions for nonlinear time-varying systems to be exponentially stable with respect to balls that can be arbitrarily reduced by a convenient tuning of gains.

Integrator backstepping was utilized by Bondhus *et al.* (2005) to prove asymptotic stability for relative attitude in leader-follower formations, Kristiansen *et al.* (2009) obtained uniform practical asymptotic stability[4] using a lead filter based on approximate differentiation, and Krogstad and Gravdahl (2009) obtained similar stability results based on a sliding surface design using the followers angular velocity to estimate the relative angular velocity. An alternative solution was presented by Tayebi (2006) using a unit quaternion observer and a linear feedback control law leading to a passive mapping between the observer input and the vector part of the estimation-error quaternion, claiming global asymptotic stability without the use of a lead filter for regulation and almost global asymptotic stability results for tracking (Tayebi, 2008). In (Abdessameud and Tayebi, 2009) auxiliary dynamical systems were introduced to generate the individual and relative damping terms in the absence of the actual angular velocities and relative angular velocities, obtaining asymptotically convergence of all members to a given reference or in the spirit of consensus when no reference attitude is specified.

1.4 Contributions and scope of thesis

The scope of this thesis is control of rigid bodies and synchronization of rigid bodies and spacecraft formations, that is, when analyzing coordination through leader-follower formations it is natural to also analyze the behavior of the leader. Our main focus has been to make leader-follower spacecraft formations more suitable for the technology of today by, among other things, reducing the amount of energy required for control for fixed formations and reducing the overall workload for the ground station crew by increasing the degree of autonomy through autonomously generated references. We also try to fill a gap in previous work where the term global stability, as we see it, has been widely misused and "reintroduce" the property *stability in the large* which is not very commonly used but, in our view, is more precise when working with stability on manifolds. All control laws presented throughout this thesis are based on the robotic control laws of Paden and Panja (1988) and Slotine and Li (1987) adapted for quaternion representation.

1.4.1 Contributions and summary

- Chapter 2: Previous modeling results of relative rotation, translation and disturbances are collected in this chapter along with a derived model of relative translational represented in the follower body frame. The reason for

[4]See (Hahn, 1967) or Appendix A.2.2 for definition of practical stability.

the latter is because the control forces applied to the follower originate from use of physically mounted thruster(s), thus producing a thrust vector which orientation is constant relative to the body frame. Since simulation results might be confusing with this representation we have added functions rotating the state vectors to leader orbit coordinates.

- Chapter 3: Especially when working with attitude control it is difficult not to get obsessed with the nature of quaternions and the difficulties following by applying them. Different solutions have been worked out throughout the years with different results, not all of them applicable from a practical point of view, while others have either quietly brushed the problems under the rug or not mentioned them at all. In this chapter we have applied techniques previously presented by Kristiansen (2008) assuming that the quaternion never leaves the half of the sphere where it initially starts and almost-global results of Rantzer (2001) adapted for quaternions for control of a single rigid body. Two state-feedback controllers are derived, and stability analysis shows that both controllers renders the equilibrium point uniformly exponentially stable in the large, and uniformly asymptotically stable in the large when scalar non-linear state dependent proportional and derivative gains are introduced; the latter to reduce sensitivity to measurement noise. Furthermore, a controller-observer scheme is derived and shown to be uniformly practically asymptotically stable without angular velocity measurements, with similar but simpler structure compared to the scheme presented in Caccavale and Villani (1999). This control solution is also proven to have similar stability properties when exponentially growing state dependent gains are introduced. Through simulations we show that both controllers and observers are less affected by measurement noise when nonlinear gains are introduced.

- Chapter 4: In this chapter we introduce hybrid switching based on the framework of Goebel *et al.* (2009) to solve the problem of dual equilibrium points for quaternion representation using a hysteresis based approach similar to the results reported in (Mayhew *et al.*, 2009) where backstepping design was utilized. The two derived control laws are then combined through a hysteresis based supervisor originally presented in (Efimov *et al.*, 2009) to combine the best properties of each controller improving the overall performance and achieve "certain optimality". The controller-observer scheme from Chapter 3 is also revisited where we include an additional jump set for the estimated attitude in the observer to solve a technicality which in previous results such as Caccavale and Villani (1999) has been addressed by restricting the norm of allowed initial states. We have also presented numerous simulation results trying to compare the behavior and performance between the continuous and hybrid control approaches.

- Chapter 5: The performance issue in the previous chapter caught our attention; in previous work typically the shortest rotational direction is preferred when an equilibrium point is chosen (Kristiansen *et al.*, 2008). Although this scheme is very easy to implement we investigated if there were anything to gain by also including initial angular velocities into the analysis. The results

were two-fold: first we found general rules to determine preferable equilibrium based on numerous simulations of the system, while secondly, we utilized a simple optimization technique to find the optimal choice. Although the result rely on a solution based on the linearized equations, a series of simulations show that the approach is able to predict the preferable equilibrium in all the applied cases.

- Chapter 6: The leader-follower synchronization problem is analyzed in this chapter. We start out by proposing two different control laws for a designated follower to synchronize with its leader which in turn is tracking a given reference, where the first is proven to be uniformly asymptotically stable in the large while we obtain similar but practical results for the latter through use of analysis tools for cascaded systems. We also use a similar technique to analyze the relative synchronization of a leader-follower formation where both members are utilizing switching controllers and confirm through simulation that both members do not need to settle at the same[5] equilibrium point. The relative translational case is also studied where first, we show uniform global practical asymptotic stability applying a sliding surface-based control law, while secondly, we present an adaptive version of the controller. For the latter, it is assumed that a part of the unknown perturbation vector is constant mean and nonlinear gains which are based on matrices instead of scalars, further improving performance compared to the scheme presented for attitude control. The reason lies in the fact that since both relative position and velocity are represented along the same axis the gains can be split up in accordance and thus gains increase along axes where the tracking error is large and vice versa for small tracking error.

- Chapter 7: This chapter is devoted to the study of autonomously generated references. In the first scheme we assume that the leader spacecraft is pointing its instrument towards the center of the Earth (nadir-pointing) while references are generated for the follower based on relative coordinates such that it autonomously points its instrument at the same target. The scheme is then generalized to include target-tracking which means that by choosing target coordinates based on longitude and latitude, references are generated for both the leader and follower spacecraft ensuring that they both point their instruments at the same target. Since we combine this scheme with tracking controllers, the input might be constant or time-varying. Note that the first scheme is a particular case of the last by using the nadir foot-print of the leader as input.

- Chapter 8: The topic of collision avoidance is addressed in this chapter where the concept of Null-space based (NSB) behavioral control is utilized to avoid collisions between spacecraft during formation reconfiguration. In particular we want to improve previous work by combining the control law with the behavioral control in the stability analysis to ensure that no collision will occur.

[5] Using the word *same* is not very precise since the two systems have different closed-loop dynamics, but what we try to express is that the system is stable even if the spacecraft are not rotating in similar directions.

In general, two different strategies are examined; first we scale the output vector of NSB-approach such that the derivative part of the control law dominates the proportional part to ensure that members move away from each other when they enter a fixed sized collision sphere, and secondly we develop the results by introducing dynamically sized spheres. Simulation results show that the second scheme might reduce fuel consumption and furthermore, since the dynamical sphere reduces relative spacecraft velocity based on whether they are on collision course or moving in parallel, the minimum allowed passing distance may be reduced further, decreasing the fuel consumption.

1.4.2 Delimitations

In this thesis we have made several implicit assumptions for purpose of analyzing the problems at hand to avoid getting nested into peripheral/out of scope problems which are commonly encountered for control of rigid bodies and spacecraft formations. These problems include but is not limited to:

- We have not treated control saturation explicitly, only included it in some simulations where it seems appropriate; thus, practical stability does not hold *per se* since tuning the gains to infinity will not reduce the radius of the ball (residual) obtained from practical stability to zero exactly.

- Throughout the thesis we have only presented model-based control laws without considering uncertainties in mass, inertia, thruster alignment *etc.*, although these types of considerations are well treated throughout literature.

- Only leader-follower formations have been considered for control purposes except for the collision avoidance scheme presented in Chapter 8 where it is combined with a behavioral strategy although the behavioral control solution is more similar to a guidance scheme.

- Full actuation of both rotational and translational control torque and force have been considered for all presented control solutions. Especially for translational control available thrust is typically available in one direction along a single axis only.

- When considering spacecraft formations, no communication constraints as in available bandwidth, delays, uncertainties in information/packet loss *etc.* have been considered which is especially evident for large formations, both in number and relative distance.

1.4.3 Publications

The following list includes all submitted, accepted and published material based on the work contained in this thesis.

Refereed conference papers

- Schlanbusch, R., E. I. Grøtli, A. Loría and P. J. Nicklasson (2011). Hybrid Attitude Tracking of Output Feedback Controlled Rigid Bodies. In: *Proceedings of the 50th IEEE Conference on Decision and Control (CDC)*, Orlando, FL.

- Schlanbusch, R., A. Loría, R. Kristiansen and P. J. Nicklasson (2011). PD+ Based Output Feedback Attitude Control of Rigid Bodies with Improved Performance. In: *Proceedings of the American Control Conference (ACC)*, San Francisco, CA.

- Schlanbusch, R., A. Loría and P. J. Nicklasson (2010). Hybrid Stabilization of Controlled Spacecraft. In: *Proceedings of the 49th IEEE Conference on Decision and Control (CDC)*, Atlanta, GA.

- Schlanbusch, R., A. Loría, R. Kristiansen and P. J. Nicklasson (2010). PD+ Attitude Control of Rigid Bodies with Improved Performance. In: *Proceedings of the 49th IEEE Conference on Decision and Control (CDC)*, Atlanta, GA.

- Schlanbusch, R., R. Kristiansen and P. J. Nicklasson (2010). Considerations choosing the Optimal Equilibrium Point on the Rotational Sphere. In: *Proceedings of the American Control Conference (ACC)*, Baltimore, MD.

- Schlanbusch, R., R. Kristiansen and P. J. Nicklasson (2010). Attitude Reference Generation for Leader-Follower Formation with Nadir Pointing Leader. In: *Proceedings of the American Control Conference (ACC)*, Baltimore, MD.

- Schlanbusch, R., R. Kristiansen and P. J. Nicklasson (2010). On Choosing Quaternion Equilibrium Point in Attitude Stabilization. In: *Proceedings of the 31th IEEE Aerospace Conference*, Big Sky, Montana.

- Schlanbusch, R., R. Kristiansen, and P. J. Nicklasson (2008). Spacecraft formation reconfiguration with collision avoidance. In: *Proceedings of the 3rd International Symposium on Formation Flying, Missions and Technologies (ISFF)*, Estec, Holland.

Journal papers

- Schlanbusch, R., E. I. Grøtli, A. Loría and P. J. Nicklasson (2011). Hybrid Attitude Tracking of Output Feedback Controlled Rigid Bodies. *Accepted for Systems & Control Letters.*

- Schlanbusch, R., A. Loría, R. Kristiansen, and P. J. Nicklasson (2011). PD+ Based Output Feedback Attitude Control of Rigid Bodies. *Accepted for IEEE Transactions on Automatic Control.*

- Schlanbusch, R., A. Loría, and P. J. Nicklasson (2011). On the stability and stabilization of quaternion equilibria of rigid bodies. *Conditionally accepted for Automatica.*

- Schlanbusch, R., A. Loría, and P. J. Nicklasson (2011). Cascades-based controlled synchronization and tracking of spacecraft in leader-follower formation. *International Journal of Aerospace Engineering, special issue on Formation Flight Control,* **2011**, 12 pages.

- Schlanbusch, R., R. Kristiansen, and P. J. Nicklasson (2011). Spacecraft formation reconfiguration with collision avoidance. *Automatica,* **24**(7), 1443–1449.

Book chapters

- Schlanbusch, R. and P. J. Nicklasson (2011). Synchronization of Target Tracking Cascaded Leader-Follower Spacecraft Formation. *Advances in Spacecraft Technologies*, Chap. 25, pp. 563–584, InTech, ISBN 978-953-307-551-8.

Related work

- Schlanbusch, R., R. Kristiansen, and P. J. Nicklasson (2011). Spacecraft Magnetic Control Using Dichotomous Coordinate Descent Algorithm with Box Constraints. *Modeling, Identification and Control (MIC)*, **31**(4), 123–131.

- Schlanbusch, R., E. Oland and P. J. Nicklasson (2009). Modeling and Simulation of a CubeSat Using Nonlinear Control in an Elliptic Orbit. In: *Proceedings of the 4th International Conference on Recent Advances in Space Technologies (RAST)*, Istanbul, Turkey.

- Oland, E., R. Schlanbusch (2009). Reaction Wheel Design for CubeSats. In: *Proceedings of the 4th International Conference on Recent Advances in Space Technologies (RAST)*, Istanbul, Turkey.

- Mathisen, S. V., R. Schlanbusch and P. J. Nicklasson (2009). Real-time Inertial Navigation System for Educational Use. In: *Proceedings of the 4th International Conference on Recent Advances in Space Technologies (RAST)*, Istanbul, Turkey.

- Schlanbusch, R., T. M. Steihaug and P. J. Nicklasson (2008). Target Reference Generator for the European Student Moon Orbiter Satellite. *Presentation at Multiphysics conference*, Narvik, Norway.

Part I

Modeling of leader-follower spacecraft formations

Chapter 2

Modeling

In this chapter we start by defining basic notations in Section 2.1 and proceed with orbital dynamics in Section 2.2, reference frames in Section 2.3, frame transformations in Section 2.4, mathematical modeling of relative translational and rotational motion in Section 2.5 and 2.6, respectively, orbital perturbations in Section 2.7 and simulation results of a spacecraft formation with uncontrolled follower in Section 2.8.

2.1 Basic notations

In the following, we denote $\mathbb{R}$ as the set of all real numbers which are expressed by italic small letters, occasionally Greek letters, and $\mathbb{N}$ as the set of natural numbers, that is, the set of all positive integers. We denote $\mathbb{R}_{\geq 0} = \{\alpha \in \mathbb{R} : \alpha \in [0, \infty)\}$ as the set of all non-negative numbers, $\mathbb{R}_{+} = \{\alpha \in \mathbb{R} : \alpha \in (0, \infty)\}$ as the set of all positive numbers, and the absolute value of a real number $x \in \mathbb{R}$ is denoted $|x|$. The Euclidian n-dimensional space is denoted $\mathbb{R}^n$, that is, the set of all vectors $\mathbf{x}$ of dimension n formed by n real numbers in the column form

$$\mathbf{x} = \begin{bmatrix} x_1 \\ x_2 \\ \vdots \\ x_n \end{bmatrix} = [x_1,\ x_2,\ \ldots, x_n]^\top \in \mathbb{R}^n, \tag{2.1}$$

where $x_1,\ x_2,\ \ldots,\ x_n \in \mathbb{R}$. The associated vectors are denoted by small bold letters. We denote $\mathbb{R}^{n \times m}$ the set of real matrices formed by n rows and m columns,

$$\mathbf{A} = \{a_{ij}\} = \begin{bmatrix} a_{11} & a_{12} & \cdots & a_{1m} \\ a_{21} & a_{22} & \cdots & a_{2m} \\ \vdots & \vdots & \ddots & \vdots \\ a_{n1} & a_{n2} & \cdots & a_{nm} \end{bmatrix}. \tag{2.2}$$

The transpose matrix $\mathbf{A}^\top = \{a_{ji}\} \in \mathbb{R}^{m \times n}$ is obtained by interchanging the rows and columns of A. The associated matrices are denoted by capitalized bold letters. We denote by $\dot{\mathbf{x}}$ the time derivative of a vector $\mathbf{x}$, i.e. $\dot{\mathbf{x}} = d\mathbf{x}/dt =$

$[dx_1/dt,\ dx_2/dt,\ \ldots,\ dx_n/dt]^\top$, and moreover, $\ddot{\mathbf{x}} = d^2\mathbf{x}/dt^2$. We denote functions f with domain $\mathcal{D}$ and taking values in a set $\mathcal{R}$ by $f : \mathcal{D} \to \mathcal{R}$ or alternatively by $f(\mathbf{x})$ where $\mathbf{x} \in \mathcal{D}$, and the solution of a nonlinear differential equation $\dot{\mathbf{x}} = f(t, \mathbf{x})$ with initial conditions $(t_0, \mathbf{x}_0)$ where $\mathbf{x}_0 = \mathbf{x}(t_0)$ is denoted by $\mathbf{x}(t, t_0, \mathbf{x}_0)$. Two different gradient operators are defined as $\nabla g = \left[\frac{\partial g}{\partial x_1}\ \ldots\ \frac{\partial g}{\partial x_1}\right]$, $g : \mathbb{R}^n \to \mathbb{R}$, and $\nabla \cdot h = \frac{\partial h_1}{\partial x_1} + \cdots + \frac{\partial h_n}{\partial x_n}$, $h : \mathbb{R}^n \to \mathbb{R}^n$. We denote by $\|\cdot\|$ the Euclidian norm of a vector and the induced $\mathcal{L}_2$ norm (spectral norm) of a matrix (*cf.* Section A.1 for more details on norms). For the open ball in $\mathbb{R}^n$ centered at the origin we denote $\mathcal{B}_\delta := \{\mathbf{x} \in \mathbb{R}^n : \|\mathbf{x}\| < \delta\}$, and $\bar{\mathcal{B}}_\gamma = \{\mathbf{x} \in \mathbb{R}^n : \|\mathbf{x}\| \leq \gamma\}$ for the closed ball with $\delta \in \mathbb{R}_+$ and $\gamma \in \mathbb{R}_{\geq 0}$. The Euclidian distance from a given point $\mathbf{y}$ to the set associated with the closed ball $\bar{\mathcal{B}}_\delta$ is given as

$$\|\mathbf{y}\|_\delta = \inf_{\mathbf{x} \in \bar{\mathcal{B}}_\delta} \|\mathbf{y} - \mathbf{x}\|. \tag{2.3}$$

We use the notation $\mathcal{H}(\delta, \Delta) := \{\mathbf{x} \in \mathbb{R}^n : \delta \leq \|\mathbf{x}\| \leq \Delta\}$ for a spherical shell with inner radius δ and outer radius Δ, or strictly speaking $\mathcal{H}(\delta, \Delta) = \bar{\mathcal{B}}_\Delta \backslash \bar{\mathcal{B}}_\delta$. $\mathbf{I}$ denotes the identity matrix of appropriate dimension, and the cross-product operator is denoted $\mathbf{S}(\cdot)$, such that $\mathbf{S}(\mathbf{x})\mathbf{y} = \mathbf{x} \times \mathbf{y}$ with the property $\mathbf{S}(\mathbf{x})\mathbf{y} = -\mathbf{S}(\mathbf{y})\mathbf{x}$ for all $\mathbf{x}, \mathbf{y} \in \mathbb{R}^3$.

Reference frames are denoted by $\mathcal{F}^{(\cdot)}$, and we denote by $\boldsymbol{\omega}^c_{b,a}$ the angular velocity of $\mathcal{F}^a$ relative to $\mathcal{F}^b$, referenced in $\mathcal{F}^c$. Matrices representing rotation or coordinate transformation from $\mathcal{F}^a$ to $\mathcal{F}^b$ are denoted $\mathbf{R}^b_a$.

When the context is sufficiently explicit, we may omit to write arguments of a function, vector or matrix.

2.2 Orbit dynamics

Orbit dynamics are based on the *Laws of Kepler* and the *Laws of Newton*, where the first presents three basic empirical laws describing motion in unperturbed planetary orbits, while the latter formulates the more general physical laws governing the motion of planets –*cf.* (Sidi, 1997).

Laws of Kepler

1. The orbit of a planet is an ellipse with the sun at one focus;

2. the radius vector from the sun to the planet sweeps out equal areas in equal time intervals;

3. planetary periods of revolution are proportional to the [mean distance to sun]$^{3/2}$.

Laws of Newton

1. Every particle remains in a state of rest or uniform motion in a straight line with constant velocity, unless acted upon by an external force;

2. the rate of change of linear momentum of a body equals the force $\mathbf{f}$ applied to it, where $m\mathbf{v}$ is the linear momentum and

$$\mathbf{f} = \frac{d(m\mathbf{v})}{dt}; \tag{2.4}$$

3. if a particle exerts a force $\mathbf{f}$ on another particle, the other particle exerts an equal force with opposite direction, on the first particle;

4. the gravitational force between any two particles with mass m_1 and m_2 is given by

$$\mathbf{f} = \frac{Gm_1m_2}{r^3}\mathbf{r}, \ where\ G = 6.667 \times 10^{-11} m^3/kg - s^2. \tag{2.5}$$

To fully describe an orbit we make use of the *classical orbit parameters* which are sufficient to describe the orbit in the plane, the position of the spacecraft in the orbit as in Figure 2.1 and the position of the orbit as in Figure 2.2 (Sidi, 1997), where the parameters are defined follows:

Classical orbit parameters

a, the semimajor axis;

e, the eccentricity;

i, the inclination;

Ω, the right ascension of the ascending node;

ω, the argument of perigee;

M, the mean anomaly;

where

$$M = n(t - t_0) = \psi - e\sin(\psi) \tag{2.6}$$

is the *mean anomaly*, n is the *mean motion* defined as $n = \sqrt{\mu/a^3}$, $\mu = Gm$ is the gravitational constant, t is time, t_0 is the time of passage at the perigee and ψ is the *eccentric anomaly* as shown in Figure 2.1. All parameters may be used to described the vector $\boldsymbol{\alpha} = [a,\ e,\ i,\ \Omega,\ \omega,\ M]^\top$. The angle Ω is defined in the *equatorial plane* which separates the *node line* and $\mathbf{X}\Upsilon$[1], which is called the *vernal equinox* vector, and ω is the angle between $\mathbf{r}_p$ and the node line. The node line is the line of intersection between the equatorial and orbit plane. The *semimajor axis* can be written as

$$a = \frac{r_a + r_p}{2} = \frac{p}{a - e^2}, \tag{2.7}$$

[1]The *vernal equinox* vector intersect the celestial sphere at a point named the *first point of the Aries*, Υ, which corresponds to the vector pointing from the center of the Earth toward the center of the Sun during the vernal equinox.

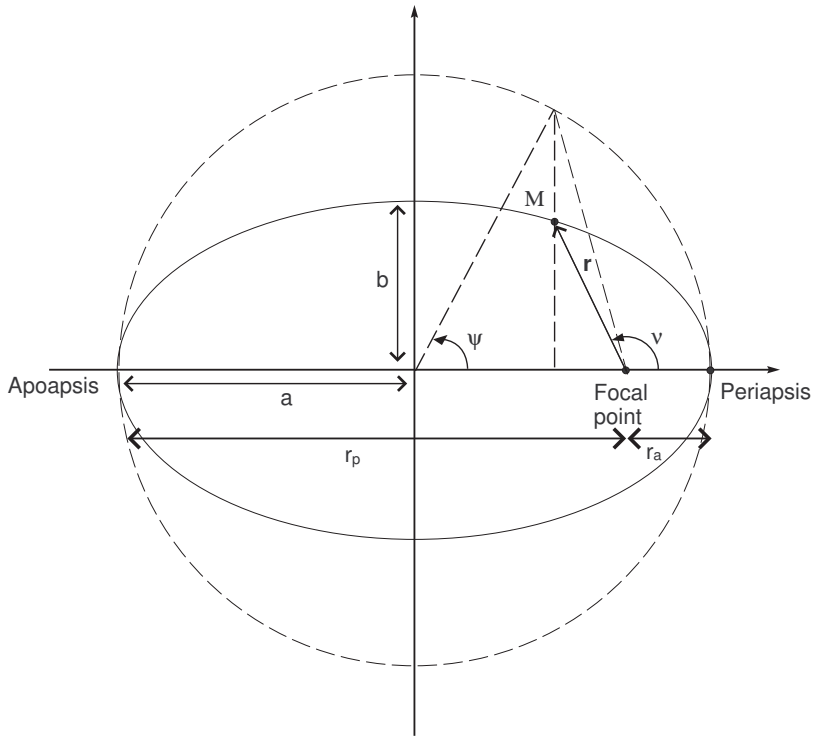

Figure 2.1: Orbit parameters (Sidi, 1997).

where p is called the *semi-latus rectum* and is defined as

$$p = a(q - e^2) = \frac{h^2}{\mu}, \tag{2.8}$$

where $h = \|\mathbf{h}\|$ is the length of the *momentum of momentum* vector $\mathbf{h} = \mathbf{S}(\mathbf{r})m\mathbf{v}$. The *apogee* distance r_a is defined as

$$r_a = \frac{p}{1+e} \tag{2.9}$$

and the *perigee* distance r_p as

$$r_p = \frac{p}{1-e}. \tag{2.10}$$

The *eccentricity* can be defined as

$$e = \frac{r_a - r_p}{r_a + r_p} \tag{2.11}$$

and the *total energy* of a body with unit mass in an orbit can be written as

$$E = \frac{v^2}{2} - \frac{\mu}{r} = -\frac{\mu}{2a}, \tag{2.12}$$

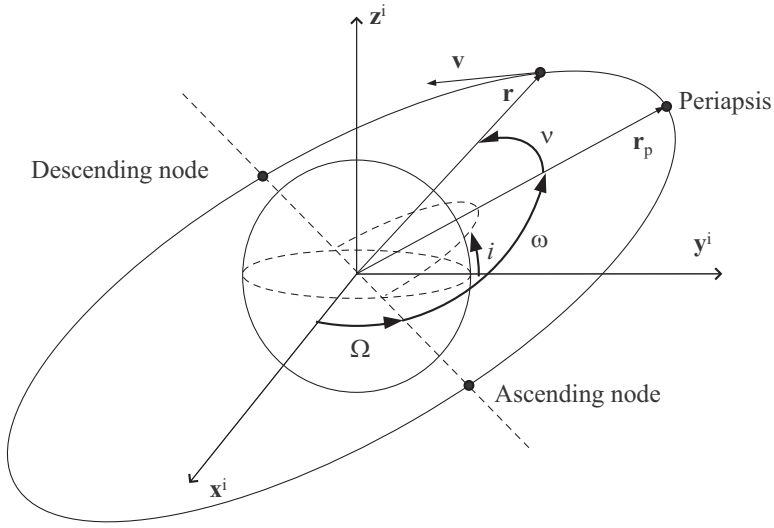

Figure 2.2: Orbit location parameters (Sidi, 1997).

where $v = \|\mathbf{v}\|$. By reorganizing equation (2.6), ψ can be found by iteration of

$$\psi_{n+1}(t) = M(t) + e\sin(\psi_n(t)), \tag{2.13}$$

but note that this algorithm only converges for elliptical orbits ($0 < e < 1$) Sidi (1997). The orbital position angle or *true anomaly* ν, as shown in Figure 2.1, can then be found by

$$\cos(\nu) = \frac{\cos(\psi) - e}{1 - e\cos(\psi)}. \tag{2.14}$$

The true orbit rate can be found using

$$\dot{\nu} = \frac{n(1 + e\cos(\nu))^2}{(1 - e^2)^{\frac{3}{2}}} \tag{2.15}$$

and the rate of change may be written as

$$\ddot{\nu} = \frac{-2n^2 e(1 + e\cos(\nu))^3 \sin(\nu)}{(1 - e^2)^3}. \tag{2.16}$$

2.3 Cartesian coordinate frames

The coordinate reference frames utilized throughout this thesis are presented throughout this section and some of them are shown in Figures 2.3 and 2.4.

2.3.1 Earth-centered inertial frame

The Earth-centered inertial (ECI) frame is denoted $\mathcal{F}^i$, and has its origin fixed at the center of the Earth. The axes are denoted $\mathbf{x}^i$, $\mathbf{y}^i$, and $\mathbf{z}^i$, where the $\mathbf{z}^i$ axis is directed along the axis of rotation of the Earth toward the celestial North Pole, the $\mathbf{x}^i$ axis is pointing in the direction of the vernal equinox vector, $\mathbf{X}_\Upsilon$, which is the vector pointing from the center of the sun toward the center of the Earth during the vernal equinox, and finally the $\mathbf{y}^i$ axis complete the right handed orthonormal frame.

2.3.2 Earth-centered Earth fixed

The Earth-centered Earth-fixed reference frame (ECEF) is denoted $\mathcal{F}^{ef}$, and has its origin fixed at the center of the Earth. The axes are denoted $\mathbf{x}^{ef}$, $\mathbf{y}^{ef}$ and $\mathbf{z}^{ef}$, where $\mathbf{z}^{ef}$ is parallel to the $\mathbf{z}^i$ axis, and rotates about this axis with a constant angular rate of $\omega_e = 7.292115 \times 10^{-5}$ rad/s, thus $\mathcal{F}^{ef}$ coincides with $\mathcal{F}^i$ once per day. This frame can typically be used for describing position of targets which are located on the Earth's surface.

2.3.3 North-east-down frame

The north-east-down frame (NED), denoted $\mathcal{F}^n$, is defined relative to the Earths' reference ellipsoid at the tangent plane of the surface of the Earth, where the $\mathbf{x}^n$ axis is pointing toward true north, $\mathbf{y}^n$ towards true east, and $\mathbf{z}^n$ points downwards normal to the surface of the Earth.

2.3.4 Leader orbit reference frame

The leader orbit frame, denoted $\mathcal{F}^l$ and depicted in Figure 2.3, has its origin located in the center of mass of the leader spacecraft. The $\mathbf{e}_r$ axis in the frame coincide with the vector $\mathbf{r}_l \in \mathbb{R}^3$ from the center of the Earth to the spacecraft, and the $\mathbf{e}_h$ axis is parallel to the orbital angular momentum vector, pointing in the orbit normal direction. The $\mathbf{e}_\theta$ axis completes the right-handed orthonormal frame. The basis vectors of the frame can be defined as

$$\mathbf{e}_r := \frac{\mathbf{r}_l}{\|\mathbf{r}_l\|}, \qquad \mathbf{e}_\theta := \mathbf{S}(\mathbf{e}_h)\mathbf{e}_r \qquad \text{and} \qquad \mathbf{e}_h := \frac{\mathbf{h}}{\|\mathbf{h}\|}, \tag{2.17}$$

where $\mathbf{h} = \mathbf{S}(\mathbf{r}_l)\dot{\mathbf{r}}_l$ is the angular momentum vector of the orbit; see (Schaub and Junkins, 2003) for description.

2.3.5 Follower orbit reference frame

The follower orbit frame has its origin in the center of mass of the follower spacecraft, is denoted $\mathcal{F}^f$ and depicted in Figure 2.3. The vector pointing from the center of the Earth to the frame origin is denoted $\mathbf{r}_f \in \mathbb{R}^3$, and the frame is specified by a relative orbit position vector $\mathbf{p} = [x,\ y,\ z]^\top$ expressed in $\mathcal{F}^l$ components, and its unit vectors align with the basis vectors of $\mathcal{F}^l$. Accordingly,

$$\mathbf{p} = \mathbf{R}_i^l(\mathbf{r}_f - \mathbf{r}_l) = x\mathbf{e}_r + y\mathbf{e}_\theta + z\mathbf{e}_h \Rightarrow \mathbf{r}_f = \mathbf{R}_l^i\mathbf{p} + \mathbf{r}_l. \tag{2.18}$$

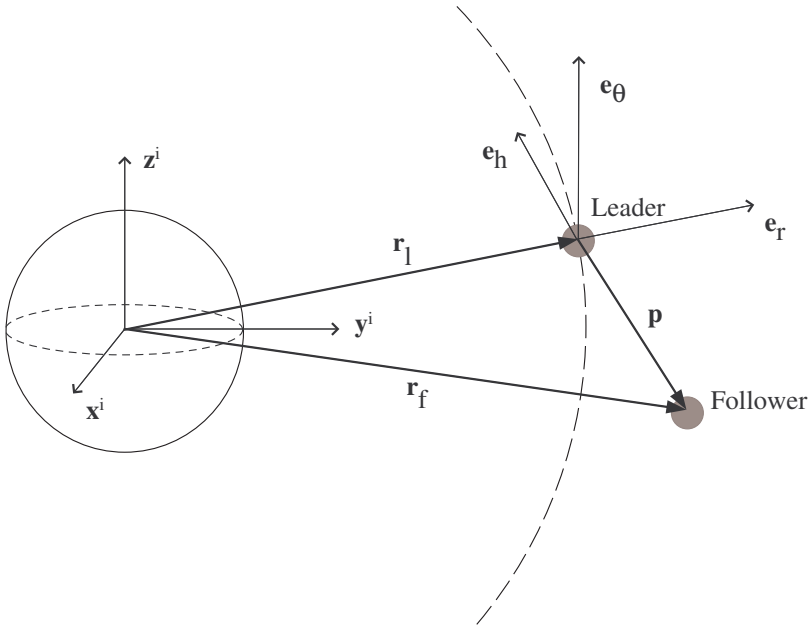

Figure 2.3: Inertial and leader-orbit reference frames (Schaub and Junkins, 2003).

2.3.6 Body fixed frames

The body axis frame of a spacecraft is denoted either $\mathcal{F}^{lb}$ or $\mathcal{F}^{fb}$ for leader and follower spacecraft respectively. The axes are denoted $\mathbf{x}^{lb}$, $\mathbf{y}^{lb}$ and $\mathbf{z}^{lb}$ for the leader spacecraft and $\mathbf{x}^{fb}$, $\mathbf{y}^{fb}$ and $\mathbf{z}^{fb}$ for the follower spacecraft and coincide with its principal axes of inertia. The frames have their origins in the center of mass of the spacecraft.

2.3.7 Auxiliary frame

Because of the nature of the aerodynamic drag and the fact that it always acts along the velocity vector of the spacecraft we need an auxiliary orbit frame, denoted $\mathcal{F}^a$, when elliptic orbits are considered; see Figure 2.4. The first basis vector is parallel with the orbit frame $\mathbf{e}_r$, $\mathbf{e}_v$ is pointing in the direction of the spacecraft velocity vector, and $\mathbf{e}_n$ is completing the right-handed orthonormal frame such that $\mathbf{e}_n = \mathbf{S}(\mathbf{e}_v)\mathbf{e}_h$.

2.4 Frame transformations

Since the spacecraft rotation and translation are presented in different frames, it is important to define proper transformations between the appropriate frames. The

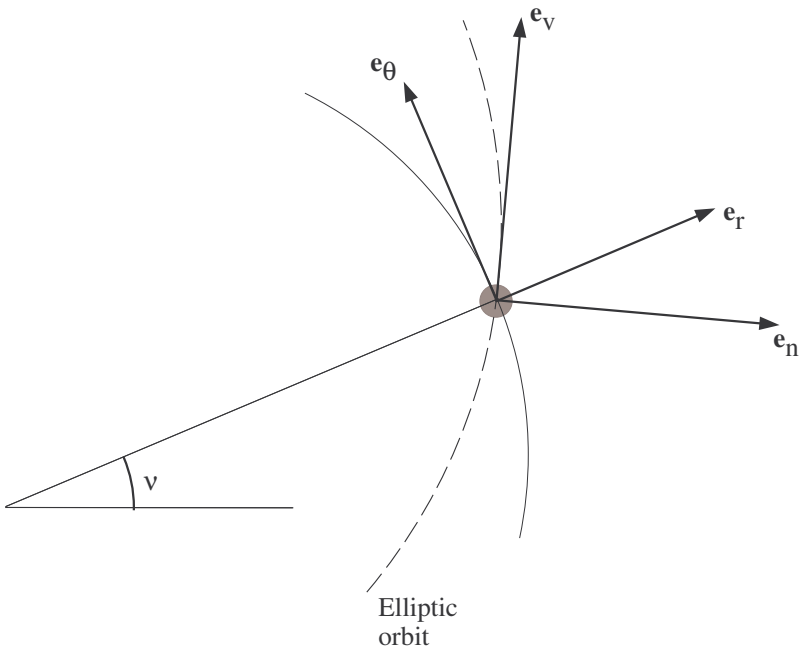

Figure 2.4: Auxiliary reference frame (Schaub and Junkins, 2003).

attitude of a rigid body can be represented by a rotation matrix $\mathbf{R} \in SO(3)$ fulfilling

$$SO(3) = \{\mathbf{R} \in \mathbb{R}^{3\times 3} \ : \ \mathbf{R}^\top \mathbf{R} = \mathbf{I}, \ \det(\mathbf{R}) = 1\} \ , \tag{2.19}$$

which is the special orthogonal group of order three, where $\mathbf{I}$ denotes the identity matrix. An important property for rotation matrices is that $(\mathbf{R}_a^b)^{-1} = (\mathbf{R}_a^b)^\top = \mathbf{R}_b^a$, and coordinate transformation of a vector $\mathbf{r}$ from frame a to frame b is written as $\mathbf{r}^b = \mathbf{R}_a^b \mathbf{r}^a$.

2.4.1 NED to ECEF frame

The rotation from $\mathcal{F}^n$ to $\mathcal{F}^{ef}$ can be expressed as (Fossen, 2002)

$$\mathbf{R}_n^{ef} = \begin{bmatrix} -\cos\lambda\sin\phi & -\sin\lambda & -\cos\lambda\cos\phi \\ -\sin\lambda\sin\phi & \cos\lambda & -\sin\lambda\cos\phi \\ \cos\phi & 0 & -\sin\mu \end{bmatrix}, \tag{2.20}$$

where λ is the longitude[2] while ϕ is the latitude[3].

[2]Longitude is the angular distance of a point's meridian from the Greenwich meridian expressed in degrees, minutes and seconds.

[3]Latitude of a point is the angular distance of that point north or south of the equator expressed in degrees, from 90° N, 0° at the equator and −90° S.

2.4.2 ECEF to ECI frame

The rotation from $\mathcal{F}^{ef}$ to $\mathcal{F}^{i}$ can be expressed as

$$\mathbf{R}_{ef}^{i} = \begin{bmatrix} \cos(\omega_e t + \alpha) & -\sin(\omega_e t + \alpha) & 0 \\ \sin(\omega_e t + \alpha) & \cos(\omega_e t + \alpha) & 0 \\ 0 & 0 & 1 \end{bmatrix}, \tag{2.21}$$

where t is time and α is an initial phase between the $\mathbf{x}^{ef}$ and $\mathbf{x}^{i}$ at $t = 0$, and $\omega_e = 7.292115 \times 10^{-5}$ rad/s is the constant angular rate of the Earth around its rotation axis $\mathbf{z}^{ef}$.

2.4.3 ECI to orbit frame

The rotation from the ECI frame $\mathcal{F}^{i}$ to the orbit frame $\mathcal{F}^{s}$, where $s = f, l$ for leader and follower, respectively, can be described by three composite rotations (Sidi, 1997), *e.g.*

$$\mathbf{R}_{i}^{s} = \mathbf{R}_z(\omega + \nu)\mathbf{R}_x(i)\mathbf{R}_z(\Omega) \tag{2.22}$$

$$= \begin{bmatrix} c(\omega+\nu) & s(\omega+\nu) & 0 \\ -s(\omega+\nu) & c(\omega+\nu) & 0 \\ 0 & 0 & 1 \end{bmatrix} \begin{bmatrix} 1 & 0 & 0 \\ 0 & ci & si \\ 0 & -si & ci \end{bmatrix} \begin{bmatrix} c\Omega & s\Omega & 0 \\ -s\Omega & c\Omega & 0 \\ 0 & 0 & 1 \end{bmatrix} \tag{2.23}$$

$$= \begin{bmatrix} c(\omega+\nu)+c\Omega-cis(\omega+\nu)s\Omega & c(\omega+\nu)s\Omega+s(\omega+\nu)cic\Omega & s(\omega+\nu)si \\ -s(\omega+\nu)c\Omega-cis\Omega c(\omega+\nu) & -s(\omega+\nu)s\Omega+c(\omega+\nu)cic\Omega & c(\omega+\nu)si \\ sis\Omega & -sic\Omega & ci \end{bmatrix},$$

where ν is the true anomaly defined as the angle between the major axis pointing to the perigee and the vector $\mathbf{r}$ pointing at the appropriate spacecraft, from the prime focus F and $c(\cdot)$ and $s(\cdot)$ denotes cosine and sine, respectively. The inverse rotation is obtained by reversing the order of rotations (Sidi, 1997)

$$\mathbf{R}_{s}^{i} = \mathbf{R}_z^{-1}(\Omega)\mathbf{R}_x^{-1}(i)\mathbf{R}_z^{-1}(\omega + \nu). \tag{2.24}$$

Since $\mathbf{R}_{s}^{i} = (\mathbf{R}_{i}^{s})^{-1} = (\mathbf{R}_{i}^{s})^{T}$, (2.24) can be written as

$$\mathbf{R}_{s}^{i} = \mathbf{R}_z^{T}(\Omega)\mathbf{R}_x^{T}(i)\mathbf{R}_z^{T}(\omega + \nu). \tag{2.25}$$

2.4.4 Orbit to body frame

Because of the singularity issue in the kinematics using *Euler angles –cf.* (Sidi, 1997) *unit quaternions* are often preferred to parameterize members of $SO(3)$. The rotation matrix can be described as a rotation by an angle θ about the corresponding unit eigenvector $\mathbf{k}$ as (Egeland and Gravdahl, 2002)

$$\mathbf{R} = \cos(\theta)\mathbf{I} + \sin(\theta)\mathbf{S}(\mathbf{k}) + [1 - \cos(\theta)]\mathbf{k}\mathbf{k}^{\top}, \tag{2.26}$$

which is called the *angle-axis parameterization* of the rotation matrix. *Euler parameters* are often used to parameterize members of $SO(3)$, defined by $\eta = \cos(\theta/2) \in$

$\mathbb{R}$ as the scalar part and $\boldsymbol{\epsilon} = \mathbf{k}\sin(\theta/2) \in \mathbb{R}^3$ as the vector part, leading to a corresponding rotation matrix

$$\mathbf{R} = \mathbf{I} + 2\eta\mathbf{S}(\boldsymbol{\epsilon}) + 2\mathbf{S}^2(\boldsymbol{\epsilon}). \tag{2.27}$$

The vector $\mathbf{q} = [\eta,\ \boldsymbol{\epsilon}^\top]^\top$ of Euler parameters can be treated as a *unit quaternion* vector defined as $\mathbf{q} \in S^3 = \{\mathbf{x} \in \mathbb{R}^4 \ :\ \mathbf{x}^\top\mathbf{x} = 1\}$, where the set S^3 forms a group with quaternion multiplication, which is distributive and associative, but not commutative, and the quaternion product defined as

$$\mathbf{q}_1 \otimes \mathbf{q}_2 = \begin{bmatrix} \eta_1\eta_2 - \boldsymbol{\epsilon}_1^\top\boldsymbol{\epsilon}_2 \\ \eta_1\boldsymbol{\epsilon}_2 + \eta_2\boldsymbol{\epsilon}_1 + \mathbf{S}(\boldsymbol{\epsilon}_1)\boldsymbol{\epsilon}_2 \end{bmatrix}. \tag{2.28}$$

The inverse rotation can be performed by using the conjugate of $\mathbf{q}$ given by $\bar{\mathbf{q}} = [\eta,\ -\boldsymbol{\epsilon}^\top]^\top$ and the rotation can be expressed as

$$\mathbf{q}_{c,a} = \bar{\mathbf{q}}_{b,a} \otimes \mathbf{q}_{b,c} = \mathbf{q}_{a,b} \otimes \mathbf{q}_{b,c}. \tag{2.29}$$

Note that because of the unit length of the quaternion vector, we have that $\mathbf{q}^\top\mathbf{q} = \eta^2 + \boldsymbol{\epsilon}^\top\boldsymbol{\epsilon} = 1$ where it follows that $\mathbf{R} = \mathbf{I} \Leftrightarrow \mathbf{q} = [\pm 1,\ \mathbf{0}]^\top$ often expressed as $\mathbf{q} = \pm\mathbf{q}_{id}$.

2.4.5 Auxiliary to orbit frame

The rotation from the auxiliary frame to the orbit frame can be expressed as (Schaub and Junkins, 2003)

$$\mathbf{C}_a^s = \frac{h}{pv}\begin{bmatrix} \frac{p}{r} & e\sin\nu & 0 \\ -e\sin\nu & \frac{p}{r} & 0 \\ 0 & 0 & \frac{pv}{h} \end{bmatrix}, \tag{2.30}$$

where $p = h^2/\mu$ is the semi-latus rectum of the spacecraft orbit, μ is the geocentric gravitational constant of the Earth, v is the magnitude of the velocity vector, e is the orbit eccentricity, and ν is the true anomaly. Note that $\mathbf{C}_a^s$ is not in general a proper rotation matrix since

$$\det(\mathbf{C}_a^s) = 1 + e^2 + 2e\cos(\nu), \tag{2.31}$$

thus only holds for circular orbits where the rotation matrix becomes identity.

2.5 Relative translation

In this Section we will present different types of translational models for leader-follower spacecraft formations in elliptic orbits. What is common is that they are all derived from the N-body problem based on the Newtonian mechanics.

2.5.1 The N-body problem

Objects in space are affected by gravitational attraction from celestial bodies, where the sum of all forces working on an object can be written as (Sidi, 1997)

$$\mathbf{f}_i = G\sum_{j=1}^{j=n}\frac{m_i m_j}{r_{ij}^3}(\mathbf{r}_j - \mathbf{r}_i), \quad i \neq j, \tag{2.32}$$

where G is the universal constant of gravity, and r_{ij} is the distance between any to particles defined as

$$r_{ij} := \|\mathbf{r}_j - \mathbf{r}_i\|. \tag{2.33}$$

Using Newton's second law of motion (2.4), (2.32) can be written as

$$\frac{d^2\mathbf{r}_i}{dt^2} = G\sum_{j=1}^{j=n}\frac{m_j}{r_{ij}^3}(\mathbf{r}_j - \mathbf{r}_i), \quad i \neq j. \tag{2.34}$$

From the N-body problem, (2.34) can be reduced to the differential equation of the two body problem

$$\frac{d^2\mathbf{r}}{dt^2} + \frac{\mu}{r^3}\mathbf{r} = 0, \tag{2.35}$$

where

$$\mathbf{r} := \mathbf{r}_2 - \mathbf{r}_1 \tag{2.36}$$

is the relative position between the two masses, and

$$\mu = G(m_1 + m_2), \tag{2.37}$$

where G is the gravitational constant, and m_1 and m_2 are the masses of the two bodies.

2.5.2 Formation dynamics using true anomaly

The orbit equation describes the dynamics of the spacecraft under ideal conditions, but conditions like solar wind, uneven gravity field *etc.* contribute with external disturbances. These disturbances are denoted $\mathbf{f}_{dl}$ and $\mathbf{f}_{df}$ for the leader and follower spacecraft respectively, and the input vectors from actuators on board the spacecraft are denoted $\mathbf{f}_{al}$ and $\mathbf{f}_{af}$ for leader and follower, respectively; (2.35) may then be expressed as

$$\ddot{\mathbf{r}}_l = -\frac{\mu}{r_l^3}\mathbf{r}_l + \frac{\mathbf{f}_{dl}}{m_l} + \frac{\mathbf{f}_{al}}{m_l} \tag{2.38}$$

$$\ddot{\mathbf{r}}_f = -\frac{\mu}{r_f^3}\mathbf{r}_f + \frac{\mathbf{f}_{df}}{m_f} + \frac{\mathbf{f}_{af}}{m_f}. \tag{2.39}$$

The relative position vector can according to Schaub and Junkins (2003) be written as $\mathbf{p} = \mathbf{r}_f - \mathbf{r}_l = x\mathbf{e}_r + y\mathbf{e}_\theta + z\mathbf{e}_h$, thus obtaining

$$\ddot{\mathbf{p}} = \ddot{\mathbf{r}}_f - \ddot{\mathbf{r}}_l = -\frac{\mu}{r_f^3}\mathbf{r}_f + \frac{\mathbf{f}_{df}}{m_f} + \frac{\mathbf{f}_{af}}{m_f} + \frac{\mu}{r_l^3}\mathbf{r}_l - \frac{\mathbf{f}_{dl}}{m_l} - \frac{\mathbf{f}_{al}}{m_l}, \tag{2.40}$$

and by manipulation we obtain

$$m_f\ddot{\mathbf{p}} = -m_f\mu\left[\frac{\mathbf{r}_l+\mathbf{p}}{(r_l+p)^3} - \frac{\mathbf{r}_l}{r_l^3}\right] + \mathbf{f}_{af} + \mathbf{f}_{df} - \frac{m_f}{m_l}(\mathbf{f}_{al}+\mathbf{f}_{dl}). \tag{2.41}$$

The dynamics of the follower orbit frame can be expressed in the leader orbit frame according to

$$\mathbf{r}_f = \mathbf{r}_l + \mathbf{p} = (r_l+x)\mathbf{e}_r + y\mathbf{e}_\theta + z\mathbf{e}_h, \tag{2.42}$$

and by differentiating twice we obtain

$$\ddot{\mathbf{r}}_f = (\ddot{r}_l+\ddot{x})\mathbf{e}_r + 2(\dot{r}_l+\dot{x})\dot{\mathbf{e}}_r + (r_l+x)\ddot{\mathbf{e}}_r + \ddot{y}\mathbf{e}_\theta + 2\dot{y}\dot{\mathbf{e}}_\theta + y\ddot{\mathbf{e}}_\theta + \ddot{z}\mathbf{e}_h + 2\dot{z}\dot{\mathbf{e}}_h + z\ddot{\mathbf{e}}_h. \tag{2.43}$$

The following relations can be shown (Kristiansen *et al.*, 2007)

$$\dot{\mathbf{e}_r} = \dot{\nu}\mathbf{e}_\theta \qquad \ddot{\mathbf{e}_r} = \ddot{\nu}\mathbf{e}_\theta - \dot{\nu}^2\mathbf{e}_r \tag{2.44}$$

$$\dot{\mathbf{e}_\theta} = -\dot{\nu}\mathbf{e}_r \qquad \ddot{\mathbf{e}_\theta} = -\ddot{\nu}\mathbf{e}_r - \dot{\nu}^2\mathbf{e}_\theta, \tag{2.45}$$

where it should be noted that $\mathbf{e}_h$ is pointing out of the plane, thus

$$\ddot{\mathbf{e}}_h = \dot{\mathbf{e}}_h = 0 \tag{2.46}$$

since out-of-plane motion is not considered. Then by inserting (2.44)–(2.46) into (2.43) we obtain

$$\ddot{\mathbf{r}}_f = (\ddot{r}_l+\ddot{x}-2\dot{y}\dot{\nu}-\dot{\nu}^2(r_l+x)-y\ddot{\nu})\mathbf{e}_r + (\ddot{y}+2\dot{\nu}(\dot{r}_l+\dot{x})+\ddot{\nu}(r_l+x)-y\dot{\nu}^2)\mathbf{e}_\theta + \ddot{z}\mathbf{e}_h. \tag{2.47}$$

Note that the position of the leader spacecraft can be expressed as

$$\mathbf{r}_l = r_l\mathbf{e}_r, \tag{2.48}$$

and when differentiated twice we obtain

$$\ddot{\mathbf{r}}_l = \ddot{r}_l\mathbf{e}_r + 2\dot{r}_l\dot{\mathbf{e}}_r + r_l\ddot{\mathbf{e}}_r, \tag{2.49}$$

and by inserting (2.44) into (2.49) we obtain

$$\ddot{\mathbf{r}}_l = (\ddot{r}_l - r_l\dot{\nu}^2)\mathbf{e}_r + (2\dot{r}_l\dot{\nu} + r_l\ddot{\nu})\mathbf{e}_\theta. \tag{2.50}$$

Subtracting (2.50) from (2.43) formulates the second order derivative of the relative position vector written as

$$\ddot{\mathbf{p}} = \ddot{\mathbf{r}}_f - \ddot{\mathbf{r}}_l = (\ddot{x} - 2\dot{y}\dot{\nu} - \dot{\nu}^2x - y\ddot{\nu})\mathbf{e}_r + (\ddot{y} + 2\dot{\nu}\dot{x} + \ddot{\nu}x - y\dot{\nu}^2)\mathbf{e}_\theta + \ddot{z}\mathbf{e}_h. \tag{2.51}$$

Substituting equation (2.51) into (2.40) leads to the final position dynamics model (Kristiansen *et al.*, 2007)

$$m_f\ddot{\mathbf{p}} + \mathbf{C}_t(\dot{\nu})\dot{\mathbf{p}} + \mathbf{D}_t(\dot{\nu},\ddot{\nu},r_f)\mathbf{p} + \mathbf{n}_t(r_l,r_f) = \mathbf{F}_a + \mathbf{F}_d, \tag{2.52}$$

where

$$\mathbf{C}_t(\dot{\nu}) = 2m_f\dot{\nu}\begin{bmatrix} 0 & -1 & 0 \\ 1 & 0 & 0 \\ 0 & 0 & 0 \end{bmatrix} \tag{2.53}$$

is a skew-symmetric *Coriolis*-like matrix,

$$\mathbf{D}_t(\dot{\nu},\ddot{\nu},r_f)\mathbf{p} = m_f \begin{bmatrix} \frac{\mu}{r_f^3} - \dot{\nu}^2 & -\ddot{\nu} & 0 \\ \ddot{\nu} & \frac{\mu}{r_f^3} - \dot{\nu}^2 & 0 \\ 0 & 0 & \frac{\mu}{r_f^3} \end{bmatrix} \mathbf{p} \tag{2.54}$$

may be viewed as a time-varying potential force, and

$$\mathbf{n}_t(r_l,r_f) = m_f\mu \begin{bmatrix} \frac{r_l}{r_f^3} - \frac{1}{r_l^2} \\ 0 \\ 0 \end{bmatrix} \tag{2.55}$$

as a nonlinear term. The disturbance force and relative control force can be expressed as

$$\mathbf{F}_d = \mathbf{f}_{df} - \frac{m_f}{m_l}\mathbf{f}_{dl}, \quad \mathbf{F}_a = \mathbf{f}_{af} - \frac{m_f}{m_l}\mathbf{f}_{al}, \tag{2.56}$$

respectively.

2.5.3 Formation dynamics using Euclidian parameters in leader orbit coordinates

The time derivative of the rotation matrix can be expressed as

$$\dot{\mathbf{R}}_b^a = \mathbf{S}\left(\boldsymbol{\omega}_{a,b}^a\right)\mathbf{R}_b^a = \mathbf{R}_b^a\mathbf{S}\left(\boldsymbol{\omega}_{a,b}^b\right). \tag{2.57}$$

According to (2.18) the relative position between the leader and follower spacecraft may be expressed as

$$\mathbf{R}_l^i\mathbf{p} = \mathbf{r}_f - \mathbf{r}_l, \tag{2.58}$$

and by differentiating twice and inserting (2.57) we obtain

$$\mathbf{R}_l^i\ddot{\mathbf{p}} + 2\mathbf{R}_l^i\mathbf{S}(\boldsymbol{\omega}_{i,l}^l)\dot{\mathbf{p}} + \mathbf{R}_l^i\left(\mathbf{S}^2(\boldsymbol{\omega}_{i,l}^l) + \mathbf{S}(\dot{\boldsymbol{\omega}}_{i,l}^l)\right)\mathbf{p} = \ddot{\mathbf{r}}_f - \ddot{\mathbf{r}}_l. \tag{2.59}$$

By inserting (2.38)–(2.39), the right hand side of (2.59) may be written as

$$\ddot{\mathbf{r}}_f - \ddot{\mathbf{r}}_l = -\frac{\mu}{r_f^3}\mathbf{r}_f + \frac{\mathbf{f}_{fd}}{m_f} + \frac{\mathbf{f}_{fa}}{m_f} + \frac{\mu}{r_l^3}\mathbf{r}_l - \frac{\mathbf{f}_{ld}}{m_l} - \frac{\mathbf{f}_{la}}{m_l}, \tag{2.60}$$

and by inserting (2.18) into (2.60), we find that

$$m_f(\ddot{\mathbf{r}}_f - \ddot{\mathbf{r}}_l) = -m_f\mu\left[\left(\frac{1}{r_f^3} - \frac{1}{r_l^3}\right)\mathbf{r}_l + \frac{\mathbf{R}_l^i\mathbf{p}}{r_f^3}\right] + \mathbf{f}_{fa} + \mathbf{f}_{fd} - \frac{m_f}{m_l}(\mathbf{f}_{la} + \mathbf{f}_{ld}). \tag{2.61}$$

Moreover, by inserting (2.61) into (2.59), and rearranging the terms we obtain

$$m_f\ddot{\mathbf{p}} + \mathbf{C}_t(\boldsymbol{\omega}_{i,l}^l)\dot{\mathbf{p}} + \mathbf{D}_t(\dot{\boldsymbol{\omega}}_{i,l}^l,\boldsymbol{\omega}_{i,l}^l,r_f)\mathbf{p} + \mathbf{n}_t(\mathbf{r}_l,r_f) = \mathbf{F}_a + \mathbf{F}_d, \tag{2.62}$$

where

$$\mathbf{C}_t(\boldsymbol{\omega}_{i,l}^l) = 2m_f\mathbf{S}(\boldsymbol{\omega}_{i,l}^l) \tag{2.63}$$

is a skew-symmetric matrix,

$$\mathbf{D}_t(\dot{\boldsymbol{\omega}}_{i,l}^l, \boldsymbol{\omega}_{i,l}^l, r_f) = m_f\left[\mathbf{S}^2(\boldsymbol{\omega}_{i,l}^l) + \mathbf{S}(\dot{\boldsymbol{\omega}}_{i,l}^l) + \frac{\mu}{r_f^3}\mathbf{I}\right] \tag{2.64}$$

may be viewed as a time-varying potential force, and

$$\mathbf{n}_t(\mathbf{r}_l, r_f) = \mu m_f\mathbf{R}_i^l\left[\frac{1}{r_f^3} - \frac{1}{r_l^3}\right]\mathbf{r}_l \tag{2.65}$$

is a nonlinear term. The composite perturbation force $\mathbf{F}_d$ and the composite relative control force $\mathbf{F}_a$ are respectively written as

$$\mathbf{F}_d = \mathbf{R}_i^l\left(\mathbf{f}_{fd} - \frac{m_f}{m_l}\mathbf{f}_{ld}\right) \quad \text{and} \quad \mathbf{F}_a = \mathbf{R}_i^l\left(\mathbf{f}_{fa} - \frac{m_f}{m_l}\mathbf{f}_{la}\right). \tag{2.66}$$

Note that all forces $\mathbf{f}$ are presented in the inertial frame. If the forces are computed in another frame, the rotation matrices in (2.66) should be replaced accordingly. The orbital angular velocity and angular acceleration can be expressed as

$$\boldsymbol{\omega}_{i,l}^i = \mathbf{S}(\mathbf{r}_l)\mathbf{v}_l/\mathbf{r}_l^\top\mathbf{r}_l, \tag{2.67}$$

and

$$\dot{\boldsymbol{\omega}}_{i,l}^i = \frac{\mathbf{r}_l^\top\mathbf{r}_l\mathbf{S}(\mathbf{r}_l)\mathbf{a}_l - 2\mathbf{v}_l^\top\mathbf{r}_l\mathbf{S}(\mathbf{r}_l^\top)\mathbf{v}_l}{(\mathbf{r}_l^\top\mathbf{r}_l)^2}\ , \tag{2.68}$$

respectively, and $\boldsymbol{\omega}_{i,l}^l = \mathbf{R}_i^l\boldsymbol{\omega}_{i,l}^i$, $\dot{\boldsymbol{\omega}}_{i,l}^l = \mathbf{R}_i^l[\mathbf{S}(\boldsymbol{\omega}_{i,l}^l) + \dot{\boldsymbol{\omega}}_{i,l}^i]$.

Note that the model presented in (2.62) have many similarities compared to (2.52) although one difference is that the assumption of out-of-plane motion has been removed.

2.5.4 Formation dynamics using Euclidian parameters in follower body coordinates

The actuator forces exercised by a spacecraft are typically represented in a fixed body frame, and along with the fact that the relative rotation also is derived in the body frame (which is presented in the next section), it seems natural also to derive the relative translation in the same frame. This becomes especially evident for 6DOF modeling since it seems natural that both models are expressed in the same frame. According to Fossen (2002) and Kyrkjebø (2007) the position of the spacecraft in the body frame does not have any immediate physical interpretation as the integral $\mathbf{p}^b = \int_0^t \mathbf{v}^b dt$, but its mathematical representation is still valid.

We start by applying a rotation of (2.18) to the follower body frame such that

$$\mathbf{R}_{fb}^i\mathbf{p} = \mathbf{r}_f - \mathbf{r}_l\ , \tag{2.69}$$

and by differentiating twice and inserting (2.57) we obtain

$$\mathbf{R}^i_{fb}\ddot{\mathbf{p}} + 2\mathbf{R}^i_{fb}\mathbf{S}(\boldsymbol{\omega}^{fb}_{i,fb})\dot{\mathbf{p}} + \mathbf{R}^i_{fb}\left(\mathbf{S}^2(\boldsymbol{\omega}^{fb}_{i,fb}) + \mathbf{S}(\dot{\boldsymbol{\omega}}^{fb}_{i,fb})\right)\mathbf{p} = \ddot{\mathbf{r}}_f - \ddot{\mathbf{r}}_l. \tag{2.70}$$

Using (2.38)–(2.39), the right hand side of (2.70) may be written as

$$\ddot{\mathbf{r}}_f - \ddot{\mathbf{r}}_l = -\frac{\mu}{r_f^3}\mathbf{r}_f + \frac{\mathbf{f}_{df}}{m_f} + \frac{\mathbf{f}_{af}}{m_f} + \frac{\mu}{r_l^3}\mathbf{r}_l - \frac{\mathbf{f}_{dl}}{m_l} - \frac{\mathbf{f}_{al}}{m_l}, \tag{2.71}$$

and by insertion of (2.18) into (2.71), we obtain

$$m_f(\ddot{\mathbf{r}}_f - \ddot{\mathbf{r}}_l) = -m_f\mu\left[\left(\frac{1}{r_f^3} - \frac{1}{r_l^3}\right)\mathbf{r_l} + \frac{\mathbf{R}^i_{fb}\mathbf{p}}{r_f^3}\right] + \mathbf{f}_{af} + \mathbf{f}_{df} - \frac{m_f}{m_l}(\mathbf{f}_{al} + \mathbf{f}_{dl}). \tag{2.72}$$

Moreover, by inserting (2.72) into (2.70), and rearranging the terms we obtain

$$m_f\ddot{\mathbf{p}} + \mathbf{C}_t(\boldsymbol{\omega}^{fb}_{i,fb})\dot{\mathbf{p}} + \mathbf{D}_t(\dot{\boldsymbol{\omega}}^{fb}_{i,fb}, \boldsymbol{\omega}^{fb}_{i,fb}, r_f)\mathbf{p} + \boldsymbol{n}_t(\mathbf{r}_l, r_f) = \mathbf{F}_a + \mathbf{F}_d, \tag{2.73}$$

where

$$\mathbf{C}_t(\boldsymbol{\omega}^{fb}_{i,fb}) = 2m_f\mathbf{S}(\boldsymbol{\omega}^{fb}_{i,fb}) \tag{2.74}$$

is a skew-symmetric matrix,

$$\mathbf{D}_t(\dot{\boldsymbol{\omega}}^{fb}_{i,fb}, \boldsymbol{\omega}^{fb}_{i,fb}, r_f) = m_f\left[\mathbf{S}^2(\boldsymbol{\omega}^{fb}_{i,fb}) + \mathbf{S}(\dot{\boldsymbol{\omega}}^{fb}_{i,fb}) + \frac{\mu}{r_f^3}\mathbf{I}\right], \tag{2.75}$$

may be viewed as a time-varying potential force, and

$$\boldsymbol{n}_t(\mathbf{r}_l, r_f) = \mu m_f\mathbf{R}^{fb}_i\left[\frac{1}{r_f^3} - \frac{1}{r_l^3}\right]\mathbf{r}_l \tag{2.76}$$

is a nonlinear term. The composite perturbation force $\mathbf{F}_d$ and the composite relative control force $\mathbf{F}_a$ are given respectively by

$$\mathbf{F}_d = \mathbf{R}^{fb}_i\left(\mathbf{f}_{df} - \frac{m_f}{m_l}\mathbf{f}_{dl}\right) \quad \text{and} \quad \mathbf{F}_a = \mathbf{R}^{fb}_i\left(\mathbf{f}_{af} - \frac{m_f}{m_l}\mathbf{f}_{al}\right). \tag{2.77}$$

Note that all forces $\mathbf{f}$ are given in the inertial frame. If the forces are computed in another frame, the rotation matrices in (2.77) should be changed accordingly. As the forces acting on a spacecraft typically are given in the body frame, (2.77) can simply be written as

$$\mathbf{F}^{fb}_d = \mathbf{f}^{fb}_{df} - \mathbf{R}^{fb}_{lb}\left(\frac{m_f}{m_l}\mathbf{f}^{lb}_{dl}\right) \quad \text{and} \quad \mathbf{F}^{fb}_a = \mathbf{f}^{fb}_{af} - \mathbf{R}^{fb}_{lb}\left(\frac{m_f}{m_l}\mathbf{f}^{lb}_{al}\right). \tag{2.78}$$

The angular velocity between the follower body frame and the inertial frame may be written as

$$\boldsymbol{\omega}^{fb}_{i,fb} = \mathbf{R}^{fb}_{lb}\mathbf{R}^{lb}_l\mathbf{R}^l_i\boldsymbol{\omega}^i_{i,l} + \mathbf{R}^{fb}_{lb}\boldsymbol{\omega}^{lb}_{l,lb} + \boldsymbol{\omega}^{fb}_{lb,fb}. \tag{2.79}$$

Note that the model presented in (2.73) are quite similar to the model presented in (2.62) except for rotation matrices and which frame the angular velocity and its derivative are represented in.

One drawback is that using follower body frame coordinates may be confusing and hard to intuitively understand and compare with other models where the relative translation is represented in the leader orbit frame. As to solve this inconvenience we may give the initial values in the leader orbit frame as $\mathbf{p}_l = [a,\ b,\ c]^\top = a\mathbf{e}_r + b\mathbf{e}_\theta + c\mathbf{e}_h$, and utilize a rotation such as

$$\mathbf{p} = \mathbf{R}_l^{fb}\mathbf{p}_l, \tag{2.80}$$

and by differentiation of (2.80) we obtain

$$\dot{\mathbf{p}} = -\mathbf{S}(\boldsymbol{\omega}_{l,fb}^{fb})\mathbf{R}_l^{fb}\mathbf{p}_l + \mathbf{R}_l^{fb}\dot{\mathbf{p}}_l. \tag{2.81}$$

For plotting we solve (2.80) for $\mathbf{p}_l$ and differentiate for $\dot{\mathbf{p}}_l$.

2.6 Relative rotation

In this section we present rigid body kinematics and dynamics along with a model of relative rotation for a leader-follower system, which is derived from Euler's momentum equations using unit quaternion attitude representation.

2.6.1 Rigid body kinematics

The kinematic differential equations based on the rotation from $\mathcal{F}^b$ to $\mathcal{F}^a$ can according to Egeland and Gravdahl (2002) be expressed as

$$\dot{\mathbf{q}} = \mathbf{T}(\mathbf{q})\boldsymbol{\omega}_{a,b}^{b}, \quad \mathbf{T}(\mathbf{q}) = \frac{1}{2}\begin{bmatrix} -\boldsymbol{\epsilon}^T \\ \eta\mathbf{I} + \mathbf{S}(\boldsymbol{\epsilon}) \end{bmatrix} \in \mathbb{R}^{4\times 3}. \tag{2.82}$$

2.6.2 Rigid body dynamics

With the assumptions of rigid body movement, the dynamical model can be found from Euler's momentum equations as (Sidi, 1997)

$$\mathbf{J}_s\dot{\boldsymbol{\omega}}_{i,sb}^{sb} = -\mathbf{S}(\boldsymbol{\omega}_{i,sb}^{sb})\mathbf{J}_s\boldsymbol{\omega}_{i,sb}^{sb} + \boldsymbol{\tau}_{sd}^{sb} + \boldsymbol{\tau}_{sa}^{sb} \tag{2.83}$$

where $\mathbf{J}_s = \mathrm{diag}\{J_{sx}, J_{sy}, J_{sz}\} \in \mathbb{R}^{3\times 3}$ is the rigid body moment of inertia matrix, $\boldsymbol{\tau}_{sd}^{sb} \in \mathbb{R}^3$ is the total disturbance torque, $\boldsymbol{\tau}_{sa}^{sb} \in \mathbb{R}^3$ is the total actuator torque and sub-/super-script $s = l, f$ denotes the leader and follower spacecraft, respectively. For a spacecraft it might be preferable to control relative to the orbit frame *i.e.* for *nadir* pointing spacecraft. Then the angular velocity might be expressed as

$$\boldsymbol{\omega}_{s,sb}^{sb} = \boldsymbol{\omega}_{i,sb}^{sb} - \mathbf{R}_i^{sb}\boldsymbol{\omega}_{i,s}^{i}, \tag{2.84}$$

where $\boldsymbol{\omega}_{i,s}^{i}$ can be expressed as in (2.67). To obtain the dynamical model we differentiate (2.84) and insert (2.83), leading to

$$\mathbf{J}\dot{\boldsymbol{\omega}}_{s,sb}^{sb} = -\mathbf{S}(\boldsymbol{\omega}_{i,sb}^{sb})\mathbf{J}_s\boldsymbol{\omega}_{i,sb}^{sb} + \mathbf{J}_s\mathbf{S}(\boldsymbol{\omega}_{i,sb}^{sb})\mathbf{R}_i^{sb} - \mathbf{J}_s\mathbf{R}_i^{sb}\dot{\boldsymbol{\omega}}_{i,s}^{i} + \boldsymbol{\tau}_{sd} + \boldsymbol{\tau}_{sa}, \tag{2.85}$$

where $\dot{\boldsymbol{\omega}}^{i}_{i,s}$ can be expressed as in (2.68). Utilizing the model (2.85) leads to more complex control laws, that is, the control structure gets more complicated because of the extra terms compared to (2.83). Instead, the relation can be applied to the references although, the inconvenience is only moved, but from a practical viewpoint the manipulation can be performed on ground before sending the references to the spacecraft, saving valuable computational resources on board the spacecraft. Furthermore, the stability analysis' as presented in this thesis are not altered because we do not consider guidance-in-the-loop hence, we only use this relationship to define reference trajectories if otherwise is not stated.

2.6.3 Relative attitude

The attitude of the leader body frame relative to the inertial frame is denoted $\mathbf{q}_{i,lb}$, while the attitude of the follower body frame relative to the inertial frame is denoted $\mathbf{q}_{i,fb}$. Relative attitude between the follower and leader body frame is found by applying the quaternion product (*cf.* (2.28)) expressed as

$$\mathbf{q}_{lb,fb} = \bar{\mathbf{q}}_{i,lb} \otimes \mathbf{q}_{i,fb} \ , \tag{2.86}$$

and from now on, with a slightly abuse of notation we denote $\mathbf{q}_l = \mathbf{q}_{i,lb}$ and $\mathbf{q}_f = \mathbf{q}_{lb,fb}$. The relative attitude dynamics may be expressed as (Yan *et al.*, 2000*a*; Kristiansen, 2008)

$$\begin{aligned} &\mathbf{J}_f\dot{\boldsymbol{\omega}} + \mathbf{J}_f\mathbf{S}(\mathbf{R}^{fb}_{lb}\boldsymbol{\omega}^{lb}_{i,lb})\boldsymbol{\omega} - \mathbf{J}_f\mathbf{R}^{fb}_{lb}\mathbf{J}_l^{-1}\mathbf{S}(\boldsymbol{\omega}^{lb}_{i,lb})\mathbf{J}_l\boldsymbol{\omega}^{lb}_{i,lb} \\ &\quad + \mathbf{S}(\boldsymbol{\omega} + \mathbf{R}^{fb}_{lb}\boldsymbol{\omega}^{lb}_{i,lb})\mathbf{J}_f(\boldsymbol{\omega} + \mathbf{R}^{fb}_{lb}\boldsymbol{\omega}^{lb}_{i,lb}) = \boldsymbol{\Upsilon}_d + \boldsymbol{\Upsilon}_a, \end{aligned} \tag{2.87}$$

where

$$\boldsymbol{\omega} := \boldsymbol{\omega}^{fb}_{lb,fb} = \boldsymbol{\omega}^{fb}_{i,fb} - \mathbf{R}^{fb}_{lb}\boldsymbol{\omega}^{lb}_{i,lb} \tag{2.88}$$

is the relative angular velocity between the $\mathcal{F}^{fb}$ and $\mathcal{F}^{lb}$ expressed in $\mathcal{F}^{fb}$, and

$$\boldsymbol{\Upsilon}_d = \boldsymbol{\tau}^{fb}_{fd} - \mathbf{J}_f\mathbf{R}^{fb}_{lb}\mathbf{J}_l^{-1}\boldsymbol{\tau}^{lb}_{ld}, \quad \boldsymbol{\Upsilon}_a = \boldsymbol{\tau}^{fb}_{fa} - \mathbf{J}_f\mathbf{R}^{fb}_{lb}\mathbf{J}_l^{-1}\boldsymbol{\tau}^{lb}_{la} \tag{2.89}$$

are the relative perturbation torque and actuator torque, respectively. For simplicity (2.87) may be rewritten as

$$\mathbf{J}_f\dot{\boldsymbol{\omega}} + \mathbf{C}_r(\boldsymbol{\omega})\boldsymbol{\omega} + \mathbf{n}_r(\boldsymbol{\omega}) = \boldsymbol{\Upsilon}_d + \boldsymbol{\Upsilon}_a, \tag{2.90}$$

where

$$\mathbf{C}_r(\boldsymbol{\omega}) = \mathbf{J}_f\mathbf{S}(\mathbf{R}^{fb}_{lb}\boldsymbol{\omega}^{lb}_{i,lb}) + \mathbf{S}(\mathbf{R}^{fb}_{lb}\boldsymbol{\omega}^{lb}_{i,lb})\mathbf{J}_f - \mathbf{S}(\mathbf{J}_f(\boldsymbol{\omega} + \mathbf{R}^{fb}_{lb}\boldsymbol{\omega}^{lb}_{i,lb})) \tag{2.91}$$

is a skew-symmetric matrix, and

$$\mathbf{n}_r(\boldsymbol{\omega}) = \mathbf{S}(\mathbf{R}^{fb}_{lb}\boldsymbol{\omega}^{lb}_{i,lb})\mathbf{J}_f\mathbf{R}^{fb}_{lb}\boldsymbol{\omega}^{lb}_{i,lb} - \mathbf{J}_f\mathbf{R}^{fb}_{lb}\mathbf{J}_l^{-1}\mathbf{S}(\boldsymbol{\omega}^{lb}_{i,lb})\mathbf{J}_l\boldsymbol{\omega}^{lb}_{i,lb} \tag{2.92}$$

is a nonlinear term.

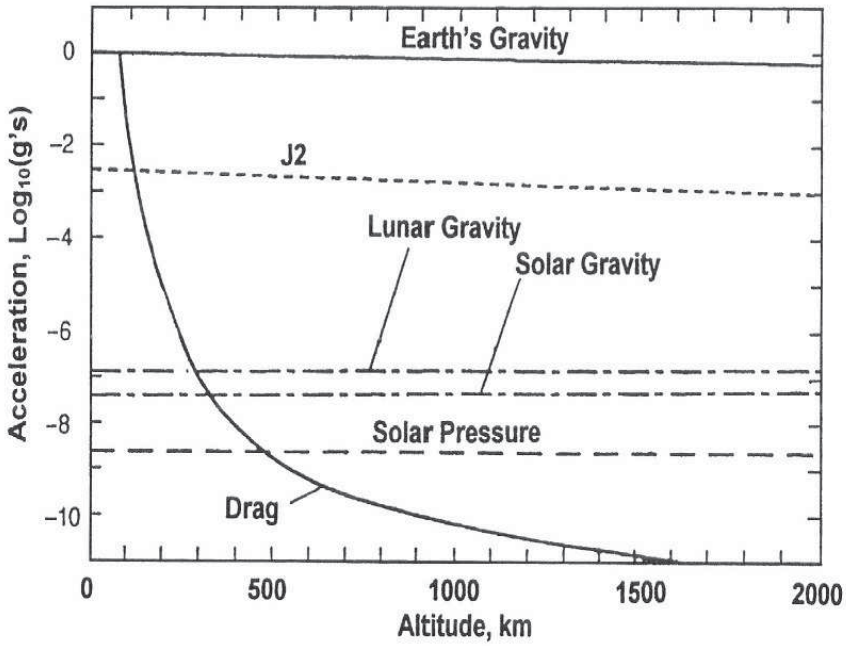

Figure 2.5: Influence of different disturbing forces at different altitude. Reproduced with courtesy to Wiley; (Fortescue *et al.*, 2007).

2.7 Orbital perturbations

In this section we present modeling of orbital perturbing forces and torques made by external sources working on Earth orbiting spacecraft including aerodynamic drag, J_2, gravitational forces from other bodies, solar radiation and solar wind, gravity gradient and torques produced by forces working on a spacecraft with displacement of the center of mass. Accurate models of the perturbations are important because of the high precision required in *e.g.* formation flying guidance and control applications, and because of the relative distances between members and possibly differences in design the perturbations may act differently on each individual spacecraft participating in the formation, causing a challenging problem to the control of the overall formation. Although the disturbances are small, they have to be considered because over time large deviations will occur, thus small velocity vectors have to be produced by each spacecraft to cope with the disturbances on each satellite individually. Some of these disturbances are shown in Figure 2.5 where it can be seen that most of the disturbing forces are near constant at low Earth orbits (LEO) except atmospheric drag which is reduced rapidly with increasing altitude.

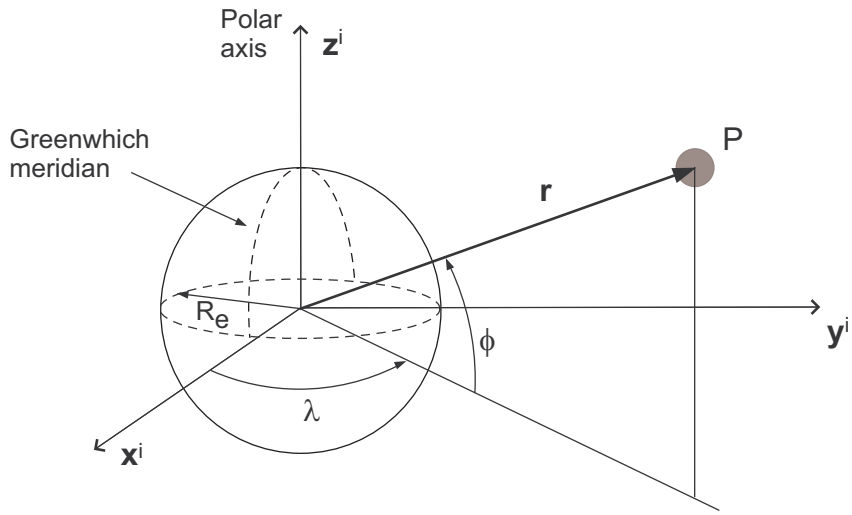

Figure 2.6: Coordinates for the derivation of the Earths' external gravitational potential.

2.7.1 Orbital perturbing forces

In this section we will present disturbance forces working on a spacecraft in orbit. The main disturbance forces are caused by gravitational perturbations, atmospheric drag, solar radiation, solar wind and third-body perturbing forces.

Gravitational perturbation

A spacecraft is attracted by the gravitation force of the Earth which can be described by a gradient of a scalar depending on the distance between the Earth and the spacecraft by the function $U(\mathbf{r}) = -\mu/r$. The Earth is not a mass concentrated in a single point or a perfect sphere, but rather an oblate body without homogeneous mass distribution. Because of this correction factors have to be added to the gravitational potential and may be expressed as (Wertz, 1978)

$$U(\mathbf{r}, \phi, \lambda) = -\frac{\mu}{r} + B(\mathbf{r}, \phi, \lambda), \tag{2.93}$$

where $\mu = Gm$, r is the geocentric distance to any point P outside the sphere of the Earth, and $B(\mathbf{r}, \phi, \lambda)$ is the appropriate spherical harmonic expansion used to correct the scalar gradient because of the uneven mass distribution of the Earth. The parameter ϕ denotes the geocentric latitude and λ the geographical longitude of the body position as shown in Figure 2.6.

Table 2.1: Tesseral and sectoral harmonic coefficients up to degree and order three.

n	m	S_{nm}	C_{nm}
2	1	0	0
2	2	-0.9×10^{-6}	1.57×10^{-6}
3	1	0.27×10^{-6}	2.19×10^{-6}
3	2	-0.21×10^{-6}	0.31×10^{-6}

Table 2.2: Zonal harmonic coefficients of order 0.

n	J_n
2	1082.6×10^{-6}
3	-2.53×10^{-6}
4	$= -1.61 \times 10^{-6}$

The spherical harmonic expansion can be written as

$$B(\mathbf{r},\phi,\lambda) = \frac{\mu}{r}\Big\{\sum_{n=2}^{\infty}\Big[\left(\frac{R_e}{r}\right)^n J_n P_n(\sin(\phi)) + \sum_{m=1}^{n}\left(\frac{R_e}{r}\right)^n \times (C_{nm}\cos(m\lambda) + S_{nm}\sin(m\lambda))P_{nm}(\sin(\phi))\Big]\Big\}, \tag{2.94}$$

which is the infinite series of the *geopotential* function at any point P. Utilizing the coordinates shown in Figure 2.6, the parameters are defined as follows

R_e - mean equatorial radius of the earth;

$\cos(m\lambda)$ and $\sin(m\lambda)$ - harmonics in λ;

J_{nm} - zonal harmonic coefficients;

J_n - zonal harmonic coefficients of order 0;

P_{nm} - associated Legendre polynomial of degree n and order m;

P_n - Legendre polynomial degree n and order 0;

C_{nm} - tesseral harmonic coefficients for $n \neq m$; and

S_{nm} - sectoral harmonic coefficients for $n = m$.

These coefficients are a result of the Earth's oblateness, and the values are found by satellite observation and appropriate measurements. Note that the values are changing with time; some of the values for the World Geodetic Survey (WGS) from 1984 are presented in Tables 2.1 and 2.2.

It is important to notice that the coefficients doesn't necessarily decrease when the order increases however, the factor $(R_e/r)^n$ in (2.94) has great influence on

Table 2.3: Legendre polynomials.

n	m	$P_{nm}(u)$	$P_{nm}(\sin(\phi))$
0	0	1	1
1	0	u	$\sin(\phi)$
1	1	$(1-u^2)^{\frac{1}{2}}$	$\cos(\phi)$
2	0	$\frac{1}{2}(3u^2-1)$	$\frac{1}{2}(3\sin^2(\phi)-1)$
2	1	$3u(1-u^2)^{\frac{1}{2}}$	$3\cos(\phi)\sin(\phi)$
2	2	$3(1-u^2)$	$3\cos^2(\phi)$

the series. The magnitude of J_2 is at least 400 times larger then the other J_n coefficients. For engineering purposes a simplified form of (2.94) may be used.

$$U \approx -\frac{\mu}{r}\left[1-\sum_{n=2}^{\infty}\left(\frac{R_e}{r}\right)^n J_n P_n \sin(\phi)\right] = \frac{\mu}{r}[U_0 + U_{J2} + U_{J3} + \ldots], \tag{2.95}$$

where the *Legendre polynomials* P_{nm} are polynomials of $\cos(\phi)$ and $\sin(\phi)$ and are defined as

$$P_{nm}(u) = (1-u^2)^{\frac{m}{2}}\frac{d^m}{du^m}P_n(u). \tag{2.96}$$

A number of Legendre polynomials is presented in Table 2.3 calculated based on (2.96), and based on these, the terms in (2.95) are obtained as

$$U_0 = -1, \tag{2.97}$$

$$U_{J2} = \frac{1}{2}J_2\left(\frac{R_e}{r}\right)^2(3\sin^2(\phi)-1), \tag{2.98}$$

$$U_{J3} = \frac{1}{2}J_3\left(\frac{R_e}{r}\right)^3(5\sin^3(\phi)-3\sin(\phi)), \tag{2.99}$$

where $P_2 = P_{02}$ and $P_3 = P_{03}$ were used. By considering that J_2 is so much larger then the other coefficients it is the most important factor to be used. By inserting (2.97) and (2.98) into (2.95) we obtain an approximated gravitational potential function written as

$$U = \frac{\mu}{r}[U_0 + U_{J2}] = \frac{\mu}{r}\left\{-1+\left(\frac{R_e}{r}\right)^2 J_2\frac{1}{2}[3\sin^2(\phi)-1]\right\}. \tag{2.100}$$

As can be seen from (2.100) the perturbing potential is only dependent on the latitude of the spacecraft. The term $\sin(\phi)$ expressed in $\mathcal{F}^i$ can be written as

$$\sin(\phi) = \frac{z}{r} = \frac{z}{\sqrt{x^2+y^2+z^2}}, \tag{2.101}$$

where x, y and z are the components of $\mathbf{r}$ which is the vector pointing from the center of Earth to a point P in space. The gravitational force acting on the spacecraft is then found by

$$\mathbf{F} = -\nabla U(x,y,z), \tag{2.102}$$

and by combining (2.102) with (2.100) and (2.101) we find the gravitational forces on vector form as

$$F_x = -\frac{\partial U}{\partial x} = \mu\left[-\frac{x}{r^3} + \frac{1}{2}J_2R_e^2\left(15\frac{xz^2}{r^7} - 3\frac{x}{r^5}\right)\right] \tag{2.103}$$

$$F_y = -\frac{\partial U}{\partial y} = \mu\left[-\frac{y}{r^3} + \frac{1}{2}J_2R_e^2\left(15\frac{yz^2}{r^7} - 3\frac{y}{r^5}\right)\right] \tag{2.104}$$

$$F_z = -\frac{\partial U}{\partial z} = \mu\left[-\frac{z}{r^3} + \frac{1}{2}J_2R_e^2\left(15\frac{z^3}{r^7} - 9\frac{z}{r^5}\right)\right]. \tag{2.105}$$

Eq. (2.103)–(2.105) may also be written on a more compact form

$$\mathbf{F} = \mu\begin{bmatrix} -\frac{x}{r^3} + \frac{1}{2}J_2R_e^2\left(15\frac{xz^2}{r^7} - 3\frac{x}{r^5}\right) \\ -\frac{y}{r^3} + \frac{1}{2}J_2R_e^2\left(15\frac{yz^2}{r^7} - 3\frac{y}{r^5}\right) \\ -\frac{z}{r^3} + \frac{1}{2}J_2R_e^2\left(15\frac{z^3}{r^7} - 9\frac{z}{r^5}\right) \end{bmatrix}, \tag{2.106}$$

and the perturbation caused by the J_2 gravitation force for Earth is the latter terms of (2.106) and may be written as

$$\mathbf{f}_{grav} = \frac{1}{2}\mu J_2R_e^2\mathbf{R}_i^{sb}\begin{bmatrix} 15\frac{xz^2}{r^7} - 3\frac{x}{r^5} \\ 15\frac{yz^2}{r^7} - 3\frac{y}{r^5} \\ 15\frac{z^3}{r^7} - 9\frac{z}{r^5} \end{bmatrix}. \tag{2.107}$$

Note that the J_2 perturbation causes changes in the orbital parameters Ω, ω and M over time.

Atmospheric drag

Atmospheric drag is a disturbance which exists only in the lower orbits, especially low earth orbits (LEO) are affected, that is, orbits of 600 km or less altitude, because the atmospheric density decreases exponentially with increasing altitude. The density of the atmosphere ρ is defined as

$$\rho(r) = \rho_0 e^{\left[\frac{(r-r_0)}{h}\right]}, \tag{2.108}$$

where ρ_0 is reference density and r_0 is the reference orbit radius; if a circular orbit is assumed, the density ρ is constant. The perturbing force F_{atm}, working in opposite direction of the spacecraft velocity, can be expressed as (Sidi, 1997)

$$F_{atm} = \frac{1}{2}\rho v^2 C_d S, \tag{2.109}$$

where v is the spacecraft velocity, C_d is the drag coefficient of the spacecraft and S is the equivalent spacecraft surface in the direction of the motion. The acceleration of the spacecraft caused by the atmospheric drag can be found by

$$\mathbf{f}_{atm}^a = \frac{\mathbf{F}_{atm}}{m_s}, \tag{2.110}$$

where m_s is the spacecraft mass and $\mathbf{F}_{atm} = [0, \ -F_{atm}, \ 0]^\top$. Rearranging and substituting (2.110) and (2.109) leads to

$$\mathbf{v} \cdot \mathbf{f}^a_{atm} = \frac{-v(\rho v^2 C_d S)}{2m_s}, \tag{2.111}$$

where the term $C_d S/2m_s$ is known as the *ballistic coefficient*. The aerodynamic drag can be expressed as

$$\mathbf{f}_{atm} = -\mathbf{R}^{sb}_s \mathbf{C}^s_a \frac{1}{2}\rho v^2 C_d S \mathbf{e}_v = \mathbf{R}^{sb}_s \mathbf{C}^s_a \begin{bmatrix} 0 \\ -\frac{1}{2}\rho v^2 C_d S \\ 0 \end{bmatrix}, \tag{2.112}$$

where $\mathbf{f}_{atm}$ is the perturbing force acting in opposite to the direction of motion of the spacecraft, $\mathbf{C}^s_a$ denotes the transformation matrix from auxiliary to orbit frame, and $\mathbf{e}_v$ denotes the unit velocity vector. By further manipulation the relationship

$$\frac{da}{dt} = -\rho\sqrt{a\mu}\frac{C_d S}{m_s} \tag{2.113}$$

can be obtained showing that the semi-major axis a is decreasing over time because of the atmospheric drag and extra force is needed to counteract the disturbance force to maintain a constant spacecraft orbit.

Solar radiation and solar wind

Solar radiation is an aggregate expression for all the electromagnetic waves radiated by the Sun, while the *Solar wind* is mainly ionized nuclei and electrons radiated by the Sun. The radiation from both phenomena produces a physical pressure on the spacecraft body causing a disturbance force; the pressure is proportional to the *momentum flux* (momentum per unit area per unit time) of the radiation. Note that the solar radiation momentum flux is 100 to 1000 times greater than the solar wind (Sidi, 1997). The mean *solar energy flux* at the Earth's position can be expressed as

$$F_e = \frac{1358}{1.0004 + 0.0334\cos(D)}, \tag{2.114}$$

where D is the "phase" of the year, which is calculated as starting on July 4 (Wertz, 1978). The typical value for the mean solar energy flux at Earth is $F_e \approx 1367$ Wm^{-2}. The total perturbation from solar radiation can be written as

$$\mathbf{f}_{rad} = -\mathbf{R}^{sb}_s \frac{F_e}{c}\cos(\theta_{sun})A[(1-\varepsilon)\mathbf{e}_{Sun} + 2\varepsilon\cos(\theta_{sun})\mathbf{n}], \tag{2.115}$$

where c is the velocity of light, A is the cross-sectional area of the spacecraft perpendicular to the Sun line, $\mathbf{n}$ is the normal vector of the body, $\mathbf{e}_{Sun}$ is the vector pointing towards the Sun, θ_{Sun} denotes the angle between the vector $\mathbf{e}_{Sun}$ and the normal vector $\mathbf{n}$, and ε is the absorption characteristic of the spacecraft. The value of ε lies between 0 and 1 where $\varepsilon = 0$ is a *black body*[4] while $\varepsilon = 1$ is describing a body which is perfectly reflecting all light. Typical values ranges from $0.2 - 0.9$ for spacecraft materials.

[4] A black body is a physical body which is considered perfectly absorbing, that is, it absorbs all incident electromagnetic radiation.

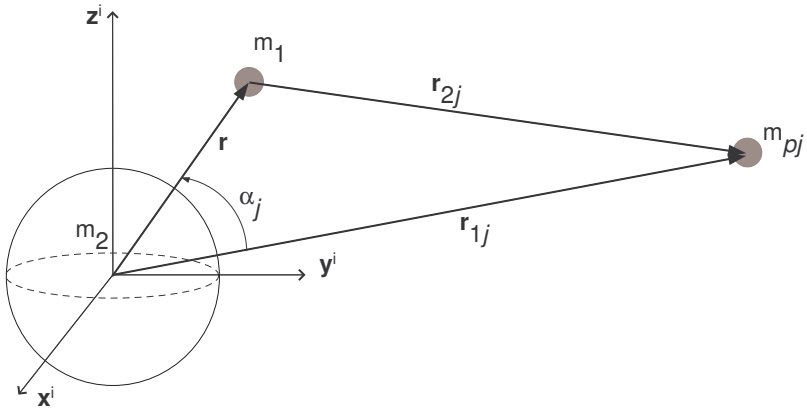

Figure 2.7: Simplified model for the n-body dynamics perturbing forces.

Third-Body perturbing force

A third-body, like the Sun or the Moon, creates a perturbing force with respect to an orbiting spacecraft which can cause changes to its nominal Keplerian orbit. A generalization of this problem leads to the *n-body problem* which is a system including n different bodies as derived in Section 2.5.1. Based on (2.32) the accelerations for m_1 and m_2 are found as

$$\frac{d^2\mathbf{r}_1}{dt^2} = G\frac{m_1}{r_{12}^3}(\mathbf{r}_2 - \mathbf{r}_1) + G\sum_{j=3}^{j=n}\frac{m_j}{r_{1j}^3}(\mathbf{r}_j - \mathbf{r}_1) \tag{2.116}$$

$$\frac{d^2\mathbf{r}_2}{dt^2} = G\frac{m_2}{r_{21}^3}(\mathbf{r}_1 - \mathbf{r}_2) + G\sum_{j=3}^{j=n}\frac{m_j}{r_{2j}^3}(\mathbf{r}_j - \mathbf{r}_2), \tag{2.117}$$

where (2.116)–(2.117) represents the motion with respect to the inertial coordinate axis. For an Earth orbiting spacecraft we denote $m_1 = M_e$ the mass of the Earth, $m_2 = m_s$ the mass of the spacecraft and m_j the mass of the j-th perturbing body *e.g.* Moon or Sun. Since $\mathcal{F}^i$ is located at the center of the Earth we have that $\mathbf{r}_1 = 0$, and by subtracting (2.116) from (2.117) we obtain

$$\frac{d^2\mathbf{r}}{dt^2} + G\frac{\mathbf{r}}{r^3}(M_e + m_s) = G\sum_{j=3}^{j=n} m_j\left[\frac{\mathbf{r}_{2j}}{r_{2j}^3} - \frac{\mathbf{r}_{1j}}{r_{1j}^3}\right] \tag{2.118}$$

where we in general denote $\mathbf{r}_{ij} := \mathbf{r}_j - \mathbf{r}_i$ for all $i \neq j$. The perturbing force due to the $n-2$ perturbing bodies can then be written as

$$\mathbf{f}_{body} = \mathbf{R}_i^{sb}\sum_{j=3}^{j=n}\mu_j\left[\frac{\mathbf{r}_{2j}}{r_{2j}^3} - \frac{\mathbf{r}_{1j}}{r_{1j}^3}\right], \tag{2.119}$$

where $\mu_j = Gm_j$.

Total perturbation force

The total perturbation force working on an Earth orbiting spacecraft may be summarized as

$$\mathbf{f}_d = \mathbf{f}_{atm} + \mathbf{f}_{grav} + \mathbf{f}_{rad} + \mathbf{f}_{body}, \tag{2.120}$$

where $\mathbf{f}_{atm}$ is caused by aerodynamic drag, $\mathbf{f}_{grav}$ is caused by mass distribution of the Earth, $\mathbf{f}_{rad}$ caused by solar radiation and $\mathbf{f}_{body}$ is a gravitational perturbation caused by a third body. The total disturbance force can be included in the spacecraft control law to counteract the external forces working on the spacecraft.

Remark 2.1 *Disturbances working on spacecraft such as aerodynamic drag, J_2 effect caused by uneven mass distribution of the Earth and third-body perturbing forces can all be seen as state dependent, slow varying and even in some cases constant. In the control laws and simulations presented throughout this thesis we will assume that all constants are unknown but bounded such as $\|\mathbf{f}_d(t)\| \leq \beta_d$, but as many of the disturbances for spacecraft can be reasonably well modeled as shown in this section,* e.g. *$\hat{\mathbf{f}}_d(t)$, we could add this to the overall analysis such that $\tilde{\mathbf{f}}_d(t) = \mathbf{f}_d(t) - \hat{\mathbf{f}}_d(t)$. This strategy could reduce the upper bound such that $\|\tilde{\mathbf{f}}_d(t)\| \leq \beta_{\tilde{d}} < \beta_d$, based on the quality of the disturbance modeling.*

2.7.2 Orbital perturbing torques

In this section we will present disturbances torques working on a spacecraft in orbit as in Section 2.7.1. The main disturbance torques are caused by gravity gradient and perturbing forces working on a spacecraft where the center of mass is displaced.

Gravity gradient

Gravity gradient torque is forcing the spacecraft to align its axis of minimum moment of inertia vertically and can be expressed as (Sidi, 1997)

$$\boldsymbol{\tau}_{gg} = \mathbf{R}_i^{sb} 3\frac{\mu}{r^5}\mathbf{S}(\mathbf{r})\mathbf{J}\mathbf{r} \tag{2.121}$$

Note that $\boldsymbol{\tau}_{gg} = \mathbf{0}$ if the inertia matrix is on the form $\mathbf{J} = \alpha\mathbf{I}$ where $\alpha \in \mathbb{R}_+$ or if the position vector is parallel with any of the principal body axes.

Perturbing torque caused by perturbing forces

The rotational torque caused by perturbing forces can be found from the relation (Egeland and Gravdahl, 2002)

$$\boldsymbol{\tau}_j = \mathbf{S}(\mathbf{r}_c)\mathbf{f}_j, \tag{2.122}$$

where $\mathbf{r}_c$ is the vector from the spacecraft center of mass to the line of action of the force $\mathbf{f}_j$.

Total perturbation torque

The total perturbation torque working on an Earth orbiting spacecraft may be summarized as

$$\boldsymbol{\tau}_d = \boldsymbol{\tau}_{gg} + \mathbf{S}(\mathbf{r}_c)(\mathbf{f}_d). \tag{2.123}$$

Remark 2.1 also holds for modeled disturbance torques.

2.8 Simulations

In this section we present simulation parameters utilized throughout this thesis in Section 2.8.1 and simulation results based on the derived models for relative translation presented in Section 2.5.3 and 2.5.4 in Section 2.8.2. Simulation results for the relative translational model presented in Section 2.5.2 and the model for relative rotation presented in Section 2.6 can be seen in (Kristiansen *et al.*, 2007).

2.8.1 Simulation parameters

Simulation results will be included in each succeeding chapter throughout this thesis to validate the mathematical results. For simplicity, the authors have tried to utilize similar simulation parameters for all simulations to make comparison between results easier. Therefore, if nothing else is explicitly stated, we make use of the following parameters.

All simulations were performed in Simulink$^{\text{TM}}$ using either a variable sample-time Runge-Kutta ODE45 solver with relative and absolute tolerance of 10^{-9} for simulations without noise or a fixed time Runge-Kutta ODE4 solver with step size of 1×10^{-3} s when noise is included. The rigid body moments of inertia were chosen as $\mathbf{J}_s = \text{diag}\{4.35,\ 4.33,\ 3.664\}$ kgm^2 and masses as $m_s = 100$ kg, and for simulations of spacecraft the orbit was chosen with perigee at 600 km, apogee at 750 km, inclination at 71°, and the argument of perigee and the right ascension of the ascending node at 0°. For leader-follower formations it was assumed both perfect control and that all perturbations were known and accounted for regarding the leader spacecraft.

Measurement noise was introduced as $\sigma\mathbb{B}^n = \{x \in \mathbb{R}^n : \|x\| \leq \sigma\}$ and were added to the error functions so that the measured states $\mathbf{q}_n$ satisfies $\mathbf{q}_n = (\mathbf{q} + 0.05\mathbb{B}^4)/\|\mathbf{q} + 0.05\mathbb{B}^4\|$ and $\boldsymbol{\omega}_n = \boldsymbol{\omega} + 0.01\mathbb{B}^3$ for rotational control and $\mathbf{p}_n = \mathbf{p} + 1 \times 10^{-3}\mathbb{B}^3$ and $\dot{\mathbf{p}}_n = \dot{\mathbf{p}} + 5 \times 10^{-4}\mathbb{B}^3$ for translational control. The major contributors for disturbance forces and torques in LEO were added to the simulations including atmospheric drag, J_2 and gravity gradient with a displacement in center of gravity by $\mathbf{r}_c^b = [0.1,\ 0,\ 0]^\top$.

To evaluate and compare the performance of the rotational controllers we have defined performance functionals

$$J_q = \int_{t_0}^{t_f} \tilde{\boldsymbol{\epsilon}}^\top \tilde{\boldsymbol{\epsilon}} dt, \quad J_\omega = \int_{t_0}^{t_f} \mathbf{e}_\omega^\top \mathbf{e}_\omega dt, \quad J_p = \int_{t_0}^{t_f} \boldsymbol{\tau}_a^\top \boldsymbol{\tau}_a dt, \tag{2.124}$$

where t_0 and t_f defines the start and end of the simulation window, respectively. The functionals J_q and J_ω describe the integral of the attitude and angular velocity error, while J_p describes the integral of the applied control torque.

To evaluate and compare the performance of the translational controllers we use the functionals

$$J_{pos} = \int_{t_0}^{t_f} \tilde{\mathbf{p}}^\top \tilde{\mathbf{p}} dt,\ J_{vel} = \int_{t_0}^{t_f} \dot{\tilde{\mathbf{p}}}^\top \dot{\tilde{\mathbf{p}}} dt,\quad J_{pow} = \int_{t_0}^{t_f} \mathbf{f}_{af}^\top \mathbf{f}_{af} dt, \tag{2.125}$$

where the functional J_{pos} and J_{vel} describes the integral functional error of the relative position and velocity error, while J_{pow} describes the integral of the applied control force.

2.8.2 Simulation results

The simulation results presented in this section are based on the results derived in Section 2.5.3 and Section 2.5.4. We have chosen to compare these results with the simulation results presented by Kristiansen *et al.* (2007) where the model derived in Section 2.5.2 were utilized. Therefore, we have chosen for the leader spacecraft a circular Earth orbit with an altitude of 250 km, inclination at 22.5° and the argument of perigee and the right ascension of the ascending node at 0°. The initial relative position and velocity were chosen as standstill ($\dot{\mathbf{p}}(t_0) = \mathbf{0}$ m/s) at $\mathbf{p}(t_0) = [0,\ -100,\ 0]^\top$m.

Figure 2.8 shows a plot over four orbital revolutions of the relative position and velocity without any orbit perturbations. As can be seen, the follower spacecraft trails the leader spacecraft with a more or less constant relative position and velocity, that is, since the leader orbit is circular and the point -100 m along the $\mathbf{e}_\theta$ vector is not part of the same circular orbit and since both have same initial velocity, the follower follows a slightly elliptic orbit which deviates compared to the circular one as can be seen from the topmost plot in Figure 2.9, along with the relative angular velocity between the leader and follower orbit as the bottommost plot.

Figure 2.10 represents simulation results applying the perturbation model for atmospheric drag working on the follower spacecraft. The equivalent spacecraft area and drag coefficient are both set to 1 for simplicity. The plot shows that the altitude of the follower spacecraft decreases because of the negative evolution along $\mathbf{e}_r$, which probably means that it starts to loose altitude because of the aerodynamic drag working opposite of the velocity vector. This effect causes the orbital angular velocity of the follower spacecraft to increase, while the orbital period is decreasing, which reflects the increasing position along $\mathbf{e}_\theta$. The same effect is also seen from the plot of the relative velocity. The main reason why the aerodynamic drag causes such a large impact on the follower orbit is because of the high density of the local atmosphere at 250 km orbit altitude.

In Figure 2.11 simulation results including atmospheric drag and J_2 perturbation force are presented. The J_2 perturbing force increases the effect from the previous simulation, that is, the effect causes the follower spacecraft to be pulled towards the Earth in an oscillating way, thereby increasing the distance along $\mathbf{e}_r$. The effect also causes an oscillation about the $\mathbf{e}_h$-axis because of the inclined orbit.

Lastly, simulation results for an elliptic orbit with perigee at 250 km and apogee at 500 km are presented in Figure 2.12 including atmospheric drag and J_2 perturbation. The effect caused by the perturbations on the follower spacecraft is reduced

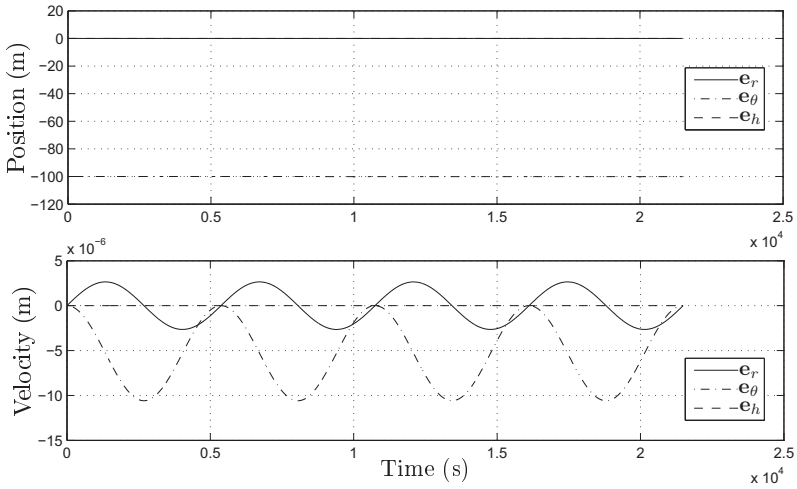

Figure 2.8: Relative position and velocity between leader and follower spacecraft without perturbations.

compared to the circular orbit of 250 km altitude because the density of the local atmosphere is lower in all parts of the elliptic orbit except the perigee, while the increased distance also have negative impact on the contribution from the J_2 perturbation.

By utilizing the same initial condition as described in this section and transforming them according to (2.81), along with the model presented in follower body (2.73) and transforming them back to leader orbit coordinates for representation, we obtain the exact same results as presented above and conclude that the models are in some sense equal.

By comparing the results presented above with the results presented by Kristiansen *et al.* (2007) where the model presented in Section 2.5.2 were utilized we see that the behavior is different. In (Kristiansen *et al.*, 2007) the follower obtain an increasing altitude (growth along $\mathbf{e}_r$) while decreasing along cross-track ($\mathbf{e}_\theta$), which is natural since since the orbital period is increasing with the growth in altitude. After a close inspection it might seem that the results are quite alike except for opposite signs.

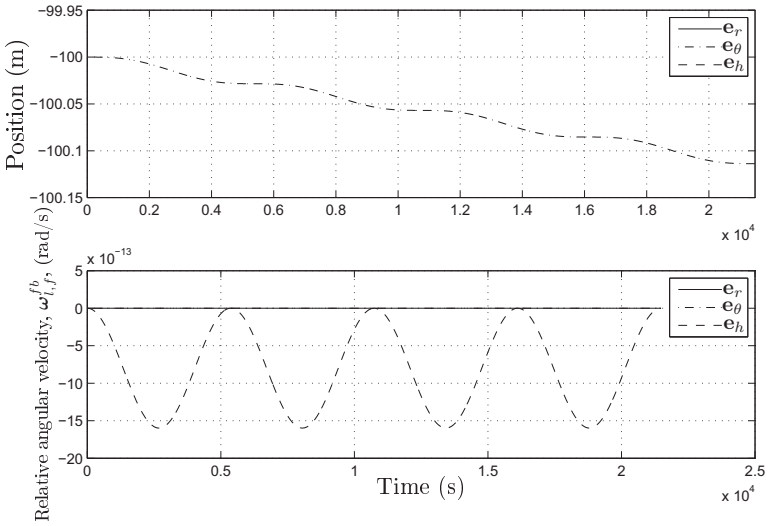

Figure 2.9: Relative position (zoomed) between leader and follower spacecraft and relative angular velocity between leader orbit and follower orbit frame without perturbations.

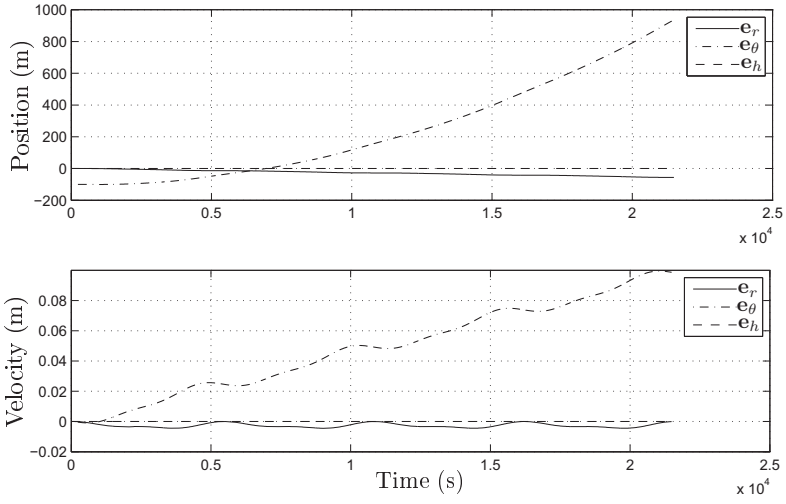

Figure 2.10: Relative position and velocity between leader and follower spacecraft including aerodynamic drag.

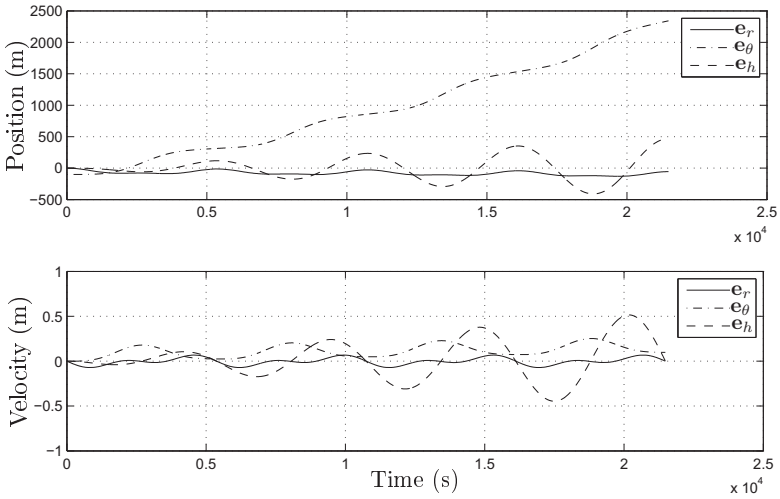

Figure 2.11: Relative position and velocity between leader and follower spacecraft including aerodynamic drag and J_2 perturbation force.

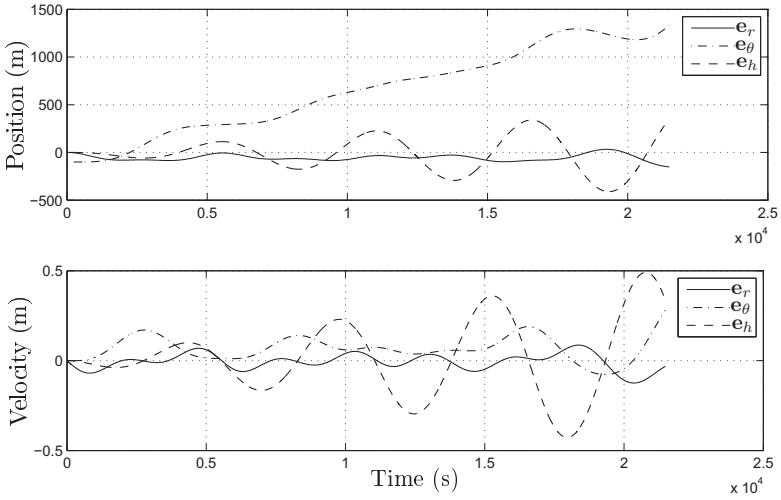

Figure 2.12: Relative position and velocity between leader and follower spacecraft including aerodynamic drag and J_2 perturbation force in an elliptic orbit.

Part II

Control of rigid bodies

Chapter 3

Continuous attitude control of rigid bodies

In this chapter we present different control strategies for continuous attitude control of rigid bodies. The control laws are reminiscent of classic controllers for robot manipulators, adapted to the topology of the quaternion space, in which the model of rigid bodies are expressed. The controllers in question are the passivity-based PD+ controller presented by Paden and Panja (1988) and the wrongly-called "sliding-mode" controller of Slotine and Li (1987), which is *continuous* and may rather be casted in the passivity-based framework (Slotine and Li, 1988), while the *sliding-mode* controller alters the dynamics of a nonlinear system by application of a *discontinuous* control signal (switching function). The rest of this chapter is organized as follows: we start by discussing different solutions from previous work on the tracking problem formulation and give a formal definition in Section 3.1, present exponential stability results and stability almost in the large for state feedback control in Section 3.2. We present a state feedback controller utilizing nonlinear gains in Section 3.3, which is extended to output feedback control in Section 3.4 and wrap up with simulation results and discussion in Section 3.5. The results presented in this chapter are based on (Schlanbusch *et al.*, 2010*b*, 2011*b*,*d*,*c*).

3.1 Tracking problem formulation

The attitude control problem consists of making the actual attitude converge towards a given reference attitude $\mathbf{q}_d$ satisfying the kinematic equation

$$\dot{\mathbf{q}}_d = \mathbf{T}(\mathbf{q}_d)\boldsymbol{\omega}_d. \tag{3.1}$$

We define the quaternion error as $\tilde{\mathbf{q}} := \bar{\mathbf{q}}_d \otimes \mathbf{q}$ where $\tilde{\mathbf{q}} = [\tilde{\eta},\ \tilde{\boldsymbol{\epsilon}}^\top]^\top$ yielding the error kinematics according to (2.82) to be expressed as

$$\dot{\tilde{\mathbf{q}}} = \mathbf{T}(\tilde{\mathbf{q}})\tilde{\boldsymbol{\omega}}, \tag{3.2}$$

where $\mathbf{T}(\tilde{\mathbf{q}})$ is defined as in (2.82) and $\tilde{\boldsymbol{\omega}}(t) := \boldsymbol{\omega}^b_{i,b} - \boldsymbol{\omega}^b_{i,d}(t)$. The tracking control goal is then to steer $\tilde{\boldsymbol{\epsilon}}(t)$ and $\tilde{\boldsymbol{\omega}}(t)$ to zero. Due to the mapping from S^3 to $SO(3)$,

for each point on $SO(3)$ there exists two unit quaternions, and therefore we are not able to achieve global representation using continuous control, and furthermore, since the term global refers to the whole state space $\mathbb{R}^n$ according to Hahn (1967) while S^3 is a covering *manifold* only; see also discussion on globality in Section 1.1.

To overcome this particular difficulty several strategies have been proposed. In (Fjellstad, 1994) an approach was presented for control of unmanned underwater vehicles and properties for a scalar function was presented as

- $H(\cdot) \ : \ [-1,1] \to \mathbb{R}_+$; (non-negative)
- $H(-1) = 0$ and/or $H(1) = 0$;
- $H(\cdot)$ is Lipschitz on $[-1,1]$:

$$|H(\tilde{\eta}_1) - H(\tilde{\eta}_2)| \leq L|\tilde{\eta}_1 - \tilde{\eta}_2|; \text{ (L finite, positive)},$$

and a function was chosen as $H(\tilde{\eta}) = 1 - |\tilde{\eta}|$ yielding a corresponding feedback vector

$$\mathbf{z}(\tilde{\mathbf{q}}) = -\frac{\partial H}{\partial \tilde{\eta}}\tilde{\boldsymbol{\epsilon}} = \text{sgn}(\tilde{\eta})\tilde{\boldsymbol{\epsilon}} \ , \tag{3.3}$$

where the signum function is defined as

$$sgn(x) = \begin{cases} -1, & \text{if } x < 0 \\ 1, & \text{if } x \geq 0 \end{cases} \ . \tag{3.4}$$

Using this feedback results in two asymptotically stable equilibrium points in $\tilde{\mathbf{q}} = [\pm 1, \ \mathbf{0}]^\top$, but the solution is not robust when measurement noise is introduced. Letting $E := \{\mathbf{q} \in S^3 \ : \ \eta = 0\}$, and $\boldsymbol{\nu}(\mathbf{x}) := [0, \mathbf{x}^\top]^\top$, the non-robustness issue was defined by Mayhew *et al.* (2009) as

Theorem 3.1 (Mayhew *et al.* (2009)) *Let $\sigma > 0$. Then, for each $\mathbf{q}(t_0) \in (E + \sigma\mathbb{B}^4) \cap S^3$, there exist a piecewise constant function $\mathbf{e} : [0,\infty) \to \sigma\mathbb{B}^4$ and an absolutely continuous $\mathbf{q} : [0,\infty) \to S^3$ satisfying $\dot{\mathbf{q}}(t) = 1/2\mathbf{q}(t) \otimes \nu(-\mathbf{z}(\mathbf{q}(t) + \mathbf{e}(t)))$ for almost all $t \in [0,\infty)$, and $\mathbf{q}(t) \in (E + \sigma\mathbb{B}^4) \cap S^3$ for all $t \in [0,\infty)$.*

Theorem 3.1 states that for initial values arbitrary close to E, there is a possibility that the solution stays close to E for finite time.

Another approach was presented in (Kristiansen, 2008) for control of a leader-follower spacecraft formation, where the equilibrium point which require the shortest rotation was chosen *a priori*, minimizing the path length. Hence $\tilde{\mathbf{q}}_+ := [1, \ \mathbf{0}^\top]^\top$ was chosen if $\tilde{\eta}(t_0) \geq 0$, and $\tilde{\mathbf{q}}_- := [-1, \ \mathbf{0}^\top]^\top$ was chosen if $\tilde{\eta}(t_0) < 0$. Then for stability purposes, the equilibrium points were shifted to the origin using error functions defined as $\mathbf{e}_{q+} := [1 - \tilde{\eta}, \ \tilde{\boldsymbol{\epsilon}}^\top]^\top$ for the positive equilibrium, while for the negative equilibrium point the error function was chosen as $\mathbf{e}_{q-} := [1 + \tilde{\eta}, \ \tilde{\boldsymbol{\epsilon}}^\top]^\top$, thus $\|\mathbf{e}_{q\pm}\| \in [0,2]$, and the angular velocity error vector was denoted $\mathbf{e}_\omega = \tilde{\boldsymbol{\omega}}$. In accordance with general kinematic relations

$$\dot{\mathbf{e}}_{q\pm} = \mathbf{T}_e(\mathbf{e}_{q\pm})\mathbf{e}_\omega \ , \tag{3.5}$$

where

$$\mathbf{T}_e(\mathbf{e}_{q\pm}) = \frac{1}{2}\begin{bmatrix} \pm\tilde{\boldsymbol{\epsilon}}^\top \\ \tilde{\eta}\mathbf{I} + S(\tilde{\boldsymbol{\epsilon}}) \end{bmatrix}. \tag{3.6}$$

The drawback of this method is that once the appropriate error function is chosen, $\tilde{\eta}$ is not allowed to switch sign as can be formalized as follows.

Assumption 3.1 *We assume that* $\text{sgn}(\tilde{\eta}(t_0)) = \text{sgn}(\tilde{\eta}(t))$ *for all* $t \geq t_0$.

Note that although $\tilde{\mathbf{q}} \in S^3$ this is not true for $\mathbf{e}_q$, thus we define two sets, one for each half of the rotational sphere, as $\mathbf{e}_{q+} \in S^3_{e+} := \{[1-\tilde{\eta},\ \tilde{\boldsymbol{\epsilon}}^\top]^\top : \tilde{\eta} \geq 0, \tilde{\mathbf{q}} \in S^3\}$ and $\mathbf{e}_{q-} \in S^3_{e-} := \{[1+\tilde{\eta},\ \tilde{\boldsymbol{\epsilon}}^\top]^\top : \tilde{\eta} < 0, \tilde{\mathbf{q}} \in S^3\}$ and find that $\mathbf{e}_{q\pm} \in S^3_{e+} \cup S^3_{e-} = S^3_e := \{[1-|\tilde{\eta}|,\ \tilde{\boldsymbol{\epsilon}}^\top]^\top : \tilde{\mathbf{q}} \in S^3\}$. The tracking control problem can then be described as follows.

$$\lim_{t\to\infty} \tilde{\boldsymbol{\epsilon}} \to \tilde{\boldsymbol{\epsilon}}_d(t) \Leftrightarrow \lim_{t\to\infty} \bar{\mathbf{q}}_d(t) \otimes \mathbf{q} \to [\pm 1, \mathbf{0}^\top]^\top \Leftrightarrow \lim_{t\to\infty} \|\mathbf{e}_{q\pm}\| \to 0, \tag{3.7}$$

$$\lim_{t\to\infty} \boldsymbol{\omega} \to \boldsymbol{\omega}_d(t) \Leftrightarrow \lim_{t\to\infty} \|\boldsymbol{\omega} - \boldsymbol{\omega}_d(t)\| = 0 \Leftrightarrow \lim_{t\to\infty} \|\mathbf{e}_\omega\| \to 0. \tag{3.8}$$

For our stability results we also make the following hypothesis'.

Assumption 3.2 *There exists* $\beta_{\boldsymbol{\omega}_d}$, $\beta_{\dot{\boldsymbol{\omega}}_d} > 0$ *such that* $\|\boldsymbol{\omega}_d(t)\| < \beta_{\boldsymbol{\omega}_d}$ *and* $\|\dot{\boldsymbol{\omega}}_d(t)\| < \beta_{\dot{\boldsymbol{\omega}}_d}$ *for all* $t \geq t_0$.

Assumption 3.3 *There exists* $\beta_j, \beta_J > 0$ *such that the inertia matrix* $\mathbf{J}$ *is constant, symmetric and positive definite, and satisfies the inequality*

$$\beta_j \leq \|\mathbf{J}\| \leq \beta_J. \tag{3.9}$$

To complete the proofs presented in this chapter we make use of the following technical lemmas.

Lemma 3.1 *Let* $\mathbf{e}_{q\pm}$ *and* $\mathbf{T}_e(\mathbf{e}_{q\pm})$ *be defined as in* (3.5) *and* (3.6). *Then, the inequality*

$$\mathbf{e}_{q\pm}^\top \mathbf{T}_e \mathbf{T}_e^\top \mathbf{e}_{q\pm} \geq \frac{1}{8}\mathbf{e}_{q\pm}^\top \mathbf{e}_{q\pm} \tag{3.10}$$

holds for $\mathbf{e}_{q+}\ \forall\ 0 \leq \tilde{\eta} \leq 1$ *and* $\mathbf{e}_{q-}\ \forall\ -1 \leq \tilde{\eta} \leq 0$.

Proof: See Appendix B.1.

Thus, Lemma 3.1 hold because of Assumption 3.1. The assumption of sign-definiteness was discussed in (Kristiansen, 2008) though no analytical proof that the assumption holds could be found. Following the lines of Caccavale and Villani (1999) a bound on the initial states could be introduced such as in the extreme case if $\tilde{\eta}(t_0) = 0$ then $\boldsymbol{\omega}(t_0) = \mathbf{0}$ has to be fulfilled, or more generally, let $\mathbf{x} = [\mathbf{e}_q^\top, \mathbf{e}_\omega^\top]^\top$, and $\|\mathbf{x}(t_0)\| \leq \rho\sqrt{c_m/c_M} := \Delta$ where $0 < \rho < 1$ and c_m and c_M are the lower and upper bound, respectively, fulfilling $c_m\|\mathbf{x}\|^2 \leq V(\mathbf{x}) \leq c_M\|\mathbf{x}\|^2$ where $V(\mathbf{x})$ is a Lyapunov function. Then, $\text{sign}(\tilde{\eta}(\text{t})) = \text{sign}(\tilde{\eta}(\text{t}_0))$ for all $t \geq t_0$ for all initial values starting in the domain

$$\mathbf{x}(t_0) \in \bar{\mathcal{B}}_\Delta := \left\{ \mathbf{x} \in S^3_e \times \mathbb{R}^3 : \|\mathbf{x}\| \leq \rho\sqrt{\frac{c_m}{c_M}} \right\}, \tag{3.11}$$

and a similar line of arguments can be used for $\tilde{\eta}(t_0) < 0$.

Based on the findings of Kristiansen (2008) we pose the following lemma.

Lemma 3.2 *The derivative of* $\dot{\mathbf{T}}_e(q\pm)$ *satisfies*

$$\dot{\mathbf{T}}_e(\mathbf{e}_{q\pm})\mathbf{e}_{q\pm} = \mathbf{G}_{\pm}\mathbf{e}_{\omega}, \tag{3.12}$$

where

$$\mathbf{G}_{\pm} = \frac{1}{4}\{\pm[\tilde{\eta}\mathbf{I} + \mathbf{S}(\tilde{\boldsymbol{\epsilon}})] - \mathbf{I}\}. \tag{3.13}$$

Proof: See Appendix B.2.

3.2 State feedback control

In this section we present continuous state feedback control of rigid bodies based on the previously mentioned PD+ and sliding surface controllers.

3.2.1 Passivity-based PD+ control

Theorem 3.2 *Let Assumptions 3.1, 3.2 and 3.3 hold. Then, the dual equilibria* $(\mathbf{e}_{q\pm}, \mathbf{e}_{\omega}) = (\mathbf{0}, \mathbf{0})$ *of system* (2.82) *and* (2.83)*, in closed loop with the controller*

$$\boldsymbol{\tau}_a = \mathbf{J}\dot{\boldsymbol{\omega}}_d - \mathbf{S}(\mathbf{J}\boldsymbol{\omega})\boldsymbol{\omega}_d - k_q\mathbf{T}_e^{\top}\mathbf{e}_q - k_{\omega}\mathbf{e}_{\omega} - \boldsymbol{\tau}_d, \tag{3.14}$$

where $k_q > 0$ *and* $k_{\omega} > 0$*, are uniformly asymptotically stable in the large with set of initial conditions* $\Gamma = S_e^3 \times \mathbb{R}^3$.

Proof: See Appendix B.3.

Remark 3.1 *In words, Theorem 3.2 establishes that the desired attitude* $\mathbf{q}_d$ *may be reached from any initial posture and any initial velocity. However, it must be clear from the previous proof that it is wrong to conclude global asymptotic stability since besides the fact that the system possesses two equilibria, the trajectories are supposed to remain in a manifold where* $\tilde{\eta}$ *(which is part of the state) does not change sign; –see Definition A.3.*

Furthermore, by invoking (Panteley *et al.*, 2001, Lemma 3) the result of Theorem 3.2 can be shown to hold exponentially.

Theorem 3.3 *Let Assumptions 3.1, 3.2 and 3.3 hold. Then, the dual equilibria* $(\mathbf{e}_{q\pm}, \mathbf{e}_{\omega}) = (\mathbf{0}, \mathbf{0})$ *of system* (2.82) *and* (2.83)*, in closed loop with the controller* (3.14) *are uniformly exponentially stable in the large with set of initial conditions* $\Gamma = S_e^3 \times \mathbb{R}^3$.

Proof: See Appendix B.4.

Remark 3.2 *Note that Remark 3.1 also holds for Theorem 3.3.*

In Theorem 3.2 uniform asymptotic stability clearly follows under the assumption that $\boldsymbol{\tau}_d$ is known and accounted for in the control law. This assumption can be relaxed by replacing it with the following assumption.

Assumption 3.4 *Assume there exists $\beta_d > 0$ such that $\|\boldsymbol{\tau}_d(t)\| \leq \beta_d$ for all $t \geq t_0$.*

We then obtain the following result.

Corollary 3.1 *Let Assumptions 3.1–3.4 hold. Then, the dual equilibria $(\mathbf{e}_{q\pm}, \mathbf{e}_\omega) = (\mathbf{0}, \mathbf{0})$ of system (2.82) and (2.83), in closed loop with the controller*

$$\boldsymbol{\tau}_a = \mathbf{J}\dot{\boldsymbol{\omega}}_d - \mathbf{S}(\mathbf{J}\boldsymbol{\omega})\boldsymbol{\omega}_d - k_q \mathbf{T}_e^\top \mathbf{e}_q - k_\omega \mathbf{e}_\omega, \tag{3.15}$$

where $k_q > 0$ and $k_\omega > 0$, are uniformly practically asymptotically stable in the large with set of initial conditions $\Gamma = S_e^3 \times \mathbb{R}^3$.

The proof is omitted, but follows along the same lines as the proof of Theorem 3.9; see Appendix A.2.2 for definition and sufficient conditions for practical stability.

Remark 3.3 *Note that Remark 3.1 also holds for Corollary 3.1.*

3.2.2 Sliding surface control

Theorem 3.4 *Let Assumptions 3.1, 3.2 and 3.3 hold. Then, the dual equilibria $(\mathbf{e}_{q\pm}, \mathbf{s}) = (\mathbf{0}, \mathbf{0})$ of system (2.82) and (2.83), in closed loop with the controller*

$$\begin{aligned}
\boldsymbol{\tau}_a &= \mathbf{J}\dot{\boldsymbol{\omega}}_r - \mathbf{S}\left(\mathbf{J}\boldsymbol{\omega}\right)\boldsymbol{\omega}_r - k_q \mathbf{T}_e^\top \mathbf{e}_q - k_\omega \mathbf{s} - \boldsymbol{\tau}_d && \text{(3.16a)}\\
\boldsymbol{\omega}_r &= \boldsymbol{\omega}_d - \gamma \mathbf{T}_e^\top \mathbf{e}_q && \text{(3.16b)}\\
\dot{\boldsymbol{\omega}}_r &= \dot{\boldsymbol{\omega}}_d \mp \frac{\gamma}{4}[\tilde{\eta}\mathbf{I} + \mathbf{S}(\tilde{\boldsymbol{\epsilon}})] && \text{(3.16c)}\\
\mathbf{s} &= \boldsymbol{\omega} - \boldsymbol{\omega}_r = \mathbf{e}_\omega + \gamma \mathbf{T}_e^\top \mathbf{e}_q, && \text{(3.16d)}
\end{aligned}$$

where $k_q > 0$, $k_\omega > 0$ and $\gamma > 0$, are uniformly exponentially stable in the large with set of initial conditions $\Gamma = S_e^3 \times \mathbb{R}^3$.

Proof: See Appendix B.5.

Remark 3.4 *Note that Remark 3.1 also holds for Theorem 3.4.*

The reference vector $\boldsymbol{\omega}_r$ represents a notational manipulation that allows translation of energy-related properties expressed in terms of the actual velocity vector $\boldsymbol{\omega}$ into trajectory control properties expressed in terms of the virtual velocity error vector $\mathbf{s}$. This is performed by shifting the desired velocities $\boldsymbol{\omega}_d$ according to the attitude error $\tilde{\mathbf{q}}$ $(\mathbf{e}_q)$, *–cf.* (Slotine and Li, 1987; Berghuis and Nijmeijer, 1993).

By relaxing the assumption of known disturbances with Assumption 3.4 we have the following.

Theorem 3.5 *Let Assumptions 3.1, 3.2 and 3.3 hold. Then, the dual equilibria $(\mathbf{e}_{q\pm}, \mathbf{s}) = (\mathbf{0}, \mathbf{0})$ of system (2.82) and (2.83), in closed loop with the controller*

$$\boldsymbol{\tau}_a = \mathbf{J}\dot{\boldsymbol{\omega}}_r - \mathbf{S}\left(\mathbf{J}\boldsymbol{\omega}\right)\boldsymbol{\omega}_r - k_q \mathbf{T}_e^\top \mathbf{e}_q - k_\omega \mathbf{s}, \tag{3.17}$$

(3.16b) *and* (3.16d) *where $k_q > 0$, $k_\omega > 0$ and $\gamma > 0$, are uniformly practically exponentially stable in the large with set of initial conditions $\Gamma = S_e^3 \times \mathbb{R}^3$.*

Proof: See Appendix B.6.

Remark 3.5 *Note that Remark 3.1 also holds for Theorem 3.5.*

3.2.3 Sliding surface - almost in the large

In this section we relax the assumption that the sign of $\tilde{\eta}(t)$ is constant for all t and consider that the state space of the closed-loop system is $S_e^3 \times \mathbb{R}^3$. In this space, the closed-loop system possesses two equilibria: the positive equilibrium $(\mathbf{e}_{q+}, \mathbf{e}_\omega) = (\mathbf{0}, \mathbf{0})$ and the negative equilibrium $(\mathbf{e}_{q-}, \mathbf{e}_\omega) = (\mathbf{0}, \mathbf{0})$.

As in (Rantzer, 2001; Angeli, 2004, 2001), we use a notion of stability for all initial states except for a zero-measure set. For systems with state space $\mathbb{R}^n$, we speak of *almost* global asymptotic stability –see (Rantzer, 2001) if the origin is asymptotically stable for all *all* initial states in $\mathbb{R}^n$ except for a set of measure zero. If not because the system's state space is a subset of $\mathbb{R}^6$ (hence, we cannot use the qualifier 'global') this is the property that we establish in Theorem A.6, relying on a refinement of the main theorem in (Rantzer, 2001) for non-autonomous systems and restated from[1] (Monzón, 2006).

Theorem 3.6 *Let Assumptions 3.2 and 3.3 hold. Then, the equilibrium point* $(\mathbf{e}_{q+}, \mathbf{e}_\omega) = (\mathbf{0}, \mathbf{0})$ [respectively, the equilibrium $(\mathbf{e}_{q-}, \mathbf{e}_\omega) = (\mathbf{0}, \mathbf{0})$] *of system* (2.82) *and* (2.83)*, in closed loop with the controller* (3.16) *is asymptotically stable in the large with respect to* $S_e^3 \times \mathbb{R}^3$*, taken away a set of measure zero which includes the dual equilibrium* $\{(\mathbf{e}_{q-}, \mathbf{e}_\omega) = (\mathbf{0}, \mathbf{0})\}$ [respectively, with respect to $S_e^3 \times \mathbb{R}^3$, taken away a set of measure zero including the dual equilibrium $\{(\mathbf{e}_{q+}, \mathbf{e}_\omega) = (\mathbf{0}, \mathbf{0})\}$].

Proof: See Appendix B.7.

Remark 3.6 *In other words, the equilibrium point* $(\mathbf{e}_{q+}, \mathbf{e}_\omega) = (\mathbf{0}, \mathbf{0})$ [respectively, the equilibrium $(\mathbf{e}_{q-}, \mathbf{e}_\omega) = (\mathbf{0}, \mathbf{0})$] *is stable and attracts almost all trajectories in* $S_e^3 \times \mathbb{R}^3$.

3.3 State feedback control with nonlinear gains

In this section we present similar control laws as in Section 3.2.1 but with added nonlinearities in the controller gains for improved performance in the sense of reduced sensibility to sensor noise. The control law ensures faster convergence to the desired operating point during attitude maneuver, while keeping the gains small for station keeping. A direct consequence is a drop in energy consumption when affected by sensor noise.

Assume, for the time-being that the disturbances $\boldsymbol{\tau}_d$ are known. The following theorem establishes uniform asymptotic stability of the closed-loop system under a modified version of the PD+ controller presented in Section 3.2.1.

Theorem 3.7 *Let Assumptions 3.1, 3.2 and 3.3 hold. Then, the dual equilibrium points* $(\mathbf{e}_{q\pm}, \mathbf{e}_\omega) = (\mathbf{0}, \mathbf{0})$ *of the system* (2.82) *and* (2.83)*, in closed-loop with the control law*

$$\boldsymbol{\tau}_a = \mathbf{J}\dot{\boldsymbol{\omega}}_d - \mathbf{S}(\mathbf{J}\boldsymbol{\omega})\boldsymbol{\omega}_d - \boldsymbol{\tau}_d - k_p e^{k_1 \mathbf{e}_q^\top \mathbf{e}_q} \mathbf{T}_e^\top \mathbf{e}_q - k_d e^{k_2 \mathbf{e}_\omega^\top \mathbf{e}_\omega} \mathbf{e}_\omega, \tag{3.18}$$

where $k_p > 0$*,* $k_d > 0$*,* $k_1 > 0$ *and* $k_2 > 0$ *are feedback gains, are uniformly asymptotically stable in the large with set of initial conditions* $\Gamma = S_e^3 \times \mathbb{R}^3$.

[1] In Theorem A.6 we enforce the integrability assumption on ρ to be uniform in t.

Proof: see Appendix B.8

Remark 3.7 *Note that Remark 3.1 also holds for Theorem 3.7.*

To obtain increasing gains when the error is increasing we need to choose $k_1 > 0$ and $k_2 > 0$. By choosing $k_1 = k_2 = 0$ we see that (3.18) is reduced to (3.14).

Now we want to generalize the previous results. First, we want to design a control law with a special set of properties considering the proportional and derivative gains; we want the proportional gain to be large and derivative gain to be small when the attitude error is large independent of the angular velocity; we want the proportional gain to be small and the derivative gain large when the attitude error is small and angular velocity error is large; and we want both gains to be small when the attitude and angular velocity errors are small. These properties are chosen such that the system will have fast response, little overshoot and low gains when the error is small to reduce the effect of measurement noise on the system. Secondly, we introduce a number of scalar gain dependent nonlinear feedback functions such that the behavior of the system can be altered based on the choice of functions.

Theorem 3.8 *Let Assumptions 3.1, 3.2 and 3.3 hold. Let $\alpha, \beta : [0, a) \to [1, \infty)$ be strictly increasing continuous functions where $\alpha(0) = \beta(0) = 1$ and $\alpha(r), \beta(r) \to \infty$ as $r \to \infty$, and let $\upsilon : [0, a) \to (0, 1]$ be a strictly decreasing continuous function where $\upsilon(0) = 1$ and $\upsilon(s) \to 0$ as $s \to \infty$. Then, the dual equilibrium points $(\mathbf{e}_{q\pm}, \mathbf{e}_\omega) = (\mathbf{0}, \mathbf{0})$ of the system (2.82) and (2.83), in closed-loop with the control law*

$$\begin{aligned}\boldsymbol{\tau}_a =& \mathbf{J}\dot{\boldsymbol{\omega}}_d - \mathbf{S}(\mathbf{J}\boldsymbol{\omega})\boldsymbol{\omega}_d - \boldsymbol{\tau}_d - k_p\alpha(\|\mathbf{e}_q\|^2)\mathbf{T}_e^\top\mathbf{e}_q \\ & - k_d\beta(\|\mathbf{e}_\omega\|^2)\upsilon(\|\mathbf{e}_q\|^2)\mathbf{e}_\omega,\end{aligned} \tag{3.19}$$

where $k_p > 0$ and $k_d > 0$ are feedback gains, are uniformly asymptotically stable in the large with set of initial conditions $\Gamma = S_e^3 \times \mathbb{R}^3$.

Proof: see Appendix B.9.

Remark 3.8 *Note that Remark 3.1 also holds for Theorem 3.8.*

Some example functions for α, β, υ and related ξ are given in Table 3.1 which can be chosen arbitrarily for the controller.

In the next two theorems we extend the results presented in Theorem 3.7 and 3.8 by relaxing the assumption of known disturbances.

Theorem 3.9 *Let Assumptions 3.1–3.4 hold. Then, the dual equilibrium points $(\mathbf{e}_{q\pm}, \mathbf{e}_\omega) = (\mathbf{0}, \mathbf{0})$ of the system (2.82) and (2.83), in closed loop with the control law*

$$\boldsymbol{\tau}_a = \mathbf{J}\dot{\boldsymbol{\omega}}_d - \mathbf{S}(\mathbf{J}\boldsymbol{\omega})\boldsymbol{\omega}_d - k_p e^{k_1\mathbf{e}_q^\top\mathbf{e}_q}\mathbf{T}_e^\top\mathbf{e}_q - k_d e^{k_2\mathbf{e}_\omega^\top\mathbf{e}_\omega}\mathbf{e}_\omega, \tag{3.20}$$

where $k_p > 0$, $k_d > 0$, $k_1 > 0$ and $k_2 > 0$ are feedback gains, are uniformly practically asymptotically stable in the large with set of initial conditions $\Gamma = S_e^3 \times \mathbb{R}^3$.

Table 3.1: Sample functions for convergence and divergence of gains and related Lyapunov function terms.

$\alpha\left(\|\mathbf{x}\|^2\right), \beta\left(\|\mathbf{x}\|^2\right)$	$\xi\left(\|\mathbf{x}\|^2\right)$	$\upsilon\left(\|\mathbf{x}\|^2\right)$
$e^{k_1\mathbf{x}^\top\mathbf{x}}$	$(1/k_1)\left(e^{k_1\mathbf{x}^\top\mathbf{x}}-1\right)$	$e^{-k_2\mathbf{x}^\top\mathbf{x}}$
$a^{k_1\mathbf{x}^\top\mathbf{x}},\ a>0$	$1/(k_1\ln(a))\left(a^{k_1\mathbf{x}^\top\mathbf{x}}-1\right)$	$a^{-k_2\mathbf{x}^\top\mathbf{x}},\ a>0$
$\cosh\left(k_1\mathbf{x}^\top\mathbf{x}\right)$	$(1/k_1)\sinh\left(k_1\mathbf{x}^\top\mathbf{x}\right)$	$\cos\left(\frac{\pi}{2}\tanh(k_2\mathbf{x}^\top\mathbf{x})\right)$
$1+\sinh\left(k_1\mathbf{x}^\top\mathbf{x}\right)$	$(1/k_1)\cosh\left(k_1\mathbf{x}^\top\mathbf{x}\right)+\|\mathbf{x}\|-1$	$1-\tanh\left(k_2\mathbf{x}^\top\mathbf{x}\right)$
$\ln\left(e+k_1\mathbf{x}^\top\mathbf{x}\right)$	$(1/k_1)\big[\left(e+k_1\mathbf{x}^\top\mathbf{x}\right)\ln\left(e+k_1\mathbf{x}^\top\mathbf{x}\right)-\left(e+k_1\mathbf{x}^\top\mathbf{x}\right)\big]$	$1-\frac{2}{\pi}\text{atan}\left(k_2\mathbf{x}^\top\mathbf{x}\right)$

Proof: see Appendix B.10.

Remark 3.9 *Note that Remark 3.1 also holds for Theorem 3.9.*

Theorem 3.10 *Let Assumptions 3.1–3.4 hold. Let $\alpha,\beta:[1,a)\to[1,\infty)$ be strictly increasing continuous functions where $\alpha(0)=\beta(0)=1$ and $\alpha(r),\beta(r)\to\infty$ as $r\to\infty$, and let $\upsilon:[0,a)\to(0,1]$ be a strictly decreasing continuous function where $\upsilon(0)=1$ and $\upsilon(s)\to 0$ as $s\to\infty$. Then, the dual equilibrium points $(\mathbf{e}_{q\pm},\mathbf{e}_\omega)=(\mathbf{0},\mathbf{0})$ of the system (2.82) and (2.83), in closed-loop with the control law*

$$\begin{aligned}\boldsymbol{\tau}_a =&\mathbf{J}\dot{\boldsymbol{\omega}}_d-\mathbf{S}(\mathbf{J}\boldsymbol{\omega})\boldsymbol{\omega}_d-k_p\alpha(\|\mathbf{e}_q\|^2)\mathbf{T}_e^\top\mathbf{e}_q\\&-k_d\beta(\|\mathbf{e}_\omega\|^2)\upsilon(\|\mathbf{e}_q\|^2)\mathbf{e}_\omega,\end{aligned}\tag{3.21}$$

where $k_p>0$ and $k_d>0$ are feedback gains, are uniformly practically asymptotically stable in the large with set of initial conditions $\Gamma=S_e^3\times\mathbb{R}^3$.

Proof: see Appendix B.11.

Remark 3.10 *Note that Remark 3.1 also holds for Theorem 3.10.*

3.4 Output feedback control

As mentioned in the introduction, we want to stress that by using the expression *output feedback* we strictly speak of *without measurement of the angular velocity*, thus we start by defining the estimation error $\mathbf{e}_{e\omega}:=\boldsymbol{\omega}_{i,b}^b-\boldsymbol{\omega}_{i,e}^b$, where super-/subscript e denotes the estimated frame, together with an attitude estimation error defined as $\mathbf{q}_{e,b:}=[\eta_{e,b},\ \boldsymbol{\epsilon}_{e,b}^\top]^\top=\bar{\mathbf{q}}_{i,e}\otimes\mathbf{q}_{i,b}$.

The desired angular velocity of a rigid body is usually given with reference to the inertial frame as $\boldsymbol{\omega}_{i,d}^i$. By rotating to the body frame we obtain

$$\boldsymbol{\omega}_{i,d}^b=\mathbf{R}_i^b\boldsymbol{\omega}_{i,d}^i\tag{3.22}$$

hence,

$$\dot{\boldsymbol{\omega}}^b_{i,d} = \dot{\mathbf{R}}^b_i \boldsymbol{\omega}^i_{i,d} + \mathbf{R}^b_i \dot{\boldsymbol{\omega}}^i_{i,d} \tag{3.23}$$

$$= -\mathbf{S}(\boldsymbol{\omega}^b_{i,b})\boldsymbol{\omega}^b_{i,d} + \mathbf{R}^b_i \dot{\boldsymbol{\omega}}^i_{i,d}. \tag{3.24}$$

We see that to evaluate the derivative of the reference $\dot{\boldsymbol{\omega}}^b_{i,d}$ we need to know the actual angular velocity of the rigid body $\boldsymbol{\omega}^b_{i,b}$. For control purposes we use the modified acceleration vector where $\boldsymbol{\omega}^b_{i,b}$ is substituted with $\boldsymbol{\omega}^b_{i,d}$, obtaining (Caccavale and Villani, 1999)

$$\mathbf{a}_d = -\mathbf{S}(\boldsymbol{\omega}^b_{i,d})\boldsymbol{\omega}^b_{i,d} + \mathbf{R}^b_i \dot{\boldsymbol{\omega}}^i_{i,d} \tag{3.25}$$

$$= \mathbf{R}^b_i \dot{\boldsymbol{\omega}}^i_{i,d}. \tag{3.26}$$

We also make use of the following assumption.

Assumption 3.5 *We assume that there exists a constant δ_η such that $\eta_{e,b}(t) \geq \delta_\eta > 0 \; \forall \; t \geq t_0 \geq 0$.*

Assumption 3.5 is similar to Assumption 3.1 for $\tilde{\eta}$ and its necessity will become evident during the proof of the following theorem. Since this state is measured we can choose $\mathbf{q}_{e,b}(t_0) = [1, \mathbf{0}]^\top$, and thus define the error vector as $\mathbf{e}_{eq} := [1 - \eta_{e,b}, \; \boldsymbol{\epsilon}^\top_{e,b}]^\top$ with $\mathbf{T}_{eq}$ accordingly. The state only evolves on the positive half of the rotational sphere thus, $\mathbf{e}_{eq} \in S^3_{eq} := \{[1 - \eta_{e,b}, \; \boldsymbol{\epsilon}^\top_{e,b}]^\top : \eta_{e,b} \geq \delta_\eta, \mathbf{q}_{e,b} \in S^3\}$.

Theorem 3.11 *Let Assumptions 3.1–3.5 hold. Then, the dual equilibria $(\mathbf{e}_{q\pm}, \mathbf{e}_\omega, \mathbf{e}_{eq}, \mathbf{e}_{e\omega}) = (\mathbf{0}, \mathbf{0}, \mathbf{0}, \mathbf{0})$ of the system (2.82) and (2.83), in closed-loop with the control law*

$$\boldsymbol{\tau}_a = \mathbf{J}\mathbf{a}_d - \mathbf{S}(\mathbf{J}\boldsymbol{\omega}^b_{i,e})\boldsymbol{\omega}^b_{i,d} - k_p e^{k_1 \mathbf{e}_q^\top \mathbf{e}_q} \mathbf{T}_e^\top \mathbf{e}_q - k_d e^{-k_2 \mathbf{e}_q^\top \mathbf{e}_q} \boldsymbol{\omega}^b_{d,e}, \tag{3.27}$$

with $k_p, k_d, k_1, k_2 > 0$ as constant gains, and the observer

$$\dot{\mathbf{z}} = \mathbf{a}_d + \mathbf{J}^{-1}\left[l_p e^{k_3 \mathbf{e}_{eq}^\top \mathbf{e}_{eq}} \mathbf{T}_{eq}^\top \mathbf{e}_{eq} - k_p e^{k_1 \mathbf{e}_q^\top \mathbf{e}_q} \mathbf{T}_e^\top \mathbf{e}_q\right], \tag{3.28}$$

$$\boldsymbol{\omega}^b_{i,e} = \mathbf{z} + 2\mathbf{J}^{-1} l_d \mathbf{T}_{eq}^\top \mathbf{e}_{eq}, \tag{3.29}$$

with $l_p, l_d, k_3 > 0$ considered as constant gains, are uniformly practically asymptotically stable.

Proof: see Appendix B.12.

Remark 3.11 *Remark 3.1 does not hold for Theorem 3.11 because of Assumption 3.5 where $\eta_{e,b}$ is not allowed to go to zero.*

Remark 3.12 *In (3.18) a PD+ based state feedback control law was presented using exponential gains with the derivative term as $-k_d e^{k_2 \mathbf{e}_\omega^\top \mathbf{e}_\omega} \mathbf{e}_\omega$. One difference is that in (3.27) the damping has a relatively small effect on the system while the solutions are located 'far' away from the equilibrium point, and increases when the attitude error is going towards zero. This helps in reducing trajectories overshoot.*

Remark 3.13 *Note that instead of using $\boldsymbol{\omega}^b_{i,d}$ in the modified acceleration vector* (3.25)*, the estimated angular velocity $\boldsymbol{\omega}^b_{i,e}$ might be utilized. This will lead to added restrictions for the l_d gain, but might result in better performance when the estimation error has converged.*

Assumptions 3.1 and 3.5 might look restrictive, but in fact they are not; they are only an *ad hoc* hypothesis that is made for the purpose of the analysis, and can be removed at the price of restricting the domain of attraction as we do next.

Theorem 3.12 *Let Assumptions 3.2, 3.3 and 3.4 hold and let $\mathbf{e}_q$ be defined either by $\mathbf{e}_q = \mathbf{e}_{q+}$ or $\mathbf{e}_q = \mathbf{e}_{q-}$. Then, the closed-loop system is uniformly practically asymptotically stable on $\mathbb{R}^7_{>0}$. That is, for any positive numbers δ, a, b, any $\delta_\eta \in (0,1)$ and any subset Γ of $\mathcal{R} = \{\mathbf{x} \in S^3_e \times \mathbb{R}^3 \times S^3_{eq} \times \mathbb{R}^3 : |\tilde{\eta}| > 0,\ \|\mathbf{e}_\omega\| \in [0,a), \eta_{e,b} \geq \delta_\eta > 0,\ \|\mathbf{e}_{e\omega}\| \in [0,b)\}$ there exist control gains in $\mathbb{R}^7_{>0}$ such that the set $\mathcal{B}_\delta = \{\mathbf{x} \in \mathcal{R} : \|\mathbf{x}\| < \delta\}$ is uniformly stable for all initial conditions in Γ. Furthermore, all trajectories originating in Γ converge to $\mathcal{B}_\delta$ asymptotically and uniformly in the initial conditions.*

Proof: see Appendix B.13.

Remark 3.14 *Remark 3.1 does not hold for Theorem 3.12 because $\tilde{\eta}$ and $\eta_{e,b}$ are not allowed to be zero.*

For purpose of comparison we pose the following controller-observer structure without variable gains.

Corollary 3.2 *Assume that all assumptions made in Theorem 3.11 hold. Then, the set of equilibrium points $(\mathbf{e}_{q\pm}, \mathbf{e}_\omega, \mathbf{e}_{eq\pm}, \mathbf{e}_{e\omega}) = (\mathbf{0},\mathbf{0},\mathbf{0},\mathbf{0})$ of the system* (2.82) *and* (2.83)*, in closed-loop with the control law*

$$\boldsymbol{\tau}_a = \mathbf{J}\mathbf{a}_d - \mathbf{S}(\mathbf{J}\boldsymbol{\omega}^b_{i,e})\boldsymbol{\omega}^b_{i,d} - k_q \mathbf{T}_e^\top \mathbf{e}_q - k_\omega \boldsymbol{\omega}^b_{d,e}, \tag{3.30}$$

with $k_q, k_\omega > 0$ considered as constant gains, and the observer

$$\dot{\mathbf{z}} = \mathbf{a}_d + \mathbf{J}^{-1}\left[l_q \mathbf{T}^\top_{eq}\mathbf{e}_{eq} - k_q \mathbf{T}_e^\top \mathbf{e}_q\right], \tag{3.31}$$

$$\boldsymbol{\omega}^b_{i,e} = \mathbf{z} + 2\mathbf{J}^{-1} l_\omega \mathbf{T}^\top_{eq}\mathbf{e}_{eq}, \tag{3.32}$$

with $l_q, l_\omega > 0$ considered as constant gains, are uniformly practically asymptotically stable.

The proof is omitted, but follows along the same lines as the proof of Theorem 3.11.

3.5 Simulation results

In this section we present simulation results based on the control laws presented in this chapter. Our main focus is to compare performance of the control laws using linear gains (static) with nonlinear gains (exponential/variable). We utilize simulation data as presented in Section 2.8.1 if otherwise is not stated.

Table 3.2: Values of performance functionals for attitude maneuver.

	J_p	J_q	J_ω
Static PD+	2.409	4.202	0.767
Exponential PD+	2.719	4.015	0.765

Table 3.3: Values of performance functionals for attitude maneuver over one orbital period (5896 s).

	J_p	J_q	J_ω
Static PD+	6.476	4.489	0.850
Exponential PD+	3.961	4.171	0.797

Table 3.4: Average value of performance functionals for rigid-body over $10,000$ simulations.

	J_p	J_q	J_ω
Static PD+	2.140	2.060	0.947
Exponential PD+	4.174	1.382	0.916

3.5.1 State feedback PD+ versus PD+ with exponential gains

For our simulations we have chosen the initial conditions as $\mathbf{q}(t_0) = [-0.3772,\ -0.4329,\ 0.6645,\ 0.4783]^\top$, $\boldsymbol{\omega}(t_0) = [0.1,\ -0.3,\ 0.2]^\top$, $t_0 = 0$ s and $t_f = 30$ s. The control laws were tuned to achieve similar performance for sake of comparison thus using parameters $k_q = k_\omega = 2$ for (3.15), and $k_p = 1$, $k_d = 1.6$ and $k_1 = k_2 = 1$ for (3.20).

The simulation results are summarized in Table 3.2 and depicted in Figures 3.1 and 3.2. The performance functionals show that both controllers have similar performance though the static controller has slightly higher attitude and angular velocity error while the power consumption is slightly lower, while the maximum control torque is similar.

The simulation results for one orbital period (5896 s) is presented in Table 3.3 and as can be seen the performance functionals are less affected for the controller (3.20) compared to the controller (3.15). This is because as $\mathbf{e}_q \approx \mathbf{0}$ and $\mathbf{e}_\omega \approx \mathbf{0}$, the controller gains for (3.20) are $k_p e^{k_1 \mathbf{e}_q^\top \mathbf{e}_q} \approx k_p$ and $k_d e^{k_2 \mathbf{e}_\omega^\top \mathbf{e}_\omega} \approx k_d$ and since the gains k_p and k_d are smaller for (3.20) compared to k_q and k_ω for (3.15) for a similar maneuver, the sensitivity to measurement noise is reduced as can be seen from the performance functionals.

In table 3.4 we present simulation results from a wide number of simulations for a general rigid-body without disturbances and noise with controller gains $k_q = k_p = 2$, $k_\omega = k_d = 1$ for (3.14) and (3.18), and using random initial values for the quaternion vector, while the initial angular velocity was found randomly with standard deviation in equal steps from 0.01 to 0.5 rad/s during $10,000$ consecutive runs. This is done to show that the exponential gains makes the trajectories converge faster than constant gains, at the price of increased power consumption, without increasing the sensitivity to measurement noise.

Table 3.5: Values of performance functionals for attitude maneuver.

	J_p	J_q	J_ω
Static PD+	0.839	4.147	0.468
Variable PD+	0.833	4.151	0.822

Table 3.6: Values of performance functionals for attitude maneuver over one orbital period (5896 s).

	J_p	J_q	J_ω
Static PD+	1.005	4.149	0.469
Variable PD+	0.850	4.152	0.822

Table 3.7: Average value of performance functionals for rigid-body over $10,000$ simulations.

	J_p	J_q	J_ω
Static PD+	3.6435	1.6795	1.1596
Variable PD+	4.2109	1.3939	1.0880

3.5.2 State feedback PD+ versus PD+ with nonlinear gains

For our simulations we have chosen the same initial conditions as in Section 3.5.1 with $t_0 = 0$ s, $t_f = 50$ s. The control laws were tuned to achieve similar performance for sake of comparison thus using parameters $k_q = 1.8$ and $k_\omega = 3$ for (3.15), and $\alpha(\|\mathbf{x}\|^2) = \beta(\|\mathbf{x}\|^2) = \cosh(k_1\|\mathbf{x}\|^2)$, $\upsilon(\|\mathbf{x}\|^2) = 1 - \tanh(k_2\|\mathbf{x}\|^2)$ with $k_p = 0.7$, $k_d = 2.3$ and $k_1 = k_2 = 1$ for (3.21).

The simulation results are summarized in Table 3.5 and depicted in Figures 3.3 and 3.4. The performance functionals show that both controllers have similar performance except that the angular velocity error for the static gain controller are lower, while Figure 3.4 shows that a higher absolute torque is needed.

The simulation results for one orbital period (5896 s) is presented in Table 3.6 and as can be seen the performance functionals are much less affected for (3.21) compared to (3.15) as expected based on the results presented in Section 3.5.1 where similar reasoning is used. The noise have thus less effect on both the energy consumption, and the attitude and angular velocity error as depicted in Figure 3.5.

In Table 3.7 we present simulation results from a wide number of simulations for a general rigid-body without disturbances and noise with variable functions as $\alpha(\|\mathbf{e}_q\|^2) = \log(e + \mathbf{e}_q^\top \mathbf{e}_q)$, $\beta(\|\mathbf{e}_\omega\|^2) = e^{\mathbf{e}_\omega^\top \mathbf{e}_\omega}$ and $\upsilon(\|\mathbf{e}_q\|^2) = \cos((\pi/2)\tanh(\mathbf{e}_q^\top \mathbf{e}_q))$ with controller gains $k_q = k_p = 3$, $k_\omega = k_d = 1$ for both (3.15) and (3.19), and using random initial values for the quaternion vector, while the initial angular velocity was found randomly with standard deviation in equal steps from 0.01 to 0.5 rad/s during $10,000$ consecutive runs. Notice the difference in the performance functionals in Table 3.5/3.6 compared to Table 3.7, which is a result obtained by choosing different α, β and υ leading to different behaviors for the solution trajectories.

Table 3.8: Values of performance functionals for attitude maneuver.

	J_p	J_q	J_{eq}
Static gains	96.3	0.778	0.013
Variable gains	96.1	0.800	0.013

Table 3.9: Values of performance functionals for attitude maneuver over one orbital period (5896 s).

	J_p	J_q	J_{eq}
Static gains	236.9	0.785	0.014
Variable gains	156.7	0.803	0.013

3.5.3 Output feedback PD+ versus PD+ with exponential gains

We introduce the performance functional

$$J_{eq} = \int_{t_0}^{t_f} \tilde{\boldsymbol{\epsilon}}_{e,b}^{\top} \tilde{\boldsymbol{\epsilon}}_{e,b} dt \tag{3.33}$$

which is an expression of the integral attitude estimation error similar to J_q, and we apply measurement noise $\sigma_q = \sigma_\omega = 0.01$. For our simulations we have chosen the initial conditions as $\mathbf{q}_{i,b}(t_0) = \mathbf{q}_{i,e}(t_0) = [0.3772,\ -0.4329,\ 0.6645,\ 0.4783]^\top$, $\boldsymbol{\omega}_{i,b}^b(t_0) = [0.1,\ 0.2,\ -0.3]^\top$ rad/s, $\mathbf{z}(t_0) = [0\ 0\ 0]^\top$, $t_0 = 0$ s and $t_f = 15$ s. The control laws are tuned to achieve similar performance for sake of comparison thus using parameters $k_p = 10$, $k_d = 7$, $l_p = 100$, $l_d = 75$, and $k_1 = k_2 = k_3 = 1$ for (3.27)–(3.29), and $k_q = 49$, $k_\omega = 11$, $l_q = 240$ and $l_\omega = 150$ for (3.30)–(3.32). The spacecraft is commanded to follow smooth sinusoidal trajectories around the origin with velocity profile

$$\begin{aligned} \boldsymbol{\omega}_{i,d}^i(t) = [&3.2\cos(2\times 10^{-3}t),\ 0.12\sin(1\times 10^{-3}t), \\ &-3.2\sin(4\times 10^{-3}t)]^\top \times 10^{-6}\ \text{rad/s}. \end{aligned} \tag{3.34}$$

The simulation results are summarized in Table 3.8 and depicted in Figures 3.6 and 3.7. From the performance functionals we see that both controllers lead to similar performance, as imposed. One difference is that the controller with variable gains utilizes lower maximum torque as seen in Figure 3.7, but experiences larger overall angular velocity errors.

Simulation results for one orbital period (5896 s) is presented in Table 3.9 and Figures 3.8 and 3.9, and as can be seen from the performance functionals the control law containing variable gains is less effected by the measurement noise compared to the control law using static gains, as expected based on the results presented in Section 3.5.1 where similar reasoning is used. From Figure 3.9 we see similar behavior for the observer; the noise has less effect on both attitude and angular velocity between estimated and body frame.

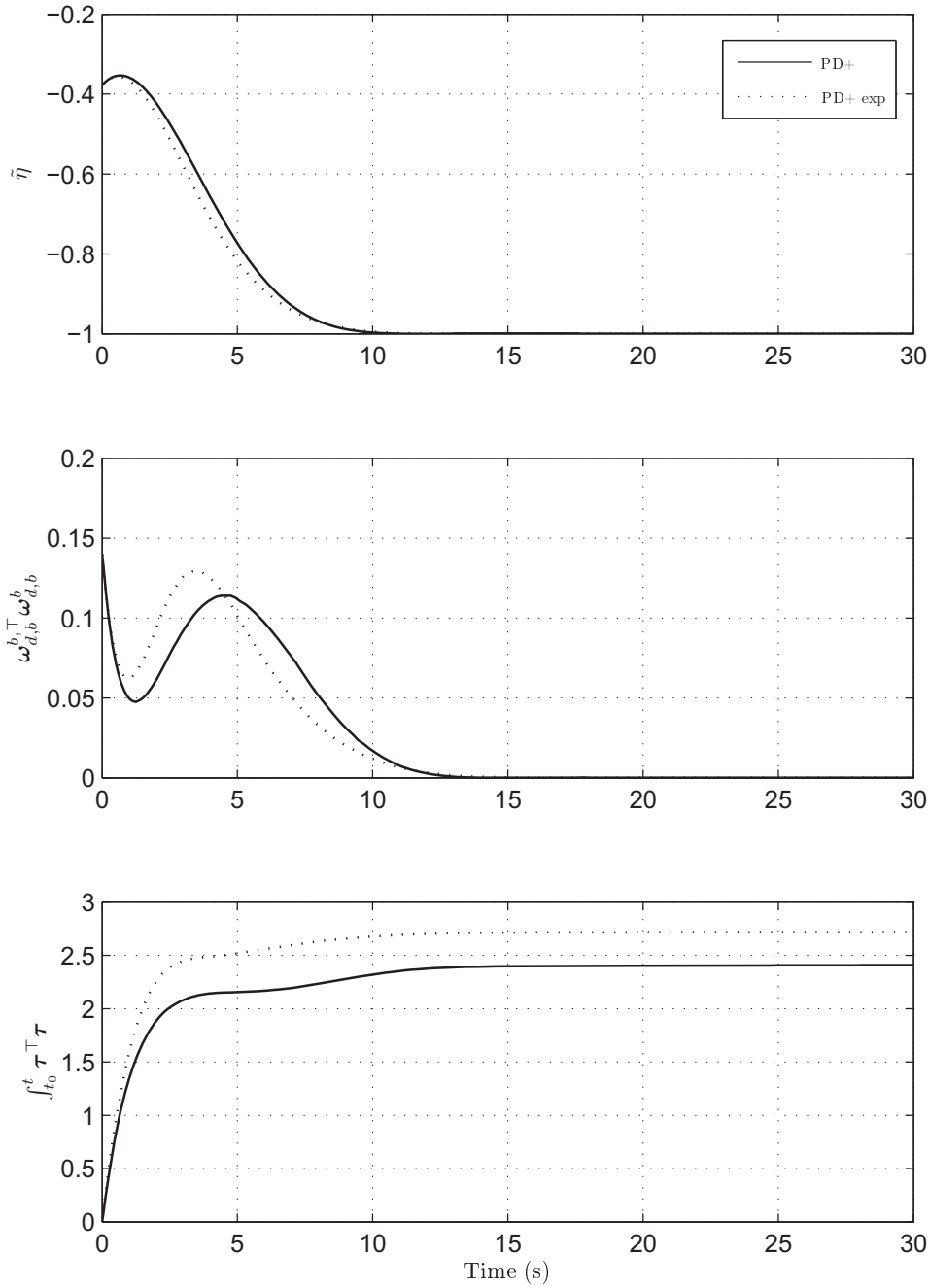

Figure 3.1: Attitude and angular velocity error, and power consumption using PD+ controller and PD+ controller with exponential gains controllers during spacecraft attitude maneuver.

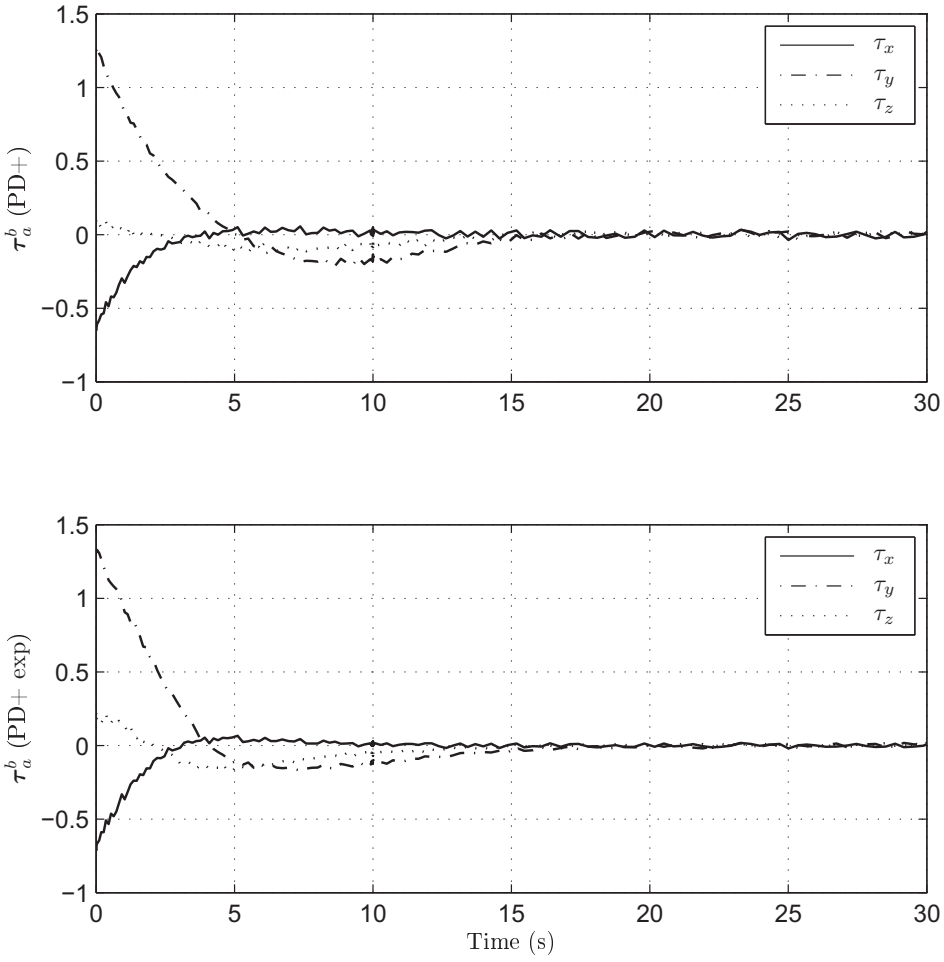

Figure 3.2: Control torque using PD+ controller and PD+ controller with exponential gains during spacecraft attitude maneuver.

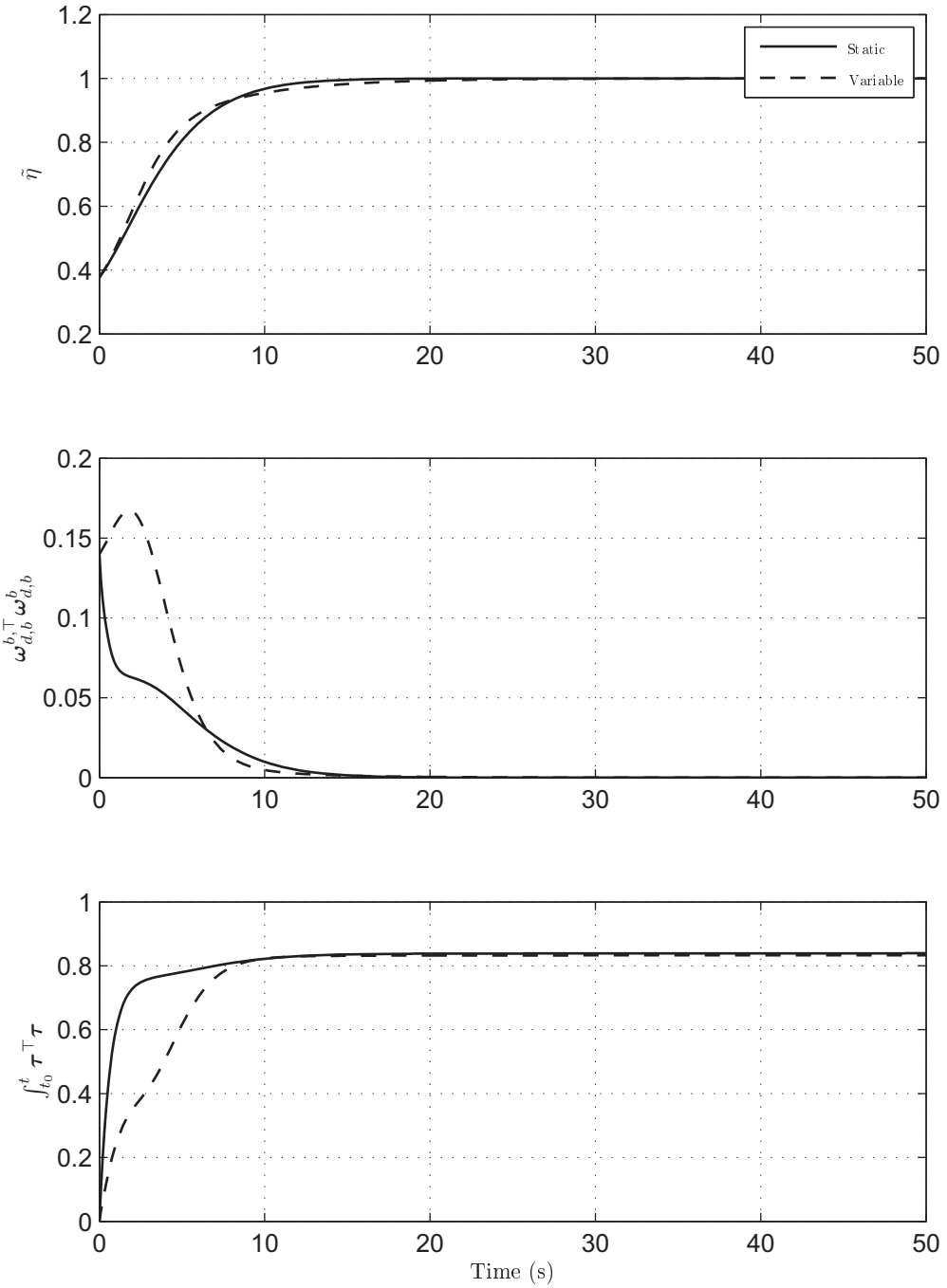

Figure 3.3: Attitude and angular velocity error, and power consumption using PD+ controllers with static and variable gains during spacecraft attitude maneuver.

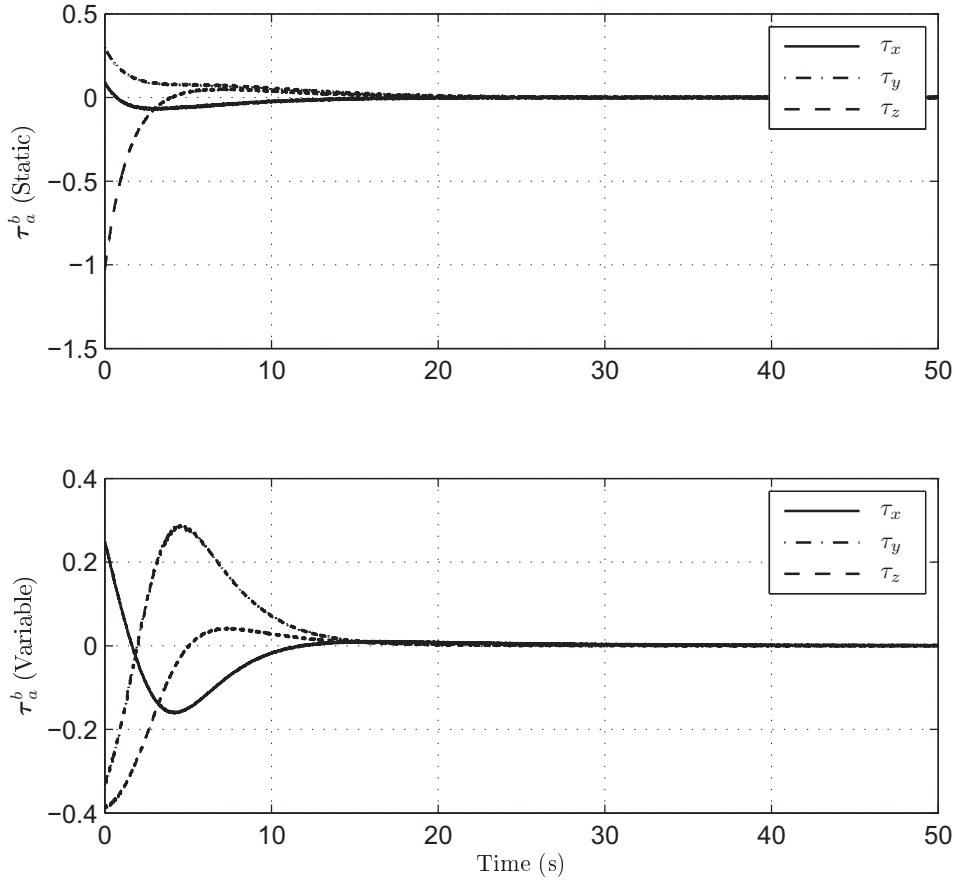

Figure 3.4: Control torque using PD+ controllers with static and variable gains during spacecraft attitude maneuver.

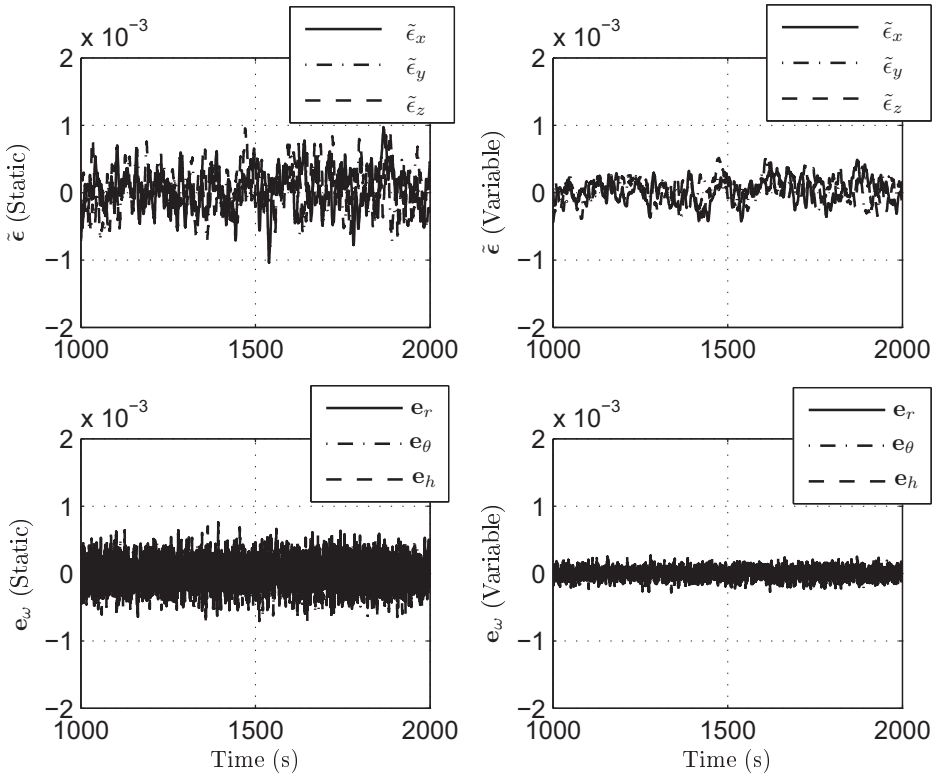

Figure 3.5: Attitude and angular velocity error for PD+ controller with static (left) and variable (right) gains.

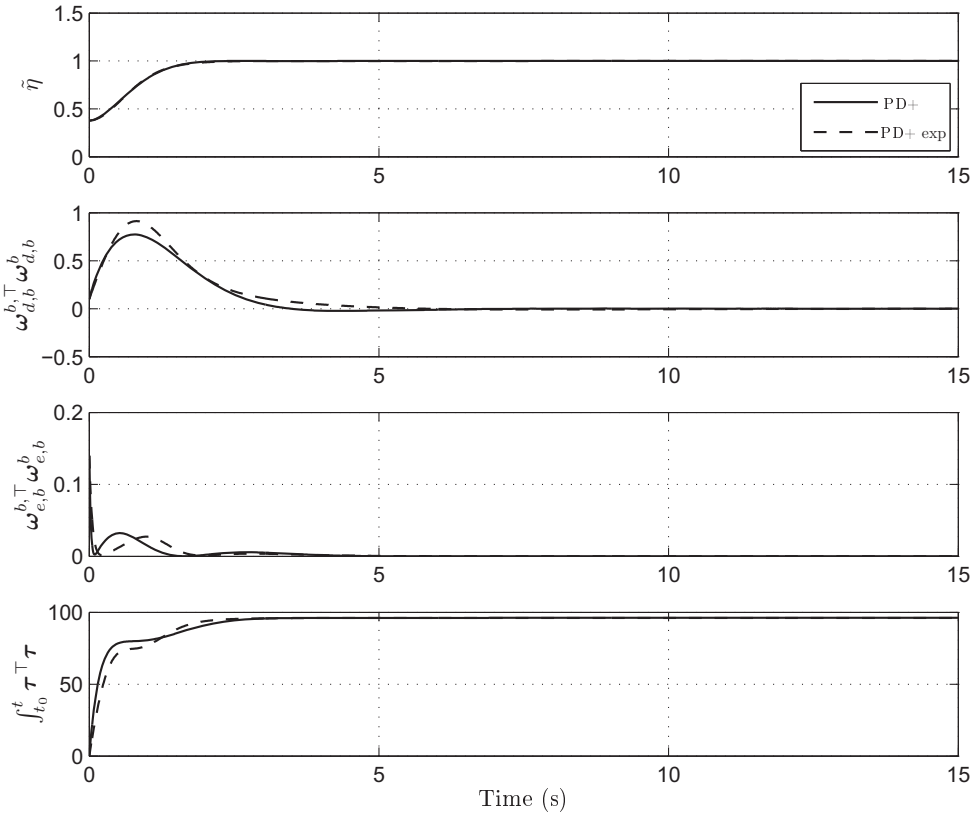

Figure 3.6: Attitude, angular velocity and angular velocity estimation error, and power consumption using PD+ based output feedback with static and variable gains during spacecraft attitude maneuver.

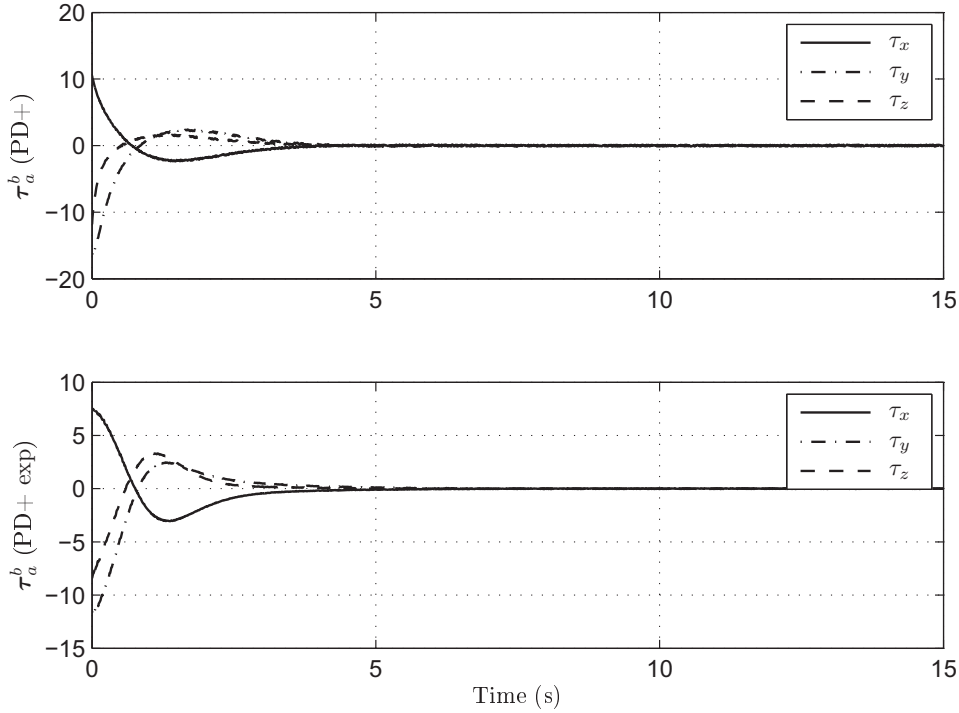

Figure 3.7: Control torque for PD+ based output feedback with static and variable gains during spacecraft attitude maneuver.

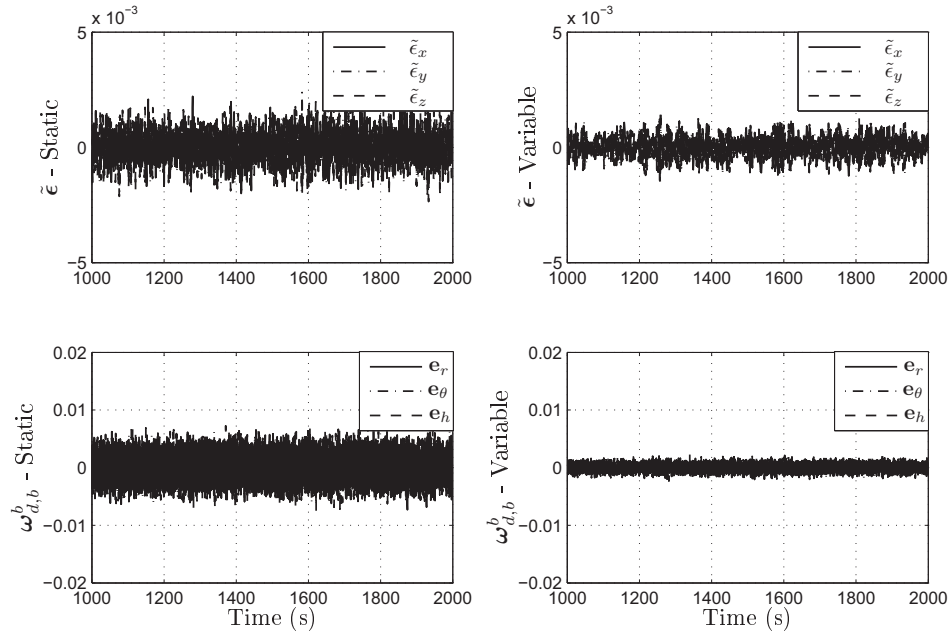

Figure 3.8: Attitude and angular velocity error for static gains (left) and variable gains (right).

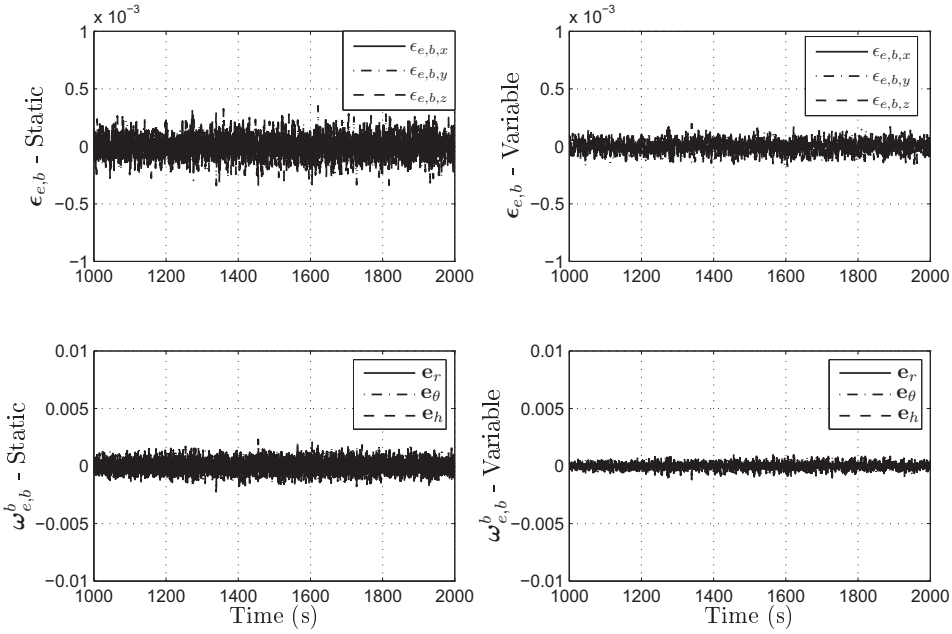

Figure 3.9: Attitude and angular velocity estimation error for static gains (left) and variable gains (right).

Chapter 4

Hybrid attitude control of rigid bodies

In this chapter we will present different control strategies for hybrid attitude control of rigid bodies based on the general framework briefly presented in Appendix A.3. The control laws treated are modified versions of the same classical control laws as presented in Chapter 3. The rest of the chapter is organized as follows: we start by presenting the problem formulation in Section 4.1 along with some technical lemmas utilized throughout this chapter. In Section 4.2 we present hybrid state feedback versions of the controllers and combine them through a supervisor. Then we revise the output feedback controller for the hybrid approach in Section 4.3 and end with simulation results and discussion in Section 4.4. The results presented in this chapter are based on (Schlanbusch *et al.*, 2010*a*; Schlanbusch and Nicklasson, 2011; Schlanbusch *et al.*, 2011*b*,*e*,*f*).

4.1 Problem formulation

The problem at hand is tracking of a given reference similar to what is presented in Section 3.1 except that in order to use the methods of (Sanfelice *et al.*, 2007) for the controlled rigid bodies we define the error variable

$$\mathbf{e}_{hq} = [1 - h\tilde{\eta}, \tilde{\boldsymbol{\epsilon}}^\top]^\top, \tag{4.1}$$

fulfilling the kinematic equation

$$\dot{\mathbf{e}}_{hq} := \mathbf{T}_h^\top(\mathbf{e}_{hq})\mathbf{e}_\omega, \tag{4.2}$$

where

$$\mathbf{T}_h^\top(\mathbf{e}_{hq}) = \begin{bmatrix} -h\tilde{\boldsymbol{\epsilon}}^\top \\ \tilde{\eta}\mathbf{I} + \mathbf{S}(\tilde{\boldsymbol{\epsilon}}) \end{bmatrix}, \tag{4.3}$$

$h \in H := \{-1, 1\}$ is the hybrid switching parameter and $\mathbf{e}_{hq} \in S_h^3 := \{[1 - h\tilde{\eta},\ \tilde{\boldsymbol{\epsilon}}^\top]^\top : \mathbf{q} \in S^3,\ h \in H\}$. To complete the proofs presented in this chapter we make use of two technical lemmas adopted for hybrid systems. The first one is a version of Lemma 3.1 while the latter is a version of Lemma 3.2 adapted to the sliding surface closed-loop equations.

Lemma 4.1 *Let* $\mathbf{e}_{hq}$ *and* $\mathbf{T}_h(\mathbf{e}_{hq})$ *be defined as in* (4.1) *and* (4.3). *Then the inequality*

$$\mathbf{e}_{hq}^\top \mathbf{T}_h \mathbf{T}_h^\top \mathbf{e}_{hq} \geq \frac{1}{8}\mathbf{e}_{hq}^\top \mathbf{e}_{hq} \tag{4.4}$$

holds for all $\tilde{\mathbf{q}} \in S^3$ *and* $h \in H$.

Proof: See Appendix B.14.

Lemma 4.2 *The derivative of* $\dot{\mathbf{T}}_h(\mathbf{e}_{hq})$ *satisfies*

$$\dot{\mathbf{T}}_h(\mathbf{e}_{hq})\mathbf{e}_{hq} = \mathbf{H}(\mathbf{e}_{hq}, \mathbf{s}), \tag{4.5}$$

where

$$\mathbf{H} = \frac{1}{4}\left\{h[\tilde{\eta}\mathbf{I} + \mathbf{S}(\tilde{\boldsymbol{\epsilon}})] - \mathbf{I}\right\}\left[\mathbf{s} - \frac{1}{2}\gamma h\tilde{\boldsymbol{\epsilon}}\right]. \tag{4.6}$$

Proof: See Appendix B.15.

We see from (3.12) and (3.13) that by replacing h for $\pm$ and $\mathbf{e}_\omega = \mathbf{s} - \gamma\mathbf{T}_h^\top \mathbf{e}_{hq} = \mathbf{s} - 1/2\gamma h\tilde{\boldsymbol{\epsilon}}$ from the sliding surface control structure, we obtain (4.6). A hybrid version of Lemma 3.2 can be stated as follows.

Corollary 4.1 *The derivative of* $\dot{\mathbf{T}}_h(\mathbf{e}_{hq})$ *satisfies*

$$\dot{\mathbf{T}}_h(\mathbf{e}_{hq})\mathbf{e}_{hq} = \mathbf{G}_h\mathbf{e}_\omega, \tag{4.7}$$

where

$$\mathbf{G}_h = \frac{1}{4}\{h[\tilde{\eta}\mathbf{I} + \mathbf{S}(\tilde{\boldsymbol{\epsilon}})] - \mathbf{I}\}. \tag{4.8}$$

4.2 State feedback control

In this section we will present hybrid state feedback control of rigid bodies based on the previously mentioned PD+ and sliding surface controllers.

4.2.1 Passivity-based PD+ control

We start by considering a switching controller based on Paden & Panja's controller. Let the input control torque be given by

$$\boldsymbol{\tau}_a = \mathbf{J}\dot{\boldsymbol{\omega}}_d - \mathbf{S}\left(\mathbf{J}\boldsymbol{\omega}\right)\boldsymbol{\omega}_d - \boldsymbol{\tau}_d - k_p\mathbf{T}_h^\top \mathbf{e}_{hq} - k_d\mathbf{e}_\omega, \tag{4.9}$$

where $k_p, k_d > 0$ are constant feedback gains, and the state $\mathbf{x} := [\mathbf{e}_{hq}^\top, \mathbf{e}_\omega^\top, h]^\top$. The switching law is defined as follows. Let C and D denote the flow and jump sets respectively and be defined as

$$C := \{\mathbf{x} \in S_h^3 \times \mathbb{R}^3 \times H : h\tilde{\eta} \geq -\sigma\} \tag{4.10a}$$

$$D := \{\mathbf{x} \in S_h^3 \times \mathbb{R}^3 \times H : h\tilde{\eta} \leq -\sigma\}, \tag{4.10b}$$

for a given value $\sigma \in (0, 1)$ which determines the hysteresis margin to ensure robustness to measurement noise along the lines of Theorem 3.1. Note that both the

flow and jump sets are closed, thus there exists a point $h\tilde{\eta} = -\sigma$ were the sets are overlapping, and that by setting $\sigma = 0$ leads to feedback similar to (3.3) using a sign function. To ensure robustness to measurement noise we need to choose $\sigma \geq 2\sigma_n \mathbb{B}^7$, where $\sigma_n \mathbb{B}^7$ denotes the noise vector for the total state. If $\sigma \geq 1$ switching of h will never occur. Also note that $C \cup D = S_h^3 \times \mathbb{R}^3 \times H$. The switching law is defined as

$$\dot{h} = 0 \qquad \mathbf{x} \in C \tag{4.11a}$$

$$\mathbf{x}^+ = G(\mathbf{x}) := [\mathbf{e}_{hq}^\top, \mathbf{e}_\omega^\top, -h]^\top \qquad \mathbf{x} \in D. \tag{4.11b}$$

We then have the following.

Theorem 4.1 *Let Assumptions 3.2 and 3.3 hold. Then, the equilibrium set*

$$\mathcal{A} = \{\mathbf{x} \in S_h^3 \times \mathbb{R}^3 \times H : (\mathbf{e}_{hq}, \mathbf{e}_\omega) = (\mathbf{0}, \mathbf{0})\} \tag{4.12}$$

for (2.83) *and* (4.2)–(4.3) *in closed-loop with the hybrid controller* (4.9)–(4.11) *is uniformly asymptotically stable in the large on the set*[1] $S_h^3 \times \mathbb{R}^3$.

Proof: See Appendix B.16.

What we see here is that the "sphere" described by the quaternion in S^3 is roughly divided in half by $\tilde{\eta} = 0$ plus hysteresis, such that the switching control law always will choose the rotational direction based on the shortest path. Note also that by applying switching we do not need to consider Assumption 3.1 and Remark 3.1. By removing the assumption of known disturbances we obtain the following result.

Corollary 4.2 *Let Assumptions 3.2, 3.3 and 3.4 hold. Then, the equilibrium set*

$$\mathcal{A} = \{\mathbf{x} \in S_h^3 \times \mathbb{R}^3 \times H : (\mathbf{e}_{hq}, \mathbf{s}) \in \bar{\mathcal{B}}_\delta\} \tag{4.13}$$

for (2.83) *and* (4.2)–(4.3) *in closed-loop with the hybrid controller*

$$\boldsymbol{\tau}_a = \mathbf{J}\dot{\boldsymbol{\omega}}_d - \mathbf{S}(\mathbf{J}\boldsymbol{\omega})\boldsymbol{\omega}_d - k_p \mathbf{T}_h^\top \mathbf{e}_{hq} - k_d \mathbf{e}_\omega, \tag{4.14}$$

and (4.10)–(4.11) *is uniformly asymptotically stable in the large on the set* $S_h^3 \times \mathbb{R}^3$.

The proof is omitted, but follows along the same lines as the proof of Theorem 3.9 with $k_1 = k_2 = 0$ adapted for hybrid control according to the proof of Theorem 4.1.

Note that uniform asymptotic stability of a set as defined in (4.13) is equivalent to uniform practical asymptotical stability of the origin for $\delta > 0$, while for $\delta = 0$ the set is reduced to the origin, which corresponds to uniform asymptotic stability of the origin.

[1] Note that throughout literature, the stability of sets are defined in many different ways; see for instance (Goebel *et al.*, 2009) for set convergence and (Chaillet and Panteley, 2006) for stability of sets. Our understanding is that all trajectories $\mathbf{x}(t, t_0, \mathbf{x}_0)$ will enter the closed set $\mathcal{A}$ at $t = t_0 + T$ and stay in $\mathcal{A}$ for all $t \geq t_0 + T$.

4.2.2 Sliding surface control

The hybrid controller is composed of the continuous-time control law

$$\boldsymbol{\tau}_a = \mathbf{J}\dot{\boldsymbol{\omega}}_{hr} - \mathbf{S}\left(\mathbf{J}\boldsymbol{\omega}\right)\boldsymbol{\omega}_{hr} - \boldsymbol{\tau}_d - k_q\mathbf{T}_h^\top\mathbf{e}_{hq} - k_\omega\mathbf{s}_h, \tag{4.15a}$$

$$\boldsymbol{\omega}_{hr} = \boldsymbol{\omega}_d - \gamma\mathbf{T}_h^\top\mathbf{e}_{hq}, \tag{4.15b}$$

$$\mathbf{s}_h = \boldsymbol{\omega} - \boldsymbol{\omega}_{hr} = \boldsymbol{\omega} - \boldsymbol{\omega}_d + \gamma\mathbf{T}_h^\top\mathbf{e}_{hq}, \tag{4.15c}$$

where $k_q,\ k_\omega,\ \gamma > 0$ are considered constant gains, the switching law

$$\mathbf{x}^+ = G(\mathbf{x}) := [\mathbf{e}_{hq}^\top, \mathbf{s}_h^\top, -h]^\top \quad \mathbf{x} \in D \tag{4.16}$$

where $\mathbf{x} =: [\mathbf{e}_{hq}^\top, \mathbf{s}_h^\top, h]^\top$, and the flow and jump sets

$$C := \left\{\mathbf{x} \in S_h^3 \times \mathbb{R}^3 \times H : h\left[k_q\tilde{\eta} - \frac{1}{2}\gamma\tilde{\boldsymbol{\epsilon}}^\top\mathbf{J}\mathbf{e}_\omega\right] \geq -\sigma\right\} \tag{4.17a}$$

$$D := \left\{\mathbf{x} \in S_h^3 \times \mathbb{R}^3 \times H : h\left[k_q\tilde{\eta} - \frac{1}{2}\gamma\tilde{\boldsymbol{\epsilon}}^\top\mathbf{J}\mathbf{e}_\omega\right] \leq -\sigma\right\}, \tag{4.17b}$$

where again σ defines the switching hysteresis. We state the following theorem.

Theorem 4.2 *Let Assumptions 3.2 and 3.3 hold. Consider the system* (2.83) *and* (4.2)–(4.3) *in closed-loop with the controller* (4.15)–(4.17)*. Then, the set*

$$\mathcal{A} = \{\mathbf{x} \in S_h^3 \times \mathbb{R}^3 \times H : (\mathbf{e}_{hq}, \mathbf{s}_h) = (\mathbf{0}, \mathbf{0})\} \tag{4.18}$$

is asymptotically stable in the large on the set $S_h^3 \times \mathbb{R}^3$*.*

Proof: See Appendix B.17.

By removing the assumption of known disturbances we obtain the following result.

Corollary 4.3 *Let Assumptions 3.2, 3.3 and 3.4 hold. Consider the system* (2.83) *and* (4.2)–(4.3) *in closed-loop with the controller*

$$\boldsymbol{\tau}_a = \mathbf{J}\dot{\boldsymbol{\omega}}_{hr} - \mathbf{S}\left(\mathbf{J}\boldsymbol{\omega}\right)\boldsymbol{\omega}_{hr} - k_q\mathbf{T}_h^\top\mathbf{e}_{hq} - k_\omega(\boldsymbol{\omega} - \boldsymbol{\omega}_{hr}), \tag{4.19}$$

(4.15b), (4.15c) *and* (4.17)*. Then, the set*

$$\mathcal{A} = \{\mathbf{x} \in S_h^3 \times \mathbb{R}^3 \times H : (\mathbf{e}_{hq}, \mathbf{s}_s) \in \bar{\mathcal{B}}_\delta\} \tag{4.20}$$

is asymptotically stable in the large on the set $S_h^3 \times \mathbb{R}^3$*.*

The proof is omitted, but follows along the same lines as the proof of Theorem 4.2.

A notable difference with respect to the controller in Section 4.2.1 is that the switching condition depends on both the attitude and angular velocities, which may lead to different behaviors as pointed out by Mayhew *et al.* (2009). Another notable point is that the flow and jump sets (4.17) for the sliding surface controller are very similar to the ones derived in (Mayhew *et al.*, 2009) using backstepping technique. In (Kristiansen, 2008) an analysis of the structures of the two mentioned controllers were given, and vast similarities were shown, which also seems to be evident for the hybrid case as well.

4.2.3 Hybrid supervisor

We now introduce a supervisor to take advantage of the features of each of the switching controllers presented in Section 4.2 in order to improve performance in closed-loop, where our primary goal is to reduce energy consumption *i.e.* control effort. As we show, this may be achieved by designing a second switching law which determines which hybrid controller to use at which instant. The supervisor is based on the work of Efimov *et al.* (2009). According to the latter, the design method consists in defining a partition of the real positive semi-line with respect to the values of the norm of the output to be controlled. Then, the semi-line is divided in regions, for which each of them a controller is associated. For instance, one may want to apply "controller 3" which provides fast convergence on "region 4" which corresponds to 'large' errors. In the actual context *i.e.*, the attitude control problem, the real positive semi-line consists on the line $\tilde{\eta} \in [-1, 1]$.

We start by dividing the line of values for $\tilde{\eta}$ into suitable domains with local optimality[2] according to

$$[-1, 1] = \bigcup_{p=0}^{M} [\Delta_p, \Delta_{p+1}),\ \Delta_0 = -1,\ \Delta_M = 1. \tag{4.21}$$

The approach is to use controller 1 to reduce large angular velocities and then to switch to controller 2 when the attitude error is small thus, the following imposed partition is set in an intuitive manner and then tuned based on simulation results

$$\Delta_0 = -1,\ \Delta_1 = -0.8,\ \Delta_2 = 0.05,\ \Delta_3 = 0.85,\ \Delta_4 = 1. \tag{4.22}$$

We also introduce hysteresis to the switching logic by defining

$$\chi_{\theta_0}(\Delta_1) = -0.85,\ \chi_{\theta_1}(\Delta_2) = -0.05,\ \chi_{\theta_2}(\Delta_3) = 0.80, \tag{4.23}$$

where $\theta_p = i$ if controller i is used. Based on simulations we assign the sliding surface controller for θ_0 and θ_3 for negative and positive h respectively, and the PD+ for θ_1 and θ_2 again for negative and positive h respectively, since the sliding surface controller behaved better close to the equilibrium, while the latter behaved well during stabilization, thus obtaining a partition as illustrated in Figure 4.1.

The hysteresis supervisor is given by

$$t_0 = 0,\ i(t_0) = r, r \in \{0, \ldots, M\},\ \tilde{\eta} \in [\Delta_r, \Delta_{r+1}); \tag{4.24}$$

$$t'_k = \arg_{t \geq t_j} \inf\{\tilde{\eta} \in [\Delta_k, \chi_{\theta_k}(\Delta_{k+1}))\},\quad k \in \{i(t_j) - 1, i(t_j) + 1\} \tag{4.25}$$

$$t_{j+1} = \min_{k \in \{i(t_j)-1, i(t_j)+1\}} \{t'_k\}; \tag{4.26}$$

$$i(t_{j+1}) = k \text{ such that } \tilde{\eta} \in [\Delta_k, \chi_{\theta_k}(\Delta_{k+1})) \subset [\Delta_k, \Delta_{k+1}). \tag{4.27}$$

where t_j, with $j = 1, 2, 3, \ldots$, are switching times; j is the number of the last switch and the signal $i(t)$ has constant value in the hysteresis set

$$\mathcal{N} = \bigcup_{p=0}^{2} [\chi_{\theta_p}(\Delta_{p+1}), \Delta_{p+1}). \tag{4.28}$$

[2]It should be noted that strictly speaking, we do not obtain an optimal solution of the total system but, by carefully choosing the switching conditions the switched control leads, if not in general to optimal performance, to an improvement.

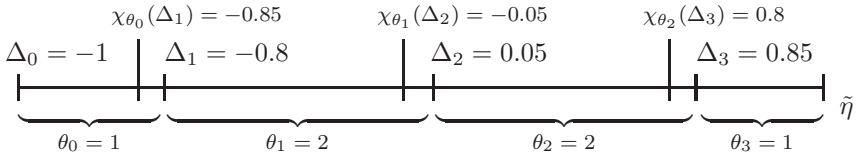

Figure 4.1: Illustration of the $\tilde{\eta}$ partitions.

The switching works as follows: the system starts in a mode $i(t_0)$ based on the initial value of $\tilde{\eta}$. Then, at t'_k the value of $\tilde{\eta}$ leaves the specified interval (including hysteresis), and t_{j+1} denotes the shortest time where this interval is abandoned, thus a switch occur to the appropriate interval $i(t_{j+1}) = k$ where k denotes either a switch "left" or "right" based on an decrease or increase of $\tilde{\eta}$.

4.3 Output feedback control

In the control laws presented in this section we have used hybrid feedback to remove the assumption of no sign change of $\tilde{\eta}(t)$ as suggested by Assumption 3.1 based on the analysis due to Lemma 3.1 similar to what was presented in the previous sections. One challenge is still left, the assumption that $\eta_{e,b}(t) \geq \delta_\eta$ for all $t \geq t_0$ describing the rotation between the body and estimated frame as suggested in Assumption 3.5. Based on this discussion we propose the following controller

$$\boldsymbol{\tau}_a = \mathbf{J}\mathbf{a}_d - \mathbf{S}(\mathbf{J}\boldsymbol{\omega}^b_{i,e})\boldsymbol{\omega}^b_{i,d} - k_p\mathbf{T}_h^\top \mathbf{e}_{hq} - k_d\boldsymbol{\omega}^b_{d,e}, \tag{4.29}$$

with $k_p, k_d > 0$ considered as constant gains and $\boldsymbol{\omega}^b_{d,e} := \boldsymbol{\omega}^b_{i,e} - \boldsymbol{\omega}^b_{i,d}$ as the angular velocity of the estimated frame relative to the desired frame presented in the body frame, and the observer

$$\dot{\mathbf{z}} = \mathbf{a}_d + \mathbf{J}^{-1}\left[l_p\mathbf{T}_{eq}^\top \mathbf{e}_{eq} - k_p\mathbf{T}_h^\top \mathbf{e}_{hq}\right], \tag{4.30}$$

$$\boldsymbol{\omega}^b_{i,e} = \mathbf{z} + 2\mathbf{J}^{-1}l_d\mathbf{T}_{eq}^\top \mathbf{e}_{eq}, \tag{4.31}$$

with $l_p, l_d > 0$ constants to be defined. Next, let $\mathbf{x} := [\mathbf{e}_{hq}^\top,\ \mathbf{e}_\omega^\top,\ \mathbf{e}_{eq}^\top,\ \mathbf{e}_{e\omega}^\top, h]^\top$ and define the flow sets as

$$C_1 := \{\mathbf{x} \in S^3 \times \mathbb{R}^3 \times S^3 \times \mathbb{R}^3 \times H : h\left(\tilde{\eta} - \frac{1}{2k_p}\lambda\tilde{\boldsymbol{\epsilon}}^\top \mathbf{J}\mathbf{e}_\omega\right) \geq -\delta_m\} \tag{4.32}$$

$$C_2 := \{\mathbf{x} \in S^3 \times \mathbb{R}^3 \times S^3 \times \mathbb{R}^3 \times H : \eta_{e,b} \geq \delta_\eta\}, \tag{4.33}$$

where $C = C_1 \cap C_2$, and δ_m and δ_η are constants to be defined. The set (4.32) can be seen as hysteresis such that if $\tilde{\eta}$ switches sign, it has to grow larger than some constant δ_m before the trajectory leaves the flow set. The second set (4.33)

is introduced to ensure that $\eta_{e,b}$ remains separated from zero. Then, the jump sets should be assigned according to

$$D_1 := \{\mathbf{x} \in S^3 \times \mathbb{R}^3 \times S^3 \times \mathbb{R}^3 \times H : h\left(\tilde{\eta} - \frac{1}{2k_p}\lambda\tilde{\boldsymbol{\epsilon}}^\top \mathbf{J}\mathbf{e}_\omega\right) \leq -\delta_m\} \tag{4.34}$$

$$D_2 := \{\mathbf{x} \in S^3 \times \mathbb{R}^3 \times S^3 \times \mathbb{R}^3 \times H : \eta_{e,b} \leq \delta_\eta\}, \tag{4.35}$$

where $D = D_1 \cup D_2$, and the switching laws defined as

$$\dot{h} = 0 \ \forall \mathbf{x} \in C \tag{4.36}$$

$$\mathbf{x}^+ := G_1(\mathbf{x}) = [\mathbf{e}_{hq}^\top, \mathbf{e}_\omega^\top, \mathbf{e}_{eq}^\top, \mathbf{e}_{e\omega}^\top, -h]^\top \ \forall \mathbf{x} \in D_1 \tag{4.37}$$

$$\mathbf{x}^+ := G_2(\mathbf{x}) = [\mathbf{e}_{hq}^\top, \mathbf{e}_\omega^\top, \mathbf{0}, \mathbf{e}_{e\omega}^\top, h]^\top \ \forall \mathbf{x} \in D_2. \tag{4.38}$$

$G_1(\mathbf{x})$ ensures that h switches sign when the hysteresis value is passed such that the product $h\tilde{\eta}$ is positive, while $G_2(\mathbf{x})$ ensures that $\mathbf{e}_{eq} = \mathbf{0} \Rightarrow \eta_{e,b} = 1$. During flows (that is $\forall \mathbf{x} \in C$), we have $\dot{h} = 0$. We can now state the following theorem.

Theorem 4.3 *Consider the system* (4.2) *and* (2.83)*, in closed loop with the hybrid controller* (4.29)–(4.38)*. Let Assumptions 3.2, 3.3 and 3.4 hold. Then, for each* δ*,* Δ *there exist control gains* k_p*,* k_d*,* l_p *and* l_d *such that the set* $\mathcal{A}_\delta = \{\mathbf{x} \in S^3 \times \mathbb{R}^3 \times S^3 \times \mathbb{R}^3 \times H : \|\boldsymbol{\chi}\| \leq \delta\}$ *is uniformly asymptotically stable for all initial conditions in* $\mathcal{A}_\Delta := \{\mathbf{x} \in S^3 \times \mathbb{R}^3 \times S^3 \times \mathbb{R}^3 \times H : \|\boldsymbol{\chi}\| \leq \Delta\}$.

Proof: See Appendix B.18.

Remark 4.1 *Note that Remark 3.13 also hold for Theorem 4.3.*

Corollary 4.4 *If in addition to the conditions of Theorem 4.3, the disturbances* $\boldsymbol{\tau}_d \equiv \mathbf{0}$ *the equilibrium* $\boldsymbol{\chi} = \mathbf{0}$ *is uniformly asymptotically stable.*

4.4 Simulation results

In this section we present simulation results based on the control laws presented in this section. Our main focus is to compare performance between continuous and hybrid control laws, and between different hybrid controllers compared with a combination through supervisory control. We utilize simulation data as presented in Section 2.8.1 if otherwise is not stated.

4.4.1 Continuous versus hybrid state feedback

We have performed several series of simulations to compare the hybrid controller of Section 4.2.2 to the continuous controller of Section 3.2.2. In the simulations setting we assume that the rigid body is a spacecraft and naturally, the primary goal is to improve performance. The latter is measured in terms of (reducing) fuel consumption *i.e.*, control effort.

For the continuous controller in Section 3.2.3 the reference equilibrium point is chosen *a priori* according to the method presented in Chapter 5. This is done considering both initial rotation and orientation for 'small' initial values,

$$\mathbf{e}_q = \left\{ \begin{array}{ll} \mathbf{e}_{q+} & \text{if} \quad k_{\tilde{\eta}}\tilde{\eta}(t_0) + k_{\dot{\tilde{\eta}}}\dot{\tilde{\eta}}(t_0) \geq 0 \\ \mathbf{e}_{q-} & \text{if} \quad k_{\tilde{\eta}}\tilde{\eta}(t_0) + k_{\dot{\tilde{\eta}}}\dot{\tilde{\eta}}(t_0) < 0 \end{array} \right\}, \tag{4.39}$$

where $\tilde{\eta}(t_0)$ and $\dot{\tilde{\eta}}(t_0)$ are initial values and $k_{\tilde{\eta}}$ and $k_{\dot{\tilde{\eta}}}$ are chosen parameters. Note that $\dot{\tilde{\eta}} = -1/2\tilde{\boldsymbol{\epsilon}}^\top \mathbf{e}_\omega$. By this rule of choice we can make a fair comparison with the hybrid sliding surface controller as presented in Section 4.2.2. Also, an appropriate tuning is made; for the continuous controller the parameters $k_{\tilde{\eta}}$ and $k_{\dot{\tilde{\eta}}}$ can be tuned to fit a given system while for the switching strategy tuning consists in choosing appropriately the hysteresis threshold σ and the gains k_q and γ. Note that when choosing equilibrium point a priori we only need to tune external parameters while for the hybrid approach controller gains have to be chosen which reduces the tuning flexibility of the control law itself.

An interesting natural scenario to consider is when the initial conditions are 'large'; particularly, when the spacecraft's attitude is 'close' to the desired one but turning rapidly away from it that is, $\|\boldsymbol{e}_\omega(t_0)\| \gg 1$ and $\tilde{\boldsymbol{\epsilon}}(t_0) \approx 0$. Note that the switching law in (4.17) consists in verifying whether

$$\varsigma := h\left(k_q\tilde{\eta} - \frac{1}{2}\gamma\tilde{\boldsymbol{\epsilon}}^\top \mathbf{J}\mathbf{e}_\omega\right) \geq -\sigma\,. \tag{4.40}$$

Hence, if we have $\tilde{\boldsymbol{\epsilon}}^\top \mathbf{e}_\omega \approx 0$ the effect of (large) angular velocities may be transparent to the hybrid controller.

The simulations are made for two cases of initial angular velocities. Figure 4.2 shows simulation results using $(\mathbf{q}(t_0), \boldsymbol{\omega}(t_0)) = ([1, \mathbf{0}]^\top, 1.5\mathbf{v}^\top)$ where $\mathbf{v} = [3, -4, 5]^\top / \|[3, -4, 5]^\top\|$, and the gains are set to $k_q = 1$, $k_\omega = 2$, $\gamma = 1$. The switching threshold (hysteresis) is chosen as $\sigma = 0.1$. As it may be appreciated the negative equilibrium point is preferable but the switching threshold for the hybrid controller is never met; the state trajectory never enters the jump set. One may think that the hysteresis switching threshold is not chosen properly however, Figure 4.3 illustrates the opposite, showing that the value of the switching condition (4.40) does not reach the switching threshold for any $\sigma > 0$. It may be argued that the initial angular velocity may not be recognized by the continuous controller (3.2.2) based on the prediction (4.39) either. Yet, this expression only accounts for small initial angular velocity errors; for large initial angular velocity errors the equilibrium point giving the largest initial rotational error is in generally preferred.

Next, we increase the initial velocity to $\mathbf{e}_\omega(t_0) = 3.5\mathbf{v}^\top$ to provoke switching; see Figure 4.4 for simulation results. Now, the system under either controller, that is continuous or hybrid, eventually settles at the negative equilibrium point, although the continuous controller has lower power consumption compared to the hybrid controller while the integrated attitude and angular velocity errors are larger.

To compare further the performances of the hybrid versus the continuous controller we performed a simulation decreasing the derivative gain to $k_\omega = 1$. On one hand, this entails a change in the preferred reference equilibrium point when using

Table 4.1: Values of performance functionals.

	J_q	J_ω	J_p
Continuous controller (Fig. 4.2)	2.80	7.19	9.50
Hybrid controller (Fig. 4.2)	1.47	1.15	21.07
Continuous controller (Fig. 4.4)	1.86	18.00	70.11
Hybrid controller (Fig. 4.4)	1.69	13.44	76.89
Continuous controller (Fig. 4.5)	4.52	20.02	83.16
Hybrid controller (Fig. 4.5)	4.53	19.44	80.95

Table 4.2: Values of performance functionals without noise.

	J_q	J_ω	J_p
Sliding surface	4.040	0.774	5.021
PD+	3.861	0.556	4.439
Supervisor	4.002	0.556	4.438

Table 4.3: Values of performance functionals including noise and perturbations for one orbital period (5896 s).

	J_q	J_ω	J_p
Sliding surface	4.058	0.7776	10.840
PD+	3.874	0.561	22.780
Supervisor	4.024	0.533	7.921

the continuous controller (3.2.2). On the other hand, using the hybrid controller with less damping results in lower energy consumption compared to the continuous controller while the integrated attitude error is similar for both controllers; see Figure 4.5 for plotted results. The energy consumption under hybrid control may be further diminished by increasing the hysteresis threshold σ.

A comparison of the controllers in function of the performance indexes J_q, J_ω and J_p for all three simulations discussed above is presented in Table 4.1.

4.4.2 Hybrid versus supervisory control

In this section we compare the hybrid controllers presented in Section 4.2.1 and 4.2.2 with the supervisory strategy presented in Section 4.2.3, where the primary goal is to compare performance features.

The initial conditions were set to $\mathbf{q}(t_0) = [-0.3772,\ -0.4329,\ 0.6645,\ 0.4783]^\top$ and $\boldsymbol{\omega}^b_{i,b}(t_0) = [0.1\ \ -0.3\ 0.2]^\top$. The controller gains were chosen as $k_p = 4$, $k_d = 5$ for the PD+ controller, and $k_q = 1$, $k_\omega = 2$ and $\gamma = 1$ for the sliding surface controller, while the supervisor gains were chosen as $k_p = 4$, $k_d = 5$, $k_q = 0.5$ $k_\omega = 1$ and $\gamma = 1$. Our objective for the tuning process was to obtain similar performance for the different controllers.

We ran two series of simulations to compare the hybrid sliding surface controller, the PD+ hybrid controller and the supervisor-based controller. The simulation results from the first simulation are summarized in Table 4.2 and depicted

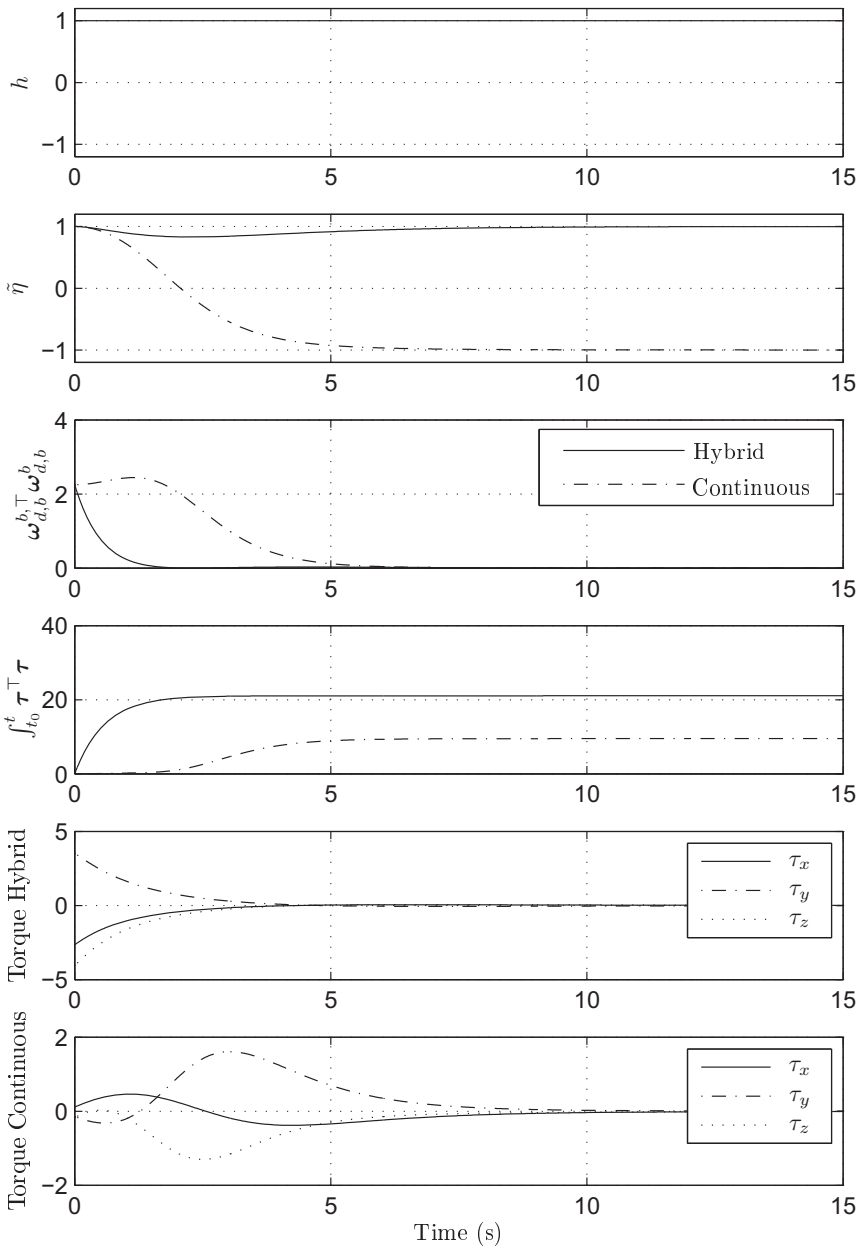

Figure 4.2: Switching value, attitude error, total angular velocity error, power consumption and actuator torque for switching and continuous sliding surface control of a rigid body. ($k_q = 1,\ k_\omega = 2,\ \boldsymbol{\omega} = 1.5\mathbf{v}$).

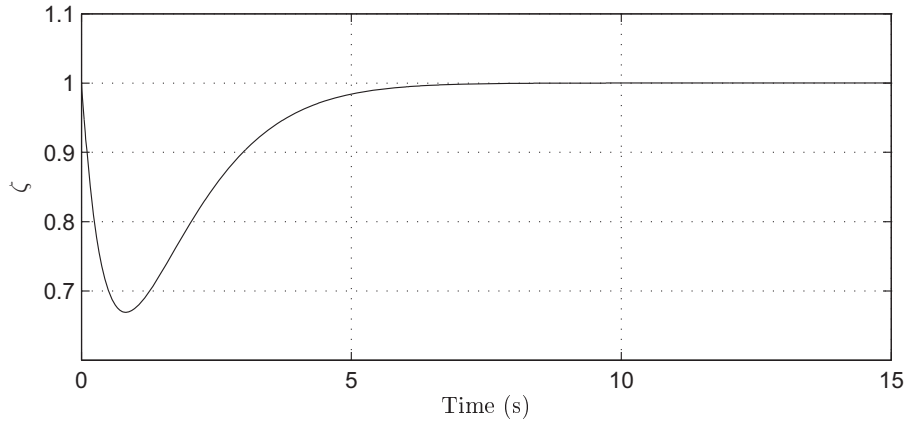

Figure 4.3: Switching criterion evolving over time.

in Figure 4.6. The performance for each controller is similar; the hybrid sliding surface controller lead to slightly higher power consumption and slower transient. Yet, regarding instant-power overshoot, it is worth remarking that the maximal torque required from the actuators was a little smaller as can be seen in Figure 4.7.

In a second run of simulations we introduced measurement noise and input disturbances. The simulation time was set to one orbital period (5896 s) to show the effect of the noise and disturbances on the error functionals. The results are summarized in Table 4.3. The attitude and angular velocity errors were very similar to those showed in Figure 4.6 and therefore is not showed here. The difference is better appreciated in regards to the input torques; see Figure 4.8. As it may be expected, supervisory control again yielded the lowest power consumption. One important property which should be noted is that for the controller working far away from the equilibrium the gains are picked large while the controller working close to the equilibrium has smaller gains. This strategy is not too different from the control strategy presented in Section 3.3 where the variable terms in the gains caused the same effect, though in a continuous manner, but the result of reduced sensibility to measurement noise is similar.

4.4.3 Output feedback control

In this section we show that the controller presented in Section 4.3 works properly. For our simulations we have chosen the initial conditions as $\mathbf{q}_{i,b}(t_0) = [1,\ 0,\ 0,\ 0]$, $\boldsymbol{\omega}^b_{i,b} = [4,\ 0.2,\ -0.3]^\top$, $h(t_0) = 1$, $\mathbf{z}(t_0) = [0,\ 0,\ 0]^\top$ and $\mathbf{q}_{i,e}(t_0) = \mathbf{q}_{i,b}(t_0)$, controller and estimator gains as $k_p = 1$, $k_d = 3$, $l_p = 40$, $l_d = 25$, and switching variables as $\delta_m = 0.1$ and $\delta_\eta = 0.9$. The spacecraft was commanded to follow smooth sinusoidal trajectories around the origin with velocity profile

$$\boldsymbol{\omega}^i_{i,d} = [3.2\cos(2\times10^{-3}t),\ 0.12\sin(1\times10^{-3}t), \\ -3.2\sin(4\times10^{-3}t)]^\top \times 10^{-6}\ \text{rad/s}. \tag{4.41}$$

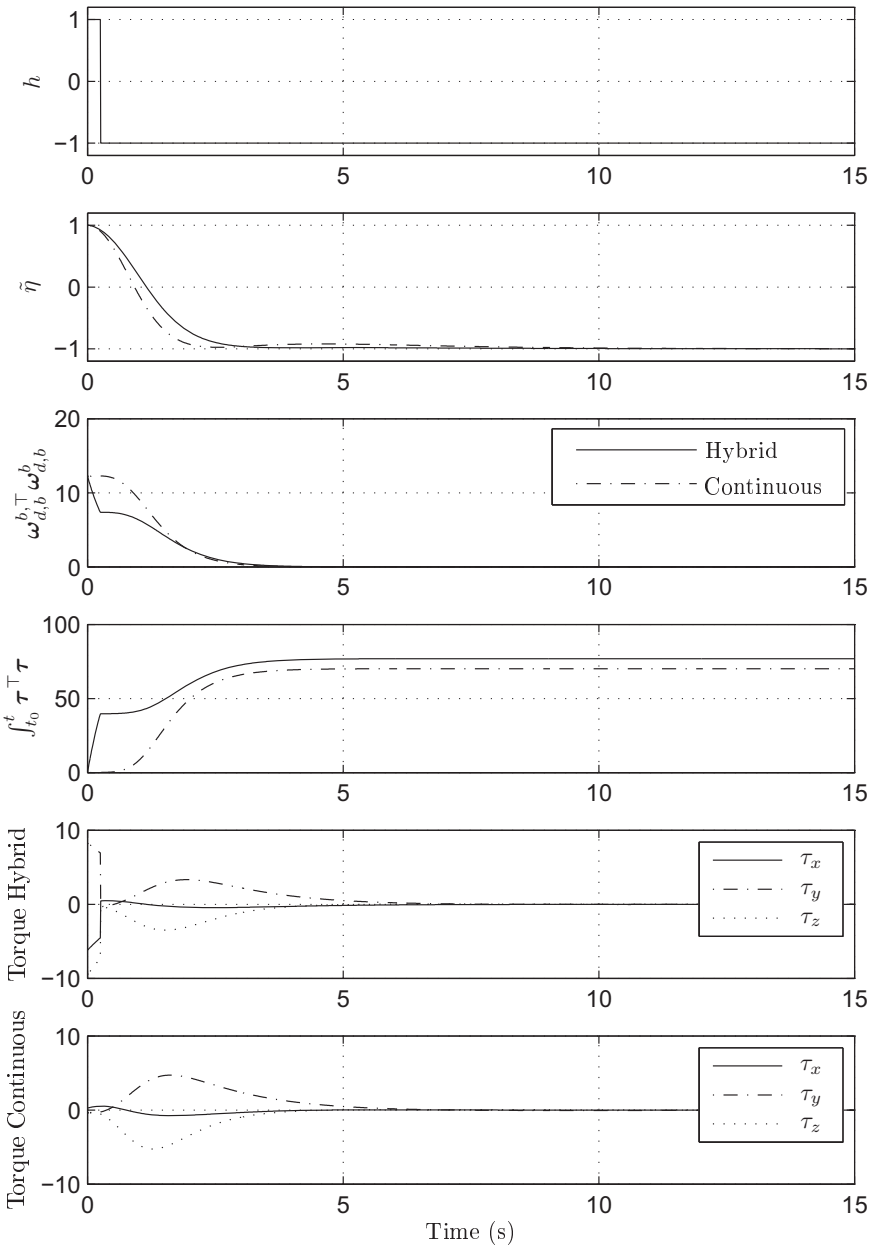

Figure 4.4: Switching value, attitude error, total angular velocity error, power consumption and actuator torque for switching and continuous sliding surface control of a rigid body. ($k_q = 1,\ k_\omega = 2,\ \boldsymbol{\omega} = 3.5\mathbf{v}$).

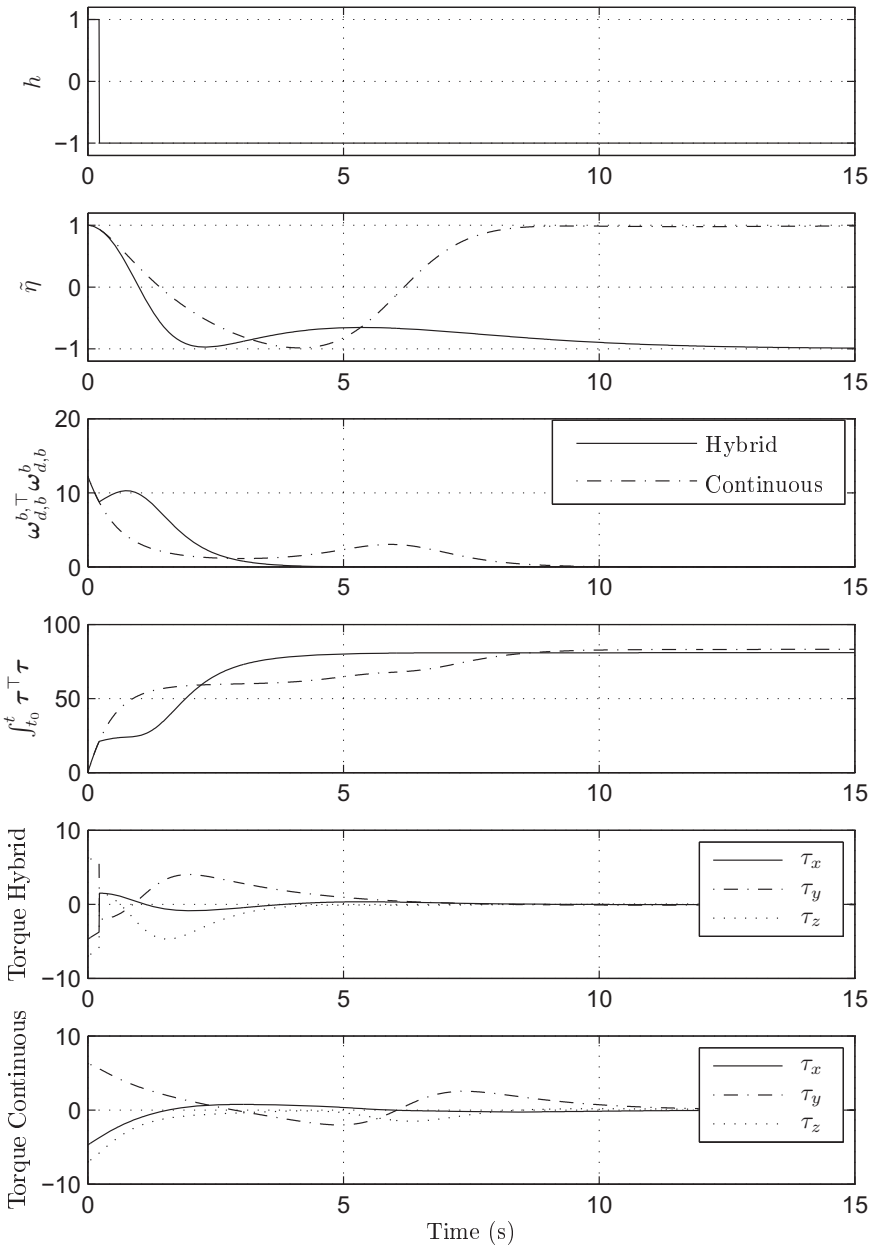

Figure 4.5: Switching value, attitude error, total angular velocity error, power consumption and actuator torque for switching and continuous sliding surface control of a rigid body. ($k_q = 1,\ k_\omega = 1,\ \boldsymbol{\omega} = 3.5\mathbf{v}$).

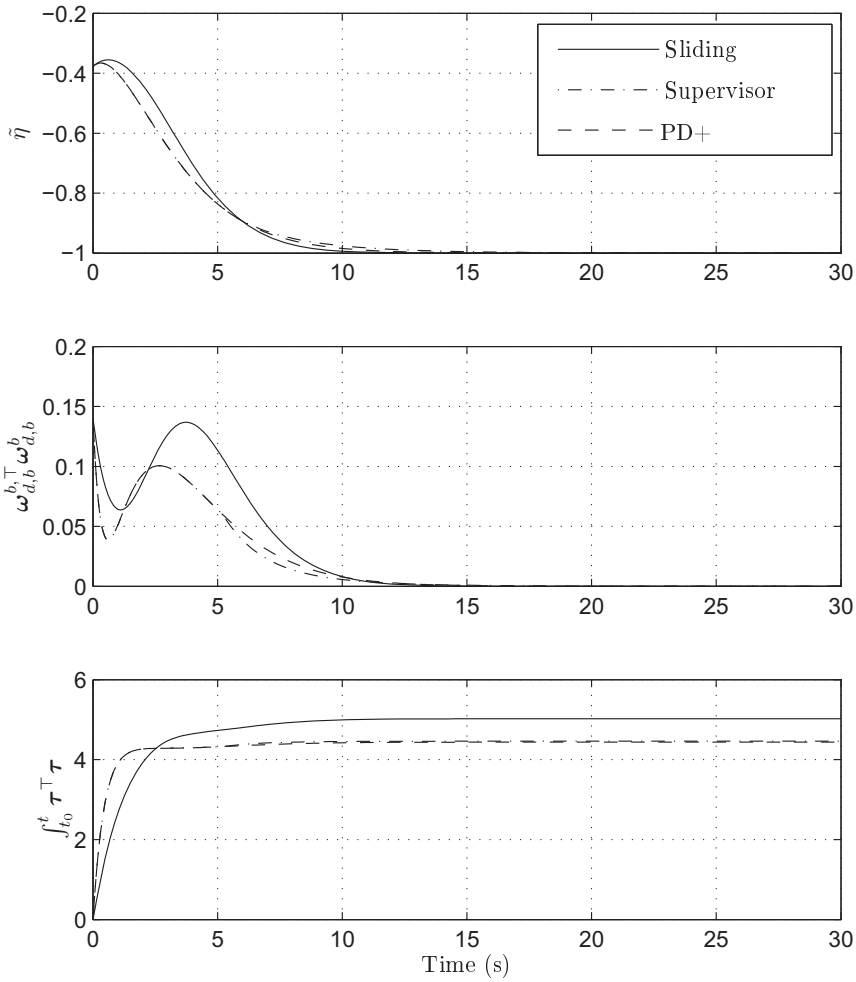

Figure 4.6: Attitude and angular velocity error, and power consumption using sliding surface, PD+ and combination of both by supervisory control during spacecraft rotational maneuver.

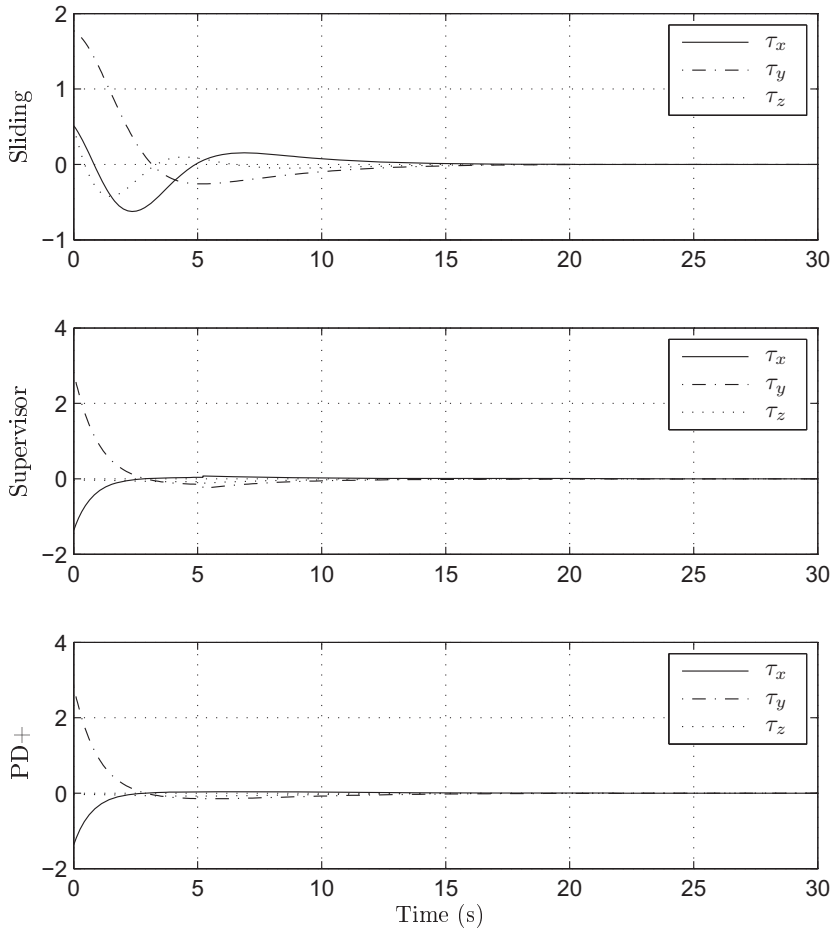

Figure 4.7: Control torque using sliding surface, PD+, and combination of both by supervisory control during spacecraft rotational maneuver.

The simulation results are depicted in Figure 4.9 and show that the large initial velocity error provoked switching for both the dynamical system and the observer after about 1 s and 0.4 s, respectively, as can be seen in the topmost plot, which means that h is set to -1 and $\eta_{e,b}$ is set to 1, respectively. In the second plot it is shown that the angular velocity of the body frame relative to the estimated frame converges faster than the angular velocity of the body frame relative to the desired frame, as is expected since from (B.223) we observe that $l_d > k_d$ and we can expect that in most cases $l_p^\star > k_d^\star$. When both angular velocity errors have converged, we conclude that also $\boldsymbol{\omega}_{d,e}^b \approx \mathbf{0}^3$ since $\boldsymbol{\omega}_{d,e}^b = \boldsymbol{\omega}_{d,b}^b - \boldsymbol{\omega}_{e,b}^b$. The actuator torques are depicted in the bottommost plot where it can be seen that the applied torques were

[3]We denote approximate zero because unknown disturbances and measurement noise are added.

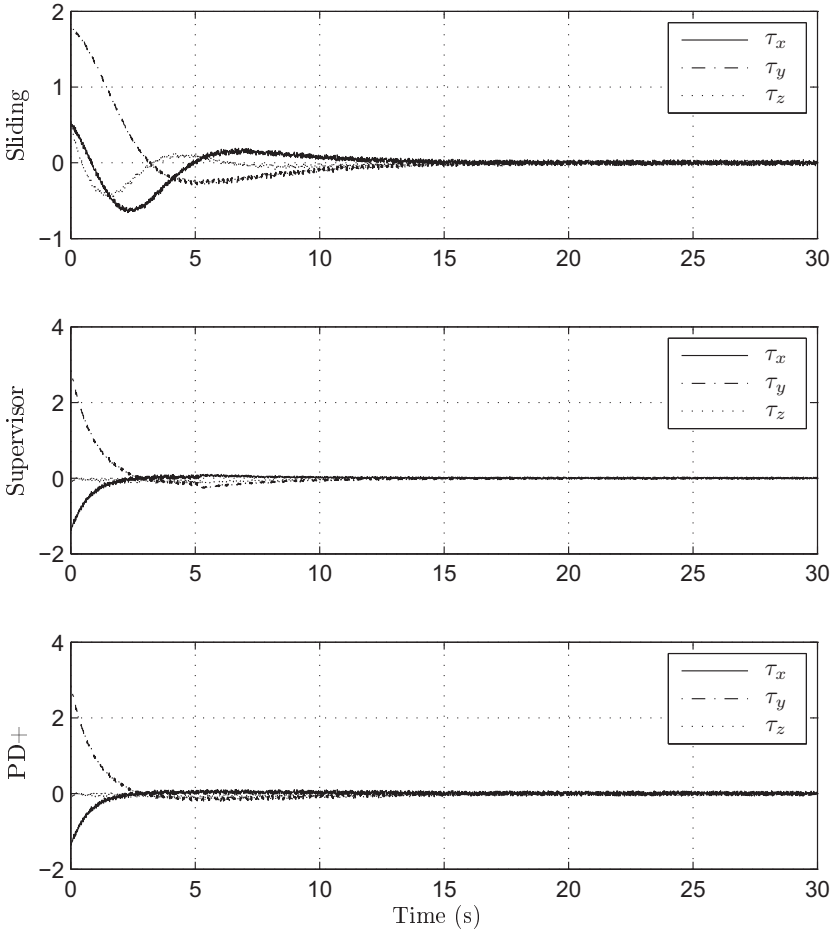

Figure 4.8: Control torque using sliding surface, PD+ and combination of both by supervisory control during spacecraft rotational maneuver including noise and disturbances.

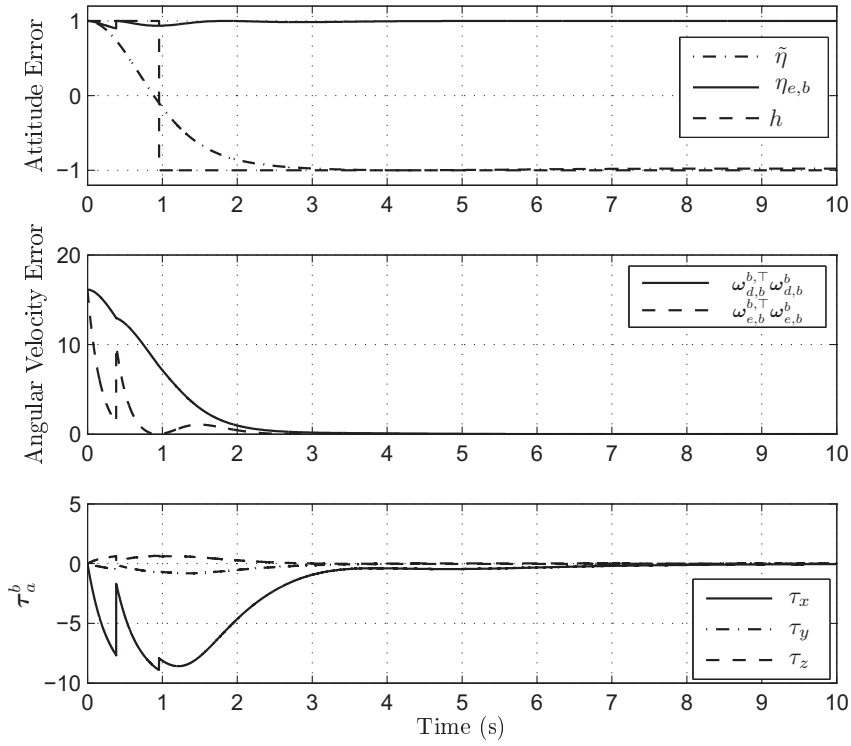

Figure 4.9: Attitude error, angular velocity error and control torque during spacecraft maneuver with hybrid PD+ based output feedback tracking controller.

consequently reduced after each jump. Note that if $\eta_{e,b}(t_0) < \delta_\eta$, then $\mathbf{x}(t_0) \in D_2$ which will provoke a switch before any control torque is calculated, thus $\dot{V}(\mathbf{x})$ is negative and the same is then also true for $\dot{\mathcal{V}}(\mathbf{x})$ for all time (see Appendix B.18 for details).

Chapter 5

Considerations choosing attitude equilibrium point

Based on the discussion in Section 3.1, in general three different strategies are presented for stabilization of the attitude equilibrium points; continuous feedback with choice of either shortest path, almost any initial condition (almost "global" stability) and through hybrid feedback. For a system which is standstill at t_0, the equilibrium point leading to the shortest path is the obvious best choice, but the problem at hand gets more complicated when initial angular velocity is introduced. In Section 5.1 we present a motivating example of a cart moving along a line to give a better understanding of the problem. Next, we analyze the system behavior of rigid body attitude control by an extensive amount of simulations to look for patterns leading to general rules in Section 5.2, and then we utilize an optimization technique to find the optimal equilibrium point based on a cost function in Section 5.3. In Section 5.4 we present simulation results showing that the proposed schemes are able to predict which choice of equilibrium leads to the cheapest rotation based on energy consumption. The results presented in this chapter are based on (Schlanbusch *et al.*, 2010*e*,*d*).

5.1 Cart example

To clearly illustrate the main motivation of this topic, we present an example where a cart needs to choose between two ending points causing the cheapest travel as illustrated in Figure 5.1. The dynamics of a cart moving in one direction without influence of friction is expressed as $F = ma$, where F is the control force, m is the mass of the cart, and a is the acceleration. The velocity of the cart is expressed as the time derivative of the position, which leads to the state space representation

$$\dot{x}_1(t) = x_2(t) \ , \quad \dot{x}_2(t) = \frac{1}{m} u(t) \ , \tag{5.1}$$

where $x_1(t)$ is the position and $x_2(t)$ the velocity of the cart, and $u(t)$ is the control signal. The initial states of the cart at t_0 are given as $x_1(t_0) = x_{10}$ and $x_2(t_0) = x_{20}$, and the final states at t_f are $x_1(t_f) = x_{1f}$ and $x_2(t_f) = x_{2f}$ for simplicity of

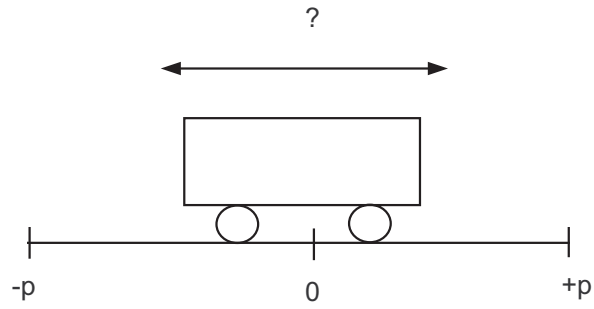

Figure 5.1: Cart moving along a line, a linear view of traveling on a circle.

notation. Assume that the cart starts at a position restricted by $-p \leq x_{10} \leq p$, where $p \in \mathbb{R}\backslash\{0\}$ is an arbitrary distance. The problem is to find which way the cart should be moving, either towards $-p$ or p to minimize the position error at time t_f and energy consumption for the total maneuver, *–cf.* Appendix A.4 for a short review on solving linear optimal control problems. This is done by considering two cost functionals, one for each ending point

$$J = \frac{1}{2}q(x_{1f} \pm p)^2 + \int_{t_0}^{t_f} \frac{1}{2}ru^2 dt \ , \tag{5.2}$$

where q and r are weighting constants. The final value of the adjoint vector is

$$\boldsymbol{\lambda}(t_f) = \begin{bmatrix} q(x_{1f} \pm p) \\ 0 \end{bmatrix} = \begin{bmatrix} \lambda_1(t_f) \\ \lambda_2(t_f) \end{bmatrix}, \tag{5.3}$$

while the differential equation that describes the time history of the adjoint vector is according to (A.63)

$$\dot{\boldsymbol{\lambda}}(t) = -\begin{bmatrix} 0 & 0 \\ 1 & 0 \end{bmatrix}\begin{bmatrix} \lambda_1(t) \\ \lambda_2(t) \end{bmatrix} - \begin{bmatrix} 0 \\ 0 \end{bmatrix} = -\begin{bmatrix} 0 \\ \lambda_1(t) \end{bmatrix}. \tag{5.4}$$

Solving (5.4) by integration from t_f to t, results in

$$\lambda_1(t) = \lambda_1(t_f) + \int_{t_f}^{t} (0)dt = q(x_{1f} \pm p) \tag{5.5}$$

$$\lambda_2(t) = \lambda_2(t_f) - \int_{t_f}^{t} \lambda_1(t)dt = q(x_{1f} \pm p)(t_f - t), \tag{5.6}$$

and then the control history is found by applying (A.64), such that

$$ru(t) + \begin{bmatrix} 0 & \frac{1}{m} \end{bmatrix}\begin{bmatrix} q(x_{1f} \pm p) \\ q(x_{1f} \pm p)(t_f - t) \end{bmatrix} = 0$$

$$u(t) = -\frac{q}{rm}(x_{1f} \pm p)(t_f - t). \tag{5.7}$$

Inserting the control signal (5.7) into the dynamics of (5.1), leads to

$$\dot{\mathbf{x}}(t) = \begin{bmatrix} 0 & 1 \\ 0 & 0 \end{bmatrix} \mathbf{x}(t) - \begin{bmatrix} 0 \\ \frac{q}{rm^2}(x_{1f} \pm p)(t_f - t) \end{bmatrix}, \tag{5.8}$$

and solving (5.8) for the final position at $t = t_f$ yields

$$x_{1f} = \frac{x_{10} + x_{20}(t_f - t_0) \pm pT}{1 + T}, \tag{5.9}$$

where

$$T = \frac{q}{rm^2}\left[-\frac{1}{3}t_f^3 + t_f^2 t_0 - t_f t_0^2 + \frac{1}{3}t_0^3\right]. \tag{5.10}$$

We define the ending position error as $\tilde{x}_\pm = |\pm p - x_f|$, and assume that the cart starts standstill at $x_{10} = 0$ where $t_0 = 0$ with $q = r = m = 1$, $p = 100$ and $t_f = 10$. This gives an error of 0.3009 for both $\pm p$, in other words it is indifferent which way the cart moves, which seems logical. If the cart starts standstill at $x_{10} = 10$ the error for $-p$ is 0.3310 while for p it is 0.2708, which means that the closest point is the optimal one, which also seems logical. If the cart now starts at the exact same spot but has an initial velocity of $x_{20} = -3$ we get an error of 0.2407 for $-p$ while 0.3611 for p. Hence, because of the initial velocity the farthest point is the optimal one. To verify the results we ran simulation for both the positive and negative p with (5.7) as control signal, which can be seen in Figure 5.2 where we see that both points are reached at the specified time although the initial velocity makes $-p$ the preferable ending point as can be seen from the total applied control signal. Note that the above example easily can be extended to also include ending velocity as well.

5.2 Statistical choice of equilibrium point

In this section we present a scheme developed to choose the favorable equilibrium point based on statistical analysis such that the criteria described as

$$J = \min\{J_{p+}, J_{p-}\} \tag{5.11}$$

is satisfied where $J_{p\pm}$ is called a *performance functional* defined as

$$J_{p\pm} = \int_{t_0}^{t_f} \boldsymbol{\tau}_a^\top(\mathbf{e}_{q\pm})\boldsymbol{\tau}_a(\mathbf{e}_{q\pm})dt, \tag{5.12}$$

where t_0 and t_f are the respective start- and end-time of the maneuver. Notice that the argument $\mathbf{e}_{q\pm}$ now is used to denote if the positive or negative equilibrium is chosen according to $\mathbf{e}_{q\pm} = [1 \mp \tilde{\eta},\ \tilde{\boldsymbol{\epsilon}}^\top]^\top$. We start by presenting simulation results from a wide variety of randomly generated initial values, where a maneuver on $SO(3)$ is considered with desired values as $\mathbf{q}_d = [\pm 1,\ \mathbf{0}^\top]^\top$ and $\boldsymbol{\omega}_d = \dot{\boldsymbol{\omega}}_d = \mathbf{0}$ using simulation parameters as described in Section 2.8.1 utilizing the control law (3.14)

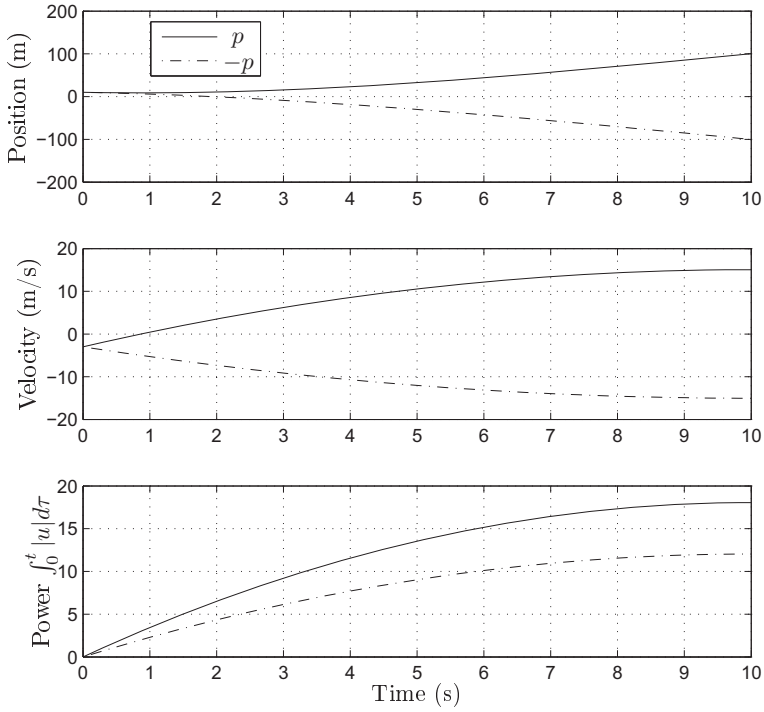

Figure 5.2: Simulation results including position, velocity and power consumption for the example cart moving towards $\pm p = \pm 100$ with initial conditions $x_{10} = 10$ and $x_{20} = -3$.

with $k_p = 1$, $k_d = 2$ constant gains. We did not apply disturbances or measurement noise.

Figure 5.3, 5.4 and 5.5 shows 1000 simulation results; each where the initial quaternion was randomly generated and initial angular velocity was generated as normal values with zero radians per second mean and standard deviation of 0.01, 0.1 and 1 rad/s respectively. We have plotted the results such that $z = 1$ and $z = -1$ if stabilization at the positive and negative equilibrium point requires least energy, respectively. From the figures we can identify some features; in essence we have obtained three different behaviors: in Figure 5.3 the distribution of preferred equilibrium points is such that $\tilde{\eta}$ is the dominant part, in Figure 5.4 we see that choice of preferred equilibrium is dominated by the $\dot{\tilde{\eta}}$ parameter, while in Figure 5.5 the preferred equilibrium is opposed to the initially closer one.

The ideal approach is to use one single function to describe the behavior of the system; a positive result would indicate that the positive equilibrium is preferable while a negative result would indicate that the negative equilibrium is preferable. However, since we have detected three different behaviors we split into three dif-

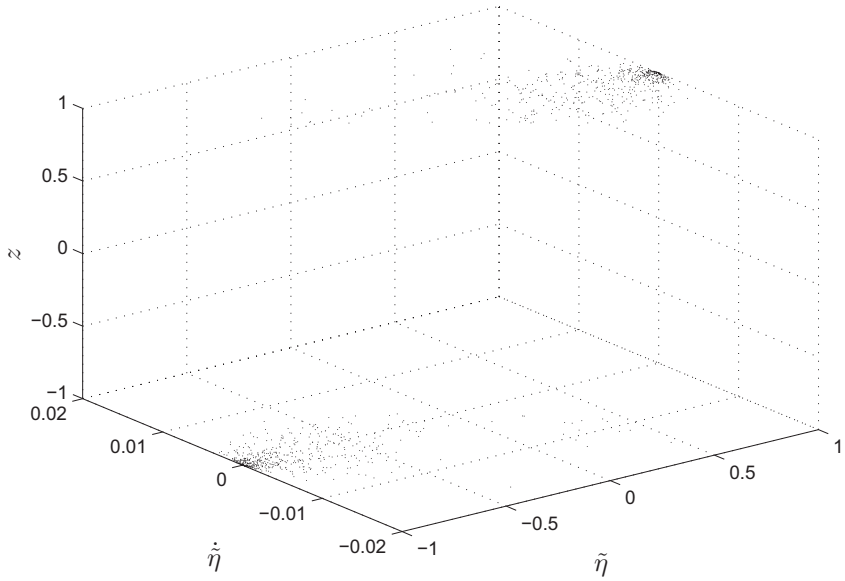

Figure 5.3: Simulation results from random initial values with 0.01 rad/s standard deviation for angular velocity.

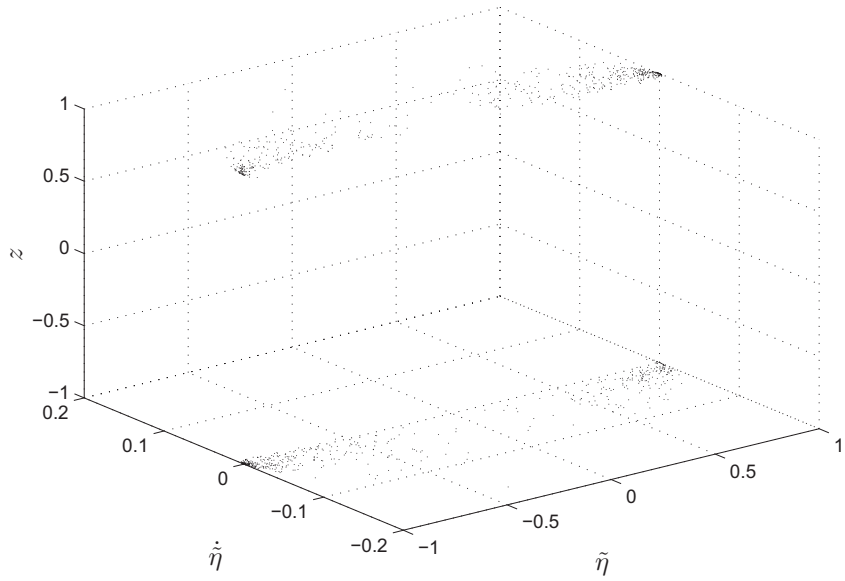

Figure 5.4: Simulation results from random initial values with 0.1 rad/s standard deviation for angular velocity.

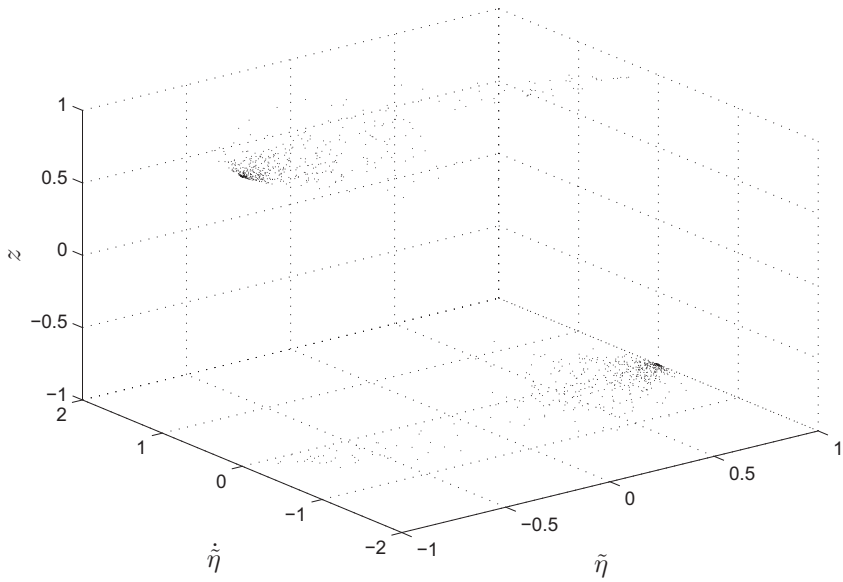

Figure 5.5: Simulation results from random initial values with 1 rad/s standard deviation for angular velocity.

ferent rules depending on the initial angular velocity. Case 1 is for small initial angular velocities and the choice is made according to

$$\mathbf{e}_q = \begin{cases} \mathbf{e}_{q+} & \text{if} \quad k_{\tilde{\eta}}\tilde{\eta}(t_0) + k_{\dot{\tilde{\eta}}}\dot{\tilde{\eta}}(t_0) \geq 0 \\ \mathbf{e}_{q-} & \text{if} \quad k_{\tilde{\eta}}\tilde{\eta}(t_0) + k_{\dot{\tilde{\eta}}}\dot{\tilde{\eta}}(t_0) < 0 \end{cases}, \tag{5.13}$$

where $\tilde{\eta}(t_0)$ and $\dot{\tilde{\eta}}(t_0)$ are initial values, and $k_{\tilde{\eta}}$ and $k_{\dot{\tilde{\eta}}}$ could be considered as scaling constants. The idea is to tune the gains based on trial and error or statistical analysis such that we obtain the equilibrium point from (5.13) that results in fulfillment of (5.11).

As simulation results show in Figure 5.3, (5.13) leads to a good approximation for small $\mathbf{e}_\omega(t_0)$, while when larger initial angular velocities are considered (Case 2), as can be seen in Figure 5.4, the system tends to prefer the equilibrium point based solely on $\dot{\tilde{\eta}}(t_0)$; a plane is splitting up the accumulated points through $\dot{\tilde{\eta}}(t_0) = 0$ and thus an alternative function for choosing equilibrium point can be expressed as

$$\mathbf{e}_q = \begin{cases} \mathbf{e}_{q+} & \text{if} \quad \dot{\tilde{\eta}}(t_0) > 0 \\ \mathbf{e}_{q-} & \text{if} \quad \dot{\tilde{\eta}}(t_0) < 0 \end{cases} \quad \forall\ \dot{\tilde{\eta}}(t_0) \neq 0, \tag{5.14}$$

while for $\dot{\tilde{\eta}}(t_0) = 0$ we choose according to

$$\mathbf{e}_q = \begin{cases} \mathbf{e}_{q+} & \text{if} \quad \tilde{\eta}(t_0) \geq 0 \\ \mathbf{e}_{q-} & \text{if} \quad \tilde{\eta}(t_0) < 0 \end{cases}, \tag{5.15}$$

When even larger initial angular velocities are considered, the system tends to prefer the opposite equilibrium compared to $\tilde{\eta}(t_0)$ independently to the sign of

$\dot{\tilde{\eta}}(t_0)$ as can be seen in Figure 5.5. This behavior (Case 3) can be described by the function

$$\mathbf{e}_q = \begin{cases} \mathbf{e}_{q+} & \text{if} \quad \tilde{\eta}(t_0) > 0 \\ \mathbf{e}_{q-} & \text{if} \quad \tilde{\eta}(t_0) > 0 \end{cases} \quad \forall\ \tilde{\eta}(t_0) \neq 0, \tag{5.16}$$

while for $\tilde{\eta}(t_0) = 0$ we choose according to

$$\mathbf{e}_q = \begin{cases} \mathbf{e}_{q+} & \text{if} \quad \dot{\tilde{\eta}}(t_0) \geq 0 \\ \mathbf{e}_{q-} & \text{if} \quad \dot{\tilde{\eta}}(t_0) < 0 \end{cases} . \tag{5.17}$$

The rationale for this may be explained as follows: if the system starts with an initial attitude close to the desired attitude, but the initial angular velocity is large, it is more fuel efficient to use this initial velocity to do one rotation and then stop instead of first stopping the initial rotation, reverse the rotation and then stop again at the originally closest equilibrium. What is observed in Figure 5.5 is that the system tends to favor the opposite equilibrium point even if $\dot{\tilde{\eta}} \approx 0$, in contrast with the results shown in Figure 5.3. The reason for this is the relation $\dot{\tilde{\eta}} = -0.5\tilde{\boldsymbol{\epsilon}}^\top \mathbf{e}_\omega$ which means that the system may initially have a large initial angular velocity error, but since $\tilde{\boldsymbol{\epsilon}} \approx \mathbf{0}$, it cannot be observed by the $\dot{\tilde{\eta}}$ parameter, which is similar for the switching sliding surface controller as presented and discussed in Section 4.2.2 and 4.4.1, respectively.

As we now have rules that cover all initial values we need to determine which case is appropriate based on a given set of initial values. The angular velocity seems to be a key element and therefore we suggest to introduce two "cut-off"-frequencies named ω_{c1} and ω_{c2} accordingly; dividing such that we apply: Case 1 when $\|\mathbf{e}_\omega(t_0)\| \leq \omega_{c1}$, Case 2 when $\omega_{c1} < \|\mathbf{e}_\omega(t_0)\| < \omega_{c2}$, and Case 3 when $\|\mathbf{e}_\omega(t_0)\| \geq \omega_{c2}$.

Remark 5.1 *An alternative approach is to let the goal (5.11) instead be described by a performance functional such as*

$$J_{q\pm} = \int_{t_0}^{t_f} \tilde{\boldsymbol{\epsilon}}^\top(\mathbf{e}_{q\pm})\tilde{\boldsymbol{\epsilon}}(\mathbf{e}_{q\pm})dt. \tag{5.18}$$

Then a similar technique as presented above can be used to find the equilibrium point giving the least attitude error, and furthermore, the functionals can be combined as

$$\min\left\{\theta J_{p+} + (1-\theta)J_{q+}, \theta J_{p-} + (1-\theta)J_{q-}\right\}, \tag{5.19}$$

where $0 \leq \theta \leq 1$ *is a weighting constant.*

5.3 Optimal choice of equilibrium point

As the obvious choice of equilibrium point would be to define two cost functions $J_1 = \mathbf{e}_{q+}^\top \mathbf{Q}\mathbf{e}_{q+} + \int_{t_0}^{t_f} \boldsymbol{\tau}_a^\top \mathbf{R}\boldsymbol{\tau}_a dt$ and $J_2 = \mathbf{e}_{q-}^\top \mathbf{Q}\mathbf{e}_{q-} + \int_{t_0}^{t_f} \boldsymbol{\tau}_a^\top \mathbf{R}\boldsymbol{\tau}_a dt$, where $\mathbf{Q} \in \mathbb{R}^{4\times 4} = \text{diag}\{Q_1,\ Q_2,\ Q_3,\ Q_4\}$ and $\mathbf{R} \in \mathbb{R}^{7\times 7} = \text{diag}\{R_1,\ \ldots,\ R_7\}$, and then choose the equilibrium point requiring the cheapest rotation, such that $J = \min\{J_1, J_2\}$, but this would require to solve two nonlinear optimal control problems which is far too computationally consuming for most tasks such as spacecraft attitude maneuvers;

a long computation time would change the initial conditions thus possibly ruining the end result when initial angular velocity is considered. Instead we linearize the equations of motion. The system equations can be written as

$$\dot{\tilde{\mathbf{q}}} = \mathbf{T}_e(\tilde{\mathbf{q}})\tilde{\boldsymbol{\omega}} \tag{5.20}$$

$$\mathbf{J}\dot{\tilde{\boldsymbol{\omega}}} = \boldsymbol{\tau}_a - \mathbf{S}(\boldsymbol{\omega})\mathbf{J}\boldsymbol{\omega} - \mathbf{J}\dot{\boldsymbol{\omega}}_d(t), \tag{5.21}$$

and by linearization we obtain (Schaub and Junkins, 2003)

$$\dot{\mathbf{x}}(t) \approx \mathbf{A}\mathbf{x}(t) + \mathbf{B}\boldsymbol{\tau}_a(t), \tag{5.22}$$

where $\mathbf{x}_1(t) = \tilde{\mathbf{q}}(t)$, $\mathbf{x}_2(t) = \tilde{\boldsymbol{\omega}}(t)$, $\mathbf{x}(t) = [\mathbf{x}_1(t)^\top,\ \mathbf{x}_2(t)^\top]^\top$,

$$\mathbf{A} = \frac{\partial \mathbf{f}(\mathbf{x}, \boldsymbol{\tau}_a)}{\partial \mathbf{x}}, \quad \mathbf{B} = \frac{\partial \mathbf{f}(\mathbf{x}, \boldsymbol{\tau}_a)}{\partial \boldsymbol{\tau}_a} \tag{5.23}$$

around the equilibrium points $(\tilde{\mathbf{q}}, \tilde{\boldsymbol{\omega}}) = (\pm 1,\ \mathbf{0},\ \mathbf{0})$, where

$$\mathbf{A} = \pm\frac{1}{2}\begin{bmatrix} \mathbf{0}_{4\times4} & \mathbf{0}_{1\times3} \\ \mathbf{0}_{3\times4} & \mathbf{I}_{3\times3} \\ & \mathbf{0}_{3\times3} \end{bmatrix}, \quad \mathbf{B} = \begin{bmatrix} \mathbf{0}_{4\times7} \\ \mathbf{0}_{3\times4} \quad \mathbf{J}^{-1} \end{bmatrix}. \tag{5.24}$$

By introducing an attitude error vector defined as $\mathbf{e}_{q\pm} = [1 \mp \tilde{\eta},\ \tilde{\boldsymbol{\epsilon}}^\top]^\top$ we evaluate both the positive and negative rotation around the rotational axis. Linearization causes the first row of $\mathbf{A}$ to disappear, resulting in a loss of $\tilde{\eta}$. Instead of doing the normal rotation from $\tilde{\mathbf{q}}(t_0)$ to $\tilde{\mathbf{q}} = [\pm 1,\ \mathbf{0}^\top]^\top$ we rotate by θ for the positive equilibrium and for the opposite rotation we rotate by $\psi = \theta - 2\pi$ yielding $-\tilde{\mathbf{q}}$, (see Section 2.4.4 for more on angle-axis parametrerization and Euler parameters), and thus utilize an error vector defined as $\mathbf{e}_{q\pm}(t_0) = [1 - \tilde{\eta}(t_0),\ \pm\tilde{\boldsymbol{\epsilon}}^\top(t_0)]^\top$. A cost function is defined as

$$J = \frac{1}{2}\mathbf{e}_{q\pm}^\top \mathbf{Q}\mathbf{e}_{q\pm} + \frac{1}{2}\int_{t_0}^{t_f} \boldsymbol{\tau}_a^\top \mathbf{R}\boldsymbol{\tau}_a dt, \tag{5.25}$$

the final value of the adjoint vector is found to be

$$\boldsymbol{\lambda}(t_f) = \begin{bmatrix} \mathbf{Q}\mathbf{e}_{q\pm}(t_f) \\ \mathbf{0} \end{bmatrix}, \tag{5.26}$$

and solving the adjoint vector according to (A.63) yields

$$\boldsymbol{\lambda}_1(t) = \mathbf{Q}\mathbf{e}_{q\pm}(t_f), \quad \boldsymbol{\lambda}_2(t) = \frac{1}{2}\tilde{\mathbf{Q}}\tilde{\boldsymbol{\epsilon}}_f(t_f - t), \tag{5.27}$$

where $\tilde{\mathbf{Q}} = \mathrm{diag}\{Q_2,\ Q_3,\ Q_4\}$ and $\tilde{\boldsymbol{\epsilon}}_f = \tilde{\boldsymbol{\epsilon}}(t_f)$. The control history is found by applying (A.64) resulting in

$$\mathbf{R}\boldsymbol{\tau}_a + \mathbf{B}^\top \begin{bmatrix} \mathbf{Q}\mathbf{e}_{q\pm} \\ \frac{1}{2}\tilde{\mathbf{Q}}\tilde{\boldsymbol{\epsilon}}_f(t_f - t) \end{bmatrix} = 0 \tag{5.28}$$

$$\boldsymbol{\tau}_a = -\frac{1}{2}\mathbf{R}^{-1}\begin{bmatrix} \mathbf{0} \\ \mathbf{J}^{-1}\tilde{\mathbf{Q}}\tilde{\boldsymbol{\epsilon}}_f \end{bmatrix}(t_f - t), \tag{5.29}$$

which leads to the state equation

$$\dot{\mathbf{x}}(t) = \mathbf{A}\mathbf{x} - \frac{1}{2}\mathbf{B}\mathbf{R}^{-1}\begin{bmatrix} \mathbf{0} \\ \mathbf{J}^{-1}\tilde{\mathbf{Q}}\tilde{\boldsymbol{\epsilon}}_f \end{bmatrix}(t_f - t). \tag{5.30}$$

Solving (5.30) yields

$$\mathbf{x}_2(t) = \mathbf{x}_2(t_0) - \frac{1}{2}\mathbf{J}^{-1}\tilde{\mathbf{R}}^{-1}\mathbf{J}^{-1}\tilde{\mathbf{Q}}\tilde{\boldsymbol{\epsilon}}_f\left[t_f(t-t_0) - \frac{1}{2}(t^2 - t_0^2)\right], \tag{5.31}$$

where $\tilde{\mathbf{R}} = \text{diag}\{R_5,\ R_6,\ R_7\}$, and

$$\mathbf{x}_1(t) = \mathbf{x}_1(t_0) \pm \frac{1}{2}\int_{t_0}^{t_f}\begin{bmatrix} 0 \\ \mathbf{x}_2(t) \end{bmatrix} dt\ . \tag{5.32}$$

As we are interested in finding which equilibrium point we want the dynamical system to converge to resulting in the smallest attitude error, we consider $\tilde{\boldsymbol{\epsilon}}_f$ since $\tilde{\eta}_f$ is lost, evaluated at $t = t_f$ yielding

$$\tilde{\boldsymbol{\epsilon}}_{f\pm} = \mathbf{H}^{-1}\left[\tilde{\boldsymbol{\epsilon}}_0 \pm \frac{1}{2}\tilde{\boldsymbol{\omega}}_0 t_f\right]\ , \tag{5.33}$$

where $\tilde{\boldsymbol{\epsilon}}_0 = \tilde{\boldsymbol{\epsilon}}(t_0)$ and $\tilde{\boldsymbol{\omega}}_0 = \tilde{\boldsymbol{\omega}}(t_0)$, and

$$\mathbf{H} = \mathbf{I} \pm \frac{1}{6}\mathbf{J}^{-1}\tilde{\mathbf{R}}^{-1}\mathbf{J}^{-1}\tilde{\mathbf{Q}}t_f^3\ . \tag{5.34}$$

The weighting matrices $\tilde{\mathbf{Q}}$ and $\tilde{\mathbf{R}}$ and time constant t_f should be selected such that $\text{rank}(\mathbf{H}) = 3$.

To sum up we have the following. To find the cheapest rotational direction for the system (2.82) and (2.83) in closed-loop with a state feedback control law according to the cost function (5.25) we choose the equilibrium point satisfying either $\mathbf{e}_{q+}$ if $\tilde{\eta}(t_0) \geq 0$ or $\mathbf{e}_{q-}$ if $\tilde{\eta}(t_0) < 0$ for $\tilde{\boldsymbol{\omega}}(t_0) = \mathbf{0}$, or $\mathbf{e}_{q+}$ if $\|\tilde{\boldsymbol{\epsilon}}_{f+}\| \leq \|\tilde{\boldsymbol{\epsilon}}_{f-}\|$ or $\mathbf{e}_{q-}$ if $\|\tilde{\boldsymbol{\epsilon}}_{f-}\| < \|\tilde{\boldsymbol{\epsilon}}_{f+}\|$ for $\tilde{\boldsymbol{\omega}}(t_0) \neq \mathbf{0}$, according to (5.33) and (5.34), where $\mathbf{e}_{q\pm}$ denotes positive and negative equilibrium point, respectively.

Remark 5.2 *The time constant t_f can be considered as a weighting variable between initial attitude and initial angular velocity; a large time constant tends to utilize the initial angular velocity more.*

Remark 5.3 *As our result is achieved by performing linearization of the system equations the resulting equilibrium point will not necessarily be the optimal one. Nevertheless, we observe that the preferable equilibrium is chosen in most cases when simulations of the full nonlinear model are performed, and solutions in the boundary area ($\|\tilde{\boldsymbol{\epsilon}}_{f+}\| \approx \|\tilde{\boldsymbol{\epsilon}}_{f-}\|$) tends to provide little saving of power consumption or none at all if either point is chosen compared to the other.*

Remark 5.4 *It is assumed that the rigid body has available torque and is tuned to stop the rotation at the chosen equilibrium point given the initial conditions.*

5.4 Simulation results

In this section we present simulation results based on the two different schemes of finding the cheapest rotation from an energy consumption point of view as presented in this section. We utilize simulation data as presented in Section 2.8.1 if otherwise is not stated.

5.4.1 Statistical method

In the following, results are presented to illustrate the performance of our equilibrium test by presenting simulation results of a rigid body with arbitrary initial values, where power consumption is compared for both equilibrium points according to (5.11). The simulations were performed using the same parameters as described in Section 5.2 except for the standard deviation which was varying for the different simulations. The simulations were performed in the following way: first the initial values were randomly generated, and we proceeded by predicting which equilibrium was the preferable according to the rules in Section 5.2. Subsequently, two maneuvers were performed utilizing the control law (3.14); one for each equilibrium, and the preferable equilibrium, that is, the equilibrium leading to the cheapest maneuver was noted and compared with the prediction.

We start by presenting simulation results for a single case as an example. For all simulations the following parameters were used: $k_{\tilde{\eta}} = 1$, $k_{\dot{\tilde{\eta}}} = 70$, $\omega_{c1} = 0.1$ and $\omega_{c2} = 0.4$. The initial values were chosen as $\mathbf{q}(t_0) = [-0.3772, \ -0.4329, \ 0.6645, \ 0.4783]^\top$ and $\boldsymbol{\omega}(t_0) = [0.0212, \ -0.0283, \ 0.0354]^\top$. Since the initial angular velocity $\|\boldsymbol{\omega}(t_0)\| = 0.05 < \omega_{c1}$ we applied the rule in Case 1. Using (5.13) and (3.2) we obtain $1 \cdot (-0.3772) - 70 \cdot 0.5 \cdot [-0.4329, \ 0.6645, \ 0.4783][0.0212, \ -0.0283, \ 0.0354]^\top = 0.0096 \geq 0$. Thus the positive equilibrium point should give the cheapest rotation, and therefore we chose $\mathbf{e}_{q+} = \mathbf{e}_q$. The simulation results including attitude error, angular velocity error, power consumption and control torque are depicted in Figures 5.6 and 5.7, and we find that even if the negative equilibrium point was initially the closest, the maneuver using the positive equilibrium point lead to the cheapest rotation, as expected from the calculation. It is also interesting to note that the positive rotation was performed with a smaller peak torque, which is preferable especially in cases when actuator saturation is introduced.

The simulation results for statistically purposes are summarized in Table 5.1 where the three different cases were simulated using standard deviation for the randomized angular velocities of 0.01, 0.1 and 1 rad/s for case 1, 2 and 3 respectively. The simulation denoted total was performed using varying standard deviation in equal steps from 0.01 to 1.5 rad/s during 100,000 consecutive runs. As can be seen, each simulation were run numerous times and 'Hits' are the number of times we were able to predict which equilibrium point that gave the cheapest rotation. The percentage of hits for all cases and the number of runs indicate that there is a relationship between prediction and actual results.

Remark 5.5 *It should be noted that the presentations and discussions presented in this section are based on maneuvers with well-defined initial moments tracking*

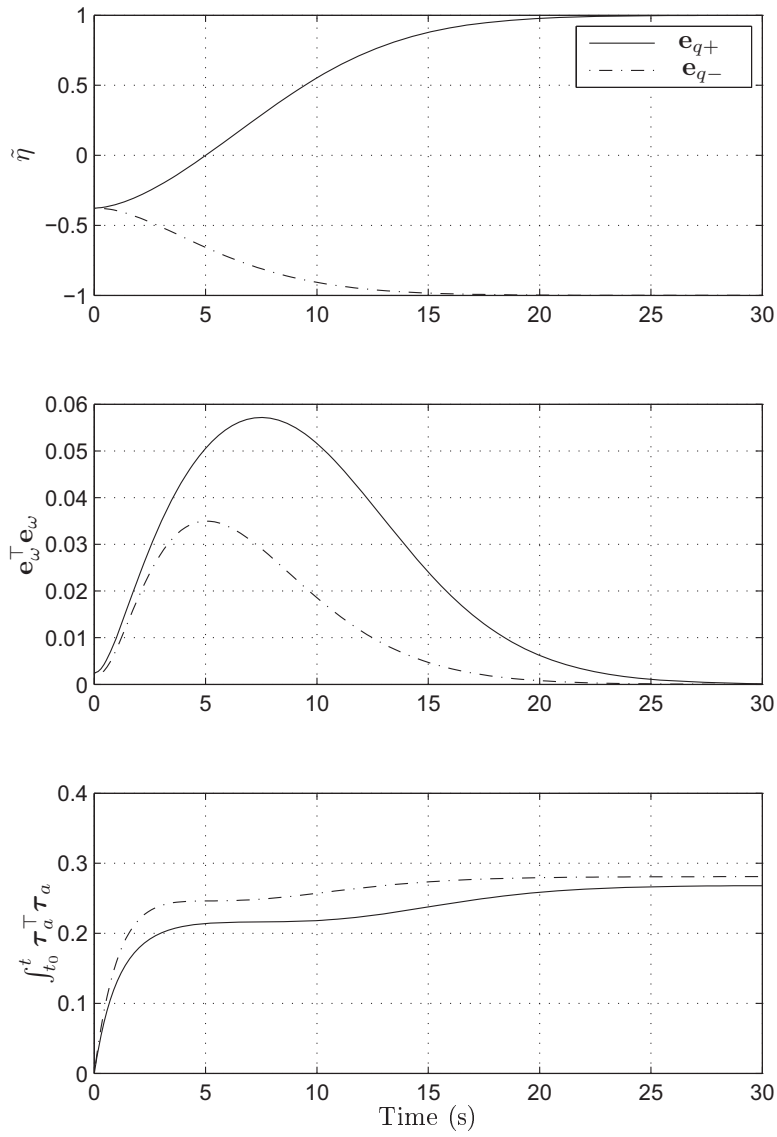

Figure 5.6: A comparison of attitude, angular velocity and power consumption for attitude maneuver of a rigid body using both positive and negative equilibrium.

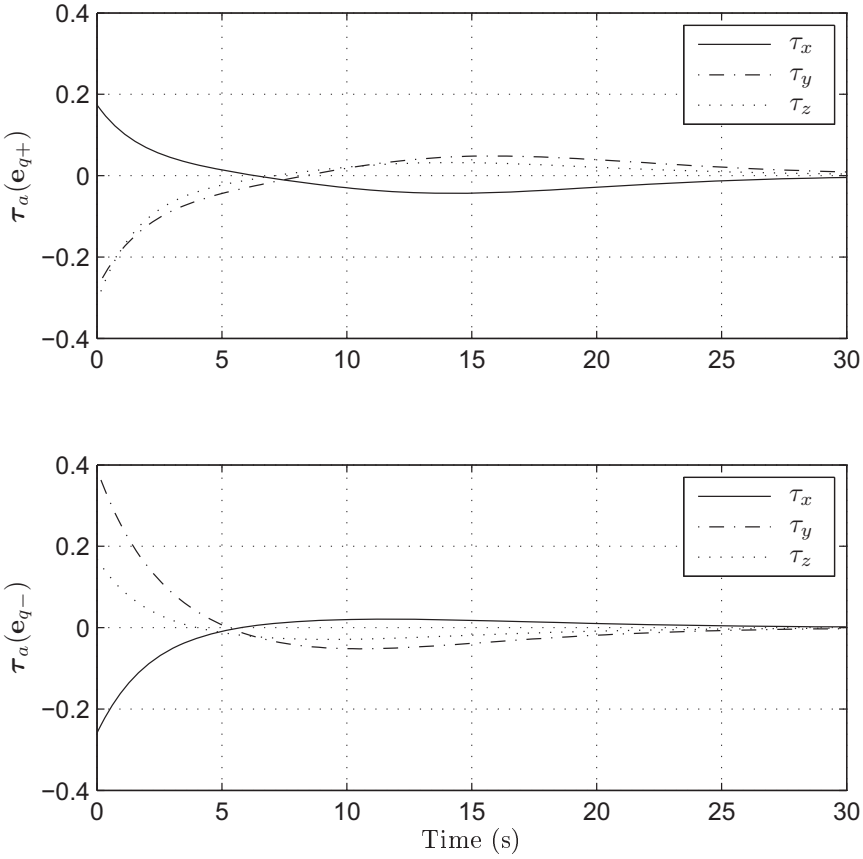

Figure 5.7: A comparison of control torques for attitude maneuver of a rigid body using both positive and negative equilibrium point.

Table 5.1: Simulation results.

	Trials	Hits	Percentage
Case 1	10,000	9969	99.7%
Case 2	10,000	8554	85.5%
Case 3	10,000	9201	92.0%
Total	100,000	89,234	89.2%

Table 5.2: Initial values and results for three set of simulations predicting optimal equilibrium point.

	Sim. 1	Sim. 2	Sim. 3
ϕ [deg]	180	0	30
θ [deg]	0	90	-130
ψ [deg]	0	0	150
ω_x [rad/s]	0.01	0.01	-0.01
ω_y [rad/s]	0	0	0.04
ω_z [rad/s]	0	0	0.02
$\|\epsilon_{f+}\|$	8.12×10^{-3}	5.10×10^{-3}	7.82×10^{-3}
$\|\epsilon_{f-}\|$	6.09×10^{-3}	5.18×10^{-3}	9.39×10^{-3}
P_{f+}	0.3358	0.1402	0.3015
P_{f-}	0.2923	0.2221	0.3109

a given reference where the equilibrium point is chosen in advance of the maneuver. However, if the control goal is tracking of a given reference, also running the presented algorithms continuously, care should be taken. This is because if we end up with situations where the result of (5.13) ≈ 0 *and by adding a suitable amount of measurement noise, the system might theoretically get stuck for infinite time switching between the equilibrium points. This problem can be solved by introducing hysteresis, but will lead to a result more similar to switching control* –cf. *(Liberzon, 2003).*

5.4.2 Optimal method

In the following, the performance of our equilibrium test is illustrated by presenting simulation results of a rigid body with arbitrary initial values, where power consumption were compared for both equilibrium points. Again, the controller (3.14) was utilized with gains chosen as $k_p = 1$, $k_d = 2$, the simulation time was chosen as $t_0 = 0$ and $t_f = 30$ and all disturbances were omitted to better illustrate the purpose of the scheme.

All simulation results are summarized in Table 5.2 where we have presented the initial attitude as Euler angles in degrees to give a better understanding of the physical orientation and initial angular velocities. The total power consumption was calculated using $P_{f\pm} = \int_{t_0}^{t_f} \boldsymbol{\tau}_{\pm}^{\top}\boldsymbol{\tau}_{\pm}dt$ for choosing the positive and negative equilibrium point, and $\|\boldsymbol{\epsilon}_{f\pm}\|$ was found according to (5.33). We do not present simulation results without initial velocities because the result is obvious; shortest rotation gives cheapest maneuver.

The results from the first simulation is presented in Figure 5.8 where the quantity of initial rotational error was equal for both equilibrium points, but with a small initial velocity favoring the negative equilibrium point. Choosing the optimal equilibrium gave 14.88 % energy saving which is a considerable amount especially for applications such as spacecraft maneuvers where the fuel cost is extremely high.

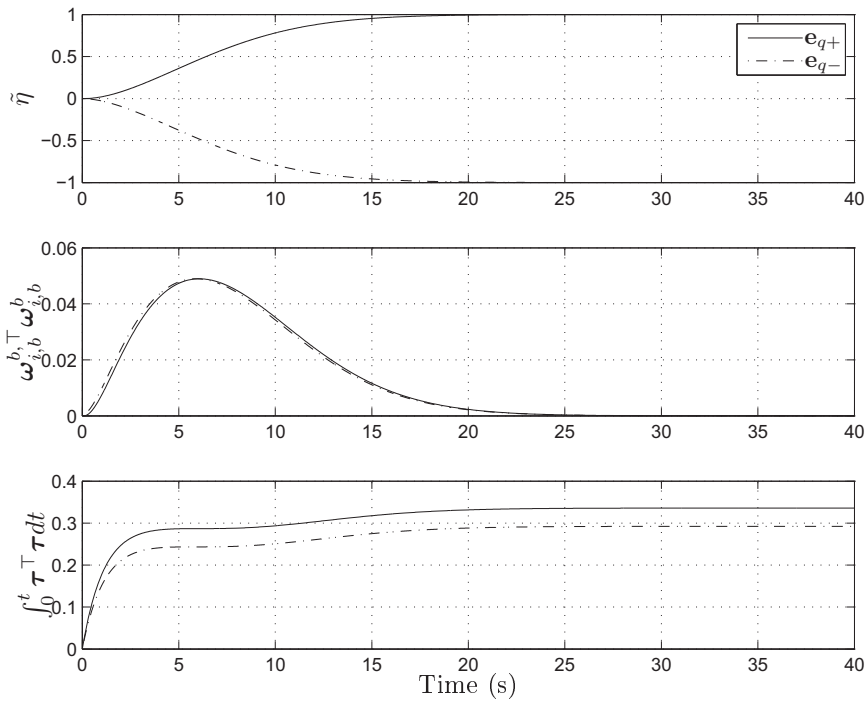

Figure 5.8: Comparison in power consumption between choosing positive and negative equilibrium during an attitude maneuver where rotational error is equal but with initial angular velocity error of $\tilde{\boldsymbol{\omega}} = [0.01,\ 0,\ 0]^\top$.

The results from the second simulation is presented in Figure 5.9 showing a maneuver where the positive equilibrium had the shortest path and the initial velocity was about a different axis. The result shows that the positive equilibrium also was the optimal one, which is of no surprise.

In the third simulation presented in Figure 5.10 we chose an arbitrary attitude and angular velocity where it apparently is hard to tell which equilibrium is the optimal one. Even though the path length for the positive equilibrium was larger and the angular velocity was higher during all parts of the simulation, it was confirmed that the positive equilibrium was the optimal equilibrium and resulted in 3.12 % energy saving.

The choice of optimal equilibrium tends to favor the positive equilibrium point when small initial angular velocities are considered combined with a low value for t_f, even if the path length is larger. An initial value of $\boldsymbol{\omega} = [10^{-4},\ 0,\ 0]^\top$ using initial attitude as in the first simulation will favor the positive equilibrium even if the negative is the optimal, but simulation result shows that the energy consumption is 0.3138 and 0.3134 for the positive and negative equilibrium point respectively, only a 0.13 percent difference. By increasing to $t_f = 300$ s the switch of equilibrium point is moved down to about $\boldsymbol{\omega} = [10^{-8},\ 0,\ 0]^\top$ before the non-optimal is chosen,

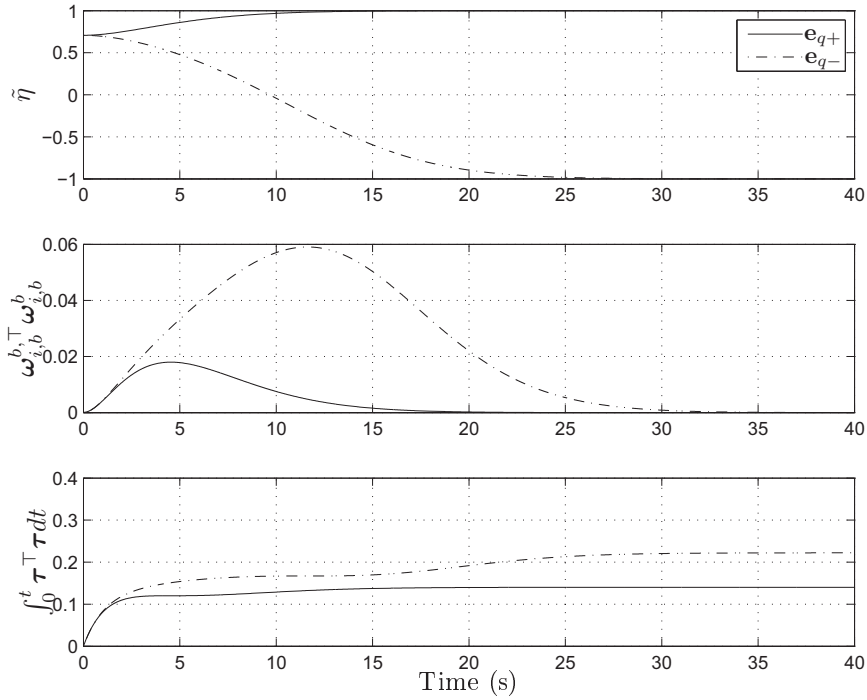

Figure 5.9: Comparison in power consumption between choosing positive and negative equilibrium during an attitude maneuver where with initial rotational and angular velocity error of $\tilde{\mathbf{q}} = [\sqrt{2},\ 0,\ \sqrt{2},\ 0]^\top$ and $\tilde{\boldsymbol{\omega}} = [0.01,\ 0,\ 0]^\top$.

which will result in theoretical difference in energy consumption.

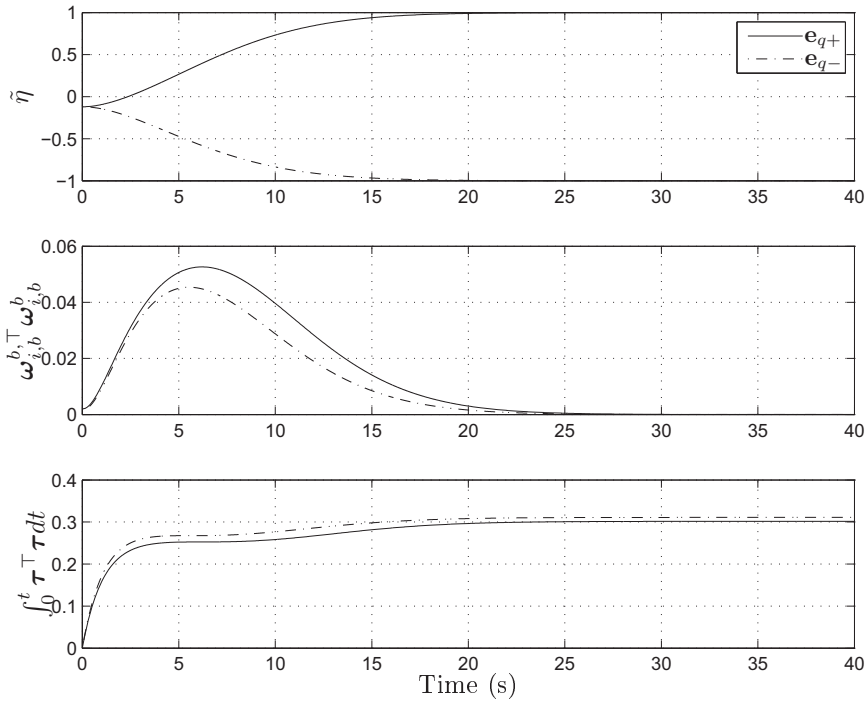

Figure 5.10: Comparison in power consumption between choosing positive and negative equilibrium during an attitude maneuver where with initial rotational and angular velocity error of $\tilde{\mathbf{q}} = [-1.209,\ 0.8739,\ -0.1209,\ 0.4550]^\top$ and $\tilde{\boldsymbol{\omega}} = [-0.01,\ 0.04,\ 0.02]^\top$.

Part III

Applications

Chapter 6

Leader-follower synchronization

In this chapter we present two different results on synchronization. First, we start by introducing the problem formulation in Section 6.1, and then continue in Section 6.2 by presenting two different control laws for attitude synchronization of two rigid bodies based on the framework of cascaded systems presented in Appendix A.5. In Section 6.3 we study the synchronization problem of two spacecraft in leader-follower formation for both translational and rotational control where a hybrid solution is incorporated for the latter. One main difference is that in Section 6.2 we show that two similar systems can be synchronized via control, while in Section 6.3 we work on relative coordinates. Furthermore, in Section 6.4 we extend the results using exponential gains presented in Section 3.3 for translational control where each axis is weighted differently and also include I^2 action in the control law to reduce the residual for constant mean disturbances. In the end we present simulation results in Section 6.5 to verify our results along with discussions. The results presented in this chapter are based on (Schlanbusch *et al.*, 2011*a*; Schlanbusch and Nicklasson, 2011).

6.1 Synchronization problem formulation

The control problem at hand is a combined tracking and synchronization problem, that is, we want the leader to track a certain reference $\mathbf{q}_d(t) \in S^3$ as presented in Section 3.1, that is, we want the state $\mathbf{q}_l \in S^3$ and $\boldsymbol{\omega}_{i,lb}^{lb} \in \mathbb{R}^3$ to fulfill (3.7) and (3.8), respectively, while at the same time, we want the follower rigid body represented by the states $\mathbf{q}_f \in S^3$, $\boldsymbol{\omega}_{i,fb}^{fb} \in \mathbb{R}^3$ to synchronize with its leader such that

$$\lim_{t\to\infty} \tilde{\boldsymbol{\epsilon}}_f \to \tilde{\boldsymbol{\epsilon}}_l \Leftrightarrow \lim_{t\to\infty} \bar{\mathbf{q}}_l \otimes \mathbf{q}_f \to [\pm 1,\ \mathbf{0}^\top]^\top, \tag{6.1}$$

$$\lim_{t\to\infty} \boldsymbol{\omega}_{i,fb}^{fb} \to \mathbf{R}_{lb}^{fb}\boldsymbol{\omega}_{i,lb}^{lb} \Leftrightarrow \lim_{t\to\infty} \|\boldsymbol{\omega}_{i,fb}^{fb} - \mathbf{R}_{lb}^{fb}\boldsymbol{\omega}_{i,lb}^{lb}\| \to 0. \tag{6.2}$$

Alternatively, the follower can track a second reference $\mathbf{q}'_d(t) \in S^3$, $\boldsymbol{\omega}'_d(t) \in \mathbb{R}^3$ *relative* to the leader, thus we require that

$$\lim_{t\to\infty} \tilde{\boldsymbol{\epsilon}} \to \boldsymbol{\epsilon}'_d(t) \Leftrightarrow \lim_{t\to\infty} \bar{\mathbf{q}}'_d(t) \otimes \mathbf{q} \to [\pm 1,\ \mathbf{0}^\top]^\top, \tag{6.3}$$

$$\lim_{t\to\infty} \boldsymbol{\omega} \to \boldsymbol{\omega}'_d(t) \Leftrightarrow \lim_{t\to\infty} \|\boldsymbol{\omega} - \boldsymbol{\omega}'_d(t)\| \to 0, \tag{6.4}$$

where $\mathbf{q} = \bar{\mathbf{q}}_l \otimes \mathbf{q}_f$ and $\boldsymbol{\omega} = \boldsymbol{\omega}^{fb}_{i,fb} - \mathbf{R}^{fb}_{lb}\boldsymbol{\omega}^{lb}_{i,lb}$ are relative attitude and angular velocity, respectively.

6.2 Synchronization of two rigid-bodies

For meaningful stability analysis, we make use of error functions $\mathbf{e}_{sq\pm} = [1 \mp \tilde{\eta}_s,\ \tilde{\boldsymbol{\epsilon}}_s^\top]^\top$ where $\tilde{\mathbf{q}}_s = [\tilde{\eta}_s,\ \tilde{\boldsymbol{\epsilon}}_s^\top]^\top = \bar{\mathbf{q}}_d(t) \otimes \mathbf{q}_s$ and $s = l, f$ for the leader and the follower rigid body, respectively, and $\mathbf{T}_{se\pm}(\mathbf{e}_{sq\pm})$ is defined according to (3.6), thus we obtain the error kinematics

$$\dot{\mathbf{e}}_{sq\pm} = \mathbf{T}_{se\pm}(\mathbf{e}_{sq\pm})\mathbf{e}_{s\omega}\ , \tag{6.5}$$

where $\mathbf{e}_{s\omega} = \boldsymbol{\omega}^{sb}_{i,sb} - \mathbf{R}^{sb}_{i}\boldsymbol{\omega}^{i}_{i,d}(t)$. For leader-follower tracking and synchronization we pose the following theorem.

Theorem 6.1 *Let Assumptions 3.1, 3.2 and 3.3 hold for both the leader and follower rigid bodies. Then, each of the equilibria* $(\mathbf{e}_{lq\pm}, \mathbf{e}_{l\omega}, \mathbf{e}_{fq\pm}, \mathbf{e}_{f\omega}) = (\mathbf{0}, \mathbf{0}, \mathbf{0}, \mathbf{0})$ *of the two systems described by* (2.82) *and* (2.83)*, in closed-loop with the control law* (3.14) *for the leader and*

$$\begin{aligned}\boldsymbol{\tau}^{fb}_{fa} =& \mathbf{J}_f\dot{\boldsymbol{\omega}}^{fb}_{i,d} - \mathbf{S}(\mathbf{J}_f\boldsymbol{\omega}^{fb}_{i,fb})\boldsymbol{\omega}^{fb}_{i,d} \\ &- k_{fp}\left(\mathbf{T}^\top_{fe}\mathbf{e}_{fq} - \mathbf{T}^\top_{le}\mathbf{e}_{lq}\right) - k_{fd}\left(\mathbf{e}_{f\omega} - \mathbf{R}^{fb}_{lb}\mathbf{e}_{l\omega}\right) - \boldsymbol{\tau}^{fb}_{fd}\end{aligned} \tag{6.6}$$

for the follower, where $k_{fp} > 0$ *and* $k_{fd} > 0$ *are feedback gain scalars, are uniformly asymptotically stable in the large with the set of initial conditions* $\Gamma = S^3_e \times \mathbb{R}^3 \times S^3_e \times \mathbb{R}^3$.

Proof: See Appendix B.19.

Remark 6.1 *Note that Remark 3.1 also holds for Theorem 6.1 for both the leader and follower.*

Again we note that the result is based on removing all disturbances in the control law. The result can be extended by introducing unknown bounded disturbances as suggested in Assumption 3.4. We use a control law reminiscent of the Slotine & Li controller as presented in Section 3.2.2, based on a control structure which has often shown to be favorable from a stability analysis point of view as in this case. In the case of bounded additive non-vanishing disturbances, a steady-state error is unavoidable, hence only practical asymptotic stability may be obtained. The previous theorem for stability must be adapted to this case, however their extension is involved and therefore the technical tools that we use are presented in Appendix A.5.2. We pose the following theorem.

Theorem 6.2 *Let Assumptions 3.1–3.4 hold for both the leader and follower rigid bodies. Then, each of the equilibria* $(\mathbf{e}_{lq\pm}, \mathbf{e}_{l\omega}, \mathbf{e}_{fq\pm}, \mathbf{e}_{f\omega}) = (\mathbf{0}, \mathbf{0}, \mathbf{0}, \mathbf{0})$ *of the two systems described by* (2.82) *and* (2.83)*, in closed-loop with the control law* (3.17) *for the leader and*

$$\boldsymbol{\tau}_{fa}^{lb} = \mathbf{J}_f \dot{\boldsymbol{\omega}}_{i,r}^{fb} - \mathbf{S}\left(\mathbf{J}_f \boldsymbol{\omega}_{i,fb}^{fb}\right) \boldsymbol{\omega}_{i,r}^{fb} - k_{fq}\left(\mathbf{T}_{ef}^{\top}\mathbf{e}_{fq} - \mathbf{T}_{le}^{\top}\mathbf{e}_{lq}\right) - k_{f\omega}\left(\mathbf{s}_f - \mathbf{s}_l\right) \quad (6.7)$$

for the follower, where $\boldsymbol{\omega}_{i,r}^{fb}$ *and* $\mathbf{s}_f$ *are defined similar to* (3.16b)-(3.16d)*, and* $k_{fq} > 0$ *and* $k_{f\omega} > 0$ *are feedback gain scalars, is uniformly asymptotically stable in the large with the set of initial conditions* $\Gamma = S_e^3 \times \mathbb{R}^3 \times S_e^3 \times \mathbb{R}^3$*.*

Proof: See Appendix B.20.

Remark 6.2 *Note that Remark 3.1 also holds for Theorem 6.7 for both the leader and follower.*

6.3 Synchronization of spacecraft formations

In this section we present state feedback control laws for relative attitude switching control of a leader-follower spacecraft formation in cascade with a separately controlled leader, similar to what was presented in Section 6.2 for two arbitrarily rigid bodies with similar dynamics, and relative translational control of a leader-follower spacecraft formation with assumed perfectly controlled leader.

6.3.1 Rotational control

In this section we make use of the results on hybrid control presented in Chapter 4 for synchronized attitude control of a leader-follower formation. The main difference between the approach presented in this section and what was presented in Chapter 4 is that now we make use of relative coordinates for the follower spacecraft, thus the two models of the hybrid system (A.65)–(A.66) will in general differ, along with the connection term. Furthermore, we incorporate reasoning similar to what was used for cascaded systems for analysis of the synchronization part.

The spacecraft error quaternions $\tilde{\mathbf{q}}_s = [\tilde{\eta}_s,\ \tilde{\boldsymbol{\epsilon}}_s^{\top}]^{\top}$ are found by applying the quaternion product –*cf.* (2.28)

$$\tilde{\mathbf{q}}_s = \bar{\mathbf{q}}_{sd} \otimes \mathbf{q}_s = \begin{bmatrix} \eta_s\eta_{sd} + \boldsymbol{\epsilon}_s^{\top}\boldsymbol{\epsilon}_{sd}^{\top} \\ \eta_{sd}\boldsymbol{\epsilon}_s - \eta_s\boldsymbol{\epsilon}_{sd} - \mathbf{S}(\boldsymbol{\epsilon}_{sd})\boldsymbol{\epsilon}_s \end{bmatrix}. \quad (6.8)$$

It is important to notice that $\mathbf{q}_l$ is the rotation between leader body and inertial frame while $\mathbf{q}_f$ is the (relative) rotation between the follower body and the leader body frame, and thus the leader is commanded to follow one reference while for the follower a second reference *relative* to the leader. We define error variables as $\mathbf{e}_{shq} = [1 - h_s\tilde{\eta}_s,\ \tilde{\boldsymbol{\epsilon}}_s^{\top}]^{\top}$ where the *state* variables $h_s \in H = \{-1, 1\}$ determines the choice of desired equilibrium points, and the error kinematics may be presented analogous to (4.2) as

$$\dot{\mathbf{e}}_{shq} = \mathbf{T}_{sh}(\mathbf{e}_{shq})\mathbf{e}_{sh\omega}, \quad (6.9)$$

where

$$\mathbf{T}_{sh}(\mathbf{e}_{shq}) = \frac{1}{2}\begin{bmatrix} h_s\tilde{\boldsymbol{\epsilon}}_s^\top \\ \tilde{\eta}_s\mathbf{I} + \mathbf{S}(\tilde{\boldsymbol{\epsilon}}_s) \end{bmatrix} \tag{6.10}$$

$$\mathbf{e}_{lh\omega} = \boldsymbol{\omega}_{i,lb}^{lb} - \mathbf{R}_i^{lb}\boldsymbol{\omega}_{i,ld}^{i} \tag{6.11}$$

$$\mathbf{e}_{fh\omega} = \boldsymbol{\omega}_{lb,fb}^{fb} - \mathbf{R}_i^{fb}\boldsymbol{\omega}_{lb,fd}^{i} = \boldsymbol{\omega}_{lb,fb}^{fb} - \mathbf{R}_i^{fb}\left(\boldsymbol{\omega}_{i,fd}^{i} - \boldsymbol{\omega}_{i,lb}^{i}\right), \tag{6.12}$$

where we from now on denote $\boldsymbol{\omega} = \boldsymbol{\omega}_{lb,fb}^{fb}$. The control law for the follower spacecraft is expressed as

$$\boldsymbol{\tau}_{fa} = \mathbf{J}_f\dot{\boldsymbol{\omega}}_{fr} + \mathbf{C}_r(\boldsymbol{\omega})\boldsymbol{\omega}_{fr} + \mathbf{n}_r(\boldsymbol{\omega}) - k_{fq}\mathbf{T}_{fh}^\top\mathbf{e}_{fhq} - k_{f\omega}\mathbf{s}_{fh}, \tag{6.13a}$$

$$\boldsymbol{\omega}_{fr} = \boldsymbol{\omega}_{lb,fd}^{fb} - \gamma_f\mathbf{T}_{fh}^\top(\mathbf{e}_{fhq})\mathbf{e}_{fhq}, \tag{6.13b}$$

$$\mathbf{s}_{fh} = \boldsymbol{\omega} - \boldsymbol{\omega}_{fr} = \mathbf{e}_{fh\omega} + \gamma_f\mathbf{T}_{fh}^\top(\mathbf{e}_{fhq})\mathbf{e}_{fhq}, \tag{6.13c}$$

where $k_{fq} > 0$, $k_{f\omega} > 0$ and $\gamma_f > 0$ are constant gains. Next, let $\mathbf{x}_1 = [\mathbf{e}_{fhq}^\top, \mathbf{s}_{fh}^\top, h_f]^\top \in S_h^3 \times \mathbb{R}^3 \times H$ and, for a given hysteresis margin $\sigma_f > 0$ define the flow and jump sets, respectively as

$$C_f := \{\mathbf{x}_1 \in S_h^3 \times \mathbb{R}^3 \times H : h_f(k_{fq}\tilde{\eta}_f - \frac{1}{2}\gamma_f\tilde{\boldsymbol{\epsilon}}_f^\top\mathbf{J}_f\mathbf{e}_{fh\omega}) \geq -\sigma_f\}\ , \tag{6.14a}$$

$$D_f := \{\mathbf{x}_1 \in S_h^3 \times \mathbb{R}^3 \times H : h_f(k_{fq}\tilde{\eta}_f - \frac{1}{2}\gamma_f\tilde{\boldsymbol{\epsilon}}_f^\top\mathbf{J}_f\mathbf{e}_{fh\omega}) \leq -\sigma_f\}\ . \tag{6.14b}$$

Then, the switching law is defined by

$$\dot{h}_f = 0 \quad \mathbf{x}_1 \in C_f\ , \tag{6.15a}$$

$$\mathbf{x}_1^+ = G_f(\mathbf{x}_1) = [\mathbf{e}_{fq}^\top, \mathbf{s}_{fh}^\top, -h_f]^\top \quad \mathbf{x}_1 \in D_f\ . \tag{6.15b}$$

For the leader spacecraft we make use of the results presented in Section 4.2.2 and thus define $\mathbf{x}_2 = [\mathbf{e}_{lhq}^\top, \mathbf{s}_{lh}^\top, h_l]^\top \in S_h^3 \times \mathbb{R}^3 \times H$ as the leader state, and the state of the total system is defined as $\mathbf{x} = [\mathbf{x}_1^\top, \mathbf{x}_2^\top]^\top$. We now state the following theorem.

Theorem 6.3 *Let Assumptions 3.2, 3.3 and 3.4 hold for both the leader and follower spacecraft. Consider the system* (2.82) *and* (2.83) *in closed-loop with the controller* (4.15)–(4.17) *for the leader spacecraft, as input for the system* (6.9) *and* (2.90) *in closed-loop with the controller* (6.13)–(6.15) *for the follower spacecraft. Then, the set*

$$\mathcal{A} := \{\mathbf{x} \in S_h^3 \times \mathbb{R}^3 \times H \times S_h^3 \times \mathbb{R}^3 \times H : (\mathbf{e}_{lhq}, \mathbf{e}_{lh\omega}, \mathbf{e}_{fhq}, \mathbf{e}_{fh\omega}) \in \bar{\mathcal{B}}_{\delta_r}\}, \tag{6.16}$$

where $\delta_r > 0$, is uniformly asymptotically stable in the large on the set $S_h^3 \times \mathbb{R}^3 \times S_h^3 \times \mathbb{R}^3$.

Proof: See Appendix B.21.

Remark 6.3 *The cascaded system in Theorem 6.3 is in fact two practically stable systems which are interconnected. Therefore, we state in the proof that* for any given $\delta_l > 0$, *the set of the total system is asymptotically stable instead of the usual notation for practical systems, because when* $\lim_{\delta_l \to \infty} \beta_{la}(\boldsymbol{\theta}_2) \to \infty$.

6.3.2 Translational Control

For the translational case we start by making the following assumptions.

Assumption 6.1 *There exists* $\alpha_{\mathbf{p}_d}$, $\alpha_{\dot{\mathbf{p}}_d}$, $\alpha_{\ddot{\mathbf{p}}_d} > 0$ *such that* $\|\mathbf{p}_d(t)\| < \alpha_{\mathbf{p}_d}$, $\|\dot{\mathbf{p}}_d(t)\| < \alpha_{\dot{\mathbf{p}}_d}$, *and* $\|\ddot{\mathbf{p}}_d(t)\| < \alpha_{\ddot{\mathbf{p}}_d}$ *for all* $t \geq t_0$.

Assumption 6.2 *It is assumed that the mass* m_s *of each spacecraft is positive, constant and bounded.*

Assumption 6.3 *Assume there exists* $\alpha_{sd} > 0$ *such that* $\|\mathbf{f}_{sd}(t)\| \leq \alpha_{sd}$ *for all* $t \geq t_0$, *where* $s = l, f$ *denotes the leader and follower spacecraft, respectively.*

In this case we only consider control of the follower spacecraft since orbital maneuvers for the leader spacecraft is not considered in this thesis, which means that the synchronization can be viewed as tracking of a disturbed reference trajectory. Furthermore, we assume that the leader spacecraft compensates for disturbances such that $\mathbf{f}_{al} = -\mathbf{f}_{dl}$.

The control goal is to make the follower synchronize with its leader according to the given time varying reference $\mathbf{p}_d(t)$, $\dot{\mathbf{p}}_d(t)$, $\ddot{\mathbf{p}}_d(t) \in \mathbb{R}^3$ similar to the rotational case described in Section 6.1, *i.e.*

$$\lim_{t\to\infty} \mathbf{p} \to \mathbf{p}_d(t) \Leftrightarrow \lim_{t\to\infty} \|\tilde{\mathbf{p}}\| \to 0 \tag{6.17}$$

$$\lim_{t\to\infty} \dot{\mathbf{p}} \to \dot{\mathbf{p}}_d(t) \Leftrightarrow \lim_{t\to\infty} \|\dot{\tilde{\mathbf{p}}}\| \to 0, \tag{6.18}$$

where $\tilde{\mathbf{p}} = \mathbf{p} - \mathbf{p}_d(t)$ is the relative position error and $\dot{\tilde{\mathbf{p}}} = \dot{\mathbf{p}} - \dot{\mathbf{p}}_d(t)$ is the relative velocity error. We state the following theorem.

Theorem 6.4 *Let Assumptions 6.1, 6.2 and 6.3 hold. Then, the equilibrium point* $(\tilde{\mathbf{p}},\ \dot{\tilde{\mathbf{p}}}) = (\mathbf{0},\ \mathbf{0})$ *of the system* (2.62) *in closed-loop with the control law*

$$\mathbf{f}_{af} = m_f \ddot{\mathbf{p}}_r + \mathbf{C}_t(\boldsymbol{\omega}^l_{i,l})\dot{\mathbf{p}}_r + \mathbf{D}_t(\dot{\boldsymbol{\omega}}^l_{i,l}, \boldsymbol{\omega}^l_{i,l}, r_f)\mathbf{p} + \mathbf{n}_t(\mathbf{r}_l, r_f) - \mathbf{K}_p\tilde{\mathbf{p}} - \mathbf{K}_d\mathbf{s} \tag{6.19}$$

$$\dot{\mathbf{p}}_r = \dot{\mathbf{p}}_d - \gamma\tilde{\mathbf{p}}, \tag{6.20}$$

$$\mathbf{s} = \dot{\mathbf{p}} - \dot{\mathbf{p}}_r = \dot{\tilde{\mathbf{p}}} + \gamma\tilde{\mathbf{p}}, \tag{6.21}$$

where $\mathbf{K}_p$ *and* $\mathbf{K}_d$ *both are symmetric positive definite constant matrices, and there exist* $k_{pm},\ k_{pM},\ k_{dm},\ k_{dM} > 0$ *such that* $k_{pm} \leq \mathbf{K}_p \leq k_{pM}$ *and* $k_{dm} \leq \mathbf{K}_d \leq k_{dM}$ *and* $\gamma > 0$, *is uniformly globally practically exponentially stable.*

Proof: See Appendix B.22.

Remark 6.4 *We note that even if we state global stability, this is not precise from a theoretical viewpoint since when* $\mathbf{R}^i_l\mathbf{p} = -\mathbf{r}_l$, i.e.*when the follower is located at the center of the orbit, there is a singularity in* (2.62) *and according to (Hahn, 1967) the adjective* global *pertains to the case and only to the case when the state space is* $\mathbb{R}^n$. *From a practical viewpoint this is not an issue because a physical body will never reach this point because of the celestial body* i.e. *Earth centered at this point.*

Remark 6.5 *The assumption of perfectly control leader and its bounded orbital angular velocity can be relaxed by following the lines of Grøtli (2010), where a control law for the leader is utilized in closed-loop with the dynamics leading to a stability proof based on cascaded system and instead a bound on the leader references similar to Assumption 6.1 for the follower spacecraft.*

6.4 Spacecraft formation control with improved performance

In this section we will extend the results from Section 6.3.2 by introducing different kinds of exponential gains than presented in Section 3.3 and adaptivity for disturbance rejection. We pose the following assumption.

Assumption 6.4 *The perturbation vector can be written as*

$$\mathbf{f}_{df}(t) = \mathbf{a} + \mathbf{b}(t) \tag{6.22}$$

where $\mathbf{a}$ *is considered a constant mean while* $\mathbf{b}(t)$ *is considered as a continuous higher frequency component, and the latter is assumed upper bounded such that* $\|\mathbf{b}(t)\| \leq \alpha_d$ *(and* $\|\dot{\mathbf{b}}(t)\| \leq \alpha_{\dot{d}}$ *because of continuity) for all* $t \geq t_0$.

The assumption given in (6.22) holds for typical disturbances working on spacecraft such as aerodynamic drag, J_2 effect caused by uneven mass distribution of the Earth, Solar radiation and third-body perturbing forces which all can be seen as state dependent, slow varying and even in some cases constant.

Theorem 6.5 *Let Assumptions 6.1, 6.2 and 6.3 hold. Then, the solution trajectories of the system* (2.62) *in closed-loop with the control law*

$$\begin{aligned}
\mathbf{f}_{af} =& m_f \ddot{\mathbf{p}}_r + \mathbf{C}_t(\boldsymbol{\omega}^l_{i,l})\dot{\mathbf{p}}_r + \mathbf{D}(\dot{\boldsymbol{\omega}}^l_{i,l}, \boldsymbol{\omega}^l_{i,l}, r_f)\mathbf{p} + \mathbf{n}_t(\mathbf{r}_l, r_f) \\
& - \mathbf{K}_p\tilde{\mathbf{p}} - k_i\boldsymbol{\zeta} - k_a\boldsymbol{\xi} - \mathbf{K}_d\mathbf{s} && (6.23)\\
\dot{\boldsymbol{\zeta}} =& \tilde{\mathbf{p}}, && (6.24)\\
\dot{\boldsymbol{\xi}} =& k_a\dot{\tilde{\mathbf{p}}}, && (6.25)\\
\mathbf{s} =& [s_x,\ s_y,\ s_z]^\top = \dot{\mathbf{p}} - \dot{\mathbf{p}}_r = \dot{\tilde{\mathbf{p}}} + \gamma\tilde{\mathbf{p}}, && (6.26)\\
\dot{\mathbf{p}}_r =& \dot{\mathbf{p}}_d - \gamma\tilde{\mathbf{p}}, && (6.27)\\
\ddot{\mathbf{p}}_r =& \ddot{\mathbf{p}}_d - \gamma\dot{\tilde{\mathbf{p}}}, && (6.28)
\end{aligned}$$

where $\mathbf{K}_p = k_p \operatorname{diag}\{e^{k_1\tilde{p}_x^2},\ e^{k_1\tilde{p}_y^2},\ e^{k_1\tilde{p}_z^2}\} = \mathbf{K}_p^\top$ *and* $\mathbf{K}_d = k_d \operatorname{diag}\{e^{k_2 s_x^2},\ e^{k_2 s_y^2},\ e^{k_2 s_z^2}\} = \mathbf{K}_d^\top$, *tuning parameters* $k_p,\ k_i,\ k_a,\ k_d \in \mathbb{R}_+$, *and* $\gamma := k_i/k_a^2$, *uniformly converge to the set* $\{(\tilde{\mathbf{p}}, \dot{\tilde{\mathbf{p}}}, \boldsymbol{\zeta}, \boldsymbol{\xi}) \in \mathbb{R}^{12} \ :\ \|[\tilde{\mathbf{p}},\ \dot{\tilde{\mathbf{p}}}]\| \leq \delta\}$, *where* δ *can be made arbitrarily small by increasing the controller gains, for all initial values as* $t \to \infty$.

Proof: See Appendix B.23.

Remark 6.6 *By inserting* (6.26) *and* $\gamma = k_i/k_a^2$ *into* (6.23) *we obtain a proportional term on the form* $-(\mathbf{K}_d k_i/k_a^2 + \mathbf{K}_p)\tilde{\mathbf{p}}$ *which means that the proportional gain will increase by increasing the gain for the integral of the position error, while decrease with fast integration of the velocity error.*

Remark 6.7 *The results of Theorem 6.5 might be further extended showing uniform asymptotic stability by following along the lines of (Loría* et al.*, 2005) where* persistency of excitation *is utilized, thus also guaranteeing certain robustness vis-a-vis disturbances. Also, the result can be generalized by introducing functions similar as in* (3.21).

For convenience, the system equations for relative rotation and translation may be "stacked" as a 6DOF (3+3DOF) system –*cf.* (Kristiansen *et al.*, 2008).

6.5 Simulation results

In this section we present simulation results based on the control laws presented in this chapter. Our main focus is to show that the follower spacecraft is able to synchronize with its leader, along with showing that by utilizing exponential gains independent for each axis we can reduce energy consumption without hampering the position and velocity errors and furthermore, showing that the residual can be decreased by introducing I^2 action. We utilize simulation data as presented in Section 2.8.1 if otherwise is not stated.

6.5.1 Synchronization of two rigid bodies

In this section we present two different simulation results to verify the two synchronizing controllers presented in Section 6.2. The initial conditions for both simulations were chosen as $\mathbf{q}_l(t_0) = [-0.3772,\ -0.4329, 0.6645,\ 0.4783]^\top$, $\mathbf{q}_f(t_0) = 0.5[1,\ 1,\ 1,\ 1]^\top$, $\boldsymbol{\omega}_l(t_0) = [0.1,\ -0.3,\ 0.2]^\top$ and $\boldsymbol{\omega}_f(t_0) = [0.2,\ -0.3,\ 0.1]^\top$. The controller gains for the first simulation were chosen as $k_{sp} = 1$, $k_{sd} = 2$ for the leader (3.14) and follower (6.6) controllers, and for the second simulation we chose $k_{sq} = 1$, $k_{s\omega} = 2$ and $\boldsymbol{\Gamma}_s = \mathbf{I}$ for the leader (3.17) and follower (6.7) controllers. The desired trajectory used for both simulations was chosen as $\dot{\boldsymbol{\omega}}_d(t) = 0.1[-10c_0^2\cos(8c_0t),\ 48c_0^2\sin(16c_0t),\ -8c_0^2\cos(4c_0t)]$, $\boldsymbol{\omega}_d(t_0) = \mathbf{0}$, and $\mathbf{q}_d(t_0) = [1,\ \mathbf{0}^\top]^\top$, where $c_0 = \pi/t_o$ and t_o denotes the orbital period.

In Figure 6.1 simulation results are presented where the PD+ based control laws for the leader and follower spacecraft were applied without added disturbances and noise. From the top left we see that the leader spacecraft settles at the negative equilibrium, the angular velocity error goes towards zero, while the actuator torque is presented in the bottommost plot. On the right hand side we see that the relative attitude and angular velocity error goes towards zero and thus the follower spacecraft is able to synchronize with the leader spacecraft. The bottommost plot on the right hand depicts the follower actuator torque.

In the second set of simulation results we introduce measurement noise and disturbances as presented in Section 2.8.1, and as it can be seen from Figure 6.2 the sliding surface-based control laws derived for unknown disturbances are also able to make the leader track the reference and make the follower synchronize with the leader, similar to the results from the first simulation. One notable difference is that these control laws are in general faster than the results presented in Figure 6.1, though demanding larger absolute control torque.

Table 6.1: Values of performance functionals (6.29) and (6.30) without disturbances.

	J_q	J_p
Synchronizing	8.302	0.977
Tracking	10.158	0.884

Table 6.2: Values of performance functionals (6.29) and (6.30) including disturbances on leader spacecraft.

	J_q	J_p
Synchronizing (100 s)	4.452	3.190
Tracking (100 s)	5.189	6.341
Synchronizing (1 orbit)	4.529	13.151
Tracking (1 orbit)	8.448	14.52

Now we compare the presented control laws with a more naive approach where two spacecraft are tracking a common reference using the same control law to show that synchronization does not necessarily follow. For sake of comparison between the two control strategies we use performance functionals defined as

$$J_{\mathrm{q,sy/tr}} = \int_{t_0}^{t_f} \tilde{\boldsymbol{\epsilon}}_{\mathrm{sy/tr}}^{\top} \tilde{\boldsymbol{\epsilon}}_{\mathrm{sy/tr}} dt \tag{6.29}$$

$$J_{\mathrm{p,sy/tr}} = \int_{t_0}^{t_f} \boldsymbol{\tau}_{\mathrm{sy/tr}}^{\top} \boldsymbol{\tau}_{\mathrm{sy/tr}} dt \tag{6.30}$$

where the subscripts sy and tr means either synchronization (the follower utilize the control law presented in Section 6.2 and utilized in the previous presented simulation) or tracking (the follower uses the same control law as the leader) for the follower spacecraft, respectively. The parameters $\tilde{\boldsymbol{\epsilon}}_{\mathrm{sy}}$ and $\tilde{\boldsymbol{\epsilon}}_{\mathrm{tr}}$ are found by applying $\tilde{\mathbf{q}}_{\mathrm{sy/tr}} = \bar{\mathbf{q}}_l \otimes \mathbf{q}_{\mathrm{sy/tr}}$.

Table 6.1 show the performance functionals for an unperturbed and noiseless system where the synchronizing and tracking controllers are compared (note that we now control the leader spacecraft as a set point at the origin). What can be seen is that the synchronizing controller is able to achieve its objective with a smaller integral attitude error with a slightly increase in power consumption, which makes sense because of the added synchronizing terms in the control law, compared with using two similar tracking controllers.

Now we add disturbances to the leader spacecraft as $\boldsymbol{\tau}_{ld}^{lb} = [0.02\sin(0.005t), -0.04\cos(0.005t), 0.02\sin(0.01t)]^{\top}$, and from Figure 6.3 and the performance functionals in Table 6.2 it can be seen that the tracking follower is not able to synchronize with its leader because of the rise in $J_{q,tr}$ over one orbital period. Thus we conclude that having two spacecraft following the same reference does not necessarily mean that they are synchronized.

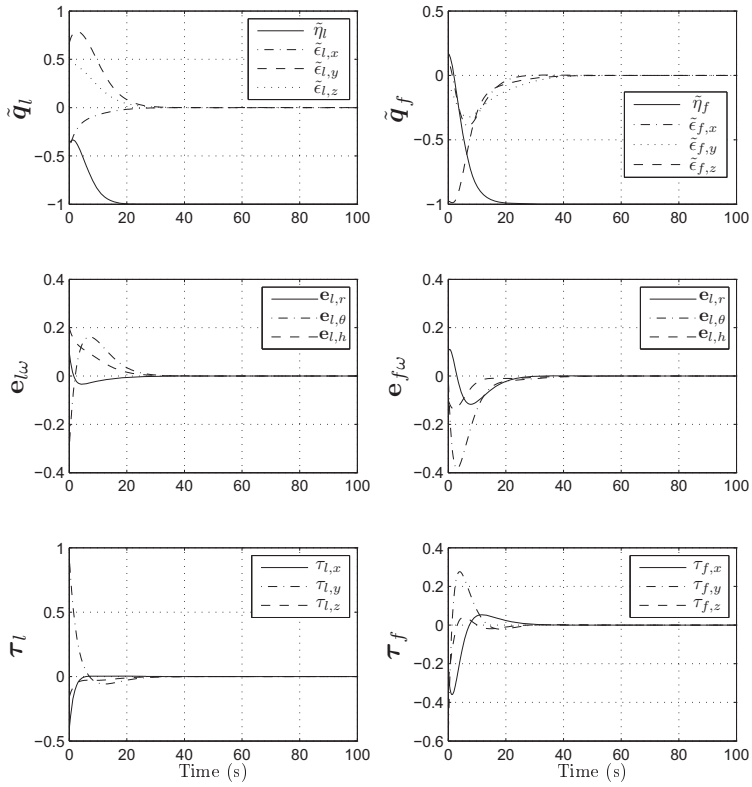

Figure 6.1: Attitude and angular velocity error and control torque for leader (left) and synchronizing follower (right) spacecraft during attitude maneuver without measurement noise and disturbances.

6.5.2 Synchronization of spacecraft formation

We have run a set of simulations to verify the hybrid synchronizing attitude controller presented in Section 6.3.1 and the translational controller presented in Section 6.3.2. The initial conditions were chosen as $\mathbf{q}_{i,lb}(t_0) = 0.5[1,\ 1,\ 1,\ 1]^\top$, $\mathbf{q}_{i,fb}(t_0) = [-0.866,\ 0.5,\ 0,\ 0]^\top$, $\boldsymbol{\omega}^{lb}_{i,lb}(t_0) = [0.8,\ -0.2,\ 0.05]^\top$ and $\boldsymbol{\omega}^{fb}_{i,fb}(t_0) = [0.8,\ -0.2,\ 1]^\top$. The desired trajectory was chosen as $\dot{\boldsymbol{\omega}}^i_{i,ld}(t) = \dot{\boldsymbol{\omega}}^i_{lb,fd}(t) = 0.1[-10c_0^2\cos(8c_0t), 48c_0^2\sin(16c_0t),\ -8c_0^2\cos(4c_0t)]$, with $\boldsymbol{\omega}^i_{i,ld}(t_0) = \boldsymbol{\omega}^i_{lb,fd}(t_0) = \mathbf{0}$, and $\mathbf{q}_{i,ld}(t_0) = \mathbf{q}_{lb,fd}(t_0) = [1,\ \mathbf{0}^\top]^\top$, where $c_0 = \pi/t_o$ and t_o denotes the orbital period. For relative position the follower started standstill at $\mathbf{p}(t_0) = [0,\ -100,\ 0]^\top$ with desired values as standstill at $\mathbf{p}_d = [0,\ -1000,\ 500]^\top$. As gains we used $k_{sq} = 1$, $k_{s\omega} = 2$ and $\gamma_s = 1$ for control of relative rotation using control laws (4.15) and (6.13) for leader and follower, respectively, and $\mathbf{K}_p = 0.1\mathbf{I}$ and $\mathbf{K}_d = 2\mathbf{I}$ for

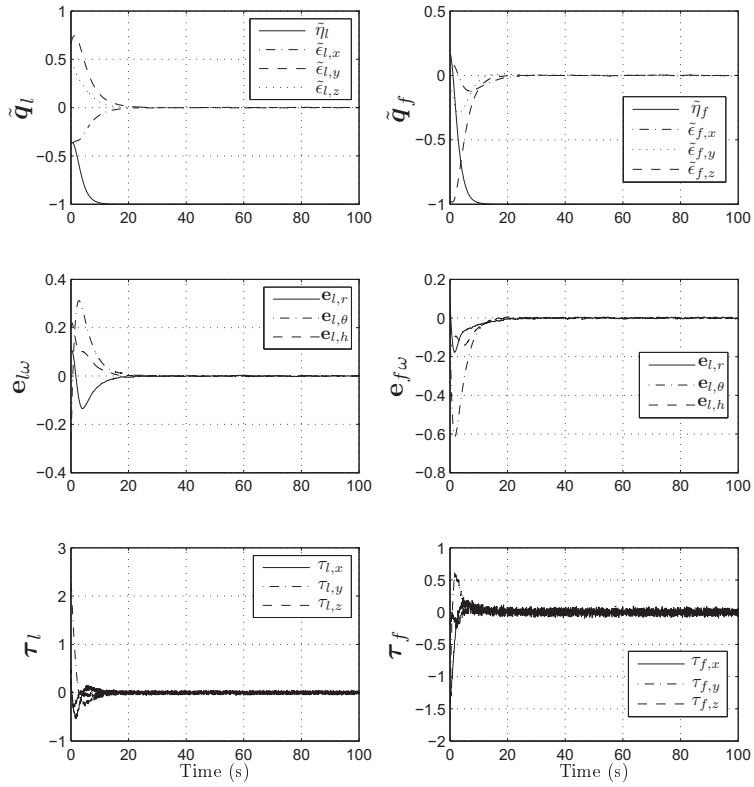

Figure 6.2: Attitude and angular velocity error and control torque for leader (left) and synchronizing follower (right) spacecraft during attitude maneuver including measurement noise and disturbances.

control of relative translation (6.19). The measurement noise was added according to $\mathbf{r}_{ln} = \mathbf{r}_l + 0.01\mathbb{B}^3$, $\mathbf{p}_n = \mathbf{p} + 0.01\mathbb{B}^3$, $\mathbf{v}_{ln} = \mathbf{v}_l + 5\times10^{-3}\mathbb{B}^3$, $\dot{\mathbf{p}}_n = \dot{\mathbf{p}} + 5\times10^{-3}\mathbb{B}^3$.

The simulation results for rotational control are presented in Figure 6.4 and it can be seen that the high initial angular velocities of the leader and follower spacecraft provokes switching for both controllers. What we want to show in these simulations is that there is no connection between h_l and h_f, that is, if the leader settles at a specified equilibrium point, the follower can without problem settle at the opposite because the equilibrium points are only separated mathematically and not physically. What also can be seen is that because of the cross-term defined in the jump sets (4.17) for the leader and (6.14) for the follower, the switching occurred even if $\tilde{\eta}_s$ was on the "correct" side of the rotational sphere. This is easiest seen on the topmost plot on the right hand side where $\tilde{\eta}_f$ was about -0.6 when h_f switched from -1 to $+1$. This was possible because there were still high angular velocities

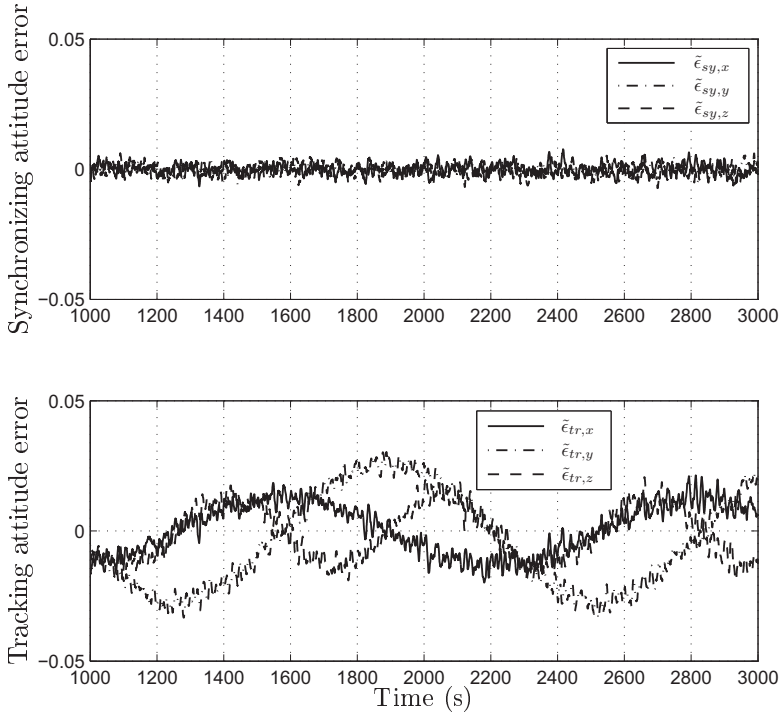

Figure 6.3: Relative attitude error error for synchronizing (top) and tracking (bottom) controlled follower spacecraft during station keeping including measurement noise and periodic disturbances on leader spacecraft.

present at this time instant, as also was discussed in Section 4.4.1. In Figure 6.5 the relative position and velocity error and control force are depicted and it can be seen that the state variables settled close to the origin even if perturbations were present.

6.5.3 Adaptive spacecraft formation with improved performance

In this section we have performed several simulations to validate the control law presented in Section 6.4. Furthermore, for sake of comparison regarding performance, we included the sliding surface control law (6.19) and

$$\begin{aligned}\mathbf{f}_{af} =& m_f \ddot{\mathbf{p}}_r + \mathbf{C}_t(\boldsymbol{\omega}_{i,l}^l)\dot{\mathbf{p}}_r + \mathbf{D}(\dot{\boldsymbol{\omega}}_{i,l}^l, \boldsymbol{\omega}_{i,l}^l, r_f)\mathbf{p} + \mathbf{n}_t(\mathbf{r}_l, r_f) \\ & - k_p e^{k_1 \|\tilde{\mathbf{p}}\|^2} \tilde{\mathbf{p}} - k_d e^{k_2 \|\mathbf{s}\|^2} \mathbf{s} \end{aligned} \tag{6.31}$$

in the simulations, where the latter has similar exponential gains as the controller (3.20), which can be shown uniformly globally practically exponentially stable by following the lines of proof of Theorem 6.5. Our idea is to show that by weighting

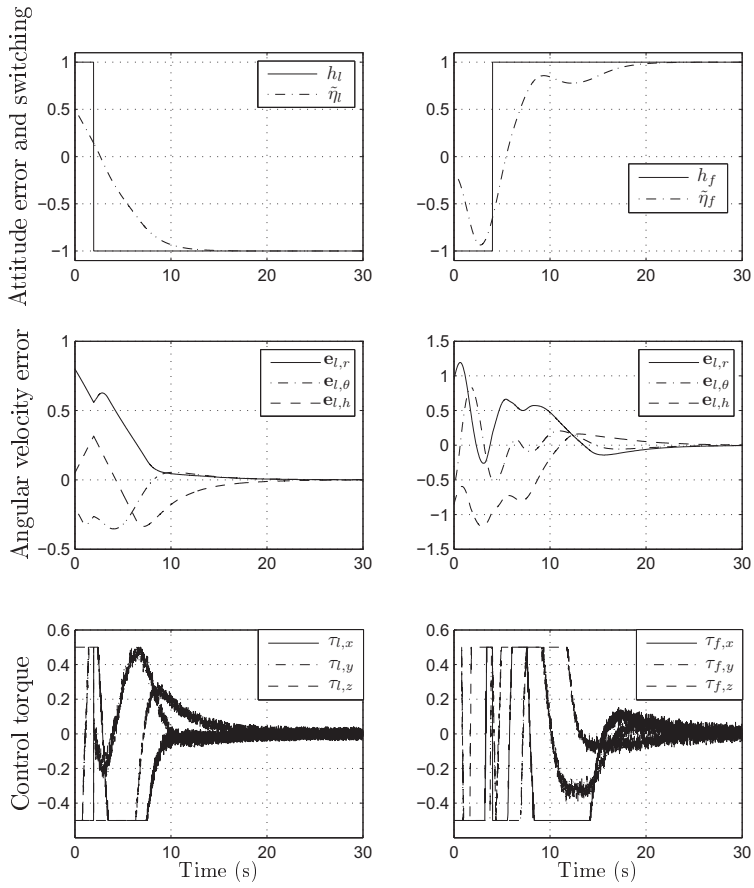

Figure 6.4: Attitude and angular velocity error and control torque for leader (left) and follower (right) spacecraft during attitude maneuver including measurement noise and disturbances.

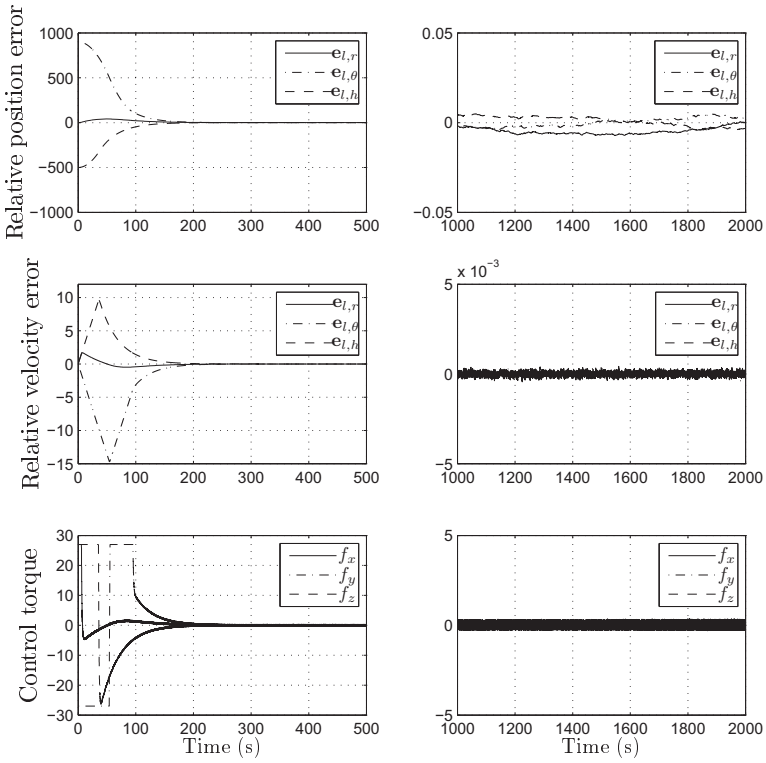

Figure 6.5: Relative position and velocity error and control force during stabilization left) and station keeping (right).

the gains along each axis individually, the overall performance increases compared to (6.31) where the gains are scalar based on the norm of the whole relative position and velocity (sliding) vector.

Two different scenarios are presented to show the features of the derived control law. First we present simulation results to show that the integral action manages to reduce the residual of the practical result, while the latter results show that by utilizing the variable gain matrix, the energy consumption can be reduced without increasing the response time of the system compared to (6.31).

All perturbations were added according to Section 2.8.1 which typically are (state dependent) continuous and slowly varying, while atmospheric drag often can be considered close to constant for near circular orbits. For our simulations we have chosen the initial conditions as $\mathbf{p}(t_0) = [20, \ -80, \ 0]^\top$, $\dot{\mathbf{p}}(t_0) = \mathbf{0}$, $\mathbf{p}_d = [10, \ 20, \ -30]^\top$ and $\dot{\mathbf{p}}_d = \mathbf{0}$. What we compare is the control law (6.23) with a version where the integral action is removed, *i.e.* $k_a = k_i = 0$. Simulation results for a translational maneuver is depicted in Figure 6.6 and performance functionals

Table 6.3: Values of performance functionals for translational maneuver.

	J_{pos}	J_{vel}	J_{pow}
Controller (6.23)	3.43×10^5	133	5803
Controller (6.23), $k_a = k_i = 0$	2.40×10^5	159	5551

Table 6.4: Average value of performance functionals for rigid-body over 10,000 simulations.

	J_{pos}	J_{vel}	J_{pow}
Controller (6.23)	1.29×10^6	1.13×10^3	3.76×10^4
Controller (6.19)	2.01×10^6	884	2.67×10^4
Controller (6.31)	1.25×10^6	1.37×10^3	5.48×10^4

presented in Table 6.3, which both show that introducing integral action leads to a slower system response, while looking at Figure 6.7 it can be seen that the residual of the physical state vector is reduced. One of the reasons that the result looks like this, might be because the atmospheric density is divided into regions (*cf.* (Wertz, 1978)) where it is constant within each region, thus, since the spacecraft is following an elliptic orbit the disturbance will wary in steps when the orbit altitude moves between two regions, in addition to the sinusoidal variations caused by the J_2 effect. The issue regarding atmospheric density could be solved differently by introducing a continuous function of the density using altitude as argument or interpolate between the centers of each neighboring regions.

In Table 6.4 we present simulation results from 10,000 simulations for translational maneuvers without disturbances and noise using controller gains $k_p = 0.1$, $k_d = 10$ and $\gamma = 0.001$ for (6.19), and including $k_1 = 1 \times 10^{-4}$ and $k_2 = 1 \times 10^{-2}$ for (6.31), and furthermore including $k_i = k_a = 0$ for (6.23), with random initial values for the initial relative position and velocity, with standard deviation of 50 and 5, respectively. This was done to show two different properties; first we see that the exponential gains makes the system work faster, though consuming more energy without increasing sensitivity to measurement noise compared to using static gains; and furthermore, we see that by using gain matrices where each axis is weighted differently, we obtained a marginal increase in J_{pos} while the power consumption J_{pow} was reduced by over 30 percent without increasing the sensitivity to measurement noise; –*cf.* Section 3.5.

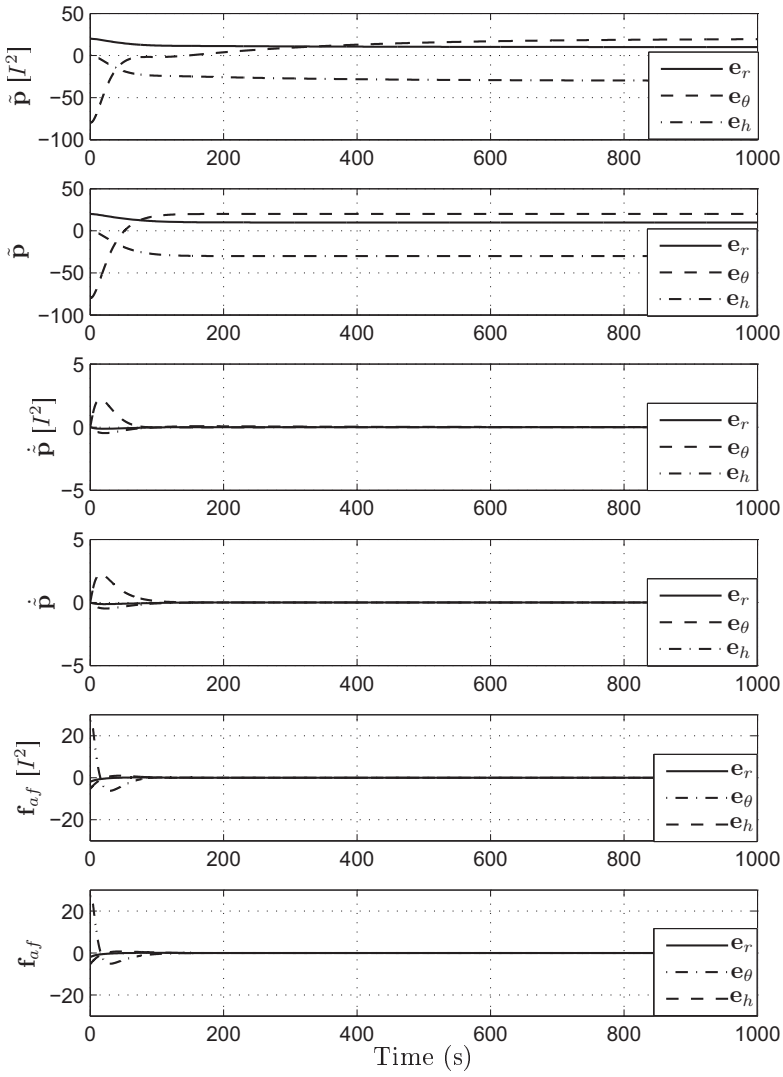

Figure 6.6: Relative position and velocity error and control force for translational maneuver by sliding surface control with exponential gains with and without I^2 action.

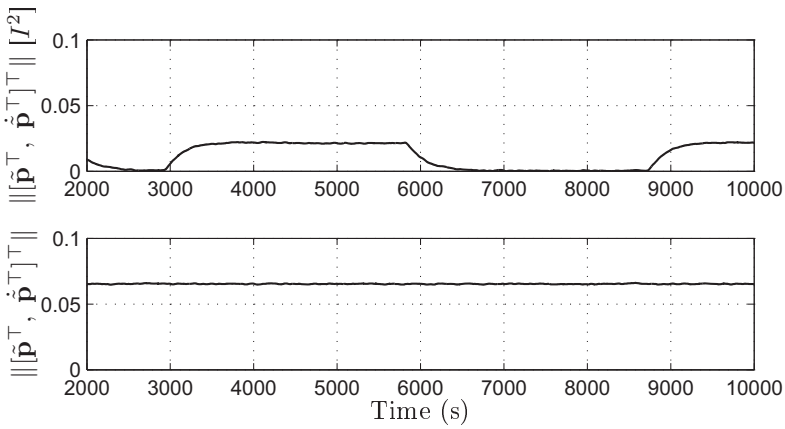

Figure 6.7: Norm of physical states ($\|[\tilde{\mathbf{p}}^\top,\ \dot{\tilde{\mathbf{p}}}^\top]^\top\|$) by sliding surface control with exponential gains with (top) and without (bottom) I^2 action during station keeping.

Chapter 7

Autonomous attitude reference generation for leader-follower formations

For minimizing the workload on the ground station operator it is important for a spacecraft formation to be as autonomous as possible. The topic of reference generation is to have the spacecraft themselves generate their needed references to fulfill the mission requirements in real-time. In this chapter we present two different solutions on how to generate rotational references for both the leader and follower spacecraft. In the first scheme presented in Section 7.1 we assume that the leader spacecraft is pointing its instrument towards the center of the Earth (nadir pointing leader), while in the second scheme presented in Section 7.2 we assume that the leader is assigned a target (target pointing leader). In both cases, references are generated such that the leader and follower are able to track the common target point on the Earth surface which could be either constant or time varying which is verified through simulations in Section 7.3. The results presented in this chapter are based on (Schlanbusch *et al.*, 2008*b*, 2010*c*; Schlanbusch and Nicklasson, 2011).

7.1 Nadir pointing leader

The target reference frame $\mathcal{F}^t$ with unit vectors $[\mathbf{x}^t,\ \mathbf{y}^t,\ \mathbf{z}^t]$, as depicted in Figure 7.1, is located at the Earth surface specified by the vector $r_e\mathbf{r}_l/\|\mathbf{r}_l\|$ relative to $\mathcal{F}^i$, where r_e is the Earth radius. It is assumed a perfect spherical Earth; alternatively a function $r_e(\lambda,\phi)$ of the Earth radius may be used with longitude and latitude as arguments. Unit vectors of the target reference frame align with the basis vectors of the leader orbit reference frame $\mathcal{F}^l$. A vector pointing from the follower spacecraft towards the target is first derived in target and follower orbit frames as

$$\mathbf{l}^t = -\varpi(\mathbf{r}_l)\mathbf{e}_r - \mathbf{R}_l^t\mathbf{p}, \quad \mathbf{l}^f = -\varpi(\mathbf{r}_l)\mathbf{R}_t^f\mathbf{e}_r^t - \mathbf{R}_l^f\mathbf{p}, \tag{7.1}$$

respectively, where $\varpi(\mathbf{r}_l) = \|\mathbf{r}_l\| - r_e$ is the orbit height. A desired reference frame $\mathcal{F}^d$, as depicted in Figure 7.1, is located at the center of mass of the follower spacecraft, and defined as $\mathbf{z}_d = \mathbf{l}^f/\|\mathbf{l}^f\|$, $\mathbf{y}_d = \mathbf{S}(\mathbf{z}_d)\mathbf{p}/\|\mathbf{S}(\mathbf{z}_d)\mathbf{p}\|$ and $\mathbf{x}_d = \mathbf{S}(\mathbf{y}_d)\mathbf{z}_d$.

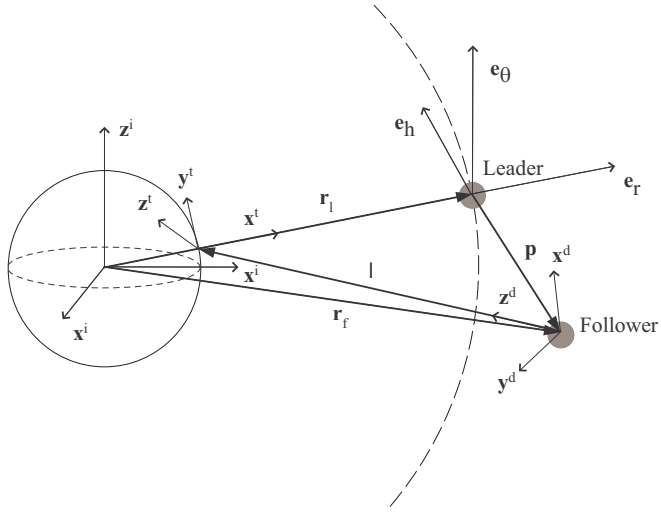

Figure 7.1: Inertial, leader, desired and target reference frames.

It should be noted that the vectors $\mathbf{p}$ and $\mathbf{l}^t$ are not necessarily perpendicular, and in some instances, when $\mathbf{p} = [c,\ 0,\ 0]^\top$, $c \in \mathbb{R}$, the vectors are parallel, which will give a zero vector in the defined reference frame. When this occur it means that the two spacecraft are lined along the $\mathbf{r}_l$ vector and one of the spacecraft is blocking the field of view for the other. As a solution for this instance the generated rotational reference is set to nadir pointing.

7.1.1 Angular velocity reference

The angular velocity of the desired frame relative the target frame is expressed in the desired reference frame as $\boldsymbol{\omega}_{t,d}^d = [\omega_{dx},\ \omega_{dy},\ \omega_{dz}]^\top$. The derivative of the target pointing vector in the follower orbit frame can be expressed in the desired frame as (Tsiotras *et al.*, 2001)

$$\dot{\mathbf{l}}^d = (\dot{\mathbf{l}}^f \cdot \mathbf{x}_d)\mathbf{x}_d + (\dot{\mathbf{l}}^f \cdot \mathbf{y}_d)\mathbf{y}_d + (\dot{\mathbf{l}}^f \cdot \mathbf{z}_d)\mathbf{z}_d. \tag{7.2}$$

Alternatively the vector may be expressed as

$$\dot{\mathbf{l}}^f = \frac{{}^d d\mathbf{l}}{dt} + \mathbf{S}(\boldsymbol{\omega}_{f,d}^d)\mathbf{l}, \tag{7.3}$$

where ${}^d d\mathbf{l}/dt$ is the derivative taken in the desired reference frame, and $\mathbf{l} = \|\mathbf{l}^t\|\mathbf{z}_d$. By combining (7.2) and (7.3) we obtain the expression

$$\boldsymbol{\omega}_{f,d}^d = \left[\frac{-\dot{\mathbf{l}}^f \cdot \mathbf{y}_d}{\|\mathbf{l}^f\|}, \frac{\dot{\mathbf{l}}^f \cdot \mathbf{x}_d}{\|\mathbf{l}^f\|}, 0\right]^\top. \tag{7.4}$$

It should be noted that the desired angular velocity about the $\mathbf{z}_d$-axis is set to zero to ensure that the instrument is not rotating while performing measurements

e.g. causing blurry pictures when a camera is utilized. The derivative of (7.1) is

$$\dot{\mathbf{l}}^f = -\varpi(\mathbf{r}_l)\mathbf{S}(\boldsymbol{\omega}_{t,f}^f)\mathbf{R}_t^f\mathbf{e}_r - \mathbf{R}_t^f(\dot{\varpi}(\mathbf{r}_l,\mathbf{v}_l)\mathbf{e}_r + \varpi(\mathbf{r}_l)\dot{\mathbf{e}}_r) - \mathbf{S}(\boldsymbol{\omega}_{f,l}^f)\mathbf{R}_l^f\mathbf{p} - \mathbf{R}_l^f\dot{\mathbf{p}}. \quad (7.5)$$

Since $\mathcal{F}^f$ and $\mathcal{F}^l$ are aligned, the relative velocity $\boldsymbol{\omega}_{l,f}^f = \mathbf{0}$ and $\mathbf{R}_l^f = \mathbf{I}$. The same is also true for $\mathcal{F}^t$ and $\mathcal{F}^l$ which means that $\mathbf{R}_t^l = \mathbf{I}$ and $\boldsymbol{\omega}_{t,f}^f = \boldsymbol{\omega}_{t,i}^f + \boldsymbol{\omega}_{i,l}^f + \boldsymbol{\omega}_{l,f}^f = -\boldsymbol{\omega}_{i,t}^f + \boldsymbol{\omega}_{i,l}^f + \boldsymbol{\omega}_{l,f}^f = 0$, since $\boldsymbol{\omega}_{i,t}^f = \boldsymbol{\omega}_{i,l}^f$, as both reference frames are located along the same vector $\mathbf{r}_l$ rotating about $\mathcal{F}^i$ with equal angular velocity. Finally, $\dot{\mathbf{e}}_r = 0$ since a change in the radial vector will have no impact on the angular velocity between the target and follower orbit frames. Equation (7.5) is then rewritten as

$$\dot{\mathbf{l}}^f = -\dot{\varpi}(\mathbf{r}_l,\mathbf{v}_l)\mathbf{e}_r - \dot{\mathbf{p}}. \quad (7.6)$$

7.1.2 Angular acceleration reference

The angular acceleration reference $\dot{\boldsymbol{\omega}}_{t,d}^d = [\dot{\omega}_{dx},\ \dot{\omega}_{dy},\ \dot{\omega}_{dz}]^\top$ is obtained by differentiating the angular velocity reference (7.4) leading to

$$\dot{\boldsymbol{\omega}}_{f,d}^d = \begin{bmatrix} -\frac{\ddot{\mathbf{l}}^f\cdot\mathbf{y}_d + 2\omega_{dx}\|\mathbf{l}^f\|}{\|\mathbf{l}^f\|} + \omega_{dy}\omega_{dz} \\ \frac{\ddot{\mathbf{l}}^f\cdot\mathbf{x}_d - 2\omega_{dy}\|\mathbf{l}^f\|}{\|\mathbf{l}^f\|} - \omega_{dx}\omega_{dz} \\ 0 \end{bmatrix}. \quad (7.7)$$

Since the angular velocity about the z-axis is set to zero in (7.4), the last terms of $\dot{\omega}_{dx}$ and $\dot{\omega}_{dy}$ are zero. The derivative of (7.6) is

$$\ddot{\mathbf{l}}^f = -\ddot{\varpi}(\mathbf{r}_l,\mathbf{v}_l,\mathbf{a}_l)\mathbf{e}_r - \dot{\varpi}(\mathbf{r}_l,\mathbf{v}_l)\dot{\mathbf{e}}_r - \ddot{\mathbf{p}} = -\ddot{\varpi}(\mathbf{r}_l,\mathbf{v}_l,\mathbf{a}_l)\mathbf{e}_r - \ddot{\mathbf{p}}. \quad (7.8)$$

7.2 Target pointing leader

In this scheme our objective for the spacecraft formation is to have each spacecraft, including the leader, tracking a fixed point located at the surface of *e.g.* the Earth by specifying a tracking direction of the selected pointing axis where a measurement instrument is mounted such as a camera or antenna. The target is chosen by the spacecraft operator as a given set of coordinates such as longitude (λ) and latitude (ϕ). The vector pointing from the center of Earth to the target in an Earth Centered Earth Fixed (ECEF) frame is obtained by applying

$$\mathbf{r}_t^{ef} = r_e \begin{bmatrix} \cos(\phi)\cos(\lambda) \\ \cos(\phi)\sin(\lambda) \\ \sin(\phi) \end{bmatrix}, \quad (7.9)$$

where $r_e = 6378.137 \times 10^3$ m is the Earth radius. It is assumed a perfect spherical Earth; alternatively a function of the Earth radii may be used as $r_e(\lambda,\phi)$ with longitude and latitude as arguments. We rotate the target vector to ECI coordinates by utilizing

$$\mathbf{r}_t = \mathbf{R}_{ef}^i\mathbf{r}_t^{ef}, \quad (7.10)$$

where $\mathbf{R}_{ef}^i$ can be found in (2.21).

7.2.1 Leader reference

For the leader spacecraft we start by defining a target pointing vector in inertial coordinates as

$$\mathbf{l}_{ld} = \mathbf{r}_t - \mathbf{r}_l, \tag{7.11}$$

which is used to construct a leader desired frame called $\mathcal{F}^{ld}$ as

$$\mathbf{x}_{ld} = -\frac{\mathbf{l}_{ld}}{\|\mathbf{l}_{ld}\|}, \qquad \mathbf{y}_{ld} = \frac{\mathbf{S}(\mathbf{x}_{ld})(-\mathbf{h}_l)}{\|\mathbf{S}(\mathbf{x}_{ld})(-\mathbf{h}_l)\|} \qquad \text{and} \qquad \mathbf{z}_{ld} = \mathbf{S}(\mathbf{x}_{ld})\mathbf{y}_{ld}, \tag{7.12}$$

and thus we can obtain a desired quaternion vector by transforming the constructed rotation matrix and require continuity of solution to ensure a smooth vector over time. By differentiating (7.11) twice we obtain

$$\dot{\mathbf{l}}_{ld} = \dot{\mathbf{r}}_t - \dot{\mathbf{r}}_i \tag{7.13}$$

$$\ddot{\mathbf{l}}_{ld} = \ddot{\mathbf{r}}_t - \ddot{\mathbf{r}}_i, \tag{7.14}$$

where

$$\dot{\mathbf{r}}_t = \mathbf{S}(\boldsymbol{\omega}^i_{i,ef})\mathbf{R}^i_{ef}\mathbf{r}^{ef}_t \tag{7.15}$$

$$\ddot{\mathbf{r}}_t = \mathbf{S}^2(\boldsymbol{\omega}^i_{i,ef})\mathbf{R}^i_{ef}\mathbf{r}^{ef}_t, \tag{7.16}$$

and $\boldsymbol{\omega}^i_{i,e} = [0,\ 0,\ \omega_e]^\top$ which is constant along with $\mathbf{r}^{ef}_t$. According to Wertz (1978) the relationship between the desired angular velocity and the normalized target vector is

$$\dot{\boldsymbol{\ell}}_{ld} = \mathbf{S}(\boldsymbol{\omega}^i_{i,ld})\boldsymbol{\ell}_{ld}, \tag{7.17}$$

where

$$\boldsymbol{\ell}_{ld} = [\ell_{ldx},\ \ell_{ldy},\ \ell_{ldz}]^\top = \mathbf{l}_{ld}/\|\mathbf{l}_{ld}\|. \tag{7.18}$$

The set of equations in (7.17) are linearly dependent, thus the desired angular velocity is not uniquely specified. On component form (7.17) is written as

$$\dot{\ell}_{ldx} = -\omega_{lzd}\ell_{ldy} + \omega_{lyd}\ell_{ldz} \tag{7.19a}$$

$$\dot{\ell}_{ldy} = \omega_{lzd}\ell_{ldx} - \omega_{lxd}\ell_{ldz} \tag{7.19b}$$

$$\dot{\ell}_{ldz} = -\omega_{lyd}\ell_{ldx} + \omega_{lxd}\ell_{ldy}, \tag{7.19c}$$

where $\boldsymbol{\omega}^i_{i,ld} = [\omega_{ldx},\ \omega_{ldy},\ \omega_{ldz}]^\top$. This particular problem was solved by Chen *et al.* (2000) by adding a cost constraint to minimize the amplitude of $\boldsymbol{\omega}^i_{i,ld}$ such as

$$J = \frac{1}{2}k\boldsymbol{\omega}^{i,\top}_{i,ld}\boldsymbol{\omega}^i_{i,ld}, \tag{7.20}$$

where k is a positive scalar. We then define a Hamiltonian function based on (7.19b) and (7.19c) leading to

$$\mathcal{H} = \frac{1}{2}k\boldsymbol{\omega}^{i,\top}_{i,ld}\boldsymbol{\omega}^i_{i,ld} + \lambda_1(\dot{\ell}_{ldy} - \omega_{ldz}\ell_{ldx} + \omega_{ldx}l_{ldz}) + \lambda_2(\dot{\ell}_{ldz} + \omega_{ldy}\ell_{ldx} - \omega_{ldx}\ell_{ldy}), \tag{7.21}$$

where λ_1, λ_2 are constant adjoint scalars. By differentiating (7.21) with respect to $\boldsymbol{\omega}^i_{i,ld}$ and setting the result to zero, we obtain

$$k\omega_{ldx} + \lambda_1 \ell_{ldz} - \lambda_2 \ell_{ldy} = 0 \tag{7.22a}$$
$$k\omega_{ldy} + \lambda_2 \ell_{ldx} = 0 \tag{7.22b}$$
$$k\omega_{ldz} - \lambda_1 \ell_{ldx} = 0. \tag{7.22c}$$

By inserting (7.22b) and (7.22c) into (7.22a) we obtain the relation

$$\boldsymbol{\omega}^i_{i,ld} \cdot \boldsymbol{\ell}_{ld} = 0, \tag{7.23}$$

which implies that the desired angular velocity will be orthogonal to the desired tracking direction. By solving (7.17) and (7.23) for the angular velocity, we obtain

$$\boldsymbol{\omega}^i_{i,ld} = \mathbf{S}(\boldsymbol{\ell}_{ld})\dot{\boldsymbol{\ell}}_{ld}, \tag{7.24}$$

which is a solution resulting in no rotation about the desired pointing direction during tracking maneuvers. By inserting (7.18) and its differentiated into (7.24), it can be shown that

$$\boldsymbol{\omega}^i_{i,ld} = \frac{\mathbf{S}(\mathbf{l}_{ld})\dot{\mathbf{l}}_{ld}}{\|\mathbf{l}_{ld}\|^2}, \tag{7.25}$$

and obtain the desired angular acceleration we differentiate (7.25), which leads to the expression

$$\dot{\boldsymbol{\omega}}^i_{i,ld} = \frac{\mathbf{S}(\mathbf{l}_{ld})\ddot{\mathbf{l}}_{ld}\|\mathbf{l}_{ld}\|^2 - 2\mathbf{l}_{ld}^\top \mathbf{S}(\mathbf{l}_{ld})\dot{\mathbf{l}}_{ld}}{\|\mathbf{l}_{ld}\|^2}. \tag{7.26}$$

Since the leader body frame is utilized in the dynamic equations (2.83), we simply rotate (7.25) and (7.26), obtaining

$$\boldsymbol{\omega}^{lb}_{i,ld} = \mathbf{R}^{lb}_i \boldsymbol{\omega}^i_{i,ld} \tag{7.27}$$
$$\dot{\boldsymbol{\omega}}^{lb}_{i,ld} = -\mathbf{S}(\boldsymbol{\omega}^{lb}_{i,lb})\mathbf{R}^{lb}_i \boldsymbol{\omega}^i_{i,ld} + \mathbf{R}^{lb}_i \dot{\boldsymbol{\omega}}^i_{i,ld}. \tag{7.28}$$

7.2.2 Follower reference

The procedure to generate a follower reference is similar to the one presented in Section 7.2.1. We start by defining a target pointing vector in the inertial frame as

$$\mathbf{l}_{fd} = \mathbf{r}_t - \mathbf{r}_l - \mathbf{R}^i_{lo}\mathbf{p}, \tag{7.29}$$

which is used to construct a follower desired reference frame called $\mathcal{F}^{fd}$ as

$$\mathbf{x}_{fd} = -\frac{\mathbf{l}_{fd}}{\|\mathbf{l}_{fd}\|}, \qquad \mathbf{y}_{fd} = \frac{\mathbf{S}(\mathbf{x}_{fd})(-\mathbf{h}_l)}{\|\mathbf{S}(\mathbf{x}_{fd})(-\mathbf{h}_l)\|} \qquad \text{and} \qquad \mathbf{z}_{fd} = \mathbf{S}(\mathbf{x}_{fd})\mathbf{y}_{fd}. \tag{7.30}$$

We can now construct a rotation matrix between $\mathcal{F}^{fd}$ and $\mathcal{F}^i$, and because the relative rotation is between $\mathcal{F}^{fb}$ and $\mathcal{F}^{lb}$ we apply composite rotation, thus obtaining

$$\mathbf{R}^{lb}_{fd} = \mathbf{R}^{lb}_i \mathbf{R}^i_{fd}, \tag{7.31}$$

and transform the rotation matrix (7.31) to the desired quaternion –*cf.* (Sidi, 1997). By differentiating (7.29) twice, we obtain

$$\dot{\mathbf{l}}_{fd} = \dot{\mathbf{r}}_t - \dot{\mathbf{r}}_l - \mathbf{S}(\boldsymbol{\omega}^i_{i,lo})\mathbf{R}^i_{lo}\mathbf{p} - \mathbf{R}^i_{lo}\dot{\mathbf{p}} \tag{7.32}$$

$$\ddot{\mathbf{l}}_{fd} = \ddot{\mathbf{r}}_t - \ddot{\mathbf{r}}_l - (\mathbf{S}(\dot{\boldsymbol{\omega}}^i_{i,lo}) + \mathbf{S}^2(\boldsymbol{\omega}^i_{i,lo}))\mathbf{R}^i_{lo}\mathbf{p} - 2\mathbf{S}(\boldsymbol{\omega}^i_{i,lo})\mathbf{R}^i_{lo}\dot{\mathbf{p}} - \mathbf{R}^i_{lo}\ddot{\mathbf{p}}. \tag{7.33}$$

The same optimization technique as presented in Section 7.2.1 can then be applied, leading to

$$\boldsymbol{\omega}^i_{i,fd} = \frac{\mathbf{S}(\mathbf{l}_{fd})\dot{\mathbf{l}}_{fd}}{\|\mathbf{l}_{fd}\|^2} \tag{7.34}$$

$$\dot{\boldsymbol{\omega}}^i_{i,fd} = \frac{\mathbf{S}(\mathbf{l}_{fd})\ddot{\mathbf{l}}_{fd}\|\mathbf{l}_{fd}\|^2 - 2\mathbf{l}^\top_{fd}\mathbf{S}(\mathbf{l}_{fd})\dot{\mathbf{l}}_{fd}}{\|\mathbf{l}_{fd}\|^2}, \tag{7.35}$$

and the desired angular rotation and acceleration vectors can be transformed according to the relative dynamics of (2.87), resulting in

$$\boldsymbol{\omega}^{fb}_{lb,fd} = \mathbf{R}^{fb}_i\boldsymbol{\omega}^i_{i,fd} - \mathbf{R}^{fb}_{lb}\boldsymbol{\omega}^{lb}_{i,lb}\ , \tag{7.36}$$

$$\dot{\boldsymbol{\omega}}^{fb}_{lb,fd} = -\mathbf{S}(\boldsymbol{\omega}^{fb}_{i,fb})\mathbf{R}^{fb}_i\boldsymbol{\omega}^i_{i,fd} + \mathbf{R}^{fb}_i\dot{\boldsymbol{\omega}}^i_{i,fd} + \mathbf{S}(\boldsymbol{\omega}^{fb}_{lb,fb})\mathbf{R}^{fb}_{lb}\boldsymbol{\omega}^{lb}_{i,lb} - \mathbf{R}^{fb}_{lb}\dot{\boldsymbol{\omega}}^{lb}_{i,lb}. \tag{7.37}$$

7.3 Simulation results

In this section we present simulation results based on the reference generation schemes presented in this chapter. Our main focus is to show that the presented schemes are generating smooth and correct references which the followers are able to track by utilizing translational and rotational synchronizing control laws presented in Section 6.3. We utilize simulation data as presented in Section 2.8.1 if otherwise is not stated.

7.3.1 Nadir pointing leader

In this section we present simulation results where the leader was commanded to be nadir pointing while the follower spacecraft were tracking the same point on the Earth surface during a translational maneuver, based on the reference generation scheme presented in Section 7.1. For the leader spacecraft we chose a circular Earth orbit with an altitude of 600 km, with an inclination of 79°, and the maximum available force and torque was limited to 0.2 N and 0.05 Nm respectively, while for control we utilized a 3+3DOF PD+ controller

$$\mathbf{u}_f = \mathbf{M}_f\dot{\mathbf{x}}_{d2} + \mathbf{C}(\dot{\nu},\boldsymbol{\omega})\mathbf{x}_{d2} + \mathbf{D}(\dot{\nu},\ddot{\nu},r_f)\mathbf{x}_1 + \mathbf{n}(\boldsymbol{\omega},r_f,r_l) - \mathbf{w}_f - \mathbf{K}_p\Lambda^\top_e\mathbf{e}_1 - \mathbf{K}_d\mathbf{e}_2,$$

with gains $\mathbf{K}_p = \mathrm{diag}\{0.003\mathbf{I},\mathbf{I}\}$ and $\mathbf{K}_d = 2\mathrm{diag}\{\mathbf{I},\mathbf{I}\}$, which can be proven to lead to uniform asymptotic stability of the equilibrium point of the closed-loop system; –*cf.* (Kristiansen, 2008) for details on the controller and stability analysis. The initial relative position and attitude for the follower spacecraft were chosen as standstill at $\mathbf{p}(t_0) = [200,\ 100,\ -300]^\top$, and $\mathbf{q}(t_0) = [1,\ \mathbf{0}^\top]^\top$, while the desired

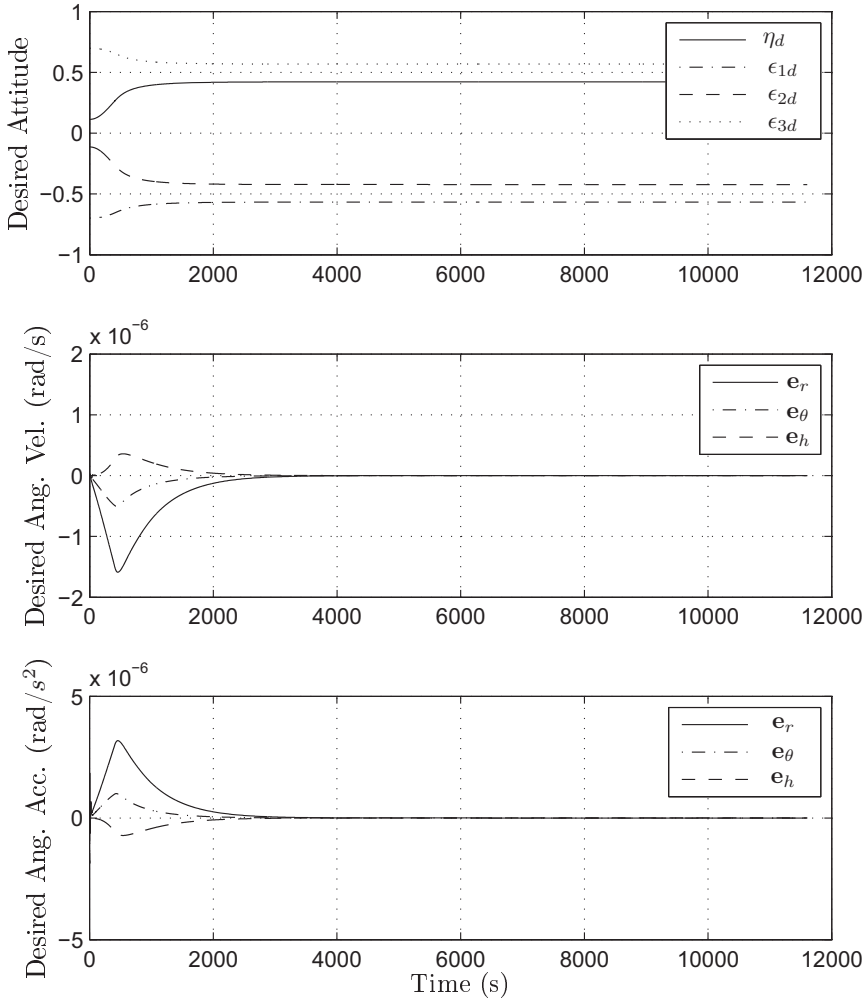

Figure 7.2: Generated attitude, angular velocity and angular acceleration.

relative position was chosen as standstill at $\mathbf{p}_d = [-200,\ 1000,\ -300]^\top$ and desired attitude and rotational motion according to what was presented in Section 7.1. The simulation was performed without perturbations to better illustrate its purpose. Also note that the generated references are presented with respect to the leader orbit frame.

Figure 7.2 shows the generated references for relative attitude, angular velocity and angular acceleration which are transient in the first 3000 s because of the translational motion of the follower spacecraft and, because of the circular orbit, the reference is constant when the translational maneuver is completed because the representation is relative to the orbit frame. In Figure 7.3 the relative position and

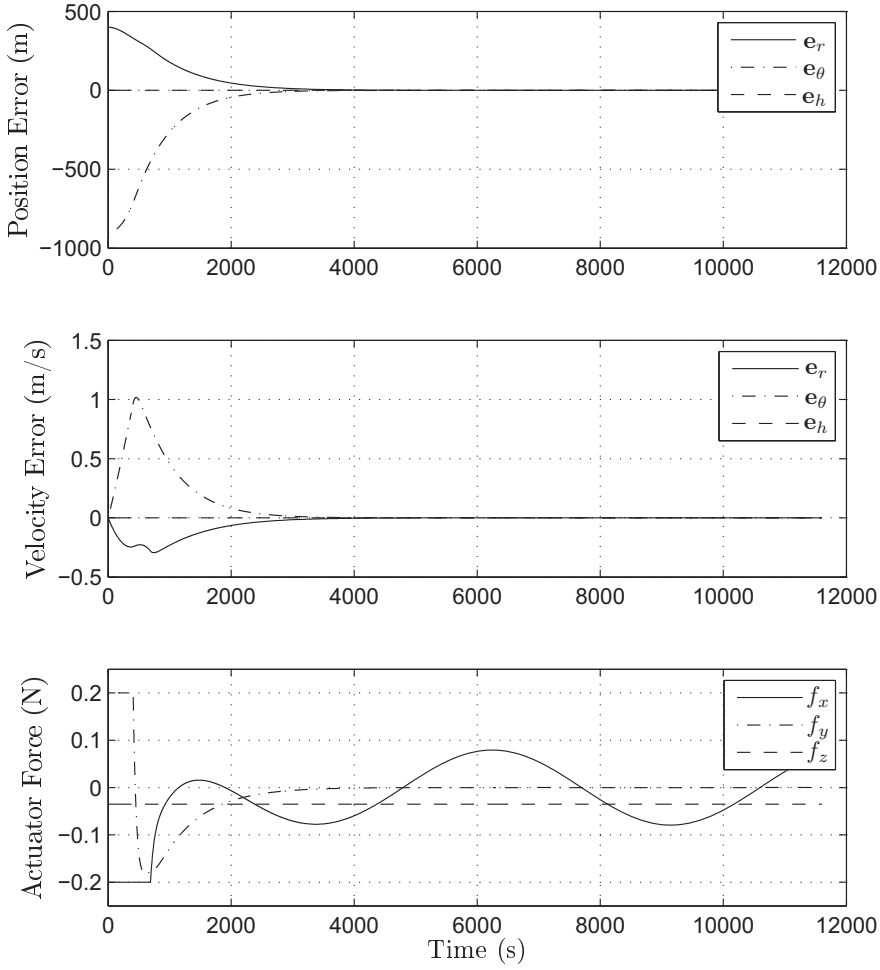

Figure 7.3: Settling of relative position and velocity error, and actuator force.

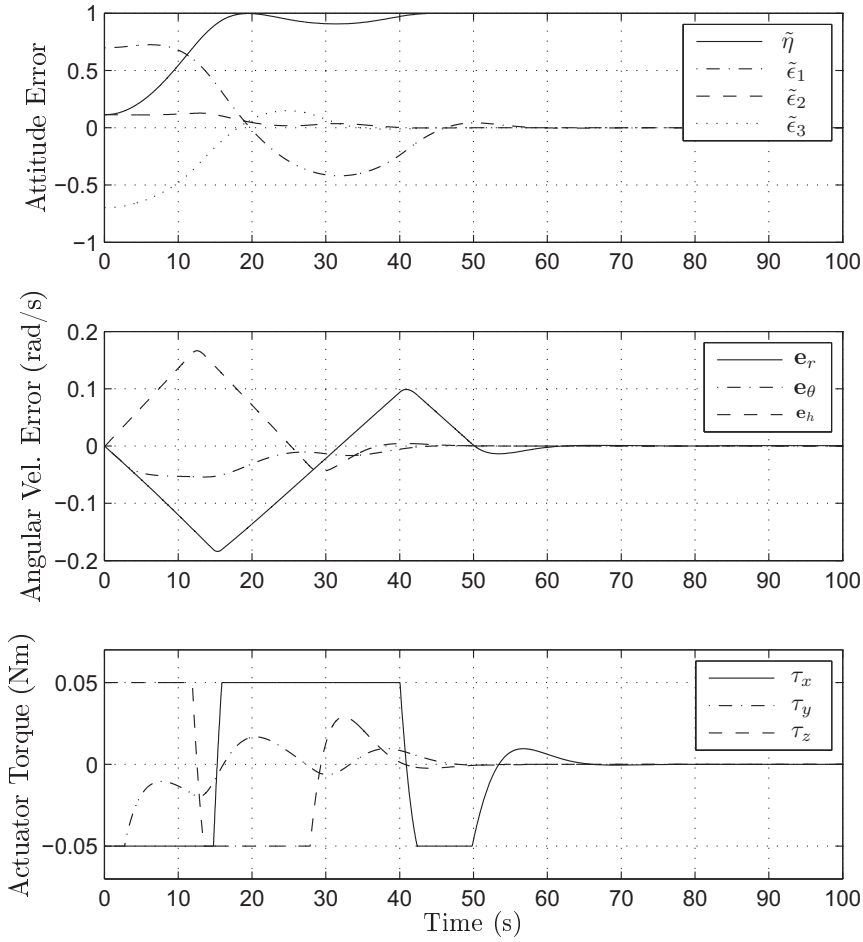

Figure 7.4: Settling of relative attitude and angular velocity, and actuator torque.

velocity errors are presented showing the translational motion during the reconfiguration. The bottommost plot depicts the actuator force during two consecutive orbits and as can be seen, is quite active during all parts of the simulation, which is because the follower spacecraft is commanded to keep a fixed relative position to the leader spacecraft thus challenging the natural orbital motion. The relative attitude and angular velocity is depicted in Figure 7.4 which shows that the controller is able to track the generated reference. Lastly, Figure 7.5 shows both latitude and longitude on the Earth surface of where the follower and leader spacecraft are pointing their instruments. The follower spacecraft is not pointing at the Earth surface during the first eight seconds, and after this it can be seen that both measuring points coincides even as the follower is performing a translational maneuver.

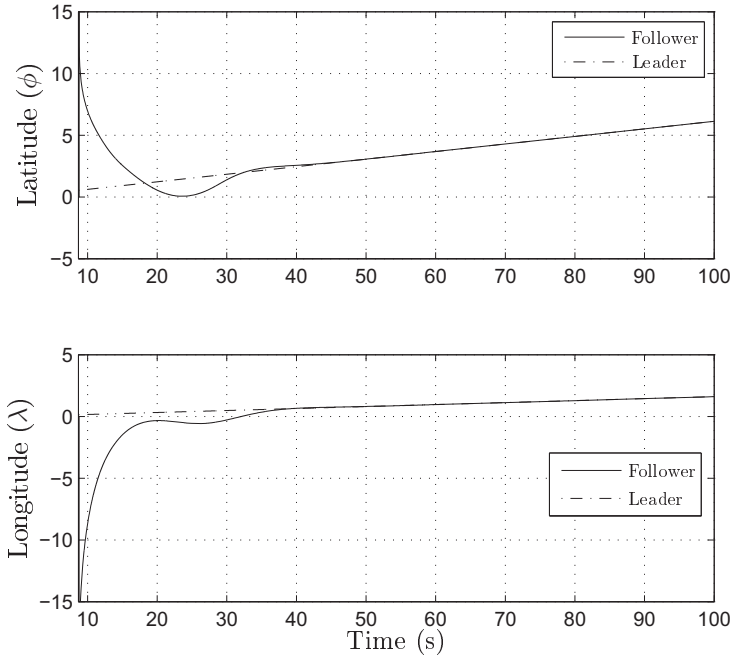

Figure 7.5: Latitude and longitude of intersection point between instrument pointing vector and Earth surface during maneuver for leader and follower spacecraft.

7.3.2 Target pointing leader

In this section we present simulation results where one leader and one follower spacecraft were tracking a common point on the Earth surface based on the reference generation scheme presented in Section 7.2. For this simulation we utilized an inclination of 79°, and the tracking point was located at the Earth surface at zero degrees latitude (ϕ) and longitude (λ), and both spacecraft continued tracking the point even if it was outside the field of view. The initial conditions were set to $\mathbf{p}(t_0) = [0,\ -100,\ 0]^\top$, $\dot{\mathbf{p}}(t_0) = \ddot{\mathbf{p}}(t_0) = \mathbf{0}$, $\mathbf{q}_l(t_0) = \mathbf{q}_f(t_0) = [0.9437,\ 0.1277,\ 0.1449,\ -0.2685]^\top$, $\boldsymbol{\omega}_{i,lb}^{lb}(t_0) = [1.745\ -3.491\ 0.873]^\top \times 10^{-3}$ and $\boldsymbol{\omega}_{i,fb}^{fb}(t_0) = [0,\ 0,\ 0]^\top$. The desired conditions for relative translation were set to $\mathbf{p}_d = [0,\ -1000,\ 500]^\top$ m, $\dot{\mathbf{p}}_d = \ddot{\mathbf{p}}_d = \mathbf{0}$, while the desired values for relative rotation were calculated based on the results presented in Section 7.2. We utilized the control laws presented in Section 6.3 for this simulation where the controller gains were set to $\mathbf{K}_p = \mathbf{K}_d = 0.5\mathbf{I}$ for control of relative translation, and $k_{lq} = k_{fq} = 5$, $k_{l\omega} = k_{f\omega} = 10$ and $\gamma_l = \gamma_f = 1$ for control of relative rotation.

Noise was added to the measured vectors such that $\mathbf{r}_{ln} = \mathbf{r}_l + 0.01\mathbb{B}^3$, $\mathbf{p}_n = \mathbf{p}+0.01\mathbb{B}^3$, $\mathbf{v}_{ln} = \mathbf{v}_l+5\times10^{-3}\mathbb{B}^3$, $\dot{\mathbf{p}}_n = \dot{\mathbf{p}}+5\times10^{-3}\mathbb{B}^3$. The measured states $\mathbf{q}_{ln}$ and $\mathbf{q}_n$ satisfies $\mathbf{q}_{ln} \in (\mathbf{q}_l+[0,\ (0.001\mathbb{B}^3)^\top]^\top)\cap\mathcal{S}^{3,1}$ and $\mathbf{q}_n \in (\mathbf{q}+[0,\ (0.001\mathbb{B}^3)^\top]^\top)\cap\mathcal{S}^3$,

[1] Noise is added to the vector $\boldsymbol{\epsilon}_l$ and the quaternion is normalized through η_l.

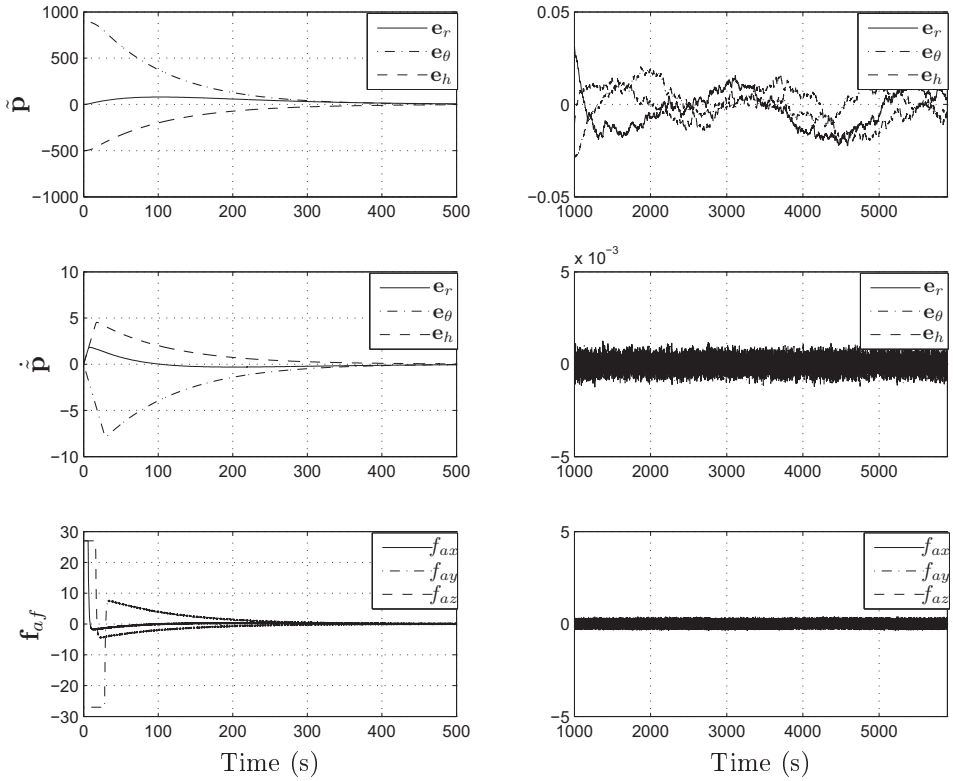

Figure 7.6: Relative position error, relative velocity error and control force with uncompensated disturbances and unfiltered sensor noise.

and $\boldsymbol{\omega}_{ln} = \boldsymbol{\omega}_{i,lb}^{lb} + 2 \times 10^{-3}\mathbb{B}^3$ and $\boldsymbol{\omega}_n = \boldsymbol{\omega} + 2 \times 10^{-3}\mathbb{B}^3$. The simulation time is set to one orbital period (5896 s) to show the performance of the reference generation scheme. Note that the generated references are presented with respect to the inertial frame.

Figure 7.6 shows the relative position, velocity and control force during both settling and station keeping phase. As can be seen the position of the follower spacecraft converged to the desired position and kept within a few centimeters during one orbital period. Figure 7.7 shows the relative attitude, angular velocity and control torque during settling and station keeping phase, and results similar to the relative translation can be observed for relative rotation as well thus, all states are converging towards the equilibrium point and kept close during the following orbit. The three topmost plots in Figure 7.8 shows the desired attitude, angular velocity and angular acceleration for the follower spacecraft during one orbit. What can be seen is that there is no rotation about the x-axis during the orbital period which is expected because of the assumption of no rotation along the pointing axis. It should also be mentioned that the desired angular velocity and acceleration is smaller during the second pass compared to the first. This is because the Earth is

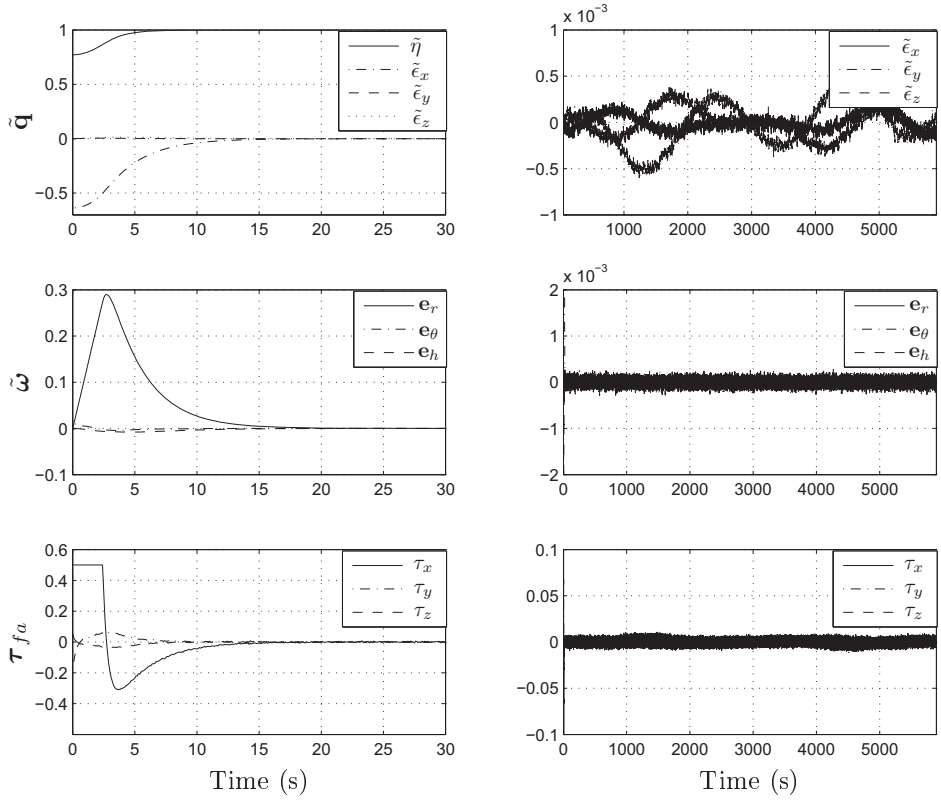

Figure 7.7: Relative attitude error, relative angular velocity error and control torque with uncompensated disturbances and unfiltered sensor noise.

rotating, thus the distance between the spacecraft and target is longer, causing less fluctuation of the components. Also note that $\tilde{\eta}_{fd}$ is negative after one revolution which is because the rotation is generated with respect to the inertial frame, thus leading close to a 2π rotation. The bottommost plot in Figure 7.8 shows the $\tilde{\boldsymbol{\epsilon}}_d$ components of the difference in desired attitude between the leader and follower, defined as $\tilde{\mathbf{q}}_d = \eta_{ld}\boldsymbol{\epsilon}_{fd} - \eta_{fd}\boldsymbol{\epsilon}_{ld} - \mathbf{S}(\boldsymbol{\epsilon}_{fd})\boldsymbol{\epsilon}_{ld}$. Here it can be seen that the follower spacecraft was moving away from the leader spacecraft during the first 500 seconds because of the increasing desired relative attitude during the same period.

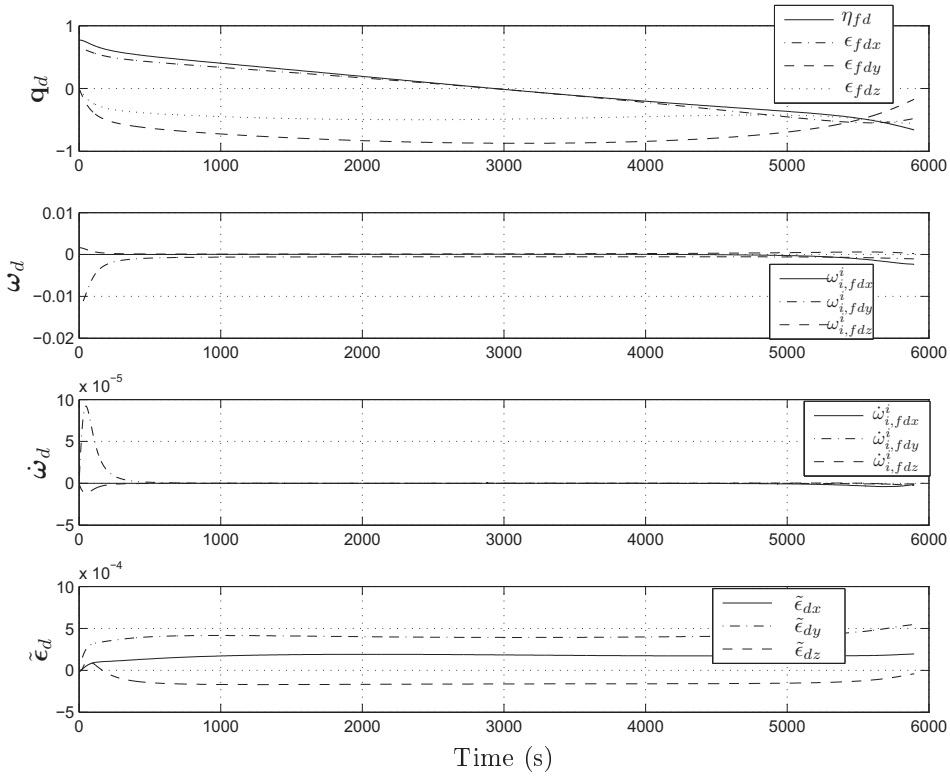

Figure 7.8: Follower desired attitude, angular velocity, angular acceleration and relative desired attitude with uncompensated disturbances and unfiltered sensor noise.

Chapter 8

Leader-follower formation reconfiguration with collision avoidance

In this chapter we utilize a concept called Null-Space Based (NSB) behavioral control for collision avoidance and reconfiguration of spacecraft formations, which is a concept based on work done for control of robot manipulators. For correctness we start by extending our previous model and control for n followers in Section 8.1 and present the framework of inverse kinematics which the NSB concept is based on in Section 8.2, following with several different collision avoidance tasks in Section 8.3. A thorough stability analysis of the leader-follower dynamics, control law and NSB-guidance in closed-loop is presented in Section 8.4 and validated in Section 8.5 through simulations. The results presented in this chapter are based on (Schlanbusch *et al.*, 2008*a*, 2011*g*).

8.1 Multiple followers

In this section we expand the translational modeling presented in Section 2.5.3 for multiple followers, and similar for sliding surface control of multiple followers as presented in Section 6.3.2.

8.1.1 Modeling of multiple followers

We start by expanding the model presented in Section 2.5.3 for a formation consisting of multiple follower spacecraft. In the following, we consider a formation consisting of one leader and n followers and denote the dynamics for each follower $\iota \in \{1, \ldots, n\}$ as

$$m_{f,\iota}\ddot{\mathbf{p}}_\iota + \mathbf{C}_{t,\iota}(\boldsymbol{\omega}^l_{i,l})\dot{\mathbf{p}}_\iota + \mathbf{D}_{t,\iota}(\dot{\boldsymbol{\omega}}^l_{i,l}, \boldsymbol{\omega}^l_{i,l}, r_{f,\iota})\mathbf{p}_\iota + \mathbf{n}_{t,\iota}(\mathbf{r}_l, r_{f,\iota}) = \mathbf{F}_{a,\iota} + \mathbf{F}_{d,\iota}, \quad (8.1)$$

where

$$\mathbf{C}_{t,\iota}(\boldsymbol{\omega}_{i,l}^{l}) = 2m_{f,\iota}\mathbf{S}(\boldsymbol{\omega}_{i,l}^{l}) \tag{8.2}$$

$$\mathbf{D}_{t,\iota}(\dot{\boldsymbol{\omega}}_{i,l}^{l}, \boldsymbol{\omega}_{i,l}^{l}, r_{f,\iota}) = m_{f,\iota}[\mathbf{S}^2(\boldsymbol{\omega}_{i,l}^{l}) + \mathbf{S}(\dot{\boldsymbol{\omega}}_{i,l}^{l}) + \mathbf{I}\mu/r_{f,\iota}^3] \tag{8.3}$$

$$\mathbf{n}_{t,\iota}(\mathbf{r}_l, r_{f,\iota}) = \mu m_{f,\iota}\mathbf{R}_i^l[1/r_{f,\iota}^3 - 1/r_l^3]\mathbf{r}_l. \tag{8.4}$$

The composite perturbation force $\mathbf{F}_{d,\iota}$ and the composite relative control force $\mathbf{F}_{a,\iota}$ are expressed as

$$\mathbf{F}_{d,\iota} = \mathbf{R}_i^l(\mathbf{f}_{df,\iota} - \mathbf{f}_{dl}m_{f,\iota}/m_l), \quad \mathbf{F}_{a,\iota} = \mathbf{R}_i^l(\mathbf{f}_{af,\iota} - \mathbf{f}_{al}m_{f,\iota}/m_l), \tag{8.5}$$

respectively. Note that all forces $\mathbf{f}$ are expressed in the inertial frame. If the forces are computed in another frame, the rotation matrix should be replaced accordingly.

8.1.2 Control of multiple followers

The control problem is to design controllers such that each follower is tracking a desired trajectory $\mathbf{p}_d(t) = [\mathbf{p}_{d,1}^\top(t), \ldots, \mathbf{p}_{d,n}^\top(t)]^\top$ with corresponding $\dot{\mathbf{p}}_d(t)$ and $\ddot{\mathbf{p}}_d(t)$ defined likewise, which are all bounded functions. Reference trajectories[1] are defined for each follower as $\dot{\mathbf{p}}_{\rho,\iota}(t) = \dot{\mathbf{p}}_{d,\iota}(t) - \gamma_\iota\tilde{\mathbf{p}}_\iota$, $\dot{\mathbf{p}}_\rho(t) = [\dot{\mathbf{p}}_{\rho,1}^\top(t), \ldots, \dot{\mathbf{p}}_{\rho,n}^\top(t)]^\top$ and $\ddot{\mathbf{p}}_\rho(t) = [\ddot{\mathbf{p}}_{\rho,1}^\top(t), \ldots, \ddot{\mathbf{p}}_{\rho,n}^\top(t)]^\top$ its derivative, $\gamma_\iota > 0$ is a constant gain, $\tilde{\mathbf{p}}_\iota = \mathbf{p}_\iota - \mathbf{p}_{d,\iota}(t)$ is the position error and $\tilde{\mathbf{p}} = [\tilde{\mathbf{p}}_1\top, \ldots, \tilde{\mathbf{p}}_n^\top]^\top$. The sliding surface is defined as

$$\mathbf{s}_\iota = \dot{\mathbf{p}}_\iota - \dot{\mathbf{p}}_{\rho,\iota} = \dot{\tilde{\mathbf{p}}}_\iota + \gamma_\iota\tilde{\mathbf{p}}_\iota, \tag{8.6}$$

and we denote $\mathbf{s} = [\mathbf{s}_1^\top, \ldots, \mathbf{s}_n^\top]^\top$. Model based control laws based on (6.19) for each spacecraft individually are expressed as

$$\begin{aligned}\mathbf{f}_{af,\iota} =& m_{f,\iota}\ddot{\mathbf{p}}_{\rho,\iota} + \mathbf{C}_{t,\iota}(\boldsymbol{\omega}_{i,l}^{l})\dot{\mathbf{p}}_{\rho,\iota} + \mathbf{D}_{t,\iota}(\dot{\boldsymbol{\omega}}_{i,l}^{l}, \boldsymbol{\omega}_{i,l}^{l}, r_{f,\iota})\mathbf{p}_\iota \\ &+ \mathbf{n}_{t,\iota}(\mathbf{r}_l, r_{f,\iota}) - \mathbf{f}_{df,\iota} - \mathbf{K}_{p,\iota}\tilde{\mathbf{p}}_\iota - \mathbf{K}_{d,\iota}\mathbf{s}_\iota,\end{aligned} \tag{8.7}$$

where $\mathbf{K}_{p,\iota}$ and $\mathbf{K}_{d,\iota}$ are both symmetric positive definite matrices and $\mathbf{K}_{p,\iota}, \mathbf{K}_{d,\iota} \in \mathbb{R}^{3\times3}$. By inserting (8.6) and (8.7) into (8.1) and stack the resulting systems, the closed-loop dynamics may be written as

$$m_f\dot{\mathbf{s}} + (\mathbf{C}_t + \mathbf{K}_d)\,\mathbf{s} + \mathbf{K}_p\tilde{\mathbf{p}} = \mathbf{0}, \tag{8.8}$$

where $\mathbf{K}_p = \mathrm{diag}\{\mathbf{K}_{p,1}, \ldots, \mathbf{K}_{p,n}\} \in \mathbb{R}^{3n\times3n}$, $\mathbf{K}_d = \mathrm{diag}\{\mathbf{K}_{d,1}, \ldots, \mathbf{K}_{d,n}\} \in \mathbb{R}^{3n\times3n}$ and $\mathbf{C}_t(\boldsymbol{\omega}_{i,l}^{l}) = \mathrm{diag}\{\mathbf{C}_{t,1}(\boldsymbol{\omega}_{i,l}^{l}), \ldots, \mathbf{C}_{t,n}(\boldsymbol{\omega}_{i,l}^{l})\} \in \mathbb{R}^{3n\times3n}$.

8.2 Inverse kinematics

The general goal is to control each spacecraft while performing different tasks. For compactness we use the notation $\mathbf{p} = [\mathbf{p}_1^\top, \ldots, \mathbf{p}_n^\top]^\top \in \mathbb{R}^{3n}$ and $\dot{\mathbf{p}} = [\dot{\mathbf{p}}_1^\top, \ldots, \dot{\mathbf{p}}_n^\top]^\top \in$

[1] We denote reference trajectories by ρ instead of r.

$\mathbb{R}^{3n}$. The tasks to be controlled are represented by a task variable defined as $\boldsymbol{\sigma} = f(\mathbf{p}_1, \ldots, \mathbf{p}_n) \in \mathbb{R}^m$, and its derivative can be expressed as

$$\dot{\boldsymbol{\sigma}} = \sum_{i=1}^{n} \frac{\partial \mathbf{f}(\mathbf{p})}{\partial \mathbf{p}_i} \dot{\mathbf{p}}_i = \mathbf{J}(\mathbf{p})\dot{\mathbf{p}}, \tag{8.9}$$

where $\mathbf{J} \in \mathbb{R}^{m \times 3n}$ is the configuration-dependent Jacobian matrix. Often $3n > m$, and thus we achieve infinite number of solutions, and an optimization technique is required. This is usually solved for by requiring minimum-norm velocity using least-square solution

$$\dot{\mathbf{p}}_d = \mathbf{J}^{\dagger}\dot{\boldsymbol{\sigma}}_d = \mathbf{J}^{\top}(\mathbf{J}\mathbf{J}^{\top})^{-1}\dot{\boldsymbol{\sigma}}_d, \tag{8.10}$$

where $\boldsymbol{\sigma}_d(t)$ is the desired time history of $\boldsymbol{\sigma}(t)$, and $\dot{\mathbf{p}}_d(t)$ is the desired relative velocity between the leader and follower spacecraft. Position references can be obtained by time integration of $\dot{\mathbf{p}}_d$ utilizing the Closed-Loop Inverse Kinematics (CLIK)-algorithm (Antonelli and Chiaverini, 2006). By defining $\tilde{\boldsymbol{\sigma}} = \boldsymbol{\sigma}_d - \boldsymbol{\sigma}$, we obtain

$$\dot{\mathbf{p}}_d(t_k) = \mathbf{J}^{\dagger}(\dot{\boldsymbol{\sigma}}_d + \boldsymbol{\Lambda}\tilde{\boldsymbol{\sigma}})|_{t=t_k} \tag{8.11}$$

and

$$\mathbf{p}_d(t_k) = \mathbf{p}_d(t_{k-1}) + \dot{\mathbf{p}}_d(t_k)\Delta t, \tag{8.12}$$

where t_k is the k-th time sample, Δt is the sampling period, and $\boldsymbol{\Lambda}$ is a constant positive definite matrix of gains. By projecting the different sub-task velocities onto the null-space created by the Jacobian matrices of higher prioritized sub-tasks, the competitive problem is solved. Each sub-task first has to calculate the desired velocity as

$$\dot{\mathbf{p}}_{jd} = \mathbf{J}_j^{\dagger}(\dot{\boldsymbol{\sigma}}_{jd} + \boldsymbol{\Lambda}_j\tilde{\boldsymbol{\sigma}}_j), \tag{8.13}$$

where j denotes the j-th task, such that $\dot{\boldsymbol{\sigma}}_{jd}$ and $\tilde{\boldsymbol{\sigma}}_j$ is $\dot{\boldsymbol{\sigma}}_d$ and $\tilde{\boldsymbol{\sigma}}$ for the j-th task, respectively. By solving each sub-task individually the tasks can be merged together using

$$\dot{\mathbf{p}}_d^{(j)} = \dot{\mathbf{p}}_{jd} + (\mathbf{I} - \mathbf{J}_j^{\dagger}\mathbf{J}_j)\dot{\mathbf{p}}_d^{(j+1)}, \qquad j = m, \ldots, 1 \tag{8.14}$$

where $\dot{\mathbf{p}}_d^{(j)}$ is the current vehicles velocity vector including the tasks with priority from m to j. The initial condition is set to be $\dot{\mathbf{p}}_d^{(m+1)} = \mathbf{0}$, and the final desired velocity $\dot{\mathbf{p}}_d = \dot{\mathbf{p}}_d^{(1)}$. By putting together three different sub-tasks we obtain

$$\dot{\mathbf{p}}_d = \dot{\mathbf{p}}_1 + (\mathbf{I} - \mathbf{J}_1^{\dagger}\mathbf{J}_1)[\dot{\mathbf{p}}_2 + (\mathbf{I} - \mathbf{J}_2^{\dagger}\mathbf{J}_2)\dot{\mathbf{p}}_3]. \tag{8.15}$$

A sketch of the architecture of the NSB method is depicted in Figure 8.1 where the supervisor may change the priority (and weighting) of the different sub-tasks throughout the mission if new requirements are given. This architecture leads to a velocity output as shown in Figure 8.2. The process is performed individually by each follower.

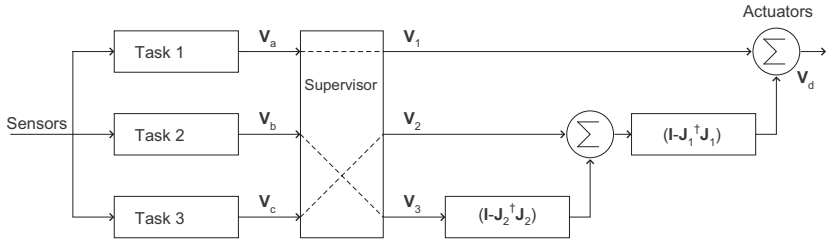

Figure 8.1: Sketch of NSB control using three different tasks.

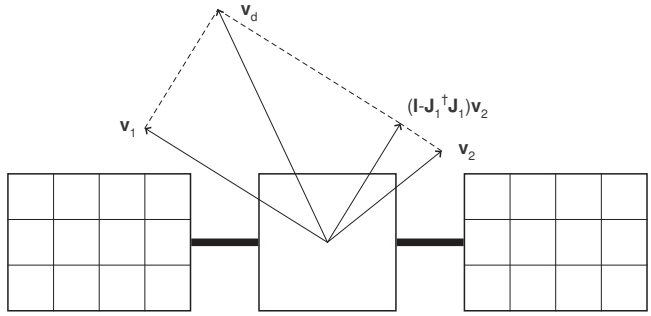

Figure 8.2: Velocity output using null space projection.

8.3 NSB tasks

With the general dynamics for the NSB approach introduced, we proceed to present the sub-tasks for controlling the spacecraft. Two different tasks will be presented in this chapter, but additional tasks can be introduced according to other mission requirements. Each task function is presented as $\boldsymbol{\sigma}_j,\ j \in \{m, \ldots, 1\}$, where the subscript describes the priority of the task, ranging from m (lowest) to one (highest). All task functions for each follower $\iota \in \{1, \ldots, n\}$ produces a driving velocity $\dot{\mathbf{p}}_{jd,\iota}$ for each task j.

8.3.1 Collision avoidance

The collision and obstacle avoidance task function is used to ensure that collision between spacecraft does not occur during formation reconfiguration. If one or more of the spacecraft is out of control, it is treated as an obstacle which the remaining spacecraft must avoid. The task is built individually for each spacecraft, and not as an aggregate task function. The current obstacle for each follower is chosen as the *closest* obstacle at any given time. An alternative approach to choosing the nearest obstacle is to introduce a weighting function considering *each obstacle*,

but this could lead to cases where *e.g.* the output velocity is equal to zero, and thus the mission can be delayed while control is lost, or even worse; consider a formation of three followers positioned along a line intersecting all three, where two of the followers both are moving towards the central follower, a collision might be unavoidable.

We present two different approaches: by static collision avoidance we mean that the sphere surrounding each obstacle is of constant size d, while by dynamical collision avoidance we speak of a state dependent sphere surrounding each obstacle where the size is determined by the relative position and velocity between the follower and the respective obstacle. In each case, a unit vector is calculated pointing at the closest obstacle expressed as

$$\hat{\mathbf{r}}_\iota = \frac{\mathbf{p}_\iota - \mathbf{p}_o}{\|\mathbf{p}_\iota - \mathbf{p}_o\|} \tag{8.16}$$

where $\mathbf{p}_o$ is the obstacle *closest* to the ι-th spacecraft which position is given relative to the leader spacecraft. The Jacobian matrix can be written as $\mathbf{J}_{o,\iota} = \hat{\mathbf{r}}_\iota^\top$, and for compactness we write $\dot{\mathbf{p}}_{od} = [\dot{\mathbf{p}}_{od,1}^\top, \ldots, \dot{\mathbf{p}}_{od,n}^\top]^\top \in \mathbb{R}^{3n}$ and $\mathbf{J}_o = [\mathbf{J}_{o,1}^\top, \ldots, \mathbf{J}_{o,n}^\top]^\top \in \mathbb{R}^{1\times 3n}$.

Static collision avoidance with constant gain

The task function for each follower $\iota \in \{1, \ldots, n\}$ produces a driving velocity away from an obstacle, represented as

$$\sigma_{o,\iota} = \|\mathbf{p}_\iota - \mathbf{p}_o\|, \tag{8.17}$$

and each obstacle is covered by a virtual sphere

$$\bar{\mathcal{B}}_{o,\iota} = \{\mathbf{p}_\iota, \mathbf{p}_o \in \mathbb{R}^3 : \|\mathbf{p}_\iota - \mathbf{p}_o\| \leq d_\iota\}, \tag{8.18}$$

where we denote $\sigma_{od,\iota} = d_\iota$ where d_ι is the minimum allowed distance between the spacecraft and the obstacle. The general equation (8.13) can then be written as

$$\dot{\mathbf{p}}_{od,\iota} = \mathbf{J}_{o,\iota}^\dagger \lambda_{o,\iota} \tilde{\sigma}_{o,\iota} = \lambda_{o,\iota}(d - \|\mathbf{p}_\iota - \mathbf{p}_o\|)\hat{\mathbf{r}}_\iota. \tag{8.19}$$

That is, if a follower enters the static safety sphere d_ι of an obstacle, a desired velocity vector based on the *relative* position $\mathbf{p}_{o,\iota} := \mathbf{p}_\iota - \mathbf{p}_o$ scaled by the constant gain $\lambda_{o,\iota}$ is produced.

Static collision avoidance with variable gain

The task function for each follower $\iota \in \{1, \ldots, n\}$ produces a driving velocity away from an obstacle, represented as

$$\sigma_{o,\iota} = \left(\max\{\|\mathbf{p}_\iota - \mathbf{p}_o\|, d_\iota\} + d_\iota - \|\dot{\mathbf{p}}_\iota - \dot{\mathbf{p}}_o\|\right), \tag{8.20}$$

where each spacecraft is surrounded by a virtual sphere

$$\bar{\mathcal{B}}_{o,\iota} = \{\mathbf{p}_\iota, \mathbf{p}_o \in \mathbb{R}^3 : \|\mathbf{p}_\iota - \mathbf{p}_o\| \leq d_\iota\}. \tag{8.21}$$

Then the general equation (8.13) can then be written as

$$\begin{aligned}\dot{\mathbf{p}}_{od,\iota} &= \mathbf{J}_{o,\iota}^{\dagger}\lambda_{o,\iota}\tilde{\sigma}_{o,\iota} \\ &=\lambda_{o,\iota}(\|\tilde{\mathbf{p}}_{\iota}\|,\|\dot{\mathbf{p}}_{\iota}\|)\left(\max\{d_{\iota}-\|\mathbf{p}_{\iota}-\mathbf{p}_{o}\|,0\}+\|\dot{\mathbf{p}}_{\iota}-\dot{\mathbf{p}}_{o}\|\right)\hat{\mathbf{r}}_{\iota},\end{aligned} \tag{8.22}$$

where $\lambda_{o,\iota}(\|\tilde{\mathbf{p}}_{\iota}\|,\|\dot{\mathbf{p}}_{\iota}\|) > 0$ is a variable gain to be defined. Note that $\tilde{\sigma}_{o,\iota} > 0$ when the task is active and we define $\tilde{\sigma}_{o,\iota} = 0$ when the task is inactive. That is, if a follower enters the static safety sphere d_{ι} of an obstacle, a desired velocity vector based on relative position $\mathbf{p}_{o,\iota}$ and velocity $\dot{\mathbf{p}}_{o,\iota}$ scaled by the variable gain $\lambda_{o,\iota}(\|\tilde{\mathbf{p}}_{\iota}\|,\|\dot{\mathbf{p}}_{\iota}\|)$ is produced.

Dynamic collision avoidance with constant gain

The task function for each follower $\iota \in \{1,\ldots,n\}$ produces a driving velocity away from an obstacle, represented as

$$\sigma_{o,\iota} = \|\mathbf{p}_{\iota}-\mathbf{p}_{o}\|, \tag{8.23}$$

and each obstacle is covered by a virtual sphere

$$\bar{\mathcal{B}}_{o,\iota}(\mathbf{p}_{o,\iota},\dot{\mathbf{p}}_{o,\iota}) = \left\{\mathbf{p}_{o,\iota},\dot{\mathbf{p}}_{o,\iota}\in\mathbb{R}^{3} : \|\mathbf{p}_{\iota}-\mathbf{p}_{o}\| \le \sigma_{od,\iota}(\mathbf{p}_{o,\iota},\dot{\mathbf{p}}_{o,\iota})\right\}, \tag{8.24}$$

where we denote

$$\sigma_{od,\iota}(\mathbf{p}_{o,\iota},\dot{\mathbf{p}}_{o,\iota}) := \max\left\{d_{\iota}-k_{o,\iota}\frac{m_{f,\iota}}{m_{l}}\mathbf{p}_{o,\iota}\cdot\dot{\mathbf{p}}_{o,\iota},\ d_{\iota}\right\}, \tag{8.25}$$

where $k_{o,\iota} > 0$ is determining the growth rate of the sphere, *i.e.* the sphere is centered at the obstacle and d_{ι} is the minimum radius of the sphere. The term $-\mathbf{p}_{o,\iota}\cdot\dot{\mathbf{p}}_{o,\iota}$ is positive when the spacecraft and obstacle are on collision course, zero when their relative position and velocity are perpendicular, and negative when they move away from each other. This enables us to reduce the size of the constant d_{ι} compared with static collision avoidance, such that the spacecraft can pass closer to another spacecraft without increasing the danger of collision. The general equation (8.13) can then be written as

$$\begin{aligned}\dot{\mathbf{p}}_{od,\iota} &= \mathbf{J}_{o,\iota}^{\dagger}\lambda_{o,\iota}(\mathbf{p}_{o,\iota},\dot{\mathbf{p}}_{o,\iota})\tilde{\sigma}_{o,\iota}(\mathbf{p}_{o,\iota},\dot{\mathbf{p}}_{o,\iota}) \\ &= \lambda_{o,\iota}(\mathbf{p}_{o,\iota}\dot{\mathbf{p}}_{o,\iota})[\sigma_{od,\iota}(\mathbf{p}_{o,\iota},\dot{\mathbf{p}}_{o,\iota}) - \|\mathbf{p}_{\iota}-\mathbf{p}_{o}\|]\hat{\mathbf{r}}_{o,\iota},\end{aligned} \tag{8.26}$$

where $\lambda_{o,\iota} > 0$ is considered a constant gain. Note that we have assumed $\dot{\sigma}_{od,\iota} = 0$ for simplicity since differentiation also includes relative acceleration which can be challenging to measure[2]. Nevertheless, this term can be added according to (8.13) by differentiation of (8.25). Also note that because of the relative velocity considered in the desired task variable $\sigma_{od,\iota}$, a collision can be detected between the spacecraft and an obstacle which is not necessarily the closest one because of variations in size of the spheres, thus each follower now calculates spheres for all

[2]Relative acceleration between two bodies can be found *e.g.* by differentiation of relative velocity although sensor noise is amplified.

obstacles/members and only consider each obstacle which has a sphere covering the follower in question. Furthermore, we choose the appropriate obstacle as the one which gives the lowest relationship between relative distance and size of sphere. That is, if a follower $\iota \in \{1, \ldots, n\}$ is considered a threat according to (8.26), we assign it to a set $\iota' = \{1, \ldots, n'\} \subset i$ (the follower in question can not consider itself as an obstacle) such that $n' < n$. Then we choose the target fulfilling

$$\min \left\{ \frac{\|\mathbf{p}_{o,1}\|}{\sigma_{od,1}(\mathbf{p}_{o,1}, \dot{\mathbf{p}}_{o,1})}, \ \ldots, \ \frac{\|\mathbf{p}_{o,n'}\|}{\sigma_{od,n'}(\mathbf{p}_{o,n'}, \dot{\mathbf{p}}_{o,n'})} \right\}. \tag{8.27}$$

8.3.2 Rigid formation

The rigid body sub-task is used to ensure that each follower moves to the designated location forming a given formation. This task can be performed in several different ways; we propose two different strategies, one where the formation is formed around the barycenter and another where the formation is formed around the leader spacecraft.

Barycenter

This task performs the movement of each spacecraft to a predefined position relative to the formation barycenter. The task function is defined as $\boldsymbol{\sigma}_r = [(\mathbf{p}_1 - \mathbf{p}_b)^\top \ldots (\mathbf{p}_n - \mathbf{p}_b)^\top]^\top$, where $\mathbf{p}_b = 1/n \sum_{\iota=1}^{n} \mathbf{p}_\iota$ is the coordinate of the barycenter, and $\boldsymbol{\sigma}_{rd}$ denotes the desired formation for all the follower spacecraft, such that $\tilde{\boldsymbol{\sigma}}_r = \boldsymbol{\sigma}_{rd} - \boldsymbol{\sigma}_r$. The Jacobian matrix can be written as

$$\mathbf{J}_r = \begin{bmatrix} \mathbf{A} & \mathbf{0} & \mathbf{0} \\ \mathbf{0} & \mathbf{A} & \mathbf{0} \\ \mathbf{0} & \mathbf{0} & \mathbf{A} \end{bmatrix} \tag{8.28}$$

where $\mathbf{J}_r \in \mathbb{R}^{3n \times 3n}$, $\mathbf{0} \in \mathbb{R}^{n \times n}$, and

$$\mathbf{A} = \begin{bmatrix} 1 - \frac{1}{n} & -\frac{1}{n} & \cdots & -\frac{1}{n} \\ -\frac{1}{n} & 1 - \frac{1}{n} & \cdots & -\frac{1}{n} \\ \vdots & \vdots & \ddots & \vdots \\ -\frac{1}{n} & -\frac{1}{n} & \cdots & 1 - \frac{1}{n} \end{bmatrix} \in \mathbb{R}^{n \times n}. \tag{8.29}$$

It can be shown that $\mathbf{A}$ has one zero eigenvalue and $(n-1)$ eigenvalues equal to one, thus the Jacobian matrix is singular with $\text{rank}(\mathbf{J}_r) = 2n$, but a pseudo-inverse $\mathbf{J}_r^\dagger$ exists. Since $\mathbf{J}_r$ is symmetric and idempotent as shown in Appendix B.24, we have that $\mathbf{J}_r^\dagger = \mathbf{J}_r$. The velocity-vector from this task can then be written as $\dot{\mathbf{p}}_{rd} = \mathbf{J}_r^\dagger \boldsymbol{\Lambda}_r \tilde{\boldsymbol{\sigma}}_r$ where $\dot{\boldsymbol{\sigma}}_{rd} = 0$ when a fixed formation is desired.

Leader spacecraft

This task performs the movement of each spacecraft to a predefined position relative to the leader spacecraft which is an easier strategy compared to the task above. The task function is defined as $\boldsymbol{\sigma}_r = [\mathbf{p}_1^\top, \ldots, \mathbf{p}_n^\top]^\top$ leading to the Jacobian matrix

$\mathbf{J}_r = \mathbf{I} \in \mathbb{R}^{3n\times 3n}$ and by denoting $\boldsymbol{\sigma}_{rd}$ as the desired position for all the follower spacecraft such that $\tilde{\boldsymbol{\sigma}}_r = \boldsymbol{\sigma}_{rd} - \boldsymbol{\sigma}_r$. The velocity vector from this task can then be written as $\dot{\mathbf{p}}_{rd} = \mathbf{J}_r^{\dagger}\boldsymbol{\Lambda}_r\tilde{\boldsymbol{\sigma}}_r$ where $\dot{\boldsymbol{\sigma}}_{rd} = 0$ for fixed formations. Note that this task has an obvious drawback which makes it suited (only) for lowest priority since $(\mathbf{I} - \mathbf{J}_r^{\dagger}\mathbf{J}_r) = (\mathbf{I} - \mathbf{I}^{\dagger}\mathbf{I}) = \mathbf{0}$ which means that lower prioritized tasks will be completely removed through projection onto the null space since $\text{rank}(\mathbf{J}_r) = 3n$ (full rank). This can be shown to hold in general by seeing that since for any $\mathbf{A} \in \{\mathbf{X} \in \mathbb{R}^{n\times n} : \text{rank}(\mathbf{X}) = n\}$ we have that $\mathbf{A}\mathbf{A}^{\top}$ has a non-zero determinant and thus we can apply (A.15) obtaining $(\mathbf{I} - \mathbf{A}^{\dagger}\mathbf{A}) = (\mathbf{I} - (\mathbf{A}^{\top}\mathbf{A})^{-1}\mathbf{A}^{\top}\mathbf{A}) = \mathbf{0}$.

8.4 NSB stability analysis

In this section we will analyze the stability of the NSB behavioral approach. In general, the proof is quite straight forward, but it gets more involved when some assumptions are removed or new elements are considered.

8.4.1 Task error analysis

To analyze the convergence of the global task, each task may be evaluated to check for convergence to the desired value. The output of (8.15) is considered, multiplying both members by $\mathbf{J}_1$ which is supposed to be full rank and observing that $\mathbf{J}_1(\mathbf{I} - \mathbf{J}_1^{\dagger}\mathbf{J}_1) = \mathbf{0}$, then

$$\dot{\boldsymbol{\sigma}}_1 = \dot{\boldsymbol{\sigma}}_{1,d} + \boldsymbol{\Lambda}_1(\boldsymbol{\sigma}_{1,d} - \boldsymbol{\sigma}_1), \tag{8.30}$$

which can be rewritten as

$$\dot{\tilde{\boldsymbol{\sigma}}}_1 = -\boldsymbol{\Lambda}_1(\tilde{\boldsymbol{\sigma}}_1) \tag{8.31}$$

where $\tilde{\boldsymbol{\sigma}}_1 := \boldsymbol{\sigma}_1 - \boldsymbol{\sigma}_{1,d}$. Consider the Lyapunov function candidate

$$V(\boldsymbol{\sigma}_1) = \frac{1}{2}\tilde{\boldsymbol{\sigma}}_1^{\top}\tilde{\boldsymbol{\sigma}}_1 \tag{8.32}$$

yielding

$$\dot{V} = -\tilde{\boldsymbol{\sigma}}_1^{\top}\boldsymbol{\Lambda}_1\tilde{\boldsymbol{\sigma}}_1, \tag{8.33}$$

which proves (uniform) global asymptotic stability of the equilibrium point, thus the primary task is always fulfilled where rate of convergence of the kinematic error is influenced by the constant positive definite NSB gain $\boldsymbol{\Lambda}_1$.

The lower level tasks can only be fulfilled if they do not conflict with the higher level tasks. The relationship between non-conflicting tasks can be evaluated by considerations of the Jacobians of the task functions. These can be evaluated mathematically by considering the range $\mathcal{R}(\cdot)$ and null-spaces $\mathcal{N}(\cdot)$. By multiplying both members of the secondary task of (8.15) by $\mathbf{J}_2$, then (Arrichiello, 2006)

$$\dot{\boldsymbol{\sigma}}_2 = \mathbf{J}_2\mathbf{J}_1^{\dagger}(\dot{\boldsymbol{\sigma}}_{1,d} + \boldsymbol{\Lambda}_1(\boldsymbol{\sigma}_{1,d} - \boldsymbol{\sigma}_1)) + \dot{\boldsymbol{\sigma}}_{2,d} + \boldsymbol{\Lambda}_2(\boldsymbol{\sigma}_{2,d} - \boldsymbol{\sigma}_2). \tag{8.34}$$

Assume that there is no conflict between the two tasks, then an interesting property of the Jacobian matrices is utilized saying that the non-conflicting relationship between two tasks can be expressed as

$$\mathbf{J}_2\mathbf{J}_1^{\dagger} = \mathbf{0}, \tag{8.35}$$

which means that two tasks re-projected onto the spacecraft velocity space are orthogonal and therefore may be fulfilled simultaneously –*cf.* (Chiaverini, 1997). The property of (8.35) may also be expressed as

$$\mathcal{R}(\mathbf{J}_2^\dagger) \perp \mathcal{R}(\mathbf{J}_1^\dagger). \tag{8.36}$$

By substituting (8.35) with (8.34), we obtain

$$\dot{\boldsymbol{\sigma}}_2 = \dot{\boldsymbol{\sigma}}_{2,d} + \boldsymbol{\Lambda}_2(\boldsymbol{\sigma}_{2,d} - \boldsymbol{\sigma}_2), \tag{8.37}$$

and thus (uniform) global asymptotic stability of the equilibrium point of the task can be shown by applying a quadratic Lyapunov function candidate. It should be noted that this condition is implied by

$$\mathcal{R}(\mathbf{J}_2^\dagger) \subseteq \mathbf{I} - \mathbf{J}_1^\dagger \mathbf{J}_1 = \mathcal{N}(\mathbf{J}_1). \tag{8.38}$$

If a third task is to be added, the stability of the first two tasks is unchanged because of the higher priority of the tasks and the projection into the null-space of the lower tasks. Following the procedure for two tasks, a third task can be analyzed the same way. This implies that the third task is decoupled from the first two tasks if

$$\mathcal{R}(\mathbf{J}_3^\dagger) \subseteq [\mathcal{N}(\mathbf{J}_1) \cap \mathcal{N}(\mathbf{J}_2)] \tag{8.39}$$

is fulfilled.

8.4.2 NSB general stability

The task functions of the NSB produce desired velocity vectors for the spacecraft as described in section 8.2. The desired relative velocity for two tasks is found by using (8.13) merged with (8.14), where in our case $i = 2$, expressed as

$$\dot{\mathbf{p}}_d = \mathbf{J}_1^\dagger(\dot{\boldsymbol{\sigma}}_{1,d} + \boldsymbol{\Lambda}_1\tilde{\boldsymbol{\sigma}}_1) + (\mathbf{I} - \mathbf{J}_1^\dagger\mathbf{J}_1)\mathbf{J}_2^\dagger(\dot{\boldsymbol{\sigma}}_{2,d} + \boldsymbol{\Lambda}_2\tilde{\boldsymbol{\sigma}}_2). \tag{8.40}$$

Assuming that each spacecraft is perfectly following the desired trajectory, $\dot{\mathbf{p}} = \dot{\mathbf{p}}_d(t)$, the stability analysis is reduced to only prove convergence of each task function to the desired value. A suitable LFC is chosen as

$$V_1(\tilde{\boldsymbol{\sigma}}_1) = \frac{1}{2}\tilde{\boldsymbol{\sigma}}_1^\top\tilde{\boldsymbol{\sigma}}_1, \tag{8.41}$$

and by differentiating along (8.9), $\dot{V}_1$ can be written as

$$\begin{aligned}
\dot{V}_1 &= \tilde{\boldsymbol{\sigma}}_1^T\dot{\tilde{\boldsymbol{\sigma}}}_1 && (8.42)\\
&= \tilde{\boldsymbol{\sigma}}_1^T(\dot{\boldsymbol{\sigma}}_{1,d} - \mathbf{J}_1\dot{\mathbf{p}}_d) && (8.43)\\
&= \tilde{\boldsymbol{\sigma}}_1^T[\dot{\boldsymbol{\sigma}}_{1,d} - \mathbf{J}_1\mathbf{J}_1^\dagger(\dot{\boldsymbol{\sigma}}_{1,d} + \boldsymbol{\Lambda}_1\tilde{\boldsymbol{\sigma}}_1) - \mathbf{J}_1(\mathbf{I} - \mathbf{J}_1^\dagger\mathbf{J}_1)\mathbf{J}_2^\dagger(\dot{\boldsymbol{\sigma}}_{2,d} + \boldsymbol{\Lambda}_2\tilde{\boldsymbol{\sigma}}_2)] && (8.44)\\
&= \tilde{\boldsymbol{\sigma}}_1^T[\dot{\boldsymbol{\sigma}}_{1,d} - \mathbf{J}_1\mathbf{J}_1^\dagger(\dot{\boldsymbol{\sigma}}_{1,d} + \boldsymbol{\Lambda}_1\tilde{\boldsymbol{\sigma}}_1)] && (8.45)\\
&= -\tilde{\boldsymbol{\sigma}}_1^T\boldsymbol{\Lambda}_1\tilde{\boldsymbol{\sigma}}_1. && (8.46)
\end{aligned}$$

Because $\mathbf{\Lambda}_1$ is positive definite, the convergence of $\tilde{\boldsymbol{\sigma}}_1$ to $\mathbf{0}$ is proved. In other words, the first task is always achieved. For the second task, a suitable LFC is chosen as

$$V_2 = \frac{1}{2}\tilde{\boldsymbol{\sigma}}_2^\top \tilde{\boldsymbol{\sigma}}_2 \tag{8.47}$$

and again by differentiating along (8.9), we obtain

$$\begin{aligned}
\dot{V}_2 &= \tilde{\boldsymbol{\sigma}}_2^T \dot{\tilde{\boldsymbol{\sigma}}}_2 \\
&= \tilde{\boldsymbol{\sigma}}_2^T (\dot{\boldsymbol{\sigma}}_{2,d} - \mathbf{J}_2 \dot{\mathbf{p}}_d) \\
&= \tilde{\boldsymbol{\sigma}}_2^T [\dot{\boldsymbol{\sigma}}_{2,d} - \mathbf{J}_2 \mathbf{J}_2^\dagger (\dot{\boldsymbol{\sigma}}_{1,d} + \mathbf{\Lambda}_1 \tilde{\boldsymbol{\sigma}}_1) - \mathbf{J}_2 (\mathbf{I} - \mathbf{J}_1^\dagger \mathbf{J}_1) \mathbf{J}_2^\dagger (\dot{\boldsymbol{\sigma}}_{2,d} + \mathbf{\Lambda}_2 \tilde{\boldsymbol{\sigma}}_2)] \\
&= \tilde{\boldsymbol{\sigma}}_2^T [-\mathbf{\Lambda}_2 \tilde{\boldsymbol{\sigma}}_2 - \mathbf{J}_2 \mathbf{J}_1^\dagger (\dot{\boldsymbol{\sigma}}_{1,d} + \mathbf{\Lambda}_1 \tilde{\boldsymbol{\sigma}}_1) + \mathbf{J}_2 \mathbf{J}_1^\dagger \mathbf{J}_1 \mathbf{J}_2^\dagger (\dot{\boldsymbol{\sigma}}_{2,d} + \mathbf{\Lambda}_2 \tilde{\boldsymbol{\sigma}}_2)].
\end{aligned} \tag{8.48}$$

As explained in Section 8.4.1, the secondary task is only accomplished when it is not conflicting with the primary task. By inserting (8.35) into (8.48), the last two expressions are zero, leading to

$$\dot{V}_2 = -\tilde{\boldsymbol{\sigma}}_2^T \mathbf{\Lambda}_2 \tilde{\boldsymbol{\sigma}}_2, \tag{8.49}$$

where $\mathbf{\Lambda}_2$ is positive definite, and convergence of $\tilde{\boldsymbol{\sigma}}_2$ to $\mathbf{0}$ is proved. Thus, we conclude that the primary task is always stable, and the secondary task is also stable when it is not conflicting with the primary task.

8.4.3 NSB stability for collision avoidance

Now we present a more involved stability analysis. First of all, since the collision avoidance task function is not a vector but a scalar, the proof of general stability does not hold, and therefore we define $\tilde{\sigma}_o = \sum_{\iota=1}^{n} \tilde{\sigma}_{o,\iota}$ where $\tilde{\sigma}_o = 0$ when collision avoidance is inactive for all followers, and $\tilde{\sigma}_o > 0$ when it is active for one or more followers. Secondly, we remove the assumption that $\dot{\mathbf{p}} = \dot{\mathbf{p}}_d(t)$, and thus we need to show that collisions do not occur during reconfiguration, and lastly, we tie the NSB behavioral control approach with the control law by scaling the length of the desired relative velocity vector produced by the collision avoidance task. The reason for this is that $\dot{\mathbf{p}}_{od,\iota} = \mathbf{J}_{o,\iota}^\dagger \lambda_{o,\iota} \tilde{\boldsymbol{\sigma}}_{o,\iota}$ and since $\|\mathbf{J}_{o,\iota}\| = 1$, $\lambda_{o,\iota}$ is constant and $\tilde{\boldsymbol{\sigma}} \leq d$ for static collision avoidance, $\|\dot{\mathbf{p}}_{od,\iota}\| < c$, and in the typical PD control structure there are terms $-k_p \tilde{\mathbf{p}} - k_d \dot{\tilde{\mathbf{p}}}$, where the last term can be dominated by the first term if the current spacecraft is far away from the desired position. Or, in other words, for any given $\lambda_{o,\iota}$, k_p and k_d there exists initial conditions such that the proportional term of the control law can push the spacecraft towards an obstacle.

In this particular analysis we utilize the sliding surface control structure as presented in Section 6.3.2 for each follower individually. We start by finding the desired relative velocity by utilizing (8.13) together with (8.14), where $m = 2$, $o = 1$ and $r = 2$, where we utilize the static sphere with variable gain presented in Section 8.3.1, thus obtaining

$$\dot{\mathbf{p}}_d = \dot{\mathbf{p}}_{od} + (\mathbf{I} - \mathbf{J}_o^\dagger \mathbf{J}_o) \mathbf{J}_r^\dagger \mathbf{\Lambda}_r \tilde{\boldsymbol{\sigma}}_r. \tag{8.50}$$

A suitable LFC is chosen as

$$V(\mathbf{x}) = \frac{1}{2}\Big(\lambda_1 \tilde{\sigma}_o^2 + \tilde{\boldsymbol{\sigma}}_r^\top \lambda_2 \tilde{\boldsymbol{\sigma}}_r + \mathbf{s}^\top m_f \mathbf{s} + \tilde{\mathbf{p}}^\top \mathbf{K}_p \tilde{\mathbf{p}}\Big), \tag{8.51}$$

where $\mathbf{x} = [\tilde{\mathbf{p}}^\top, \mathbf{s}^\top, \tilde{\sigma}_o, \tilde{\boldsymbol{\sigma}}_r^\top]^\top$ and $\lambda_1, \lambda_2 > 0$ are considered as design parameters. By differentiation and insertion of (8.8) and (8.9), we obtain

$$\begin{aligned}\dot{V} = &- \tilde{\sigma}_o \lambda_1 \mathbf{J}_o \dot{\mathbf{p}}_d - \tilde{\boldsymbol{\sigma}}_r^\top \lambda_2 \mathbf{J}_r \dot{\mathbf{p}}_d - \mathbf{s}^\top \mathbf{C}_t \mathbf{s} - \mathbf{s}^\top \mathbf{K}_p \tilde{\mathbf{p}} \\ &- \mathbf{s}^\top \mathbf{K}_d \mathbf{s} + \tilde{\mathbf{p}}^\top \mathbf{K}_p \dot{\tilde{\mathbf{p}}}. \end{aligned} \tag{8.52}$$

Using the fact that $\mathbf{C}_t(\boldsymbol{\omega}_{i,l}^l)$ is skew-symmetric, we further obtain

$$\begin{aligned}\dot{V} = &- \tilde{\sigma}_o \lambda_1 \left[\mathbf{J}_o \mathbf{J}_o^\dagger \lambda_o \tilde{\sigma}_o + \mathbf{J}_o \left(\mathbf{I} - \mathbf{J}_o^\dagger \mathbf{J}_o\right) \mathbf{J}_r^\dagger \boldsymbol{\Lambda}_r \tilde{\boldsymbol{\sigma}}_r\right] \\ &- \tilde{\boldsymbol{\sigma}}_r^\top \lambda_2 \left[\mathbf{J}_r \mathbf{J}_o^\dagger \lambda_o \tilde{\sigma}_o + \mathbf{J}_r \left(\mathbf{I} - \mathbf{J}_o^\dagger \mathbf{J}_o\right) \mathbf{J}_r^\dagger \boldsymbol{\Lambda}_r \tilde{\boldsymbol{\sigma}}_r\right] \\ &- (\mathbf{s}^\top - \dot{\tilde{\mathbf{p}}}^\top) \mathbf{K}_p \tilde{\mathbf{p}} - \mathbf{s}^\top \mathbf{K}_d \mathbf{s} \end{aligned} \tag{8.53}$$

$$\begin{aligned}= &- \lambda_o \lambda_1 \tilde{\sigma}_o \tilde{\sigma}_o - \tilde{\boldsymbol{\sigma}}_r^\top \lambda_2 \Big[\mathbf{J}_r \mathbf{J}_o^\dagger \lambda_o \tilde{\sigma}_o + \mathbf{J}_r \mathbf{J}_r^\dagger \boldsymbol{\Lambda}_r \tilde{\boldsymbol{\sigma}}_r \\ &- \mathbf{J}_r \mathbf{J}_o^\dagger \mathbf{J}_o \mathbf{J}_r^\dagger \boldsymbol{\Lambda}_r \tilde{\boldsymbol{\sigma}}_r\Big] - \tilde{\mathbf{p}}^\top \boldsymbol{\Gamma} \mathbf{K}_p \tilde{\mathbf{p}} - \mathbf{s}^\top \mathbf{K}_d \mathbf{s}, \end{aligned} \tag{8.54}$$

where $\boldsymbol{\Gamma} = \text{diag}\{\gamma_1 \mathbf{I}, \ldots, \gamma_n \mathbf{I}\} \in \mathbb{R}^{3n \times 3n}$. From this point the proof goes in two different directions; conflicting and non-conflicting tasks, which will be discussed separately. By assuming that there are no conflict tasks we can apply the property (8.35), and by inserting (8.35) into (8.54), we obtain

$$\dot{V} = -\mathbf{x}^\top \mathbf{P} \mathbf{x} \tag{8.55}$$

where $\mathbf{P} = \text{diag}\{\boldsymbol{\Gamma}\mathbf{K}_p, \mathbf{K}_p, \lambda_o \lambda_1, \boldsymbol{\Lambda}_r \lambda_2\}$. Thus the secondary task is only accomplished when there is no conflict with the primary task. Hence, convergence of V towards the origin is proved. Accordingly, from the above analysis and according to standard Lyapunov analysis –*cf.* (Khalil, 2002), we find that the primary task, which is the collision avoidance task, is always stable, and the secondary task performing formation shaping is also stable when it is not conflicting with the primary task. Thus we find that the equilibrium point of the closed-loop system is uniformly globally exponentially stable.

On the other hand, if the collision avoidance task is active and the tasks are conflicting we see that the system is on the form

$$\dot{V} = -\mathbf{x}^\top \mathbf{Q} \mathbf{x}, \tag{8.56}$$

where $\mathbf{Q} = [\mathbf{q}_{ij}], \quad i, j = 1, 2, 3, 4$, with sub-matrices given by $\mathbf{q}_{11} = \boldsymbol{\Gamma}\mathbf{K}_p$, $\mathbf{q}_{22} = \mathbf{K}_p$, $\mathbf{q}_{33} = \lambda_o \lambda_1$, $\mathbf{q}_{43} = \mathbf{q}_{34}^\top = \lambda_o \lambda_2 \mathbf{J}_f \mathbf{J}_o^\dagger$, $\mathbf{q}_{44} = \lambda_2 \mathbf{J}_f \mathbf{J}_f^\dagger \boldsymbol{\Lambda}_f - \lambda_2 \mathbf{J}_f \mathbf{J}_o^\dagger \mathbf{J}_o \mathbf{J}_f^\dagger \boldsymbol{\Lambda}_f$ and the rest of the sub-matrices are equal to zero. Next, we apply $2|ab| \leq a^2 + b^2$ for any $a, b \in \mathbb{R}$ to obtain

$$\begin{aligned}\mathbf{x}^\top \mathbf{Q} \mathbf{x} \geq &(q_{11,m} - q_{12,M} - q_{13,M} - q_{14,M}) \|\tilde{\mathbf{p}}\|^2 \\ &+ (q_{22,m} - q_{21,M} - q_{23,M} - q_{24,M}) \|\mathbf{s}\|^2 \\ &+ (q_{33,m} - q_{31,M} - q_{32,M} - q_{34,M}) \tilde{\sigma}_o^2 \\ &+ (q_{44,m} - q_{41,M} - q_{42,M} - q_{43,M}) \|\tilde{\boldsymbol{\sigma}}_f\|^2 \end{aligned} \tag{8.57}$$

where $q_{ij,m}$ and $q_{ij,M}$ denote lower and upper bounds on the induced norms of the sub-blocks $\mathbf{q}_{ij}$ of $\mathbf{Q}$ respectively. Hence, $\mathbf{x}^\top \mathbf{Q}\mathbf{x} \geq \frac{1}{2}(q_{11,m}\|\tilde{\mathbf{p}}\|^2 + q_{22,m}\|\mathbf{s}\|^2 + q_{33,m}\tilde{\sigma}_o^2 + q_{44,m}\|\tilde{\boldsymbol{\sigma}}_f\|^2)$. We see that since $\mathbf{J}_o^\dagger \mathbf{J}_o = \mathbf{I}$, $\|\mathbf{J}_o\| = \|\mathbf{J}_r\| = 1$, we obtain $q_{44,m} = q_{44,M} = 0$, and thus control of $\tilde{\boldsymbol{\sigma}}_f$ is lost. Also we need $q_{33,m} \geq 2q_{34,M}$ resulting in $\lambda_1 \geq 2\lambda_2$. This analysis show that when the collision avoidance task is active, we may end up with moving away from the desired position which is a necessity; consider for example a scenario where the spacecraft is located at its equilibrium and has to move away when an obstacle is passing close by to avoid collision. Since the NSB method is acting on the dynamics through the desired relative velocity and not also the desired relative position, we have to ensure that the relative velocity error is dominating the relative position error in the control law, thus avoiding being "pulled" towards an obstacle. This is done by scaling the length of the desired relative velocity vector utilizing the collision avoidance task gain $\lambda_{o,\iota}(\mathbf{p}_{o,\iota}, \dot{\mathbf{p}}_{o,\iota})$. The sliding surface (8.6) is containing both position and velocity error. By inserting $\dot{\mathbf{p}}_{d,\iota}$ from (8.50) into (8.6) and applying the fact that if the second task is conflicting with the first, the counteracting components are removed by projection, meaning that the contribution from $\tilde{\boldsymbol{\sigma}}_r$ can be removed. Therefore we require that

$$\begin{aligned}&(\dot{\mathbf{p}}_\iota - \mathbf{J}_{o,\iota}^\dagger \lambda_{o,\iota}\tilde{\sigma}_{o,\iota})^\top \mathbf{K}_{d,\iota}(\dot{\mathbf{p}}_\iota - \mathbf{J}_{o,\iota}^\dagger \lambda_{o,\iota}\tilde{\sigma}_{o,\iota}) > \\ &k_{dM,\iota}\gamma\tilde{\mathbf{p}}_\iota^\top \left[2(\dot{\mathbf{p}}_\iota - \mathbf{J}_{o,\iota}^\dagger \lambda_{o,\iota}\tilde{\sigma}_{o,\iota}) + \tilde{\mathbf{p}}_\iota\right] + k_{pM,\iota}\tilde{\mathbf{p}}_\iota^\top \gamma_\iota^2 \tilde{\mathbf{p}}_\iota,\end{aligned} \tag{8.58}$$

where $k_{pm,\iota} \leq \|\mathbf{K}_{p,\iota}\| \leq k_{pM,\iota}$ and $k_{dm,\iota} \leq \|\mathbf{K}_{d,\iota}\| \leq k_{dM,\iota}$. By taking the norm on each side of (8.58) and manipulate as an equality from a conservative point of view[3], we obtain

$$\begin{aligned}&\left(\lambda_{o,\iota}^\star\right)^2 k_{dm,\iota}\tilde{\sigma}_{o,\iota}^2 - \lambda_{o,\iota}^\star 2k_{dM,\iota}\tilde{\sigma}_{o,\iota}\left(\|\dot{\mathbf{p}}_\iota\| + \|\tilde{\mathbf{p}}_\iota\|\right) \\ &- k_{dM,\iota}\|\dot{\mathbf{p}}_\iota\|^2 - 2k_{dM,\iota}\|\dot{\mathbf{p}}_\iota\|\|\tilde{\mathbf{p}}_\iota\| \\ &- \gamma_\iota\left(\gamma_\iota k_{pM,\iota} + k_{dM,\iota}\right)\|\tilde{\mathbf{p}}_\iota\|^2 = 0\end{aligned} \tag{8.59}$$

and solve for the largest value of $\lambda_{o,\iota}^\star$, leading to

$$\lambda_{o,\iota}^\star(\|\tilde{\mathbf{p}}_\iota\|, \|\dot{\mathbf{p}}_\iota\|) = \frac{b_\iota + \sqrt{b_\iota^2 + 4a_\iota c_\iota}}{2a_\iota}, \tag{8.60}$$

where $a_\iota = k_{dm,\iota}\tilde{\sigma}_{o,\iota}^2$, $b_\iota = 2k_{dM,\iota}\tilde{\sigma}_{o,\iota}(\|\dot{\mathbf{p}}_\iota\| + \|\tilde{\mathbf{p}}_\iota\|)$ and $c_\iota = k_{dM,\iota}\|\dot{\mathbf{p}}_\iota\|^2$ $+2k_{dM,\iota}\|\dot{\mathbf{p}}_\iota\|\|\tilde{\mathbf{p}}_\iota\| + \gamma_\iota\left(k_{pM,\iota} + \gamma_\iota k_{dM,\iota}\right)\|\tilde{\mathbf{p}}_\iota\|^2$. Thus by choosing $\lambda_{o,\iota}(\|\tilde{\mathbf{p}}_\iota\|, \|\dot{\mathbf{p}}_\iota\|) = \lambda_{o,\iota}^\star(\|\tilde{\mathbf{p}}_\iota\|, \|\dot{\mathbf{p}}_\iota\|) + \delta_\iota$, where $\delta_\iota > 0$ is chosen based on robustness to *e.g.* measurement noise, it is ensured that the derivative part of the control law is dominating the proportional part, and therefore the task function will make the spacecraft move away from the obstacle. Note that the state dependent gain only scales the desired velocity vector produced by the obstacle avoidance task when a safety sphere is entered and does not influence the size of the sphere itself.

[3] By this we mean that the inequality in (8.58) will hold if we substitute the left side with the minimum eigenvalue and makes it equal to the maximum eigenvalue of the right side.

Remark 8.1 *What we have proved in this section is that if we have no conflicting tasks, the equilibrium point of the closed-loop system is uniformly globally exponentially stable for each follower spacecraft. For tasks to be conflicting, the collision avoidance has to be activated, which may lead to situations where a spacecraft is forced to move such that the position error increases, thus the exponential/asymptotical property does not hold. Arrichiello (2006) states that this is especially evident for robots if the robot is going to frontally collide with the obstacle (the velocity elaborated by the other tasks is in the vehicle-obstacle direction), then the projection along the tangential direction is null. This particular situation gives rise to a local minimum that makes the robot stop. Nevertheless, the experimental results showed that the presence of measurement noise allows the vehicle to avoid the local minima; this is, in fact, an unstable stationary point. Another requirement related to this consideration is that each spacecraft can only reach their equilibrium point if it is not located within a collision sphere for all time. In other words, the desired relative distance between each spacecraft has to be greater than d.*

Remark 8.2 *If the assumption of known disturbances of the follower spacecraft is reduced to unknown but bounded disturbances such that* $\|\mathbf{f}_{df}\| \leq \beta$*, a similar analysis as above can be performed leading to*

$$\dot{V} \leq -\mathbf{x}^\top \mathbf{P}\mathbf{x} + \mathbf{s}^\top \mathbf{f}_{df} \tag{8.61}$$

$$\leq -p_m \|\mathbf{x}\|^2 + \beta \|\mathbf{x}\| \ , \tag{8.62}$$

where $p_m > 0$ *is the smallest eigenvalue of* $\mathbf{P}$*. Thus* $\dot{V} < 0$ *when* $\|\mathbf{x}\| > \delta = \beta/p_m$ *and* δ *can be diminished by increasing* p_m *which is done by increasing the controller gains, and we can conclude that equilibrium point of the closed-loop system is uniformly globally practically exponentially stable (cf. (Grøtli, 2010)), when Remark 8.1 is considered.*

Remark 8.3 *Note that Remark 6.4 also holds for the present analysis.*

A similar analysis can be given utilizing the dynamic collision avoidance with variable gain task as presented in Section 8.3.1 scaling the size of the safety sphere through the gain $k_{o,\iota}$ instead of the desired relative velocity vector.

8.5 Simulation results

In this section we present simulation results based on the NSB behavioral control method presented in this chapter comparing the different obstacle avoidance schemes presented in Section 8.3.1, where our main focus is to show the difference in performance.

We assumed a perfectly controlled leader spacecraft in a circular Low Earth Orbit (LEO) at 600 km altitude, inclination (i), the argument of perigee (ω) and the right ascension of the ascending node (Ω) at 0°. Since we are considering a LEO, we only model the disturbance forces which are the major contributors to these kind of orbits; namely, atmospheric drag and the J_2 effect. All disturbances are considered continuous and bounded. The noise is considered to be contained in

a compact set $\sigma\mathbb{B}^n = \{\mathbf{x} \in \mathbb{R}^n : \|\mathbf{x}\| \leq \sigma\}$ and is added to the the measured states according to $\mathbf{p}_n = \mathbf{p} + 0.1\mathbb{B}^3$ and $\dot{\mathbf{p}}_n = \dot{\mathbf{p}}_n + 0.02\mathbb{B}^3$. The parameter for minimum length between two objects is set to $d = 10$ m. If the distance between objects is higher, the velocity output for the current object is set to zero, and if one or more objects are closer than the minimum distance, the closest object is given highest priority.

In the simulations, the obstacle avoidance task was set as first priority while the rigid formation task as second, where for simplicity the task presented as *Leader spacecraft* in Section 8.3.2 was utilized since the task had lowest priority. The rigid body task gain was chosen as $\mathbf{\Lambda}_r = 0.1\mathbf{I}$ while for collision avoidance we chose $\lambda_{o,\iota} = 0.5$ for constant gain or calculated according to (8.60) with $\delta_\iota = 1$ for all ι for dynamic gain. The controller gains were chosen as $\mathbf{K}_p = 0.8\mathbf{I}$, $\mathbf{K}_d = \mathbf{I}$, and $\mathbf{\Gamma} = \mathbf{I}$, and the maximum control force (if saturation was introduced) as 27 N for each spacecraft. For comparison of performance we utilize the performance functional $J_{pow,\iota}$ as defined in (2.125) for each follower ι.

Two different scenarios are considered. In the first scenario, a formation of six spacecraft is reconfigured from an initial state to a desired configuration while avoiding collisions between spacecraft. In the second scenario, one spacecraft is assumed to malfunction and start drifting through the formation, and is therefore considered an obstacle that is avoided by evasive maneuvers of the other spacecraft.

8.5.1 Formation shaping

In this scenario five followers were relocating and shaping a new formation while avoiding collisions by setting the collision avoidance task as first priority and rigid formation as second, relative to a leader spacecraft. In this simulation the initial relative positions and velocities were chosen as standstill at

$$\mathbf{p}(t_0) = [(-40\ -30\ 0),\ (-15\ -40\ 5),\ (0\ -40\ 0),\ (15\ -40\ -5),\ (30\ -40\ 0)]^\top \text{ m}$$

and the desired relative positions and velocities for the follower spacecraft were standstill at

$$\boldsymbol{\sigma}_{f,d} = [(-20\ 20\ 0),\ (0\ 30\ 0),\ (-15\ -20\ 0),\ (15\ -20\ 0),\ (20\ 20\ 0)]^\top \text{ m}.$$

As some of the followers never encounter a possible collision we only present the results where the collision avoidance task is enabled during the maneuver.

Static collision avoidance with constant gain

Figure 8.3 shows the result of the formation shaping maneuver without saturated control force where relative position between the second follower and leader are depicted in the first and second (zoomed) plot, while control torque for the second follower in the bottommost plot. As can be seen, the control torque is quite large because of the relative initial errors and controller gains. After about six seconds, the second follower enters the safety sphere centered on the leader spacecraft (relative distance drops below 10 m), and thus the collision avoidance task is activated as can be seen in the bottommost plot where a spike occur. It should be noted that

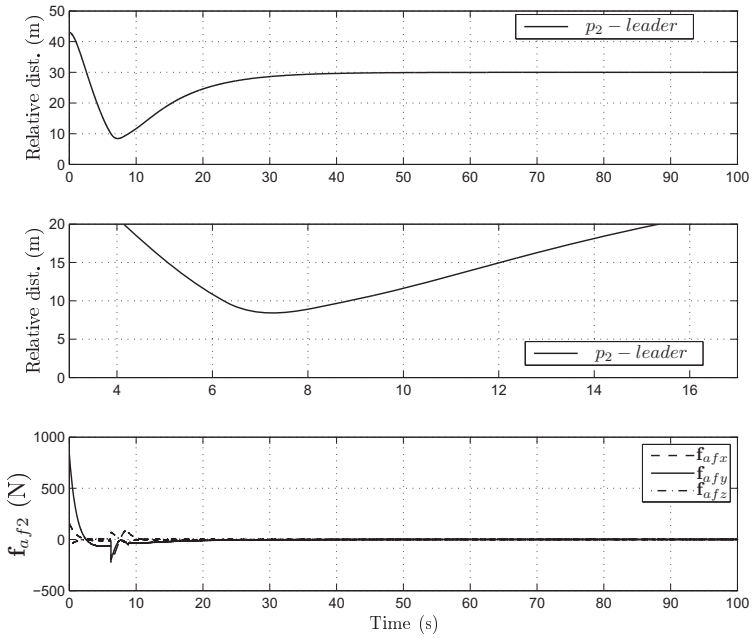

Figure 8.3: Formation reconfiguration without saturated control force and constant obstacle avoidance task gain where switching in actuator force is provoked when relative distance between spacecraft is less than 10 m due to the static collision avoidance task. The plots from the top represents relative distance between the second follower and the leader, a zoomed version of the topmost plot and actuator force for the second follower.

the relative distance drops to about eight meters because of the inertia present in the dynamics.

Figure 8.4 shows the results of the same maneuver as above with saturated control force. First of all, we now see that more spacecraft are involved with collision avoidance, that is, the topmost plot (left) shows relative distance between the second follower and the third follower, and the second follower and the leader, while the third plot shows the relative distance between the forth follower and the fifth follower. The actuator force of the second (top) to the fifth follower are shown on the right side. What can be seen now is that switching in the actuator force is located at the same time instant as the respective followers are entering each others (and the leaders) safety zones. Another important difference compared to the results without saturation is that the minimal relative distance drops to about six meters, and it can be concluded that if the relative velocity is to high when the collision avoidance task is activated, collisions might be unavoidable because of the saturation along with the inertia.

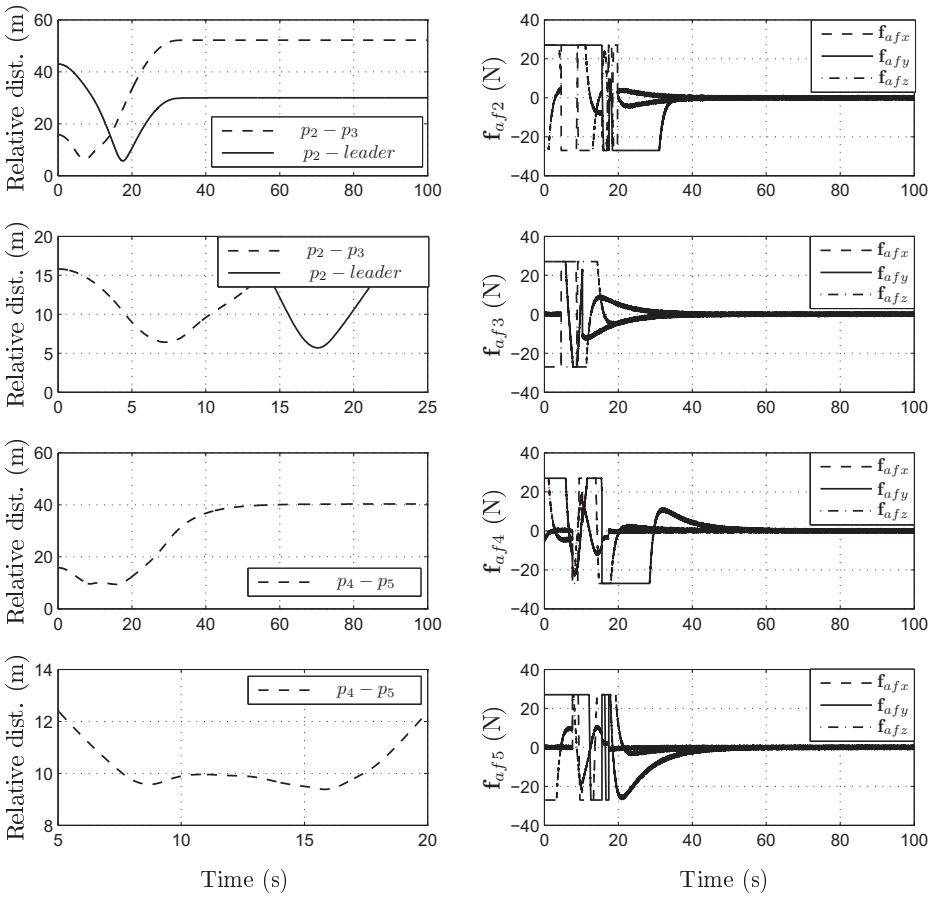

Figure 8.4: Formation reconfiguration with saturated control force and constant obstacle avoidance task gain where switching in actuator force is provoked when relative distance between spacecraft is less than 10 m due to the static collision avoidance task. The plots from the left top represents relative distance between second and third follower, and second follower and leader, and relative distance between forth and fifth followers, both with zoom. The plots from the right top represents actuator force for second, third, fourth and fifth follower.

Static collision avoidance with variable gain

Figure 8.5 shows the result of the formation shaping maneuver without saturated control force where relative position between the second follower and leader are depicted in the first and second (zoomed) plot, while control torque for the second follower in the bottommost plot. As can be seen, the control torque is quite large because of the relative initial errors and controller gains. After about six seconds, the second follower enters the safety sphere centered on the leader spacecraft (relative distance drops below 10 m), and thus the collision avoidance task is activated as can be seen in the bottommost plot where a spike occurs. As was shown in the proof of Section 8.4.3 the scaling of the desired velocity vector (variable task gain) is calculated to ensure that the spacecraft are instantaneously driven away from each other, which is seen in the zoomed plot, though at the cost of high actuator output.

Figure 8.6 shows the results of the same maneuver as above with saturated control force. First of all, we now see that more spacecraft are involved with collision avoidance, that is, the topmost plot (left) shows relative distance between the second follower and the third follower, and the second follower and the leader, while the third plot shows the relative distance between the forth follower and the fifth follower. The actuator force of the second (top) to the fifth follower are shown on the right side. What can be seen now is that switching in the actuator force is located at the same time instant as the respective followers are entering each others (and the leaders) safety zones. Another important difference compared to the results without saturation is that the minimal relative distance drops to about five meters, which is the same as the results presented in the previous section. Thus, the method can secure that collision will not occur at the cost of high actuator output, which is hampered by saturation.

Dynamic collision avoidance with constant gain

Replacing the fixed d with the dynamical sphere from (8.25) with $k_o = 0.15$ it can be seen in Figure 8.7 that the relative distance between each spacecraft never was below 10 m, and furthermore, the spike shown in the bottommost plot in Figure 8.3 is replaced by a more smooth behavior.

Figure 8.8 shows the results of the same maneuver as above with saturated control force. The topmost plot (left) shows relative distance between the second follower and the third follower, and the second follower and the leader, while the third plot shows the relative distance between the forth follower and the fifth follower. The actuator force of the second (top) to the fifth follower are shown on the right side. What can be seen now is that switching in the actuator force is located at the same time instant as the respective followers are entering each others (and the leaders) safety zones. It should be noted that even when including saturation force, the relative distance between all followers never dropped below 10 meters which is what is truly sought in this work. It should also be noted that in Table 8.1 it is shown that the energy consumption is slightly reduced for all followers compared to using static collision avoidance.

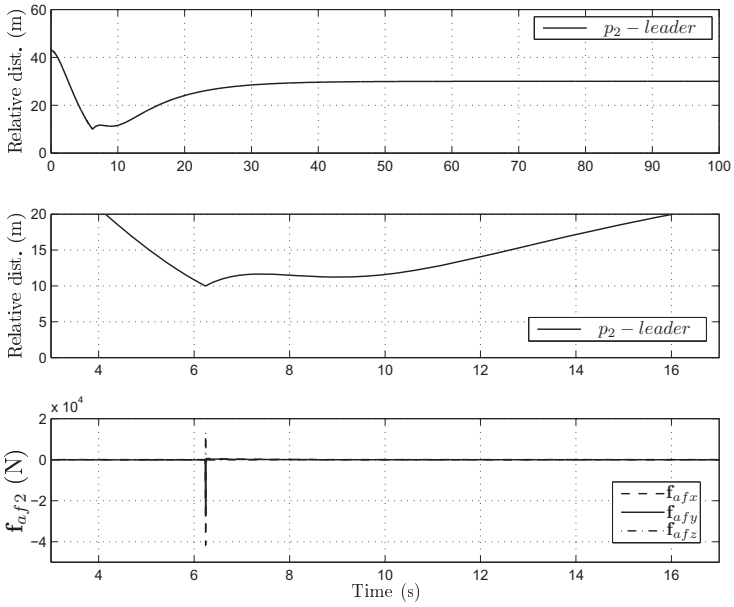

Figure 8.5: Formation reconfiguration without saturated control force and variable obstacle avoidance task gain where switching in actuator force is provoked when relative distance between spacecraft is less than 10 m due to the static collision avoidance task. The plots from the top represents relative distance between the second follower and the leader, a zoomed version of the topmost plot and actuator force for the second follower.

Table 8.1: Simulation results, $J_{pow,\iota}(\times 10^4)$

	1	2	3	4	5
Static (10m)	2.125	5.406	2.721	1.311	2.629
Dynamic (10m)	2.114	5.223	2.273	1.162	2.537
Dynamic (5m)	2.114	3.852	1.835	0.722	2.185

By reducing the minimum distance to $d = 5$ m we see from Table 8.1 that the energy consumption for all followers involved with the collision avoidance task is greatly reduced. This is because the spacecraft now can travel closer together because close maneuvers are only allowed when spacecraft do not move directly towards each other. It can again be shown through simulations that the spacecraft never are within five meters of each other during the reconfiguration, which is similar to the results for static collision avoidance with $d = 10$ m.

Note that we do not present dynamic collision avoidance with variable gain since the variable gain causes very long desired velocity vectors when a safety sphere is entered which in turn leads to large actuator forces. This in turn leads to large

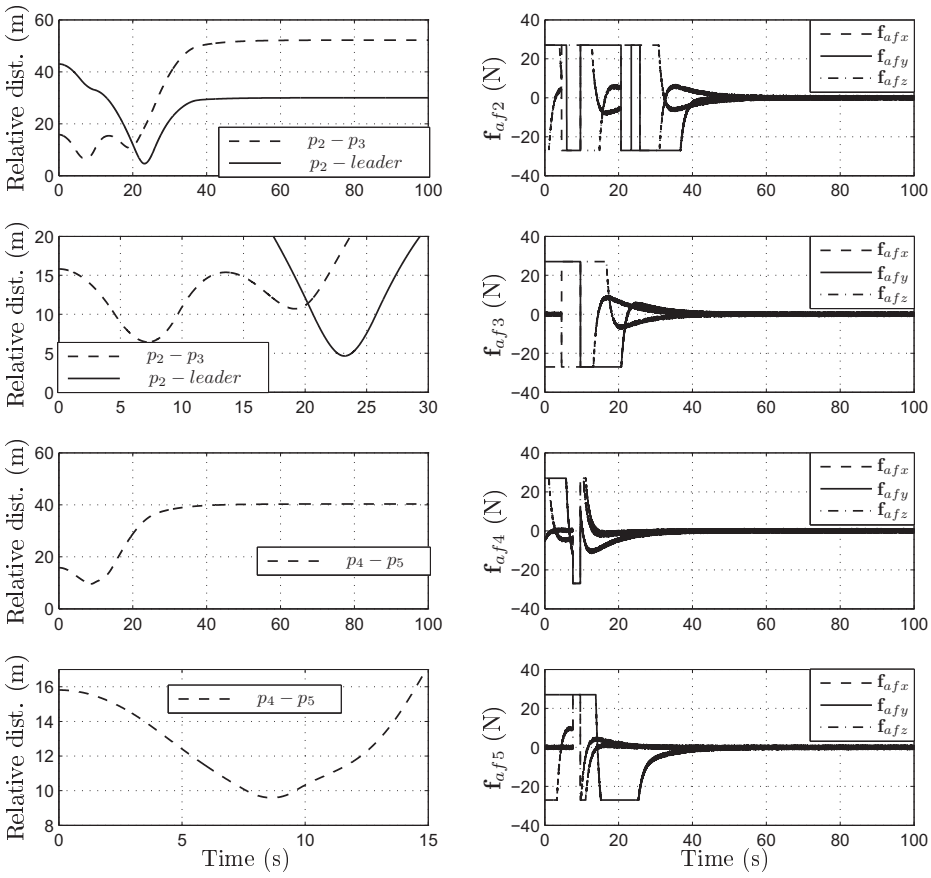

Figure 8.6: Formation reconfiguration with saturated control force and variable obstacle avoidance task gain where switching in actuator force is provoked when relative distance between spacecraft is less than 10 m due to the static collision avoidance task. The plots from the left top represents relative distance between second and third follower, and second follower and leader, and relative distance between forth and fifth followers, both with zoom. The plots from the right top represents actuator force for second, third, fourth and fifth follower.

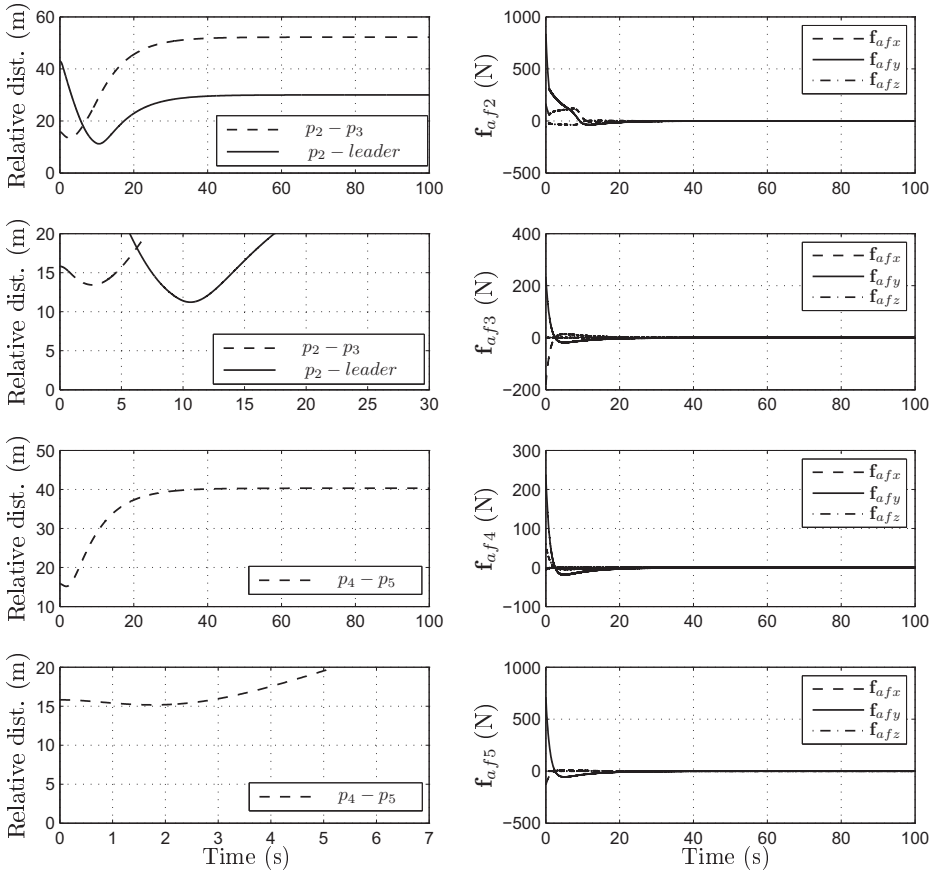

Figure 8.7: Formation reconfiguration where switching in actuator force is provoked when relative distance between spacecraft is less than 10 m due to the static collision avoidance task. The plots from the left top represents relative distance between second and third follower, and second follower and leader, and relative distance between forth and fifth followers, both with zoom. The plots from the right top represents actuator force for second, third, fourth and fifth follower.

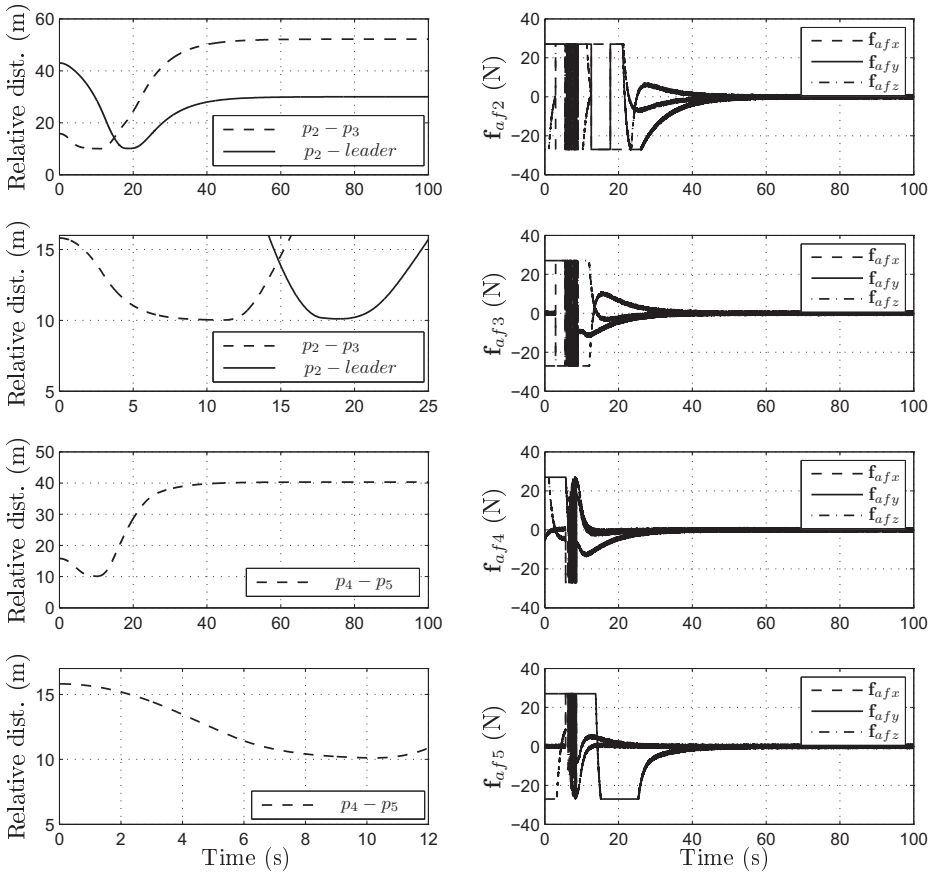

Figure 8.8: Formation reconfiguration where switching in actuator force is provoked when relative distance between spacecraft is less than $\sigma_{od,\iota}(\mathbf{p}_{o,\iota}, \dot{\mathbf{p}}_{o,\iota})$ due to the dynamic collision avoidance task. The plots from the left top represents relative distance between second and third follower, and second follower and leader, and relative distance between forth and fifth followers, both with zoom. The plots from the right top represents actuator force for second, third, fourth and fifth follower.

velocities which increases the dynamic spheres leading to bad behavior during reconfiguration, especially without saturation in available control force.

8.5.2 Drifting spacecraft

The initial configuration for this scenario was an arrowhead formation, maintained by the rigid formation task. One of the spacecraft was assumed to malfunction and loose actuator control, thus drifting through the formation due to orbital mechanics and perturbations. The individual positions of the followers relative to the leader where $\mathbf{p}_{init} = [(-50 \;\; -0 \;\; 0),\; (-25 \;\; 15 \;\; 0),\; (0 \;\; 30 \;\; 0),\; (25 \;\; 15 \;\; 0),\; (50 \;\; 0 \;\; 0)]^\top$, and $\boldsymbol{\sigma}_{f,d} = \mathbf{p}_{init}$, while the leader spacecraft was located at the origin. The simulation results are presented in Figure 8.9, and shows that when the drifting spacecraft entered the sphere of another spacecraft, the latter moved away from the desired position in a looping motion to avoid collision. This behavior was maintained until the drifting spacecraft exited the area presented by a sphere with radius 10 m centered at the desired position for the first follower, thus the controlled spacecraft moved back to its desired position in the formation.

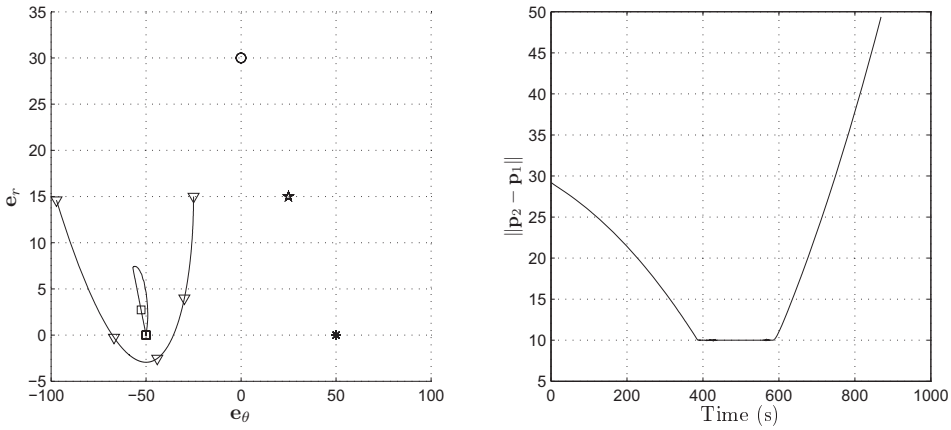

Figure 8.9: The left plot shows follower one, marked by □, avoiding the second follower, marked by ∇, which is out-of-control and drifting. The right plot shows the relative distance between spacecraft one and two.

Chapter 9

Conclusions and future work

9.1 Conclusions

Since this thesis in some sense is a continuation of the work by Kristiansen (2008) we have tried to expand the results in several different directions where appropriate challenges for leader-follower spacecraft formation have been sought to be solved. All the control laws presented in this thesis are based on the classical controllers for robot manipulators introduced as passivity-based PD+ by Paden and Panja (1988) and passivity-based sliding surface by Slotine and Li (1987).

In the first part of this thesis we presented previous work on modeling of leader-follower spacecraft formations for relative translational motion based on orbital parameters and relative rotation. Furthermore, we derived the relative translational dynamics using Euclidian parameters represented in the leader orbit frame and follower body frame. The latter was developed because a real spacecraft typically measures the relative position to the leader spacecraft using body mounted instruments, thus obtaining measurements represented in the body frame, and similar for actuation.

In the second part we focused our attention on attitude tracking control of rigid bodies which in our applied case represents the leader spacecraft. We presented exponentially growing proportional and derivative gains to reduce sensitivity to measurement noise during station keeping, and thus reduction in energy consumption and improved pointing accuracy which is crucial for orbiting spacecraft, without reducing the performance during attitude maneuvers. This method was solved for both state feedback and output feedback control and generalized for different kinds of nonlinear gain functions. Another problem which received some of our attention was the assumption that in previous work the attitude error is not allowed to increase beyond π rad during attitude maneuvers which is quite restrictive. This problem was solved in two different ways; by proving stability almost in the large for continuous control, or using hybrid feedback, both for state feedback and output feedback. The solution of stability almost in the large opens the door for a new problem which was considered, namely choosing the preferable rotational direction from an energy consumption point of view. This was solved for based on statistical analysis and an optimal control approach. For hybrid control we also presented

work where a supervisor was introduced switching between the two previously mentioned control laws to further increase the performance regarding maneuvers and sensitivity to measurement noise.

The third part of this thesis treated problems of rotational and translational synchronization of rigid bodies in the leader-follower framework for both absolute and relative coordinates. Based on the work from the second part, we proved uniform global asymptotic stability for the formation as a whole where the leader and follower are controlled separately through use of cascaded system theory. This was done for both the continuous and hybrid case. The technique using variable gains was also investigated, and it turned out that further improvements were provided for systems where the position and velocity works along the same axis compared to rotations where this is not necessarily true. Furthermore, we developed a scheme for autonomously generating references for either nadir or target tracking leader where the follower tracks the exact same point based on relative coordinates. In the last chapter we presented results for real-time autonomous collision avoidance by the null space based (NSB) behavioral control approach. Based on stability analysis of the coupling between the control law and NSB approach we were able to prove that collisions will not occur during configurational maneuvers, and furthermore, we developed different kind of strategies to increase safety while reducing energy consumption during these maneuvers.

9.2 Recommendations for future work

Although the authors feel they obtained adequate results for the specific problems which were analyzed, there are a lot of remaining issues still unanswered which would be interesting to solve in future work.

9.2.1 Choosing equilibrium point based on energetic function

The results in Chapter 5 may be further developed by also consider the angular velocity at t_f or utilizing an energetic function based on *e.g.* potential and kinetic energy to improve the accuracy of estimating the preferable equilibrium point.

9.2.2 Synchronization through output feedback control

In 6.3.1 we develop results for switching state feedback synchronization of a leader-follower formation. This result could be extended to the output-feedback case utilizing the results presented in Section 4.3 for the leader and a similar control structure for the follower.

9.2.3 Underactuated control

Based on the results in Section 6.3.2 a possible extension would be to consider thrust only available along one axis, and thus for proving stability a 6DOF analysis where relative attitude is coupled with relative translation needs to be provided.

9.2.4 Guidance in-the-loop

In Chapter 7 we presented autonomously generated references based on the spacecraft states and showed through simulations that our scheme behaved as expected for both nadir pointing and target tracking using a derived control law from Section 6.3. One possible extension would be to present a more complete stability analysis by including the guidance law in the loop as feedback for the control law.

Bibliography

Aamo, O. M., M. Arcak, T. I. Fossen and P. V. Kokotović (2000). Global output tracking control of a class of Euler-Lagrange systems. In: *Proceedings of the 39th IEEE Conference on Decision and Control*. Sydney, Australia.

Abdessameud, A. and A. Tayebi (2009). Attitude synchronization of a group of spacecraft without velocity measurements. *Automatic Control, IEEE Transactions on* **54**(11), 2642–2648.

Aeyels, Dirk (1985). Stabilization by smooth feedback of the angular velocity of a rigid body. *Systems & Control Letters* **6**(1), 59–63.

Aeyels, Dirk and Marek Szafranski (1988). Comments on the stabilizability of the angular velocity of a rigid body. *Systems & Control Letters* **10**(1), 35–39.

Akella, M. R. (2001). Rigid body attitude tracking without angular velocity feedback. *Systems & Control Letters* **42**(4), 321–326.

Alfriend, K. T., S. R. Vadali, P. Gurfil, J. P. How and L. S. Breger (2010). *Spacecraft Formation Flying - Dynamics, Control and Navigation*. Elsevier Astrodynamics Series. Elsevier.

Angeli, D. (2001). Almost global stabilization of the inverted pendulum via continuous state feedback. *Automatica* **37**(7), 1103–1108.

Angeli, D. (2004). An almost global notion of input-to-state stability. *IEEE Transactions on Automatic Control* **49**(6), 866–874.

Antonelli, G. and S. Chiaverini (2006). Kinematic control of platoons of autonomous vehicles. *IEEE Transactions on Robotics* **22**(6), 1285–1292.

Arrichiello, F. (2006). Coordination Control of Multiple Mobile Robots. PhD thesis. Cassino University. Cassino, Italy.

Arrichiello, F., S. Chiaverini and T. I. Fossen (2006). Formation control of marine surface vessels using the null-space-based behavioral control. In: *Group Coordination and Cooperative Control* (K. Y. Pettersen, J. T. Gravdahl and H. Nijmeijer, Eds.). Vol. 336 of *Lecture Notes in Control and Information Sciences*. Chap. 1, pp. 1–19. Springer Verlag. ISBN 3-540-33468-8.

Astolfi, A. (1999). Output feedback stabilization of the angular velocity of a rigid body. *Systems & Control Letters* **36**(3), 181–192.

Astolfi, A. and M. Lovera (2002). Global spacecraft attitude control using magnetic actuators. In: *Proceedings of the American Control Conference*.

Astolfi, A., D. Chhabra and R. Ortega (2002). Asymptotic stabilization of some equilibria of an underactuated underwater vehicle. *Systems & Control Letters* **45**(3), 193–206.

Bai, H., M. Arcak and J. T. Wen (2007). A decentralized design for group alignment and synchronous rotation without inertial frame information. In: *Proceedings of the 46th IEEE Conference on Decision and Control*.

Bai, H., M. Arcak and J. T. Wen (2008). Rigid body attitude coordination without inertial frame information. *Automatica* **44**(12), 3170–3175.

Bai, H., M. Arcak and J. T. Wen (2009). Adaptive motion coordination: Using relative velocity feedback to track a reference velocity. *Automatica* **45**(4), 1020–1025.

Bang, H. and C.-S. Oh (2004). Predictive control for the attitude maneuver of a flexible spacecraft. *Aerospace Science and Technology* **8**(5), 443–452.

Beard, R. W., J. Lawton and F. Y. Hadaegh (1999). A feedback architecture for formation control. In: *Proceedings of the American Control Conference*. San Diego, CA.

Beard, R. W., J. Lawton and F. Y. Hadaegh (2001). A coordination architecture for spacecraft formation control. *IEEE Transactions on Control Systems Technology* **9**(6), 777–790.

Beard, R. W., T. W. McLain and F. Y. Hadaegh (1998). Fuel equalized retargeting for separated spacecraft interferometry. In: *Proceedings of the American Control Conference*. Philadelphia, PA.

Belikov, S. A. (1981). Effect of gyroscopic forces on stability of uniform rotation of a rigid body about a principal axis. *Izv. Akad. Nauk SSSR* **16**(4), 3–10.

Bennett, M., M. F. Schatz, H. Rockwood and K. Wiesenfeld (2002). Huygen's clocks. *Proceedings of the Royal Society of London* **458**(2019), 563–579.

Berghuis, H. and H. Nijmeijer (1993). A passivity approach to controller-observer design for robots. *IEEE Transactions on Robotics and Automation* **9**(6), 740–754.

Bertrand, S., T. Hamel, H. Piet-Lahanier and R. Mahoney (2009). Attitude tracking of rigid bodies on the special orthogonal group with bounded partial state feedback. In: *Proceedings of the 48th IEEE Conference on Decision and Control, held jointly with the 28th Chinese Control Conference*.

Bhat, S. P. (2005). Controllability of nonlinear time-varying systems: Applications to spacecraft attitude control using magnetic actuation. *IEEE Transactions on Automatic Control* **50**(11), 1725–1735.

Bhat, S. P. and D. S. Bernstein (2000). A topological obstruction to continuous global stabilization of rotational motion and the unwinding phenomenon. *Systems & Control Letters* **39**(1), 63–70.

Blekhman, I.I. (1988). *Synchronization in Science and Technology*. ASME Press Translations. ASME Press. New York.

Blekhman, I.I., A.L. Fradkov, H. Nijmeijer and Yu.A. Pogromsky (1997). On self-synchronization and controlled synchronization. *Systems & Control Letters* **31**(5), 299–305.

Bloch, A. M., P. S. Krishnaprasad, J. E. Marsden and G. Sánchez de Alvarez (1992). Stabilization of rigid body dynamics by internal and external torques. *Automatica* **28**(4), 745–756.

Bondhus, A. K., K. Y. Pettersen and H. Nijmeijer (2004). Master-slave synchronization of robot manipulators. In: *Proceedings of the IFAC Symposium on Nonlinear Control Systems Design*. Stuttgart, Germany.

Bondhus, A. K., K. Y. Pettersen and J. T. Gravdahl (2005). Leader/follower synchronization of satellite attitude without angular velocity measurements. In: *Proceedings of the IEEE Conference on Decision and Control*. Seville, Spain.

Brockett, R. W. (1983). Asymptotic stability and feedback stabilization. In: *Differential Geometric Control Theory* (R. W. Brockett, R. S. Millmann and H. J. Sussmann, Eds.). pp. 181–191. Birkhauser.

Bullo, F. and M. Murray, R (1999). Tracking for fully actuated mechanical systems: a geometric framework. *Automatica* **35**(1), 17–34.

Byrnes, C. I. and A. Isidori (1989). New results and examples in nonlinear feedback stabilization. *Systems & Control Letters* **12**(5), 437–442.

Byrnes, C. I. and A. Isidori (1991). On the attitude stabilization of rigid spacecraft. *Automatica* **27**(1), 87–95.

Caccavale, F. and L. Villani (1999). Output feedback control for attitude tracking. *Systems & Control Letters* **38**(2), 91–98.

Camazine, S., J.-L. Deneubourg, N. R. Franks, J. Sneyd, G. Theraulaz and E. Bonabeau (2003). *Self-Organization in Biological Systems*. Princeton Studies in Complexity. Princeton University Press. ISBN 0-691-11624-5.

Casagrande, D., A. Astolfi and R. Ortega (2011). Asymptotic stabilization of passive systems without damping injection: A sampled integral technique. *Automatica* **47**(2), 262–271.

Casagrande, D., A. Astolfi and T. Parisini (2008). Global asymptotic stabilization of the attitude and the angular rates of an underactuated non-symmetric rigid body. *Automatica* **44**(7), 1781–1789.

Cassini, G. D. (1693). Traité de l'origine ede progrès de l'astronomie. Paris, France.

Chaillet, A. (2006). On Stability and Robustness of Nonlinear Systems: Applications to Cascaded Systems. PhD thesis. UFR Scientifique D'Orsay. Paris, France.

Chaillet, A. and A. Loría (2008). Uniform semiglobal practical asymptotic stability for non-autonomous cascaded systems and applications. *Automatica* **44**(2), 337–347.

Chaillet, A. and E. Panteley (2006). Stability of sets for nonlinear systems in cascade. In: *Proceedings of the 17th International Symposium on Mathematical Theory of Networks and Systems*. Kyoto, Japan.

Chang, I., S.-J. Chung and L. Blackmore (2010). Cooperative control with adaptive graph laplacians for spacecraft formation flying. In: *Proceedings of the 49th Conference on Decision and Control*.

Chen, X., W. H. Steyn and Y. Hashida (2000). Ground-target tracking control of earth-pointing satellites. In: *AIAA Guidance, Navigation, and Control Conference and Exhibit*. Denver, CO.

Chiaverini, S. (1997). Singularity-robust task-priority redundancy resolution for real-time kinematic control of robot manipulators. *Robotics and Automation, IEEE Transactions on* **13**(3), 398–410.

Clohessy, W. H. and R. S. Wiltshire (1960). Terminal guidance system for satellite rendezvous. *Journal of Aerospace Sciences* **27**(9), 653–658.

Cong, B.-L., X.-D. Liu and Z. Chen (2011). Distributed attitude synchronization of formation flying via consensus-based virtual structure. *Acta Astronautica* **68**(11-12), 1973–1986.

Costic, B., D. Dawson, M. de Queiroz and V. Kapila (2000). A quaternion-based adaptive attitude tracking controller without velocity measurements. In: *Proceedings of the IEEE Conference on Decision and Control*. Sydney, Australia. pp. 2429–2434.

Crouch, P. (1984). Spacecraft attitude control and stabilization: Applications of geometric control theory to rigid body models. *Automatic Control, IEEE Transactions on* **29**(4), 321 – 331.

Crouch, P. E., A. J. Pritchard, N. Carmichael and C. Lobry (1980). An appraisal of linear systems theory with applications to attitude control. report to estec. *NASA STI/Recon Technical Report N*.

Crowley, J. L. (1989). Asynchronous control of orientation and displacement in a robot vehicle. In: *Proceedings of the IEEE International Conference on Robotics and Automation*. Vol. 3. Scottsdale, AZ, USA. pp. 1277–1282.

Cui, Rongxin, Shuzhi Sam Ge, Bernard Voon Ee How and Yoo Sang Choo (2010). Leader-follower formation control of underactuated autonomous underwater vehicles. *Ocean Engineering* **37**(17-18), 1491 – 1502.

Cunha, Rita, Carlos Silvestre and João Hespanha (2008). Output-feedback control for stabilization on SE(3). *Systems & Control Letters* **57**(12), 1013 – 1022.

de Queiroz, M., V. Kapila and Q. Yan (2000). Adaptive nonlinear control of multiple spacecraft formation flying. *AIAA Journal of Guidance, Control and Dynamics* **23**(3), 385–390.

de Queiroz, M.S., Q. Yan, G. Yang and V. Kapila (1999). Global output feedback tracking control of spacecraft formation flying with parametric uncertainty. In: *Decision and Control, 1999. Proceedings of the 38th IEEE Conference on*. Vol. 1. pp. 584 –589 vol.1.

Di Gennaro, S. (2003). Passive attitude control of flexible spacecraft from quaternion measurements. *Journal of Optimization Theory and Applications* **116**(1), 41–60.

Dimarogonas, Dimos V., Panagiotis Tsiotras and Kostas J. Kyriakopoulos (2009). Leader-follower cooperative attitude control of multiple rigid bodies. *Systems & Control Letters* **58**(6), 429 – 435.

Edwards, C. H. and D. E. Penney (1988). *Elementary Linear Algebra*. Prentice Hall. ISBN 0-13-258260-0.

Efimov, D., E. Panteley and A. Loría (2009). Robust output stabilization: improving performance via supervisory control. arXiv.org. http://arxiv.org/abs/0906.0437.

Efimov, D. V. (2005). Dynamical adaptive synchronization. In: *Proceedings of the 44th IEEE Conference on Decision and Control and European Control Conference*. Sevilla, Spain.

Egeland, O. and J.-M. Godhavn (1994). Passivity-based adaptive attitude control of a rigid spacecraft. *IEEE Transactions on Automatic Control* **39**(4), 842–846.

Egeland, O. and J. T. Gravdahl (2002). *Modeling and Simulation for Automatic Control*. Marine Cybernetics. Trondheim, Norway. ISBN 82-92356-01-0.

Egerstedt, M., X. Hu and A. Stotsky (2001). Control of mobile platforms using a virtual vehicle approach. *IEEE Transactions on Automatic Control* **46**(11), 1777–1782.

El-Gohary, A.I. and T.S. Tawfik (2010). Optimal control of a rigid body motion using euler parameters without angular velocity measurements. *Mechanics Research Communications* **37**(3), 354 – 359.

Erdong, Jin and Sun Zhaowei (2010). Passivity-based control for a flexible spacecraft in the presence of disturbances. *International Journal of Non-Linear Mechanics* **45**(4), 348 – 356.

Euler, L. (1752). Découverte d'un nouveau principe de mécanique. *Histoire de l'Académie Royale des Science et Belles Lettres, Berlin* **6**, 185–217.

Fjellstad, O.-E. (1994). Control of Unmanned Underwater Vehicles in Six Degrees of Freedom. PhD thesis. Department of Engineering Cybernetics, Norwegian University of Science and Technology. Trondheim, Norway.

Fjellstad, O.-E. and T. I. Fossen (1994*a*). Position and attitude tracking of AUV's: A quaternion feedback approach. *IEEE Journal of Oceanic Engineering* **19**(4), 512–518.

Fjellstad, O.-E. and T. I. Fossen (1994*b*). Quaternion feedback regulation of underwater vehicles. In: *Proceedings of the IEEE Conference on Control Applications*. Glasgow, Scotland.

Fortescue, P., Stark, J. and Swinerd, G., Eds. (2007). *Spacecraft Systems Engineering, third edition*. Wiley. ISBN 0-471-61951-5.

Fossen, T. I. (2002). *Marine Control Systems: Guidance, Navigation, and Control of Ships, Rigs and Underwater Vehicles*. Marine Cybernetics. Trondheim, Norway. ISBN 82-92356-00-2.

Fossen, T. I. and O.-E. Fjellstad (1993). Cascaded adaptive control of ocean vehicles with significant actuator dynamics. In: *Proceedings of the IFAC World Congress*. Sydney, Australia.

Fragopoulos, D. and M. Innocenti (2004). Stability considerations in quaternion attitude control using discontinuous lyapunov functions. *Control Theory and Applications, IEE Proceedings* - **151**(3), 253–258.

Fu, S. H., C. C. Cheng and C. Y. Yin (2004). Nonlinear adaptive tracking control for underway replenishment process. In: *Proceedings of the IEEE International Conference on Networking, Sensing and Control*. Taipei, Taiwan.

Furasov, V. D. (1977). *Ustoichivost' dvijeniya, otzenki i stabilizatsia*. Nauka. Moscow. Translated title: Stability of motion, estimates and stabilization.

Glad, T. and L. Ljung (2000). *Control Theory*. Taylor & Francis. ISBN 0-7484-0878-9.

Goebel, R., R. G. Sanfelice and A. R. Teel (2009). Hybrid dynamical systems. *IEEE Control Systems Magazine* **29**(2), 28–93.

Goerre, B. B. and B. Shucker (1999). Geometric attitude control of a small satellite for ground tracking maneuvers. In: *Proceedings of the 13th AIAA/USU Conference on Small Satellites*. Utah State University.

Grøtli, E. I. (2010). Robust stability and control of spacecraft formations. PhD thesis. Department of Engineering Cybernetics, Norwegian University of Science & Technology.

Grøtli, E. I. and J. T. Gravdahl (2007). Passivity based controller-observer schemes for relative translation of a formation of spacecraft. In: *Proceedings of the American Control Conference*.

Grøtli, I. E., A. Chaillet and J.T. Gravdahl (2008). Output control of spacecraft in leader follower formation. In: *Proceedings of 47th IEEE Conference on Decision and Control*.

Gu, Y., B. Seanor, G. Campa, M. R. Napolitano, L. Rowe, S. Gururajan and S. Wan (2006). Design and flight testing evaluation of formation control laws. *IEEE Transactions on Control Systems Technology* **14**(6), 1105–1112.

Hadaegh, F. Y., W. M. Lu and P. K. C. Wang (1998). Adaptive control of formation flying spacecraft for interferometry. In: *Proceedings of the IFAC Conference on Large Scale Systems*. Rio Patras, Greece.

Hahn, W. (1963). *Theory and Application of Liapunov's Direct Method*. Prentice Hall. New York.

Hahn, W. (1967). *Stability of Motion*. Springer-Verlag. Berlin, Germany.

Hamilton, W. R. (1844). On quaternions: Or a new system of imaginaries in algebra. *Philosophical Magazine* **25**, 489–495.

Hill, G. W. (1878). Researches in the lunar theory. *American Journal of Mathematics* **1**(1), 5–26.

Horn, R. A. and C. R. Johnson (1985). *Matrix Analysis*. Cambridge University Press. ISBN 0-521-38632-2.

Hughes, P. C. (1986). *Spacecraft Attitude Dynamics*. John Wiley & Sons, Inc. USA. ISBN 0-486-43925-9.

Huygens, C. (1669). Instructions concerning the use of pendulum-watches, for finding the longitude at sea. *Philosophical Transactions of the Royal Society of London* (47), 937–953.

Huygens, C. (1673). *Horoloquium Oscilatorium*. Paris, France.

Ioslovich, I. (2003). Arbitrary fuel-optimal attitude maneuvering of a non-symmetric space vehicle in a vehicle-fixed coordinate frame. *Automatica* **39**(3), 557–562.

Janković, M., R. Sepulchre and P. V. Kokotović (1996). Constructive Lyapunov stabilization of non linear cascaded systems. *IEEE Transactions on Automatic Control* **41**(12), 1723–1736.

Jensen, H. B. and R. Wisniewski (2001). Quaternion feedback control for rigid-body spacecraft. In: *Proceedings of the AIAA Guidance, Navigation and Control Conference*. Montreal, Canada.

Jiang, Z. P. and I. Mareels (1997). A small gain control method for nonlinear cascaded systems with dynamic uncertainties. *IEEE Transaction on Automatic Control* **42**(3), 1–17.

Joshi, S. M., A. G. Kelkar and J. T.-Y. Wen (1995). Robust attitude stabilization of spacecraft using nonlinear quaternion feedback. *IEEE Transactions on Automatic Control* **40**(10), 1800–1803.

Junkins, J. L. and J. D. Turner (1986). *Optimal Spacecraft Rotational Maneuvers*. Vol. 3 of *Studies in Astronautics*. Elsevier Science Publishers. Amsterdam. ISBN 0-444-42619-1.

Kelly, R., V. Santibáñez and A. Loria (2005). *Control of robot manipulators in joint space*. Advanced textbooks in control engineering. Springer Verlag. ISBN 1-85233-994-2.

Khalil, H. K. (2002). *Nonlinear Systems, third edition*. Pearson Education International Inc.. Upper Saddle River, New Jersey, USA. ISBN 0-13-067389-7.

Koditschek, D.E. (1988). Application of a new Lyapunov function to global adaptive attitude tracking. In: *Proceedings of the 27th IEEE Conference on Decision and Control*.

Kovalev, A. and A. Savchenko (1975). Stability of uniform rotations of a rigid body about a principal axis. *Journal of Applied Mathematics and Mechanics* **39**(4), 623–633.

Kovalev, A. and A. Savchenko (2001). On the state and development perspectives of rigid body dynamics. *Multibody System Dynamics* **6**, 73–98.

Kreyzig, E. (1993). *Advanced Engineering Mathematics*. John Wiley & Sons Ltd.. New York. ISBN 0-471-50459-9.

Krishnan, H., N. H. McClamroch and M. Reyhanoglu (1995). Attitude stabilization of a rigid spacecraft using two momentum wheel actuators. *Journal of Guidance, Control and Dynamics* **18**(2), 256–263.

Kristiansen, R. (2008). Dynamic Synchronization of Spacecraft - Modeling and Coordinated Control of Leader-Follower Spacecraft Formations. PhD thesis. Department of Engineering Cybernetics, Norwegian University of Science and Technology. Trondheim, Norway.

Kristiansen, R., A. Loría, A. Chaillet and P. J. Nicklasson (2009). Spacecraft relative rotation tracking without angular velocity measurements. *Automatica* **45**(3), 750–756.

Kristiansen, R., A. Loría, A. Chaillet and P. J. Nicklasson (2006). Adaptive output feedback control of spacecraft relative translation. In: *Proceedings of the 45th IEEE Conference on Decision and Control*. San Diego, CA.

Kristiansen, R., E. I. Grøtli, P. J. Nicklasson and J. T. Gravdahl (2007). A model of relative translation and rotation in leader-follower spacecraft formations. *Modeling, Identification and Control* **28**(1), 3–14.

Kristiansen, R., P. J. Nicklasson and J. T. Gravdahl (2008). Spacecraft coordination control in 6DOF: Integrator backstepping vs passivity-based PD+. *Automatica* **44**(11), 2896–2901.

Kristiansen, Raymond and Per Johan Nicklasson (2009). Spacecraft formation flying: A review and new results on state feedback control. *Acta Astronautica* **65**(11-12), 1537–1552.

Krogstad, T. R. and J. T. Gravdahl (2006*a*). 6-DOF mutual synchronization of formation flying spacecraft. In: *Proceedings of the 45th Conference on Decision & Control*. San Diego, CA.

Krogstad, T. R. and J. T. Gravdahl (2006*b*). Coordinated attitude control of satellites in formation. In: *Group Coordination and Cooperative Control* (K. Y. Pettersen, J. T. Gravdahl and H. Nijmeijer, Eds.). Vol. 336 of *Lecture Notes in Control and Information Sciences*. pp. 153–170. Springer-Verlag. ISBN 3-540-33468-8.

Krogstad, T. R. and J. T. Gravdahl (2009). Output feedback control of relative spacecraft attitude. In: *Proceedings of the European Control Conference*.

Krstić, M. and P. Tsiotras (1997). Inverse optimality results for the attitude motion of a rigid spacecraft. In: *Proceedings of the American Control Conference*. Alburquerque, NM.

Krstić, M., I. Kanellakopoulos and P. Kokotović (1995). *Nonlinear and Adaptive Control Design*. John Wiley & Sons. New York. ISBN 0-471-12732-9.

Kuang, J., P. A. Meehan, A. Y. T. Leung and S. Tan (2004). Nonlinear dynamics of a satellite with deployable solar panel arrays. *International Journal of Non-Linear Mechanics* **39**(7), 1161–1179.

Kyrkjebø, E. (2007). Motion Coordination of Mechanical Systems: Leader-Follower Synchronization of Euler-Lagrange Systems using Output Feedback Control. PhD thesis. Department of Engineering Cybernetics, Norwegian University of Science and Technology. Trondheim, Norway.

Kyrkjebø, E., E. Panteley, A. Chaillet and K. Y. Pettersen (2006). A virtual vehicle approach to underway replenishment. In: *Group Coordination and Cooperative Control* (K. Y. Pettersen, J. T. Gravdahl and H. Nijmeijer, Eds.). Vol. 336 of *Lecture Notes in Control and Information Sciences*. pp. 171–189. Springer-Verlag.

Lalish, E., K.A. Morgansen and T. Tsukamaki (2006). Formation tracking control using virtual structures and deconfliction. In: *Proceedings of the 45th IEEE Conference on Decision and Control*.

LaSalle, J. and S. Lefschetz (1961). *Stability by Lyapunovs's direct method*. Mathematics in science and engineering. Academic Press.

Lawden, D. (1954). Fundamentals of space navigation. *Journal of the British Interplanetary Society* **13**(2), 87–101.

Lawton, J. and R. W. Beard (2000). Elementary attitude formation maneuver via leader-following and behaviour-based control. In: *Proceedings of the AIAA Guidance, Navigation and Control Conference*. Denver, CO.

Lawton, J., B. J. Young and R. W. Beard (2000). A decentralized approach to elementary formation maneuvers. In: *Proceedings of IEEE International Conference on Robotics and Automation*. San Fransisco, CA.

Lawton, J. R. (2000). A Behaviour-based approach for spacecraft formation flying. PhD thesis. Bringham Young University. Provo, UT.

Lawton, J. R. and R. W. Beard (2002). Synchronized multiple spacecraft rotations. *Automatica* **38**(8), 1359–1364.

Lawton, J., R. W. Beard and F. Y. Hadaegh (1999). An adaptive control approach to satellite formation flying with relative distance constraints. In: *Proceedings of the American Control Conference*. San Diego, CA.

Lebedev, D. V. (1981). On the control of a rigid body's triaxial orientation in the presence of constraints on the controls. *Journal of Applied Mathematics and Mechanics* **45**(3), 398–402.

Lee, T., M. Leok and N. H. McClamroch (2008). Time optimal attitude control for a rigid body. In: *Proceedings of the American Control Conference*.

Lefferts, E. J., F. L. Markley and M. D. Shuster (1982). Kalman filtering for spacecraft attitude estimation. *Journal of Guidance, Control and Dynamics* **5**(5), 417–429.

Leonard, N. E. and E. Fiorelli (2001). Virtual leaders, artificial potentials and coordinated control of groups. In: *Proceedings of the 40th IEEE Conference on Decision and Control*. Orlando, FL.

Lewis, F. L. and V. L. Syrmos (1995). *Optimal Control*. John Wiley & Sons, Inc. ISBN 0-471-03378-2.

Li, C., G. Ma and B. Song (2006). Passivity-based nonlinear attitude regulation of rigid spacecraft subject to control saturation. In: *Proceedings of The 6th World Congress on Intelligent Control and Automation*.

Liberzon, D. (2003). *Switching in Systems and Control*. Birkhäuser. ISBN 0-8176-4297-8.

Lizarralde, F. and J. T. Wen (1996). Attitude control without angular velocity measurement: a passivity approach. *IEEE Transactions on Automatic Control* **41**(3), 468–472.

Loría, A. and E. Panteley (2005). Cascaded nonliear time-varying systems: Analysis and design. In: *Advanced Topics in Control Systems Theory*. Vol. 311 of *Lecture Notes in Control and Information Sciences*. Chap. 2, pp. 23–64. Springer Verlag. ISBN 1-85233-923-3.

Loría, A. and E. Panteley (2006). Stability, told by its developers. In: *Advanced Topics in Control Theory* (A. Loría, F. Lamnabhi-Lagarrigue and E. Panteley, Eds.). Vol. 328 of *Lecture Notes in Control and Information Sciences*. Chap. 6, pp. 199–258. Springer Verlag. London. ISBN 1-84628-313-2.

Loría, A., H. Nijmeijer and Egeland O. (1998). Cascaded synchronization of two pendula. In: *Proceedings of the American Control Conference*.

Loría, A., R. Kelly and A. R. Teel (2005). Uniform parametric convergence in the adaptive control of mechanical systems. *European Journal of Control* **11**(2), 1–14.

Loría, A., T. I. Fossen and E. Panteley (2000). A separation principle for dynamic positioning of ships: Theoretical and experimental results. *IEEE Transactions on Control Systems Technology* **8**(2), 332–343.

Lovera, M. and A. Astolfi (2004). Spacecraft attitude control using magnetic actuators. *Automatica* **40**(8), 1405–1414.

Maithripala, D.H.S., J.M. Berg and W.P. Dayawansa (2004). An intrinsic observer for a class of simple mechanical systems on a Lie group. In: *Proceedings of the American Control Conference*.

Maithripala, D.H.S., J.M. Berg and W.P. Dayawansa (2006). Almost-global tracking of simple mechanical systems on a general class of lie groups. *Automatic Control, IEEE Transactions on* **51**(2), 216–225.

Matrosov, V. M. (1962). On the stability of motion. *Journal of Applied Mathematics and Mechanics* **26**(5), 1337–1353.

Mayhew, C. G., R. G. Sanfelice and A. R. Teel (2009). Robust global asymptotic attitude stabilization of a rigid body by quaternion-based hybrid feedback. In: *Proceedings of the IEEE Conference on Decision and Control*.

Mazenc, F., L. Praly and W. P. Dayawansa (1994). Global stabilization by output feedback: examples and counterexamples. *Systems & Control Letters* **23**(2), 119–125.

McInnes, C. R. (1995). Autonomous ring formation for a planar constellation of satellites. *AIAA Journal of Guidance, Control and Dynamics* **18**(5), 1215–1217.

Meng, Z., W. Ren and Z. You (2010). Distributed finite-time attitude containment control for multiple rigid bodies. *Automatica* **46**(12), 2092–2099.

Meyer, G. (1971). Design and global analysis of spacecraft attitude control systems. NASA TR R-361. Ames Research Center.

Monzón, P. (2006). Almost global stability of time-varying systems. In: *Proceedings of the Congresso Brasileiro de Automatica*. Bahia, Brasil. pp. 198–201.

Morin, P. and C. Samson (1997). Time-varying exponential stabilization of a rigid spacecraft with two control torques. *Automatic Control, IEEE Transactions on* **42**(4), 528–534.

Morin, P., C. Samson, J. B. Pomet and Z. P. Jiang (1995). Time-varying feedback stabilization of the attitude of a rigid spacecraft with two controls. *Systems & Control Letters* **25**(5), 375–385.

Mortensen, R. E. (1963). On system for automatic control of the rotation of a rigid body. *Electronics Reaserach Lab., University of California*.

Mortensen, R. E. (1968). A globally stable linear attitude regulator. *Journal of Control* **8**(3), 297–302.

Nair, S. and N. E. Leonard (2007). Stable synchronization of rigid body networks. *Networks and Heterogeneous Media* **2**(4), 595–624.

Nijmeijer, H. and A. Rodriguez-Angeles (2003). *Synchronization of Mechanical Systems*. Vol. 46 of *World Scientific Series on Nonlinear Science, Series A*. World Scientific Publishing Co. Pte. Ltd. ISBN 981-238-605-X.

Ögren, P., E. Fiorelli and N. E. Leonard (2004). Cooperative control of mobile sensor networks: Adaptive gradient climbing in a distributed environment. *IEEE Transactions on Automatic Control* **49**(8), 1292–1302.

Ortega, R., A. Loría, P. J. Nicklasson and H. Sira-Ramírez (1998). *Passivity-based Control of Euler-Lagrange Systems: Mechanical, Electrical and Electromechanical Applications*. Series Comunications and Control Engineering. Springer Verlag. London. ISBN 1-85233-016-3.

Ortega, R., A. Loría, R. Kelly and L. Praly (1994). On passivity-based output feedback global stabilization of Euler-Lagrange systems. In: *Proceedings of the 33rd Conference on Decision and Control*. Buena Vista, FL.

Outbib, R. and G. Sallet (1992). Stabilizability of the angular velocity of a rigid body revisited. *Systems & Control Letters* **18**(2), 93–98.

Paden, B. and R. Panja (1988). Globally asymptotically stable 'PD+' controller for robot manipulators. *International Journal of Control* **47**(6), 1697–1712.

Pan, H. and V. Kapila (2001). Adaptive nonlinear control for spacecraft formation flying with coupled translational and attitude dynamics. In: *Proceedings of the Conference on Decision and Control*. Orlando, FL.

Pan, H., H. Wong and V. Kapila (2004). Output feedback control for spacecraft with coupled translation and attitude dynamics. In: *Proceedings of the 43rd IEEE Conference on Decision and Control*. Vol. 4. pp. 4453 – 4458 Vol.4.

Panteley, E., A. Loría and A. R. Teel (2001). Relaxed persistency of excitation for uniform asymptotic stability. *IEEE Transactions on Automatic Control* **46**(12), 1874–1886.

Panteley, E. and A. Loría (1998). On global uniform asymptotic stability of nonlinear time-varying systems in cascade. *Systems & Control Letters* **33**(2), 131–138.

Pettersen, K. Y. and O. Egeland (1999). Time-varying exponential stabilization of the position and attitude of an underactuated autonomous underwater vehicle. *IEEE Transactions on Automatic Control* **44**(1), 112–115.

Ploen, S. R., D. P. Scharf, F. Y. Hadaegh and A. B. Acikmese (2004*a*). Dynamics of Earth orbiting formations. In: *Proceedings ot he AIAA Guidance, Navigation and Control Conference*.

Ploen, S. R., F. Y. Hadaegh and D. P. Scharf (2004*b*). Rigid body equations of motion for modeling and control of spacecraft formations - part 1: Absolute equations of motion. In: *Proceedings of the American Control Conference*. Boston, MA.

Pongvthithum, R., S. M. Veres, S. B. Gabriel and E. Rogers (2005). Universal adaptive control of satellite formation flying. *International Journal of Control* **78**(1), 45–52.

Quottrup, M. M., J. Krogh-Sørensen and R. Wiśniewski (2001). Passivity based nonlinear attitude control of the Rømer satellite. In: *Proceedings of the 15th IFAC Symposium on Automatic Control in Aerospace*. Bologna, Italy.

Rantzer, A. (2001). A dual to Lyapunov's stability theorem. *Systems & Control Letters* **42**(3), 161–168.

Ren, W. and R. W. Beard (2004). A decentralized scheme for spacecraft formation flying via the virtual structure approach. *AIAA Journal of Guidance, Control and Dynamics* **27**(1), 73–82.

Ren, W. and R. W. Beard (2008). *Distributed Consensus in Multi-vehicle Cooperative Control*. Springer-Verlag. ISBN 978-1-84800-014-8.

Rodriguez-Angeles, A. (2002). Synchronization of Mechanical Systems. PhD thesis. Eindhoven University of Technology. The Netherlands.

Rodriguez-Angeles, A. and H. Nijmeijer (2001). Coordination of two robot manipulators based on position measurements only. *International Journal of Control* **74**(13), 1311–1323.

Rouch, N. and J. Mawhin (1980). *Ordinary Differential Equations - Stability and Periodic Solutions*. Pitman Publishing Limited. ISBN 0-273-08419-4.

Sabol, C., R. Burns and C. A. McLaughlin (2001). Satellite formation flying design and evolution. *AIAA Journal of Spacecraft and Rockets* **38**(2), 270–278.

Salcudean, S. E. (1991). A globally convergent angular velocity observer for rigid body motion. *IEEE Transactions on Automatic Control* **36**(12), 1493–1497.

Sanfelice, R. G. and A. R. Teel (2008). A nested Matrosov theorem for hybrid systems. In: *Proceedings of the American Control Conference*.

Sanfelice, R. G., R. Goebel and A. R. Teel (2007). Invariance principles for hybrid systems with connections to detectability and asymptotic stability. *IEEE Transactions on Automatic Control* **52**(12), 2282–2297.

Sarlette, A., R. Sepulchre and N. E. Leonard (2007). Cooperative attitude synchronization in satellite swarms: A consensus approach. In: *Proceedings of the 17th IFAC Symposium on Automatic Control in Aerospace*.

Sarlette, A., R. Sepulchre and N. E. Leonard (2009). Autonomous rigid body attitude synchronization. *Automatica* **45**(2), 572–577.

Sarlette, A., S. Bonnabel and R. Sepulchre (2010). Coordinated motion design on Lie groups. *Automatic Control, IEEE Transactions on* **55**(5), 1047–1058.

Scharf, D. P., F. Y. Hadaegh and S. R. Ploen (2003). A survey of spacecraft formation flying guidance and control (part i): Guidance. In: *Proceedings of the American Control Conference*. Denver, CO.

Scharf, D. P., F. Y. Hadaegh and S. R. Ploen (2004). A survey of spacecraft formation flying guidance and control (part ii): Control. In: *Proceedings of the American Control Conference*. Boston, MA.

Schaub, H. and J. L. Junkins (2003). *Analytical Mechanics of Space Systems*. AIAA Education Series. American Institute of Aeronautics and Astronautics. Reston, VA. ISBN 1-56347-563-4.

Schlanbusch, R., A. Loría and P. J. Nicklasson (2010*a*). Hybrid stabilization of controlled spacecraft. In: *Proceedings of the 49th IEEE Conference on Decision and Control*. Atlanta, GA.

Schlanbusch, R., A. Loría and P. J. Nicklasson (2011*a*). Cascade-based controlled synchronization and tracking of spacecraft in leader-follower formation. *International Journal of Aerospace Engineering, special issue on Formation Flight Control*.

Schlanbusch, R., A. Loría and P. J. Nicklasson (2011*b*). On the stability and stabilization of quaternion equilibria of rigid bodies. Conditionally accepted for Automatica.

Schlanbusch, R., A. Loría, R. Kristiansen and P. J. Nicklasson (2010*b*). PD+ attitude control of rigid bodies with improved performance. In: *Proceedings of the 49th IEEE Conference on Decision and Control*. Atlanta, GA.

Schlanbusch, R., A. Loría, R. Kristiansen and P. J. Nicklasson (2011*c*). PD+ based output feedback attitude control of rigid bodies. Accepted for IEEE Transactions on Automatic Control.

Schlanbusch, R., A. Loría, R. Kristiansen and P. J. Nicklasson (2011*d*). PD+ based output feedback attitude control of rigid bodies with improved performance. In: *Proceedings of the American Control Conference*. San-Francisco, CA.

Schlanbusch, R. and P. J. Nicklasson (2011). Synchronization of target tracking cascaded leader-follower spacecraft formation. In: *Advances in Spacecraft Technologies* (J.Hall, Ed.). Chap. 25, pp. 563–584. InTech. ISBN 978-953-307-551-8.

Schlanbusch, R., E. I. Grøtli, A. Loría and P. J. Nicklasson (2011*e*). Hybrid attitude tracking of output feedback controlled rigid bodies. In: *Proceedings of the 50th IEEE Conference on Decision and Control*. Orlando, FL.

Schlanbusch, R., E. I. Grøtli, A. Loría and P. J. Nicklasson (2011*f*). Hybrid attitude tracking of rigid bodies without angular velocity measurements. Accepted for Systems & Control Letters.

Schlanbusch, R., R. Kristiansen and P. J. Nicklasson (2008*a*). Spacecraft formation reconfiguration with collision avoidance. In: *Proceedings of the 3rd International Symposium on Formation Flying, Missions and Technologies (ISFF)*. Estec, Holland.

Schlanbusch, R., R. Kristiansen and P. J. Nicklasson (2010*c*). Attitude reference generation for leader-follower formation with nadir pointing leader. In: *Proceedings of the American Control Conference*. Baltimore, MD.

Schlanbusch, R., R. Kristiansen and P. J. Nicklasson (2010*d*). Considerations choosing the optimal equilibrium point on the rotational sphere. In: *Proceedings of the American Control Conference*. Baltimore, MD.

Schlanbusch, R., R. Kristiansen and P. J. Nicklasson (2010*e*). On choosing quaternion equilibrium point in attitude stabilization. In: *Proceedings of the 31th IEEE Aerospace Conference*. Big Sky, MO.

Schlanbusch, R., R. Kristiansen and P. J. Nicklasson (2011*g*). Spacecraft formation reconfiguration with collision avoidance. *Automatica* **47**(7), 1443–1449.

Schlanbusch, R., T. M. Steihaug and P. J. Nicklasson (2008*b*). Target reference generator for the European Student Moon Orbiter (ESMO) satellite. Presentation at Multiphysics conference, Narvik, Norway.

Seibert, P. and R. Suarez (1990). Global stabilization of nonlinear cascade systems. *Systems & Control Letters* **14**(4), 347–352.

Serrani, A. (2003). Robust coordinated control of satellite formations subject to gravity perturbations. In: *Proceedings of the American Control Conference*.

Shan, J. (2008). Six-degree-of-freedom synchronised adaptive learning control for spacecraft formation flying. *Control Theory Applications, IET* **2**(10), 930 –949.

Shuster, M. D. (1993). A survey of attitude representations. *The Journal of the Astronautical Sciences* **41**(4), 439–517.

Shuster, M. D. (2008). The nature of the quaternion. *The Journal of the Astronautical Sciences*.

Shuster, M. D. and S. D. Oh (1981). Three-axis attitude determination from vector observations. *Journal of Guidance, Control and Dynamics* **4**(1), 70–77.

Sidi, M. J. (1997). *Spacecraft Dynamics and Control*. Cambridge University Press. New York. ISBN 0-521-78780-7.

Skjetne, R., T.I. Fossen and P. V. Kokotović (2002). Output maneuvering for a class of nonlinear systems. In: *Proceedings of the IFAC World Congress*. Barcelona, Spain.

Slotine, J. J.-E. and M. D. Di Benedetto (1990). Hamiltonian adaptive control of spacecraft. *IEEE Transactions on Automatic Control* **35**(7), 848–852.

Slotine, J. J.-E. and W. Li (1987). On the adaptive control of robot manipulators. *International Journal of Robotics Research* **6**(3), 49–59.

Slotine, J. J.-E. and W. Li (1988). Adaptive manipulator control: A case study. *Automatic Control, IEEE Transactions on* **33**(11), 995–1003.

Smirnov, E. Ya. (1974). Control of the rotational motion of a rigid body. *Izv. Akad. Nauk SSSR* **9**(3), 5–10.

Song, G. and B. N. Agrawal (2001). Vibration suppression of flexible spacecraft during attitude control. *Acta Astronautica* **49**(2), 73–83.

Sontag, E. D. and H. J. Sussmann (1988). Further comments on the stabilizability of the angular velocity of a rigid body. *Systems & Control Letters* **12**(3), 437–442.

Spindler, K. (1996). Optimal attitude control of a rigid body. *Applied Mathematics and Optimization* **34**(1), 79–90.

Steyn, W. H. (2006). A view finder control system for an Earth observation satellite. *Aerospace Science and Technology* **10**(3), 248–255.

Strutt, J. W. (Lord Rayleigh) (1896). *The Theory of Sound*. Vol. II. London, Macmillan.

Sun, D. (2003). Position synchronization of multiple motion axes with adaptive coupling control. *Automatica* **39**(6), 997–1005.

Svendsen, L. M., R. Kristiansen, P. J. Nicklasson and R. Schlanbusch (2007). Modelling of leader-follower spacecraft formations in 6DOF. In: *Proceedings of the 6th EUROSIM Congress on Modelling and Simulation*.

Takegaki, M. and S. Arimoto (1981). A new feedback method for dynamic control of manipulators. *ASME Journal of Dynamical Systems, Measurement and Control* **102**(2), 119–125.

Tan, K.-H. and M.A. Lewis (1996). Virtual structures for high-precision cooperative mobile robotic control. In: *Proceedings of the IEEE/RSJ International Conference on Intelligent Robots and Systems*.

Tayebi, A. (2006). Unit quaternion observer based attitude stabilization of a rigid spacecraft without velocity measurement. In: *Proceedings of the 45th IEEE Conference on Decision and Control*.

Tayebi, A. (2008). Unit quaternion-based output feedback for the attitude tracking problem. *Automatic Control, IEEE Transactions on* **53**(6), 1516–1520.

Tillerson, M., L. Breger and J. P. How (2003). Distributed coordination and control of formation flying spacecraft. In: *Proceedings of the American Control Conference*. Denver, CO.

Tschauner, J. (1967). Elliptic orbit rendezvous. *AIAA Journal* **5**(6), 1110–1113.

Tsiotras, P. (1996). On the choice of coordinates for control problems on SO(3). In: *Proceedings of the 30th Annual Conference on Information Sciences and Systems*.

Tsiotras, P. (1998). Further passivity results for the attitude control problem. *IEEE Transactions on Automatic Control* **43**(11), 1597–1600.

Tsiotras, P. and J. Luo (2000). Control of underactuated spacecraft with bounded inputs. *Automatica* **36**(8), 1153–1169.

Tsiotras, P. and J. M. Longuski (1995). A new parametrization of the attitude kinematics. *Journal of the Astronautical Sciences* **43**(3), 243–262.

Tsiotras, P. and J. M. Longuski (1996). Analytical solution of Euler's equations of motion for an asymmetric rigid body. *ASME Journal of Applied Mechanics* **63**(1), 149–155.

Tsiotras, P. and V. Doumtchenko (2000). Control of spacecraft subject to actuator failures: state-of-the-art and open problems. *Journal of the Astronautical Sciences* **48**(2), 337–358.

Tsiotras, P., H. Shen and C. Hall (2001). Satellite attitude control and power tracking with energy/momentum wheels. *AIAA Journal of Guidance, Control and Dynamics* **24**(1), 23–34.

Tsiotras, P., M. Corless and M. Rotea (1996). Optimal control of rigid body angular velocity with quadratic cost. In: *Proceedings of the IEEE Conference on Decision and Control*.

Van der Schaft, A. J. (1996). *L_2-Gain and Passivity Techniques in Nonlinear Control*. Vol. 218 of *Lecture notes in control and information science*. Springer-Verlag. ISBN 1-85233-073-2.

Van der Schaft, A. J. and H. Schumacher (2000). *An Introduction to Hybrid Dynamical Systems*. Vol. 251 of *Lecture notes in control and information science*. Springer-Verlag. ISBN 1-85233-233-6.

VanDyke, M. and C. Hall (2006). Decentralized coordinated attitude control of a formation of spacecraft. *Journal of Guidance, Control and Dynamics* **29**(5), 1101–1009.

Wang, P. K. C. and F. Y. Hadaegh (1996). Coordination and control of multiple microspacecraft moving in formation. *Journal of the Astronautical Sciences* **44**(3), 315–355.

Wang, P. K. C., F. Y. Hadaegh and K. Lau (1999). Synchronized formation rotation and attitude control of multiple free-flying spacecraft. *AIAA Journal of Guidance, Control and Dynamics* **22**(1), 28–35.

Wang, Z., F. Khorrami and W. Grossman (2000). Robust adaptive control of formationkeeping for a pair of satellites. In: *Proceedings of the American Control Conference*.

Wen, J. T.-Y. and K. Kreutz-Delgado (1991). The attitude control problem. *IEEE Transactions on Automatic Control* **36**(10), 1148–1162.

Wertz, J. R., Ed. (1978). *Spacecraft Attitude Determination and Control*. Kluwer Academic Publishers. London. ISBN 90-277-0959-9.

Wie, B. and P. M. Barba (1985). Quaternion feedback for spacecraft large angle maneuvers. *Journal of Guidance, Control and Dynamics* **8**(3), 360–365.

Wie, B., H. Weiss and A. Arapostathis (1989). Quaternion feedback regulator for spacecraft eigenaxis rotation. *Journal of Guidance, Control and Dynamics* **12**(3), 375–380.

Wiles, A. (1995). Modular elliptic curves and fermat's last theorem. *Annals of Mathematics* **141**(3), 443–551.

Wiśniewski, R. and M. Blanke (1999). Fully magnetic attitude control for spacecraft subject to gravity gradient. *Automatica* **35**(7), 1201–1214.

Wong, H., H. Pan and V. Kapila (2005). Output feedback control for spacecraft formation flying with coupled translation and attitude dynamics. In: *Proceedings of the American Control Conference*. Portland, OR.

Wong, H., H. Pan, M.S. de Queiroz and V. Kapila (2001*a*). Adaptive learning control for spacecraft formation flying. In: *Proceedings of the 40th IEEE Conference on Decision and Control*.

Wong, H., M. S. de Queiroz and V. Kapila (2001*b*). Adaptive tracking control using synthesized velocity from attitude measurements. *Automatica* **37**(6), 947–953.

Wong, H., V. Kapila and A. G. Sparks (2002). Adaptive output feedback tracking control of spacecraft formation. *International Journal of Robust and Nonlinear Control* **12**(2-3), 117–139.

Yan, Q., G. Yang, V. Kapila and M. de Queiroz (2000*a*). Nonlinear dynamics and output feedback control of multiple spacecraft in elliptical orbits. In: *Proceedings of the American Control Conference*. Chicago, Illinois.

Yan, Q., G. Yang, V. Kapila and M. de Queiroz (2000*b*). Nonlinear dynamics, trajectory generation, and adaptive control of multiple spacecraft in periodic relative orbits. In: *Proceedings of the AAS Guidance and Control Conference*. Breckenridge, CO.

Yeh, H.-H., E. Nelson and A. Sparks (2000). Nonlinear tracking control for satellite formations. In: *Proceedings of the IEEE Conference on Decision and Control*. Sydney, Australia.

Young, B. J., R. W. Beard and J. M. Kelsey (2001). A control scheme for improving multi-vehicle formation maneuvers. In: *Proceedings of the American Control Conference*. Arlington, VA.

Young, W. H. (1912). On classes of summable functions and their fourier series. *Proceedings of the Royal Society of London. Series A, Containing Papers of a Mathematical and Physical Character* **87**(594), 225–229.

Appendix A

Background material

In this chapter we present mathematical tools utilized throughout this thesis to make it self-contained. Section A.1 starts with basic linear algebra and functional properties recovered from (Horn and Johnson, 1985; Edwards and Penney, 1988; Kreyzig, 1993); Section A.2 reviews definitions and theorems for Lyapunov stability analysis recovered from (Hahn, 1967; Rouch and Mawhin, 1980; Khalil, 2002; Kelly *et al.*, 2005; Loría and Panteley, 2006); almost-global stability, recovered from (Rantzer, 2001) in Section A.2.1; and for practical and semi-global results in Section A.2.2 recovered from (Hahn, 1967; Chaillet, 2006; Grøtli, 2010). A short introduction on hybrid switching control is given in Section A.3 recovered from (Goebel *et al.*, 2009), basic optimal control theory is revisited in Section A.4 recovered from (Lewis and Syrmos, 1995; Glad and Ljung, 2000), while in Section A.5 we review results on stability analysis of cascaded systems, recovered from (Loría and Panteley, 2005; Chaillet, 2006; Grøtli, 2010).

A.1 Mathematical review

The inner product of two vectors $\mathbf{x}, \mathbf{y} \in \mathbb{R}^n$ is defined as $\mathbf{x}^\top \mathbf{y} = \sum_{i=1}^{n} x_i y_i$, where the inner product of vectors satisfy $\mathbf{x}^\top \mathbf{y} = \mathbf{y}^\top \mathbf{x}\ \forall \mathbf{x}, \mathbf{y} \in \mathbb{R}^n$ and $\mathbf{x}^\top(\mathbf{y} + \mathbf{z}) = \mathbf{x}^\top \mathbf{y} + \mathbf{x}^\top \mathbf{z},\ \forall \mathbf{x}, \mathbf{y}, \mathbf{z} \in \mathbb{R}^n$. The Euclidian norm of a vector $\mathbf{x} \in \mathbb{R}^n$ is defined as

$$\|\mathbf{x}\| := \sqrt{\sum_{i=1}^{n} x_i^2} = \sqrt{\mathbf{x}^\top \mathbf{x}}, \tag{A.1}$$

and satisfy the following axioms and properties

- $\|\mathbf{x}\| = 0$ if and only if $\mathbf{x} = \mathbf{0} \in \mathbb{R}^n$;
- $\|\mathbf{x}\| > 0$ for all $\mathbf{x} \in \mathbb{R}^n$ with $\mathbf{x} \neq \mathbf{0} \in \mathbb{R}^n$;
- $\|\alpha \mathbf{x}\| = |\alpha| \|\mathbf{x}\|$ for all $\alpha \in \mathbb{R}$ and $\mathbf{x} \in \mathbb{R}^n$ (Homogenity);

- $\|\mathbf{x}\| - \|\mathbf{y}\| \leq \|\mathbf{x}+\mathbf{y}\| \leq \|\mathbf{x}\| + \|\mathbf{y}\|$ for all $\mathbf{x}, \mathbf{y} \in \mathbb{R}^n$ (Triangle inequality);

- $|\mathbf{x}^\top \mathbf{y}| \leq \|\mathbf{x}\|\|\mathbf{y}\|$ for all $\mathbf{x}, \mathbf{y} \in \mathbb{R}^n$ (Schwartz inequality),

where $\mathbf{0}$ in general denotes the null matrix of dimension $n \times m$ which may be written as $\mathbf{0}_{n\times m} \in \mathbb{R}^{n\times m}$ where each element is zero. Other useful inequalities include Young's Inequality where for $\mathbf{x}, \mathbf{y} \in \mathbb{R}^n$ and any $p \in \mathbb{N}\backslash\{1\}$ we have that

$$|\mathbf{x}^\top \mathbf{y}| \leq \frac{1}{p}\|\mathbf{x}\|^p + \frac{p-1}{p}\|\mathbf{y}\|^{\frac{p}{p-1}}. \tag{A.2}$$

For $p = 2$, it follows from Young's inequality that for any $\lambda > 0$ we have

$$|\mathbf{x}^\top \mathbf{y}| \leq \frac{\lambda}{2}\|\mathbf{x}\|^2 + \frac{1}{2\lambda}\|\mathbf{y}\|^2. \tag{A.3}$$

The dot product $\mathbf{v} \cdot \mathbf{u}$ of the vectors $\mathbf{v} \in \mathbb{R}^n$ and $\mathbf{u} \in \mathbb{R}^n$ is defined as

$$\mathbf{v} \cdot \mathbf{u} \triangleq v_1 u_1 + v_2 u_2 + \ldots + v_n u_n. \tag{A.4}$$

The dot product is a real number and not a vector, and also sometimes called *scalar product*. If a set of vectors $\mathbf{v} \in \mathbb{R}^n$ and $\mathbf{u} \in \mathbb{R}^n$ leads to

$$\mathbf{v} \cdot \mathbf{u} = 0 \tag{A.5}$$

the vectors are *orthogonal* or *perpendicular* to each other. The zero vector $\mathbf{0}$ is orthogonal to every vector $\mathbf{v} \in \mathbb{R}^n$ because $\mathbf{v} \cdot \mathbf{0} = 0$ for all $\mathbf{v}$.

The vector cross product between vectors $\mathbf{v}$ and vector $\mathbf{u}$ is given as

$$\|\mathbf{v} \times \mathbf{u}\| = \|\mathbf{v}\|\|\mathbf{u}\| \sin\theta, \tag{A.6}$$

where θ is the angle between the vectors $\mathbf{u}$ and $\mathbf{v}$. The skew symmetric operator $\mathbf{S}(\cdot)$ is used to evaluate the cross product between two vectors $\mathbf{u} \in \mathbb{R}^3$ and $\mathbf{v} = [v_1,\ v_2,\ v_3]^\top \in \mathbb{R}^3$ and is defined as

$$\mathbf{S}(\mathbf{v}) \triangleq \begin{bmatrix} 0 & -v_3 & v_2 \\ v_3 & 0 & -v_1 \\ -v_2 & v_1 & 0 \end{bmatrix}, \tag{A.7}$$

such that $\mathbf{v} \times \mathbf{u} = \mathbf{S}(\mathbf{v})\mathbf{u}$. The properties of the skew symmetric matrix are

1. $\mathbf{S}(\alpha\mathbf{v} + \beta\mathbf{u}) = \alpha\mathbf{S}(\mathbf{v}) + \beta\mathbf{S}(\mathbf{u})$
2. $\mathbf{S}(\mathbf{v})\mathbf{S}(\mathbf{u}) = \mathbf{u}\mathbf{v}^T - \mathbf{v}^T\mathbf{u}\mathbf{I}_{3\times 3}$
3. $\mathbf{S}[\mathbf{S}(\mathbf{v})\mathbf{u}] = \mathbf{u}\mathbf{v}^T - \mathbf{v}\mathbf{u}^T$
4. $\mathbf{v}^T\mathbf{S}(\mathbf{u})\mathbf{v} = 0$
5. $\mathbf{S}(\mathbf{v})\mathbf{v} = \mathbf{0}$.

The product of matrices $\mathbf{A} \in \mathbb{R}^{m\times p}$ and $\mathbf{B} \in \mathbb{R}^{p\times n}$ denoted $\mathbf{C} = \mathbf{AB} \in \mathbb{R}^{m\times n}$ is defined as

$$\mathbf{C} = \begin{bmatrix} \sum_{k=1}^{p} a_{1k}b_{k1} & \sum_{k=1}^{p} a_{1k}b_{k2} & \cdots & \sum_{k=1}^{p} a_{1k}b_{kn} \\ \sum_{k=1}^{p} a_{2k}b_{k1} & \sum_{k=1}^{p} a_{2k}b_{k2} & \cdots & \sum_{k=1}^{p} a_{2k}b_{kn} \\ \vdots & \vdots & \ddots & \vdots \\ \sum_{k=1}^{p} a_{mk}b_{k1} & \sum_{k=1}^{p} a_{mk}b_{k2} & \cdots & \sum_{k=1}^{p} a_{mk}b_{kn} \end{bmatrix}, \tag{A.8}$$

and it may be verified that

- $(\mathbf{AB})^\top = \mathbf{B}^\top\mathbf{A}^\top$ for all $\mathbf{A} \in \mathbb{R}^{m\times p}$ and $\mathbf{B} \in \mathbb{R}^{p\times n}$;
- in general, $\mathbf{AB} \neq \mathbf{BA}$;
- for all $\mathbf{A} \in \mathbb{R}^{m\times p}, \mathbf{B} \in \mathbb{R}^{p\times n}$;
  $\mathbf{A}(\mathbf{B}+\mathbf{C}) = \mathbf{AB} + \mathbf{AC}$ with $\mathbf{C} \in \mathbb{R}^{p\times n}$;
  $\mathbf{ABC} = \mathbf{A}(\mathbf{BC}) = (\mathbf{AB})\mathbf{C}$ with $\mathbf{C} \in \mathbb{R}^{n\times r}$.

A matrix $\mathbf{A} \in \mathbb{R}^{n\times m}$ is square if it contains equal number of rows and columns, *i.e.* $m = n$. A square matrix is symmetric if $\mathbf{A} = \mathbf{A}^\top$, skew-symmetric if $\mathbf{A} = -\mathbf{A}^\top$ and an important property of skew-symmetric matrices is that

$$\mathbf{x}^\top\mathbf{Ax} = 0, \ \forall \mathbf{x} \in \mathbb{R}^n. \tag{A.9}$$

A square matrix $\mathbf{A} \in \mathbb{R}^{n\times n}$ is diagonal if $a_{ij} = 0$ for all $i \neq j$, denoted $\mathbf{A}$= diag$\{a_{11}, \ a_{22}, \ \ldots, \ a_{nn}\}$. A square matrix $\mathbf{A} \in \mathbb{R}^{n\times n}$ is singular if its determinant is zero, that is, one or more of the eigenvalues are zero –*cf.* (Edwards and Penney, 1988) for more on determinants and eigenvalues. A matrix $\mathbf{A}$ is said to be Hurwitz if all eigenvalues of $\mathbf{A}$ satisfy $\mathrm{Re}(\lambda_i) < 0$. A square matrix $\mathbf{A} \in \mathbb{R}^{n\times n}$ is said to be positive definite if

$$\mathbf{x}^\top\mathbf{Ax} > 0, \ \forall \mathbf{x} \in \mathbb{R}^n, \ \mathbf{x} \neq \mathbf{0}. \tag{A.10}$$

A square matrix $\mathbf{A} \in \mathbb{R}^{n\times n}$ is said to be positive semi-definite if

$$\mathbf{x}^\top\mathbf{Ax} \geq 0, \ \forall \mathbf{x} \in \mathbb{R}^n. \tag{A.11}$$

A square matrix $\mathbf{A} \in \mathbb{R}^{n\times n}$ is said to be negative definite if $-\mathbf{A}$ is positive definite and negative semi-definite if $-\mathbf{A}$ is positive semi-definite.

The the induced $\mathcal{L}_2$-norm of a matrix $\mathbf{A} \in \mathbb{R}^{n\times m}$ also sometimes called the spectral norm is defined as

$$\|\mathbf{A}\| = \sqrt{\lambda_{max}(\mathbf{A}^\top\mathbf{A})} \tag{A.12}$$

where $\lambda_{min}(\mathbf{Q})$ and $\lambda_{max}(\mathbf{Q})$ denotes the minimum and maximum eigenvalue of a matrix $\mathbf{Q}$, respectively. The spectral norm satisfy the following axioms and properties

- $\|\mathbf{A}\| = 0$ if and only if $\mathbf{A} = \mathbf{0} \in \mathbb{R}^{n\times m}$;

- $\|\mathbf{A}\| > 0$ for all $\mathbf{A} \in \mathbb{R}^{n\times m}$ where $\mathbf{A} \neq \mathbf{0} \in \mathbb{R}^{n\times m}$;
- $\|\mathbf{A}+\mathbf{B}\| \leq \|\mathbf{A}\| + \|\mathbf{B}\|$ for all $\mathbf{A}, \mathbf{B} \in \mathbb{R}^{n\times m}$;
- $\|\alpha\mathbf{A}\| = |\alpha|\|\mathbf{A}\|$ for all $\alpha \in \mathbb{R}$ and $\mathbf{A} \in \mathbb{R}^{n\times m}$;
- $\|\mathbf{A}^\top\mathbf{B}\| \leq \|\mathbf{A}\|\|\mathbf{B}\|$ for all $\mathbf{A}, \mathbf{B} \in \mathbb{R}^{n\times m}$.

For a matrix $\mathbf{A} \in \mathbb{R}^{m\times n}$ and a vector $\mathbf{x} \in \mathbb{R}^n$, the vector norm satisfies

$$\|\mathbf{A}\mathbf{x}\| \leq \|\mathbf{A}\|\|\mathbf{x}\|, \ \forall \mathbf{A} \in \mathbb{R}^{m\times n}, \mathbf{x} \in \mathbb{R}^n, \tag{A.13}$$

and moreover, for a vector $\mathbf{y} \in \mathbb{R}^n$, the absolute value satisfies

$$|\mathbf{y}^\top\mathbf{A}\mathbf{x}| \leq \|\mathbf{A}\|\|\mathbf{y}\|\|\mathbf{x}\|. \tag{A.14}$$

The pseudo inverse $\mathbf{A}^\dagger$ of a matrix $\mathbf{A} \in \mathbb{R}^{m\times n}$ is the unique matrix satisfying the following criteria

- $\mathbf{A}\mathbf{A}^\dagger\mathbf{A} = \mathbf{A}$;
- $\mathbf{A}^\dagger\mathbf{A}\mathbf{A}^\dagger = \mathbf{A}^\dagger$;
- $(\mathbf{A}\mathbf{A}^\dagger)^H = \mathbf{A}\mathbf{A}^\dagger$;
- $(\mathbf{A}^\dagger\mathbf{A})^H = \mathbf{A}^\dagger\mathbf{A}$;

where $(\cdot)^H$ denotes a *Hermitian* matrix (Kreyzig, 1993), leading to

$$\mathbf{A}^\dagger = (\mathbf{A}^T\mathbf{A})^{-1}\mathbf{A}^T \ \text{ and } \ \mathbf{A}^\dagger = \mathbf{A}^T(\mathbf{A}\mathbf{A}^T)^{-1}. \tag{A.15}$$

The inverse matrix does not exist if the product $\mathbf{A}\mathbf{A}^T$ or $\mathbf{A}^T\mathbf{A}$ has a zero determinant, which is not invertible.

Now we introduce some basic functional concepts which is widely used in the context of stability analysis. The system considered is

$$\dot{\mathbf{x}} = f(t, \mathbf{x}), \ \mathbf{x}(t_0) = \mathbf{x}_0. \tag{A.16}$$

A function $f : \mathbb{R}^n \to \mathbb{R}^m$ is said to be continuous at a point $\mathbf{x}$ if, given any $\epsilon > 0$, there is $\delta > 0$ such that

$$\|\mathbf{x} - \mathbf{y}\| < \delta \Rightarrow \|f(\mathbf{x}) - f(\mathbf{y})\| < \epsilon. \tag{A.17}$$

A function is uniformly continuous if, given any $\epsilon > 0$ there is a $\delta(\epsilon) > 0$ such that (A.17) holds. Furthermore, a function f is said to be continuous on the set S if it is continuous at every point $\mathbf{x} \in S$. The function

$$(a_1 f_1 + a_2 f_2)(\cdot) = a_1 f_1(\cdot) + a_2 f_2(\cdot) \tag{A.18}$$

is continuous for any two scalars a_1 and a_2 and any two continuous functions f_1 and f_2. If the functions are defined for sets such that $f_1 : S_1 \to S_2$ and $f_2 : S_2 \to S_3$, then the composition of f_1 and f_2 can be written as

$$(f_2 \circ f_1)(\cdot) = f_2(f_1), \text{ where } f_2 \circ f_1 : S_1 \to S_3. \tag{A.19}$$

A function $u : I \to \mathbb{R}$ is said to be absolutely continuous on the interval $I \subset \mathbb{R}$ if for every $\epsilon > 0$ there exists $\delta > 0$ such that

$$\sum_{k=1}^{\ell} |u(b_k) - u(a_k)| \leq \epsilon \tag{A.20}$$

for every finite number of nonoverlapping intervals (a_k, b_k), $k = 1, \ldots, \ell$, with $[a_k, b_k] \subset I$ and

$$\sum_{k=1}^{\ell} (b_k - a_k) \leq \delta. \tag{A.21}$$

A function $u : I \to \mathbb{R}$ is locally absolutely continuous if it is absolutely continuous in $[a, b]$ for every interval $[a, b] \subset I$. The system (A.16) is said to satisfy the Lipschitz condition if

$$\|f(t, \mathbf{x}) - f(t, \mathbf{y})\| \leq L\|\mathbf{x} - \mathbf{y}\| \tag{A.22}$$

for all $(t, \mathbf{x})$ and $(t, \mathbf{y})$ in some neighborhood of $(t_0, \mathbf{x}_0)$ with $L > 0$. The Lipschitz condition guarantees a unique solution in $[t_0, t_0 + \delta]$ for some $\delta > 0$. If there exists a constant $L > 0$ which hold for all $\mathbf{x}, \mathbf{y} \in \mathbb{R}^n$, then we say that (A.16) is globally Lipschitz. A continuous function $V : \mathbb{R}^n \to \mathbb{R}$ is said to be radially unbounded if $V(\mathbf{x}) \to \infty$ as $\|\mathbf{x}\| \to \infty$. A continuous function $V : [0, \infty) \times \mathbb{R}^n \to \mathbb{R}$ is said to be decrescent if there exists a positive definite function $W : \mathbb{R}^n \to \mathbb{R}$ such that $V(t, \mathbf{x}) \leq W(\mathbf{x}),\ \forall t \geq 0,\ \forall \mathbf{x} \in \mathbb{R}^n$.

A function $f : \mathbb{R} \to \mathbb{R}$ is said to be differentiable at x if the limit

$$f'(x) = \lim_{h \to 0} \frac{f(x + h) - f(x)}{h} \tag{A.23}$$

exist. A function $f : \mathbb{R}^n \to \mathbb{R}^m$ is said to be continuously differentiable at a point $\mathbf{x}^\star$ if the partial derivatives $\partial f / \partial x_i$ exist and are continuous at $\mathbf{x}^\star$ for $1 \leq i \geq m$, $1 \leq j \leq n$. A function f is continuously differentiable in a set S if it is continuously differentiable at every point in S.

A continuous function $\alpha : [0, a) \to [0, \infty)$ is said to belong to class $\mathcal{K}$ if it is strictly increasing and $\alpha(0) = 0$. A continuous function $\alpha : [0, \infty) \to [0, \infty)$ is said to belong to class $\mathcal{K}_\infty$ it is is strictly increasing and $\alpha(0) = 0$ and $\alpha(r) \to \infty$ as $r \to \infty$. A continuous function $\beta : [0, a) \times [0, \infty) \to [0, \infty)$ is said to belong to class $\mathcal{KL}$ if, for each fixed s, the mapping $\beta(r, s)$ belongs to class $\mathcal{K}$ with respect to r and, for each fixed r, the mapping $\beta(r, s)$ is decreasing with respect to s and $\beta(r, s) \to 0$ as $s \to \infty$. A constant vector $\mathbf{x}^\star \in \mathbb{R}^n$ is an equilibrium point of the system (A.16) if $f(t, \mathbf{x}^\star)) = \mathbf{0},\ \forall t \geq t_0$, and it follows that $\dot{\mathbf{x}}(t) = 0$. An equilibrium is usually located at the origin, if not, without loss of generality it can be shifted to the origin via a change of variables.

A.2 Lyapunov stability

When we speak of stability we mean stability in sense of Lyapunov, in particular the so-called second method of Lyapunov. Since the topics in this thesis mainly concern non-autonomous systems, that is, the solution of the differential equation (A.16) is dependent on both t and t_0, we state uniform stability results with respect to time. We assume that $f(t, \mathbf{x}) : \mathbb{R}_{\geq 0} \times \mathbb{R}^n \to \mathbb{R}^n$ is locally Lipschitz in $\mathbf{x}$, uniformly in t, continuous in both arguments, and the origin is an equilibrium point of (A.16).

A smooth function $V : \mathbb{R}^n \to \mathbb{R}$ is said to be *proper* if, for any $c \in \mathbb{R}$, the set $V^{-1}([0, c]) = \{\mathbf{x} \in \mathbb{R}^n : 0 \leq V(\mathbf{x}) \leq c\}$ is compact. A continuous and differentiable function $V : \mathbb{R}_{\geq 0} \times \mathbb{R}^n \to \mathbb{R}_{\geq 0}$ is said to be a Lyapunov function candidate for the equilibrium $\mathbf{x} = \mathbf{0} \in \mathbb{R}^n$ of (A.16) if

- $V(t, \mathbf{x})$ is locally positive definite;
- $\frac{\partial V(t,\mathbf{x})}{\partial t}$ is continuous with respect to t and $\mathbf{x}$;
- $\frac{\partial V(t,\mathbf{x})}{\partial \mathbf{x}}$ is continuous with respect to t and $\mathbf{x}$.

A Lyapunov function candidate for (A.16) is a Lyapunov function for (A.16) if its total time derivative along the trajectories of (A.16) satisfies $\dot{V}(t, \mathbf{x}) \leq 0$, $\forall t \geq 0$ and for small $\|\mathbf{x}\|$.

We now state the basic definitions of uniform stability.

Definition A.1 (Khalil (2002)) *The equilibrium point $\mathbf{x} = \mathbf{0}$ of (A.16) is*

- *stable if, for each $\epsilon > 0$, there is $\delta = \delta(\epsilon, t_0) > 0$ such that*

$$\|\mathbf{x}(t_0)\| < \delta \Rightarrow \|\mathbf{x}(t)\| < \epsilon, \ \forall t \geq t_0 \geq 0; \tag{A.24}$$

- *uniformly stable if, for each $\epsilon > 0$, there is $\delta = \delta(\epsilon) > 0$, independent of t_0, such that (A.24) is satisfied;*
- *unstable if not stable;*
- *asymptotically stable if it is stable and there is a positive constant $c = c(t_0)$ such that $x(t) \to 0$ as $t \to \infty$, for all $\|\mathbf{x}(t_0)\| < c$;*
- *uniformly asymptotically stable if it is uniformly stable and there is a positive constant c, independent of t_0, such that for all $\|\mathbf{x}(t_0)\| < c$, $\mathbf{x}(t) \to 0$ as $t \to \infty$, uniformly in t_0, that is, for each $\eta > 0$, there is $T = t(\eta) > 0$ such that*

$$\|\mathbf{x}(t)\| < \eta, \ \forall t \geq t_0 + T(\eta), \ \forall \|\mathbf{x}(t_0)\| < c; \tag{A.25}$$

- *uniformly globally asymptotically stable if it is uniformly stable, $\delta(\epsilon)$ can be chosen to satisfy $\lim_{\epsilon \to \infty} \delta(\epsilon) = \infty$, and, for each pair of positive numbers η and c, there is $T = T(\eta, c) > 0$ such that*

$$\|\mathbf{x}(t)\| < \eta, \ \forall t \geq t_0 + T(\eta, c), \ \|x(t_0)\| < c. \tag{A.26}$$

Definition (A.1) can also be expressed based on class $\mathcal{K}$ and $\mathcal{KL}$ functions.

Lemma A.1 (Khalil (2002)) *The equilibrium point* $\mathbf{x} = \mathbf{0}$ *of* (A.16) *is*

- *uniformly stable if and only if there exist a class* $\mathcal{K}$ *function* α *and a positive constant* c*, independent of* t_0*, such that*

$$\|\mathbf{x}(t)\| \leq \alpha(\|\mathbf{x}(t_0)\|), \ \forall t \geq t_0 \geq 0, \ \forall \|\mathbf{x}(t_0)\| < c; \tag{A.27}$$

- *uniformly asymptotically stable if and only if there exist a class* $\mathcal{KL}$ *function* β *and a positive constant* c*, independent of* t_0*, such that*

$$\|\mathbf{x}(t)\| \leq \beta(\|\mathbf{x}(t_0)\|, t - t_0), \ \forall t \geq t_0 \geq 0, \ \forall \|\mathbf{x}(t_0)\| < c; \tag{A.28}$$

- *uniformly globally asymptotically stable if and only if inequality* (A.28) *is satisfied for any initial state* $\mathbf{x}(t_0)$*.*

A special case of uniform asymptotic stability is when the class $\mathcal{KL}$ function in (A.28) is on exponential form. Then we have the following definition.

Definition A.2 (Khalil (2002)) *The equilibrium point* $\mathbf{x} = \mathbf{0}$ *of* (A.16) *is exponentially stable if there exist positive constant,* c*,* k*, and* λ *such that*

$$\|\mathbf{x}(t)\| \leq k\|\mathbf{x}(t_0)\|e^{-\lambda(t-t_0)}, \ \forall \|\mathbf{x}(t_0)\| < c \tag{A.29}$$

and globally exponentially stable if (A.29) *is satisfied for any initial state* $\mathbf{x}(t_0)$*.*

We now proceed with stating Lyapunv's stability theorems for the stability properties defined.

Theorem A.1 (Khalil (2002)) *Let* $\mathbf{x} = \mathbf{0}$ *be an equilibrium point for* (A.16) *and* $D \subset \mathbb{R}^n$ *be a domain containing* $\mathbf{x} = \mathbf{0}$*. Let* $V : [0, \infty) \times D \to \mathbb{R}$ *be a continuously differentiable function such that*

$$W_1(\mathbf{x}) \leq V(t, \mathbf{x}) \leq W_2(\mathbf{x}) \tag{A.30}$$

$$\frac{\partial V}{\partial t} + \frac{\partial V}{\partial \mathbf{x}} f(t, \mathbf{x}) \leq 0 \tag{A.31}$$

$\forall t \geq 0$ *and* $\forall \mathbf{x} \in D$*, where* $W_1(\mathbf{x})$ *and* $W_2(\mathbf{x})$ *are continuous positive definite functions on* D*. Then,* $\mathbf{x} = \mathbf{0}$ *is uniformly stable.*

Theorem A.2 (Khalil (2002)) *Suppose the assumptions of Theorem A.1 are satisfied with inequality* (A.31) *strengthened to*

$$\frac{\partial V}{\partial t} + \frac{\partial V}{\partial \mathbf{x}} f(t, \mathbf{x}) \leq -W_3(\mathbf{x}) \tag{A.32}$$

$\forall t \geq 0$ *and* $\forall \mathbf{x} \in D$*, where* $W_3(\mathbf{x})$ *is a continuous positive definite function on* D*. Then,* $\mathbf{x} = \mathbf{0}$ *is uniformly asymptotically stable. Moreover, if* r *and* c *are chosen such that* $\mathcal{B}_r = \{\mathbf{x} \in \mathbb{R}^n : \|\mathbf{x}\| < r\} \subset D$ *and* $c < \min_{\|\mathbf{x}\|=r} W_1(\mathbf{x})$*, then every trajectory starting in* $\{\mathbf{x} \in \mathcal{B}_r : W_2(\mathbf{x}) \leq c\}$ *satisfies*

$$\|\mathbf{x}(t)\| \leq \beta(\|\mathbf{x}(t_0)\|, t - t_0), \ \forall t \geq t_0 \geq 0 \tag{A.33}$$

for some class $\mathcal{KL}$ *function* β*. Finally, if* $D = \mathbb{R}^n$ *and* $W_1(\mathbf{x})$ *is radially unbounded, then* $\mathbf{x} = \mathbf{0}$ *is uniformly globally asymptotically stable.*

A similar theorem is also given for exponential stability.

Theorem A.3 (Khalil (2002)) *Let $\mathbf{x} = \mathbf{0}$ be an equilibrium point of* (A.16) *and $D \subset \mathbb{R}^n$ be a domain containing $\mathbf{x} = \mathbf{0}$. Let $V : [0, \infty) \times D \to \mathbb{R}$ be a continuously differentiable function such that*

$$k_1\|\mathbf{x}\|^a \leq V(t,x) \leq k_2\|\mathbf{x}\|^a \tag{A.34}$$

$$\frac{\partial V}{\partial t} + \frac{\partial V}{\partial \mathbf{x}} f(t,\mathbf{x}) \leq -k_3\|\mathbf{x}\|^a \tag{A.35}$$

$\forall t \geq 0$ and $\forall \mathbf{x} \in D$, where k_1, k_2, k_3 and a are positive constants. Then, $\mathbf{x} = \mathbf{0}$ is uniformly exponentially stable. If the assumptions hold globally, then $\mathbf{x} = \mathbf{0}$ is uniformly globally exponentially stable.

Furthermore, we make use of what is called Matrosov's theorem –*cf.* (Matrosov, 1962; Hahn, 1967; Rouch and Mawhin, 1980) which can be seen as an extension of the so called LaSalle's invariance principle for non-autonomous systems, stated as

Theorem A.4 (Matrosov, (Rouch and Mawhin, 1980)) *Suppose there exist three functions*

$$V : \mathcal{I} \times \mathcal{B}_\rho \to \mathbb{R}, (t,\mathbf{x}) \to V(t,\mathbf{x}); \tag{A.36}$$

$$W : \mathcal{I} \times \mathcal{B}_\rho \to \mathbb{R}, (t,\mathbf{x}) \to W(t,\mathbf{x}); \tag{A.37}$$

$$V^\star : \mathcal{B}_\rho \to \mathbb{R}, \mathbf{x} \to V^\star(\mathbf{x}), \tag{A.38}$$

where $\mathcal{I} = (\tau, \infty)$, where τ might equal $-\infty$, which are continuous along with $\dot{V}$ and $\dot{W}$ such that $V(t,0) \equiv \dot{V}(t,0) \equiv 0$ and suppose there exists ϵ, $0 < \epsilon < \rho$, such that

1. *$\|f(t,\mathbf{x})\| \leq A$ for $(t,\mathbf{x}) \in \mathcal{I} \times \bar{\mathcal{B}}_\epsilon$;*
2. *V is positive definite on $\mathcal{I} \times \bar{\mathcal{B}}_\epsilon$ with $V(t,\mathbf{x}) \to 0$ uniformly in t as $\mathbf{x} \to 0$;*
3. *$\dot{V}(t,\mathbf{x}) \leq V^\star(\mathbf{x}) \leq 0$ for $(t,\mathbf{x}) \in \mathcal{I} \times \bar{\mathcal{B}}_\epsilon$;*
4. *there exists an $L > 0$ such that $\|W(t,\mathbf{x})\| \leq L$ for $(t,\mathbf{x}) \in \mathcal{I} \times \bar{\mathcal{B}}_\epsilon$;*
5. *$\dot{W}(t,\mathbf{x})$ is non-zero definite on $E = \{\mathbf{x} \in \bar{\mathcal{B}}_\epsilon : V^\star(\mathbf{x}) = 0\}$.*

Then every solution such that $\mathbf{x}(t,t_0,x_0) \in \mathcal{B}_\epsilon$ for $t \geq t_0$ tend to 0 when $t \to +\infty$.

We say that a continuous function $W : \bar{\mathcal{B}}_\sigma \to \mathbb{R}, \mathbf{x} \to W(\mathbf{x})$ is non-zero definite on a set $E \subset \bar{\mathcal{B}}_\sigma$ if and only if $W(\mathbf{x}) \neq 0$ for all $\mathbf{x} \in \bar{E} \backslash \{0\}$. Note that the hypothesis of Theorem A.4 suffice to assure uniform asymptotic stability of the origin. The theorem is restated in (Paden and Panja, 1988) where they show that condition (5) of the theorem is satisfied if

1. $\dot{W}(t,\mathbf{x})$ is continuous in both arguments and depends on time in the following way. $\dot{W}(t,\mathbf{x}) = g(\beta(t),\mathbf{x})$ where g is continuous in both of its arguments. $\beta(t)$ is also continuous and its image lies in a bounded set K_1. (For simplicity, we simply say that $\dot{W}(t,\mathbf{x})$ depends on time continuously through a bounded function.)

2. There exists a class $\mathcal{K}$ function, k, such that $\|\dot{W}(t,\mathbf{x})\| \geq k(\|\mathbf{x}\|),\ \forall \mathbf{x} \in E$ and $t \geq t_0$.

Another type of stability property utilized in this thesis is what is called "in the large" which shouldn't be mixed up with "local" stability. Local stability means stability of the origin for initial values starting arbitrarily close to the origin while in the large means stability of the origin for initial conditions starting from a given set. A more formal definition is as follows.

Definition A.3 (Asymptotic stability in the large) *Let $\Gamma \subset \mathbb{R}^n$ be given. The trivial solution $x = 0$ of $\dot{x} = f(t,x)$ is called* asymptotically stable in the large *with respect to Γ if it is stable in the sense of Lyapunov and every other solution $x(t,t_\circ,x_\circ) \to 0$ as $t \to \infty$ for any initial states $x_\circ \in \Gamma$ and for any initial times $t_\circ \in \mathbb{R}_{\geq 0}$. The origin is uniformly asymptotically stable if it is uniformly stable and convergence is uniform in the initial times and in compact sets of the initial states.*

Remark A.1 *The previous definition is paraphrased from (Furasov, 1977, p. 29). Although the property previously defined is not unusual the terminology "in the large" has sometimes been used wrongly, as synonymous of "global" for instance, by J. L. Lasalle. However, it must be recognized that the property described in Definition A.3 does not correspond neither to (local) asymptotic stability where the mere existence of Γ is invoked*[1]*, nor to global asymptotic stability in which case $x_\circ \in \mathbb{R}^n$ –cf. Hahn (1963).*

A.2.1 Almost global stability

Stability for *all* initial states in $\mathbb{R}^n$ except for a set of measure zero is called *almost* global asymptotic stability –see (Rantzer, 2001). The concept of Almost Global Stability (AGS) is defined as follows

Theorem A.5 (Almost Global Stability, (Rantzer, 2001)) *Given the equation $\dot{x} = f(x(t))$, where $f \in \mathbb{C}^1(\mathbb{R}^n,\mathbb{R}^n)$ and $f(0) = 0$, suppose there exists a non-negative $\rho \in \mathbb{C}^1(\mathbb{R}^n\backslash\{0\},\mathbb{R})$ such that $\rho(x)f(x)\backslash|x|$ is integrable on $\{x \in \mathbb{R}^n : |x| \geq 1\}$ and*

$$[\nabla \cdot (f\rho)](x) > 0 \text{ for almost all } x. \tag{A.39}$$

Then, for almost all initial states $x(0)$ the trajectory $x(t)$ exists for $t \in [0,\infty)$ and tents to zero as $t \to \infty$. Moreover, if the equilibrium $x = 0$ is stable, then the conclusion remains valid even if ρ takes negative values.

The function $\rho(x)$ is called a density function which can be derived from a Lyapunov function V according to the following proposition.

[1] More precisely, in this case Γ corresponds to an arbitrarily small neighborhood of the origin.

Proposition A.1 (Rantzer (2001)) *Let $V(x) > 0$ for $x \neq 0$ and $\nabla V \cdot f < \alpha^{-1}(\nabla \cdot f)V$ for almost all x for some $\alpha > 0$. The $\rho(x) = V(x)^{-\alpha}$ satisfies the condition* (A.39).

To put the concept of almost global stability into the framework of asymptotic stability we make use of the following definition

Definition A.4 (Asymptotic stability, almost in the large) *Let $\Gamma \subset \mathbb{R}^n$ be given. The solution x^* of $\dot{x} = f(t,x)$ is called* asymptotically stable, almost in the large *if it is stable in the sense of Lyapunov and every other solution $x(t, t_\circ, x_\circ) \to x^*$ as $t \to \infty$ for any initial states $x_\circ \in \Gamma$ except for a zero-measure subset of Γ and for any initial times $t_\circ \in \mathbb{R}_{\geq 0}$. The equilibrium point is uniformly asymptotically stable, almost in the large if both stability and convergence are uniform in the initial conditions.*

A refinement of the main theorem in (Rantzer, 2001) for non-autonomous systems is given as follows

Theorem A.6 (Monzón (2006)) *Consider the system $\dot{x} = f(t,x)$ such that $f(t,0) = 0$ for all t and 0 is a locally stable equilibrium point. Let $\rho : \mathbb{R}^n \backslash \{0\} \to \mathbb{R}_{\geq 0}$ be once continuously differentiable and satisfy*

$$\frac{\partial}{\partial t}\rho(t,x) + [\nabla \cdot (f\rho)](t,x) > 0 \quad \forall t \geq 0,\ a.a.\ x \in \mathbb{R}^n\,.$$

Moreover, assume that $\rho(t,x)$ is integrable uniformly in t over $\{\|x\| > \varepsilon\}$ for every $\varepsilon > 0$. Then, for every initial time $t_\circ$ the set of points that are not asymptotically attracted by the origin has zero Lebesgue measure.

Remark A.2 *Stability is an assumption of Theorem A.6 hence, an implicit statement which follows directly from its conclusion is that the origin is almost globally asymptotically stable, in the sense defined in (Rantzer, 2001).*

A.2.2 Practical and semi-global stability

The need for more refined stability results based on practical systems was early identified and practical stability was suggested by LaSalle and Lefschetz (1961). The basic idea is that a practical system will be considered stable if the deviations of the motions from an equilibrium remain within certain bounds determined by the physical situation. A perturbed version of (A.16) can typically be expressed as

$$\dot{\mathbf{x}} = f(t,\mathbf{x}) + g(t,\mathbf{x}). \tag{A.40}$$

and the stability properties of the equilibrium point (A.16) are assumed to be known. A definition of practical stability was given by Hahn (1967) as follows:

Definition A.5 *The equilibrium point of* (A.16) *is called practically stable if there exist two constants k_1, k_2 with the following property: if $\|\mathbf{x}_0\| < k_1$ and if the function $g(t,\mathbf{x})$ in* (A.40) *satisfies an inequality*

$$\|g(t,\mathbf{x})\| < k_2,\ \mathbf{x} \in \mathbb{R}^n,\ t \geq t_0, \tag{A.41}$$

then the general solution of (A.40) *admits an estimate*

$$\|\mathbf{x}(t, x_0, t_0)\| < k_3 \tag{A.42}$$

where the constant k_3 *depends on the particular physical situation.*

Typically the residual caused by *e.g.* external perturbations can be diminished by tuning of some parameters. For more formal definitions we need to establish the following definition

Definition A.6 (Carathéodory conditions) *Let* $G \subset \mathbb{R}^n$ *be an open set and* $\mathcal{I} = [a, b] \subset \mathbb{R}$, $a < b$. *One say that* $f : \mathcal{I} \times G \to \mathbb{R}^m$ *satisfies the Carathéodory conditions on* $\mathcal{I} \times G$ *if*

1. $f(\cdot, \mathbf{x}) : \mathcal{I} \to \mathbb{R}^m$ *is measurable for every* $\mathbf{x} \in G$;
2. $f(t, \cdot) : G \to \mathbb{R}^m$ *is continuous for almost every* $t \in \mathcal{I}$;
3. *for each compact set* $K \subset G$ *the function*

$$h_K(t) = \sup\{\|f(t, \mathbf{x})\| : x \in K\} \tag{A.43}$$

is Lebesgue integrable on $\mathcal{I}$.

Semi-global and practical stability properties can now be described by introducing parameterized nonlinear time-varying systems on the form

$$\dot{\mathbf{x}} = f(t, \mathbf{x}, \boldsymbol{\theta}), \tag{A.44}$$

where $\mathbf{x} \in \mathbb{R}^n$, $t \in \mathbb{R}_{\geq 0}$ and $\boldsymbol{\theta} \in \mathbb{R}^m$ is a constant parameter, and $f : \mathbb{R}_{\geq 0} \times \mathbb{R}^n \times \mathbb{R}^m \to \mathbb{R}^n$ is locally Lipschitz in $\mathbf{x}$ and satisfies Carathéodory conditions for any parameter $\boldsymbol{\theta}$ under consideration.

Definition A.7 (UGPAS, (Chaillet, 2006)) *Let* $\Theta \subset \mathbb{R}^m$ *be a set of parameters. The system* (A.44) *is said to be uniformly globally practically asymptotically stable on* Θ *if, given any* $\delta > 0$, *there exists* $\theta^\star(\delta) \in \Theta$ *such that the ball* $\mathcal{B}_\delta$ *is uniformly globally asymptotically stable for the system* $\dot{x} = f(t, x, \theta^\star)$.

Definition A.8 (USPAS, (Chaillet, 2006)) *Let* $\Theta \subset \mathbb{R}^m$ *be a set of parameters. The system* (A.44) *is said to be uniformly semi-globally practically asymptotically stable on* Θ *if, given any* $\Delta > \delta > 0$, *there exists* $\theta^\star(\delta, \Delta) \in \Theta$ *such that the ball* $\mathcal{B}_\delta$ *is uniformly asymptotically stable on* $\mathcal{B}_\Delta$ *for the system* $\dot{x} = f(t, x, \theta^\star)$.

Definition A.9 *Let* $\Theta \subset \mathbb{R}^m$ *be a set of parameters. The system* $\dot{x} = f(t, x, \theta)$, *where* $x \in \mathbb{R}^n$, $t \geq 0$, $\theta \in \mathbb{R}^m$ *is a constant parameter and* $f(t, x, \theta)$ *is locally Lipschitz in* x *and piecewise continuous in* t *for all* $\theta \in \mathbb{R}^m$, *is said to be uniformly practically asymptotically stable if given any* $\Delta > \delta > 0$, *there exists* $\theta^\star(\delta, \Delta) \in \Theta$ *such that* $\mathcal{B}_\delta$ *is uniformly asymptotically stable on* $\mathcal{B}_\Delta$ *for the system*[2] $\dot{x} = f(t, x, \theta^\star)$.

[2]The set $\mathcal{B}_\delta$ is uniformly asymptotically stable on $\mathcal{B}_\Delta$ if there exists a number Δ and a class $\mathcal{KL}$ function β such that $\|x(t_0)\|_\delta < \Delta$, $t_0 \in \mathbb{R}_{>0} \implies \|x(t)\|_\delta \leq \beta(\|x(t_0)\|_\delta, t - t_0)$, where $\|x\|_\delta := \inf_{z \in \mathcal{B}_\delta} \|x - z\|$.

Remark A.3 *The property above implies but is not implied by ultimate boundedness. The definition is adapted from Chaillet and Loría (2008) –we removed the qualifier "semiglobal" which pertains to systems evolving in $\mathbb{R}^n$. However, note that the parameter θ depends on the residual set $\mathcal{B}_\delta$ and the estimate of the domain of attraction $\mathcal{B}_\Delta$. In the context of this thesis θ corresponds to design parameters.*

For exponential systems similar definitions are given as follows:

Definition A.10 (UGPES, (Grøtli, 2010)) *Let $\Theta \subset \mathbb{R}^m$ be a set of parameters. The system* (A.44) *is said to be uniformly globally practically exponentially stable on Θ if, given any $\delta > 0$, there exists a parameter $\theta^\star(\delta) \in \Theta$, and positive constants $k(\delta)$ and $\gamma(\delta)$ such that, for any $x_0 \in \mathbb{R}^n$ and any $t_0 \in \mathbb{R}_{\geq 0}$ the solution of* (A.44) *satisfies, for all $t \geq t_0$,*

$$\|x(t, t_0, x_0, \theta^\star)\| \leq \delta + k(\delta)\|x_0\|e^{-\gamma(\delta)(t-t_0)}. \tag{A.45}$$

Definition A.11 (UPES, (Grøtli, 2010)) *Let $\Theta \subset \mathbb{R}^m$ be a set of parameters. The system* (A.44) *is said to be uniformly (locally) practically exponentially stable on Θ if there exists $\Delta > 0$, and given any $\delta > 0$, there exists a parameter $\theta^\star(\delta, \Delta) \in \Theta$ and positive constants $k(\delta, \Delta)$ and $\gamma(\delta, \Delta)$ such that, for any $\mathbf{x}_0 \in \bar{\mathcal{B}}_\Delta$ and any $t_0 \in \mathbb{R}_{\geq 0}$ the solution of* (A.44) *satisfies, for all $t \geq t_0$,*

$$\|\mathbf{x}(t, t_0, \mathbf{x}_0, \theta^\star)\| \leq \delta + k(\delta, \Delta)\|\mathbf{x}_0\|e^{-\gamma(\delta,\Delta)(t-t_0)}. \tag{A.46}$$

In the above definitions θ can be seen as the tuning parameters such as gains, while Θ can be seen as the set of available parameters which could be limited by physical constraints such as actuator saturation and quantization. The parameter Δ can be seen as an estimate of the region of attraction, while δ represents the ball to where solutions converge. It is therefore favorable to have a large Δ while keeping δ as small as possible to decrease steady-state errors. A related popular concept for instance in control of mechanical systems, is that of ultimate boundedness –*cf.* (Khalil, 2002). However, practical asymptotic stability is stronger than ultimate boundedness since the latter is only a notion of convergence and does not imply stability in the sense of Lyapunov. In other words, the fact that the errors converge to a bounded region does not imply that they remain always arbitrarily close to it.

We now move further by giving Lyapunov sufficient conditions for Definitions (A.7)–(A.11).

Theorem A.7 (Lyapunov sufficient condition for UGPAS, (Chaillet, 2006)) *Let Θ be a subset of $\mathbb{R}^m$ and suppose that, given any $\delta > 0$, there exist a parameter $\theta^\star(\delta) \in \Theta$, a continuously differentiable Lyapunov function $V_\delta : \mathbb{R}_{\geq 0} \times \mathbb{R}^n \to \mathbb{R}_{\geq 0}$ and class $\mathcal{K}_\infty$ functions $\underline{\alpha}_\delta$, $\overline{\alpha}_\delta$, α_δ such that, for all $\mathbf{x} \in \mathbb{R}^n \backslash \bar{\mathcal{B}}_\delta$ and all $t \in \mathbb{R}_{\geq 0}$,*

$$\underline{\alpha}_\delta(\|\mathbf{x}\|) \leq V_\delta(t, \mathbf{x}) \leq \overline{\alpha}_\delta(\|\mathbf{x}\|) \tag{A.47}$$

$$\frac{\partial V_\delta}{\partial t}(t, \mathbf{x}) + \frac{\partial V_\delta}{\partial \mathbf{x}}(t, \mathbf{x}) f(t, \mathbf{x}, \theta^\star) \leq -\alpha_\delta(\|\mathbf{x}\|) \tag{A.48}$$

$$\lim_{\delta \to 0} \underline{\alpha}_\delta^{-1} \circ \overline{\alpha}_\delta(\delta) = 0. \tag{A.49}$$

Then the system $\dot{\mathbf{x}} = f(t, \mathbf{x}, \theta)$ introduced in (A.44) *is UGPAS on the parameter set Θ.*

Theorem A.8 (Lyapunov sufficient condition for USPAS, (Chaillet, 2006)) *Suppose that, given any $\Delta > \delta > 0$, there exist a parameter $\theta^\star(\delta, \Delta) \in \Theta$, a continuously differentiable Lyapunov function $V_{\delta,\Delta} : \mathbb{R}_{\geq 0} \times \mathbb{R}^n \to \mathbb{R}_{\geq 0}$, and class $\mathcal{K}_\infty$ functions $\underline{\alpha}_{\delta,\Delta}$, $\overline{\alpha}_{\delta,\Delta}$, $\alpha_{\delta,\Delta}$ such that, for all $\mathbf{x} \in \mathcal{H}(\delta, \Delta)$ and all $t \in \mathbb{R}_{\geq 0}$,*

$$\frac{\partial V_{\delta,\Delta}}{\partial t}(t, \mathbf{x}) + \frac{\partial V_{\delta,\Delta}}{\partial \mathbf{x}}(t, \mathbf{x}) f(t, \mathbf{x}, \theta^\star) \leq -\alpha_{\delta,\Delta}(\|\mathbf{x}\|). \tag{A.50}$$

Assume further that, for any $\Delta_\star > \delta_\star > 0$, there exist $\Delta > \delta > 0$ such that

$$\underline{\alpha}^{-1}_{\delta,\Delta} \circ \overline{\alpha}_{\delta,\Delta}(\delta) \leq \delta_\star \tag{A.51}$$

$$\overline{\alpha}^{-1}_{\delta,\Delta} \circ \underline{\alpha}_{\delta,\Delta}(\Delta) \geq \Delta_\star. \tag{A.52}$$

Then, the system $\dot{\mathbf{x}} = f(t, \mathbf{x}, \theta)$ introduced in (A.44) is USPAS on the parameter set Θ.

Theorem A.9 (Sufficient condition for UGPES, (Grøtli, 2010)) *Let Θ be a subset of $\mathbb{R}^m$ and suppose that, given any $\delta > 0$, there exist a parameter $\theta^\star(\delta) \in \Theta$, a continuously differentiable Lyapunov function $V_\delta : \mathbb{R}_{\geq 0} \times \mathbb{R}^n \to \mathbb{R}_{\geq 0}$ and positive constants $\kappa(\delta)$, $\underline{\kappa}(\delta)$, $\overline{\kappa}(\delta)$ such that, for all $x \in \mathbb{R}^n \backslash \bar{\mathcal{B}}_\delta$ and all $t \in \mathbb{R}_{\geq 0}$,*

$$\underline{\kappa}(\delta)\|x\|^p \leq V_\delta(t, x) \leq \overline{\kappa}(\delta)\|x\|^p, \tag{A.53}$$

$$\frac{\partial V_\delta}{\partial t}(t, x) + \frac{\partial V_\delta}{\partial x}(t, x) f(t, x, \theta^\star) \leq -\kappa(\delta)\|x\|^p, \tag{A.54}$$

where p denotes a positive constant. Then, under the condition that

$$\lim_{\delta \to 0} \frac{\overline{\kappa}(\delta)\delta^p}{\underline{\kappa}(\delta)} = 0, \tag{A.55}$$

the system $\dot{\mathbf{x}} = f(t, \mathbf{x}, \theta)$ introduced in (A.44) is UGPES on the parameter set Θ

Theorem A.10 (Sufficient condition for UPES, (Grøtli, 2010)) *Let Θ be a subset of $\mathbb{R}^m$ and suppose that, there exists $\Delta > 0$, and given any $\Delta > \delta > 0$, there exist a parameter $\theta^\star(\delta) \in \Theta$, a continuously differentiable Lyapunov function $V_\delta : \mathbb{R}_{\geq 0} \times \bar{\mathcal{B}}_{\geq 0} \to \mathbb{R}_{\geq 0}$ and positive constants $\kappa(\delta)$, $\underline{\kappa}(\delta)$, $\overline{\kappa}(\delta)$ such that, for all $\mathbf{x} \in \bar{\mathcal{B}}_\Delta \backslash \bar{\mathcal{B}}_\delta$ and all $t \in \mathbb{R}_{\geq 0}$,*

$$\underline{\kappa}(\delta)\|\mathbf{x}\|^p \leq V_\delta(t, \mathbf{x}) \leq \overline{\kappa}(\delta)\|\mathbf{x}\|^p \tag{A.56}$$

$$\frac{\partial V_\delta}{\partial t}(t, \mathbf{x}) + \frac{\partial V_\delta}{\partial \mathbf{x}} f(t, \mathbf{x}, \theta^\star) \leq -\kappa(\delta)\|\mathbf{x}\|^p, \tag{A.57}$$

where p denotes a positive constant. Then, under the condition that

$$\lim_{\delta \to 0} \frac{\overline{\kappa}(\delta)\delta^p}{\underline{\kappa}(\delta)} = 0, \tag{A.58}$$

the system $\dot{\mathbf{x}} = f(t, \mathbf{x}, \theta)$ introduced in (A.44) is UPES on the parameter set Θ.

A.3 Hybrid systems

A hybrid system is usually written on the form

$$\mathcal{H} = \begin{cases} \dot{x} \in F(x), & x \in C \\ x^+ \in G(x), & x \in D \end{cases} , \tag{A.59}$$

where $F : \mathbb{R}^n \to \mathbb{R}^n$ and $G : \mathbb{R}^n \to \mathbb{R}^n$ are set-valued mappings for the flow map and jump map respectively, while C and D are the flow set and jump set. A subset E of $\mathbb{R}_{\geq 0} \times \mathbb{N}$ is a hybrid time domain if it is the union of infinitely many intervals of the form $[t_j, t_{j+1}] \times \{j\}$, where $0 = t_0 \leq t_1 \leq t_2 \leq \ldots$, or of finitely many such intervals, with the last one possible of the form $[t_j, t_{j+1}] \times \{j\}, [t_j, t_{j+1}) \times \{j\}$, or $[t_j, \infty) \times \{j\}$. A hybrid arc is a function $x : \text{dom } x \to \mathbb{R}^n$, where dom x is a hybrid time domain and, for each fixed j, $t \to x(t, j)$ is a locally absolutely continuous function in on the interval $I_j\{t : (t, j) \in \text{dom } x\}$. The hybrid arc is a solution to the hybrid system $\mathcal{H} = (C, F, D, G)$ if $x(0, 0) \in C \cup D$ and the following conditions are satisfied.

- For each $j \in \mathbb{N}$ such that I_j has nonempty interior, $\dot{x}(t, j) \in F(x(t, j))$ for almost all $t \in I_j$, $x(t, j) \in C$ for all $t \in [\min I_j, \sup I_j)$.
- For each $(t, j) \in \text{dom } x$ such that $(t, j + 1) \in \text{dom } x$, $x(t, j + 1) \in G(x(t, j))$, $x(t, j) \in D$.

The solution x to a hybrid system is nontrivial if dom x contains at least one point different from $(0, 0)$; maximal if it cannot be extended; and complete if dom x is unbounded. Every complete solution is maximal. We assume that the system fulfills the basic assumptions [A1-A3] in Goebel *et al.* (2009) thus C and D are closed sets in $\mathbb{R}^n$, and $F(x)$ and $G(x)$ are continuous and locally bounded. A compact set $\mathcal{A}$ is stable for $\mathcal{H}$ if for each $\epsilon > 0$ there exists $\sigma > 0$ such that $\|x(0, 0)\|_{\mathcal{A}} \leq \sigma$ implies $\|x(t, j)\|_{\mathcal{A}} \leq \epsilon$ for all solutions x to $\mathcal{H}$ and all $(t, j) \in \text{dom } x$. A compact set is pre-attractive if there exists a neighborhood of $\mathcal{A}$ from which each solution is bounded and the complete solutions converge to $\mathcal{A}$, that is $\|x(t, j)\|_{\mathcal{A}} \to 0$ as $t + j \to \infty$, where $(t, j) \in \text{dom } x$. A compact set $\mathcal{A}$ is pre-asymptotically stable if it is stable and pre-attractive. For a pre-asymptotically stable compact set $\mathcal{A} \subset \mathbb{R}^n$, its basin of pre-attraction is the set of points in $\mathbb{R}^n$ from which each solution is bounded and the complete solutions converge to $\mathcal{A}$. Each point in $\mathbb{R}^n \backslash (C \cup D)$ belongs to the basin of pre-attraction since no solution starts at a point in $\mathbb{R}^n \backslash (C \cup D)$. If the basin of pre-attraction is $\mathbb{R}^n$ then the set $\mathcal{A}$ is globally pre-asymptotically stable. If all solutions that are starting in the basin of pre-attraction are complete, the set $\mathcal{A}$ is globally asymptotically stable.

A.4 Optimal control theory

To solve a continuous nonlinear optimal control problem, a set of known equations are solved based on the system model which can be written as

$$\dot{x} = f(x, u, t), \qquad t \geq t_0 , \tag{A.60}$$

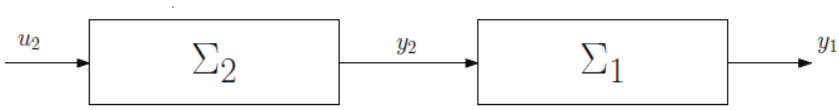

Figure A.1: Cascade interconnection of two dynamical systems.

and a performance index may be defined as

$$J(t_0) = \phi(x(T), T) + \int_{t_0}^{T} \mathcal{L}(x, u, t)dt \ . \tag{A.61}$$

A Hamiltonian is defined as

$$\mathcal{H}(x, u, t) = \mathcal{L}(x, u, t) + \lambda^\top f(x, u, t) \ , \tag{A.62}$$

while the costate equation is expressed as

$$-\dot{\lambda} = \frac{\partial \mathcal{H}}{\partial x} = \frac{\partial f^\top}{\partial x}\lambda + \frac{\partial \mathcal{L}}{\partial x} \ , \qquad t \leq T \tag{A.63}$$

and the stationary condition is defined as

$$0 = \frac{\partial \mathcal{H}}{\partial u} = \frac{\partial \mathcal{L}}{\partial u} + \frac{\partial f^\top}{\partial u}\lambda \ . \tag{A.64}$$

As most nonlinear problems are impossible to solve in an analytical way we usually have two options: either linearize the system model, or use a numerical algorithm. Both methods have pros and cons, a linearized problem is fast and easy to solve but will not perform well for highly nonlinear equations, while a numerical algorithm for a large set of equations usually requires a lot of computations to solve.

A.5 Cascaded systems theory

Cascaded-systems theory consists in analyzing complex systems by dividing them into sub-systems which are simpler to control and to analyze –see (Loría and Panteley, 2005) and references within. It must be emphasized that such representation is purely schematic, for the purpose of analysis only. Generally speaking the stability analysis problem consists in finding conditions for two systems as in Figure A.1 so that, considering that both sub-systems separately are stable, they conserve that property when interconnected. A typical nonlinear cascaded time-varying system on closed-loop dynamical form is expressed as

$$\Sigma_1 : \dot{x}_1 = f_1(t, x_1) + g(t, x)x_2 \tag{A.65}$$

$$\Sigma_2 : \dot{x}_2 = f_2(t, x_2), \tag{A.66}$$

where $x_1 \in \mathbb{R}^n$, $x_2 \in \mathbb{R}^m$, $x = [x_1^\top, \ x_2^\top]^\top$ and the functions $f_1(\cdot, \cdot)$, $f_2(\cdot, \cdot)$ and $g(\cdot, \cdot)$ are continuous in their arguments, locally Lipschitz in x, uniformly in t, and $f_1(\cdot, \cdot)$

is continuously differentiable in both arguments. Note that (A.66) is decoupled from (A.65) hence, it will be called the *driving* system, its state enters as an input to the upper system with state x_1 through the *interconnection* term $g(t,x)x_2$, and

$$\dot{x}_1 = f_1(t, x_1). \tag{A.67}$$

will then be called the *driven* system.

A.5.1 Uniform global asymptotic stability

An important fact for nonlinear time-varying cascaded systems is that

Lemma A.2 (Loría and Panteley (2005)) *The cascade* (A.65)-(A.66) *is said to be UGAS if and only if the systems* (A.66) *and* (A.67) *are UGAS and the solutions of the cascade is uniformly globally bounded (UGB).*

A useful result for cascaded system was presented by (Loría and Panteley, 2005, Theorem 1) which proves uniform asymptotic stability of the equilibrium point of a closed-loop system on the form (A.65)–(A.66) under a series of assumptions.

The first condition states that the unperturbed dynamics is stable and that one knows a Lyapunov function for that system satisfying certain mild regularity properties:

Assumption A.1 *There exist constants c_1, c_2, $\delta' > 0$ and a Lyapunov function $V(t,x_1)$ for* (A.67) *such that $V : \mathbb{R}_{\geq 0} \times \mathbb{R}^n \to \mathbb{R}_{\geq 0}$ is positive definite, radially unbounded, $\dot{V}(t,x_1) \leq 0$ and*

$$\|\frac{\partial V}{\partial x_1}\|\|x_1\| \leq c_1 V(t,x_1) \quad \forall \|x_1\| \geq \delta' \tag{A.68}$$

$$\|\frac{\partial V}{\partial x_1}\| \leq c_2 \qquad \forall \|x_1\| \leq \delta'. \tag{A.69}$$

It is to be noted that Lyapunov functions bounded by polynomials satisfy the latter. The second condition is instrumental to ensure that the interconnection does not destabilize the system. It is demanded that the dependence of the interconnection on the state x_1 is not stronger than linear:

Assumption A.2 *There exist two continuous functions ξ_1, $\xi_2 : \mathbb{R}_{\geq 0} \to \mathbb{R}_{\geq 0}$ such that $g(t,x)$ satisfies*

$$\|g(t,x)\| \leq \xi_1(\|x_2\|) + \xi_2(\|x_2\|)\|x_1\|. \tag{A.70}$$

Finally, the third condition imposes a minimal convergence rate to the state of the perturbing system. This is expressed by an integrability assumption. Notice that systems enjoying local exponential stability satisfy this condition. In contrast, if $x_2(t)$ decays sufficiently slowly say, at the rate $1/t$ stability cannot be guaranteed:

Assumption A.3 *There exists a class $\mathcal{K}$ function $\alpha(\cdot)$ such that, for all $t_0 \geq 0$, the trajectories of the system* (A.66) *satisfy*

$$\int_{t_0}^{\infty} \|x_2(t; t_0, x_2(t_0))\| dt \leq \alpha(\|x_2(t_0)\|). \tag{A.71}$$

Theorem A.11 *Under Assumptions A.1–A.3 the origin of the cascaded system is uniformly asymptotically stable if the respective origins of* (A.66), (A.67) *are uniformly asymptotically stable; –see (Panteley and Loría, 1998).*

Theorem A.11 may be extended to the case when the subsystems possess the weaker property of practical asymptotic stability as presented in Section A.2.2.

A.5.2 Uniform semi-global practical asymptotical stability

For cascades of time-varying systems that are uniformly semi-globally practically asymptotically stability (USPAS) we consider systems on the form

$$\dot{x}_1 = f_1(t, x_1, \theta_1) + g(t, x, \theta) \tag{A.72}$$

$$\dot{x}_2 = f_2(t, x_2, \theta_2), \tag{A.73}$$

where $\theta = [\theta_1^\top,\ \theta_2^\top]^\top \in \Theta$ are tuning parameters, and $\Theta = [\Theta_1^\top,\ \Theta_2^\top]^\top \subset \mathbb{R}^m$ are the sets of available tuning parameters.

Assumption A.4 *The function g is uniformly bounded both in time and in θ_2 and vanishes with x_2, i.e., for any $\theta_1 \in \Theta_1$, there exists a nondecreasing function G_{θ_1} and a class $\mathcal{K}$ function Ψ_{θ_1} such that, for all $\theta_2 \in \Theta_2$, all $x \in \mathbb{R}^{n_1} \times \mathbb{R}^{n_2}$ and all $t \in \mathbb{R}_{\geq 0}$,*

$$\|g(t, x, \theta)\| \leq G_{\theta_1}(\|x\|)\Psi_{\theta_1}(\|x_2\|). \tag{A.74}$$

Assumption A.5 *The system* (A.73) *is USPAS on Θ_2.*

Assumption A.6 *Given any $\Delta_1 > \delta_1 > 0$, there exist a parameter $\theta_1^\star(\delta_1, \Delta_1) \in \Theta_1$, a continuously differentiable Lyapunov function V_{δ_1,Δ_1}, class $\mathcal{K}_\infty$ functions $\underline{\alpha}_{\delta_1,\Delta_1}$, $\overline{\alpha}_{\delta_1,\Delta_1}$, $\alpha_{\delta_1,\Delta_1}$ and a continuous positive nondecreasing function c_{δ_1,Δ_1} such that, for all $x_1 \in \mathcal{H}(\delta_1, \Delta_1)$ and all $t \in \mathbb{R}_{\geq 0}$*

$$\underline{\alpha}_{\delta_1,\Delta_1}(\|x_1\|) \leq V_{\delta_1,\Delta_1}(t, x_1) \leq \overline{\alpha}_{\delta_1,\Delta_1}(\|x_1\|) \tag{A.75}$$

$$\frac{\partial V_{\delta_1,\Delta_1}}{\partial t}(t, x_1) + \frac{\partial V_{\delta_1,\Delta_1}}{\partial x_1}(t, x_1) f_1(t, x_1, \theta_1^\star) \leq -\alpha_{\delta_1,\Delta_1}(\|x_1\|) \tag{A.76}$$

$$\left\|\frac{\partial V_{\delta_1,\Delta_1}}{\partial x_1}(t, x_1)\right\| \leq c_{\delta_1,\Delta_1}(\|x_1\|), \tag{A.77}$$

where $\mathcal{H} = \{x \in \mathbb{R}^n : \delta \leq \|x\| \leq \Delta\}$.

Assumption A.7 *There exists a positive constant Δ_0 such that, for any given positive numbers δ_1, Δ_1, δ_2, Δ_2, satisfying $\Delta_1 > \max\{\delta_1, \Delta_0\}$ and $\Delta_2 > \delta_2$, and for the parameter $\theta_1^\star(\delta_1, \Delta_1)$ as defined in Assumption A.6, there exists a parameter $\theta_2^\star \in \mathcal{D}_{f_2}(\delta_2, \Delta_2) \cap \Theta_2$ and a positive number $\gamma(\delta_1, \delta_2, \Delta_1, \Delta_2)$ such that the trajectories of* (A.72)-(A.73) *with $\theta = \theta^\star$ satisfy*

$$\|x_0\| \leq \gamma(\delta_1, \delta_2, \Delta_1, \Delta_2) \Rightarrow \|\phi(t, t_0, x_0, \theta^\star)\| \leq \Delta_1,\ \forall t \geq t_0. \tag{A.78}$$

In addition, given any $\Delta_\star > \delta_\star > 0$, there exist some positive constants δ_1, Δ_1 and Δ_2, with $\Delta_1 > \delta_1$, such that, for all $\delta_2 \in (0, \Delta_2)$,

$$\min\{\Delta_1, \Delta_2, \gamma(\delta_1, \delta_2, \Delta_1, \Delta_2)\} \geq \Delta_\star \tag{A.79}$$

$$\max\{\delta_2, \underline{\alpha}^{-1}_{\delta_1,\Delta_1} \circ \overline{\alpha}_{\delta_1,\Delta_1}(\delta_1)\} \leq \delta_\star. \tag{A.80}$$

The following theorem provides sufficient conditions for the preservation of USPAS under cascaded interconnection:

Theorem A.12 (USPAS + USPAS + UB $\Rightarrow$ USPAS, (Chaillet, 2006)) *Under Assumptions A.4–A.7, the cascaded system* (A.72)–(A.73) *is USPAS on $\Theta_1 \times \Theta_2$.*

The following definition and proposition are also used along the proof of USPAS:

Definition A.12 ($\mathcal{D}$-set, (Chaillet, 2006)) *For any $\Delta > \delta \geq 0$, the $\mathcal{D}$-set of the dynamical system $\dot{x} = f(t, x, \theta)$, is defined as*

$$\mathcal{D}_f(\delta, \Delta) = \{\theta \in \mathbb{R}^m \ : \ \mathcal{B}_\delta \text{ is UAS on } \mathcal{B}_\Delta \text{ for } f(t, x, \theta)\}.$$

Proposition A.2 (Sufficient condition for UB, (Chaillet, 2006)) *Let b be a positive constant. Suppose that there exists a continuously differentiable function V and two class $\mathcal{K}_\infty$ functions $\underline{\alpha}$ and $\overline{\alpha}$ such that, for all $t \in \mathbb{R}_{\geq 0}$ and all $x \in \mathbb{R}^n$,*

$$\underline{\alpha}(\|x\|) \leq V(t, x) \leq \overline{\alpha}(\|x\|) \tag{A.81}$$

$$x \in \mathcal{H}(a, b) \Rightarrow \frac{\partial V}{\partial t}(t, x) + \frac{\partial V}{\partial x}(t, x) f(t, x) \leq 0, \tag{A.82}$$

where a denotes a positive number such that $\overline{\alpha}(a) < \underline{\alpha}(b)$. Then, for all $t_0 \in \mathbb{R}_{\geq 0}$, the solutions of $\dot{x} = f(t, x)$ satisfy

$$\|x_0\| \leq \overline{\alpha}^{-1} \circ \underline{\alpha}(b) \Rightarrow \|\phi(t, t_0, x_0)\| \leq b, \ \forall t \geq t_0. \tag{A.83}$$

Appendix B

Detailed proofs

B.1 Proof of Lemma 3.1

We have that

$$\mathbf{e}_{q\pm}^{\top}\mathbf{T}_e\mathbf{T}_e^{\top}\mathbf{e}_{q\pm} = \frac{1}{4}\tilde{\boldsymbol{\epsilon}}^{\top}\tilde{\boldsymbol{\epsilon}} \geq \frac{1}{8}\left((1\mp\tilde{\eta})^2 + \tilde{\boldsymbol{\epsilon}}^{\top}\tilde{\boldsymbol{\epsilon}}\right) = \frac{1}{8}\mathbf{e}_{q\pm}^{\top}\mathbf{e}_{q\pm}, \tag{B.1}$$

where the inequality from (B.1) is found by

$$\frac{1}{8}\left((1\mp\tilde{\eta})^2 + \tilde{\boldsymbol{\epsilon}}^{\top}\tilde{\boldsymbol{\epsilon}}\right) \leq \frac{1}{4}\tilde{\boldsymbol{\epsilon}}^{\top}\tilde{\boldsymbol{\epsilon}} \tag{B.2}$$

$$(1\mp\tilde{\eta})^2 \leq \tilde{\boldsymbol{\epsilon}}^{\top}\tilde{\boldsymbol{\epsilon}} = 1-\tilde{\eta}^2 \tag{B.3}$$

$$1\mp 2\tilde{\eta}+\tilde{\eta}^2 \leq 1-\tilde{\eta}^2 \tag{B.4}$$

$$\mp 2\tilde{\eta} \leq 0, \tag{B.5}$$

and we see that the inequality holds for $\mathbf{e}_{q+}\ \forall\ 0 \leq \tilde{\eta} \leq 1$ and $\mathbf{e}_{q-}\ \forall\ -1 \leq \tilde{\eta} \leq 0$.

B.2 Proof of Lemma 3.2

By multiplication we find that

$$\mathbf{T}_e^{\top}(\mathbf{e}_{q\pm})\mathbf{e}_{q\pm} = \pm\frac{1}{2}\tilde{\boldsymbol{\epsilon}} \tag{B.6}$$

and by differentiation of both sides and rearranging the terms, we obtain

$$\dot{\mathbf{T}}_e^{\top}(\mathbf{e}_{q\pm})\mathbf{e}_{q\pm} = \pm\frac{1}{2}\dot{\tilde{\boldsymbol{\epsilon}}} - \mathbf{T}_e^{\top}(\mathbf{e}_{q\pm})\dot{\mathbf{e}}_{q\pm}, \tag{B.7}$$

and from (3.5)–(3.6) we have that

$$\dot{\mathbf{T}}_e^{\top}(\mathbf{e}_{q\pm})\mathbf{e}_{q\pm} = \pm\frac{1}{4}[\tilde{\eta}\mathbf{I} + \mathbf{S}(\tilde{\boldsymbol{\epsilon}})]\mathbf{e}_{\omega} - \mathbf{T}_e^{\top}(\mathbf{e}_{q\pm})\mathbf{T}_e(\mathbf{e}_{q\pm})\mathbf{e}_{\omega}. \tag{B.8}$$

Furthermore, we find by multiplication that $\mathbf{T}_e^{\top}(\mathbf{e}_{q\pm})\mathbf{T}_e(\mathbf{e}_{q\pm}) = 1/4\mathbf{I}$ which concludes the proof.

B.3 Proof of Theorem 3.2

Without loss of generality, we show stability of the positive equilibrium point *i.e.*, let $\mathbf{e}_q = \mathbf{e}_{q+}$ and $\mathbf{T}_e = \mathbf{T}_e(\mathbf{e}_{q+})$.

By inserting (3.14) into (2.83) and applying the property $\mathbf{S}(\boldsymbol{\omega})\mathbf{J}\boldsymbol{\omega} = -\mathbf{S}(\mathbf{J}\boldsymbol{\omega})\boldsymbol{\omega}$ we obtain the closed-loop rotational dynamics

$$\mathbf{J}\dot{\mathbf{e}}_\omega + (k_\omega \mathbf{I} - \mathbf{S}(\mathbf{J}\boldsymbol{\omega}))\,\mathbf{e}_\omega + k_q \mathbf{T}_e^\top \mathbf{e}_q = \mathbf{0}. \tag{B.9}$$

A radial unbounded, positive definite Lyapunov function candidate is defined as

$$V(\mathbf{x}) := \frac{1}{2}\left(\mathbf{e}_\omega^\top \mathbf{J}\mathbf{e}_\omega + \mathbf{e}_q^\top k_p \mathbf{e}_q\right) > 0, \quad \forall\, \mathbf{e}_\omega \neq \mathbf{0},\ \mathbf{e}_q \neq \mathbf{0}, \tag{B.10}$$

where $\mathbf{x} = [\mathbf{e}_q^\top,\ \mathbf{e}_\omega^\top]^\top$, and by differentiating (B.10) and inserting (3.5) and (B.9) we obtain

$$\dot{V} = \mathbf{e}_q^\top k_q \mathbf{T}_e \mathbf{e}_\omega + \mathbf{e}_\omega^\top \left(\mathbf{S}(\mathbf{J}\boldsymbol{\omega}) - k_\omega \mathbf{I}\right)\mathbf{e}_\omega - \mathbf{e}_\omega^\top k_q \mathbf{T}_e^\top \mathbf{e}_q, \tag{B.11}$$

where the first part of the second term in equation (B.11) is zero because $\mathbf{S}\left(\mathbf{J}\boldsymbol{\omega}\right)$ is a skew-symmetric matrix, thus we have the property $\mathbf{x}^\top \mathbf{S}(\mathbf{y})\mathbf{x} = \mathbf{0}$ for all $\mathbf{x}, \mathbf{y} \in \mathbb{R}^3$, which leads to

$$\dot{V} = -\mathbf{e}_\omega^\top k_\omega \mathbf{e}_\omega\ . \tag{B.12}$$

Hence, from standard Lyapunov theorems –*cf.* (Khalil, 2002), it follows that the equilibrium point $(\mathbf{e}_q, \mathbf{e}_\omega) = (\mathbf{0}, \mathbf{0})$ is uniformly stable (US). We now apply the theorem of Matrosov (Theorem A.4), and start by introducing an auxiliary function

$$W(\mathbf{x}) := \mathbf{e}_q^\top \mathbf{T}_e \mathbf{J}\mathbf{e}_\omega, \tag{B.13}$$

which is continuous and uniformly bounded on compacts of the state. The total time derivative of $W(\mathbf{x})$ along closed-loop trajectories yields

$$\dot{W} = \dot{\mathbf{e}}_q^\top \mathbf{T}_e \mathbf{J}\mathbf{e}_\omega + \mathbf{e}_q^\top \dot{\mathbf{T}}_e \mathbf{J}\mathbf{e}_\omega + \mathbf{e}_q^\top \mathbf{T}_e \mathbf{J}\dot{\mathbf{e}}_\omega \tag{B.14}$$

$$= \mathbf{e}_\omega^\top \mathbf{T}_e^\top \mathbf{T}_e \mathbf{J}\mathbf{e}_\omega + \mathbf{e}_\omega^\top \mathbf{G}^\top \mathbf{J}\mathbf{e}_\omega - \mathbf{e}_q^\top \mathbf{T}_e \Big[\left(-\mathbf{S}(\mathbf{J}\boldsymbol{\omega}) + k_\omega \mathbf{I}\right)\mathbf{e}_\omega + k_q \mathbf{T}_e^\top \mathbf{e}_q\Big], \tag{B.15}$$

where Lemma 3.2 was applied. We now verify that $\dot{W}(\mathbf{x})$ is non-zero definite on the set $E = \{\mathbf{x} \in S_{e+}^3 \times \mathbb{R}^3 : \dot{V}(\mathbf{x}) = 0\} = \{\mathbf{x} \in S_e{+}^3 \times \mathbb{R}^3 : \mathbf{e}_\omega = \mathbf{0}\}$; to that end observe that

$$\mathbf{e}_\omega = \mathbf{0} \Rightarrow \dot{W} = -\mathbf{e}_q^\top \mathbf{T}_e k_q \mathbf{T}_e^\top \mathbf{e}_q. \tag{B.16}$$

By invoking Lemma 3.1 and employing Lyapunov arguments we find that the closed-loop system in equation (B.9) is uniformly asymptotically stable (UAS) in the equilibrium point $(\mathbf{e}_q, \mathbf{e}_\omega) = (\mathbf{0}, \mathbf{0})$.

The proof for the negative equilibrium follows *mutatis mutandis*.

B.4 Proof of Theorem 3.3

The proof follows along the lines of Proposition 3.2 until (B.12) which leads to

$$\dot{V} = -\mathbf{e}_\omega^\top k_\omega \mathbf{e}_\omega \leq 0 \tag{B.17}$$

so the origin of the system is uniformly stable and the trajectories are bounded. The rest of the proof consists in showing that the position errors and the velocity tracking errors are square-integrable. Then it suffices to invoke (Panteley *et al.*, 2001, Lemma 3).

Let $\mathcal{V}(t) = V(\mathbf{e}_q(t), \mathbf{e}_\omega(t))$ and $\mathbf{x}(t) = [\mathbf{e}_q(t)^\top,\ \mathbf{e}_\omega(t)^\top]^\top$. Then, from (B.17) we obtain by integrating on both sides

$$\int_{t_0}^{t} \dot{\mathcal{V}}(s)ds = -\int_{t_0}^{t} \mathbf{e}_\omega^\top(s) k_\omega \mathbf{e}_\omega(s) ds \tag{B.18}$$

$$-\mathcal{V}(t) + \mathcal{V}(t_0) = k_\omega \int_{t_0}^{t} \|\mathbf{e}_\omega(s)\|^2 ds. \tag{B.19}$$

Since $-\mathcal{V}_l(t) \leq 0$ we can write

$$\begin{aligned} k_\omega \int_{t_0}^{t} \|\mathbf{e}_\omega\|^2 ds \leq \mathcal{V}(t_0) =& \frac{1}{2}\left[\mathbf{e}_\omega^\top(t_0)\mathbf{J}\mathbf{e}_\omega(t_0) + \mathbf{e}_q^\top(t_0) k_q \mathbf{e}_q(t_0)\right] \\ &\leq \max\{j_M, k_q\}\|\mathbf{x}(t_0)\|^2, \end{aligned} \tag{B.20}$$

and thus

$$\int_{t_0}^{t} \|\mathbf{e}_\omega(s)\|^2 ds \leq c_1 \|\mathbf{x}(t_0)\|^2, \tag{B.21}$$

where $c_1 = \max\{j_M, k_q\}/k_\omega$. Now let $\mathcal{W}(t) = W(\mathbf{e}_q(t), \mathbf{e}_\omega(t))$ such that

$$\mathcal{W}(t) = \mathbf{e}_q(t)^\top \mathbf{T}_e(t) k_q \mathbf{J}\mathbf{e}_\omega(t), \tag{B.22}$$

and by differentiation we obtain

$$\dot{\mathcal{W}}(t) = \dot{\mathbf{e}}_q^\top(t)\mathbf{T}_e(t)k_q\mathbf{J}\mathbf{e}_\omega(t) + \mathbf{e}_q^\top(t)\dot{\mathbf{T}}_e(t)k_q\mathbf{J}\mathbf{e}_\omega(t) + \mathbf{e}_q^\top(t)\mathbf{T}_e(t)k_q\mathbf{J}\dot{\mathbf{e}}_\omega(t). \tag{B.23}$$

By applying Lemma 3.2 and inserting (3.5) and (B.9) into (B.23) we obtain

$$\begin{aligned} \dot{\mathcal{W}}(t) =& \mathbf{e}_\omega^\top(t)\mathbf{T}_e^\top(t)\mathbf{T}_e(t)k_q\mathbf{J}\mathbf{e}_\omega(t) + \mathbf{e}_\omega^\top\mathbf{G}^\top(t)k_q\mathbf{J}\mathbf{e}_\omega(t) \\ &-\mathbf{e}_q^\top(t)\mathbf{T}_e(t)k_q\left[-\mathbf{S}(\mathbf{J}\boldsymbol{\omega}_{i,b}^b(t)) + k_\omega\mathbf{I}\right]\mathbf{e}_\omega(t) - \mathbf{e}_q^\top(t)\mathbf{T}_e(t)k_q^2\mathbf{T}_e^\top(t)\mathbf{e}_q(t) \\ &\leq -c_2\|\mathbf{e}_q\|^2 + c_3\|\mathbf{e}_\omega\|^2 + c_4\|\mathbf{e}_q\|\|\mathbf{e}_\omega\|, \end{aligned} \tag{B.24}$$

where $c_2 = k_q^2/4$, $c_3 = k_q j_M \|\mathbf{G}^\top(t)\|$, $c_4 = k_q/2\left(\|\mathbf{S}(\boldsymbol{J}\boldsymbol{\omega}_{i,b}^b(t))\| + k_\omega\right)$ and $\|\mathbf{G}^\top(t)\| \leq 1/4$. The last term of (B.24) can be rewritten as

$$c_4\|\mathbf{e}_q\|\|\mathbf{e}_\omega\| \leq \kappa\|\mathbf{e}_\omega(t)\|^2 + \frac{c_4^2}{\kappa}\|\mathbf{e}_q(t)\|^2, \tag{B.25}$$

and by choosing $\kappa \gg 1$ such that $c_2 > 2c_4^2/\kappa$, we obtain

$$\dot{\mathcal{W}}(t) \leq -c_2/2\|\mathbf{e}_q(t)\|^2 + (c_3+\kappa)\|\mathbf{e}_\omega(t)\|^2. \tag{B.26}$$

By applying the same line of arguments as in (B.18)-(B.20) and inequality (B.21), (B.26) may be expressed as

$$\mathcal{W}(t_0) + (c_3+\kappa)c_1\|\mathbf{x}(t_0)\|^2 \geq \frac{c_2}{2}\int_{t_0}^{t}\|\mathbf{e}_q(s)\|^2 ds. \tag{B.27}$$

By inserting the upper bound

$$\begin{aligned}\|\mathcal{W}(t_0)\| &\leq \max\{k_q, j_M\}\|\mathbf{e}_q(t_0)\|\|\mathbf{e}_\omega(t_0)\| \\ &\leq \max\{k_q, j_M\}\|\mathbf{x}(t_0)\|^2\end{aligned} \tag{B.28}$$

into (B.27), the expression may be written as

$$\int_{t_0}^{t}\|\mathbf{e}_q(s)\|^2 ds \leq c_5\|\mathbf{x}(t_0)\|^2, \tag{B.29}$$

where $c_5 = 2\left(\max\{k_q, j_M\} + (c_3+\kappa)c_1\right)/c_2$. We conclude from Lemma 3 of (Panteley *et al.*, 2001) that the origin is uniformly exponentially stable.

B.5 Proof of Theorem 3.4

Without loss of generality, we show stability of the positive equilibrium point *i.e.*, let $\mathbf{e}_q = \mathbf{e}_{q+}$ and $\mathbf{T}_e = \mathbf{T}_e(\mathbf{e}_{q+})$.

The closed-loop equations are

$$\dot{\mathbf{x}} := \begin{bmatrix} \dot{\mathbf{e}}_q \\ \dot{\mathbf{s}} \end{bmatrix} = \begin{bmatrix} \mathbf{T}_e\mathbf{s} - \mathbf{T}_e\gamma\mathbf{T}_e^\top\mathbf{e}_q \\ \mathbf{J}^{-1}\left\{[\mathbf{S}(\mathbf{J}\boldsymbol{\omega}) - k_\omega\mathbf{I}]\mathbf{s} - k_q\mathbf{T}_e^\top\mathbf{e}_q\right\} \end{bmatrix}. \tag{B.30}$$

Consider the radially unbounded, positive definite Lyapunov function candidate

$$V(\mathbf{x}) = \frac{1}{2}\mathbf{s}^\top\mathbf{J}\mathbf{s} + \frac{1}{2}\mathbf{e}_q^\top k_q\mathbf{e}_q > 0 \;\forall\; \mathbf{s}\neq\mathbf{0},\; \mathbf{e}_q \neq \mathbf{0}, \tag{B.31}$$

which satisfies

$$\dot{V} = \mathbf{s}^\top\mathbf{J}\dot{\mathbf{s}} + \mathbf{e}_q^\top k_q\dot{\mathbf{e}}_q. \tag{B.32}$$

By inserting (B.30) into (B.32) we further obtain

$$\dot{V} = \mathbf{s}^\top\mathbf{S}(\mathbf{J}\boldsymbol{\omega})\mathbf{s} - \mathbf{s}^\top k_\omega\mathbf{s} - \mathbf{s}^\top k_q\mathbf{T}_e^\top\mathbf{e}_q + \mathbf{e}_q^\top k_q\mathbf{T}_e\mathbf{s} - \mathbf{e}_q^\top\mathbf{T}_e\gamma k_q\mathbf{T}_e^\top\mathbf{e}_q \tag{B.33}$$

$$= \mathbf{s}^\top\mathbf{S}(\mathbf{J}\boldsymbol{\omega})\mathbf{s} - \mathbf{s}^\top k_\omega\mathbf{s} - \mathbf{e}_q^\top\mathbf{T}_e\gamma k_q\mathbf{T}_e^\top\mathbf{e}_q \tag{B.34}$$

and because of the skew-symmetry of $\mathbf{S}(\cdot)$ we obtain

$$\dot{V} = -\mathbf{s}^\top k_\omega\mathbf{s} - \mathbf{e}_q^\top\mathbf{T}_e\gamma k_q\mathbf{T}_e^\top\mathbf{e}_q \tag{B.35}$$

which implies using Lemma 3.1, that

$$\dot{V} \leq -\mathbf{s}^\top k_\omega \mathbf{s} - \mathbf{e}_q^\top \frac{\gamma k_q}{8} \mathbf{e}_q \,. \tag{B.36}$$

The proof is completed invoking standard Lyapunov theory arguments. From Assumption 3.3 we have that $\beta_j \leq \|\mathbf{J}\| \leq \beta_J$. Let

$$c_6 := 1/2 \min\{k_q, \beta_j\} \tag{B.37}$$
$$c_7 := \max\{k_q, \beta_J\} \tag{B.38}$$
$$c_8 := \min\{\gamma k_q/8, k_\omega\}, \tag{B.39}$$

then, from (B.31) we have $c_7 \left[\|\mathbf{s}\|^2 + \|\mathbf{e}_q\|^2\right] \geq V(\mathbf{x}) \geq c_6 \left[\|\mathbf{s}\|^2 + \|\mathbf{e}_q\|^2\right]$ and, together with (B.36) we obtain $\dot{V} \leq -c_8/c_7 V(\mathbf{x})$. The result follows recalling that $\mathbf{e}_\omega = \gamma \mathbf{T}_e^\top \mathbf{e}_q - \mathbf{s}$.

The proof for the negative equilibrium follows *mutatis mutandis*.

B.6 Proof of Theorem 3.5

Without loss of generality, we show stability of the positive equilibrium point *i.e.*, let $\mathbf{e}_q = \mathbf{e}_{q+}$ and $\mathbf{T}_e = \mathbf{T}_e(\mathbf{e}_{q+})$.

The control law (3.17), (3.16b) and (3.16d) in closed-loop with the system (2.82) and (2.83) can be expressed as

$$\begin{bmatrix} \dot{\mathbf{e}}_q \\ \dot{\mathbf{s}} \end{bmatrix} = \begin{bmatrix} \mathbf{T}_e \mathbf{s} - \mathbf{T}_e \gamma \mathbf{T}_e^\top \mathbf{e}_q \\ \mathbf{J}^{-1} \left\{ [\mathbf{S}(\mathbf{J}\boldsymbol{\omega}) - k_\omega \mathbf{I}]\mathbf{s} - k_q \mathbf{T}_e^\top \mathbf{e}_q + \boldsymbol{\tau}_d \right\} \end{bmatrix} . \tag{B.40}$$

By utilizing the Lyapunov function candidate (B.32), we obtain the derivative along closed-loop trajectories

$$\dot{V} \leq -\mathbf{x}^\top \mathbf{Q} \mathbf{x} + \|\mathbf{x}\| \beta_d \tag{B.41}$$

where $\mathbf{Q} = \text{diag}\{\gamma k_q/8\mathbf{I}, k_\omega \mathbf{I}\}$ which is positive definite. Thus, $\dot{V} < 0$ when $\|\mathbf{x}\| > \delta = \beta_d/q_m$ where q_m is the smallest eigenvalue of $\mathbf{Q}$, hence the closed-loop trajectories converge from any ball of initial conditions in the state space to a ball in close vicinity of the origin of radius δ which can be reduced by increasing the controller gains. Furthermore,

$$\lim_{\delta \to 0} \frac{\overline{\kappa}(\delta)\delta^p}{\underline{\kappa}(\delta)} = \lim_{\delta \to 0} \frac{\max\{k_q, \beta_J\}\delta^2}{1/2 \min\{k_q, \beta_j\}} = 0 \tag{B.42}$$

shows that Theorem A.10 is fulfilled, which leads to uniform practical exponential stability with $\boldsymbol{\theta} = [k_q,\ k_\omega]^\top$ as tuning parameter.

The proof for the negative equilibrium follows *mutatis mutandis*.

B.7 Proof of Theorem 3.6

Firstly, we observe that local stability of either equilibrium follows from the proof of Theorem 3.4, and that the proof of convergence relies on Theorem A.6. Without loss

of generality, we show stability of the positive equilibrium point *i.e.*, let $\mathbf{e}_q = \mathbf{e}_{q+}$ and $\mathbf{T}_e = \mathbf{T}_e(\mathbf{e}_{q+})$ and define $\mathbf{x} = [\mathbf{e}_q^\top, \mathbf{s}^\top]^\top$. We apply Theorem A.6 with $x = \mathbf{x}$ hence, let f denote the expression on the right-hand side of (B.30), and consider the density function $\rho : S_e^3 \times \mathbb{R}^3 \backslash \{\mathbf{x} = \mathbf{0}\} \to \mathbb{R}_{\geq 0}$

$$\rho(\mathbf{x}) = \left[\frac{1}{2}\left(\mathbf{e}_q^\top k_q \mathbf{e}_q + \mathbf{s}^\top \mathbf{J}\mathbf{s}\right)\right]^{-\alpha}, \ \alpha > 2. \tag{B.43}$$

That is, we have $\rho(\mathbf{x}) = V(\mathbf{x})^{-\alpha}$ where $V : S_e^3 \times \mathbb{R}^3 \to \mathbb{R}_{\geq 0}$ is defined as in (B.31). Since $V(\mathbf{x}) = \mathcal{O}(\|\mathbf{x}\|^2)$ and ρ is independent of t the integrability condition on ρ holds provided that $\alpha > 2$. It is left to show that

$$[\nabla \cdot (f\rho)](t, \mathbf{x}) > 0 \quad \forall t \geq 0, \ a.a. \ \mathbf{x} \in S_e^3 \times \mathbb{R}^3. \tag{B.44}$$

As in the first steps of the proof of (Rantzer, 2001, Proposition 1), we have[1]

$$\begin{aligned} \nabla \cdot (f\rho) &= \nabla\rho \cdot f + (\nabla \cdot f)\rho \\ &= (\nabla \cdot f)V^{-\alpha} - \alpha V^{-(\alpha+1)} \nabla V \cdot f \\ &= V^{-(\alpha+1)} \left[(\nabla \cdot f)V - \alpha \nabla V \cdot f\right]. \end{aligned} \tag{B.45}$$

The right-hand side of the previous equality is positive if and only if so is the sum in brackets. Let us show this. On one hand we have

$$\nabla V \cdot f = -\mathbf{s}^\top k_\omega \mathbf{s} - \mathbf{e}_q^\top \mathbf{T}_e \gamma k_q \mathbf{T}_e^\top \mathbf{e}_q. \tag{B.46}$$

On the other[2],

$$[\nabla \cdot f](t, \mathbf{x}) = \nabla(\mathbf{e}_q) \cdot \dot{\mathbf{e}}_q + \nabla(\mathbf{s}) \cdot \dot{\mathbf{s}}, \tag{B.47}$$

where

$$\nabla(\mathbf{e}_q) \cdot \dot{\mathbf{e}}_q = \nabla(\mathbf{e}_q) \cdot (\mathbf{T}_e \mathbf{s} - \gamma \mathbf{T}_e \mathbf{T}_e^\top \mathbf{e}_q) \tag{B.48}$$

$$= \frac{1}{2} \nabla(\mathbf{e}_q) \cdot \left(\begin{bmatrix} \tilde{\epsilon}_x & \tilde{\epsilon}_y & \tilde{\epsilon}_z \\ \tilde{\eta} & -\tilde{\epsilon}_z & \tilde{\epsilon}_y \\ \tilde{\epsilon}_z & \tilde{\eta} & -\tilde{\epsilon}_x \\ -\tilde{\epsilon}_y & \tilde{\epsilon}_x & \tilde{\eta} \end{bmatrix} \mathbf{s} \right) - \frac{\gamma}{4} \nabla(\mathbf{e}_q) \cdot \left(\begin{bmatrix} \tilde{\epsilon}_x^2 + \tilde{\epsilon}_y^2 + \tilde{\epsilon}_z^2 \\ \tilde{\eta}\tilde{\epsilon}_x \\ \tilde{\eta}\tilde{\epsilon}_y \\ \tilde{\eta}\tilde{\epsilon}_z \end{bmatrix} \right)$$

$$= -\frac{3\gamma\tilde{\eta}}{4}. \tag{B.49}$$

Moreover,

$$\nabla(\mathbf{s}) \cdot \dot{\mathbf{s}} = \nabla(\mathbf{s}) \cdot (\mathbf{J}^{-1}\{[\mathbf{S}(\mathbf{J}\boldsymbol{\omega}(t)) - k_\omega \mathbf{I}]\mathbf{s} - k_q \mathbf{T}_e^\top \mathbf{e}_q\}). \tag{B.50}$$

Then, using $\boldsymbol{\omega}(t) = \mathbf{s} + \boldsymbol{\omega}_r(t)$ we obtain

$$\nabla(\mathbf{s}) \cdot \dot{\mathbf{s}} = \nabla \cdot (\mathbf{J}^{-1}\{[\mathbf{S}(\mathbf{J}\mathbf{s}) + \mathbf{S}(\mathbf{J}\boldsymbol{\omega}_r(t)) - k_\omega \mathbf{I}]\mathbf{s} - k_q \mathbf{T}_e^\top \mathbf{e}_q\}) \tag{B.51}$$

[1] We drop the arguments t, $\mathbf{x}$ for simplicity in the notation.

[2] With an abuse of notation we split up the gradient and the vector with respect to which the function is differentiated hence, we write $\nabla(x) \cdot f(x, y) = \frac{\partial f(x,y)}{\partial x}$.

and since

$$\nabla(\mathbf{s}) \cdot \mathbf{S}(\mathbf{J}\mathbf{s})\mathbf{s} = 0 \tag{B.52}$$

$$\nabla(\mathbf{s}) \cdot \mathbf{S}(\mathbf{J}\boldsymbol{\omega}_r(t))\mathbf{s} = 0, \tag{B.53}$$

we see that

$$\nabla(\mathbf{s}) \cdot \dot{\mathbf{s}} = -3ck_\omega, \tag{B.54}$$

where $c := (1/J_x + 1/J_y + 1/J_z)$. Therefore,

$$[\nabla \cdot f](t, \mathbf{x}) = -3(\frac{\gamma\tilde{\eta}}{4} + ck_\omega). \tag{B.55}$$

Using (B.46), (B.55) and (B.31) we see that

$$[(\nabla \cdot f)V - \alpha \nabla V \cdot f] > 0$$

if and only if

$$-\frac{3}{2}\Big(\frac{\gamma\tilde{\eta}}{4} + ck_\omega\Big)\Big[\mathbf{s}^\top \mathbf{J}\mathbf{s} + \frac{1}{2}\mathbf{e}_q^\top k_q \mathbf{e}_q\Big] + \alpha\Big[\mathbf{s}^\top k_\omega \mathbf{s} + \mathbf{e}_q^\top \mathbf{T}_e \gamma k_q \mathbf{T}_e^\top \mathbf{e}_q\Big] > 0.$$

In view of (3.10) we see that the previous inequality holds for sufficiently large values of α and provided that $\mathbf{x} \neq 0$ (which correspond to the two equilibria). According to Theorem A.6 all points in $S_e^3 \times \mathbb{R}^3$ except for a set of measure zero, generate via (B.30) with $\mathbf{T}_e = \mathbf{T}_e(\mathbf{e}_{q+})$, solutions that converge asymptotically to $(\mathbf{e}_{q+}, \mathbf{e}_\omega) = (\mathbf{0}, \mathbf{0})$. It is evident that the dual equilibrium $(\mathbf{e}_{q-}, \mathbf{e}_\omega) = (\mathbf{0}, \mathbf{0})$ also generates trajectories a trajectory which does not converge to $(\mathbf{e}_{q+}, \mathbf{e}_\omega) = (\mathbf{0}, \mathbf{0})$.

B.8 Proof of Theorem 3.7

Without loss of generality, we show stability of the positive equilibrium point *i.e.*, let $\mathbf{e}_q = \mathbf{e}_{q+}$ and $\mathbf{T}_e = \mathbf{T}_e(\mathbf{e}_{q+})$.

The closed-loop dynamics that results from substituting (3.18) in (2.83) is

$$\dot{\mathbf{e}}_\omega = \mathbf{J}^{-1}\left[\mathbf{S}(\mathbf{J}\boldsymbol{\omega})\mathbf{e}_\omega - k_p e^{k_1 \mathbf{e}_q^\top \mathbf{e}_q} \mathbf{T}_e^\top \mathbf{e}_q - k_d e^{k_2 \mathbf{e}_\omega^\top \mathbf{e}_\omega} \mathbf{e}_\omega\right]. \tag{B.56}$$

Consider the radially unbounded and positive definite Lyapunov function candidate

$$V(\mathbf{x}) := \frac{1}{2}\left[\frac{k_p}{k_1}\left(e^{k_1 \mathbf{e}_q^\top \mathbf{e}_q} - 1\right) + \mathbf{e}_\omega^\top \mathbf{J}\mathbf{e}_\omega\right] > 0 \;\forall\; \mathbf{e}_q \neq \mathbf{0},\; \mathbf{e}_\omega \neq \mathbf{0}, \tag{B.57}$$

with lower and upper bounds

$$\underline{\kappa}(\|\mathbf{x}\|) = \frac{1}{2}\min\{\frac{k_p}{k_1}, \beta_j\}\|\mathbf{x}\|^2 \tag{B.58}$$

$$\overline{\kappa}(\|\mathbf{x}\|) = \frac{1}{2}\max\{\frac{k_p}{k_1}, \beta_J\}\left(e^{k_1\|\mathbf{x}\|^2} - 1\right), \tag{B.59}$$

where $\mathbf{x} = [\mathbf{e}_q^\top,\ \mathbf{e}_\omega^\top]^\top$ and $\beta_j \leq \|\mathbf{J}\| \leq \beta_J$ from Assumption 3.3. The total time derivative of $V(\mathbf{x})$ along the closed-loop trajectories generated by (3.5) and (B.56) yields

$$\begin{aligned}\dot{V} =& k_p e^{k_1 \mathbf{e}_q^\top \mathbf{e}_q} \mathbf{e}_q^\top \mathbf{T}_e \mathbf{e}_\omega + \mathbf{e}_\omega^\top \mathbf{S}(\mathbf{J}\boldsymbol{\omega})\mathbf{e}_\omega \\ & - \mathbf{e}_\omega^\top k_p e^{k_1 \mathbf{e}_q^\top \mathbf{e}_q} \mathbf{T}_e^\top \mathbf{e}_q - \mathbf{e}_\omega^\top k_d e^{k_2 \mathbf{e}_\omega^\top \mathbf{e}_\omega} \mathbf{e}_\omega && \text{(B.60)} \\ =& - \mathbf{e}_\omega^\top k_d e^{k_2 \mathbf{e}_\omega^\top \mathbf{e}_\omega} \mathbf{e}_\omega && \text{(B.61)} \\ \leq& - \mathbf{e}_\omega^\top k_d \mathbf{e}_\omega \leq 0\,. && \text{(B.62)}\end{aligned}$$

where we have applied that $k_2 > 0$ and $\mathbf{S}(\mathbf{J}\boldsymbol{\omega})$ is skew-symmetric. We conclude that the equilibrium point $(\mathbf{e}_q, \mathbf{e}_\omega) = (\mathbf{0}, \mathbf{0})$ is uniformly stable and the solutions are uniformly bounded.

For uniform asymptotic stability we invoke Matrosov's theorem as reproduced in Theorem A.4. To that end, we introduce the auxiliary function

$$W(\mathbf{x}) := \mathbf{e}_q^\top \mathbf{T}_e \mathbf{J} \mathbf{e}_\omega \tag{B.63}$$

which is continuous and uniformly bounded on compacts of the state. The total time derivative of W along closed-loop trajectories yields

$$\begin{aligned}\dot{W} =& \dot{\mathbf{e}}_q^\top \mathbf{T}_e \mathbf{J} \mathbf{e}_\omega + \mathbf{e}_q^\top \dot{\mathbf{T}}_e \mathbf{J} \mathbf{e}_\omega + \mathbf{e}_q^\top \mathbf{T}_e \mathbf{J} \dot{\mathbf{e}}_\omega && \text{(B.64)} \\ =& \mathbf{e}_\omega^\top \mathbf{T}_e^\top \mathbf{T}_e \mathbf{J} \mathbf{e}_\omega + \mathbf{e}_q^\top \dot{\mathbf{T}}_e \mathbf{J} \mathbf{e}_\omega \\ & - \mathbf{e}_q^\top \mathbf{T}_e \Big[\Big(-\mathbf{S}(\mathbf{J}\boldsymbol{\omega}) + k_d e^{k_2 \mathbf{e}_\omega^\top \mathbf{e}_\omega} \mathbf{I} \Big) \mathbf{e}_\omega \\ & + k_p e^{k_1 \mathbf{e}_q^\top \mathbf{e}_q} \mathbf{T}_e^\top \mathbf{e}_q \Big]. && \text{(B.65)}\end{aligned}$$

We now verify that $\dot{W}$ is non-zero definite on the set $E = \{\mathbf{x} \in S^3_{e+} \times \mathbb{R}^3 : \dot{V} = 0\} = \{\mathbf{x} \in S^3_{e+} \times \mathbb{R}^3 : \mathbf{e}_\omega = \mathbf{0}\}$. To that end observe that

$$\mathbf{e}_\omega = 0 \ \Rightarrow\ \dot{W} = -\mathbf{e}_q^\top \mathbf{T}_e k_p e^{k_1 \mathbf{e}_q^\top \mathbf{e}_q} \mathbf{T}_e^\top \mathbf{e}, \tag{B.66}$$

and by applying Lemma 3.1 we obtain

$$\dot{W} \leq -\mathbf{e}_q^\top \frac{k_p}{8} \mathbf{e}_q, \tag{B.67}$$

that is, $\dot{W}$ is non-zero definite on E. Uniform asymptotic stability follows invoking Matrosov's theorem.

The proof for the negative equilibrium follows *mutatis mutandis*.

B.9 Proof of Theorem 3.8

Without loss of generality, we show stability of the positive equilibrium point *i.e.*, let $\mathbf{e}_q = \mathbf{e}_{q+}$ and $\mathbf{T}_e = \mathbf{T}_e(\mathbf{e}_{q+})$.

The closed-loop dynamics are obtained by inserting (3.19) into (2.83) such that

$$\dot{\mathbf{e}}_\omega = \mathbf{J}^{-1} \Big(\mathbf{S}(\mathbf{J}\boldsymbol{\omega})\mathbf{e}_\omega - k_p \alpha(\|\mathbf{e}_q\|^2) \mathbf{T}_e^\top \mathbf{e}_q - k_d \beta(\|\mathbf{e}_\omega\|^2) \upsilon(\|\mathbf{e}_q\|^2) \mathbf{e}_\omega \Big). \tag{B.68}$$

A radially unbounded, positive definite Lyapunov function candidate is defined as

$$V(\mathbf{x}) := \frac{1}{2}\left[k_p\xi(\|\mathbf{e}_q\|^2) + \mathbf{e}_\omega^\top \mathbf{J}\mathbf{e}_\omega\right] > 0 \;\forall\; \mathbf{e}_q \neq \mathbf{0},\; \mathbf{e}_\omega \neq \mathbf{0}, \tag{B.69}$$

where $\xi(\|\mathbf{e}_q\|^2)$ is differentiable and belongs to class $\mathcal{K}_\infty$ (*cf.* (Khalil, 2002)), and let the LFC be bounded as $\underline{\kappa}(\mathbf{x}) \leq V(x) \leq \overline{\kappa}(\mathbf{x})$, where

$$\underline{\kappa}(\mathbf{x}) = \frac{1}{2}\min\{k_p, \beta_j\}\min\{\xi(\|\mathbf{x}\|^2), \|\mathbf{x}\|^2\} \tag{B.70}$$

$$\overline{\kappa}(\mathbf{x}) = \frac{1}{2}\max\{k_p, \beta_J\}\max\{\xi(\|\mathbf{x}\|^2), \|\mathbf{x}\|^2\}, \tag{B.71}$$

with $\mathbf{x} = [\mathbf{e}_q^\top,\ \mathbf{e}_\omega^\top]^\top$ and $\beta_j \leq \|\mathbf{J}\| \leq \beta_J$ from Assumption 3.3. By differentiation and insertion of (3.5) and (B.68) we obtain

$$\begin{aligned}\dot{V} = {} & k_p\dot{\xi}(\|\mathbf{e}_q\|^2)\mathbf{e}_q^\top \mathbf{T}_e\mathbf{e}_\omega + \mathbf{e}_\omega^\top \mathbf{S}(\mathbf{J}\boldsymbol{\omega})\mathbf{e}_\omega \\ & - \mathbf{e}_\omega^\top k_p\alpha(\|\mathbf{e}_q\|^2)\mathbf{T}_e^\top \mathbf{e}_q - \mathbf{e}_\omega^\top k_d\beta(\|\mathbf{e}_\omega\|^2)\upsilon(\|\mathbf{e}_q\|^2)\mathbf{e}_\omega.\end{aligned} \tag{B.72}$$

The second term disappears since $\mathbf{S}(\mathbf{J}\boldsymbol{\omega})$ is skew-symmetric, and by choosing $\xi(r)$ such that $\dot{\xi}(r) = \alpha(r)$ we obtain

$$\begin{aligned}\dot{V} = {} & -\mathbf{e}_\omega^\top k_d\beta(\|\mathbf{e}_\omega\|^2)\upsilon(\|\mathbf{e}_q\|^2)\mathbf{e}_\omega && \text{(B.73)}\\ \leq {} & -\mathbf{e}_\omega^\top k_d\upsilon(\|\mathbf{e}_q\|^2)\mathbf{e}_\omega. && \text{(B.74)}\end{aligned}$$

Since $\mathbf{e}_q^\top \mathbf{e}_q = (1-\tilde{\eta})^2 + \tilde{\boldsymbol{\epsilon}}^\top\tilde{\boldsymbol{\epsilon}} = 2(1-\tilde{\eta}) \leq 2$ for $\tilde{\eta} \geq 0$ we have that

$$\dot{V} \leq -\mathbf{e}_\omega^\top k_d\upsilon(4)\mathbf{e}_\omega, \tag{B.75}$$

which renders the equilibrium point $(\mathbf{e}_q, \mathbf{e}_\omega) = (\mathbf{0}, \mathbf{0})$ uniformly stable according to standard Lyapunov theorems (*cf.* (Khalil, 2002)). We then apply Matrosovs theorem using an auxiliary function

$$W(\mathbf{x}) := \mathbf{e}_q^\top \mathbf{T}_e\mathbf{J}\mathbf{e}_\omega \tag{B.76}$$

which has a corresponding derivative

$$\begin{aligned}\dot{W} = {} & \dot{\mathbf{e}}_q^\top \mathbf{T}_e\mathbf{J}\mathbf{e}_\omega + \mathbf{e}_q^\top \dot{\mathbf{T}}_e\mathbf{J}\mathbf{e}_\omega + \mathbf{e}_q^\top \mathbf{T}_e\mathbf{J}\dot{\mathbf{e}}_\omega && \text{(B.77)}\\ = {} & \mathbf{e}_\omega^\top \mathbf{T}_e^\top \mathbf{T}_e\mathbf{J}\mathbf{e}_\omega + \mathbf{e}_\omega^\top\left(\frac{1}{2}[\tilde{\eta}\mathbf{I} + \mathbf{S}(\tilde{\boldsymbol{\epsilon}})] - \frac{1}{4}\mathbf{I}\right)\mathbf{J}\mathbf{e}_\omega \\ & - \mathbf{e}_q^\top \mathbf{T}_e\Big[\Big(-\mathbf{S}(\mathbf{J}\boldsymbol{\omega}) + k_p\alpha(\|\mathbf{e}_q\|^2)\mathbf{T}_e^\top \mathbf{e}_q \\ & + k_d\beta(\|\mathbf{e}_\omega\|^2)\upsilon(\|\mathbf{e}_q\|^2)\mathbf{I}\Big)\mathbf{e}_\omega\Big]. && \text{(B.78)}\end{aligned}$$

In the set $E = \{\mathbf{x} \in S_{e+}^3 \times \mathbb{R}^3 : \dot{V} = 0\} = \{\mathbf{x} \in S_{e+}^3 \times \mathbb{R}^3 : \mathbf{e}_\omega = \mathbf{0}\}$, (B.78) is reduced to

$$\dot{W} = -\mathbf{e}_q^\top \mathbf{T}_e k_p\alpha(\|\mathbf{e}_q\|^2)\mathbf{T}_e^\top \mathbf{e}_q. \tag{B.79}$$

By applying Lemma 3.1 and the fact that $\alpha(\|\mathbf{x}\|^2) \geq 1$ for all $\mathbf{x} \in \mathbb{R}^n$, we obtain

$$\dot{W} \leq -\mathbf{e}_q^\top \frac{k_p}{8} \mathbf{e}_q, \tag{B.80}$$

that is, $\dot{W}$ is non-zero definite on E. Uniform asymptotic stability follows invoking Matrosov's theorem.

The proof for the negative equilibrium follows *mutatis mutandis*.

B.10 Proof of Theorem 3.9

Without loss of generality, we show stability of the positive equilibrium point *i.e.*, let $\mathbf{e}_q = \mathbf{e}_{q+}$ and $\mathbf{T}_e = \mathbf{T}_e(\mathbf{e}_{q+})$.

By inserting the control law (3.20) into (2.83) we obtain the closed-loop dynamics

$$\dot{\mathbf{e}}_\omega = \mathbf{J}^{-1} \left(\mathbf{S}(\mathbf{J}\boldsymbol{\omega})\mathbf{e}_\omega - k_p e^{k_1 \mathbf{e}_q^\top \mathbf{e}_q} \mathbf{T}_e^\top \mathbf{e}_q - k_d e^{k_2 \mathbf{e}_\omega^\top \mathbf{e}_\omega} \mathbf{e}_\omega + \boldsymbol{\tau}_d^b \right). \tag{B.81}$$

The total time derivative of $V(\mathbf{x})$ defined in (B.57) along the closed-loop trajectories generated by (3.5) and (B.81) yields

$$\dot{V} \leq -\mathbf{e}_\omega^\top k_d \mathbf{e}_\omega + \beta_d \|\mathbf{e}_\omega\|. \tag{B.82}$$

Let $\delta := \beta_d / k_d$. From the expression above, we have $\dot{V} < 0$ if $\|\mathbf{e}_\omega\| > \delta$. Since $V(\mathbf{x})$ is positive definite and proper we obtain that $\|\mathbf{e}_\omega(t)\|$ is bounded that is, for any $r > 0$ there exists $\Delta(r) > 0$ such that $\sup_{t \geq t_0} \|\mathbf{e}_\omega(t)\| \leq \Delta$ for all initial conditions $\|\mathbf{x}(t_0)\| < r$, $t_0 \geq 0$.

For any Δ, let $\lambda(\Delta) > 0$ be a constant to be determined. Consider the Lyapunov function candidate

$$\mathcal{V} := V(\mathbf{x}) + \lambda W(\mathbf{x}), \tag{B.83}$$

which is positive definite and proper for $\lambda \leq 1$ with $W(\mathbf{x})$ as defined in (B.63). Its total time derivative along the closed-loop trajectories yields

$$\begin{aligned}
\dot{\mathcal{V}} = & - \mathbf{e}_\omega^\top k_d e^{k_2 \mathbf{e}_\omega^\top \mathbf{e}_\omega} \mathbf{e}_\omega + \beta_d \|\mathbf{e}_\omega\| + \lambda \mathbf{e}_\omega \mathbf{T}_e^\top \mathbf{T}_e \mathbf{J} \mathbf{e}_\omega \\
& + \lambda \mathbf{e}_q^\top \dot{\mathbf{T}}_e \mathbf{J} \mathbf{e}_\omega + \lambda \mathbf{e}_q^\top \mathbf{T}_e \left[\mathbf{S}(\mathbf{J}\boldsymbol{\omega}) - k_d e^{k_2 \mathbf{e}_\omega^\top \mathbf{e}_\omega} \mathbf{I} \right] \mathbf{e}_\omega \\
& - \lambda \mathbf{e}_q^\top \mathbf{T}_e k_p e^{k_1 \mathbf{e}_q^\top \mathbf{e}_q} \mathbf{T}_e^\top \mathbf{e}_q + \lambda \beta_d \|\mathbf{e}_q^\top \mathbf{T}_e\|,
\end{aligned} \tag{B.84}$$

and by applying Lemma 3.2, we obtain

$$\begin{aligned}
\dot{\mathcal{V}} \leq & - \mathbf{e}_\omega^\top k_d e^{k_2 \mathbf{e}_\omega^\top \mathbf{e}_\omega} \mathbf{e}_\omega + \frac{\lambda}{4} \mathbf{e}_\omega [\tilde{\eta}\mathbf{I} + \mathbf{S}(\tilde{\boldsymbol{\epsilon}})] \mathbf{J} \mathbf{e}_\omega \\
& + \lambda \mathbf{e}_q^\top \mathbf{T}_e \left[\mathbf{S}(\mathbf{J}\boldsymbol{\omega}) - k_d e^{k_2 \mathbf{e}_\omega^\top \mathbf{e}_\omega} \mathbf{I} \right] \mathbf{e}_\omega \\
& - \lambda \mathbf{e}_q^\top \mathbf{T}_e k_p e^{k_1 \mathbf{e}_q^\top \mathbf{e}_q} \mathbf{T}_e^\top \mathbf{e}_q + 2\beta_d \|\mathbf{x}\| \qquad \text{(B.85)} \\
= & - \mathbf{x}^\top \mathbf{P} \mathbf{x} + 2\beta_d \|\mathbf{x}\|, \qquad \text{(B.86)}
\end{aligned}$$

where we defined $\mathbf{P} := [\mathbf{p}_{ij}], \quad i,j = 1,2$ with

$$\begin{aligned}
\mathbf{p}_{11} &= \lambda \mathbf{T}_e k_p e^{k_1 \mathbf{e}_q^\top \mathbf{e}_q} \mathbf{T}_e^\top \\
\mathbf{p}_{12} = \mathbf{p}_{21}^\top &= \frac{\lambda}{2} \mathbf{T}_e \left[k_d e^{k_2 \mathbf{e}_\omega^\top \mathbf{e}_\omega} \mathbf{I} - \mathbf{S}(\mathbf{J}\boldsymbol{\omega}) \right] \\
\mathbf{p}_{22} &= k_d e^{k_2 \mathbf{e}_\omega^\top \mathbf{e}_\omega} \mathbf{I} - \frac{\lambda}{4} [\tilde{\eta} \mathbf{I} + \mathbf{S}(\tilde{\boldsymbol{\epsilon}})] \mathbf{J}
\end{aligned} \tag{B.87}$$

Notice that for any $\|\mathbf{e}_\omega\| \leq \Delta$ and $\|\boldsymbol{\omega}_d\| \leq \beta_{\omega_d}$ from Assumption 3.2 which hold under the arguments made so far, the angular velocities $\boldsymbol{\omega} = \mathbf{e}_\omega + \boldsymbol{\omega}_d$ satisfy the bound $\|\boldsymbol{\omega}\| \leq \Delta + \beta_{\omega_d} := \tilde{\Delta}$, and therefore, $\|\mathbf{S}(\mathbf{J}\boldsymbol{\omega})\| \leq \beta_J \tilde{\Delta}$. Next, we use $2|ab| \leq a^2 + b^2$ for any $a, b \in \mathbb{R}$ to obtain

$$\mathbf{x}^\top \mathbf{P} \mathbf{x} \geq (p_{11,m} - p_{12,M}) \|\mathbf{e}_q\|^2 + (p_{22,m} - p_{12,M}) \|\mathbf{e}_\omega\|^2 \tag{B.88}$$

where $p_{ij,m}$ and $p_{ij,M}$ denote lower and upper bounds on the induced norms of the sub-blocks $\mathbf{p}_{ij}$ of $\mathbf{P}$ respectively. Hence, ensuring

$$p_{11,m} \;\geq\; 2p_{12,M}\,, \qquad p_{22,m} \;\geq\; 2p_{12,M}, \tag{B.89}$$

results in

$$\mathbf{x}^\top \mathbf{P} \mathbf{x} \geq \frac{1}{2} \left(p_{11,m} \|\mathbf{e}_q\|^2 + p_{22,m} \|\mathbf{e}_\omega\|^2 \right). \tag{B.90}$$

To fulfill (B.89) we need to choose

$$\begin{aligned}
\lambda &\leq \frac{4 k_d}{\beta_J \tilde{\Delta} + k_d e^{k_2 \Delta^2} + \beta_J} \\
k_p &\geq 2 \left[\beta_J \tilde{\Delta} + k_d e^{k_2 \Delta^2} \right],
\end{aligned} \tag{B.91}$$

Thus,

$$\dot{\mathcal{V}} \leq -p_m \|\mathbf{x}\|^2 + 2\beta_d \|\mathbf{x}\|, \tag{B.92}$$

where $p_m > 0$ is a uniform lower bound on the smallest eigenvalue of $\mathbf{P}(\cdot)$. The derivative $\dot{\mathcal{V}} < 0$ for all states such that $\|\mathbf{x}\| > \delta' := 2\beta_d / p_m$. Note that p_m depends on the controller gains monotonically hence the closed-loop trajectories system converge from any ball of initial conditions in the state space to a ball in close vicinity of the origin, of radius δ'. Moreover, the latter may be reduced at will by increasing the control gains. We conclude that the equilibrium point $(\mathbf{e}_q, \mathbf{e}_\omega) \to (\mathbf{0}, \mathbf{0})$ is uniformly practically asymptotically stable.

Note that using the triangulation in (B.88) is conservative leading to bounds on the controller gains. If we instead apply Lemma 3.1 on (B.85), $\mathbf{p}_{11}$ in (B.87) is expressed as

$$\mathbf{p}_{11} = \frac{\lambda}{8} k_p e^{k_1 \mathbf{e}_q^\top \mathbf{e}_q} \mathbf{I} \tag{B.93}$$

which indeed is positive definite since $\lambda, k_p > 0$. Now, we apply Schurs compliment (Horn and Johnson, 1985) and require that

$$\begin{aligned}
\mathbf{p}_{22} &\succ \mathbf{p}_{12}^\top \mathbf{p}_{11}^{-1} \mathbf{p}_{12} \\
-\frac{\lambda}{4}[\tilde{\eta}\mathbf{I} + \mathbf{S}(\tilde{\boldsymbol{\epsilon}})]\mathbf{J} &\succ \frac{\lambda}{2}[k_d e^{k_2 \mathbf{e}_\omega^\top \mathbf{e}_\omega}\mathbf{I} + \mathbf{S}(\mathbf{J}\boldsymbol{\omega})]\mathbf{T}_e^\top \qquad \text{(B.94)} \\
&\quad \times \frac{8}{\lambda k_p e^{k_1 \mathbf{e}_q^\top \mathbf{e}_q}} \mathbf{I} \frac{\lambda}{2} \mathbf{T}_e \left[k_d e^{k_2 \mathbf{e}_\omega^\top \mathbf{e}_\omega}\mathbf{I} - \mathbf{S}(\mathbf{J}\boldsymbol{\omega})\right] \\
k_d e^{k_2 \mathbf{e}_q^\top \mathbf{e}_q}\mathbf{I} &\succ \frac{\lambda}{4}\Big\{[\tilde{\eta}\mathbf{I} + \mathbf{S}(\tilde{\boldsymbol{\epsilon}})]\mathbf{J} + \frac{2}{k_p e^{k_1 \mathbf{e}_q^\top \mathbf{e}_q}} \\
&\quad \times \left[k_d e^{k_2 \mathbf{e}_\omega^\top \mathbf{e}_\omega}\mathbf{I} - \mathbf{S}(\mathbf{J}\boldsymbol{\omega})\right]\left[k_d e^{k_2 \mathbf{e}_\omega^\top \mathbf{e}_\omega}\mathbf{I} - \mathbf{S}(\mathbf{J}\boldsymbol{\omega})\right]\Big\} \qquad \text{(B.95)} \\
&= \frac{\lambda}{4}\left\{[\tilde{\eta}\mathbf{I} + \mathbf{S}(\tilde{\boldsymbol{\epsilon}})]\mathbf{J} + \frac{2}{k_p e^{k_1 \mathbf{e}_q^\top \mathbf{e}_q}}\left[k_d^2 e^{2k_2 \mathbf{e}_\omega^\top \mathbf{e}_\omega} + \mathbf{S}^2(\mathbf{J}\boldsymbol{\omega})\right]\right\}, \qquad \text{(B.96)}
\end{aligned}$$

and by taking the norm on each side of (B.96), (B.94) is fulfilled if we choose

$$\lambda < \frac{4k_d}{\beta_J + \frac{2}{k_p}(k_d^2 e^{2k_2 \Delta^2} + \beta_J^2 \tilde{\Delta}^2)}. \qquad \text{(B.97)}$$

and by following the same lines as above, we obtain similar stability results without restricting the gains since λ is a design parameter.

The proof for the negative equilibrium follows *mutatis mutandis*.

B.11 Proof of Theorem 3.10

We start by considering the positive equilibrium point such that $\mathbf{e}_q = \mathbf{e}_{q+}$ and $\mathbf{T}_e = \mathbf{T}_e(\mathbf{e}_{q+})$. By inserting the control law (3.21) into (2.83) we obtain the closed-loop dynamics

$$\begin{aligned}
\dot{\mathbf{e}}_\omega = \mathbf{J}^{-1}\Big(&\mathbf{S}(\mathbf{J}\boldsymbol{\omega})\mathbf{e}_\omega - k_p \alpha(\|\mathbf{e}_q\|^2)\mathbf{T}_e^\top \mathbf{e}_q \qquad \text{(B.98)} \\
&- k_d \beta(\|\mathbf{e}_\omega\|)\upsilon(\|\mathbf{e}_q\|^2)\mathbf{e}_\omega + \boldsymbol{\tau}_d^b\Big). \qquad \text{(B.99)}
\end{aligned}$$

The total time derivative of $V(\mathbf{x})$ defined in (B.69) along the closed-loop trajectories generated by (3.5) and (B.98) yields

$$\dot{V} \leq -\mathbf{e}_\omega^\top k_d \upsilon(4)\mathbf{e}_\omega + \beta_d \|\mathbf{e}_\omega\|. \qquad \text{(B.100)}$$

Accordingly, $\dot{V} < 0$ for $\|\mathbf{e}_\omega\| > \beta_d/(k_d\upsilon(4)) := \delta$, and as β_d increases, it can be counteracted by increasing the controller gain k_d, or in other words: given any δ and β_d, choosing $k_d > \beta_d/(\delta\upsilon(4))$ secures that $\dot{V}(\mathbf{x}) < 0$ until $\|\mathbf{e}_\omega\| < \delta$ such that the state is secured within the open ball $\mathcal{B}_\delta$. Since V is positive definite and proper we obtain that $\|\mathbf{e}_\omega(t)\|$ is bounded that is, for any $r > 0$ there exists $\Delta(r) > 0$ such that $\sup_{t \geq t_0}\|\mathbf{e}_\omega(t)\| \leq \Delta$ for all initial conditions $\|\mathbf{x}(t_0)\| < r$, $t_0 \geq 0$. For any Δ, let $\lambda(\Delta) > 0$ be a constant to be determined. Consider the LFC

$$\mathcal{V}(\mathbf{x}) = V(\mathbf{x}) + \lambda W(\mathbf{x}) \qquad \text{(B.101)}$$

where $W(\mathbf{x})$ is defined in (B.76). By differentiation along closed-loop trajectories, we obtain

$$\begin{aligned}\dot{\mathcal{V}} =& -\mathbf{e}_\omega^\top k_d \beta(\|\mathbf{e}_\omega\|)\upsilon(\|\mathbf{e}_q\|^2)\mathbf{e}_\omega + \beta_d\|\mathbf{e}_\omega\| \\ &+ \lambda \mathbf{e}_\omega \mathbf{T}_e^\top \mathbf{T}_e \mathbf{J}\mathbf{e}_\omega + \lambda \mathbf{e}_q^\top \dot{\mathbf{T}}_e \mathbf{J}\mathbf{e}_\omega \\ &+ \lambda \mathbf{e}_q^\top \mathbf{T}_e \left(\mathbf{S}(\mathbf{J}\boldsymbol{\omega}) - k_d\beta(\|\mathbf{e}_\omega\|^2)\upsilon(\|\mathbf{e}_q\|^2)\mathbf{I}\right)\mathbf{e}_\omega \\ &- \lambda \mathbf{e}_q^\top \mathbf{T}_e k_p \alpha(\|\mathbf{e}_q\|^2)\mathbf{T}_e^\top \mathbf{e}_q + \lambda\beta_d\|\mathbf{e}_q^\top \mathbf{T}_e\|. \end{aligned} \tag{B.102}$$

By inserting $\dot{\mathbf{T}}_e\mathbf{e}_q = \mathbf{G}(\tilde{\mathbf{q}})\mathbf{e}_\omega$, where $\mathbf{G}(\tilde{\mathbf{q}}) = 1/2[\tilde{\eta}\mathbf{I} + \mathbf{S}(\tilde{\boldsymbol{\epsilon}})] - \mathbf{I}/4$, and notice that $\|\mathbf{T}_e^\top \mathbf{T}_e\| = \mathbf{I}/4$ and $\|\mathbf{e}_q\mathbf{T}_e^\top\| \leq \|\mathbf{e}_q\|$, we obtain

$$\begin{aligned}\dot{\mathcal{V}} \leq& -\mathbf{e}_\omega^\top k_d \beta(\|\mathbf{e}_\omega\|^2)\upsilon(\|\mathbf{e}_q\|^2)\mathbf{e}_\omega + \frac{\lambda}{2}\mathbf{e}_\omega[\tilde{\eta}\mathbf{I} + \mathbf{S}(\tilde{\boldsymbol{\epsilon}})]\mathbf{J}\mathbf{e}_\omega \\ &+ \lambda \mathbf{e}_q^\top \mathbf{T}_e \left(\mathbf{S}(\mathbf{J}\boldsymbol{\omega}) - k_d\beta(\|\mathbf{e}_\omega\|^2)\upsilon(\|\mathbf{e}_q\|^2)\mathbf{I}\right)\mathbf{e}_\omega \\ &- \lambda \mathbf{e}_q^\top \mathbf{T}_e k_p \alpha(\|\mathbf{e}_q\|^2)\mathbf{T}_e^\top \mathbf{e}_q + 2\beta_d\|\mathbf{x}\| \end{aligned} \tag{B.103}$$

$$= -\mathbf{x}^\top \mathbf{P}\mathbf{x} + 2\beta_d\|\mathbf{x}\|, \tag{B.104}$$

for $\lambda \leq 1$, and where $\mathbf{P} = [\mathbf{p}_{ij}]$, $i, j = 1, 2$ with

$$\begin{aligned}\mathbf{p}_{11} &= k_d\beta(\|\mathbf{e}_\omega\|^2)\upsilon(\|\mathbf{e}_q\|^2)\mathbf{I} - \frac{\lambda}{2}[\tilde{\eta}\mathbf{I} + \mathbf{S}(\tilde{\boldsymbol{\epsilon}})]\mathbf{J} \\ \mathbf{p}_{12} &= \mathbf{q}_{21}^\top = \frac{\lambda}{2}\mathbf{T}_e\left[-\mathbf{S}(\mathbf{J}\boldsymbol{\omega}) + k_d\beta(\|\mathbf{e}_\omega\|^2)\upsilon(\|\mathbf{e}_q\|^2)\mathbf{I}\right] \\ \mathbf{p}_{22} &= \lambda\mathbf{T}_e k_p \alpha(\|\mathbf{e}_q\|^2)\mathbf{T}_e^\top. \end{aligned} \tag{B.105}$$

Since $\boldsymbol{\omega} = \mathbf{e}_\omega + \boldsymbol{\omega}_d$, and both $\|\mathbf{e}_\omega\| \leq \Delta$ and $\|\boldsymbol{\omega}_d\| \leq \beta_{\omega_d}$ are bounded, we conclude that there exists a bound $\|\boldsymbol{\omega}\| \leq \zeta(\Delta, \beta_{\omega_d})$ and thus $\|\mathbf{S}(\mathbf{J}\boldsymbol{\omega})\| \leq \tilde{\zeta}(\Delta, \beta_{\omega_d})$. To find a quadratic upper-bound on $-\mathbf{x}^\top\mathbf{P}\mathbf{x}$ we use $2|ab| \leq a^2 + b^2$ for any $a, b \in \mathbb{R}$ to obtain

$$\mathbf{x}^\top \mathbf{P}\mathbf{x} \geq (p_{11,m} - p_{12,M})\|\mathbf{e}_q\|^2 + (p_{22,m} - p_{12,M})\|\mathbf{e}_\omega\|^2 \tag{B.106}$$

where $p_{ij,m}$ and $p_{ij,M}$ denotes lower and upper bounds on the induced norms of the submatrices $\mathbf{q}_{ij}$, respectively, to ensure that

$$\begin{aligned} p_{11,m} \geq& 2p_{12,M} \\ p_{22,m} \geq& 2p_{12,M}, \end{aligned} \tag{B.107}$$

resulting in

$$\mathbf{x}^\top \mathbf{P}\mathbf{x} \geq \frac{1}{2}\left(p_{11,m}\|\mathbf{e}_q\|^2 + p_{22,m}\|\mathbf{e}_\omega\|^2\right). \tag{B.108}$$

To fulfill (B.107) we need to choose

$$\begin{aligned} \lambda \leq& \frac{2k_d\upsilon(4)}{\tilde{\zeta}(\Delta, \beta_d) + k_d\beta(\Delta^2) + \beta_J} \\ k_p \geq& 2\left[\tilde{\zeta}(\Delta, \beta_d) + k_d\beta(\Delta^2)\right], \end{aligned} \tag{B.109}$$

and hence

$$\dot{\mathcal{V}} \leq -p_m\|\mathbf{x}\|^2 + 2\beta_d\|\mathbf{x}\|, \tag{B.110}$$

where p_m is the smallest eigenvalue of $\mathbf{P}$. Accordingly, $\dot{\mathcal{V}} < 0$ when $\|\mathbf{x}\| > \delta' =: 2\beta_d/p_m$, thus increasing the controller gains will ensure that the states of the closed-loop system will converge from any allowed initial conditions to a ball in close vicinity of the origin, and this ball can be diminished arbitrarily by increasing the controller gains, and thus conclude that the equilibrium point $(\mathbf{e}_q, \mathbf{e}_\omega) \to (\mathbf{0}, \mathbf{0})$ is UPAS.

The proof for the negative equilibrium follows *mutatis mutandis*.

B.12 Proof of Theorem 3.11

Without loss of generality, we show stability of the positive equilibrium point *i.e.*, let $\mathbf{e}_q = \mathbf{e}_{q+}$ and $\mathbf{T}_e = \mathbf{T}_e(\mathbf{e}_{q+})$.

We start by calculating the error dynamics. We have

$$\mathbf{e}_\omega = \boldsymbol{\omega}^b_{i,b} - \boldsymbol{\omega}^b_{i,d} \tag{B.111}$$

$$\dot{\mathbf{e}}_\omega = \dot{\boldsymbol{\omega}}^b_{i,b} - \dot{\boldsymbol{\omega}}^b_{i,d}, \tag{B.112}$$

and by inserting (2.83)and (3.24) we obtain

$$\dot{\mathbf{e}}_\omega = \mathbf{J}^{-1}[-\mathbf{S}(\boldsymbol{\omega}_{i,b})\mathbf{J}\boldsymbol{\omega}^b_{i,b} + \boldsymbol{\tau}_a + \boldsymbol{\tau}_d] + \mathbf{S}(\boldsymbol{\omega}^b_{i,b})\boldsymbol{\omega}^b_{i,d} - \mathbf{R}^b_i\dot{\boldsymbol{\omega}}^i_{i,d}. \tag{B.113}$$

Then, we insert the control law (3.27) and observe that $\mathbf{S}(\boldsymbol{\omega}^b_{i,b})\boldsymbol{\omega}^b_{i,d} = -\mathbf{S}(\boldsymbol{\omega}^b_{i,d})\boldsymbol{\omega}^b_{i,b} = -\mathbf{S}(\boldsymbol{\omega}^b_{i,d})(\mathbf{e}_\omega + \boldsymbol{\omega}^b_{i,d}) = -\mathbf{S}(\boldsymbol{\omega}^b_{i,d})\mathbf{e}_\omega$ to obtain

$$\begin{aligned}\dot{\mathbf{e}}_\omega =& \mathbf{J}^{-1}[\mathbf{S}(\mathbf{J}\boldsymbol{\omega}^b_{i,b})\boldsymbol{\omega}^b_{i,b} + \mathbf{J}\mathbf{a}_d - \mathbf{S}(\mathbf{J}\boldsymbol{\omega}^b_{i,e})\boldsymbol{\omega}^b_{i,d} - k_p e^{k_1\mathbf{e}_q^\top\mathbf{e}_q}\mathbf{T}_e^\top\mathbf{e}_q \\ & - k_d e^{-k_2\mathbf{e}_q^\top\mathbf{e}_q}\boldsymbol{\omega}^b_{d,e} + \boldsymbol{\tau}_d] - \mathbf{R}^b_i\dot{\boldsymbol{\omega}}^i_{i,d} - \mathbf{S}(\boldsymbol{\omega}^b_{i,d})\mathbf{e}_\omega.\end{aligned} \tag{B.114}$$

Next, we use $\boldsymbol{\omega}^b_{i,b} = \mathbf{e}_\omega + \boldsymbol{\omega}^b_{i,d}$, $\boldsymbol{\omega}^b_{i,e} = \boldsymbol{\omega}^b_{i,b} - \mathbf{e}_{e\omega}$ and $\boldsymbol{\omega}^b_{d,e} = \boldsymbol{\omega}^b_{d,b} + \boldsymbol{\omega}^b_{b,e} = \mathbf{e}_\omega - \mathbf{e}_{e\omega}$ to obtain

$$\begin{aligned}\dot{\mathbf{e}}_\omega =& \mathbf{J}^{-1}[\mathbf{S}(\mathbf{J}\boldsymbol{\omega}^b_{i,b})(\mathbf{e}_\omega + \boldsymbol{\omega}^b_{i,d}) - \mathbf{S}(\mathbf{J}[\boldsymbol{\omega}^b_{i,b} - \mathbf{e}_{e\omega}])\boldsymbol{\omega}^b_{i,d} \\ & - k_p e^{k_1\mathbf{e}_q^\top\mathbf{e}_q}\mathbf{T}_e^\top\mathbf{e}_q - k_d e^{-k_2\mathbf{e}_q^\top\mathbf{e}_q}(\mathbf{e}_\omega - \mathbf{e}_{e\omega}) - \mathbf{J}\mathbf{S}(\boldsymbol{\omega}^b_{i,d})\mathbf{e}_\omega + \boldsymbol{\tau}_d]\end{aligned} \tag{B.115}$$

$$\begin{aligned}=& \mathbf{J}^{-1}[\mathbf{S}(\mathbf{J}\boldsymbol{\omega}^b_{i,b})\mathbf{e}_\omega + \mathbf{S}(\mathbf{J}\mathbf{e}_{e\omega})\boldsymbol{\omega}^b_{i,d} - k_p e^{k_1\mathbf{e}_q^\top\mathbf{e}_q}\mathbf{T}_e^\top\mathbf{e}_q \\ & - k_d e^{-k_2\mathbf{e}_q^\top\mathbf{e}_q}(\mathbf{e}_\omega - \mathbf{e}_{e\omega}) - \mathbf{J}\mathbf{S}(\boldsymbol{\omega}^b_{i,d})\mathbf{e}_\omega + \boldsymbol{\tau}_d].\end{aligned} \tag{B.116}$$

For the estimator dynamics we have

$$\mathbf{e}_{e\omega} = \boldsymbol{\omega}^b_{i,b} - \boldsymbol{\omega}^b_{i,e} \tag{B.117}$$

$$\dot{\mathbf{e}}_{e\omega} = \dot{\boldsymbol{\omega}}^b_{i,b} - \dot{\boldsymbol{\omega}}^b_{i,e}, \tag{B.118}$$

and by inserting (2.83) and the derivative of (3.29) we obtain

$$\begin{aligned}\dot{\mathbf{e}}_{e\omega} =&\mathbf{J}^{-1}[-\mathbf{S}(\boldsymbol{\omega}_{i,b}^b)\mathbf{J}\boldsymbol{\omega}_{i,b}^b + \boldsymbol{\tau}_a + \boldsymbol{\tau}_d] - \dot{\mathbf{z}} \\ &- 2\mathbf{J}^{-1}l_d[\dot{\mathbf{T}}_{eq}^\top \mathbf{e}_{eq} + \mathbf{T}_{eq}^\top \dot{\mathbf{e}}_{eq}].\end{aligned} \tag{B.119}$$

Furthermore, we insert (3.27) and (3.28), obtaining

$$\begin{aligned}\dot{\mathbf{e}}_{e\omega} =&\mathbf{J}^{-1}[\mathbf{S}(\mathbf{J}\boldsymbol{\omega}_{i,b}^b)\boldsymbol{\omega}_{i,b}^b + \mathbf{J}\mathbf{a}_d - \mathbf{S}(\mathbf{J}\boldsymbol{\omega}_{i,e})\boldsymbol{\omega}_{i,d}^b - k_p e^{k_1 \mathbf{e}_q^\top \mathbf{e}_q}\mathbf{T}_e^\top \mathbf{e}_q \\ &- k_d e^{-k_2 \mathbf{e}_q^\top \mathbf{e}_q}\boldsymbol{\omega}_{d,e}^b + \boldsymbol{\tau}_d] - \mathbf{a}_d - \mathbf{J}^{-1}[l_p e^{k_3 \mathbf{e}_{eq}^\top \mathbf{e}_{eq}}\mathbf{T}_{eq}^\top \mathbf{e}_{eq} - k_p e^{k_1 \mathbf{e}_q^\top \mathbf{e}_q}\mathbf{T}_e^\top \mathbf{e}_q] \\ &- \mathbf{J}^{-1}\frac{l_d}{2}[\eta_{e,b}\mathbf{I} + \mathbf{S}(\boldsymbol{\epsilon}_{e,b})]\mathbf{e}_{e\omega}\end{aligned} \tag{B.120}$$

$$\begin{aligned}=&\mathbf{J}^{-1}\{\mathbf{S}(\mathbf{J}\boldsymbol{\omega}_{i,b}^b)(\mathbf{e}_\omega + \boldsymbol{\omega}_{i,d}^b) - \mathbf{S}(\mathbf{J}[\boldsymbol{\omega}_{i,b} - \mathbf{e}_{e\omega}])\boldsymbol{\omega}_{i,d}^b + \boldsymbol{\tau}_d \\ &- k_d e^{-k_2 \mathbf{e}_q^\top \mathbf{e}_q}(\mathbf{e}_\omega - \mathbf{e}_{e\omega}) - l_p e^{k_3 \mathbf{e}_{eq}^\top \mathbf{e}_{eq}}\mathbf{T}_{eq}^\top \mathbf{e}_{eq} - \frac{l_d}{2}[\eta_{e,b}\mathbf{I} + \mathbf{S}(\boldsymbol{\epsilon}_{e,b})]\mathbf{e}_{e\omega}\} \\ =&\mathbf{J}^{-1}\{\mathbf{S}(\mathbf{J}\boldsymbol{\omega}_{i,b}^b)\mathbf{e}_\omega - k_d e^{-k_2 \mathbf{e}_q^\top \mathbf{e}_q}\mathbf{e}_\omega + \mathbf{S}(\mathbf{J}\mathbf{e}_{e\omega})\boldsymbol{\omega}_{i,d}^b + k_d e^{-k_2 \mathbf{e}_q^\top \mathbf{e}_q}\mathbf{e}_{e\omega} \\ &- \frac{l_d}{2}[\eta_{e,b}\mathbf{I} + \mathbf{S}(\boldsymbol{\epsilon}_{e,b})]\mathbf{e}_{e\omega} - l_p e^{k_3 \mathbf{e}_{eq}^\top \mathbf{e}_{eq}}\mathbf{T}_{eq}^\top \mathbf{e}_{eq} + \boldsymbol{\tau}_d\}.\end{aligned} \tag{B.121}$$

Hence, the error dynamics can be written on state space form $\dot{\mathbf{x}} = f(t, \mathbf{x})$, $\mathbf{x} = [\mathbf{e}_q^\top,\ \mathbf{e}_\omega^\top,\ \mathbf{e}_{eq}^\top,\ \mathbf{e}_{e\omega}^\top]^\top$, with

$$f(t, \mathbf{x}) = \begin{bmatrix} \mathbf{T}_e \mathbf{e}_\omega \\ \mathbf{J}_l^{-1}\xi_1 \\ \mathbf{T}_{eq}\mathbf{e}_{e\omega} \\ \mathbf{J}_l^{-1}\xi_2 \end{bmatrix}, \tag{B.122}$$

where

$$\begin{aligned}\xi_1 =&\mathbf{S}(\mathbf{J}\boldsymbol{\omega}_{i,b}^b)\mathbf{e}_\omega + \mathbf{S}(\mathbf{J}\mathbf{e}_{e\omega})\boldsymbol{\omega}_{i,d}^b - k_p e^{k_1 \mathbf{e}_q^\top \mathbf{e}_q}\mathbf{T}_e^\top \mathbf{e}_q \\ &- k_d e^{-k_2 \mathbf{e}_q^\top \mathbf{e}_q}(\mathbf{e}_\omega - \mathbf{e}_{e\omega}) - \mathbf{J}\mathbf{S}(\boldsymbol{\omega}_{b,d}^b)\boldsymbol{\omega}_{i,d}^b + \boldsymbol{\tau}_d,\end{aligned} \tag{B.123}$$

and

$$\begin{aligned}\xi_2 =&\mathbf{S}(\mathbf{J}\boldsymbol{\omega}_{i,b}^b)\mathbf{e}_\omega - k_d e^{-k_2 \mathbf{e}_q^\top \mathbf{e}_q}\mathbf{e}_\omega + \mathbf{S}(\mathbf{J}\mathbf{e}_{e\omega})\boldsymbol{\omega}_{i,d}^b \\ &+ k_d e^{-k_2 \mathbf{e}_q^\top \mathbf{e}_q}\mathbf{e}_{e\omega} - l_d[\eta_{e,b} + \mathbf{S}(\boldsymbol{\epsilon}_{e,b})]\mathbf{e}_{e\omega} \\ &- l_p e^{k_3 \mathbf{e}_{eq}^\top \mathbf{e}_{eq}}\mathbf{T}_{eq}^\top \mathbf{e}_{eq} + \boldsymbol{\tau}_d.\end{aligned} \tag{B.124}$$

The rest of the proof consists in showing that the conditions of Theorem A.8 hold[3]. Let Assumptions 3.2, 3.3 and 3.4 generate positive real numbers β_j, β_J, β_d, $\beta_{\boldsymbol{\omega}_{i,d}^b}$, $\beta_{\dot{\boldsymbol{\omega}}_{i,d}^b}$ such that $\beta_j \leq \|\mathbf{J}\| \leq \beta_J$, $\|\boldsymbol{\tau}_d^b(t)\| \leq \beta_d$, $\|\boldsymbol{\omega}_{i,d}^b(t)\| \leq \beta_{\boldsymbol{\omega}_{i,d}^b}$ and $\|\dot{\boldsymbol{\omega}}_{i,d}^b(t)\| \leq \beta_{\dot{\boldsymbol{\omega}}_{i,d}^b}$ for all $t \geq t_0 \geq 0$.

[3] That is, with the obvious modifications. Strictly speaking, we cannot show that the conditions of A.8 (which is tailored for systems defined on $\mathbb{R}^n$) hold for arbitrarily large initial conditions in view of the topology of S_e^3 and S_{eq}^3.

Consider the Lyapunov function candidate

$$\begin{aligned}
\mathcal{V}(\mathbf{x}) &:= V(\mathbf{x}) + \lambda W(\mathbf{x}) && \text{(B.125a)}\\
V(\mathbf{x}) &:= \frac{1}{2}\Big[\Big(\frac{k_p}{k_1}e^{k_1\mathbf{e}_q^\top\mathbf{e}_q} - 1\Big) + \mathbf{e}_\omega^\top\mathbf{J}\mathbf{e}_\omega && \text{(B.125b)}\\
&\quad + \Big(\frac{l_p}{k_3}e^{k_3\mathbf{e}_{eq}^\top\mathbf{e}_{eq}} - 1\Big) + \mathbf{e}_{e\omega}^\top\mathbf{J}\mathbf{e}_{e\omega}\Big]\\
W(\mathbf{x}) &:= \mathbf{e}_q^\top\mathbf{T}_e\mathbf{J}\mathbf{e}_\omega + \mathbf{e}_{eq}^\top\mathbf{T}_{eq}\mathbf{J}\mathbf{e}_{e\omega}, && \text{(B.125c)}
\end{aligned}$$

which is positive definite and proper, as we show next. We want to find functions $\underline{\alpha}(\mathbf{x}), \overline{\alpha}(\mathbf{x}) \in \mathcal{K}_\infty$ such that $\underline{\alpha}(\mathbf{x}) \leq \mathcal{V}(\mathbf{x}) \leq \overline{\alpha}(\mathbf{x})$. For the upper bound function we write

$$\begin{aligned}
\mathcal{V}(\mathbf{x}) \leq& \frac{1}{2}\left[\frac{k_p}{k_1}\left(e^{k_1\|\mathbf{x}\|^2} - 1\right) + \frac{l_p}{k_3}\left(e^{k_3\|\mathbf{x}\|^2} - 1\right) + 2\beta_J\|\mathbf{x}\|^2\right] + \lambda 2\beta_J\|\mathbf{x}\|^2 && \text{(B.126)}\\
\leq& \max\left\{\frac{k_p}{k_1}, \frac{l_p}{k_3}, 2\beta_J, 4\lambda\beta_J\right\}\left(e^{\max\{k_1,k_3\}\|\mathbf{x}\|^2} - 1 + \|\mathbf{x}\|^2\right). && \text{(B.127)}
\end{aligned}$$

We want to find a constant c_9 such that $e^{c_9\|\mathbf{x}\|^2} - 1 \geq \|\mathbf{x}\|^2$ that is,

$$c_9 \geq \sup_{\mathbf{x}\in\mathbb{R}^{14}} \frac{\ln(\|\mathbf{x}\|^2 + 1)}{\|\mathbf{x}\|^2} = 1$$

which in turn, leads us to define

$$\overline{\alpha}(\mathbf{x}) := \; c_{10}\left(e^{c_{11}\|\mathbf{x}\|^2} - 1\right), \tag{B.128}$$

where $c_{10} := 2\max\{k_p/k_1, l_p/k_3, 2\beta_J, 4\lambda\beta_J\}$ and $c_{11} := \max\{k_1, k_3, 1\}$. Now we find a quadratic lower bound on $\mathcal{V}(\mathbf{x})$. For this we remark that

$$\left(e^{k_1\mathbf{e}_q^\top\mathbf{e}_q} - 1\right) \geq k_1\mathbf{e}_q^\top\mathbf{e}_q, \tag{B.129}$$

which can be seen recalling that

$$e^x = \sum_{n=0}^{\infty}\frac{x^n}{n!} \geq 1 + x\,. \tag{B.130}$$

Similarly for $e^{k_3\mathbf{e}_{eq}^\top\mathbf{e}_{eq}} - 1$ hence we define

$$\underline{\alpha}(\mathbf{x}) := \mathbf{x}^\top p_m\mathbf{x} \tag{B.131}$$

where $p_m > 0$ is the smallest eigenvalue of

$$\mathbf{P} := \frac{1}{2}\begin{bmatrix} k_p\mathbf{I} & \lambda\mathbf{T}_e\mathbf{J} & \mathbf{0} & \mathbf{0} \\ \lambda\mathbf{J}\mathbf{T}_e^\top & \mathbf{J} & \mathbf{0} & \mathbf{0} \\ \mathbf{0} & \mathbf{0} & l_p\mathbf{I} & \lambda\mathbf{T}_{eq}\mathbf{J} \\ \mathbf{0} & \mathbf{0} & \lambda\mathbf{J}\mathbf{T}_{eq}^\top & \mathbf{J} \end{bmatrix}. \tag{B.132}$$

Next, we evaluate the total time derivative of $\mathcal{V}(\mathbf{x})$ along the closed-loop trajectories. To that end, we first compute the derivative of $V(\mathbf{x})$. We have

$$\begin{aligned}\dot{V} =& -k_d e^{-k_2 \mathbf{e}_q^\top \mathbf{e}_q} \mathbf{e}_\omega^\top \mathbf{e}_\omega + \mathbf{e}_\omega^\top \mathbf{S}(\mathbf{J}\mathbf{e}_{e\omega})\boldsymbol{\omega}_{i,d}^b \\ &- \mathbf{e}_\omega \mathbf{J}\mathbf{S}(\boldsymbol{\omega}_{b,d}^b)\boldsymbol{\omega}_{i,d}^b + \mathbf{e}_{e\omega}^\top \mathbf{S}(\mathbf{J}\boldsymbol{\omega}_{i,b}^b)\mathbf{e}_\omega \\ &+ \mathbf{e}_{e\omega}\mathbf{S}(\mathbf{J}\mathbf{e}_{e\omega})\boldsymbol{\omega}_{i,d}^b - \left(l_d \eta_{e,b} - k_d e^{-k_2 \mathbf{e}_q^\top \mathbf{e}_q}\right) \mathbf{e}_{e\omega}^\top \mathbf{e}_{e\omega} \\ &+ \left(\mathbf{e}_\omega^\top + \mathbf{e}_{e\omega}^\top\right) \boldsymbol{\tau}_d. \end{aligned} \tag{B.133}$$

Since the matrix $\mathbf{S}(\cdot)$ is linear in its arguments, we have (Caccavale and Villani, 1999)

$$\|\mathbf{S}(\mathbf{J}\mathbf{a})\mathbf{b}\| \leq \beta_J \|\mathbf{a}\| \|\mathbf{b}\|. \tag{B.134}$$

By applying (B.134), Young's inequality (Young, 1912) and Assumptions 3.2 and 3.3 we have

$$\mathbf{e}_\omega^\top \mathbf{S}(\mathbf{J}\mathbf{e}_{e\omega})\boldsymbol{\omega}_{i,d}^b \leq \frac{1}{2}\beta_J \beta_{\boldsymbol{\omega}_{i,d}^b} (\|\mathbf{e}_\omega\|^2 + \|\mathbf{e}_{e\omega}\|^2) \tag{B.135}$$

$$\mathbf{e}_\omega \mathbf{J}\mathbf{S}(\boldsymbol{\omega}_{b,d}^b)\boldsymbol{\omega}_{i,d}^b \leq \beta_J \beta_{\boldsymbol{\omega}_{i,d}^b} \|\mathbf{e}_\omega\|^2 \tag{B.136}$$

$$\mathbf{e}_{e\omega}^\top \mathbf{S}(\mathbf{J}\boldsymbol{\omega}_{i,b}^b)\mathbf{e}_\omega \leq \frac{1}{2}\beta_J (\|\mathbf{e}_\omega\|^2 + \|\mathbf{e}_{e\omega}\|^2)(\|\mathbf{e}_\omega\| + \beta_{\boldsymbol{\omega}_{i,d}^b}) \tag{B.137}$$

$$\mathbf{e}_{e\omega}\mathbf{S}(\mathbf{J}\mathbf{e}_{e\omega})\boldsymbol{\omega}_{i,d}^b \leq \beta_J \beta_{\boldsymbol{\omega}_{i,d}^b} \|\mathbf{e}_{e\omega}\|^2. \tag{B.138}$$

Inserting the bounds (B.135)–(B.138) into (B.133), and applying the fact that $\mathbf{e}_q^\top \mathbf{e}_q < 2$ for $\tilde{\eta} > 0$ we obtain

$$\dot{V} \leq -\phi(k_d, \|\mathbf{e}_\omega\|)\|\mathbf{e}_\omega\|^2 - \psi(k_d, l_d, \|\mathbf{e}_\omega\|)\|\mathbf{e}_{e\omega}\|^2 + 2\beta_d(\|\mathbf{e}_\omega\| + \|\mathbf{e}_{e\omega}\|), \tag{B.139}$$

$$\phi(k_d, \|\mathbf{e}_\omega\|) := k_d e^{-2k_2} - \beta_J \left(6\beta_{\boldsymbol{\omega}_{i,d}^b} + \|\mathbf{e}_\omega\|\right) \tag{B.140a}$$

$$\psi(k_d, l_d, \|\mathbf{e}_\omega\|) := l_d \delta_\eta - k_d - \frac{1}{2}\beta_J (2\beta_{\boldsymbol{\omega}_{i,d}^b} + \|\mathbf{e}_\omega\|) \tag{B.140b}$$

That is, $\dot{V}$ is negative semi-definite for bounded values of $\mathbf{e}_\omega$ and sufficiently large gains. Hence, the total time derivative of $\mathcal{V}$ along the closed-loop trajectories yields[4]

$$\dot{\mathcal{V}} \leq = -\mathbf{x}^\top \mathbf{Q}(\boldsymbol{\omega}_{i,b}^b)\mathbf{x} + 2\beta_d \|\mathbf{x}\| \tag{B.141}$$

[4] Clearly, $\mathbf{Q}$ depends on other variables besides $\boldsymbol{\omega}_{i,b}^b$ however, only the dependence on the latter is made explicit for further use and to avoid a cumbersome notation.

where $\mathbf{Q} := [\mathbf{q}_{ij}]$, $i, j = 1, 2, 3, 4$ with

$$\mathbf{q}_{11} = \lambda \mathbf{T}_e k_p e^{k_1 \mathbf{e}_q^\top \mathbf{e}_q} \mathbf{T}_e^\top \tag{B.142}$$

$$\mathbf{q}_{12} = \mathbf{q}_{21}^\top = \frac{\lambda}{2} \mathbf{T}_e \left[k_d e^{-k_2 \mathbf{e}_q^\top \mathbf{e}_q} \mathbf{I} - \mathbf{S}(\mathbf{J}\boldsymbol{\omega}_{i,b}^b) - \mathbf{J}\mathbf{S}(\boldsymbol{\omega}_{i,d}^b) \right] \tag{B.143}$$

$$\mathbf{q}_{13} = \mathbf{q}_{31}^\top = \mathbf{0} \tag{B.144}$$

$$\mathbf{q}_{14} = \mathbf{q}_{41}^\top = \frac{\lambda}{2} \mathbf{T}_e \left[\mathbf{S}(\boldsymbol{\omega}_{i,d}^b)\mathbf{J} - k_d e^{-k_2 \mathbf{e}_q^\top \mathbf{e}_q} \mathbf{I} \right] \tag{B.145}$$

$$\mathbf{q}_{22} = \phi(k_d, \|\mathbf{e}_\omega\|) - \frac{\lambda}{2} \left[\tilde{\eta} \mathbf{I} + \mathbf{S}(\tilde{\boldsymbol{\epsilon}}) \right] \mathbf{J} \tag{B.146}$$

$$\mathbf{q}_{23} = \mathbf{q}_{32}^\top = \frac{\lambda}{2} \left[k_d e^{-k_2 \mathbf{e}_q^\top \mathbf{e}_q} \mathbf{I} - \mathbf{S}(\mathbf{J}\boldsymbol{\omega}_{i,b}^b) \right] \mathbf{T}_{eq}^\top \tag{B.147}$$

$$\mathbf{q}_{24} = \mathbf{q}_{42}^\top = \mathbf{0} \tag{B.148}$$

$$\mathbf{q}_{33} = \lambda \mathbf{T}_{eq} l_p e^{k_3 \mathbf{e}_{eq}^\top \mathbf{e}_{eq}} \mathbf{T}_{eq}^\top \tag{B.149}$$

$$\mathbf{q}_{34} = \mathbf{q}_{43}^\top = \frac{\lambda}{2} \mathbf{T}_{eq} \Big\{ \mathbf{S}(\boldsymbol{\omega}_{i,d}^b)\mathbf{J} + l_d \left[\eta_{e,b} \mathbf{I} + \mathbf{S}(\boldsymbol{\epsilon}_{e,b}) \right] - k_d e^{-k_2 \mathbf{e}_q^\top \mathbf{e}_q} \mathbf{I} \Big\} \tag{B.150}$$

$$\mathbf{q}_{44} = \psi(k_d, l_d, \|\mathbf{e}_\omega\|) - \frac{\lambda}{2} [\eta_{e,b} \mathbf{I} + \mathbf{S}(\boldsymbol{\epsilon}_{e,b})] \mathbf{J}. \tag{B.151}$$

We then apply Lemma 3.1 and a similar reasoning is used for $\mathbf{e}_{eq}$. We conclude that there exist lower and upper bounds $q_{ij,m}$ and $q_{ij,M}$ on the norms of the sub-blocks $\mathbf{q}_{ij}$ of $\mathbf{Q}$ respectively.

Next, we apply $2|ab| \leq a^2 + b^2$ for any $a, b \in \mathbb{R}$ to obtain

$$\begin{aligned} \mathbf{x}^\top \mathbf{Q} \mathbf{x} \geq & (q_{11,m} - q_{12,M} - q_{13,M} - q_{14,M}) \|\mathbf{e}_q\|^2 \\ & + (q_{22,m} - q_{21,M} - q_{23,M} - q_{24,M}) \|\mathbf{e}_\omega\|^2 \\ & + (q_{33,m} - q_{31,M} - q_{32,M} - q_{34,M}) \|\mathbf{e}_{eq}\|^2 \\ & + (q_{44,m} - q_{41,M} - q_{42,M} - q_{43,M}) \|\mathbf{e}_{e\omega}\|^2 \end{aligned} \tag{B.152}$$

so, for sufficiently large $q_{ii,m}$, we have

$$\mathbf{x}^\top \mathbf{Q} \mathbf{x} \ \geq \frac{1}{2} (q_{11,m} \|\mathbf{e}_q\|^2 + q_{22,m} \|\mathbf{e}_\omega\|^2 + q_{33m} \|\mathbf{e}_{eq}\|^2 + q_{44m} \|\mathbf{e}_{e\omega}\|^2). \tag{B.153}$$

Now, for any given Δ_ω let $\mathbf{e}_\omega \leq \Delta_\omega$. Hence $\boldsymbol{\omega}_{i,b}^b = \mathbf{e}_\omega + \boldsymbol{\omega}_{i,d}^b$ satisfies $\|\boldsymbol{\omega}_{i,b}^b\| \leq \Delta$ with $\Delta := \Delta_\omega + \beta_{\omega_{i,d}^b}$. It follows that (B.153) holds if, defining

$$k_p^\star := 2\beta_J \Delta, \tag{B.154}$$

$$l_p^\star := 2 \left[\beta_j (\Delta + \beta_{\omega_{i,d}^b}) + l_d \right], \tag{B.155}$$

we impose $k_p > k_p^\star$, $l_p > l_p^\star$, and

$$\lambda \leq \min \left\{ \frac{\phi(k_d, \Delta_\omega)}{k_d + \frac{1}{2}\beta_J (1 + 2\Delta + \beta_{\omega_{i,d}^b})}, \quad \frac{\psi(k_d, l_d, \Delta_\omega)}{k_d + \frac{1}{2}\beta_J (1 + 2\beta_{\omega_{i,d}^b} + l_d)}, 1 \right\}.$$

Thus,

$$\dot{\mathcal{V}} \leq -q_m\|\mathbf{x}\|^2 + 2\beta_d\|\mathbf{x}\|, \tag{B.156}$$

where $q_m(\Delta) > 0$ is a lower bound on the smallest eigenvalue of $\mathbf{Q}(\Delta)$. The derivative $\dot{\mathcal{V}}(\mathbf{x}) < 0$ for all $\mathbf{x} \in \mathcal{H} := \{\mathbf{x} \in S^3_{e+} \times \mathbb{R}^3 \times S^3_{eq} \times \mathbb{R}^3 : \delta \leq \|\mathbf{x}\| \leq \Delta\}$, where $\delta := 2\beta_d/q_m$.

According to (Chaillet and Loría, 2008, Theorem 10) we verify the growth conditions on $\underline{\alpha}^{-1} \circ \overline{\alpha}(s)$ and $\overline{\alpha}^{-1} \circ \underline{\alpha}(s)$. Given any positive constants $\delta^\star$, $\Delta^\star$ such that $\delta^\star < \Delta^\star$, there exist control gains generating $0 < \delta < \Delta$ such that

$$\underline{\alpha}^{-1} \circ \overline{\alpha}(\delta) = \sqrt{\frac{c_{10}(\Delta)\left(e^{c_{11}\delta^2} - 1\right)}{p_m}} \leq \delta^\star\,. \tag{B.157}$$

This holds because δ decreases while c_{10} and p_m increase monotonically with the gains, and c_{11} is independent of δ, c_{10} and p_m. On the other hand, Δ, c_{10} and p_m may be increased with the control gains to satisfy

$$\overline{\alpha}^{-1} \circ \underline{\alpha}(\Delta) = \sqrt{\frac{\ln\left(\frac{p_m\Delta^2+1}{c_{10}(\Delta)}\right)}{c_{11}}} \geq \Delta^\star \tag{B.158}$$

We invoke (Chaillet and Loría, 2008, Theorem 10) to conclude that the equilibrium point $(\mathbf{e}_q, \mathbf{e}_\omega, \mathbf{e}_{eq}, \mathbf{e}_{e\omega}) = (\mathbf{0}, \mathbf{0}, \mathbf{0}, \mathbf{0})$ of the closed loop system is uniformly practically asymptotically stable.

The proof for the negative equilibrium $(\mathbf{e}_{q-}, \mathbf{e}_\omega, \mathbf{e}_{eq}, \mathbf{e}_{e\omega}) = (\mathbf{0}, \mathbf{0}, \mathbf{0}, \mathbf{0})$ follows *mutatis mutandis*.

B.13 Proof of Theorem 3.12

Without loss of generality let $\mathbf{e}_q = \mathbf{e}_{q+}$, $\mathbf{T}_e = \mathbf{T}_e(\mathbf{e}_{q+})$, and $\mathbf{x} := [\mathbf{e}_q^\top,\, \mathbf{e}_\omega^\top,\, \mathbf{e}_{eq}^\top,\, \mathbf{e}_{e\omega}^\top]^\top$. The error dynamics takes the form $\dot{\mathbf{x}} = f(t, \mathbf{x})$ from (B.122)–(B.124), and the rest of the proof consists in showing that the conditions of (Chaillet and Loría, 2008, Theorem 10) hold restricted to the domain of interest.

Let Assumptions 3.2, 3.3 and 3.4 generate positive real numbers β_j, β_J, β_d, $\beta_{\omega^b_{i,d}}$, $\beta_{\dot{\omega}^b_{i,d}}$ such that $\beta_j \leq \|\mathbf{J}\| \leq \beta_J$, $\|\boldsymbol{\tau}^b_d(t)\| \leq \beta_d$, $\|\boldsymbol{\omega}^b_{i,d}(t)\| \leq \beta_{\omega^b_{i,d}}$ and $\|\dot{\boldsymbol{\omega}}^b_{i,d}(t)\| \leq \beta_{\dot{\omega}^b_{i,d}}$ for all $t \geq t_0 \geq 0$. Given any δ, δ_η, a and b let them generate a set $\mathcal{R}$ as in the statement and consider the Lyapunov function candidate $\mathcal{V} : \mathcal{R} \to \mathbb{R}$,

$$\begin{aligned}
\mathcal{V}(\mathbf{x}) &= V(\mathbf{x}) + \lambda W(\mathbf{x}) \qquad \text{where} && \text{(B.159a)}\\
V(\mathbf{x}) &= \frac{1}{2}\Big[\Big(\frac{k_p}{k_1}e^{k_1\mathbf{e}_q^\top\mathbf{e}_q} - 1\Big) + \mathbf{e}_\omega^\top\mathbf{J}\mathbf{e}_\omega && \text{(B.159b)}\\
&\quad + \Big(\frac{l_p}{k_3}e^{k_3\mathbf{e}_{eq}^\top\mathbf{e}_{eq}} - 1\Big) + \mathbf{e}_{e\omega}^\top\mathbf{J}\mathbf{e}_{e\omega}\Big]\\
W(\mathbf{x}) &= \mathbf{e}_q^\top\mathbf{T}_e\mathbf{J}\mathbf{e}_\omega + \mathbf{e}_{eq}^\top\mathbf{T}_{eq}\mathbf{J}\mathbf{e}_{e\omega}, && \text{(B.159c)}
\end{aligned}$$

where we find functions $\underline{\alpha}, \overline{\alpha} \in \mathcal{K}_\infty$ such that $\underline{\alpha}(\mathbf{x}) \leq \mathcal{V}(\mathbf{x}) \leq \overline{\alpha}(\mathbf{x})$ according to (B.131) and (B.131). Now we evaluate the total time derivative of $\mathcal{V}$ along

the closed-loop trajectories obtaining (B.133). Furthermore, by applying (B.135)–(B.138) we obtain (B.139)–(B.140), and we see that ϕ and ψ are positive definite for all $\|\mathbf{e}_\omega\| \in [0, a)$ and $\eta_{e,b} \geq \delta_\eta$. Further direct computations show that the total time derivative of $\mathcal{V}$ along the closed-loop trajectories yields (B.141) with $\mathbf{Q} = [\mathbf{q}_{ij}]$, $i, j = 1, 2, 3, 4$ as in (B.142)–(B.151). We claim that there exist lower and upper bounds $q_{ij,m}$ and $q_{ij,M}$ on the norms of each sub-block $\mathbf{q}_{ij}$ of $\mathbf{Q}$. This follows under Assumptions 3.2 and 3.3, for all $\mathbf{x} \in \mathcal{R}$ and in view of Lemma 3.1 stating that

$$\mathbf{e}_q^\top \mathbf{T}_e \mathbf{T}_e^\top \mathbf{e}_q \geq \frac{1}{8} \mathbf{e}_q^\top \mathbf{e}_q, \tag{B.160}$$

which is implied by the quaternion constraint, and $\|\mathbf{e}_\omega\| \in [0, a)$ and Assumption 3.2 imply that $\boldsymbol{\omega}_{i,b}^b = \mathbf{e}_\omega + \boldsymbol{\omega}_{i,d}^b$ satisfies $\|\boldsymbol{\omega}_{i,b}^b\| \leq \Delta$ with $\Delta := \Delta_\omega + \beta_{\omega_{i,d}^b}$. Therefore, the claim follows by applying the triangle inequality on each cross term $\mathbf{x}_k^\top \mathbf{q}_{i,j} \mathbf{x}_l$ for all suitable indexes. Next, define

$$k_p^\star := 2 j_M \Delta, \tag{B.161}$$

$$l_p^\star := 2 \left[j_m (\Delta + \beta_{\omega_{i,d}^b}) + l_d \right]; \tag{B.162}$$

let $k_p > k_p^\star$, $l_p > l_p^\star$,

$$\lambda \leq \min \left\{ \frac{\phi(k_d, \Delta_\omega)}{k_d + \frac{1}{2} j_M (1 + 2\Delta + \beta_{\omega_{i,d}^b})}, \quad \frac{\psi(k_d, l_d, \Delta_\omega)}{k_d + \frac{1}{2} j_M (1 + 2\beta_{\omega_{i,d}^b} + l_d)}, 1 \right\}$$

and let $q_m(\Delta) > 0$ be a lower bound on the smallest eigenvalue of $\mathbf{Q}(\Delta)$. It follows that

$$\dot{\mathcal{V}} \leq -q_m \|\mathbf{x}\|^2 + 2\beta_d \|\mathbf{x}\| \tag{B.163}$$

hence, provided that $q_m \geq 2\beta_d / \delta$ we have $\dot{\mathcal{V}} < 0$ for all $\mathbf{x} \in \mathcal{R} \cap \mathcal{H}$ where $\mathcal{H} := \{\mathbf{x} \in S_{e+}^3 \times \mathbb{R}^3 \times S_{eq}^3 \times \mathbb{R}^3 : \delta \leq \|\mathbf{x}\| \leq \Delta\}$.

The growth conditions can be verified to hold as in (B.157)–(B.158) and thus, the statement follows from (Chaillet and Loría, 2008, Theorem 10) by restricting the domain of attraction. The proof for the negative equilibrium $(\mathbf{e}_{q-}, \mathbf{e}_\omega, \mathbf{e}_{eq}, \mathbf{e}_{e\omega}) = (\mathbf{0}, \mathbf{0}, \mathbf{0}, \mathbf{0})$ follows *mutatis mutandis*.

B.14 Proof of Lemma 4.1

We have that

$$\mathbf{e}_{hq}^\top \mathbf{T}_h \mathbf{T}_h^\top \mathbf{e}_{hq} = \frac{1}{4} h^2 \tilde{\boldsymbol{\epsilon}}^\top \tilde{\boldsymbol{\epsilon}} = \frac{1}{4} \tilde{\boldsymbol{\epsilon}}^\top \tilde{\boldsymbol{\epsilon}}, \tag{B.164}$$

since $h^2 = (\pm 1)^2 = 1$ for all $h \in H$. Also, in view of (4.1) we have

$$\frac{1}{8} \left((1 - h\tilde{\eta})^2 + \tilde{\boldsymbol{\epsilon}}^\top \tilde{\boldsymbol{\epsilon}} \right) = \frac{1}{8} \mathbf{e}_{hq}^\top \mathbf{e}_{hq}, \tag{B.165}$$

and by inserting (B.164) and (B.165) into (4.4) we obtain

$$\frac{1}{4}\tilde{\boldsymbol{\epsilon}}^\top\tilde{\boldsymbol{\epsilon}} \geq \frac{1}{8}\left((1-h\tilde{\eta})^2 + \tilde{\boldsymbol{\epsilon}}^\top\tilde{\boldsymbol{\epsilon}}\right) \tag{B.166}$$

$$\tilde{\boldsymbol{\epsilon}}^\top\tilde{\boldsymbol{\epsilon}} \geq 1-h\tilde{\eta} \tag{B.167}$$

$$1 \geq \tilde{\boldsymbol{\epsilon}}^\top\tilde{\boldsymbol{\epsilon}}, \tag{B.168}$$

which holds for all $\tilde{\mathbf{q}} \in S^3$ because of the quaternion constraint $\tilde{\boldsymbol{\epsilon}}^\top\tilde{\boldsymbol{\epsilon}} = 1-\tilde{\eta}^2$, and thus the Lemma is proved.

B.15 Proof of Lemma 4.2

By multiplication we find that

$$\mathbf{T}_h^\top(\mathbf{e}_{hq})\mathbf{e}_{hq} = \frac{1}{2}h\tilde{\boldsymbol{\epsilon}} \tag{B.169}$$

and by differentiation of both sides and rearranging the terms, we obtain

$$\dot{\mathbf{T}}_h^\top(\mathbf{e}_{hq})\mathbf{e}_{hq} = \frac{1}{2}h\dot{\tilde{\boldsymbol{\epsilon}}} - \mathbf{T}_h^\top(\mathbf{e}_{hq})\dot{\mathbf{e}}_{hq}, \tag{B.170}$$

since $\dot{h}=0$ between jumps. From (B.30) we have that

$$\dot{\tilde{\boldsymbol{\epsilon}}} = \frac{1}{2}[\tilde{\eta}\mathbf{I} + \mathbf{S}(\tilde{\boldsymbol{\epsilon}})][\mathbf{s} - \gamma\mathbf{T}_h^\top\mathbf{e}_{hq}], \tag{B.171}$$

thus obtaining

$$\dot{\mathbf{T}}_h^\top(\mathbf{e}_{hq})\mathbf{e}_{hq} = \frac{1}{4}\left\{h[\tilde{\eta}\mathbf{I} + \mathbf{S}(\tilde{\boldsymbol{\epsilon}})]\mathbf{e}_\omega - \mathbf{I}\right\}\left[\mathbf{s} - \frac{1}{2}\gamma h\tilde{\boldsymbol{\epsilon}}\right] \tag{B.172}$$

where we find by multiplication that $\mathbf{T}_h^\top(\mathbf{e}_{hq})\mathbf{T}_h(\mathbf{e}_{hq}) = 1/4\mathbf{I}$ because $h^2=1$ for all $h \in H$, which concludes the proof.

B.16 Proof of Theorem 4.1

First we define the Lyapunov function candidate as

$$V(\mathbf{x}) := \frac{1}{2}\left(\mathbf{e}_{hq}^\top k_p\mathbf{e}_{hq} + \mathbf{e}_\omega^\top\mathbf{J}\mathbf{e}_\omega\right), \tag{B.173}$$

and note that $\mathbf{e}_{hq}^\top\mathbf{e}_{hq} = 2(1-h\tilde{\eta})$, $V(\mathbf{x} \in \{S_h^3 \times \mathbb{R}^3 \times H\}\backslash\{\mathbf{0},\mathbf{0}\} \times H) > 0$ and $V(\{\mathbf{0},\mathbf{0}\}\times H) = 0$. Also note that V is a function of $\mathbf{x}$, which includes h. However, during flows h is constant and may be regarded as a parameter in the expression (B.173). Hence, $V(\mathbf{x})$ is proper and positive definite on the projected set $\text{Proj}_{S_h^3\times\mathbb{R}^3}\mathcal{A} = \{\mathbf{x} \in S_h^3 \times \mathbb{R}^3 : (\mathbf{e}_{hq}, \mathbf{e}_\omega) = (\mathbf{0},\mathbf{0})\}$ and qualifies as a Lyapunov function candidate. Its derivative along the closed-loop trajectories of (2.83), (4.2)-(4.3) with the hybrid controller (4.9) and (4.11) yields

$$\dot{V} = \mathbf{e}_{hq}^\top k_p\mathbf{T}_h\mathbf{e}_\omega + \mathbf{e}_\omega^\top\left[\mathbf{S}(\mathbf{J}\boldsymbol{\omega})\mathbf{e}_\omega \; -k_p\mathbf{T}_h^\top\mathbf{e}_{hq} - k_d\mathbf{e}_\omega\right] \tag{B.174}$$

$$= -\mathbf{e}_\omega^\top k_d\mathbf{e}_\omega. \tag{B.175}$$

$V(\mathbf{x})$ also satisfies the difference equation

$$V(G(\mathbf{x})) - V(\mathbf{x}) = \frac{1}{2} k_p \left[\|[1 + h\tilde{\eta},\ \tilde{\boldsymbol{\epsilon}}]\|^2 - \|[1 - h\tilde{\eta},\ \tilde{\boldsymbol{\epsilon}}]\|^2 \right] \tag{B.176}$$

$$= 2hk_p\tilde{\eta} \tag{B.177}$$

so by defining the flow and jump sets as in (4.10) we ensure that $V(G(\mathbf{x})) - V(\mathbf{x}) < -2\sigma$ when $\mathbf{x} \in D$ *i.e.*, $V(\mathbf{x}(t))$ is strictly decreasing over jumps. Hence,

$$\dot{V} \leq 0 \quad \forall \mathbf{x} \in C \tag{B.178}$$

$$V(G(\mathbf{x})) - V(\mathbf{x}) < 0 \quad \forall \mathbf{x} \in D, \tag{B.179}$$

and therefore the set $\mathcal{A}$ is uniformly stable in the large on the set $S_h^3 \times \mathbb{R}^3$. The rest of the proof invokes Matrosov's theorem for hybrid systems –*cf.* (Sanfelice and Teel, 2008). To that end, define

$$u_C(\mathbf{x}) = \begin{cases} -\mathbf{e}_\omega^\top k_d \mathbf{e}_\omega & \forall\, \mathbf{x} \in C \\ -\infty & \text{otherwise} \end{cases} \tag{B.180a}$$

$$u_D(\mathbf{x}) = \begin{cases} 2hk_p\tilde{\eta} & \forall\, \mathbf{x} \in D \\ -\infty & \text{otherwise} \end{cases} \tag{B.180b}$$

and consider the auxiliary function

$$W(\mathbf{x}) := \mathbf{e}_{hq}^\top \mathbf{T}_h \mathbf{J}\mathbf{e}_\omega \,. \tag{B.181}$$

We have

$$W(G(\mathbf{x})) - W(\mathbf{x}) = \frac{1}{2} \begin{bmatrix} 1 + h\tilde{\eta} \\ \tilde{\epsilon}_x \\ \tilde{\epsilon}_y \\ \tilde{\epsilon}_z \end{bmatrix}^\top \begin{bmatrix} -h\tilde{\epsilon}_x & -h\tilde{\epsilon}_y & -h\tilde{\epsilon}_z \\ \tilde{\eta} & -\tilde{\epsilon}_z & \tilde{\epsilon}_y \\ \tilde{\epsilon}_z & \tilde{\eta} & -\tilde{\epsilon}_x \\ -\tilde{\epsilon}_y & \tilde{\epsilon}_x & \tilde{\eta} \end{bmatrix}^\top \mathbf{J}\mathbf{e}_w \tag{B.182}$$

$$- \frac{1}{2} \begin{bmatrix} 1 - h\tilde{\eta} \\ \tilde{\epsilon}_x \\ \tilde{\epsilon}_y \\ \tilde{\epsilon}_z \end{bmatrix}^\top \begin{bmatrix} h\tilde{\epsilon}_x & h\tilde{\epsilon}_y & h\tilde{\epsilon}_z \\ \tilde{\eta} & -\tilde{\epsilon}_z & \tilde{\epsilon}_y \\ \tilde{\epsilon}_z & \tilde{\eta} & -\tilde{\epsilon}_x \\ -\tilde{\epsilon}_y & \tilde{\epsilon}_x & \tilde{\eta} \end{bmatrix}^\top \mathbf{J}\mathbf{e}_w$$

$$= \frac{1}{2} \begin{bmatrix} (1 + h\tilde{\eta})(-h\tilde{\epsilon}_x) + \tilde{\epsilon}_x\tilde{\eta} + \tilde{\epsilon}_y\tilde{\epsilon}_z - \tilde{\epsilon}_z\tilde{\epsilon}_y \\ (1 + h\tilde{\eta})(-h\tilde{\epsilon}_y) - \tilde{\epsilon}_x\tilde{\epsilon}_z + \tilde{\epsilon}_y\tilde{\eta} + \tilde{\epsilon}_z\tilde{\epsilon}_x \\ (1 + h\tilde{\eta})(-h\tilde{\epsilon}_z) + \tilde{\epsilon}_x\tilde{\epsilon}_y - \tilde{\epsilon}_x\tilde{\epsilon}_y + \tilde{\eta}\tilde{\epsilon}_z \end{bmatrix}^\top \mathbf{J}\mathbf{e}_w \tag{B.183}$$

$$- \frac{1}{2} \begin{bmatrix} (1 - h\tilde{\eta})h\tilde{\epsilon}_x + \tilde{\epsilon}_x\tilde{\eta} + \tilde{\epsilon}_y\tilde{\epsilon}_z - \tilde{\epsilon}_z\tilde{\epsilon}_y \\ (1 - h\tilde{\eta})h\tilde{\epsilon}_y - \tilde{\epsilon}_x\tilde{\epsilon}_z + \tilde{\epsilon}_y\tilde{\eta} + \tilde{\epsilon}_z\tilde{\epsilon}_x \\ (1 - h\tilde{\eta})h\tilde{\epsilon}_z + \tilde{\epsilon}_x\tilde{\epsilon}_y - \tilde{\epsilon}_x\tilde{\epsilon}_y + \tilde{\eta}\tilde{\epsilon}_z \end{bmatrix}^\top \mathbf{J}\mathbf{e}_w$$

$$= - \frac{1}{2} \begin{bmatrix} -h\tilde{\epsilon}_x - h^2\tilde{\eta}\tilde{\epsilon}_x + \tilde{\eta}\tilde{\epsilon}_x \\ -h\tilde{\epsilon}_y - h^2\tilde{\eta}\tilde{\epsilon}_y + \tilde{\epsilon}_y\tilde{\eta} \\ -h\tilde{\epsilon}_z - h^2\tilde{\eta}\tilde{\epsilon}_z + \tilde{\eta}\tilde{\epsilon}_z \end{bmatrix}^\top \mathbf{J}\mathbf{e}_w \tag{B.184}$$

$$- \frac{1}{2} \begin{bmatrix} h\tilde{\epsilon}_x - h^2\tilde{\eta}\tilde{\epsilon}_x + \tilde{\epsilon}_x\tilde{\eta} \\ h\tilde{\epsilon}_y - h^2\tilde{\eta}\tilde{\epsilon}_y + \tilde{\eta}\tilde{\epsilon}_y \\ h\tilde{\epsilon}_z - h^2\tilde{\eta}\tilde{\epsilon}_z + \tilde{\eta}\tilde{\epsilon}_z \end{bmatrix}^\top \mathbf{J}\mathbf{e}_w$$

hence, since $h^2 = 1$

$$W(G(\mathbf{x})) - W(\mathbf{x}) \;=\; -h\tilde{\boldsymbol{\epsilon}}^\top \mathbf{J}\mathbf{e}_w, \tag{B.185}$$

and

$$\mathbf{e}_\omega = \;\mathbf{0} \;\Rightarrow\; W(G(\mathbf{x})) - W(\mathbf{x}) = 0\,. \tag{B.186}$$

On the other hand, its time derivative along the system's flows yields

$$\begin{aligned}
\mathbf{e}_\omega = \mathbf{0} \Rightarrow\; \dot{W} =& \dot{\mathbf{e}}_{hq}^\top \mathbf{T}_h \mathbf{J}\mathbf{e}_\omega + \mathbf{e}_{hq}^\top \dot{\mathbf{T}}_h \mathbf{J}\mathbf{e}_\omega + \mathbf{e}_{hq}^\top \mathbf{T}_h \mathbf{J}\dot{\mathbf{e}}_\omega && \text{(B.187)}\\
=& \mathbf{e}_\omega^\top \mathbf{T}_h^\top \mathbf{T}_h \mathbf{J}\mathbf{e}_\omega + \mathbf{e}_\omega^\top \mathbf{G}_h^\top \mathbf{J}\mathbf{e}_\omega && \text{(B.188)}\\
& - \mathbf{e}_{hq}^\top \mathbf{T}_h \Big[\left(-\mathbf{S}(\mathbf{J}\boldsymbol{\omega}) + k_\omega \mathbf{I}\right) \mathbf{e}_\omega + k_q \mathbf{T}_h^\top \mathbf{e}_{hq} \Big] \\
=& - \mathbf{e}_{hq}^\top \mathbf{T}_h k_p \mathbf{T}_h^\top \mathbf{e}_{hq}, && \text{(B.189)}
\end{aligned}$$

where Corollary 4.2 was applied, and by also applying Lemma 4.1 we obtain

$$\dot{W} \leq -\mathbf{e}_{hq}^\top \frac{k_p}{8} \mathbf{e}_{hq}, \tag{B.190}$$

that is, W is sign-definite on the set $\{\mathbf{x} \in S_h^3 \times \mathbb{R}^3 : \mathbf{e}_\omega = 0\} \cap C$. Thus, the set $\mathcal{A}$ is uniformly asymptotically stable in the large on the set $S_h^3 \times \mathbb{R}^3$.

B.17 Proof of Theorem 4.2

We use the Lyapunov function

$$V(\mathbf{x}) = \frac{1}{2}(\mathbf{s}_h^\top \mathbf{J}\mathbf{s}_h + \mathbf{e}_{hq}^\top k_q \mathbf{e}_{hq}), \tag{B.191}$$

which is positive definite and proper according to what was discussed in the beginning of Proof of Theorem 4.1. The total time derivative along the closed-loop flow trajectories that is generated by (2.83), (4.2)-(4.3) and (4.15), yields (under the quaternion constraint)

$$\begin{aligned}
\dot{V} =& \mathbf{s}_h^\top \mathbf{S}(\mathbf{J}\boldsymbol{\omega})\mathbf{s}_h - \mathbf{s}_h^\top k_\omega \mathbf{s}_h - \mathbf{s}_h^\top k_q \mathbf{T}_h^\top \mathbf{e}_{hq} + \mathbf{e}_{hq}^\top k_q \mathbf{T}_h \mathbf{s}_h - \mathbf{e}_{hq}^\top k_q \mathbf{T}_h \gamma \mathbf{T}_h^\top \mathbf{e}_{hq} && \text{(B.192)}\\
=& - \mathbf{s}_h^\top k_\omega \mathbf{s}_h - \mathbf{e}_{hq}^\top k_q \mathbf{T}_h \gamma \mathbf{T}_h^\top \mathbf{e}_{hq}, && \text{(B.193)}
\end{aligned}$$

and by invoking Lemma 4.1, we obtain

$$\dot{V} \leq -\mathbf{s}_h^\top k_\omega \mathbf{s}_h - \mathbf{e}_{hq}^\top \frac{\gamma k_q}{8} \mathbf{e}_{hq}. \tag{B.194}$$

Now, we evaluate $V(G(\mathbf{x})) - V(\mathbf{x})$. We have

$$\begin{aligned}
V(G(\mathbf{x})) =& \frac{1}{2}\left[(\mathbf{e}_\omega + \gamma \mathbf{T}_{-h}^\top \mathbf{e}_{-hq})^\top \mathbf{J}(\mathbf{e}_\omega + \gamma \mathbf{T}_{-h}^\top \mathbf{e}_{-hq}) + \mathbf{e}_{-hq}^\top k_q \mathbf{e}_{-hq}\right] && \text{(B.195)}\\
V(\mathbf{x}) =& \frac{1}{2}\left[(\mathbf{e}_\omega + \gamma \mathbf{T}_h^\top \mathbf{e}_{hq})^\top \mathbf{J}(\mathbf{e}_\omega + \gamma \mathbf{T}_h^\top \mathbf{e}_{hq}) + \mathbf{e}_{hq}^\top k_q \mathbf{e}_{hq}\right] && \text{(B.196)}
\end{aligned}$$

Note that $\mathbf{T}_h^\top \mathbf{e}_{hq} = 1/2h\tilde{\boldsymbol{\epsilon}}$ and that $\mathbf{e}_{hq}^\top \mathbf{e}_{hq} = (1-h\tilde{\eta})^2 + \tilde{\boldsymbol{\epsilon}}^\top \tilde{\boldsymbol{\epsilon}}$, and by inserting the unit quaternion constraint $\tilde{\eta}^2 + \tilde{\boldsymbol{\epsilon}}^\top \tilde{\boldsymbol{\epsilon}} = 1$ we have that $\mathbf{e}_{hq}^\top \mathbf{e}_{hq} = 2(1-h\tilde{\eta})$. Hence,

$$2V(G(\mathbf{x})) = \mathbf{e}_\omega^\top \mathbf{J}\mathbf{e}_\omega + \gamma(-h)\tilde{\boldsymbol{\epsilon}}^\top \mathbf{e}_\omega + \frac{1}{4}\gamma^2(-h)^2 \tilde{\boldsymbol{\epsilon}}^\top \mathbf{J}\tilde{\boldsymbol{\epsilon}} + 2k_q[1-(-h)\tilde{\eta}] \tag{B.197}$$

$$2V(\mathbf{x}) = \mathbf{e}_\omega^\top \mathbf{J}\mathbf{e}_\omega + \gamma h\tilde{\boldsymbol{\epsilon}}^\top \mathbf{e}_\omega + \frac{1}{4}\gamma^2 h^2 \tilde{\boldsymbol{\epsilon}}^\top \mathbf{J}\tilde{\boldsymbol{\epsilon}} + 2k_q[1-h\tilde{\eta}], \tag{B.198}$$

and therefore

$$V(G(\mathbf{x})) - V(\mathbf{x}) \;=\; 2h\Big[k_q\tilde{\eta} - \frac{1}{2}\gamma\tilde{\boldsymbol{\epsilon}}^\top \mathbf{J}\mathbf{e}_\omega\Big], \tag{B.199}$$

which in view of (4.17b), implies $V(G(\mathbf{x})) - V(\mathbf{x}) \leq -2\sigma < 0$ when $\mathbf{x} \in D$. Thus,

$$\begin{aligned} \dot{V} &\leq -c_8/c_7 V(\mathbf{x}) \qquad && \forall \mathbf{x} \in C \\ V(G(\mathbf{x})) - V(\mathbf{x}) &< 0 && \forall \mathbf{x} \in D, \end{aligned} \tag{B.200}$$

where c_7 and c_8 were given in Appendix B.5. Since the projection $\text{Proj}_{S_h^3 \times \mathbb{R}^3}\mathcal{A} = \{\mathbf{x} \in S_h^3 \times \mathbb{R}^3 : (\mathbf{e}_{hq}, \mathbf{s}_h) = (\mathbf{0}, \mathbf{0})\}$, according to (Sanfelice *et al.*, 2007, Corollary 7.7) we conclude that the set $\mathcal{A}$ is asymptotically stable with basin of attraction $\bar{\mathcal{B}}_\mathcal{A} = C \cup D$, thus uniform asymptotic stability in the large on the set $S_h^3 \times \mathbb{R}^3$ follows.

B.18 Proof of Theorem 4.3

The error dynamics can be derived similar to what was shown in the proof of Theorem 3.11 written on state space form $\dot{\mathbf{x}} = f(t, \mathbf{x})$ with

$$f(t,\mathbf{x}) = \begin{bmatrix} \mathbf{T}_h \mathbf{e}_\omega \\ \mathbf{J}_l^{-1}\xi_1 \\ \mathbf{T}_{eq}\mathbf{e}_{e\omega} \\ \mathbf{J}_l^{-1}\xi_2 \\ 0 \end{bmatrix}, \tag{B.201}$$

where

$$\begin{aligned} \xi_1 =& \mathbf{S}(\mathbf{J}\boldsymbol{\omega}_{i,b}^b)\mathbf{e}_\omega + \mathbf{S}(\mathbf{J}\mathbf{e}_{e\omega})\boldsymbol{\omega}_{i,d}^b - k_p \mathbf{T}_h^\top \mathbf{e}_{hq} \\ & - k_d(\mathbf{e}_\omega - \mathbf{e}_{e\omega}) - \mathbf{J}\mathbf{S}(\boldsymbol{\omega}_{i,d}^b)\mathbf{e}_\omega + \boldsymbol{\tau}_d, \end{aligned} \tag{B.202}$$

and

$$\begin{aligned} \xi_2 =& \mathbf{S}(\mathbf{J}\boldsymbol{\omega}_{i,b}^b)\mathbf{e}_\omega - k_d\mathbf{e}_\omega + \mathbf{S}(\mathbf{J}\mathbf{e}_{e\omega})\boldsymbol{\omega}_{i,d}^b \\ & + k_d\mathbf{e}_{e\omega} - \frac{l_d}{2}[\eta_{e,b} + \mathbf{S}(\boldsymbol{\epsilon}_{e,b})]\mathbf{e}_{e\omega} \\ & - l_p \mathbf{T}_{eq}^\top \mathbf{e}_{eq} + \boldsymbol{\tau}_d. \end{aligned} \tag{B.203}$$

The rest of the proof is split into two parts. Firstly we use a Lyapunov function to analyze the behaviour during flows and we show that the set $\mathcal{A}_\delta$ attracts all

trajectories generated by the flow dynamics, starting in $\mathcal{A}_\Delta$. Secondly, we show that the change in the Lyapunov function is negative over jumps.

Consider the Lyapunov function candidate

$$\begin{aligned}\mathcal{V}(\mathbf{x}) &:= V(\mathbf{x}) + \lambda W(\mathbf{x}), \\ V(\mathbf{x}) &:= \frac{1}{2}\Big[\mathbf{e}_{hq}^\top k_p \mathbf{e}_{hq} + \mathbf{e}_\omega^\top \mathbf{J}\mathbf{e}_\omega + \mathbf{e}_{eq}^\top l_p \mathbf{e}_{eq} + \mathbf{e}_{e\omega}^\top \mathbf{J}\mathbf{e}_{e\omega}\Big], \\ W(\mathbf{x}) &:= \mathbf{e}_{hq}^\top \mathbf{T}_h \mathbf{J}\mathbf{e}_\omega + \mathbf{e}_{eq}^\top \mathbf{T}_{eq}\mathbf{J}\mathbf{e}_{e\omega},\end{aligned} \tag{B.204}$$

which is positive definite and proper according to what was discussed in the beginning of the proof of Theorem 4.1, and lower and upper bounded such that $\underline{\alpha}(\mathbf{x}) \leq \mathcal{V}(\mathbf{x}) \leq \overline{\alpha}(\mathbf{x})$ where the functions $\underline{\alpha}(\mathbf{x}), \overline{\alpha}(\mathbf{x})$ are of class $\mathcal{K}_\infty$ defined as

$$\underline{\alpha}(\mathbf{x}) := \boldsymbol{\chi}^\top p_m \boldsymbol{\chi} \tag{B.205}$$

$$\overline{\alpha}(\mathbf{x}) := \boldsymbol{\chi}^\top p_M \boldsymbol{\chi}. \tag{B.206}$$

where $\boldsymbol{\chi} = [\mathbf{e}_{hq}^\top, \mathbf{e}_\omega^\top, \mathbf{e}_{eq}^\top, \mathbf{e}_{e\omega}^\top]^\top$ and $p_m \leq \|\mathbf{P}\| \leq p_M$ are the smallest and largest eigenvalues of

$$\mathbf{P} := \frac{1}{2}\begin{bmatrix} k_p\mathbf{I} & \lambda\mathbf{T}_h\mathbf{J} & \mathbf{0} & \mathbf{0} \\ \lambda\mathbf{J}\mathbf{T}_h^\top & \mathbf{J} & \mathbf{0} & \mathbf{0} \\ \mathbf{0} & \mathbf{0} & l_p\mathbf{I} & \lambda\mathbf{T}_{eq}\mathbf{J} \\ \mathbf{0} & \mathbf{0} & \lambda\mathbf{J}\mathbf{T}_{eq}^\top & \mathbf{J} \end{bmatrix}, \tag{B.207}$$

respectively. Indeed, $\mathbf{P}$ is positive definite if the Schur complements corresponding to its two 6×6 diagonal sub-blocks are positive that is, if

$$\begin{aligned} k_p\mathbf{I} &\succ \lambda^2 \mathbf{T}_e \mathbf{J}\mathbf{T}_e^\top \\ l_p\mathbf{I} &\succ \lambda^2 \mathbf{T}_{eq}\mathbf{J}\mathbf{T}_{eq}^\top. \end{aligned}$$

In view of Assumption 3.3 and the fact that $\mathbf{T}_q$ and $\mathbf{T}_{eq}$ are bounded (due to the quaternion constraint) the inequalities above hold for $\lambda < 2\sqrt{\min\{l_p, k_p\}/j_M} =: \kappa$.

Next, we evaluate the total time derivative of $\mathcal{V}(\mathbf{x})$ along the closed-loop trajectories. To that end, we first compute the derivative of $V(\mathbf{x})$. We have

$$\begin{aligned}\dot{V} = &- k_d \mathbf{e}_\omega^\top \mathbf{e}_\omega + \mathbf{e}_\omega^\top \mathbf{S}(\mathbf{J}\mathbf{e}_{e\omega})\boldsymbol{\omega}_{i,d}^b - \mathbf{e}_\omega^\top \mathbf{J}\mathbf{S}(\boldsymbol{\omega}_{i,d}^b)\mathbf{e}_\omega + \mathbf{e}_{e\omega}^\top \mathbf{S}(\mathbf{J}\boldsymbol{\omega}_{i,b}^b)\mathbf{e}_\omega \\ &+ \mathbf{e}_{e\omega}^\top \mathbf{S}(\mathbf{J}\mathbf{e}_{e\omega})\boldsymbol{\omega}_{i,d}^b - \left(\frac{l_d}{2}\eta_{e,b} - k_d\right)\mathbf{e}_{e\omega}^\top \mathbf{e}_{e\omega} + \left(\mathbf{e}_\omega^\top + \mathbf{e}_{e\omega}^\top\right)\boldsymbol{\tau}_d.\end{aligned} \tag{B.208}$$

Since the matrix $\mathbf{S}(\cdot)$ is linear in its arguments, we have (Caccavale and Villani, 1999)

$$\|\mathbf{S}(\mathbf{J}\mathbf{a})\mathbf{b}\| \leq \beta_J \|\mathbf{a}\|\|\mathbf{b}\|. \tag{B.209}$$

By applying (B.209), Young's inequality (Young, 1912)and Assumptions 3.2–3.3 we

have that

$$\mathbf{e}_{\omega}^{\top}\mathbf{S}(\mathbf{J}\mathbf{e}_{e\omega})\boldsymbol{\omega}_{i,d}^{b} \leq \frac{1}{2}\beta_J\beta_{\omega_{i,d}^{b}}(\|\mathbf{e}_{\omega}\|^2 + \|\mathbf{e}_{e\omega}\|^2) \tag{B.210}$$

$$\mathbf{e}_{\omega}^{\top}\mathbf{J}\mathbf{S}(\boldsymbol{\omega}_{i,d}^{b})\mathbf{e}_{\omega} \leq \beta_J\beta_{\omega_{i,d}^{b}}\|\mathbf{e}_{\omega}\|^2 \tag{B.211}$$

$$\mathbf{e}_{e\omega}^{\top}\mathbf{S}(\mathbf{J}\boldsymbol{\omega}_{i,b}^{b})\mathbf{e}_{\omega} \leq \frac{1}{2}\beta_J(\|\mathbf{e}_{\omega}\|^2 + \|\mathbf{e}_{e\omega}\|^2)(\|\mathbf{e}_{\omega}\| + \beta_{\omega_{i,d}^{b}}) \tag{B.212}$$

$$\mathbf{e}_{e\omega}^{\top}\mathbf{S}(\mathbf{J}\mathbf{e}_{e\omega})\boldsymbol{\omega}_{i,d}^{b} \leq \beta_J\beta_{\omega_{i,d}^{b}}\|\mathbf{e}_{e\omega}\|^2. \tag{B.213}$$

Inserting the bounds (B.210)–(B.213) into (B.208), we obtain

$$\dot{V} \leq -\phi(k_d, \|\mathbf{e}_{\omega}\|)\|\mathbf{e}_{\omega}\|^2 - \psi(k_d, l_d, \|\mathbf{e}_{\omega}\|)\|\mathbf{e}_{e\omega}\|^2 + \left(\mathbf{e}_{\omega}^{\top} + \mathbf{e}_{e\omega}^{\top}\right)\boldsymbol{\tau}_d, \tag{B.214}$$

where

$$\phi(k_d, \|\mathbf{e}_{\omega}\|) = k_d - \frac{1}{2}\beta_J\left(4\beta_{\omega_{i,d}^{b}} + \|\mathbf{e}_{\omega}\|\right), \tag{B.215a}$$

$$\psi(k_d, l_d, \|\mathbf{e}_{\omega}\|) = \frac{l_d}{2}\eta_{e,b} - k_d - \frac{1}{2}\beta_J(4\beta_{\omega_{i,d}^{b}} + \|\mathbf{e}_{\omega}\|). \tag{B.215b}$$

In view of (4.33), (4.35) we have $\eta_{e,b} \geq \delta_n$ hence, $\psi(\cdot)$ may be made positive for sufficiently large l_d. It follows that $\dot{V}$ is negative semi-definite for bounded values of $\mathbf{e}_{\omega}$.

Next, we find the total time derivative of $\mathcal{V}(\mathbf{x})$ along the closed-loop trajectories, starting with the total time derivative of $W(\mathbf{x})$ along the closed-loop trajectories yielding

$$\begin{aligned}
\dot{W} =& \dot{\mathbf{e}}_q^{\top}\mathbf{T}_e\mathbf{J}\mathbf{e}_{\omega} + \mathbf{e}_q^{\top}\dot{\mathbf{T}}_e\mathbf{J}\mathbf{e}_{\omega} + \mathbf{e}_q^{\top}\mathbf{T}_e\mathbf{J}\dot{\mathbf{e}}_{\omega} \\
&+ \dot{\mathbf{e}}_{eq}^{\top}\mathbf{T}_{eq}\mathbf{J}\mathbf{e}_{e\omega} + \mathbf{e}_{eq}^{\top}\dot{\mathbf{T}}_{eq}\mathbf{J}\mathbf{e}_{e\omega} + \mathbf{e}_{eq}^{\top}\mathbf{T}_{eq}\mathbf{J}\dot{\mathbf{e}}_{e\omega} \\
=& \mathbf{e}_{\omega}^{\top}h/4[\tilde{\eta}\mathbf{I} + \mathbf{S}(\tilde{\boldsymbol{\epsilon}})]\mathbf{e}_{\omega} + \mathbf{e}_q^{\top}\mathbf{T}_e\mathbf{S}(\mathbf{J}\boldsymbol{\omega}_{i,b}^{b})\mathbf{e}_{\omega} \\
&+ \mathbf{e}_q^{\top}\mathbf{T}_e\mathbf{S}(\mathbf{J}\mathbf{e}_{\omega})\boldsymbol{\omega}_{i,d}^{b} - \mathbf{e}_q^{\top}\mathbf{T}_e k_p\mathbf{T}_e^{\top}\mathbf{e}_q \\
&- \mathbf{e}_q^{\top}\mathbf{T}_e k_d(\mathbf{e}_{\omega} - \mathbf{e}_{e\omega}) - \mathbf{e}_q^{\top}\mathbf{T}_e\mathbf{J}\mathbf{S}(\boldsymbol{\omega}_{i,d}^{b})\mathbf{e}_{\omega} + \mathbf{e}_q^{\top}\mathbf{T}_e\boldsymbol{\tau}_d \\
&+ \mathbf{e}_{e\omega}^{\top}/4[\eta_{e,b} + \mathbf{S}(\boldsymbol{\omega}_{e,b})]\mathbf{J}\mathbf{e}_{e\omega} + \mathbf{e}_{eq}^{\top}\mathbf{T}_{eq}\mathbf{S}(\mathbf{J}\boldsymbol{\omega}_{i,b}^{b})\mathbf{e}_{\omega} \\
&- \mathbf{e}_{eq}^{\top}\mathbf{T}_{eq}k_d\mathbf{e}_{\omega} + \mathbf{e}_{eq}^{\top}\mathbf{T}_{eq}\mathbf{S}(\mathbf{J}\mathbf{e}_{e\omega})\boldsymbol{\omega}_{i,d}^{b} \\
&+ \mathbf{e}_{eq}^{\top}\mathbf{T}_{eq}k_d\mathbf{e}_{e\omega} - \mathbf{e}_{eq}^{\top}\mathbf{T}_{eq}l_d/2[\eta_{e,b}\mathbf{I} + \mathbf{S}(\epsilon_{e,b})]\mathbf{e}_{e\omega} \\
&- \mathbf{e}_{eq}^{\top}\mathbf{T}_{eq}l_p\mathbf{T}_{eq}^{\top}\mathbf{e}_{eq} + \mathbf{e}_{eq}^{\top}\mathbf{T}_{eq}\boldsymbol{\tau}_d,
\end{aligned} \tag{B.216}$$

$$\tag{B.217}$$

and by inserting (B.214) and (B.217) into (B.204), we obtain

$$\dot{\mathcal{V}} \leq = -\boldsymbol{\chi}^{\top}\mathbf{Q}(\boldsymbol{\omega}_{i,b}^{b})\boldsymbol{\chi} + 2\beta_d\|\boldsymbol{\chi}\| \tag{B.218}$$

where $\mathbf{Q}(\boldsymbol{\omega}^b_{i,b}) = [\mathbf{q}_{ij}]$, $i,j = 1,2,3,4$ with

$$\mathbf{q}_{11} = \lambda \mathbf{T}_h k_p \mathbf{T}_h^\top \tag{B.219a}$$
$$\mathbf{q}_{12} = \mathbf{q}_{21}^\top = \frac{\lambda}{2}\mathbf{T}_h \Big[k_d \mathbf{I} - \mathbf{S}(\mathbf{J}\boldsymbol{\omega}^b_{i,b}) + \mathbf{J}\mathbf{S}(\boldsymbol{\omega}^b_{i,d})\Big] \tag{B.219b}$$
$$\mathbf{q}_{13} = \mathbf{q}_{31}^\top = \mathbf{0} \tag{B.219c}$$
$$\mathbf{q}_{14} = \mathbf{q}_{41}^\top = \frac{\lambda}{2}\mathbf{T}_h \left[\mathbf{S}(\boldsymbol{\omega}^b_{i,d})\mathbf{J} - k_d \mathbf{I}\right] \tag{B.219d}$$
$$\mathbf{q}_{22} = \phi(k_d, \|\mathbf{e}_\omega\|)\mathbf{I} - \lambda \frac{1}{4}\mathbf{J} \tag{B.219e}$$
$$\mathbf{q}_{23} = \mathbf{q}_{32}^\top = \frac{\lambda}{2}\left[k_d \mathbf{I} - \mathbf{S}(\mathbf{J}\boldsymbol{\omega}^b_{i,b})\right]\mathbf{T}_{eq}^\top \tag{B.219f}$$
$$\mathbf{q}_{24} = \mathbf{q}_{42}^\top = \mathbf{0} \tag{B.219g}$$
$$\mathbf{q}_{33} = \lambda \mathbf{T}_{eq} l_p \mathbf{T}_{eq}^\top \tag{B.219h}$$
$$\mathbf{q}_{34} = \mathbf{q}_{43}^\top = \frac{\lambda}{2}\mathbf{T}_{eq}\Big[\mathbf{S}(\boldsymbol{\omega}^b_{i,d})\mathbf{J} + \frac{l_d}{2}\left[\eta_{e,b}\mathbf{I} + \mathbf{S}(\boldsymbol{\epsilon}_{e,b})\right] - k_d \mathbf{I}\Big] \tag{B.219i}$$
$$\mathbf{q}_{44} = \psi(k_d, l_d, \|\mathbf{e}_\omega\|)\mathbf{I} - \lambda \frac{1}{4}\mathbf{J}. \tag{B.219j}$$

We invoke Lemma 4.1 and 3.1 on (B.219a) and (B.219h), respectively, noting that the latter is guaranteed by the switching logic since $\eta_{e,b}(t) \geq \delta_n \in (0,1)\ \forall\ t \geq t_0$. Therefore, for all $\mathbf{e}_\omega$ such that $\|\mathbf{e}_\omega\| \leq \Delta$ there exist lower and upper bounds $q_{ij,m}$ and $q_{ij,M}$ on the norms of the sub-blocks $\mathbf{q}_{ij}$ of $\mathbf{Q}$. Next, we want to find a quadratic upper-bound on $-\mathbf{x}^\top \mathbf{Q}\mathbf{x}$, and apply $2|ab| \leq a^2 + b^2$ for any $a, b \in \mathbb{R}$ on the eigenvalues of the normed system to obtain

$$\begin{aligned}\boldsymbol{\chi}^\top \mathbf{Q}\boldsymbol{\chi} \geq &(q_{11,m} - q_{12,M} - q_{13,M} - q_{14,M})\|\mathbf{e}_q\|^2 \\ &+ (q_{22,m} - q_{21,M} - q_{23,M} - q_{24,M})\|\mathbf{e}_\omega\|^2 \\ &+ (q_{33,m} - q_{31,M} - q_{32,M} - q_{34,M})\|\mathbf{e}_{eq}\|^2 \\ &+ (q_{44,m} - q_{41,M} - q_{42,M} - q_{43,M})\|\mathbf{e}_{e\omega}\|^2\end{aligned} \tag{B.220}$$

so, if

$$q_{11,m} \geq 2(q_{12,M} + q_{13,M} + q_{14,M}) \tag{B.221a}$$
$$q_{22,m} \geq 2(q_{21,M} + q_{23,M} + q_{24,M}) \tag{B.221b}$$
$$q_{33,m} \geq 2(q_{31,M} + q_{32,M} + q_{34,M}) \tag{B.221c}$$
$$q_{44,m} \geq 2(q_{41,M} + q_{42,M} + q_{43,M}) \tag{B.221d}$$

then

$$\begin{aligned}\boldsymbol{\chi}^\top \mathbf{Q}\boldsymbol{\chi} \geq \frac{1}{2}&(q_{11,m}\|\mathbf{e}_{hq}\|^2 + q_{22,m}\|\mathbf{e}_\omega\|^2 \\ &+ q_{33,m}\|\mathbf{e}_{eq}\|^2 + q_{44,m}\|\mathbf{e}_{e\omega}\|^2).\end{aligned} \tag{B.222}$$

It follows that (B.222) holds that is, $\mathbf{Q}$ is positive definite if, defining

$$\begin{aligned} k_d^\star &:= \frac{1}{2}\beta_J(4\beta_{\omega_{i,d}^b} + \Delta) \\ k_p^\star &:= j_M(\Delta + 2\beta_{\omega_{i,d}^b}) \\ l_d^\star &:= [2k_d + \beta_J(4\beta_{\omega_{i,d}^b} + \Delta)]/\delta_\eta \qquad \text{(B.223)} \\ l_p^{\star'} &:= j_M(\Delta + \beta_{\omega_{i,d}^b}) + \frac{l_d}{2} \qquad \text{(B.224)} \\ &\geq\ j_M(\Delta + \beta_{\omega_{i,d}^b}) + \frac{l_d}{2}\eta_{e,b}, \end{aligned}$$

we choose the gains such that $k_d > k_d^\star$, $k_p > k_p^\star$, $l_d > l_d^\star$, $l_p > l_p^{\star'}$ and

$$\lambda \leq \min\left\{ \frac{\phi(k_d, \Delta)}{\frac{1}{4}j_M + 2k_d + j_M(2\Delta + \beta_{\omega_{i,d}^b})}, \right. \\ \left. \frac{\psi(k_d, l_d, \Delta)}{\frac{1}{4}j_M + 2\beta_{\omega_{i,d}^b} j_M + \frac{l_d}{2}2k_d}, \kappa \right\}.$$

Thus,

$$\dot{\mathcal{V}}(\mathbf{x}) \leq -q_m\|\boldsymbol{\chi}\|^2 + 2\beta_d\|\boldsymbol{\chi}\|, \qquad \text{(B.225)}$$

where $q_m(\Delta) > 0$ is a lower bound on the smallest eigenvalue of $\mathbf{Q}(\Delta)$. The derivative $\dot{\mathcal{V}} < 0$ for all $\mathbf{x} \in \mathcal{H} := \{\mathbf{x} \in S_h^3 \times \mathbb{R}^3 \times S_e^3 \times \mathbb{R}^3 \times H : \delta \leq \|\boldsymbol{\chi}\| \leq \Delta\}$, where

$$\delta := 2\beta_d/q_m. \qquad \text{(B.226)}$$

Given any positive constants $\delta^\star$, $\Delta^\star$ such that $\delta^\star < \Delta^\star$, we have that there exists $\Delta > \delta > 0$ such that

$$\underline{\alpha}^{-1} \circ \overline{\alpha}(\delta) = \sqrt{\frac{p_M\delta^2}{p_m}} = \sqrt{\frac{4p_M\beta_d^2}{p_m q_m^2}} \leq \delta^\star, \qquad \text{(B.227)}$$

and

$$\overline{\alpha}^{-1} \circ \underline{\alpha}(\Delta) = \sqrt{\frac{p_m\Delta^2}{p_M}} \geq \Delta^\star. \qquad \text{(B.228)}$$

We see from (B.227) that given any $\delta^\star$ we can increase the controller gains such that the inequality is fulfilled; similarly for (B.228). Hence, all conditions of (Chaillet and Loría, 2008, Theorem 10) hold; this implies that the set $\mathcal{A}_\delta$ attracts all trajectories generated by the flow dynamics, starting in the set $\mathcal{A}_\Delta$.

Next, we have to ensure that the Lyapunov function decreases over jumps (*cf.* (Goebel *et al.*, 2009)), such that

$$\mathcal{V}(G_1(\mathbf{x})) - \mathcal{V}(\mathbf{x}) < 0 \qquad \text{(B.229)}$$
$$\mathcal{V}(G_2(\mathbf{x})) - \mathcal{V}(\mathbf{x}) < 0. \qquad \text{(B.230)}$$

To that end we first see that

$$\mathcal{V}(G_1(\mathbf{x})) - \mathcal{V}(\mathbf{x}) = 2hk_p \left(\tilde{\eta} - \frac{1}{2k_p} \lambda \tilde{\boldsymbol{\epsilon}}^\top \mathbf{J} \mathbf{e}_\omega \right), \tag{B.231}$$

hence, in view of (4.34) the inequality (B.229) holds. We have that

$$\begin{aligned}
\mathcal{V}(G_2(\mathbf{x})) - \mathcal{V}(\mathbf{x}) =& \frac{1}{2} \Big[\left(\boldsymbol{\omega}_{i,b}^b - \mathbf{z} \right)^\top \mathbf{J} \left(\boldsymbol{\omega}_{i,b}^b - \mathbf{z} \right) - l_p \mathbf{e}_{eq}^\top \mathbf{e}_{eq} && \text{(B.232)} \\
& - \left(\boldsymbol{\omega}_{i,b}^b - \boldsymbol{\omega}_{i,e}^b \right)^\top \mathbf{J} \left(\boldsymbol{\omega}_{i,b}^b - \boldsymbol{\omega}_{i,e}^b \right) \Big] - \lambda \mathbf{e}_{eq}^\top \mathbf{T}_{eq} \mathbf{J} \left(\boldsymbol{\omega}_{i,b}^b - \boldsymbol{\omega}_{i,e}^b \right) \\
=& \frac{1}{2} \Big[\left(\boldsymbol{\omega}_{i,b}^b - \mathbf{z} \right)^\top \mathbf{J} \left(\boldsymbol{\omega}_{i,b}^b - \mathbf{z} \right) - l_p \mathbf{e}_{eq}^\top \mathbf{e}_{eq} && \text{(B.233)} \\
& - \left(\boldsymbol{\omega}_{i,b}^b - \mathbf{z} - 2\mathbf{J}^{-1} l_d \mathbf{T}_{eq}^\top \mathbf{e}_{eq} \right)^\top \mathbf{J} \left(\boldsymbol{\omega}_{i,b}^b - \mathbf{z} - 2\mathbf{J}^{-1} l_d \mathbf{T}_{eq}^\top \mathbf{e}_{eq} \right) \Big] \\
& - \lambda \mathbf{e}_{eq}^\top \mathbf{T}_{eq} \mathbf{J} \left(\boldsymbol{\omega}_{i,b}^b - \mathbf{z} - 2\mathbf{J}^{-1} l_d \mathbf{T}_{eq}^\top \mathbf{e}_{eq} \right),
\end{aligned}$$

where $\mathbf{e}_{e\omega} = \boldsymbol{\omega}_{i,b}^b - \boldsymbol{\omega}_{i,e}^b$ and (4.31) was inserted, and the fact that $\mathbf{T}_{eq}^\top \mathbf{e}_{eq} = \mathbf{0}$ for $\mathbf{x}^+ \in D_2$ which implies that $\mathbf{e}_{e\omega} = \boldsymbol{\omega}_{i,b}^b - \mathbf{z}$. For (B.230) to hold according to (4.35) we require that

$$\begin{aligned}
l_p \mathbf{e}_{eq}^\top \mathbf{e}_{eq} + 4 l_d^2 \mathbf{e}_{eq}^\top \mathbf{T}_{eq} \mathbf{J}^{-1} \mathbf{T}_{eq}^\top \mathbf{e}_{eq} \geq & 4 l_d \boldsymbol{\omega}_{i,b}^{b,\top} \mathbf{T}_{eq}^\top \mathbf{e}_{eq} - 4 l_d \mathbf{z}^\top \mathbf{T}_{eq}^\top \mathbf{e}_{eq} - 2\lambda \boldsymbol{\omega}_{i,b}^{b,\top} \mathbf{J} \mathbf{T}_{eq}^\top \mathbf{e}_{eq} \\
& + 2\lambda \mathbf{z}^\top \mathbf{J} \mathbf{T}_{eq}^\top \mathbf{e}_{eq} + 4\lambda l_d \mathbf{e}_{eq}^\top \mathbf{T}_{eq} \mathbf{T}_{eq}^\top \mathbf{e}_{eq}. \quad \text{(B.234)}
\end{aligned}$$

Now, for $\eta_{e,b} = \delta_\eta$ we have $\boldsymbol{\epsilon}_{eq}^\top \boldsymbol{\epsilon}_{eq} = 1 - \delta_\eta^2$, $\|\mathbf{T}_{eq}^\top \mathbf{e}_{eq}\| = 1/2 \|\boldsymbol{\epsilon}_{eq}\| = 1/2\sqrt{1-\delta_\eta^2}$ and $\mathbf{e}_{eq}^\top \mathbf{e}_{eq} = (1-\delta_\eta)^2 + \boldsymbol{\epsilon}_{eq}^\top \boldsymbol{\epsilon}_{eq} = 2(1-\delta_\eta)$ so

$$l_p^{\star''} := \frac{(2l_d + \lambda j_M)(\Delta + \Delta_z)\sqrt{1-\delta_\eta^2} - l_d \left(\frac{l_d}{j_M} - \lambda \right)(1-\delta_\eta^2)}{2(1-\delta_\eta)}, \tag{B.235}$$

where $\|\mathbf{z}\| \leq \Delta_z$ for a constant upper bound $\Delta_z > 0$. This can be argued by looking at (3.31), where $\mathbf{T}_{eq}^\top \mathbf{e}_{eq}$ and $\mathbf{T}_e^\top \mathbf{e}_q$, according to the previous part of the proof, converge towards a subset of $\mathcal{A}_\delta$ for $\mathbf{x} \in C$ and, if $\mathbf{x}$ is entering a jump set (D_1 or D_2) the value of $\mathbf{z}$ does not change abruptly during a jump hence, $\dot{\mathbf{z}}$ still converges towards $\mathbf{a}_d$ as given in (3.26), which can not be constant and sign-definite because that would violate Assumption 3.2, thus $\lim_{t\to\infty} \int_{t_0}^t \mathbf{a}_d d\tau < \infty$.

To summarize for any given requirement δ and β_d, the controller gains (including l_p) have to be chosen large enough (for instance $l_p > l_p^\star$) such that the flow enters the set $\mathcal{A}$, and $l_p > l_p^{\star'}$ for (B.224) to be fulfilled. Furthermore, for any chosen $\delta_\eta \in (0,1)$ we need to choose $l_p > l_p^{\star''}$ according to (B.235). Thus, we set $l_p > \max\{l_p^\star, l_p^{\star'}, l_p^{\star''}\}$. Now, all conditions are fulfilled according to (Sanfelice *et al.*, 2007, Corollary 7.7) and it can be concluded that the set $\mathcal{A}$ of the closed-loop system is UAS in the large, and furthermore, from (B.227)–(B.228) we have shown that the residual can be arbitrarily diminished and the set of initial angular velocities can be arbitrarily enlarged by increasing the controller gains.

Remark B.1 *Eq.* (B.234) *makes sure that the decrease in the Lyapunov function caused by attitude is larger than the increase caused by the observer angular velocity during jumps. Therefore, we want* $\delta_\eta << 1$ *to obtain* $l_p^{\star''}$ *as small as possible, but on the other hand we want* $\delta_\eta \approx 1$ *in* (B.215b) *to make* l_d *as small as possible, which leads to a small* $l_p^{\star'}$*. Note that in some cases we can find a lower bound on* l_p *by choosing* $l_p^{\star''} = \max\{l_p^\star, l_p^{\star'}\}$ *and solve* (B.235) *for* δ_η *although one has to be certain that the result is positive.*

B.19 Proof of Theorem 6.1

Without loss of generality, we show stability of the positive equilibria *i.e.*, let $\mathbf{e}_{sq} = \mathbf{e}_{sq+}$ and $\mathbf{T}_{se} = \mathbf{T}_{se}(\mathbf{e}_{sq+})$.

By insertion of (6.6) into (2.83) we obtain the closed-loop rotational dynamics

$$\dot{\mathbf{e}}_{f\omega} = \mathbf{J}_f^{-1}\left\{-\left[k_{fd}\mathbf{I} - \mathbf{S}(\mathbf{J}_f\boldsymbol{\omega}_{i,fb}^{fb})\right]\mathbf{e}_{f\omega} - k_{fp}\mathbf{T}_{fe}^\top\mathbf{e}_{fq} + k_{fp}\mathbf{T}_{le}^\top\mathbf{e}_{lq} + k_{fd}\mathbf{R}_{lb}^{fb}\mathbf{e}_{l\omega}\right\}, \tag{B.236}$$

such that the total closed-loop system can be written as

$$\dot{\mathbf{x}}_1 = f(\mathbf{x}_1) + g(\mathbf{x})\mathbf{x}_2, \tag{B.237}$$

where

$$f(\mathbf{x}_1) = \begin{bmatrix} \mathbf{T}_{fe}^\top\mathbf{e}_{f\omega} \\ \mathbf{J}_f^{-1}\left[\mathbf{S}(\mathbf{J}\boldsymbol{\omega}) - k_{fd}\mathbf{I}\right]\mathbf{e}_{f\omega} - k_{fp}\mathbf{T}_{fe}^\top\mathbf{e}_{fq} \end{bmatrix}, \tag{B.238}$$

which is similar to the closed-loop system in (B.9), and was proven uniformly exponentially stable according to Theorem 3.3, and the interconnection term is

$$g(\mathbf{x}) = \begin{bmatrix} \mathbf{J}_f^{-1}k_{fp}\mathbf{T}_{le}^\top & \mathbf{0} \\ \mathbf{0} & k_{fd}\mathbf{J}_f^{-1}\mathbf{R}_{lb}^{fb} \end{bmatrix}, \tag{B.239}$$

where $\mathbf{x}_1 = [\mathbf{e}_{fq}^\top,\ \mathbf{e}_{f\omega}^\top]^\top$, $\mathbf{x}_2 = [\mathbf{e}_{lq}^\top,\ \mathbf{e}_{l\omega}^\top]^\top$ and $\mathbf{x} = [\mathbf{x}_1^\top,\ \mathbf{x}_2^\top]^\top$. The total system is then on the cascaded form (A.65)–(A.66). In what follows we show that Assumptions A.1–A.3 hold hence, that the origin of the closed-loop system is uniformly asymptotically stable according to Theorem A.11.

Proof of Assumption A.1

We start by considering $\delta' = 1$ (where in this case δ' is the parameter given in Assumption A.1). By evaluating (A.68) on $V_f(\mathbf{x}_1) = 1/2(\mathbf{e}_{f\omega}^\top\mathbf{J}_f\mathbf{e}_{f\omega} + \mathbf{e}_{fq}^\top k_{fp}\mathbf{e}_{fq})$ we obtain

$$\|\mathbf{e}_{f\omega}^\top\mathbf{J}_f + \mathbf{e}_{fq}^\top k_{fp}\|\|\mathbf{x}_1\| \leq c_{12}V_f(\mathbf{x}_1) = \frac{c_{12}}{2}\left[\mathbf{e}_{f\omega}^\top\mathbf{J}_f\mathbf{e}_{f\omega} + \mathbf{e}_{fq}^\top k_{fp}\mathbf{e}_{fq}\right], \tag{B.240}$$

and by applying the triangular inequality on the left side of (B.240) and squaring, we obtain

$$\left(\|\mathbf{e}_{f\omega}^\top\mathbf{J}_f\| + \|\mathbf{e}_{fq}^\top k_{fp}\|\right)^2\|\mathbf{x}_1\|^2 \leq \frac{c_{12}^2}{4}\left[\mathbf{e}_{f\omega}^\top\mathbf{J}_f\mathbf{e}_{f\omega} + \mathbf{e}_{fq}^\top k_{fp}\mathbf{e}_{fq}\right]^2. \tag{B.241}$$

On the left side of (B.241) we apply $\|x\|^2 + \|y\|^2 + 2\|x\|\|y\| \leq 2(\|x\|^2 + \|y\|^2)$ and $\beta_{fj} \leq \|\mathbf{J}_f\| \leq \beta_{fJ}$ such that

$$\left(\|\mathbf{e}_{f\omega}^\top \mathbf{J}_f\| + \|\mathbf{e}_{fq}^\top k_{fp}\|\right)^2 \leq 2\varphi \left(\mathbf{e}_{f\omega}^\top \mathbf{J}_f \mathbf{e}_{f\omega} + \mathbf{e}_{fq}^\top k_{fp} \mathbf{e}_{fq}\right), \tag{B.242}$$

where $\varphi = \max\{\beta_{fJ}, k_{fp}\}$. By insertion of (B.242) in (B.241) we obtain

$$2\varphi \left(\mathbf{e}_{f\omega}^\top \mathbf{e}_{f\omega} + \mathbf{e}_{fq}^\top \mathbf{e}_{fq}\right) \leq \frac{c_{12}^2 \rho}{4} \left(\mathbf{e}_{f\omega}^\top \mathbf{e}_{f\omega} + \mathbf{e}_{fq}^\top \mathbf{e}_{fq}\right), \tag{B.243}$$

where $\rho = \min\{\beta_{fj}, k_{fp}\}$, and thus we have to choose

$$c_{12} \geq \sqrt{\frac{8\varphi}{\rho}} \tag{B.244}$$

to fulfill (A.68). For (A.69) we have that

$$\|\mathbf{e}_{f\omega}^\top \mathbf{J}_f + \mathbf{e}_{fq}^\top k_{fp}\| \leq c_{13}, \tag{B.245}$$

and by using the triangular inequality, squaring and applying (B.242) we obtain

$$2\varphi^2 \|\mathbf{x}_1\|^2 \leq c_{13}^2. \tag{B.246}$$

Since $\|\mathbf{x}_1\| \leq 1$ we have to choose

$$c_{13} \geq \sqrt{2}\varphi \tag{B.247}$$

to fulfill (A.69), and thus assumption A.1 is fulfilled.

Proof of Assumption A.2

Since $\|\mathbf{T}_{le}\| \leq 1/2$, (B.239) obviously fulfills the growth rate criteria of (A.70), such that

$$\|g(\mathbf{x})\| \leq \frac{1}{2} \left[\left(\frac{1}{J_{fx}^2} + \frac{1}{J_{fy}^2} + \frac{1}{J_{fz}^2} \right) \left(k_{fp}^2 + 4k_{fd}^2\right) \right]^{1/2} =: \xi', \tag{B.248}$$

where $\xi' > 0$ is constant, and thus assumption A.2 is fulfilled.

Proof of Assumption A.3.

This assumption holds because $\|\mathbf{x}_2(t)\|$ converges to zero exponentially fast.

We conclude that the equilibrium point $(\mathbf{e}_{lq}, \mathbf{e}_{l\omega}, \mathbf{e}_{fq}, \mathbf{e}_{f\omega}) = (\mathbf{0}, \mathbf{0}, \mathbf{0}, \mathbf{0})$ of the cascaded system is UAS.

The proof for the other equilibria follows *mutatis mutandis*.

B.20 Proof of Theorem 6.2

Without loss of generality, we show stability of the positive equilibria *i.e.*, let $\mathbf{e}_{sq} = \mathbf{e}_{sq+}$ and $\mathbf{T}_{se} = \mathbf{T}_{se}(\mathbf{e}_{sq+})$.

We start by assuming that we have available controller gains according to $\boldsymbol{\theta}_1 = [k_{fq}, k_{f\omega}]^\top \in \Theta_1 = \mathbb{R}_+^2$ and $\boldsymbol{\theta}_2 = [k_{lq}, k_{l\omega}]^\top \in \Theta_2 = \mathbb{R}_+^2$. By inserting (6.7) and $\boldsymbol{\omega}_{i,r}^{fb}$ and $\mathbf{s}_f$ into (2.83) we obtain the closed-loop dynamics

$$\dot{\mathbf{s}}_f = \mathbf{J}_f^{-1} \left\{ [\mathbf{S}(\mathbf{J_f} \boldsymbol{\omega}_{i,fb}^{fb}) - k_{f\omega} \mathbf{I}] \mathbf{s}_f - k_{fq} \mathbf{T}_{fe}^\top \mathbf{e}_{fq} + k_{fq} \mathbf{T}_{le}^\top \mathbf{e}_{lq} + k_{f\omega} \mathbf{s}_l + \boldsymbol{\tau}_d \right\} \tag{B.249}$$

such that the total closed-loop system can be written as

$$\dot{\boldsymbol{\chi}}_1 = \tilde{f}(\boldsymbol{\chi}_1) + \tilde{g}(\boldsymbol{\chi})\boldsymbol{\chi}_2, \tag{B.250}$$

where

$$\tilde{f}(\boldsymbol{\chi}_1) = \begin{bmatrix} \mathbf{T}_{fe}\mathbf{s}_f - \mathbf{T}_{fe}\gamma\mathbf{T}_{fe}^\top\mathbf{e}_{fq} \\ \mathbf{J}_f^{-1}\left\{[\mathbf{S}(\mathbf{J}_f\boldsymbol{\omega}_{i,fb}^b) - k_{f\omega}\mathbf{I}]\mathbf{s}_f - k_{fq}\mathbf{T}_{fe}^\top\mathbf{e}_{fq} + \boldsymbol{\tau}_d\right\} \end{bmatrix}, \tag{B.251}$$

which is similar to the closed-loop system in (B.40), and was proven uniformly practically exponentially stable according to Theorem 3.5, and the interconnection term is

$$\tilde{g}(\boldsymbol{\chi}) = \begin{bmatrix} \mathbf{J}_f^{-1}k_{fp}\mathbf{T}_{le}^\top & \mathbf{0} \\ \mathbf{0} & k_{fd}\mathbf{J}_f^{-1} \end{bmatrix}, \tag{B.252}$$

where $\boldsymbol{\chi}_1 = [\mathbf{e}_{fq}^\top,\ \mathbf{s}_f^\top]^\top$, $\boldsymbol{\chi}_2 = [\mathbf{e}_{lq}^\top,\ \mathbf{s}_l^\top]^\top$ and $\boldsymbol{\chi} = [\boldsymbol{\chi}_1^\top,\ \boldsymbol{\chi}_2^\top]^\top$. Along with the closed-loop system for the leader, the total system is on the form (A.72)–(A.73).

The rest of the proof consists in verifying the conditions of Theorem A.12.

Proof of Assumption A.4

The function $\tilde{g}(\boldsymbol{\chi})\boldsymbol{\chi}_2$ is uniformly bounded both in time and in $\boldsymbol{\theta}_2$ and vanishes with $\boldsymbol{\chi}_2$, thus for any $\boldsymbol{\theta}_1 \in \Theta_1$ we choose

$$\begin{aligned} G_{\boldsymbol{\theta}_1}(\|\boldsymbol{\chi}\|) =& \frac{1}{2}\left[\left(\frac{1}{J_x^2} + \frac{1}{J_y^2} + \frac{1}{J_z^2}\right)\left(k_{fq}^2 + 4k_{f\omega}^2\right)\right]^{1/2} \\ \Psi_{\boldsymbol{\theta}_1}(\|\boldsymbol{\chi}_2\|) =& \|\boldsymbol{\chi}_2\|, \end{aligned} \tag{B.253}$$

thus $G_{\boldsymbol{\theta}_1}(\|\boldsymbol{\chi}\|)$ is constant and $\Psi_{\boldsymbol{\theta}_1}(\|\boldsymbol{\chi}_2\|)$ is of class $\mathcal{K}_\infty$, and the Assumption is fulfilled for all $\boldsymbol{\theta}_2 \in \Theta_2$ and all $\boldsymbol{\chi} \in S_e^3 \times \mathbb{R}^3 \times S_e^3 \times \mathbb{R}^3$.

Proof of Assumption A.5

We recall from Theorem 3.5 that uniform practical exponential stability was obtained which holds for the leader and follower system separately. We can not claim semi-global results for the same reasons as we can not claim global results. Nevertheless, we assume that both Δ_1 and Δ_2 can be chosen arbitrary large to make it easier to follow the lines of the theorem.

Proof of Assumption A.6

By following the lines of Theorem 3.5 using the Lyapunov function candidate (B.31) we obtain $\dot{V}_f < 0$ when $\|\boldsymbol{\chi}_1\| > \beta_{fd}/q_{fm} := \delta_1$, where $q_{fm} > 0$ is the smallest eigenvalue of $\mathbf{Q}_f := \text{diag}\{\mathbf{T}_{fe}k_{fq}\gamma_f\mathbf{T}_{fe}^\top, k_{f\omega}\mathbf{I}\}$, which is defined similar to $\mathbf{Q}$ in (B.41). An increase of β_{fd} can as well be counteracted by increasing the controller gains, thus, given any $\Delta_1 > \delta_1 > 0$, there exist a parameter $\boldsymbol{\theta}_1^\star(\delta_1, \Delta_1) \in \Theta_1$. We choose $\underline{\alpha}_{\delta_1,\Delta_1}(\|\boldsymbol{\chi}_1\|) = 1/2\min\{\beta_{fj}, k_{fq}\}\|\boldsymbol{\chi}_1\|^2$ and $\overline{\alpha}_{\delta_1,\Delta_1}(\|\boldsymbol{\chi}_1\|) = 1/2\max\{\beta_{fJ}, k_{fq}\}\|\boldsymbol{\chi}_1\|^2$ and thus the first part of the assumption is fulfilled, and the second part is fulfilled for $\alpha_{\delta_1,\Delta_1}(\|\boldsymbol{\chi}_1\|) = \min\{\gamma_f k_{fq}/8, k_{f\omega}\}\|\boldsymbol{\chi}_1\|^2$. The last inequality also holds similar to (B.245)-(B.247) with $c_{\delta_1,\Delta_1}(\|\boldsymbol{\chi}_1\|)$ $= \sqrt{2}\varphi'\|\boldsymbol{\chi}_1\|^{1/2}$ where φ' are found in the same way as φ, and thus Assumption A.6 holds for all $\boldsymbol{\chi}_1 \in \mathcal{H}(\delta_1, \Delta_1)$, where Δ_1 can be chosen arbitrary large by assumption.

Proof of Assumption A.7
We define a LFC for the leader and follower spacecraft as

$$V_{lf}(\boldsymbol{\chi}) = \frac{1}{2}\Big(\mathbf{s}_l^\top \mathbf{J}_l \mathbf{s}_l + \mathbf{e}_{lq}^\top k_{lq} \mathbf{e}_{lq} + \mathbf{s}_f^\top \mathbf{J}_f \mathbf{s}_f + \mathbf{e}_{fq}^\top k_{fq} \mathbf{e}_{fq}\Big), \tag{B.254}$$

which is lower and upper bounded by

$$\underline{\alpha}_{lf} = \frac{1}{2}\min\{\beta_{lj}, \beta_{fj}, k_{lq}, k_{fq}\}\|\boldsymbol{\chi}\|^2 \tag{B.255}$$

$$\overline{\alpha}_{lf} = \frac{1}{2}\max\{\beta_{lJ}, \beta_{fJ}, k_{lq}, k_{fq}\}\|\boldsymbol{\chi}\|^2 \tag{B.256}$$

respectively, thus (A.81) is fulfilled, and it can be shown that (A.82) is fulfilled by differentiation of (B.254) fulfilling Proposition A.2. Also, there exists a positive constant Δ_0 such that for any given positive number δ_1, Δ_1, δ_2, Δ_2, satisfying $\Delta_1 > \max\{\delta_1, \Delta_0\}$ and $\Delta_2 > \delta_2$, there exist a δ_1 such that $\overline{\alpha}_{lf}(\delta_1) < \underline{\alpha}_{lf}(\Delta_1)$. Because of the practical stability shown, given any β_{ld} we can achieve any δ_2 by increasing the gains $\boldsymbol{\theta}_2$ and thus there exits a parameter $\boldsymbol{\theta}_2^\star \in \mathcal{D}_{f_2}(\delta_2, \Delta_2) \cap \Theta_2$, such that by applying (A.83) using the bounds (B.255)-(B.256), we see that the first equation of Assumption A.7 is fulfilled for

$$\gamma(\Delta_1) = \sqrt{\frac{\min\{\beta_{lj}, \beta_{fj}, k_{lq}, k_{fq}\}\Delta_1^2}{\max\{\beta_{lJ}, \beta_{fJ}, k_{lq}, k_{fq}\}}}. \tag{B.257}$$

Moreover, we have that

$$\underline{\alpha}_{\delta_1,\Delta_1}^{-1} \circ \overline{\alpha}_{\delta_1,\Delta_1}(\delta_1) = \sqrt{\frac{\max\{\beta_{fJ}, k_{fq}\}\delta_1^2}{\min\{\beta_{fj}, k_{fq}\}}}, \tag{B.258}$$

then for any $\Delta_\star > \delta_\star > 0$, there exists parameters δ_1, δ_2, Δ_1 and Δ_2 such that

$$\min\left\{\Delta_1, \Delta_2, \sqrt{\frac{\min\{\beta_{lj}, \beta_{fj}, k_{lq}, k_{fq}\}\Delta_1^2}{\max\{\beta_{lJ}, \beta_{fJ}, k_{lq}, k_{fq}\}}}\right\} \geq \Delta_\star \tag{B.259}$$

since Δ_1 and Δ_2 can be chosen arbitrarily large and the constants β_{sj}, β_{sJ}, k_{sq}, $k_{s\omega} > 0$, and

$$\max\left\{\delta_2, \sqrt{\frac{\max\{\beta_{fJ}, k_{fq}\}\delta_1^2}{\min\{\beta_{fj}, k_{fq}\}}}\right\} \leq \delta_\star, \tag{B.260}$$

is fulfilled since by decreasing δ_1, k_{fq} is increased but only of order one, and thus the two last inequalities of Assumption A.7 are fulfilled and thus Assumption A.7 holds. It can then be concluded that the equilibrium point $(\mathbf{e}_{lq}, \mathbf{e}_{l\omega}, \mathbf{e}_{fq}, \mathbf{e}_{f\omega}) = (\mathbf{0}, \mathbf{0}, \mathbf{0}, \mathbf{0})$ of the cascaded system is uniformly practically asymptotically stable.

The proof for the other equilibria follows *mutatis mutandis*.

B.21 Proof of Theorem 6.3

We start by assuming that we have available controller gains according to $\boldsymbol{\theta}_1 := [k_{fq}, k_{f\omega}]^\top \in \Theta_1 = \mathbb{R}^2_+$ and $\boldsymbol{\theta}_2 := [k_{lq}, k_{l\omega}]^\top \in \Theta_2 = \mathbb{R}^2_+$. By inserting (6.13a) into (2.90) and utilizing (6.13c), we obtain the closed-loop rotational dynamics

$$\dot{\mathbf{s}}_{fh} = \mathbf{J}_f^{-1}\left\{-[\mathbf{C}_r(\boldsymbol{\omega}) + k_{f\omega}\mathbf{I}]\mathbf{s}_{fh} - k_{fq}\mathbf{T}_{fh}^\top \mathbf{e}_{fhq} + \boldsymbol{\tau}_d + \boldsymbol{\Upsilon}_l\right\}, \tag{B.261}$$

where $\boldsymbol{\Upsilon}_l = -\mathbf{J}_f \mathbf{R}_{lb}^{fb}\mathbf{J}_l^{-1}\left(\boldsymbol{\tau}_{dl}^{lb} + \boldsymbol{\tau}_{al}^{lb}\right)$, such that the total closed-loop system can be written as

$$\dot{\mathbf{x}}_1 = f(\mathbf{x}_1) + g(\mathbf{x}_2, \boldsymbol{\theta}_2), \tag{B.262}$$

where

$$f(\mathbf{x}_1) = \begin{bmatrix} \mathbf{T}_{fh}\mathbf{s}_{fh} - \mathbf{T}_{fh}\gamma_f \mathbf{T}_{fh}^\top \mathbf{e}_{fhq} \\ \mathbf{J}_f^{-1}\left\{-[\mathbf{C}_r(\boldsymbol{\omega}) + k_{f\omega}\mathbf{I}]\mathbf{s}_{fh} - k_{fq}\mathbf{T}_{fh}\mathbf{e}_{fhq} + \boldsymbol{\tau}_d\right\} \end{bmatrix}, \tag{B.263}$$

and the interconnection term is

$$g(\boldsymbol{\chi}_2, \boldsymbol{\theta}_2) := \begin{bmatrix} 0 \\ -\mathbf{R}_{lb}^{fb}\mathbf{J}_l^{-1}(\boldsymbol{\tau}_{ld}^{lb} + \boldsymbol{\tau}_{la}^{lb}) \end{bmatrix}, \tag{B.264}$$

$\boldsymbol{\chi}_1 := [\mathbf{e}_{fhq}^\top,\ \mathbf{s}_{fh}^\top]^\top$, $\boldsymbol{\chi}_2 := [\mathbf{e}_{lhq}^\top,\ \mathbf{s}_{lh}^\top]^\top$ and $\boldsymbol{\chi} := [\boldsymbol{\chi}_1^\top,\ \boldsymbol{\chi}_2^\top]^\top$. Along with the system for the leader as presented in Appendix B.17 and Corollary 4.3, the total system is on the form (A.72)–(A.73). Note that Theorem A.12 can not be utilized because (A.74) of Assumption A.4 requires that the interconnection term is a function of the follower gains ($\boldsymbol{\theta}_1$) while clearly (B.264) is a function of $\boldsymbol{\theta}_2$ because the leader control law is part of it –*cf.* (4.19). Therefore we continue the analysis along the lines of Lemma A.2 were we already know that the driving system is uniformly practically exponentially (and therefore also asymptotically) stable. By looking at the connection term we see that since $V_l(\boldsymbol{\chi}_2)$ is positive definite and proper and $\dot{V}_l$ is negative definite for $\|\boldsymbol{\chi}_2\| > \delta_l$ we obtain that $\|\boldsymbol{\chi}_2\|$ is bounded that is, for any $r > 0$ there exists $\Delta(r) > 0$ such that $\sup_{t\geq t_0}\|\mathbf{s}_{lh}(t)\| \leq \sup_{t\geq t_0}\|\boldsymbol{\chi}_2(t)\| \leq \Delta$ for all initial conditions $\|\boldsymbol{\chi}_2(t_0)\| < r$, $t_0 \geq 0$. From Assumption 3.2 we know that $\|\boldsymbol{\omega}_{i,ld}^{lb}\| \leq \beta_{\boldsymbol{\omega}_{ld}}$ and $\|\dot{\boldsymbol{\omega}}_{i,ld}^{lb}\| \leq \beta_{\dot{\boldsymbol{\omega}}_{ld}}$ are continuous and bounded functions for some positive constants. Thus it follows from the definition of the sliding surface (4.15c) that the angular velocity of the leader spacecraft is upper bounded, *i.e.* $\|\boldsymbol{\omega}_{i,lb}^{lb}(t)\| \leq \Delta_\omega := \beta_{\boldsymbol{\omega}_{ld}} + \Delta + \gamma/2$ for all $t \geq t_0 \geq 0$. The derivative of (4.15b) can be denoted as

$$\dot{\boldsymbol{\omega}}_{lr} = \dot{\boldsymbol{\omega}}_{i,ld}^{lb} - \gamma_l(\dot{\mathbf{T}}_{lh}^\top \mathbf{e}_{lhq} + \mathbf{T}_{lh}^\top \dot{\mathbf{e}}_{lhq}), \tag{B.265}$$

where according to Lemma 4.2 we have

$$\dot{\mathbf{T}}_{lh}^\top \mathbf{e}_{lhq} = \frac{1}{4}\left\{h_l[\tilde{\eta}_l\mathbf{I} + \mathbf{S}(\tilde{\boldsymbol{\epsilon}}_l)] - \mathbf{I}\right\}\left[\mathbf{s}_l - \frac{1}{2}\gamma_l h_l \tilde{\boldsymbol{\epsilon}}_l\right], \tag{B.266}$$

and by inserting (B.266) and (4.2) into (B.265) we obtain

$$\dot{\boldsymbol{\omega}}_{lr} = \dot{\boldsymbol{\omega}}_{i,ld}^{lb} - \frac{1}{4}\gamma_l h_l[\tilde{\eta}_l\mathbf{I} + \mathbf{S}(\tilde{\boldsymbol{\epsilon}}_l)][\mathbf{s}_{lh} - \gamma_l \mathbf{T}_{lh}^\top \mathbf{e}_{lhq}]. \tag{B.267}$$

Then by inserting (4.15b), (B.267) and (4.15c) into (4.19) we obtain

$$\begin{aligned}\boldsymbol{\tau}_{la}^{lb} =&\mathbf{J}_l\left(\dot{\boldsymbol{\omega}}_{i,ld}^{lb} - \frac{1}{4}\gamma_l h_l[\tilde{\eta}_l\mathbf{I} + \mathbf{S}(\tilde{\boldsymbol{\epsilon}}_l)][\mathbf{s}_{lh} - \gamma_l\mathbf{T}_{lh}^{\top}\mathbf{e}_{lhq}]\right) \\ &- \mathbf{S}(\mathbf{J}_l\boldsymbol{\omega}_{i,lb}^{lb})[\boldsymbol{\omega}_{i,ld}^{lb} - \gamma_l\mathbf{T}_{lh}^{\top}\mathbf{e}_{lhq}] - k_{lq}\mathbf{T}_{lh}^{\top}\mathbf{e}_{lhq} - k_{l\omega}\mathbf{s}_{lh}.\end{aligned} \tag{B.268}$$

Since all terms in (B.268) are either constant or upper bounded we have that $\|\boldsymbol{\tau}_{la}^{lb}(t)\| \leq \beta_{la}(\boldsymbol{\theta}_2)$, where $\beta_{la}(\boldsymbol{\theta}_2)$ is a positive parameter, for all $t \geq t_0 \geq 0$ and finite for each $\delta_l > 0$ where δ_l denotes the size of the residual $\bar{\mathcal{B}}_{\delta_l}$ for the leader spacecraft. The interconnection term (B.264) can thus be written as

$$\|g(\boldsymbol{\chi}_2, \boldsymbol{\theta}_2)\| \leq 1/j_{lm}[\beta_{ld} + \beta_{la}(\boldsymbol{\theta}_2)], \tag{B.269}$$

and we conclude that the interconnection term is uniformly bounded *for any given* δ_l.

For the follower we define a Lyapunov function candidate as

$$V_f(\mathbf{x}_1) := \frac{1}{2}(\mathbf{s}_{fh}^{\top}\mathbf{J}_f\mathbf{s}_{fh} + \mathbf{e}_{fhq}^{\top}k_{fq}\mathbf{e}_{fhq}), \tag{B.270}$$

which is positive definite and proper according to the discussion in the beginning of proof of Theorem 4.1. Its total time derivative along the trajectories of the closed-loop system f of (B.262) is

$$\begin{aligned}\dot{V}_f =& -\mathbf{s}_{fh}^{\top}\mathbf{C}_r(\boldsymbol{\omega})\mathbf{s}_{fh} - \mathbf{s}_{fh}^{\top}k_{f\omega}\mathbf{s}_{fh} - \mathbf{s}_{fh}^{\top}k_{fq}\mathbf{T}_{fh}^{\top}\mathbf{e}_{fhq} + \mathbf{e}_{fhq}^{\top}k_{fq}\mathbf{T}_{fh}\mathbf{s}_{fh} \\ &- \mathbf{e}_{fhq}^{\top}k_{fq}\mathbf{T}_{fh}\gamma_f\mathbf{T}_{fh}^{\top}\mathbf{e}_{fhq} + \mathbf{s}_{fh}^{\top}\left[\boldsymbol{\tau}_{fd}^{fb} - \mathbf{R}_{lb}^{fb}\mathbf{J}_l^{-1}(\boldsymbol{\tau}_{ld}^{lb} + \boldsymbol{\tau}_{la}^{lb})\right]\end{aligned} \tag{B.271}$$

and by inserting (6.13c) and applying the fact that $\mathbf{C}_r(\boldsymbol{\omega})$ is skew-symmetric, we obtain

$$\dot{V}_f \leq -\boldsymbol{\chi}_1^{\top}\mathbf{Q}_f\boldsymbol{\chi}_1 + \mathbf{s}^{\top}\left[\boldsymbol{\tau}_{fd}^{fb} - \mathbf{R}_{lb}^{fb}\mathbf{J}_l^{-1}(\boldsymbol{\tau}_{ld}^{lb} + \boldsymbol{\tau}_{la}^{lb})\right], \tag{B.272}$$

where $\mathbf{Q}_f := \text{diag}\{\gamma_f k_{fq}/8\mathbf{I},\ k_{f\omega}\mathbf{I}\}$ is obtained by applying Lemma 4.1, and is therefore positive definite. Eq. (B.272) can now be written as

$$\dot{V}_f \leq -q_{fm}\|\boldsymbol{\chi}_1\|^2 + \beta_f\|\boldsymbol{\chi}_1\|\ , \tag{B.273}$$

where $\beta_f := \beta_{fd} + 1/j_{lm}(\beta_{ld} + \beta_{la}(\boldsymbol{\theta}_2))$ and $q_{fm} > 0$ is the smallest eigenvalue of $\mathbf{Q}_f$. Thus $\dot{V}_f < 0$ when $\|\boldsymbol{\chi}_1\| > \delta_f := \beta_f/q_{fm}$ and δ_f can be diminished by increasing q_{fm} which is done by increasing the controller gains. The change in V_f during jumps is expressed as

$$V_f(G_f(\mathbf{x}_1)) - V_f(\mathbf{x}_1) = 2h_f(k_{fq}\tilde{\eta}_f - \frac{1}{2}\gamma_f\tilde{\boldsymbol{\epsilon}}_f^{\top}\mathbf{J}_f\mathbf{e}_{f\omega})\ , \tag{B.274}$$

and by defining the flow and jump sets as in (6.14) we ensure that $V_f(G_f(\mathbf{x}_1)) - V_f(\mathbf{x}_2) < -2\sigma_f$ when $\mathbf{x}_1 \in D_f$, thus V_f is strictly decreasing over jumps, and then

$$\dot{V}_f \leq 0 \quad \forall \mathbf{x}_1 \in C_f/\mathcal{B}_{\delta_f}\ , \tag{B.275a}$$

$$V_f(G_f(\mathbf{x}_1)) - V_f(\mathbf{x}_1) < 0 \quad \forall \mathbf{x}_1 \in D_f\ . \tag{B.275b}$$

Thus, from Theorem 4.2, Corollary 4.3 and the above analysis we have that both the sets $\mathcal{A}_l = \{\mathbf{x}_2 \in S_h^3 \times \mathbb{R}^3 \times H : (\mathbf{e}_{lhq},\ \mathbf{s}_{lh}) \in \bar{\mathcal{B}}_{\delta_l}\}$ and $\mathcal{A}_f = \{\mathbf{x}_1 \in S_h^3 \times \mathbb{R}^3 \times H : (\mathbf{e}_{fhq},\ \mathbf{s}_{fh}) \in \bar{\mathcal{B}}_{\delta_f}\}$ are uniformly asymptotically stable, and it follows that since both the set of the *driving* system and the set of the *driven* system are uniformly asymptotically stable in the large on the set $S_h^3 \times \mathbb{R}^3$ and the *interconnection* term is uniformly bounded, the set $\mathcal{A} = \{\mathbf{x} \in S_h^3 \times \mathbb{R}^3 \times H \times S_h^3 \times \mathbb{R}^3 \times H : (\mathbf{e}_{fhq},\ \mathbf{s}_{fh},\ \mathbf{e}_{lhq},\ \mathbf{s}_{fh}) \in \bar{\mathcal{B}}_{\delta_r}\}$ where $\delta_r = \delta_f + \delta_l$ of the closed-loop system for the total cascaded system is uniformly asymptotically stable in the large on the set $S_h^3 \times \mathbb{R}^3 \times S_h^3 \times \mathbb{R}^3$.

B.22 Proof of Theorem 6.4

By inserting (6.19) into (2.62) and applying (6.21), the closed-loop dynamics may be written as

$$m_f \dot{\mathbf{s}} + (\mathbf{C}_t + \mathbf{K}_d)\,\mathbf{s} + \mathbf{K}_p \tilde{\mathbf{p}} - \mathbf{f}_{fd} + \frac{m_f}{m_l}(\mathbf{f}_{ld} + \mathbf{f}_{la}) = \mathbf{0}\,. \tag{B.276}$$

A suitable Lyapunov function candidate is chosen as

$$V_t(\mathbf{x}) := \frac{1}{2}\mathbf{s}^\top m_f \mathbf{s} + \frac{1}{2}\tilde{\mathbf{p}}^\top \mathbf{K}_p \tilde{\mathbf{p}} > 0 \quad \forall\ \mathbf{s} \neq \mathbf{0},\ \tilde{\mathbf{p}} \neq \mathbf{0}\ , \tag{B.277}$$

where $\mathbf{x} = [\mathbf{s}^\top,\ \tilde{\mathbf{p}}^\top]^\top$, which is lower and upper bounded by $\underline{\kappa} := 1/2 \min\{m_f, k_{pm}\}$ and $\overline{\kappa} := 1/2 \max\{m_f, k_{pM}\}$, respectively. By differentiation of (B.277) along the closed-loop trajectories we obtain

$$\dot{V}_t = -\mathbf{s}^\top \mathbf{C}_t \mathbf{s} - \mathbf{s}^\top \mathbf{K}_p \tilde{\mathbf{p}} - \mathbf{s}^\top \mathbf{K}_d \mathbf{s} + \tilde{\mathbf{p}}^\top \mathbf{K}_p \dot{\tilde{\mathbf{p}}} + \mathbf{s}^\top \left(\mathbf{f}_{fd} - \frac{m_f}{m_l}(\mathbf{f}_{ld} + \mathbf{f}_{la})\right), \tag{B.278}$$

and by using the fact that $\mathbf{C}_t(\boldsymbol{\omega}_{i,l}^l)$ is skew-symmetric, we further obtain

$$\begin{aligned}
\dot{V}_t &= -(\mathbf{s}^\top - \dot{\tilde{\mathbf{p}}}^\top)\mathbf{K}_p \tilde{\mathbf{p}} - \mathbf{s}^\top \mathbf{K}_d \mathbf{s} + \mathbf{s}^\top \left(\mathbf{f}_{fd} - \frac{m_f}{m_l}(\mathbf{f}_{ld} + \mathbf{f}_{la})\right) && \text{(B.279)}\\
&= -\mathbf{x}^\top \mathbf{P} \mathbf{x} + \mathbf{s}^\top \left(\mathbf{f}_{fd} - \frac{m_f}{m_l}(\mathbf{f}_{ld} + \mathbf{f}_{la})\right) && \text{(B.280)}\\
&\leq -p_m \|\mathbf{x}_t\|^2 + \alpha' \|\mathbf{x}_t\| && \text{(B.281)}
\end{aligned}$$

where $\mathbf{P} := \mathrm{diag}\{\mathbf{K}_d,\ \gamma \mathbf{K}_p\}$, $\alpha' := [\alpha_{fd} + m_f/m_l(\alpha_{ld} + \alpha_{la})]$ and $p_m > 0$ is the smallest eigenvalue of $\mathbf{P}$. Thus $\dot{V}_t(\mathbf{x}) < 0$ when $\|\mathbf{x}\| > \delta =: \alpha'/p_m$ and

$$\lim_{\delta \to 0} \frac{\overline{\kappa}(\delta)\delta^p}{\underline{\kappa}(\delta)} = \lim_{\delta \to 0} \frac{\max\{m_f, k_{pM}\}\delta^2}{\min\{m_f, k_{pm}\}} = 0, \tag{B.282}$$

which shows that δ can be diminished by increasing p_m which is done by increasing the controller gains, and we can conclude by applying Theorem A.9 that equilibrium point of the closed-loop system is uniformly globally practically exponentially stable.

B.23 Proof of Theorem 6.5

By inserting the control law (6.23) into the dynamics (2.62) and performing the coordinate transformation

$$\mathbf{z} = \boldsymbol{\xi} - \frac{1}{k_a}\mathbf{a} + \frac{k_i}{k_a}\boldsymbol{\zeta}, \tag{B.283}$$

we obtain the closed-loop dynamics

$$m_f\dot{\mathbf{s}} = -(\mathbf{C}_t + \mathbf{K}_d)\mathbf{s} - \mathbf{K}_p\tilde{\mathbf{p}} - k_a\mathbf{z} + \mathbf{b}(t). \tag{B.284}$$

A Lyapunov function candidate is defined as

$$V(\mathbf{x}) := \frac{1}{2}\left[\frac{k_p}{k_1}\left(e^{k_1\tilde{p}_x^2} + e^{k_1\tilde{p}_y^2} + e^{k_1\tilde{p}_z^2} - 3\right) + \mathbf{s}^\top m_f\mathbf{s} + \mathbf{z}^\top\mathbf{z}\right], \tag{B.285}$$

where $\mathbf{x} = [\mathbf{e}_p^\top,\ \mathbf{s}^\top,\ \mathbf{z}^\top]^\top$, which is positive definite and proper, as we show next. We want to find functions $\underline{\alpha}(\mathbf{x}), \overline{\alpha}(\mathbf{x}) \in \mathcal{K}_\infty$ such that $\underline{\alpha}(\mathbf{x}) \leq V(\mathbf{x}) \leq \overline{\alpha}(\mathbf{x})$. For the upper bound function we write

$$V(\mathbf{x}) \leq \frac{1}{2}\left[3\frac{k_p}{k_1}\left(e^{k_1\|\mathbf{x}\|^2} - 1\right) + (1 + m_f)\|\mathbf{x}\|^2\right]. \tag{B.286}$$

As typically an exponential function outgrows a squared function we want to find a constant c_{14} such that $e^{c_{14}\|\mathbf{x}\|^2} - 1 \geq \|\mathbf{x}\|^2$, *i.e.*

$$c_{14} \geq \sup_{\mathbf{x}\in\mathbb{R}^9} \frac{\ln(\|\mathbf{x}\|^2 + 1)}{\|\mathbf{x}\|^2} = 1$$

which in turn, leads us to define

$$\overline{\alpha}(\mathbf{x}) :=\ c_{15}\left(e^{c_{14}\|\mathbf{x}\|^2} - 1\right), \tag{B.287}$$

where $c_{15} := 2\max\{k_p/k_1, 1 + m_f\}$ and $c_{14} := \max\{k_1, 1\}$. Next we find a quadratic lower bound on V. Recalling that

$$e^x = \sum_{n=0}^{\infty}\frac{x^n}{n!} \geq 1 + x, \tag{B.288}$$

we obtain

$$\left(e^{k_1\tilde{p}_x^2} + e^{k_1\tilde{p}_y^2} + e^{k_1\tilde{p}_z^2} - 3\right) \geq k_1(\tilde{p}_x^2 + \tilde{p}_y^2 + \tilde{p}_z^2), \tag{B.289}$$

hence, we define

$$\underline{\alpha}(\mathbf{x}) := c_{16}\|\mathbf{x}\|^2, \tag{B.290}$$

where $c_{16} := 1/2\min\{k_p, m_f, 1\}$. Next, we evaluate the total time derivative of $V(t, \mathbf{x})$ along the closed-loop trajectories, *i.e.*

$$\begin{aligned}\dot{V}(t,\mathbf{x}) = &-\mathbf{s}^\top\left[\mathbf{C}_t(\boldsymbol{\omega}_{i,l}^l) + \mathbf{K}_d\right]\mathbf{s} - \mathbf{s}^\top\mathbf{K}_p\tilde{\mathbf{p}} - \dot{\tilde{\mathbf{p}}}^\top\mathbf{K}_p\tilde{\mathbf{p}}\\ &- \mathbf{s}^\top k_a\mathbf{z} + \mathbf{s}^\top\mathbf{b}(t) + \mathbf{z}^\top\left(k_a\dot{\tilde{\mathbf{p}}} + \frac{k_i}{k_a}\tilde{\mathbf{p}}\right).\end{aligned} \tag{B.291}$$

By inserting (6.26) and defining $\gamma := k_i/k_a^2$, we obtain

$$\begin{aligned}\dot{V}(t,\mathbf{x}) \leq & -\mathbf{s}^\top k_d \mathbf{s} - \tilde{\mathbf{p}}^\top \gamma k_p \tilde{\mathbf{p}} + \mathbf{s}^\top \mathbf{b}(t), \\ \leq & -\boldsymbol{\chi}^\top \mathbf{Q} \boldsymbol{\chi} + \alpha_d \|\boldsymbol{\chi}\|,\end{aligned} \tag{B.292}$$

where $\boldsymbol{\chi} := [\tilde{\mathbf{p}}^\top,\ \mathbf{s}^\top]^\top$ and $\mathbf{Q} := \text{diag}\{\gamma k_p \mathbf{I},\ k_d \mathbf{I}\}$. By defining $\delta := \alpha_d/q_m$ where q_m is the smallest eigenvalue of $\mathbf{Q}$ it is ensured that $\dot{V} \leq 0$ for all $\|\boldsymbol{\chi}\| \geq \delta$, and thus uniform practical stability of the equilibrium point is obtained, *i.e.* $V(t_2) \leq V(t_1)$, $\forall\, t_2 > t_1 > t_0$ when $\|\boldsymbol{\chi}\| \geq \delta$, and thus it follows that the state $\mathbf{x}$ is uniformly bounded. To prove convergence we apply Barbalat's lemma[5] (Khalil, 2002). By differentiation of (B.292) we obtain

$$\begin{aligned}\ddot{V}(t,\mathbf{x}) = & 2\mathbf{s}^\top (\mathbf{C}_t + \mathbf{K}_d)\, \mathbf{s} + 2\mathbf{s}^\top \mathbf{K}_p \tilde{\mathbf{p}} + 2\mathbf{s}^\top k_a \mathbf{z} \\ & - 2\mathbf{s}^\top \mathbf{b}(t) - 2\tilde{\mathbf{p}}^\top k_p \dot{\tilde{\mathbf{p}}} - \mathbf{s}^\top (\mathbf{C}_t^\top + \mathbf{K}_d)\mathbf{b}(t) \\ & - \tilde{\mathbf{p}} \mathbf{K}_p \mathbf{b}(t) - \mathbf{z}^\top k_a \mathbf{b}(t) + \mathbf{b}(t)^\top \mathbf{b}(t) + \mathbf{s}^\top \dot{\mathbf{b}}(t),\end{aligned} \tag{B.293}$$

where all terms are either shown to be bounded (since the equilibrium point of the closed-loop system was shown to be uniformly stable and the leader is assumed perfectly tracking a bounded reference), or are bounded by hypothesis, thus $\ddot{V}$ is bounded, which proves that $\dot{V}$ is uniformly continuous, and since V is lower bounded and $\dot{V}$ is negative semi-definite for $\|\boldsymbol{\chi}\| \geq \delta$, we apply Barbalat's lemma indicating that $\|\boldsymbol{\chi}\| \to \delta$ as $t \to \infty$.

B.24 Proof of idempotent property for $\mathbf{J}_r$

For $\mathbf{J}_r$ in (8.28)to be idempotent, the matrix has to fulfill $\mathbf{J}_r = \mathbf{J}_r^2$ which means that $\mathbf{A} = \mathbf{A}^2$. By use of mathematic induction, the matrix $\mathbf{A}^2 = [a_{ij}],\ i,j \in \{1,\ldots,n\}$ with $a_{ij} = (1-\frac{1}{n})^2 + (k-1)(\frac{1}{n})^2$ for $i = j$ and $a_{ij} = -\frac{2}{n}(1-\frac{1}{n}) + (k-2)(\frac{1}{n})^2$ for $i \neq j$. For the idempotent property to be true, each element in $\mathbf{A}$ have to be the same as in $\mathbf{A}^2$. This can be solved as

$$(1-\frac{1}{n})^2 + (k-1)(\frac{1}{n})^2 = 1 - \frac{1}{n} \tag{B.294}$$

$$1 - \frac{2}{n} + \frac{1}{n^2} + \frac{k}{n^2} - \frac{1}{n^2} = 1 - \frac{1}{n} \Rightarrow k = n \tag{B.295}$$

$$-\frac{2}{n}(1-\frac{1}{n}) + (k-2)(\frac{1}{n})^2 = -\frac{1}{n} \tag{B.296}$$

$$-\frac{2}{n} + \frac{2}{n^2} + \frac{k}{n^2} - \frac{2}{n^2} = -\frac{1}{n} \Rightarrow k = n \tag{B.297}$$

where (B.294) and (B.296) are respectively the diagonal and non-diagonal elements of $\mathbf{A}$ and $\mathbf{A}^2$. This shows that $\mathbf{A}^2 = \mathbf{A} \quad \forall\, n \in \mathbb{N}$.

[5] Note that we are imposing Barbalat's lemma in a conservative manner, *i.e.*, we are ensuring that the "physical" states converge to the set $\{\mathbf{x} \in \mathbb{R}^9 : \|\boldsymbol{\chi}\| \leq \delta\}$ which contains the origin.